

1. Report No. FHWA/TX-94/1314-1F		2. Government Accession No.		3. Recipient's Catalog No.	
4. Title and Subtitle VERIFICATION OF AN ASPHALT AGING TEST AND DEVELOPMENT OF SUPERIOR RECYCLING AGENTS AND ASPHALTS				5. Report Date November 1994	
				6. Performing Organization Code	
7. Author(s) Richard R. Davison, Jerry A. Bullin, Charles J. Glover, Jay M. Chaffin, Gerald D. Peterson, Kevin M. Lunsford, Moon S. Lin, Meng Liu, and Martha A. Ferry				8. Performing Organization Report No. Research Report 1314-1F	
9. Performing Organization Name and Address Texas Transportation Institute and Chemical Engineering Department The Texas A&M University System College Station, Texas 77843-3135				10. Work Unit No. (TRAIS)	
				11. Contract or Grant No. Study No. 0-1314	
12. Sponsoring Agency Name and Address Texas Department of Transportation Research and Technology Transfer Office P. O. Box 5080 Austin, Texas 78763-5080				13. Type of Report and Period Covered Final: May 1992 - August 1994	
				14. Sponsoring Agency Code	
15. Supplementary Notes Research performed in cooperation with the Texas Department of Transportation and the U.S. Department of Transportation, Federal Highway Administration. Research Study Title: Verification of an Asphalt Aging Test and Development of Superior Recycling Agents and Asphalts					
16. Abstract This study included an in-depth investigation of asphalt oxidation hardening and accelerated aging tests to simulate asphalt hardening on the road. A very significant finding is that the effect of both temperature and pressure on hardening rates is very asphalt dependent, so that any test run at a single elevated temperature or pressure can be very misleading. Equations are given which express asphalt oxidation as a function of both temperature and pressure which, with sufficient data, permit calculations at ambient conditions. Test section studies indicate that actual road aging is considerably slowed by diffusion resistance. Extensive studies were conducted on compositional effects in recycling. Hardening in asphalt is almost totally due to asphaltene formation. Recycling agents should be asphaltene free and low in saturates. Good mixing rules were developed for asphaltene free agents. In general, asphaltene-free agents lowered the blend viscosity more than would normally be predicted from the agent viscosity. Aging studies on recycled material produced good results with some commercial agents as well as with fractions obtained by supercritical fractionation of asphalts.					
17. Key Words Asphalt Aging, Asphalt Recycling, Supercritical Fractionation, Recycling Agent Composition			18. Distribution Statement No restrictions. This document is available to the public through NTIS: National Technical Information Service 5285 Port Royal Road Springfield, Virginia 22161		
19. Security Classif.(of this report) Unclassified		20. Security Classif.(of this page) Unclassified		21. No. of Pages 356	22. Price



VERIFICATION OF AN ASPHALT AGING TEST AND DEVELOPMENT
OF SUPERIOR RECYCLING AGENTS AND ASPHALTS

by

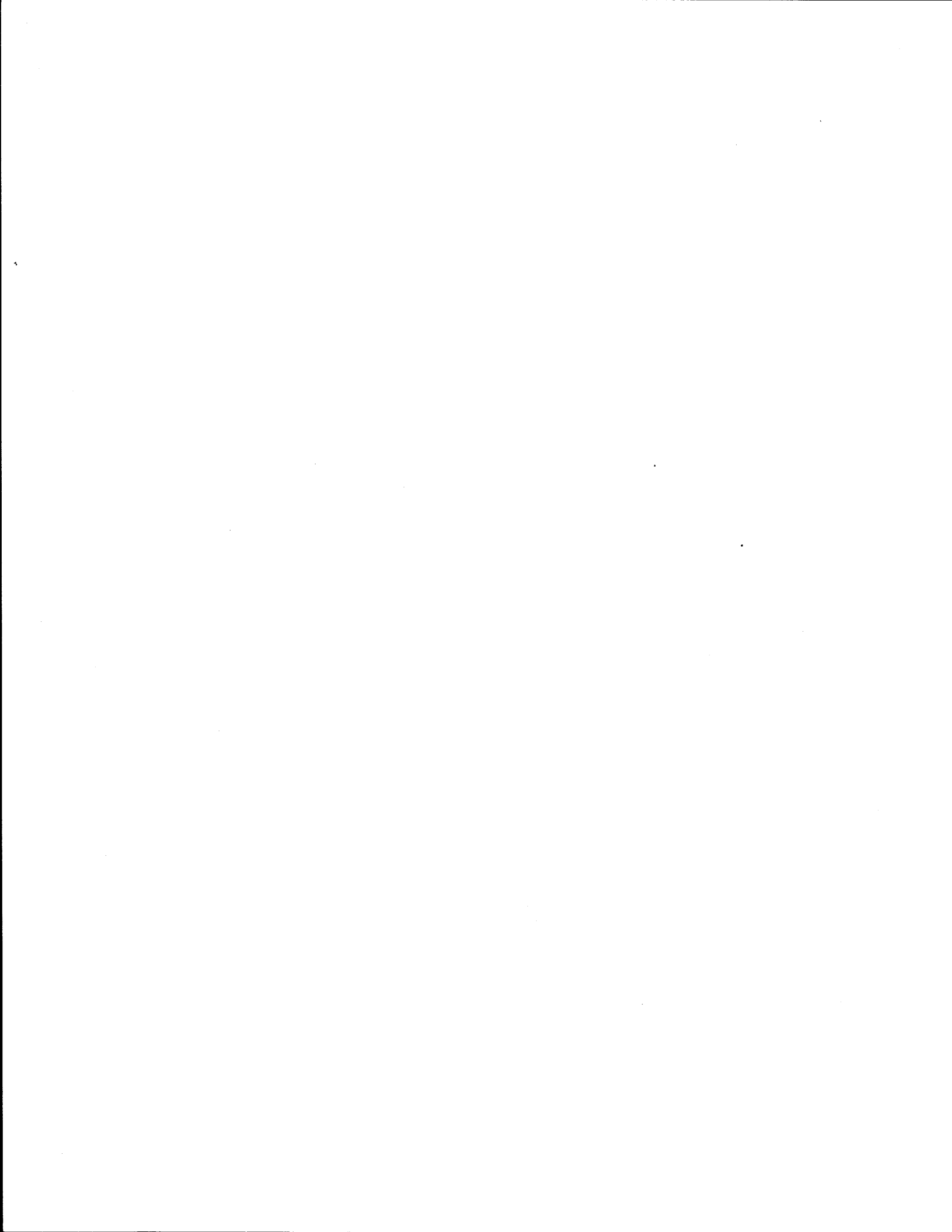
Richard R. Davison
Jerry A. Bullin
Charles J. Glover
Jay M. Chaffin
Gerald D. Peterson
Kevin M. Lunsford
Moon S. Lin
Meng Liu
Martha A. Ferry

Research Report 1314-1F
Research Study Number 0-1314
Research Study Title: Verification of an Asphalt Aging Test
and Development of Superior Recycling Agents and Asphalts

Sponsored by the
Texas Department of Transportation
In Cooperation with
U. S. Department of Transportation
Federal Highway Administration

November 1994

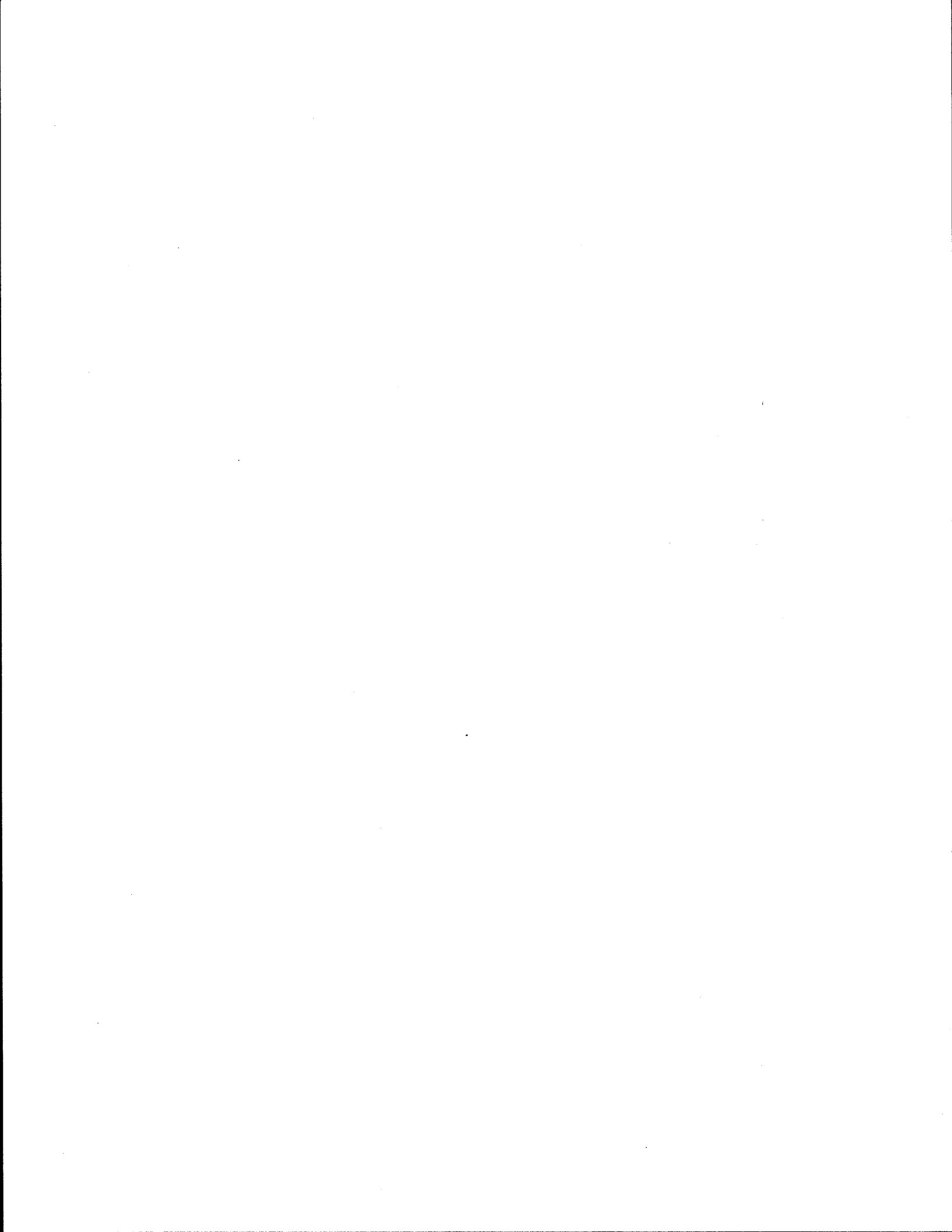
TEXAS TRANSPORTATION INSTITUTE
and
Chemical Engineering Department
The Texas A&M University System
College Station, Texas 77843-3135



IMPLEMENTATION STATEMENT

Although the Study 1314 portion of the recycling agent work has terminated, this project will continue for two more years under Department of Energy matching funds. Thus, the final recommendation for recycling agent will be presented at the end of this period. However, based on the intermediate study results available to date, the following implementation guidelines can be made for recycling agents:

- The paraffin content should be as low as possible and preferably below 10 to 15%.
- The asphaltene content should be near zero.
- Some old asphalts can be much more sensitive to the choice of recycling agent than others. Thus, the sensitivity should be examined before construction.
- The present work clearly indicates that aging tests performed at a single elevated temperature or pressure can produce misleading results.
- An equation has been developed and is present in this report to predict the viscosity for blends of old asphalt with asphaltene-free recycling agents.



DISCLAIMER

The contents of this report reflect the views of the authors, who are responsible for the facts and the accuracy of the data presented herein. The contents do not necessarily reflect the official views or policies of the Federal Highway Administration or the Texas Department of Transportation. This report does not constitute a standard, specification, or regulation. This report is not intended for construction, bidding, or permit purposes.

ACKNOWLEDGMENT

The authors wish to express their appreciation for contributions made by several individuals during the study. Mr. Darren Hazlett of the Texas Department of Transportation was very helpful in making technical suggestions and in serving as study contacts. Special thanks are extended to Mrs. Dorothy Jordan for her contribution in preparing the manuscript. The excellent staff support of the Chemical Engineering Department and the Texas Transportation Institute of Texas A&M University is greatly appreciated.

The financial support provided by the Texas Department of Transportation in cooperation with the Federal Highway Administration, the Texas Transportation Institute, the Texas Engineering Experiment Station, and the Chemical Engineering Department at Texas A&M University is also greatly appreciated.

TABLE OF CONTENTS

	Page
List of Figures	xiv
List of Tables	xxviii
Summary	xxxiii
Section I - Asphalt Aging Test Development	1
Chapter	
1 The Kinetics of Carbonyl Formation in Asphalt	3
Experimental Design	4
Order of Reaction	6
Activation Energies and Arrhenius Constants	12
Multi-Variable Parameter Estimation	18
Comparison of E_A with Literature Values	20
Hypothesized Model for CA_0 as a Function of Observable Variables	21
2 Extended Aging Studies	25
Experimental Design	25
Results	26
Section II - The Effect of Asphaltene Content on Asphalt Hardening and Recycling	55
Chapter	
3 Model Development for the Effect of Asphaltenes on Viscosity	57
Experiments and Methodology	60
Results and Discussion	61
4 Application of the Model to Mixtures of Asphaltenes and Maltenes from Diverse Sources	77

	Page
Experiments and Methodology	77
Results and Discussion	78
Section III - Recycling	97
Chapter	
5 Materials Production for Recycling	99
Supercritical Fractionation	99
Process Description	99
Operating Conditions	100
Apparatus Modifications	103
Asphalt Fractionation	105
Asphalt Properties	106
Fractionation	107
Fraction Properties	109
Fraction Uses	113
Aged Asphalt Production	114
6 Compositional Effects in Asphalt Recycling	119
Introduction	119
Methods	119
Experimental Design and Results	120
Oils and Aromatics (Experiment 1)	121
Metals and Asphaltenes (Experiment 2)	123
Supercritical Fractions as Recycling Agents	126
The Effect of Saturates on Hardening Susceptibility and Temperature Susceptibility	133
7 Recycling Agent Experiments	137
Aged Material Analyses	137
8 Mixing Rules	143

	Page
Experimental Methods	144
Aged Asphalt Production	145
Softening Agents	147
Experimental Design and Results	148
Discussion of Results	158
9 Interstate 45 Recycling	163
Sampling	163
Analyses and Sampling	166
Recycling Studies	168
Core Testing	171
Section IV - Highway Modeling	177
Chapter	
10 Fundamentals of a Highway Aging Model	179
Objectives	179
Literature Survey	180
Overview of the Thin-Film Model	183
Results	186
Estimation of Oxygen Diffusivity	190
Steady-State Variable Diffusivity	200
Unsteady-State Oxygen Diffusion and Reaction	204
Diffusion and Reaction in Asphalt Aging Tests	211
Summary	213
11 Comparison Between Laboratory and Field Aging	215
Literature Survey of Field Aging	216
Highway Samples and Laboratory Experimental Design	220
POV- and Field-Aging Comparisons:	
Experimental Data	222

	Page
Confirming Complete Solvent Removal and Coring Location	222
Comparisons Between η_o^* and CA	227
POV- and Field-Aging Comparisons: Asphalt-Aging Model	237
Experimental Design to Determine Kinetic Parameters	238
Estimation of Pavement Surface Temperature	238
Calculation of t_{theor} to Reach Measured CA	240
The Asphalt-Aging Model and Pavement Aging	242
Pavement Aging Model Development	245
Estimation of L_{eff} with Constant P_{eff}	246
Estimation of L_{eff} with Variable P_{eff}	247
Summary	251
Section V - Conclusions and Recommendations	253
Conclusions	253
Recommendations	256
References	257
Appendix A: Experimental Methods	265
Supercritical Extraction	265
Pressure Oxygen Vessel (POV) Configuration II	265
POV Configuration III	266
Corbett Analysis	268
Giant Corbett Apparatus	268
Separation of Saturates into Oils and Waxes	270
Corbett Analysis Using HPLC	270
Fourier Transform Infrared Spectroscopy, FTIR	271
Dynamic Mechanical Analysis, DMA	273

	Page
Hexane Asphaltene Determination	273
Gel Permeation Chromatography, GPC	274
Void Content of Field-Aged Cores, % V	275
Extraction and Recovery of Field-Aged Asphalt	275
Appendix B: Data for Chapter 1	277
Appendix C: Highway Aging Model and Data	301
Overview	301
Oxygen Transport and Reaction	302
Quantitative Details of the Model	304
Oxygen Film Concentration in Terms of Oxygen Pressure	304
r_{O_2} Versus r_{CA}	304
D_{O_2} as a Function of T and CA	305
Relationships Between η_0^* and CA for Multiple Temperatures	306
Carbonyl Formation Rate	309

LIST OF FIGURES

Figure		Page
1-1	C_A s of Neat and POV-Aged Cosden AC-20 at 333.3 K	7
1-2	C_A s of Neat and POV-Aged Cosden AC-20 at 344.4 K	8
1-3	C_A s of Neat and POV-Aged Cosden AC-20 at 355.5 K	8
1-4	r_{CA} Versus P at 333.3 K for POV-Aged Cosden AC-20	9
1-5	r_{CA} Versus P at 333.3 K for All POV-Aged Asphalts Studied	10
1-6	r_{CA} Versus P at 344.4 K for All POV-Aged Asphalts Studied	10
1-7	r_{CA} Versus P at 355.5 K for All POV-Aged Asphalts Studied	11
1-8	C_A s of Neat and POV-Aged Cosden AC-20 at 0.2 atm	13
1-9	C_A s of Neat and POV-Aged Cosden AC-20 at 2 atm	13
1-10	C_A s of Neat and POV-Aged Cosden AC-20 at 20 atm	14
1-11	r_{CA} Versus $(1/T)$ at 0.2 atm for POV-Aged Cosden AC-20	15
1-12	r_{CA} Versus $(1/T)$ at 0.2 atm for All POV-Aged Asphalts Studied	15
1-13	r_{CA} Versus $(1/T)$ at 2 atm for All POV-Aged Asphalts Studied	16
1-14	r_{CA} Versus $(1/T)$ at 20 atm for All POV-Aged Asphalts Studied	16
1-15	CA_o Versus POV Aging Temperature for Cosden AC-20	22

	Page
1-16 CA_o Versus POV Aging Temperature for All Asphalts Studied	23
2-1 Carbonyl Formation Rates Under Different Aging Conditions (SHRP AAA-1)	27
2-2 Carbonyl Formation Rates Under Different Aging Conditions (SHRP AAD-1)	27
2-3 Carbonyl Formation Rates Under Different Aging Conditions (SHRP AAF-1)	28
2-4 Carbonyl Formation Rates Under Different Aging Conditions (SHRP AAG-1)	28
2-5 Carbonyl Formation Rates Under Different Aging Conditions (SHRP AAM-1)	29
2-6 Carbonyl Formation Rates Under Different Aging Conditions (SHRP AAB-1)	29
2-7 Carbonyl Formation Rates Under Different Aging Conditions (SHRP AAS-1)	30
2-8 Carbonyl Formation Rates Under Different Aging Conditions (Conoco 125/150)	30
2-9 Carbonyl Formation Rates Under Different Aging Conditions (Exxon AC-20)	31
2-10 Carbonyl Formation Rates Under Different Aging Conditions (Shell AC-5)	31
2-11 Hardening Susceptibility Versus Aging Pressure (SHRP AAA-1)	33
2-12 Hardening Susceptibility Versus Aging Pressure (SHRP AAD-1)	33
2-13 Hardening Susceptibility Versus Aging Pressure (SHRP AAF-1)	34

	Page
2-14 Hardening Susceptibility Versus Aging Pressure (SHRP AAG-1)	34
2-15 Hardening Susceptibility Versus Aging Pressure (SHRP AAM-1)	35
2-16 Hardening Susceptibility Versus Aging Pressure (SHRP AAB-1)	35
2-17 Hardening Susceptibility Versus Aging Pressure (SHRP AAS-1)	36
2-18 Hardening Susceptibility Versus Aging Pressure (Conoco 125/150)	36
2-19 Hardening Susceptibility Versus Aging Pressure (Exxon AC-20)	37
2-20 Hardening Susceptibility Versus Aging Pressure (Shell AC-5)	37
2-21 Comparison of Surface and Bulk Values, AAD-1	39
2-22 Comparison of Surface and Bulk Values, AAF-1	39
2-23 Hardening Susceptibility Versus Film Thickness (SHRP AAA-1)	40
2-24 Hardening Susceptibility Versus Film Thickness (SHRP AAD-1)	40
2-25 Hardening Susceptibility Versus Film Thickness (SHRP AAF-1)	41
2-26 Arrhenius Plot of Set I Asphalts	42
2-27 Arrhenius Plot of Set II Asphalts	42
2-28 Calculated Rates Versus Pressure Corrected Experimental Rates	45

	Page
2-29 Pressure Corrected Rates and Arrhenius Plot by Linear Regression (SHRP AAA-1)	46
2-30 Pressure Corrected Rates and Arrhenius Plot by Linear Regression (SHRP AAD-1)	46
2-31 Pressure Corrected Rates and Arrhenius Plot by Linear Regression (SHRP AAF-1)	47
2-32 Pressure Corrected Rates and Arrhenius Plot by Linear Regression (SHRP AAG-1)	47
2-33 Pressure Corrected Rates and Arrhenius Plot by Linear Regression (SHRP AAM-1)	48
2-34 Pressure Corrected Rates and Arrhenius Plot by Linear Regression (SHRP AAB-1)	48
2-35 Pressure Corrected Rates and Arrhenius Plot by Linear Regression (SHRP AAS-1)	49
2-36 Pressure Corrected Rates and Arrhenius Plot by Linear Regression (Conoco 125/150)	49
2-37 Pressure Corrected Rates and Arrhenius Plot by Linear Regression (Exxon AC-20)	50
2-38 Pressure Corrected Rates and Arrhenius Plot by Linear Regression (Shell AC-5)	50
2-39 Pressure Dependence Factor Versus Activation Energy	52
2-40 Log Frequency Factor Versus Activation Energy	52
2-41 Hardening Susceptibility Versus Activation Energy	53
2-42 Initial Jump Versus Activation Energy	53
2-43 Calculated Reaction Rate Versus Activation Energy	54
2-44 Critical Time Versus Activation Energy	54

	Page
3-1 Carbonyl Area Versus Aging Time for SHRP AAA-1 Asphalt	63
3-2 Asphaltene Content Versus Aging Time for SHRP AAA-1 Asphalt	63
3-3 Total Asphaltene Versus Carbonyl Area for SHRP AAA-1 Asphalt	65
3-4 Produced Asphaltene Versus Carbonyl for SHRP AAA-1 Asphalt	65
3-5 AFS for All of SHRP Asphalts and Maltenes Studied	66
3-6 Viscosity Versus Aging Time for SHRP AAA-1 Asphalt	68
3-7 Modified Pal-Rhodes Model for SHRP AAA-1 Asphalt and Maltene	69
3-8 Modified Pal-Rhodes Model for SHRP AAC-1 Asphalt and Maltene	69
3-9 Viscosity Versus Asphaltene Content for Unaged SHRP AAA-1 Blends	72
3-10 Modified Pal-Rhodes Model for All of Asphalts Studied	72
3-11 Hardening Susceptibility of SHRP AAA-1 Asphalt and Maltene	73
3-12 Rutting Parameter Versus Asphaltene for SHRP AAA-1 Asphalt	76
4-1 Viscosities of Unaged Blends as Function of Asphaltene Content	80
4-2 Hardening Susceptibilities of SHRP AAD-1 and AAG-1	81
4-3 FT-IR Spectra of Produced Asphaltenes for SHRP AAD-1	83

	Page
4-4 Produced Asphaltene Versus Carbonyl Area for SHRP AAD-1	83
4-5 AFS for SHRP AAD-1 Asphalt and Asphaltene/Maltene Blends	84
4-6 AFS for SHRP AAG-1 Asphalt and Asphaltene/Maltene Blends	84
4-7 Comparison of AFS for SHRP AAD-1 and AAG-1	85
4-8 Viscosity/Asphaltene Relationship for Unaged DD and D Maltene	86
4-9 GPC of Original and Produced Asphaltene for SHRP AAD-1	87
4-10 Viscosity/Asphaltene Relationship for GD and D Maltene	88
4-11 Viscosity/Asphaltene Relationship for KD and D Maltene	88
4-12 Viscosity/Asphaltene Relationship for BMD and D Maltene	89
4-13 GPC of Original Asphaltenes for Four SHRP Asphalts	90
4-14 Viscosity/Asphaltene Relationship for DD, GD, KD and BMD	90
4-15 Viscosity/Asphaltene Relationship for GG and G Maltene	91
4-16 Viscosity/Asphaltene Relationship for KG and G Maltene	91
4-17 Viscosity/Asphaltene Relationship for DG and G Maltene	92
4-18 Viscosity/Asphaltene Relationship for GG, KG and DG	92
4-19 GPC of Original and Produced Asphaltene for SHRP AAG-1 ...	93
4-20 Reduced Viscosity Versus Asphaltene for Blends Studied	94
4-21 $(d \log \eta_r/d \%A)$ Versus Asphaltene for Blends Studied	95

	Page
5-1 Supercritical Unit Process Diagram	101
5-2 Legend for Supercritical Extraction Unit Diagram	102
5-3 Fraction Viscosity Versus Fraction Number	111
5-4 Asphaltene Content Versus Fraction Number	111
5-5 Aromatic Content Versus Fraction Number	112
5-6 Saturate Content Versus Fraction Number	112
5-7 Molecular Weight Versus Fraction Number	113
5-8 Effect of Air Bubbler Temperature on HS	116
6-1 Experiment 1: Hardening Susceptibilities	122
6-2 Hardening Susceptibility Versus Oil Content	122
6-3 Effect of Metals on Hardening Susceptibility	125
6-4 Effect of Asphaltenes on Hardening Susceptibilities	125
6-5 Effect of Asphaltenes on Hardening and Carbonyl Formation Rates	126
6-6 Asphalt Viscosity Frequency Sweep	129
6-7 Coastal Blend Hardening Susceptibilities	129
6-8 Effect of Paraffins on Hardening Susceptibilities	134
6-9 Effect of Paraffins on Temperature Susceptibilities	134
7-1 Blend HS Versus Initial Blend Asphaltene Content	139
7-2 Blend HS Versus Initial Blend Aromatic Content	140
7-3 Blend HS Versus Initial Blend Saturate Content	140

	Page
7-4 Blend HS Versus Initial Blend AR/SA Ratio	141
7-5 Blend HS Versus Initial Blend I_c	142
8-1 Viscosity for POV AAA-1 and AAA-AB7 Blends with Sun 125	149
8-2 Viscosity for Blends of AAF-AB2 with 8 Recycling Agents	149
8-3 Viscosity for Blends of AAF-AB2 with 3 Low Viscosity Asphalts	150
8-4 Dimensionless Log Viscosity for AAF-AB2 Blends	152
8-5 DLV Versus Aged Asphalt Mass Fraction for Blends Using AAF-AB1	154
8-6 DLV for Blends of AAF-AB2 and AAF-AB1 with Recycling Agents	155
8-7 DLV for AAA-AB7 Blends	156
8-8 DLV for AAA-AB8 Blends	157
8-9 Anomalous Behavior of AAA-AB8/DS AC-3 Blends	157
8-10 DLV for Oven Coastal Blends	159
8-11 DLV for POV ABM-1 Blends	159
8-12 DLV Mixing Rule for All Recycling Agent Blends	160
9-1 Laboratory Core Air Voids	173
9-2 Laboratory Core Hveem Stabilities	173
9-3 Laboratory Core Resilient Moduli	174
9-4 Laboratory Core Indirect Tensile Strength	174
10-1 Highway Pavement Cross-Section	183

	Page
10-2 Oxygen Diffusion and Reaction in a Thin Asphalt Film	184
10-3 Measured CA Growth at the ES and SI (333.3 K, 0.2 atm)	186
10-4 Measured CA Growth at the ES and SI (333.3 K, 2 atm)	187
10-5 Measured CA Growth at the ES and SI (344.4 K, 0.2 atm)	187
10-6 Measured CA Growth at the ES and SI (344.4 K, 2 atm)	188
10-7 Measured CA Growth at the ES and SI (355.5 K, 0.2 atm)	188
10-8 Measured CA Growth at the ES and SI (355.5 K, 2 atm)	189
10-9 Calculated Oxygen Pressure Profiles in a 1 mm Thick Film (0.2 atm)	193
10-10 Calculated Oxygen Pressure Profiles in a 1 mm Thick Film (2 atm)	193
10-11 Estimated D_{O_2} for all 1 mm Thick Films	199
10-12 Calculated Oxygen Pressure Profiles (333.3 K)	201
10-13 Calculated Oxygen Pressure Profiles (344.4 K)	203
10-14 Calculated Oxygen Pressure Profiles (355.5 K)	203
10-15 Comparisons of Measured and Calculated CA (333.3 K, 0.2 atm)	205
10-16 Comparisons of Measured and Calculated CA (333.3 K, 2 atm)	206
10-17 Comparisons of Measured and Calculated CA (344.4 K, 0.2 atm)	206
10-18 Comparisons of Measured and Calculated CA (344.4 K, 2 atm)	207

	Page
10-19 Comparisons of Measured and Calculated CA (355.5 K, 0.2 atm)	207
10-20 Comparisons of Measured and Calculated CA (355.5 K, 2 atm)	208
10-21 Calculated Oxygen Pressure Profiles Change Over Time	209
10-22 Calculated CA Growth	209
10-23 Calculated η_0^* Growth	210
10-24 Calculated D_{O_2} Decrease Over Time	210
11-1 GPC Chromatograms of Field-Aged Cores (Dickens Cosden AC-10)	223
11-2 GPC Chromatograms of Tank and POV-Aged Dickens Cosden AC-10	224
11-3 POV- and Field-Aged Dickens Cosden AC-10	225
11-4 POV- and Field-Aged Dickens Diamond Shamrock AC-20	226
11-5 POV- and Field-Aged Dickens Dorchester AC-20	226
11-6 η_0^* Versus CA for Dickens Cosden AC-10	229
11-7 η_0^* Versus CA for Dickens Cosden AC-20	229
11-8 η_0^* Versus CA for Dickens Exxon AC-20	230
11-9 η_0^* Versus CA for Dickens MacMillan AC-20	230
11-10 η_0^* Versus CA for Dickens Diamond Shamrock AC-20	231
11-11 η_0^* Versus CA for Dickens Dorchester AC-20	231
11-12 η_0^* Versus CA for Pineland Cosden AC-20	233

	Page
11-13 η_0^* Versus CA for Pineland Dorchester AC-20	233
11-14 η_0^* Versus CA for Pineland Exxon AC-20	234
11-15 η_0^* Versus CA for Pineland MacMillan AC-20	234
11-16 η_0^* Versus CA for Pineland Texaco AC-20	235
11-17 η_0^* Versus CA for Bryan Exxon AC-20	236
11-18 Temperature Effected Oxygen Pressure Profiles in Ampet AC-20	243
11-19 Temperature Effected CA Profiles in Ampet AC-20	243
11-20 Temperature Effected CA_{avg} in Ampet AC-20	244
11-21 Hypothesized P_{eff} Time Constant λ Versus Percent Air Voids	248
11-22 Hypothesized L_{eff} Versus Percent Asphalt	250
A-1 Pressure Oxygen Vessel Control Panel	266
A-2 Pressure Oxygen Vessel and Control Panel	267
A-3 Giant Corbett Apparatus	269
B-1 CAs of Tank and POV-Aged Ampet AC-20 at 333.3 K	282
B-2 CAs of Tank and POV-Aged Ampet AC-20 at 344.4 K	283
B-3 CAs of Tank and POV-Aged Ampet AC-20 at 355.5 K	283
B-4 CAs of Tank and POV-Aged Coastal AC-20 at 333.3 K	284
B-5 CAs of Tank and POV-Aged Coastal AC-20 at 344.4 K	284
B-6 CAs of Tank and POV-Aged Coastal AC-20 at 355.5 K	285
B-7 CAs of Tank and POV-Aged Exxon AC-20 at 333.3 K	285

	Page
B-8 CAs of Tank and POV-Aged Exxon AC-20 at 344.4 K	286
B-9 CAs of Tank and POV-Aged Exxon AC-20 at 355.5 K	286
B-10 CAs of Tank and POV-Aged Texaco AC-20 at 333.3 K	287
B-11 CAs of Tank and POV-Aged Texaco AC-20 at 344.4 K	287
B-12 CAs of Tank and POV-Aged Texaco AC-20 at 355.5 K	288
B-13 CAs of Tank and POV-Aged Ampet AC-20 at 0.2 atm	288
B-14 CAs of Tank and POV-Aged Ampet AC-20 at 2 atm	289
B-15 CAs of Tank and POV-Aged Ampet AC-20 at 20 atm	289
B-16 CAs of Tank and POV-Aged Coastal AC-20 at 0.2 atm	290
B-17 CAs of Tank and POV-Aged Coastal AC-20 at 2 atm	290
B-18 CAs of Tank and POV-Aged Coastal AC-20 at 20 atm	291
B-19 CAs of Tank and POV-Aged Exxon AC-20 at 0.2 atm	291
B-20 CAs of Tank and POV-Aged Exxon AC-20 at 2 atm	292
B-21 CAs of Tank and POV-Aged Exxon AC-20 at 20 atm	292
B-22 CAs of Tank and POV-Aged Texaco AC-20 at 0.2 atm	293
B-23 CAs of Tank and POV-Aged Texaco AC-20 at 2 atm	293
B-24 CAs of Tank and POV-Aged Texaco AC-20 at 20 atm	294
B-25 CAs of Tank and POV-Aged SHRP AAA-1	294
B-26 CAs of Tank and POV-Aged SHRP AAD-1	295
B-27 CAs of Tank and POV-Aged SHRP AAG-1	295
B-28 CAs of Tank and POV-Aged SHRP AAM-1	296

	Page
B-29 CAs of Tank and POV-Aged Ampet AC-20	296
B-30 CAs of Tank and POV-Aged Coastal AC-20	297
B-31 CAs of Tank and POV-Aged Cosden AC-20	297
B-32 CAs of Tank and POV-Aged Exxon AC-20	298
B-33 CAs of Tank and POV-Aged Texaco AC-20	298
B-34 Initial Jump Versus Aging Temperature for Ampet AC-20	299
B-35 Initial Jump Versus Aging Temperature for Coastal AC-20	299
B-36 Initial Jump Versus Aging Temperature for Exxon AC-20	300
B-37 Initial Jump Versus Aging Temperature for Texaco AC-20	300
C-1 CAs of Tank, <i>ES</i> and <i>SI</i> (Ampet AC-20, 333.3 K, 0.2 atm)	310
C-2 CAs of Tank, <i>ES</i> and <i>SI</i> (Ampet AC-20, 333.3 K, 2 atm)	311
C-3 CAs of Tank, <i>ES</i> and <i>SI</i> (Ampet AC-20, 344.4 K, 0.2 atm)	311
C-4 CAs of Tank, <i>ES</i> and <i>SI</i> (Ampet AC-20, 344.4 K, 2 atm)	312
C-5 CAs of Tank, <i>ES</i> and <i>SI</i> (Ampet AC-20, 355.5 K, 0.2 atm)	312
C-6 CAs of Tank, <i>ES</i> and <i>SI</i> (Ampet AC-20, 355.5 K, 2 atm)	313
C-7 CAs of Tank, <i>ES</i> and <i>SI</i> (Cosden AC-20, 333.3 K, 0.2 atm)	313
C-8 CAs of Tank, <i>ES</i> and <i>SI</i> (Cosden AC-20, 333.3 K, 2 atm)	314
C-9 CAs of Tank, <i>ES</i> and <i>SI</i> (Cosden AC-20, 344.4 K, 0.2 atm)	314
C-10 CAs of Tank, <i>ES</i> and <i>SI</i> (Cosden AC-20, 344.4 K, 2 atm)	315
C-11 CAs of Tank, <i>ES</i> and <i>SI</i> (Cosden AC-20, 355.5 K, 0.2 atm)	315
C-12 CAs of Tank, <i>ES</i> and <i>SI</i> (Cosden AC-20, 355.5 K, 2 atm)	316

	Page
C-13	<i>CAs of Tank, ES and SI (Exxon AC-20, 333.3 K, 0.2 atm)</i> 316
C-14	<i>CAs of Tank, ES and SI (Exxon AC-20, 333.3 K, 2 atm)</i> 317
C-15	<i>CAs of Tank, ES and SI (Exxon AC-20, 344.4 K, 0.2 atm)</i> 317
C-16	<i>CAs of Tank, ES and SI (Exxon AC-20, 344.4 K, 2 atm)</i> 318
C-17	<i>CAs of Tank, ES and SI (Exxon AC-20, 355.5 K, 0.2 atm)</i> 318
C-18	<i>CAs of Tank, ES and SI (Exxon AC-20, 355.5 K, 2 atm)</i> 319
C-19	<i>CAs of Tank, ES and SI (Texaco AC-20, 333.3 K, 0.2 atm)</i> 319
C-20	<i>CAs of Tank, ES and SI (Texaco AC-20, 333.3 K, 2 atm)</i> 320
C-21	<i>CAs of Tank, ES and SI (Texaco AC-20, 344.4 K, 0.2 atm)</i> 320
C-22	<i>CAs of Tank, ES and SI (Texaco AC-20, 344.4 K, 2 atm)</i> 321
C-23	<i>CAs of Tank, ES and SI (Texaco AC-20, 355.5 K, 0.2 atm)</i> 321
C-24	<i>CAs of Tank, ES and SI (Texaco AC-20, 355.5 K, 2 atm)</i> 322

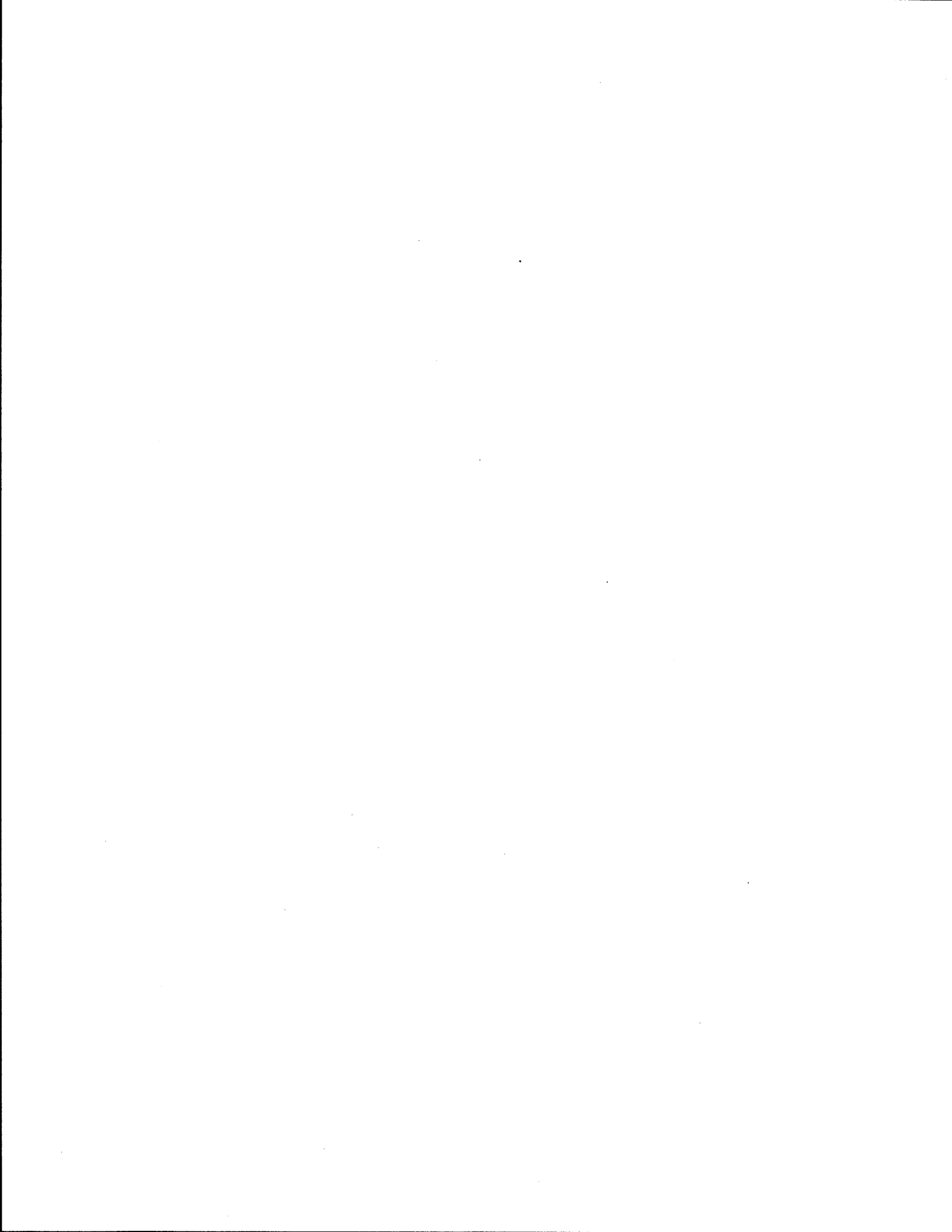
LIST OF TABLES

Table	Page
1-1 r_{CA} for All Asphalts and POV-Aging Conditions Studied	5
1-2 CA_o for All Asphalts and POV-Aging Conditions Studied	5
1-3 α for All POV-Aged Asphalts Studied	11
1-4 E_A for All POV-Aged Asphalts Studied	17
1-5 A for All POV-Aged Asphalts Studied	18
1-6 Kinetic Model Parameters for All POV-Aged Asphalts Studied	19
1-7 r_{CA} for CA_o for All POV-Aged Asphalts at 322.2 K (120°F) and 20 atm	22
2-1 List of Aging Conditions Applied	26
2-2a Aging Test Results: Kinetic Parameters	32
2-2b Aging Test Results: Hardening Susceptibility Parameters	38
2-3a Aging Tests: Time Comparisons	44
2-3b Aging Tests: Rank Comparisons	44
3-1 The Weight Percentage of n-Hexane Asphaltenes (%A), Zero Shear Rate Limiting Viscosities (η_o) and Reciprocal Loss Compliances (1/J") of Whole Asphalts, Blends and Maltenes	62
3-2 Asphaltene Formation Susceptibilities of Asphalts	67
3-3 Parameter ν and Solvation Constant (K') for Asphalts	73

	Page
3-4 The Zero Shear Limiting Viscosities (η_0^*), Weight Percentage of n-Hexane Asphaltenes (%A), and Carbonyl Areas (CA) of Asphalts at Break Point	75
4-1 The Weight Percentage of n-Hexane Asphaltenes (%A), Low Frequency Limiting Viscosities (η_0^*), and Relative Viscosity of Maltenes, Whole Asphalts, and Blends	79
5-1 Supercritical Operating Conditions and Fraction Yields	103
5-2 Tank Asphalt Data	106
5-3 SHRP Data	106
5-4 Representative Supercritical Fraction Properties	110
6-1 Asphaltenes and Metals of Starting Fractions	124
6-2 Compositions of Blends in Experiment 2	124
6-3 Compositions and Viscosities of Materials in Experiment 3	127
6-4 Viscosities and Blending Ratios for Experiment 4	130
6-5 Viscosity and Mixing Data for Experiment 5	132
7-1 Recycling Agent Table	138
7-2 Final Mixture Table	138
8-1 Representative Viscosities for Aged Asphalts and Softening Agents	146
8-2 Aged Asphalt/Agent Grunberg Interaction Parameter G_{12}	151
8-3 Comparison of Viscosities Resulting from Various Mixing Rules	161
9-1 I-45 Extraction Data	167
9-2 Blend HS and Most-Highly-Aged Sample Viscosity	170

	Page
10-1 Estimated D_{O_2} for Steady-State Constant D_{O_2} Oxygen Diffusion and Reaction	192
10-2 Estimated D_{O_2} at $\pm 40\%$ P_{SI} for Steady-State Constant D_{O_2} Oxygen Diffusion and Reaction	195
10-3 Suspect D_{O_2} and POV-Aging Conditions for Steady-State Constant D_{O_2} Oxygen Diffusion and Reaction	196
10-4 HS and $\exp(m)$ at 333.3, 344.4, and 355.5 K for All POV-Aged Asphalts Studied	197
10-5 Estimated D_{O_2} , Average CA and η_0^* , and POV-Aging Conditions for Steady-State Constant D_{O_2} Oxygen Diffusion and Reaction	198
10-6 Comparisons Between P_{SI} Estimated from r_{CA} and Calculated for Steady-State Variable D_{O_2}	202
10-7 Comparisons Between Calculated Time to Reach 500 kP η_0^* at 333.3 K (140°F), Aging at 322 K (120°F) and P_{ES} of 0.2 atm with and without Diffusion Resistance for Three Film Thicknesses	212
11-1 List of Asphalts Studied for Field Aging	221
11-2 Properties of 1987 Samples from Dickens and Pineland Test Sections	222
11-3 Arrhenius Parameters of POV- and Field-Aged Asphalts Estimated from POV Data	239
11-4 Location and Climatic Data for Dickens, Pineland, and Bryan, Texas	240
11-5 Comparisons Between t_{act} and t_{theor} for Measured CA of Field-Aged Asphalt	241

	Page
11-6 Estimated L_{eff} for Dickens and Bryan Asphalts with Constant P_{eff} of 0.2 atm	247
11-7 Hypothesized Model Between % V and λ	248
11-8 Estimated L_{eff} for Dickens, Pineland, and Bryan Asphalts with Variable P_{eff}	249
B-1 Ampet AC-20 Kinetic Data	277
B-2 Coastal AC-20 Kinetic Data	278
B-3 Cosden AC-20 Kinetic Data	279
B-4 Exxon AC-20 Carbonyl Areas	280
B-5 Texaco AC-20 Kinetic Data	281
B-6 Kinetic Data for Asphalts Aged at 322.2 K and 20 atm	282
C-1 CA and Wt% O_2 for Tank and POV-Aged SHRP AAA-1 at 344.4 K and 20 atm	305
C-2 E_v Model Parameters for All Asphalts Studied	308
C-3 CA_p Model Parameters from Measured and Estimated P for All POV-Aged Asphalts and Conditions Studied	310



SUMMARY

This study had two principal objectives: to develop a satisfactory aging test to study the effect of recycling on oxidative hardening and to study the effect of recycling agent composition on the properties of recycled blends. Perhaps the most significant finding is that the effect of temperature and pressure on asphalt oxidation is very asphalt dependent, and any test run at a single elevated temperature and pressure can be highly misleading. At the same time, equations have been developed which express asphalt oxidation rates in terms of both temperature and pressure so that with sufficient data, rates can be predicted at any road condition. These rates purposely do not include diffusion, which considerably retards roadway hardening. Some diffusion measurements were made and used in conjunction with test section aging rates to get a preliminary model of road aging in terms of asphalt properties and mix parameters.

Lengthy studies were made of asphalt hardening in connection with recycling. Rules were developed to predict the final viscosity when a recycling agent and an old asphalt are blended. In general, asphaltene-free agents gave lower blend viscosities for given starting values. Also, for the agents studied, those containing no asphaltenes followed a common relation. Hardening studies indicated that hardening increased with both asphaltene content and saturate content. Viscosity increase in asphalt is almost totally due to increase in asphaltene content, but this increase is very maltene dependent with some maltenes producing asphaltenes much more rapidly for a given degree of oxidation. Asphaltene source appears to have no effect on this nor do asphaltenes catalyze further asphaltene formation. Hardening increases exponentially with asphaltene content, so an important factor in recycling is asphaltene dilution. Optimally, then, the recycling agent should be asphaltene-free and low in saturates, but subsequent oxidation rates and asphaltene formation rates will also vary with the resulting blend aromatic composition. For some asphalts with the proper agent, recycled material may actually be superior to the original asphalt.

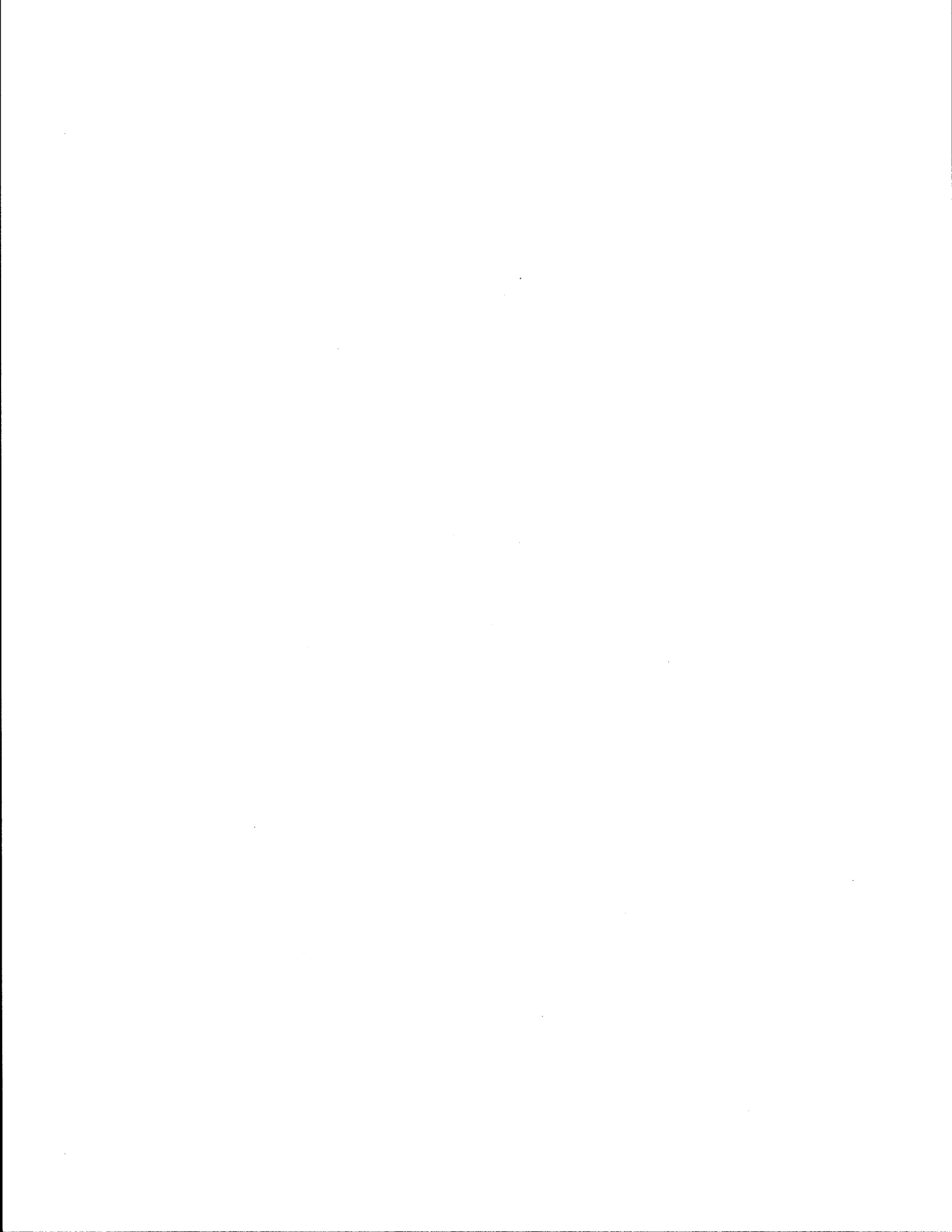


SECTION I

ASPHALT AGING TEST DEVELOPMENT

As reported in Study 1249 (Davison et al., 1992) and in Lau et al. (1992), an aging test conducted at a single elevated temperature can be misleading because differing activation energies between asphalts can cause a reversal in relative oxidation rates at road temperatures from those obtained at the test temperature. In these studies, asphalt was oxidized in a POV (pressure oxygen vessel) at several temperatures so that the oxidation rate could be extrapolated to road temperatures. To increase the oxidation rate, particularly at lower test temperatures, the data were collected at 20 atm.

The oxidation occurs in two stages: an initial rapid rate that declines to a constant rate. The oxidation is expressed in terms of the infrared measured carbonyl peak area, CA , since this correlates very well with the physical property changes. The contribution of the initial rapid oxidation, CA_o , was defined as the intercept of the extrapolation of the constant rate to zero time. This rate was found to be very asphalt dependent and also to be larger than expected. Since the effect of temperature on rate was asphalt dependent as well as the initial jump, the question arose whether there were pressure effects that were asphalt dependent. In this section we report the extensive work to determine these effects and describe the increasing complexity encountered in developing a satisfactory universal test to measure the relative rates of hardening that would be experienced by asphalts at road temperatures and pressure.



CHAPTER 1

THE KINETICS OF CARBONYL FORMATION IN ASPHALT

Several authors have reported that the carbonyl content, CA , in an asphalt as a result of oxidative aging changes the physical properties of the asphalt in a predictable way (Lee and Huang, 1973; Martin et al., 1990; Lau et al., 1992; and Petersen et al., 1993). An integrated form of the rate equation calculates CA at any time t as given in Equation 1-1.

$$CA(t) = \int_0^t r_{CA} d\theta + CA_o \quad (1-1)$$

where CA_o is a function of the initial rate. A preliminary kinetic model with an Arrhenius form was presented (Lau et al., 1992).

$$r_{CA} = A \exp\left(\frac{-E_A}{RT}\right) \quad (1-2)$$

Although Equation 1-2 describes the effect of T on r_{CA} , this model neglects any oxygen concentration or pressure effects. An improved model, accounting for both T and P , is given in Equation 1-3.

$$r_{CA} = A \exp\left(\frac{-E_A}{RT}\right) P^\alpha \quad (1-3)$$

Experimental data are required to estimate the model parameters describing the r_{CA} and CA_o . With these parameters determined, CA at any time t can be calculated. Furthermore, physical properties can be determined from the value of CA provided accurate physicochemical relationships exist. These physical properties are ultimately related to the performance of the asphalt binder. Therefore, the ability to predict CA in asphalt as a result of oxidative aging is a fundamental step toward predicting asphalt performance.

EXPERIMENTAL DESIGN

A series of aging experiments at different temperatures, oxygen pressures, and with different asphalts, is described. These experiments provide the necessary data to estimate the model parameters in Equation 1-3. Because of simultaneous diffusion and reaction of oxygen in the asphalt film, the method of data collection and analysis is critical. If steps are not taken to minimize the effect of oxygen diffusion in the data collection, the conclusions may be erroneous. Oxygen diffusion and reaction varies the oxygen concentration, or pressure, through the asphalt film. For high oxygen pressures and thin films, the diffusion problem is decreased. However, for low oxygen pressures, the diffusion problem may be significant. In an asphalt film, the exposed surface is the only location at which the oxygen pressure is known. To partially eliminate the diffusion effects at low aging pressures, only the asphalt exposed surface was analyzed.

To evaluate both T and P effects on r_{CA} , in asphalt, five AC-20 grade asphalts were POV aged. These asphalts correspond to those studied by Lau et al. (1992). The experimental design included aging at pressures of 20, 2, and 0.2 atm pure oxygen. Air was not used because complications due to oxygen diffusion through the nitrogen gas film at the asphalt surface would have to be considered in the analysis of the data. Aging temperatures were 333.3, 344.4, and 355.5 K (140, 160 and 180 °F) and aging times ranged from 2 to 80 days depending on the aging temperatures. The changes in the chemical properties of POV-aged asphalt were analyzed by FT-IR. For aging at 0.2 and 2 atm the CA at the surface of the asphalt film was measured. At 20 atm, the bulk CA was analyzed since the top surface and bulk showed the same degree of carbonyl formation. Tables B-1 through B-5 (Appendix B) show the CA values for the aging conditions and asphalts studied. Tables 1-1 and 1-2 show the rates and CA_o values for each asphalt and condition.

Table 1-1. r_{CA} for All Asphalts and POV-Aging Conditions Studied

Asphalt	$r_{CA} \times 10^3$ at 0.2 atm			$r_{CA} \times 10^3$ at 2 atm			$r_{CA} \times 10^3$ at 20 atm		
	333.3 K CA/day	344.4 K CA/day	355.5 K CA/day	333.3 K CA/day	344.4 K CA/day	355.5 K CA/day	333.3 K CA/day	344.4 K CA/day	355.5 K CA/day
Ampet AC-20	3.24	6.85	18.66	6.79	14.55	34.50	12.34	25.55	67.02
Coastal AC-20	3.73	8.91	21.32	6.36	15.74	37.92	11.46	31.19	78.21
Cosden AC-20	4.75	11.41	23.66	9.12	19.86	40.23	18.58	32.88	87.82
Exxon AC-20	4.19	7.87	19.73	8.10	13.92	32.47	12.40	29.43	60.18
Texaco AC-20	3.66	7.78	18.62	6.04	14.80	28.63	10.95	26.96	56.64

5

Table 1-2. CA_o for All Asphalts and POV-Aging Conditions Studied

Asphalt	CA_o at 0.2 atm			CA_o at 2 atm			CA_o at 20 atm		
	333.3 K CA	344.4 K CA	355.5 K CA	333.3 K CA	344.4 K CA	355.5 K CA	333.3 K CA	344.4 K CA	355.5 K CA
Ampet AC-20	0.669	0.654	0.605	0.730	0.672	0.747	0.705	0.890	0.704
Coastal AC-20	0.618	0.641	0.575	0.795	0.761	0.737	0.959	1.009	0.838
Cosden AC-20	0.667	0.638	0.649	0.839	0.756	0.819	1.145	1.382	1.200
Exxon AC-20	0.698	0.721	0.770	0.863	0.781	0.802	1.020	1.066	0.969
Texaco AC-20	0.542	0.580	0.560	0.698	0.665	0.728	0.791	0.814	0.850

ORDER OF REACTION

At isothermal aging conditions, the measure of how the change in oxygen pressure affects the change in r_{CA} is defined as the order of reaction. Ideally, the order of reaction should be independent of temperature; however, for the complex reactions of carbonyl formation in asphalts, Equation 1-3 may be too simplistic to completely separate the pressure and temperature effects. For asphalts, the order of reaction in terms of oxygen pressure is α . Low values of α suggest that pressure has little effect on r_{CA} ; high values of α suggest P has significant effects. α was determined for isothermal aging at 333.3, 344.4, and 355.5 K (140, 160 and 180 °F) for the asphalts studied. The process of determining α for one of the asphalts studied is described below.

A model describing the r_{CA} in terms of experimental data must be determined. Figure 1-1 shows CA at 0.2, 2, and 20 atm oxygen for Cosden AC-20 at 333.3 K (140 °F). Aging times ranged from 0 to 80 days. The original CA is depicted by the filled circle; the open circle, square, and diamond represent 0.2, 2, and 20 atm oxygen respectively. Initially, there is a non-linearity from the starting CA to the first recorded POV-aged sample at eight days. After that initial jump, CA increases linearly with aging time at isothermal and isobaric conditions. Furthermore, the data show that r_{CA} increases with oxygen pressure.

To quantify r_{CA} and CA_o , a linear model is used to represent the data and the estimated parameters are shown on the figure. At low pressures, 0.2 and 2 atm, the linear model provides an excellent representation of the data. However, the linear model does not describe the 20 atm data as well, perhaps due to the fact that bulk CA was measured at 20 atm, compared to the CA at the interface for the lower pressures, producing diffusion effects. Figures 1-2 and 1-3 show CA for Cosden AC-20 at aging temperatures of 344.4 and 355.5 K (160, 180 °F). Again the initial non-linearity exists, followed by a constant r_{CA} at all oxygen pressures studied. The linear model shows good agreement with the data for the long-term, constant-aging region. Data at 20 atm and higher temperatures show better linearity relative to data at 333.3 K (140 °F). Since bulk CA was measured at 20 atm aging, this suggests that the diffusion problem diminishes

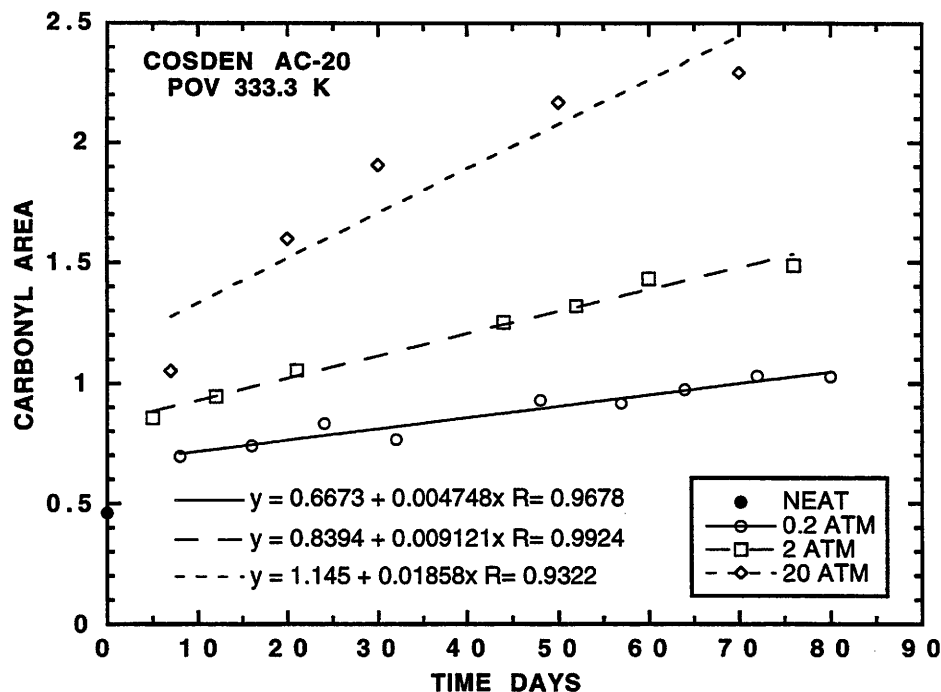


Figure 1-1. CAs of Neat and POV-Aged Cosden AC-20 at 333.3 K

with increasing temperature. With CA measured at the surface, all temperatures show excellent agreement with the linear model.

The data show that at isothermal conditions, increasing the pressure results in higher intercept. These intercepts provide an initial estimate of CA_0 . At isobaric conditions, increasing aging temperature increases r_{CA} but appears to have little effect on estimated CA_0 . The same conclusions may be drawn from Figures B-1 through B-12 in Appendix B for the other asphalts studied.

For isothermal aging, r_{CA} versus P should produce a straight line when plotted on a log-log scale, Equation 1-3. The slope of this line is α . For Cosden AC-20 at 333.3 K (140 °F), Figure 1-4 shows the log of r_{CA} versus log P . Although there are only three data points, the data suggest a linear model, and the estimated parameters are given. The order of reaction for Cosden AC-20 at 333.3 K (140 °F) is 0.296. A comparison of the effect of P on r_{CA} at 333.3 K (140 °F) for all five asphalts studied is shown in Figure 1-5. The asphalts appear to fall into two groups: Ampet AC-20 and Cosden AC-20 with $\alpha = 0.29$ in one group and Coastal AC-20, and Exxon AC-20, and Texaco AC-20 with $\alpha =$

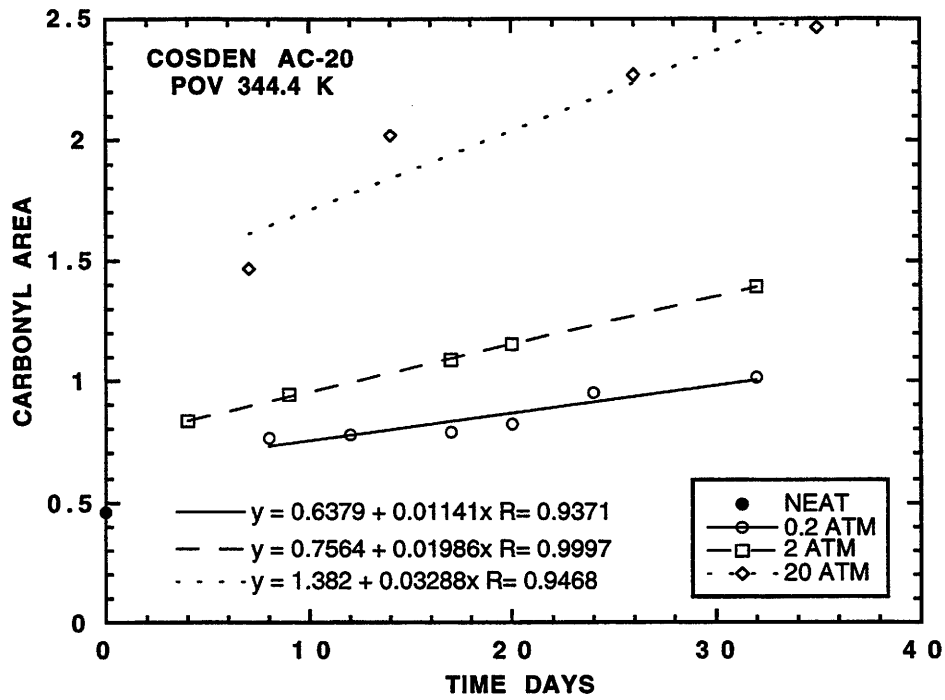


Figure 1-2. CAs of Neat and POV-Aged Cosden AC-20 at 344.4 K

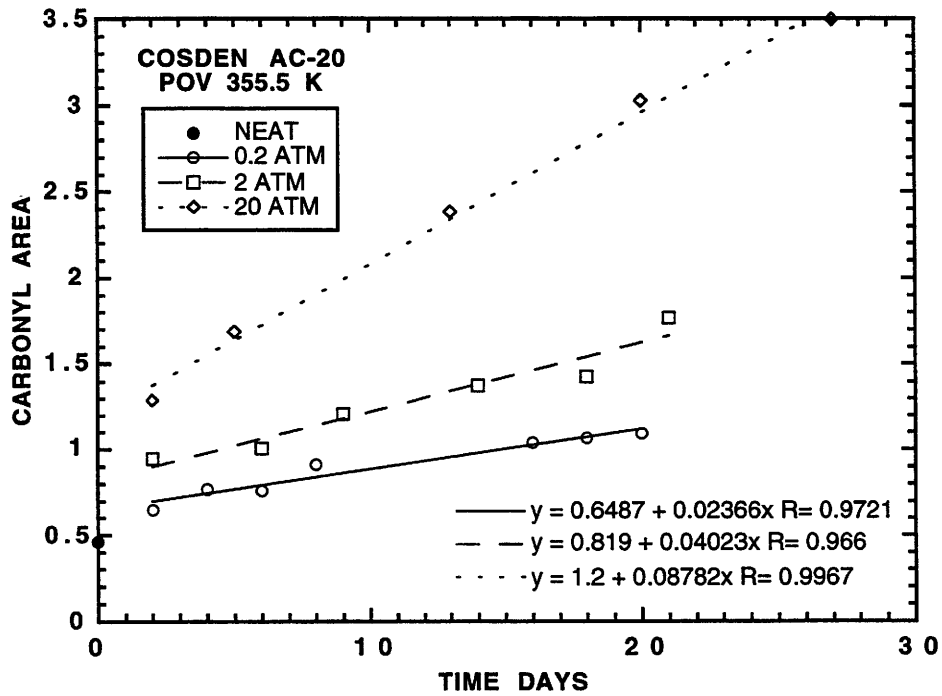


Figure 1-3. CAs of Neat and POV-Aged Cosden AC-20 at 355.5 K

0.24 in another. However, a comparison at 344.4 K (160 °F) in Figure 1-6 shows that the groupings change. All asphalts except for Cosden AC-20 have $\alpha = 0.27$; for Cosden AC-20 $\alpha = 0.23$. Finally, at 355.5 K (180 °F), Figure 1-7 suggests yet another grouping of Ampet AC-20, Coastal AC-20, and Cosden AC-20, with $\alpha = 0.28$, and Exxon AC-20 and Texaco AC-20, with $\alpha = 0.24$.

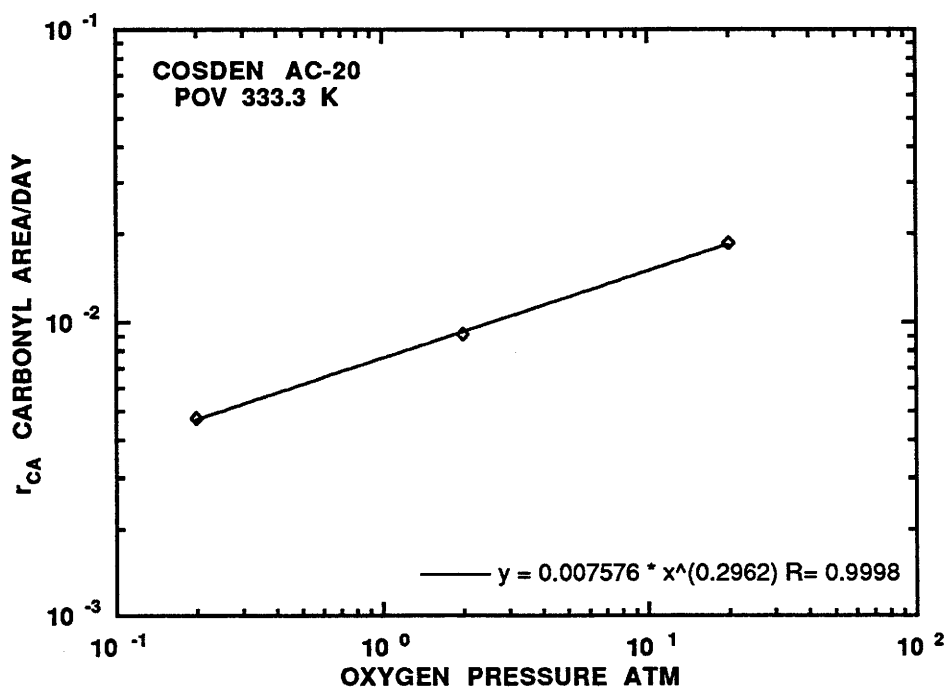


Figure 1-4. r_{CA} Versus P at 333.3 K for POV-Aged Cosden AC-20

From Figures 1-4 to 1-7 the kinetic model in equation 1-3 describes the pressure dependence on the r_{CA} for a given asphalt and temperature. Furthermore, the magnitude of α is small. From preliminary comparisons, it appears that α may be independent of asphalt composition as well as temperature.

Table 1-3 gives α for all asphalts studied at 333.3, 344.4, and 355.5 K (140, 160, 180 °F). There appears to be no correlation between T and α for a given asphalt. For example, Ampet AC-20 shows decreasing α with increasing T , Coastal AC-20 shows increasing α with increasing T , and Cosden AC-20, Exxon AC-20, and Texaco AC-20 show no recognizable trend. Although there is significant scatter, the lack of correlation between α and T suggests that α is independent of T . Furthermore, at a given aging

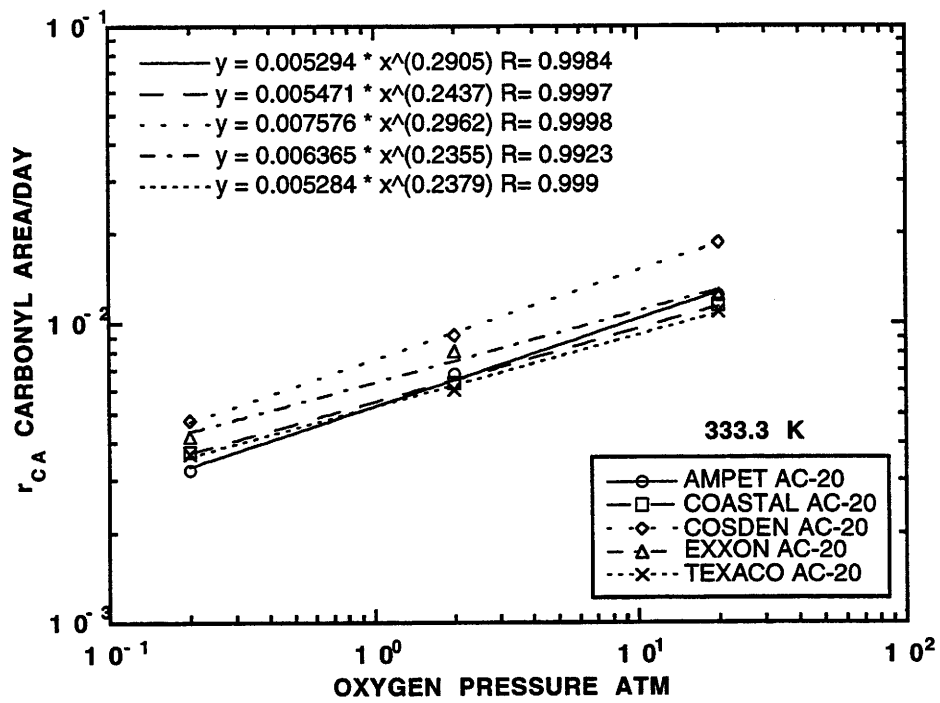


Figure 1-5. r_{CA} Versus P at 333.3 K for All POV-Aged Asphalts Studied

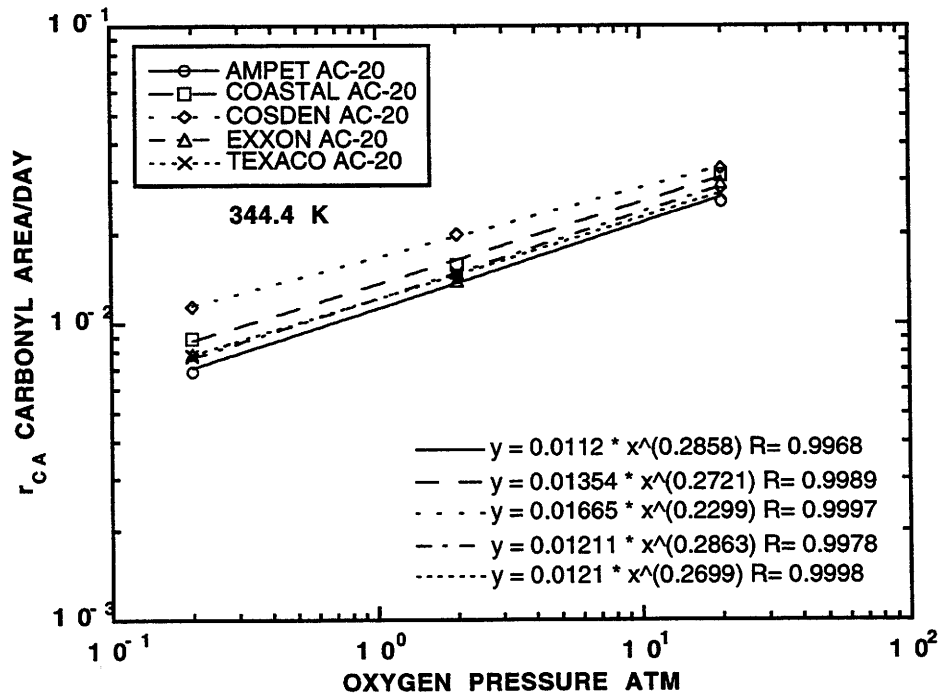


Figure 1-6. r_{CA} Versus P at 344.4 K for All POV-Aged Asphalts Studied

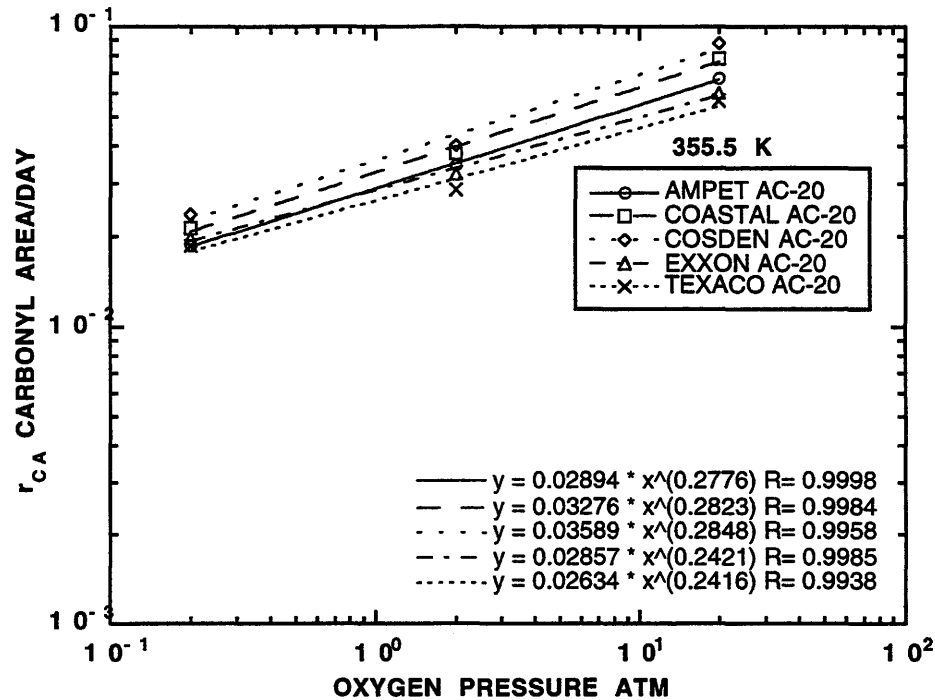


Figure 1-7. r_{CA} Versus P at 355.5 K for All POV-Aged Asphalts Studied

temperature, the values of α are somewhat independent of asphalt. Except for Ampet AC-20, which tends to be higher than the other asphalts at all temperatures, no other asphalts show a recognizable trend. The range of α for all asphalts and temperatures is 0.296 to 0.230 representing about 25% difference. Even with significant scatter, all of the data suggest a constant α , independent of aging temperature and, perhaps, crude source.

Table 1-3. α for All POV-Aged Asphalts Studied^a

Asphalt	α		
	333.3 K (140 °F)	344.4 K (160 °F)	355.5 K (180 °F)
Ampet AC-20	0.290	0.286	0.278
Coastal AC-20	0.244	0.272	0.282
Cosden AC-20	0.296	0.230	0.285
Exxon AC-20	0.236	0.286	0.242
Texaco AC-20	0.238	0.270	0.242

^a Oxygen pressures from 0.2 to 20 atm.

ACTIVATION ENERGIES AND ARRHENIUS CONSTANTS

The effect of T on r_{CA} is expressed in terms of an Arrhenius relationship having two estimated parameters, the Arrhenius constant A and activation energy E_A . R is 8.314 J/mol. At 20 atm, this model described asphalt oxidation (Lau et al., 1992). However, at lower oxygen pressures the Arrhenius relationship needs to be confirmed. For the asphalts studied, the parameters A and E_A were determined for isobaric aging at 0.2, 2.0, and 20.0 atm oxygen.

Figure 1-8 shows CA at 333.3, 344.4 and 355.5 K (140, 160, 180 °F) for Cosden AC-20 at isobaric conditions of 0.2 atm. The solid circle represents the neat or original CA , and the hollow circle, square, and diamond represent the 333.3, 344.4, and 355.5 K (140, 160, 180 °F) aging temperatures, respectively. The linear model represents the data for all temperatures; however, there is some scatter. The scatter appears to be independent of T at 0.2 atm. Figures 1-9 and 1-10 show CA as a function of t for isobaric aging of Cosden AC-20 at 2 and 20 atm, respectively. Again the linear model represents the data very well. Furthermore, the degree of scatter decreases with increasing pressure. CA values in Figure 1-10 are bulk measurements. At 333.3 K (140 °F) it appears that there is a diffusion problem compared with 344.4 (160 °F) and 355.5 K (180 °F) bulk CA . When CA values at the exposed surface are used (Figures 1-8 and 1-9) the scatter increases but the linear relationship between CA and t for long-term aging is undeniable.

From the data in Figures 1-8 to 1-10 for isobaric aging, all of the regression lines tend to intersect. This suggests that the intercept, CA_o , is independent of aging temperature. From Figures B-13 through B-24 for the other asphalts studied, similar conclusions about isobaric POV aging of asphalts are reached.

For isobaric conditions, a linear relationship must exist between the log of r_{CA} and the reciprocal of the absolute aging temperature, $(1/T)$, for the Arrhenius relationship to be valid. From the linearity shown in Figure 1-11 for POV-aged Cosden AC-20 at 0.2 atm, the Arrhenius relationship is successful, modeling the effect of T on r_{CA} at low aging pressures. Both the Arrhenius constant, A , and the slope are reported on the figure. The slope of the line is the negative of the activation energy divided by the universal gas

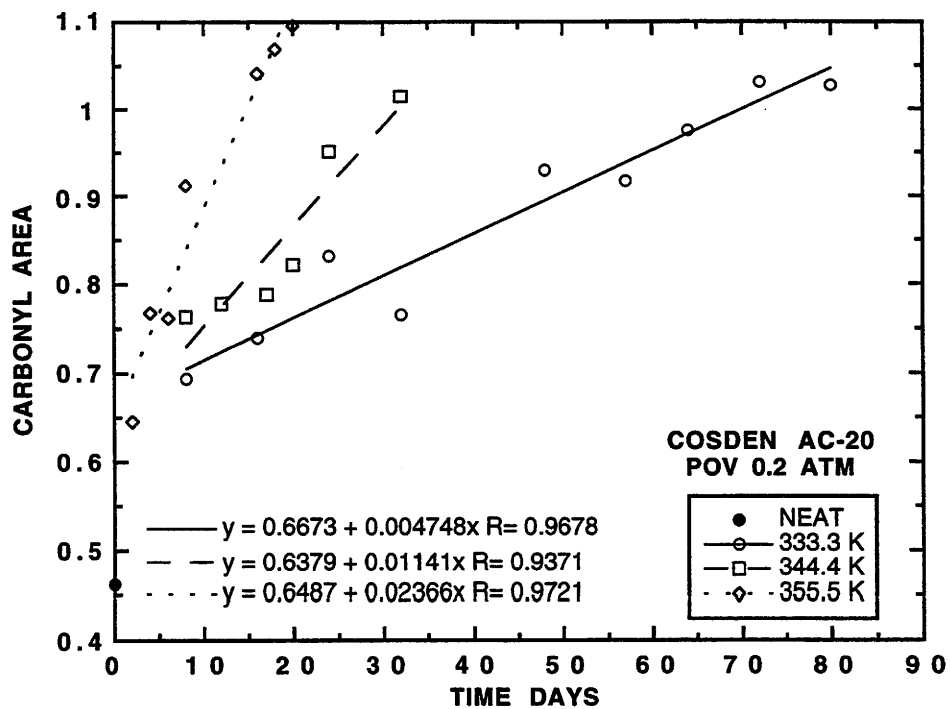


Figure 1-8. CAs of Neat and POV-Aged Cosden AC-20 at 0.2 atm

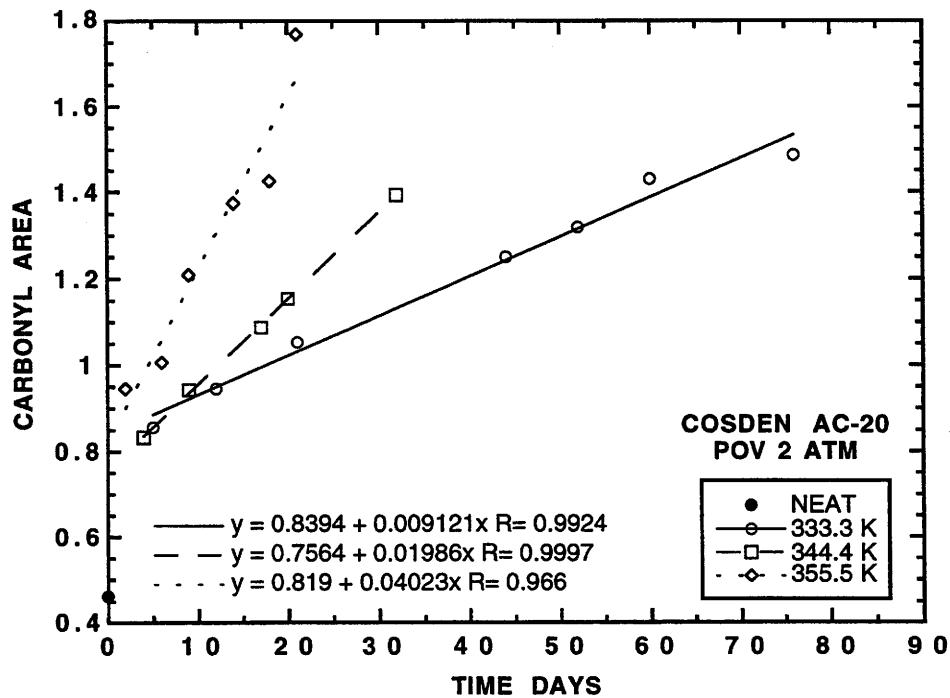


Figure 1-9. CAs of Neat and POV-Aged Cosden AC-20 at 2 atm

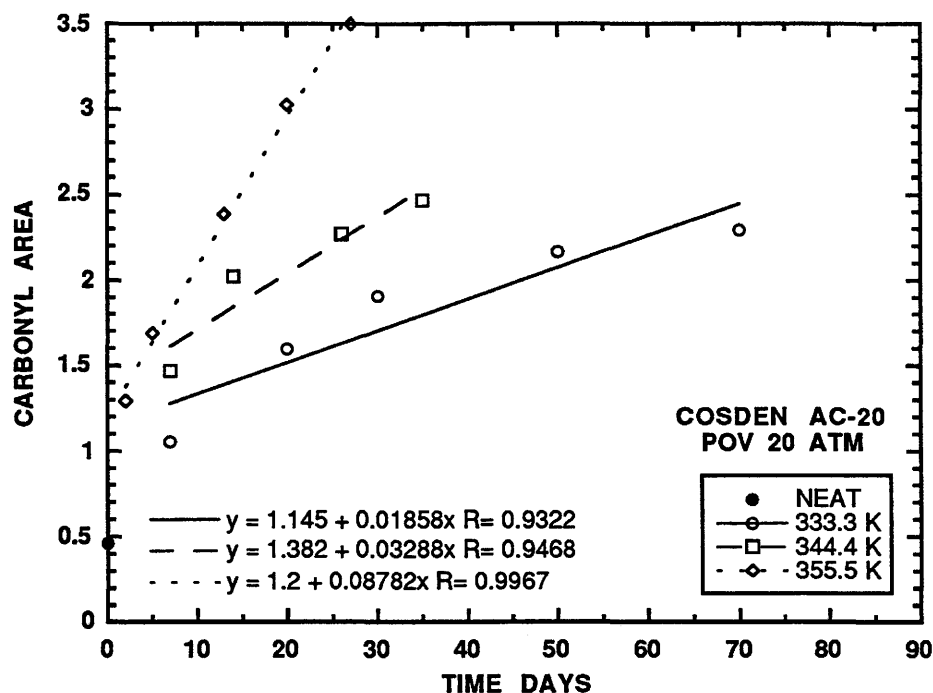


Figure 1-10. CAs of Neat and POV-Aged Cosden AC-20 at 20 atm

constant.

Previous research has shown that E_A depends on asphalt composition or crude source for POV aging at 20 atm (Lau et al., 1992). Figure 1-12 shows a comparison of the asphalts studied for isobaric POV aging at 0.2 atm. At this low oxygen pressure, it is difficult to conclude if the E_A values, or slopes, are different. The estimated slopes, also shown on the figure, range from -9330 to -8240 K, only a 13% difference. At aging pressures of 2 atm, Figure 1-13 compares the temperature dependence on the r_{CA} of the asphalts studied. In this case, the differences in the slopes are more apparent. Slope parameters range from -9520 K for Coastal AC-20 to -7380 K for Exxon AC-20. The percent difference is 30. At 20 atm, shown in Figure 1-14, the slopes range between -10200 K for Coastal AC-20 and -8250 K for Cosden AC-20, a 24% difference.

The Arrhenius model accurately describes the temperature dependence on r_{CA} at all pressures and for all asphalts studied. The effect of composition or crude source on E_A is more apparent as a result of POV aging at higher oxygen pressures. This is probably a result of the measurement of CA and the experimentally designed time periods for low

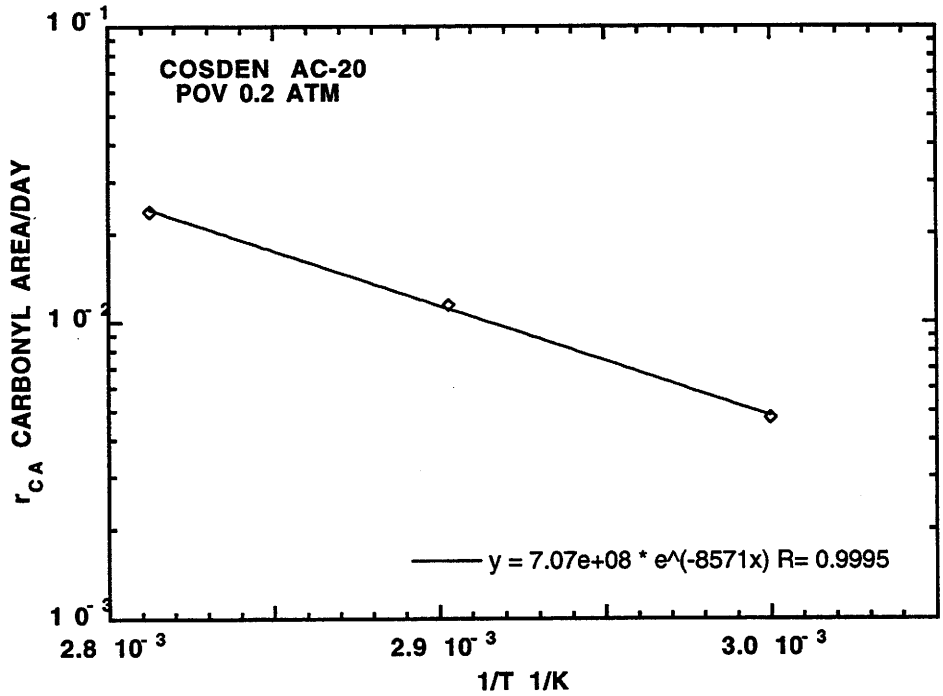


Figure 1-11. r_{CA} Versus $(1/T)$ at 0.2 atm for POV-Aged Cosden AC-20

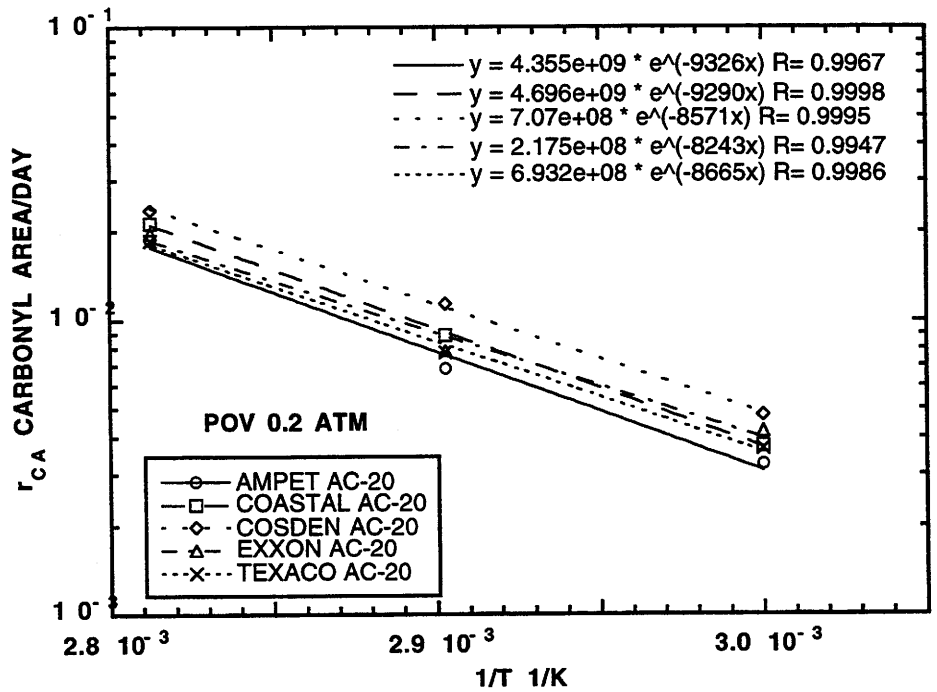


Figure 1-12. r_{CA} Versus $(1/T)$ at 0.2 atm for All POV-Aged Asphalts Studied

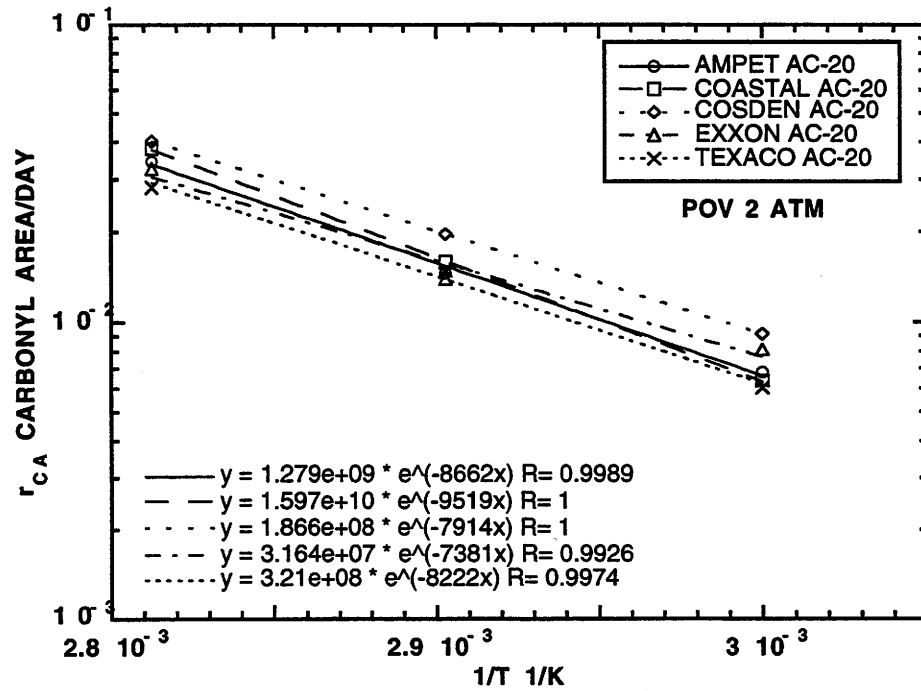


Figure 1-13. r_{CA} Versus $(1 / T)$ at 2 atm for All POV-Aged Asphalts Studied

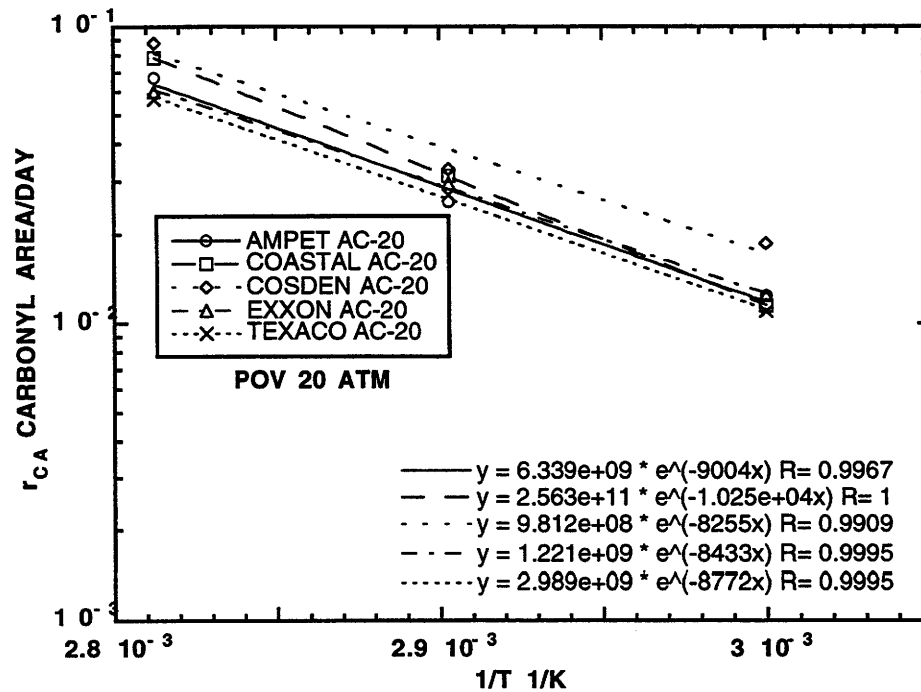


Figure 1-14. r_{CA} Versus $(1 / T)$ at 20 atm for All POV-Aged Asphalts Studied

pressures. At low P , CA changes very little for isothermal aging at 333.3, 344.4, and 355.5 K (140, 160, and 180 °F). Values of CA ranged from 0.7 to 1.1 for Cosden AC-20, Figure 1-8. For Cosden AC-20 at 20 atm, CA ranged from 1.0 to 3.5 by comparison (Figure 1-10). These ranges are representative of all of the asphalts studied by reviewing Figures B-1 through B-24. As a consequence, at low aging pressures, the ability to discriminate different asphalts by r_{CA} at different temperatures is diminished.

E_A is calculated by multiplying the slope by the universal gas constant R . Table 1-4 shows E_A s of the asphalts studied at 0.2, 2, and 20 atm. Ideally, E_A should be independent of P , and from the table, there appears to be no correlation between E_A and aging pressures. For example, Coastal AC-20 shows increasing E_A with increasing P ; however, the lowest E_A is at the aging pressure of 2 atm for the other asphalts. From the data, it appears that E_A is independent of aging pressure for a given asphalt. The magnitude of E_A for the asphalts studied indicates that the temperature effect on the r_{CA} is significant compared with the pressure effect. At constant pressure, an increase of 5.5 K (9.9 F°) roughly doubles r_{CA} ; at constant temperature, an order of magnitude change in pressure doubles r_{CA} .

Table 1-4. E_A for All POV-Aged Asphalts Studied^a

Asphalt	E_A kJ/gmol		
	0.2 atm	2 atm	20 atm
Ampet AC-20	77.5	72.0	74.8
Coastal AC-20	77.2	79.1	85.1
Cosden AC-20	71.2	65.8	68.6
Exxon AC-20	68.5	61.4	70.1
Texaco AC-20	72.0	68.3	72.9

^a Aging temperatures from 333.3 to 355.5 K (140 to 180 °F)

Figures 1-12 to 1-14 also show that the asphalts have different pre-exponential factors or Arrhenius constants, A . A represents the rate or frequency of collisions between the active sites in the asphalt and the oxygen molecules. Overall, a broad trend of increasing A with increasing P is reached by overlaying Figures 1-12 to 1-14 for the

asphalts studied. From the parameters shown in Table 1-5, only Coastal AC- 20 shows a monotonic increase in A with P . The other asphalts show a decrease in A from 0.2 to 2 atm followed by an increase in A from 2 to 20 atm over and above the value of A at 0.2 atm. Since no pressure dependency was included in the Arrhenius parameters analysis, these reported values of A contain the pressure effect. Furthermore, the large variations of several orders of magnitude in A are a direct result of the exponential relationship between the temperature dependence and the r_{CA} . Values of $\ln(A)$ obviously show significantly less variability, as shown in the next section.

Table 1-5. A for All POV-Aged Asphalts Studied^a

Asphalt	$A \times 10^{-8} \text{ CA / day}$		
	0.2 atm	2 atm	20 atm
Ampet AC-20	43.5	12.8	63.4
Coastal AC-20	47.0	160.	2560.
Cosden AC-20	7.07	1.87	9.81
Exxon AC-20	2.18	0.316	12.2
Texaco AC-20	6.93	3.21	29.9

^a Aging temperatures from 333.3 to 355.5 K (140 to 180 °F)

MULTI-VARIABLE PARAMETER ESTIMATION

For POV aging of asphalts, the effects of P and T were analyzed independently, confirming that the kinetic model, Equation 1-3, was valid. With this confirmation, a multi-variable regression of r_{CA} as a function of T and P was performed. Table 1-6 shows the estimated parameters. For each of the parameters, a 95% confidence limit is also shown. In this table, $\ln(A)$ is given and not the value of A . Reporting $\ln(A)$ provides a better comparison between asphalts and is required because the model must be linear in the parameters to provide the 95% confidence limits. The error of the estimated r_{CA} from the model parameters versus the measured r_{CA} is also given. The percent errors are all under 10%.

Table 1-6. Kinetic Model Parameters for All POV-Aged Asphalts Studied^a

Asphalt	$\ln(A)$ $\ln(CA / \text{day atm}^\alpha)$	E_A kJ/gmol	α	% Error ^b
Ampet AC-20	21.71 ± 2.95	74.8 ± 8.2	0.285 ± 0.042	7
Coastal AC-20	23.83 ± 4.40	80.5 ± 12.3	0.266 ± 0.062	4
Cosden AC-20	19.86 ± 3.10	68.6 ± 8.7	0.270 ± 0.044	7
Exxon AC-20	19.86 ± 3.39	66.7 ± 9.5	0.255 ± 0.048	8
Texaco AC-20	20.42 ± 2.02	71.1 ± 5.6	0.250 ± 0.028	5
All	20.95 ± 1.72	72.3 ± 4.9	0.270 ± 0.024	14

^a Model: $r_{CA} = A \exp(-E_A / RT) P^\alpha$
 Aging temperatures from 333.3 to 355.5 K (140 to 180 °F)
 and pressures from 0.2 to 20 atm

$$^b \text{ \% Error} = 100 \sqrt{\frac{1}{n} \sum \left(\frac{\text{meas} - \text{calc}}{\text{meas}} \right)^2}$$

A 95% confidence limit is roughly 15% of the value of the parameter. The confidence limit for Coastal AC-20 is broadest, indicating that there is more variability in this set of data. The data set with the least variability is Texaco AC-20. Unfortunately, the size of the confidence limit is such that it is difficult to determine whether the parameters are dependent on the asphalt source. Since the Arrhenius parameters describe the temperature dependence and this is the most significant factor affecting the determination of r_{CA} , it is concluded that the Arrhenius parameters are composition dependent. However, pressure dependence is far less significant than temperature and could be independent of asphalt composition.

All of the r_{CA} data for the asphalts were grouped together, and the parameters were estimated again. These parameters are given on the bottom line of the table. The percent error increased with the grouping of the data, as expected; its value is 15%. However, the 95% confidence limit for the averaged parameters decreased by roughly a factor of 2. This is a direct result of the increased number of observations in the data set. From the overall parameter estimation, the composition-independent value of α for the asphalts studied is 0.27.

COMPARISON OF E_A WITH LITERATURE VALUES

The calculated E_A values for the asphalts studied are compared with literature values. For asphalt oxidation, only a few sources report activation energies. Van Oort (1956) measured oxygen absorption in asphalts and reports an E_A of 100 kJ/mol. Verhasselt and Choquet (1991) report values between 66.9 and 87.1 kJ/mol for aging at 343.2 and 373.2 K (158 and 212 °F). The measured properties were percent asphaltenes, ring-and-ball softening point, penetration, and IR absorption in the carbonyl region. Values of E_A in this study are about 25% lower than those of Van Oort but show excellent agreement with Verhasselt and Choquet. These differences may result from the fact that only carbonyl formation is being accounted for in this study while all oxygen reactions are accounted for in Van Oort's study. Two sources (Bateman, 1954; Bolland, 1949) give E_A values of 41.8 kJ/mol for olefin oxidation. Values in this study are twice those reported for olefin oxidation because the model compound's reaction characteristics do not reflect those found in the asphalt.

Measuring oxygen absorption at different temperatures, two papers report activation energies of 29.3 and 41.7 kJ/mol (Dickinson and Nicholas, 1949; Dickinson et al., 1958). The authors conclude that the activation energies are not really values for the chemical reactions; however, the activation energy does provide a measure of the rate of acceleration of the complex aging process of diffusion and reaction. Activation energies in this work are twice as great as those reported for oxygen absorption measurements. Dickinson and Nicholas (1949) attempted to minimize diffusion resistance. Van Oort (1956) also measured oxygen absorption, but he attempted to separate reaction and diffusion and account for variable diffusivity in his model. He reports a value of 100 kJ/mol. From these comparisons with literature values, researchers who attempted to minimize diffusion resistance or account for variable diffusivity in the analysis, report higher E_A than those who did not. Overall, E_A values in this study lie in the range given by all the literature sources and are essentially identical to those reported by Verhasselt and Choquet.

HYPOTHESIZED MODEL FOR CA_o AS A FUNCTION OF OBSERVABLE VARIABLES

Since the magnitude of CA relates to the physical properties and, ultimately, to the performance of the asphalt, knowing the r_{CA} as a function of observable variables is not enough. A method to estimate the integration constant, CA_o , must also be developed. Long-term linear aging characteristics do not start from the neat material because of an initial non-linearity. Using neat asphalt CA as CA_o would result in low predictions of actual CA . For highway-pavement aging, the hot-mix process causes carbonyl formation (Jemison et al., 1991) and represents a more realistic initial condition for modeling. However, in the absence of hot-mix processed asphalt and from the standpoint of a pure laboratory test, the initial condition, CA_o , is estimated from the linear model for long-term aging.

CA_o appears to be only a function of aging pressure from experimental data. Figure 1-15 shows the intercepts for Cosden AC-20 at all aging pressures and 333.3, 344.4, and 355.5 K (140, 160, and 180 °F). Figures B-34 through B-37 show the other asphalts studied. These figures show that the intercept is only a function of aging pressure. The arithmetic averages of CA_o for each asphalt at 0.2, 2, and 20 atm were determined. Dickinson and Nicholas (1949) suggest a linear relationship between CA_o and P for aging conditions from 0.2 to 1 atm. However, the data in this study span pressures from 0.2 to 20 atm. Figure 1-16 shows each of the asphalt's arithmetically averaged CA_o versus aging P on a log-log plot. Since no fundamental theory exists for the development of a model, an empirical model of the form

$$CA_o = sP^\beta \quad (1-4)$$

was selected. This model provided the best fit for the asphalts studied, and Table 1-7 gives the model parameters.

There appear to be three distinct groups with regard to the parameter β . For Coastal AC-20, Exxon AC-20, and Texaco AC-20 it is close to 0.8. However, values of β for Ampet AC-20 and Cosden AC-20 are 0.04 and 0.14, respectively. With the limited data set and the empirical nature, it is concluded that the parameters are composition

Table 1-7. r_{CA} and CA_o for All POV-Aged Asphalts at 322.2 K (120 °F) and 20 atm^a

Asphalt	$r_{CA} \times 10^3$ CA / day	CA_o CA
Ampet AC-20	5.07	0.759
Coastal AC-20	4.41	0.761
Cosden AC-20	6.06	0.903
Exxon AC-20	5.97	0.843
Texaco AC-20	4.78	0.681

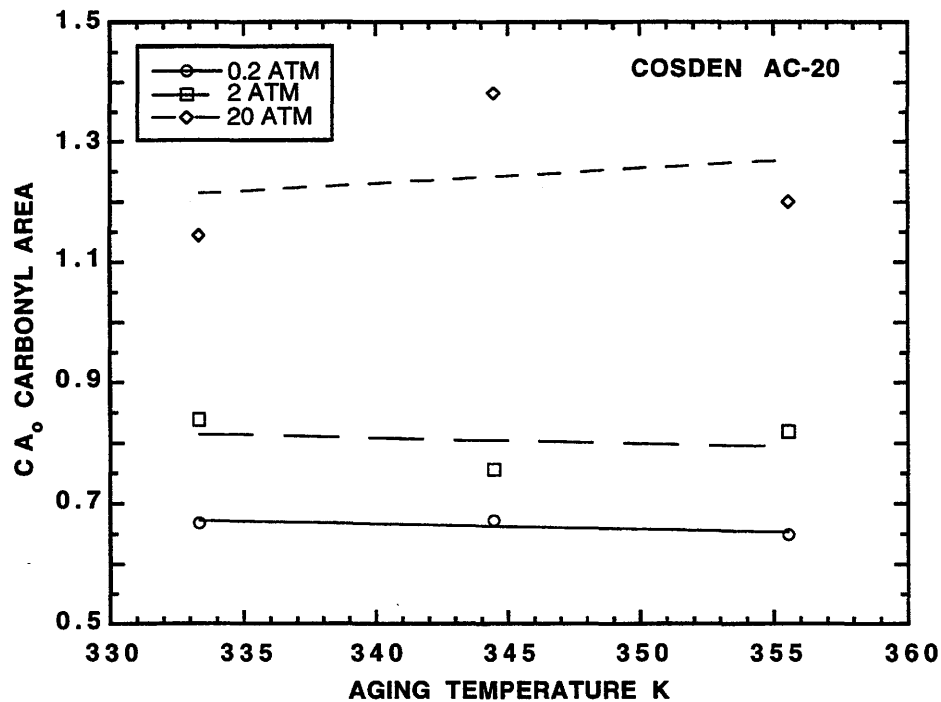


Figure 1-15. CA_o Versus POV Aging Temperature for Cosden AC-20

dependent. Unfortunately, at least one aging experiment at 0.2 atm is required to estimate CA_o for asphalt aging at highway conditions. Clearly, more asphalts, pressures, and models need to be considered to understand the pressure dependence on CA_o . The first model to look at for extending this work is that proposed by Dickinson and Nicholas (1949).

The model parameters for r_{CA} and CA_o were obtained from physical situations

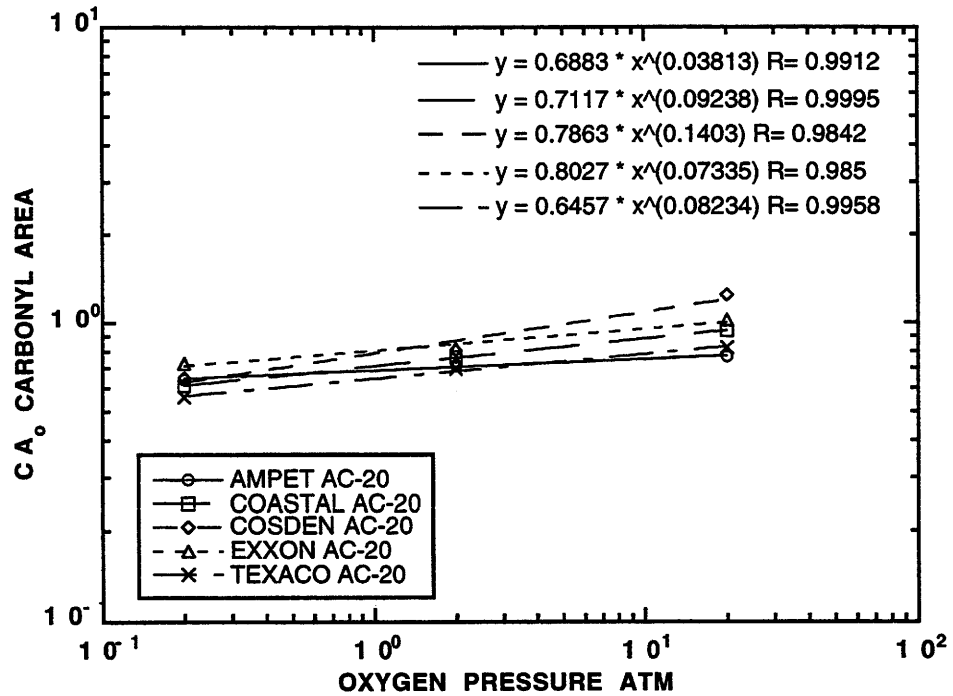


Figure 1-16. CA_o Versus POV Aging Temperature for All Asphalts Studied

that attempted to minimize oxygen diffusion problems in the asphalt film. At low oxygen pressures, only the exposed surface of the aged sample was analyzed. Even though the parameters were estimated from data at the surface, the r_{CA} and CA_o models as functions of aging T and P are valid anywhere in the asphalt film. Unfortunately, unless the diffusion of oxygen is taken into account, the oxygen pressure at points in the film are not accurately known.



CHAPTER 2

EXTENDED AGING STUDIES

The work described in the previous chapter, though extensive, left several issues in doubt. The temperature control in POV Configuration II was still less precise than desired, so the system was modified, as described, for Configuration III. The scatter in the pressure dependency factor, α , for carbonyl formation was sufficient to leave in doubt whether or not this factor was asphalt dependent. The range of α , if real, could produce significant error. It was found that the initial jump, CA_0 , is pressure dependent and asphalt dependent so that it must be measured at road pressure (0.2 atm of O_2). It was, however, independent of temperature. At 0.2 atm the rate is quite slow at lower temperatures. The five tested asphalts all had similar activation energies, but earlier work had indicated greater variation. However, accurate measurement of activation energies requires better temperature control than was obtained in many of these measurements. Finally, the discovery that the HS was pressure dependent, as described in Chapter 5, necessitated a reconsideration of the requirements for an aging procedure to accurately represent relative aging rates at road conditions.

In the SHRP PAV aging procedure, material is first aged in the TFOT before aging in the PAV. If an aging test requires multiple samples at different conditions, then running the TFOT on this material adds materially to the complexity. It would be desirable to eliminate this step if it can be justified.

EXPERIMENTAL DESIGN

Two experiments were designed, each with five asphalts and conducted in POV apparatuses at aging conditions shown in Table 2-1. Set I involved SHRP AAA-1, AAD-1, AAF-1, AAG-1 and AAM-1 at all POV conditions except C3. Both tank and RTFOT residues were included, except at condition C4, for a total of

Table 2-1. List of Aging Conditions Applied

Aging Condition	T K(°F)	P Bar(atm)
C1	349.8(170)	20.7(20)
C2	355.4(180)	20.7(20)
C3	355.4(180)	10.3(10)
C4	360.9(190)	20.7(20)
C5	360.9(190)	0.207(0.2)
C6	366.5(200)	0.207(0.2)
C7	372.0(210)	0.207(0.2)

eleven asphalts. In Set II the asphalts were SHRP AAB-1, AAS-1, Conoco 125/150, Exxon AC-20 and Shell AC-5. Only Exxon AC-20 was repeated from the work described in the previous chapter. In this set, a variety of tank and RTFOT residues were run so that the total number of asphalts ranged from seven to eleven. The POV conditions included all in Table 2-1 except condition 5. Samples were removed every few days for analysis for a total of six to eight times for each asphalt. Maximum aging times varied with conditions for a maximum of 21 days for condition 5 in Set I and 16 days for condition 3 in Set II.

All samples run at 0.2 and 2 atm were subjected to exposed surface FT-IR analysis to eliminate diffusion effects. All samples were mixed and subjected to bulk FT-IR analysis. Viscosities at 60°C (140°F) were run on all bulk samples.

RESULTS

The carbonyl formation rate results are shown in Figures 2-1 to 2-5 for Set I and Figures 2-6 to 2-10 for Set II. In the legend, RTFOT is shown by dotted lines while solid lines show results for tank asphalts. The agreement between the two is extremely close indicating that the RTFOT aging has, essentially, no effect on the subsequent oxidation rate. It may be observed that, except for some scatter, the

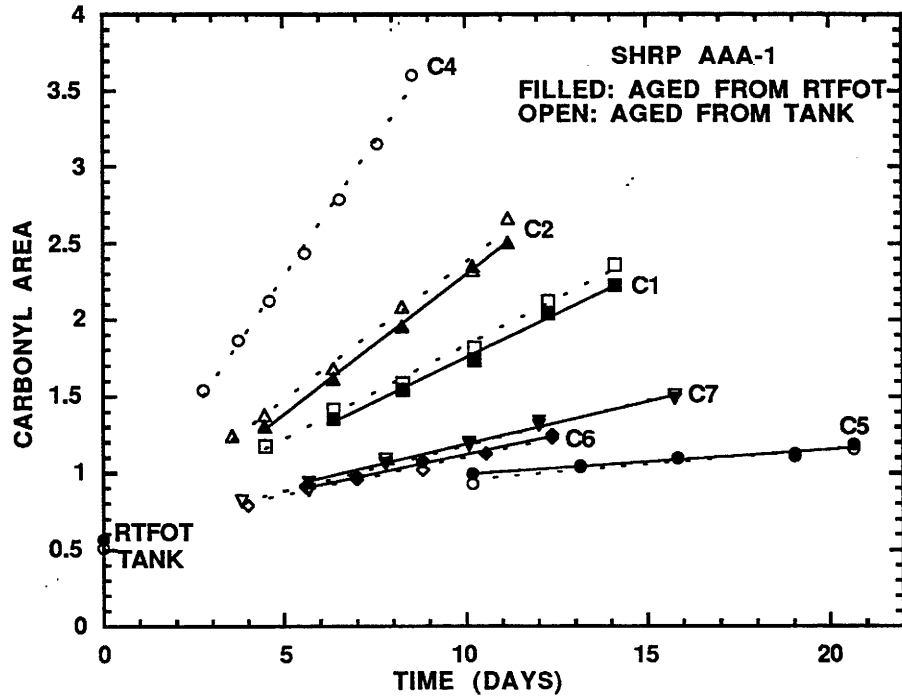


Figure 2-1. Carbonyl Formation Rates Under Different Aging Conditions

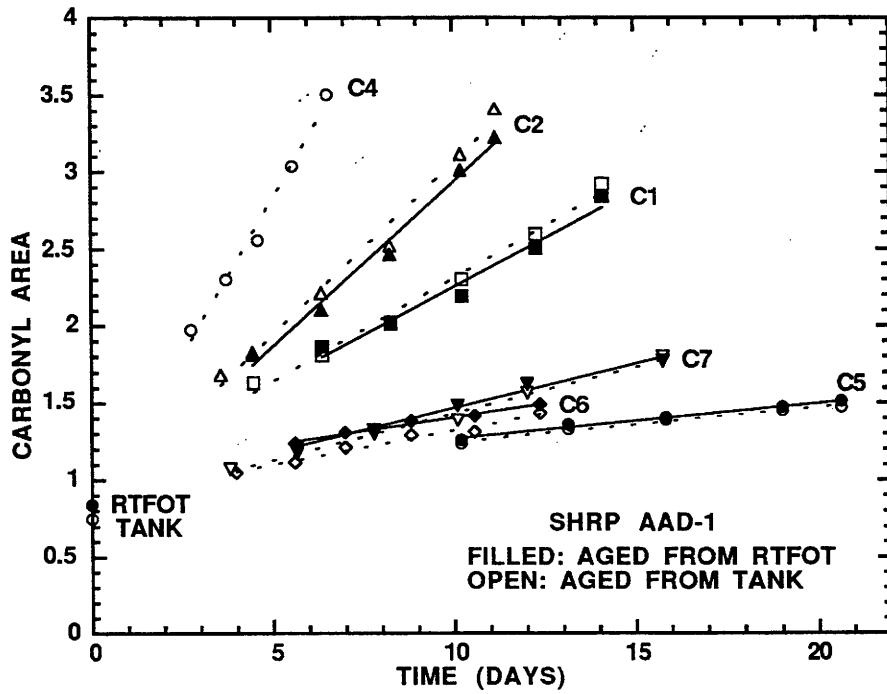


Figure 2-2. Carbonyl Formation Rates Under Different Aging Conditions

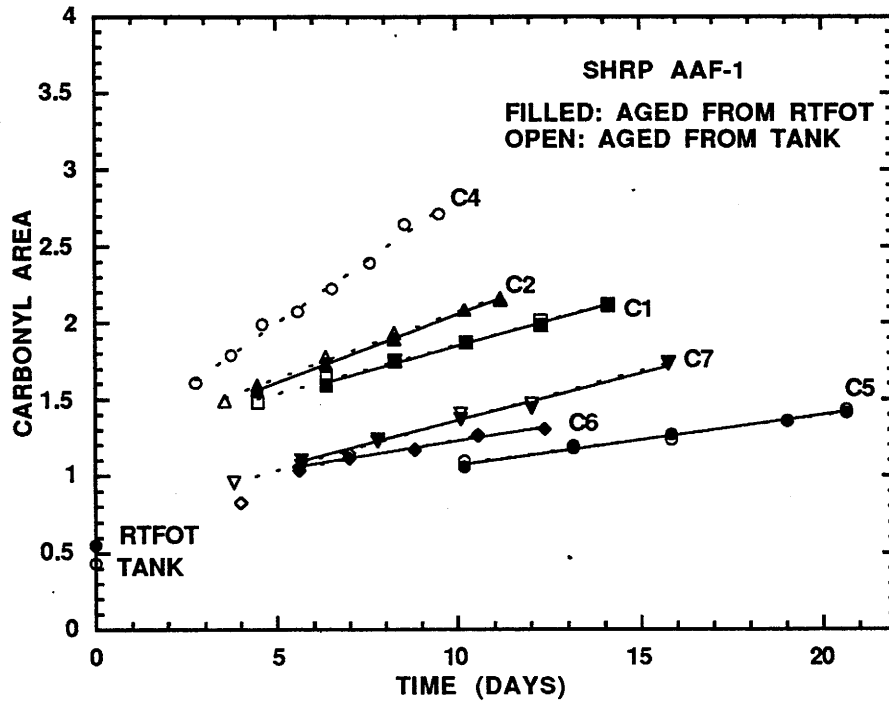


Figure 2-3. Carbonyl Formation Rates Under Different Aging Conditions

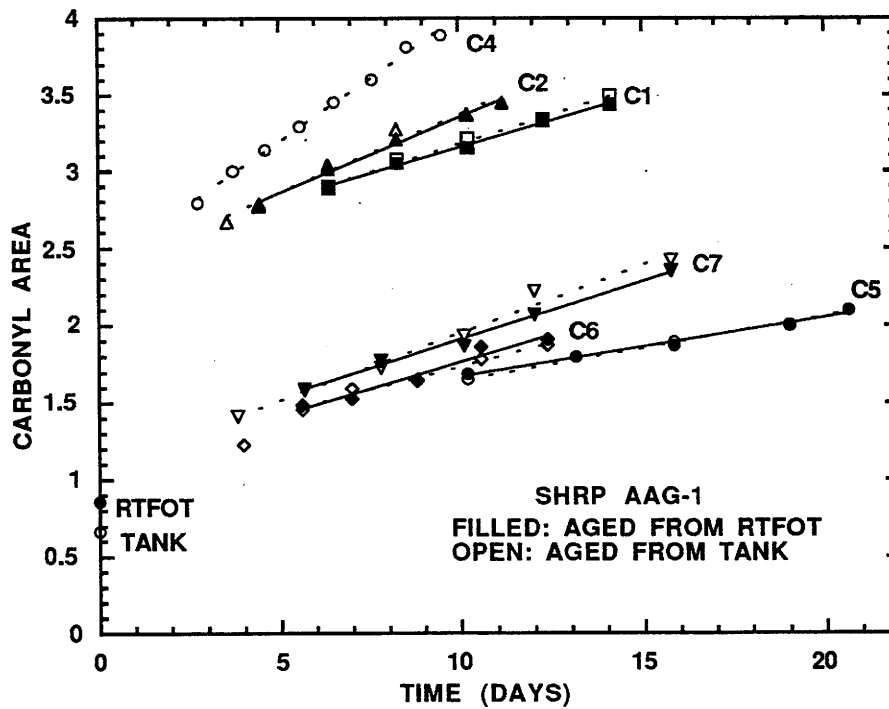


Figure 2-4. Carbonyl Formation Rates Under Different Aging Conditions

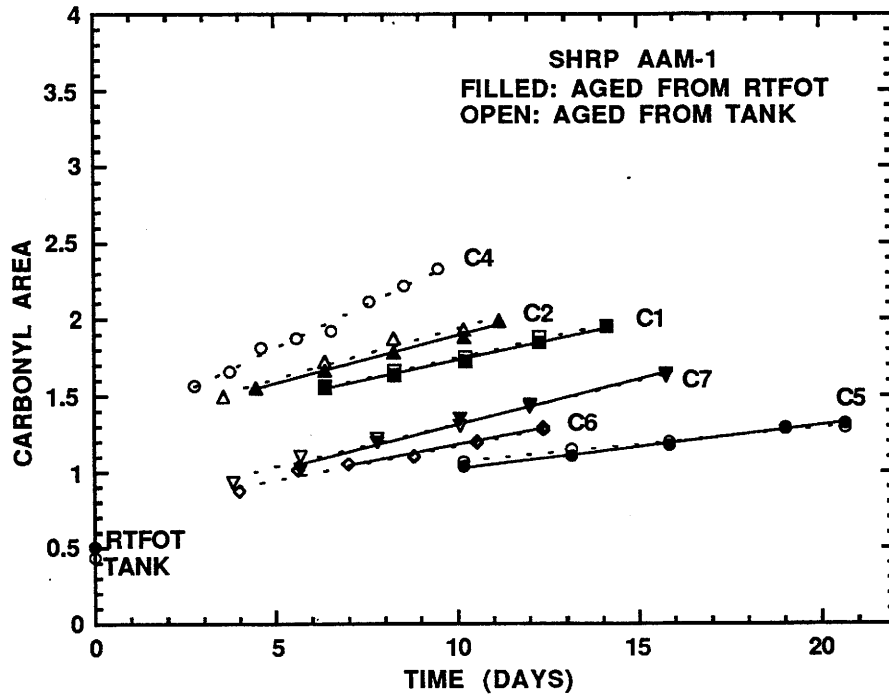


Figure 2-5. Carbonyl Formation Rates Under Different Aging Conditions

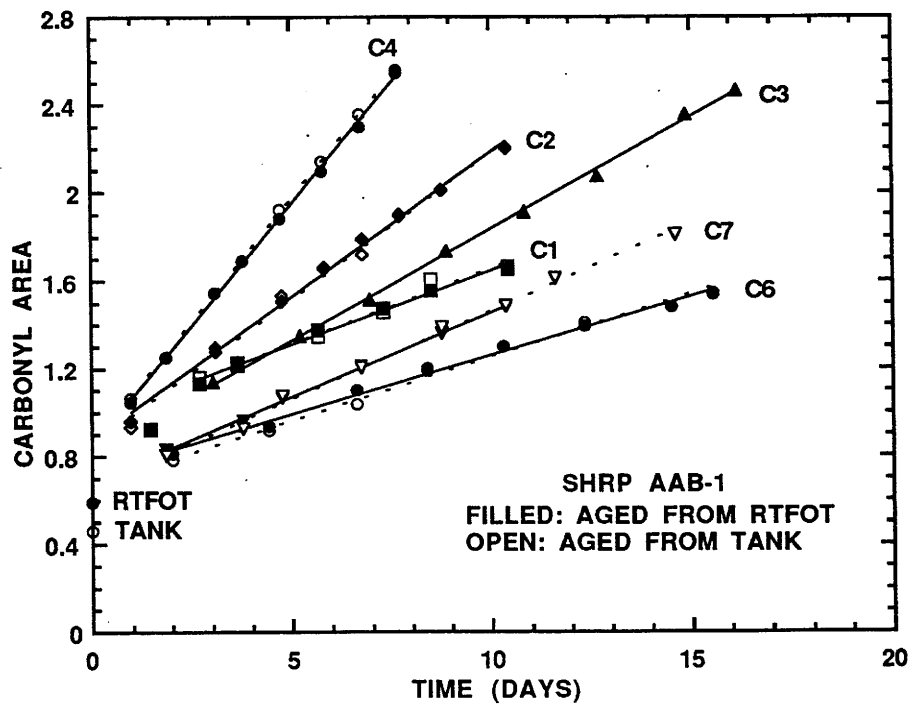


Figure 2-6. Carbonyl Formation Rates Under Different Aging Conditions

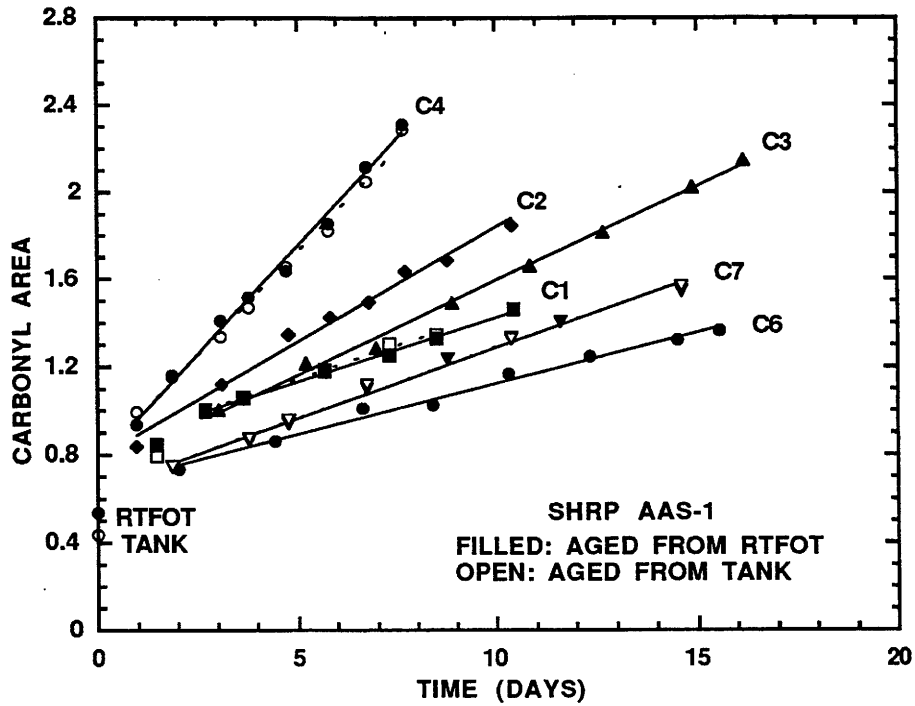


Figure 2-7. Carbonyl Formation Rates Under Different Aging Conditions

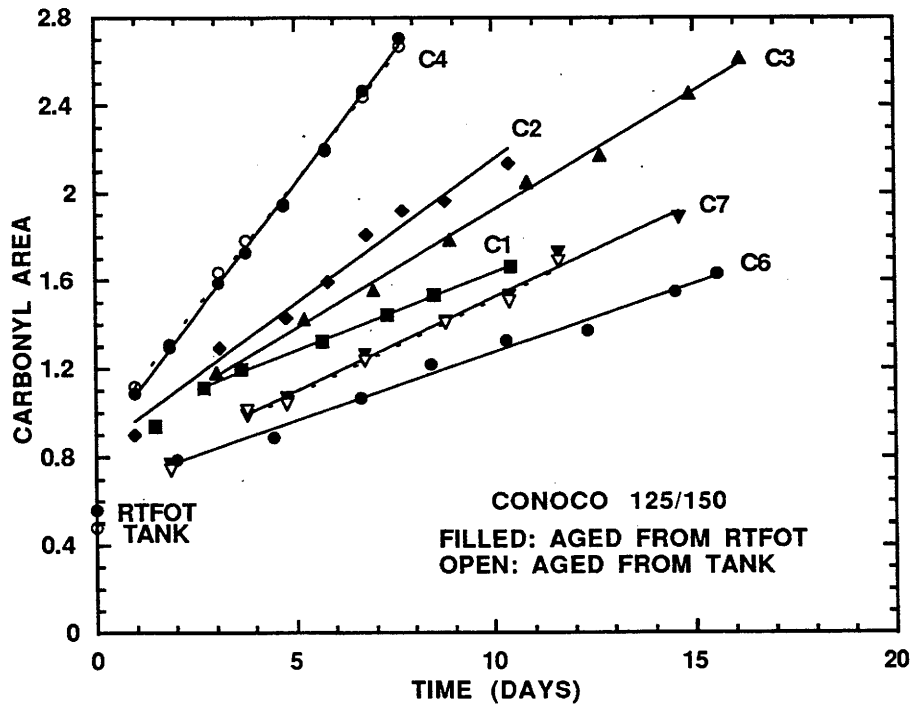


Figure 2-8. Carbonyl Formation Rates Under Different Aging Conditions

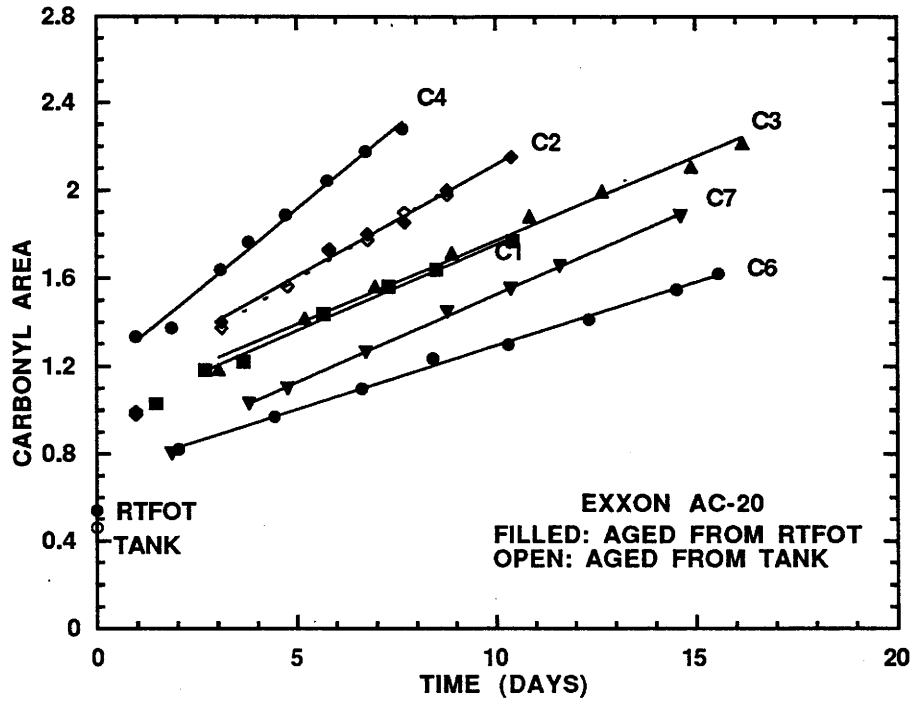


Figure 2-9. Carbonyl Formation Rates Under Different Aging Conditions

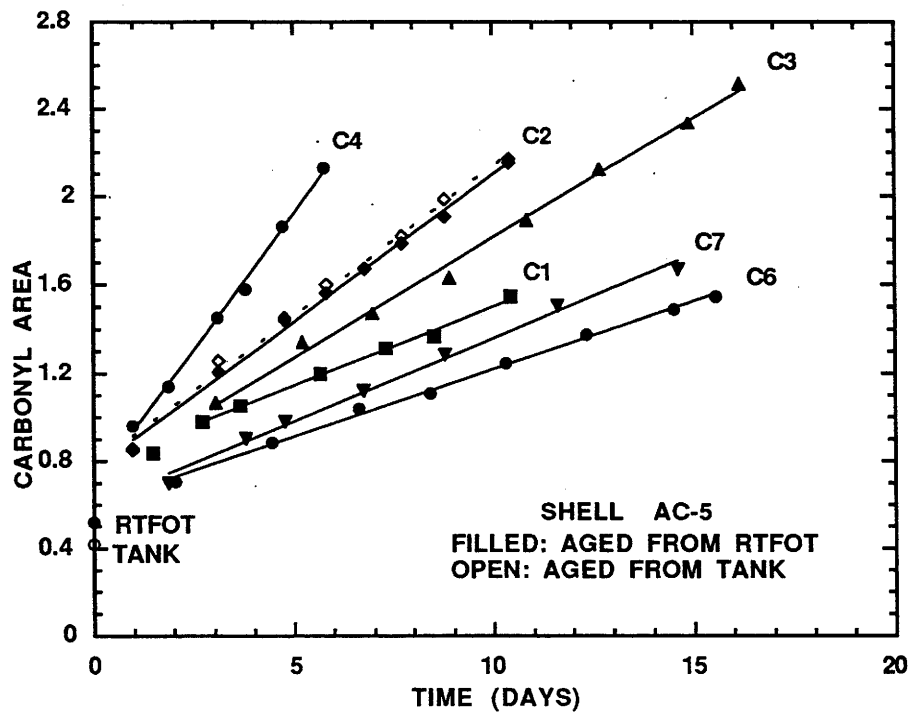


Figure 2-10. Carbonyl Formation Rates Under Different Aging Conditions

intercepts of these rate lines, CA_o , are independent of temperature but increase with pressure, as found in the work described in the previous chapter. Table 2-2a shows the average values of CA_o at 0.2 and 20 atm.

Table 2-2a. Aging Test Results: Kinetic Parameters

Asphalt	ln A	α	E kJ/mol	dCA_o at 0.2 ^a	dCA_o at 20 ^b	$r_{120, 0.2}$ ^c $\times 10^3$	$r_{200, 20}$ ^d
AAA-1	31.9	0.59	104	0.15	0.060	0.36	0.60
AAD-1	31.2	0.61	102	0.16	0.11	0.38	0.64
AAF-1	24.4	0.36	82	0.33	0.76	1.09	0.23
AAG-1	20.6	0.28	70	0.48	1.73	2.61	0.22
AAM-1	18.9	0.26	66	0.27	0.81	2.18	0.14
AAB-1	31.7	0.43	104	0.23	0.43	0.32	0.27
AAS-1	32.2	0.44	106	0.21	0.36	0.32	0.29
Conoco 125/150	32.0	0.42	105	0.18	0.39	0.39	0.31
Exxon AC-20	18.6	0.27	63	0.24	0.60	5.01	0.30
Shell AC-5	31.1	0.43	102	0.19	0.33	0.44	0.32

^a initial jump $CA_o - CA_{o,tank}$ at 0.2 atm

^b initial jump $CA_o - CA_{o,tank}$ at 20 atm

^c carbonyl area growth rate at 49°C (120°F), 0.2 atm (carbonyl area/day)

^d carbonyl area growth rate at 93.3°C (200°F), 20 atm (carbonyl area/day)

The hardening susceptibilities (HS) for Set I are shown in Figures 2-11 to 2-15 and for Set II in Figures 2-16 to 2-20 and for all asphalts at both 0.2 and 20 atm in Table 2-2b. The significant effect of pressure is apparent. There is some difference now between RTFOT and tank material. The RTFOT samples are nearly always slightly higher. Jemison et al. (1991) have shown that the RTFOT and TFOT do not give the same viscosity-carbonyl relation as results in the hot-mix operation, so it is doubtful if running the TFOT on these samples prior to POV aging is justified.

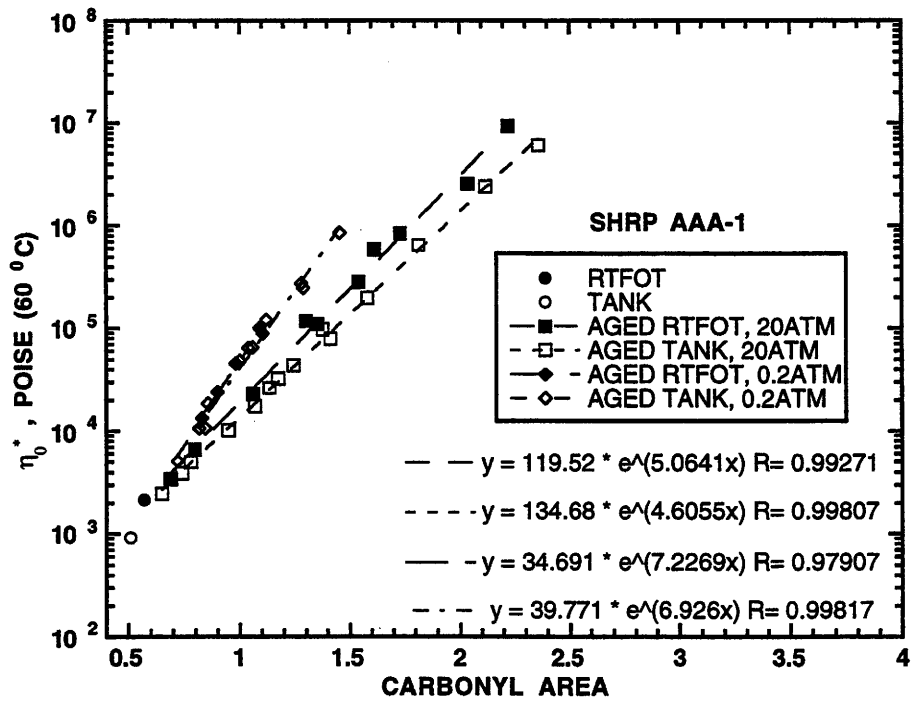


Figure 2-11. Hardening Susceptibility Versus Aging Pressure

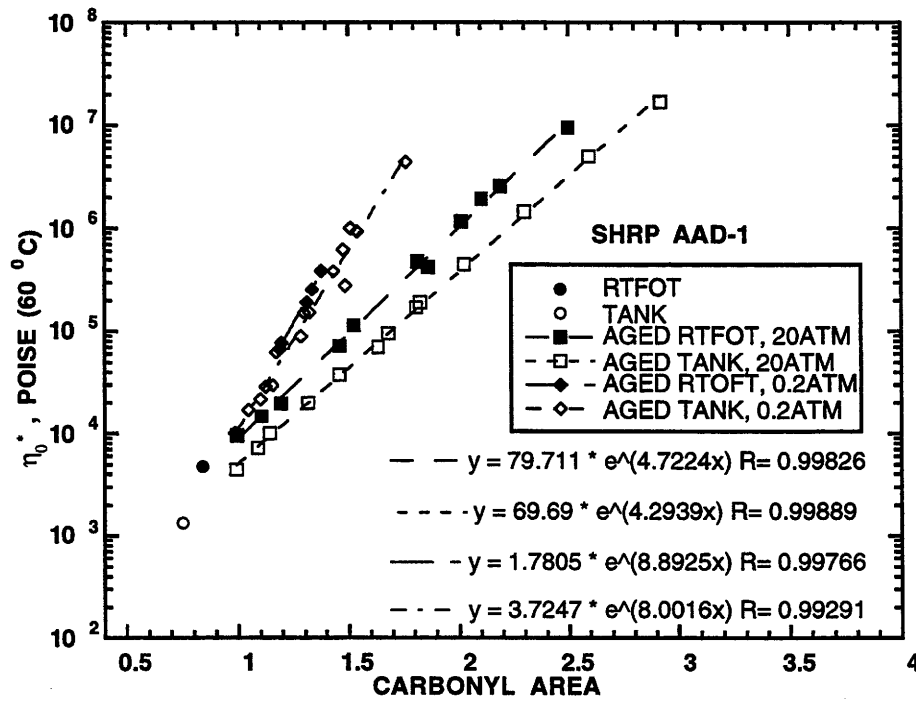


Figure 2-12. Hardening Susceptibility Versus Aging Pressure

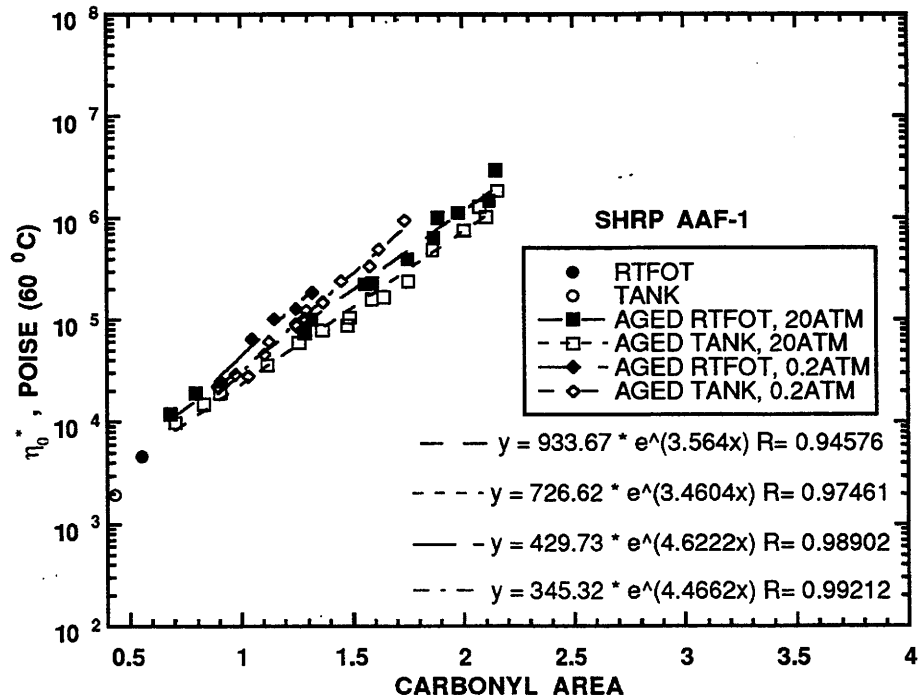


Figure 2-13. Hardening Susceptibility Versus Aging Pressure

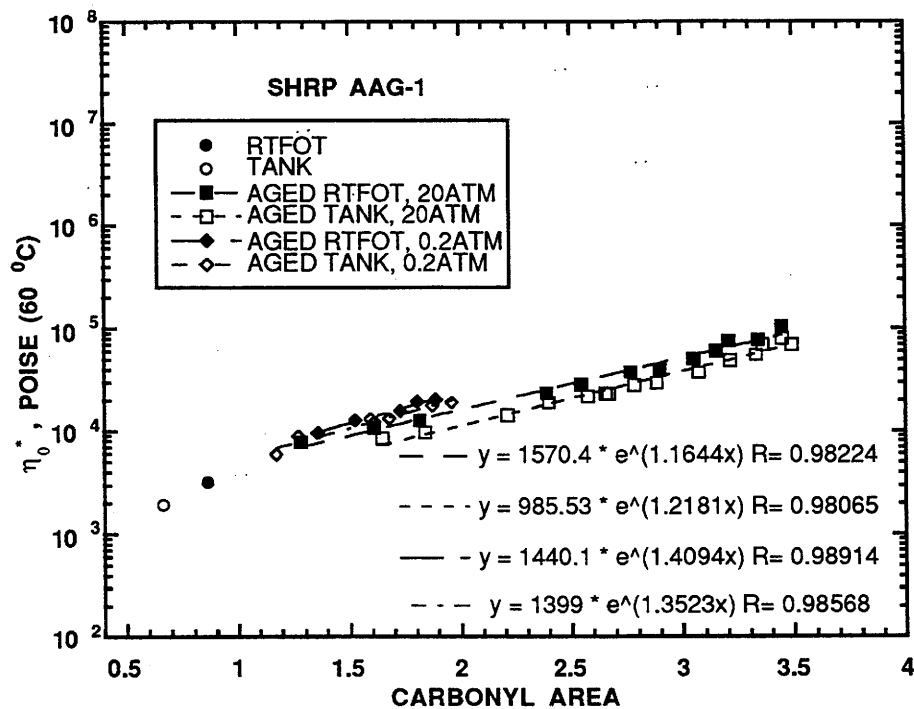


Figure 2-14. Hardening Susceptibility Versus Aging Pressure

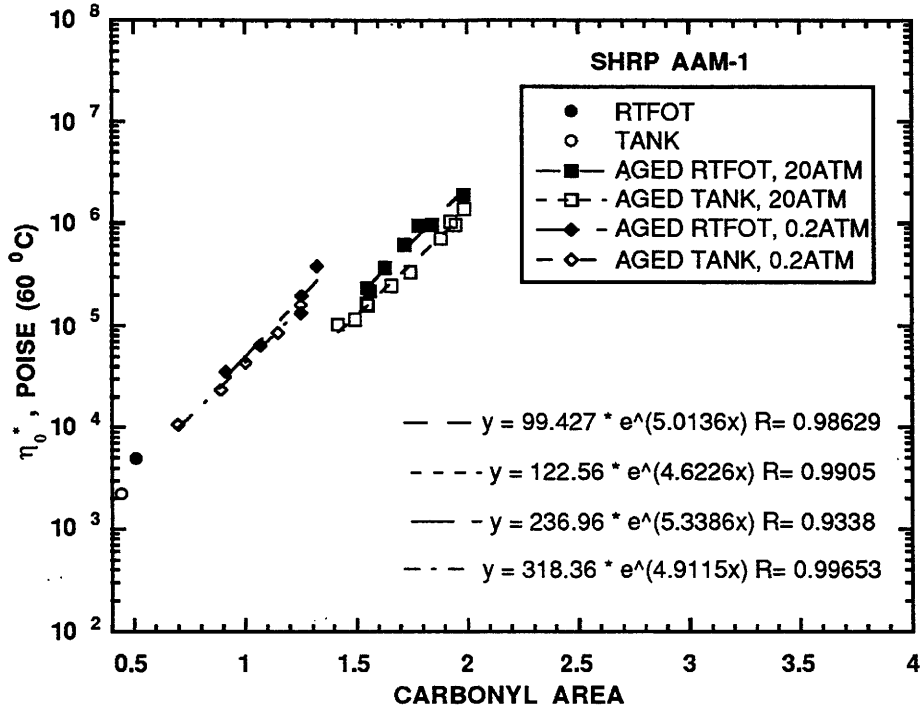


Figure 2-15. Hardening Susceptibility Versus Aging Pressure

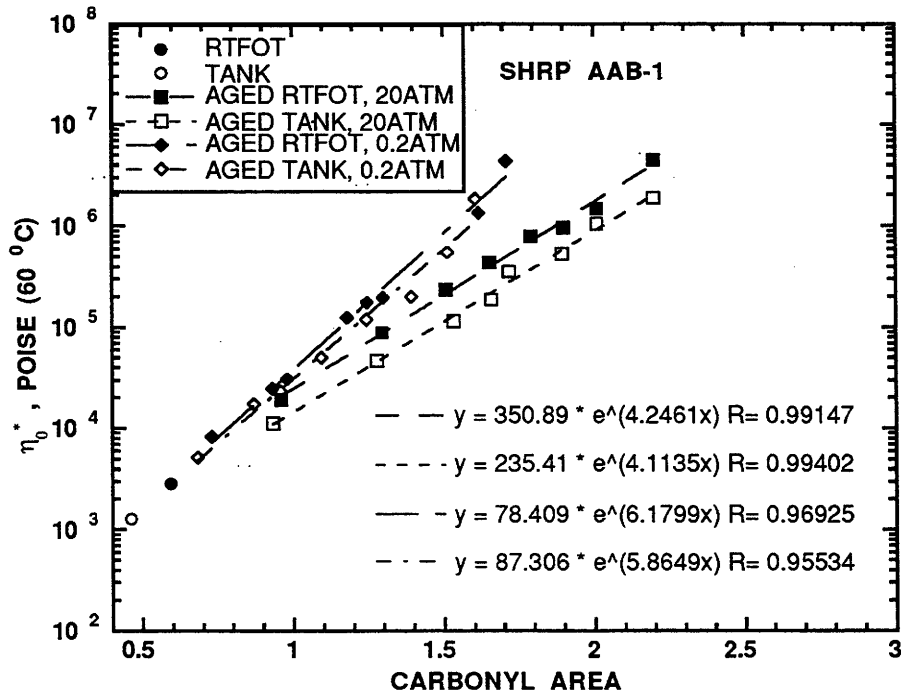


Figure 2-16. Hardening Susceptibility Versus Aging Pressure

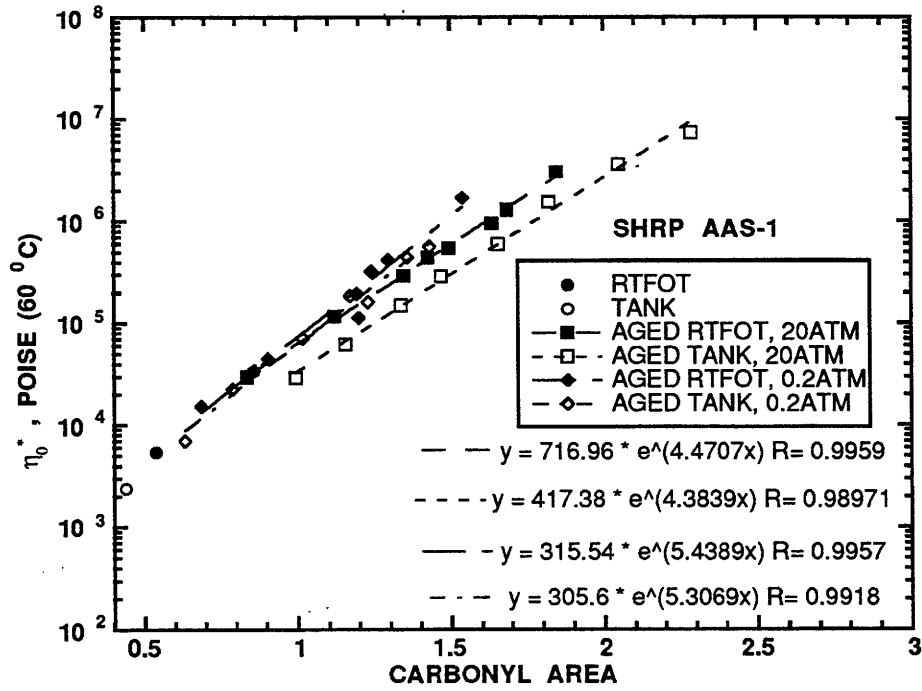


Figure 2-17. Hardening Susceptibility Versus Aging Pressure

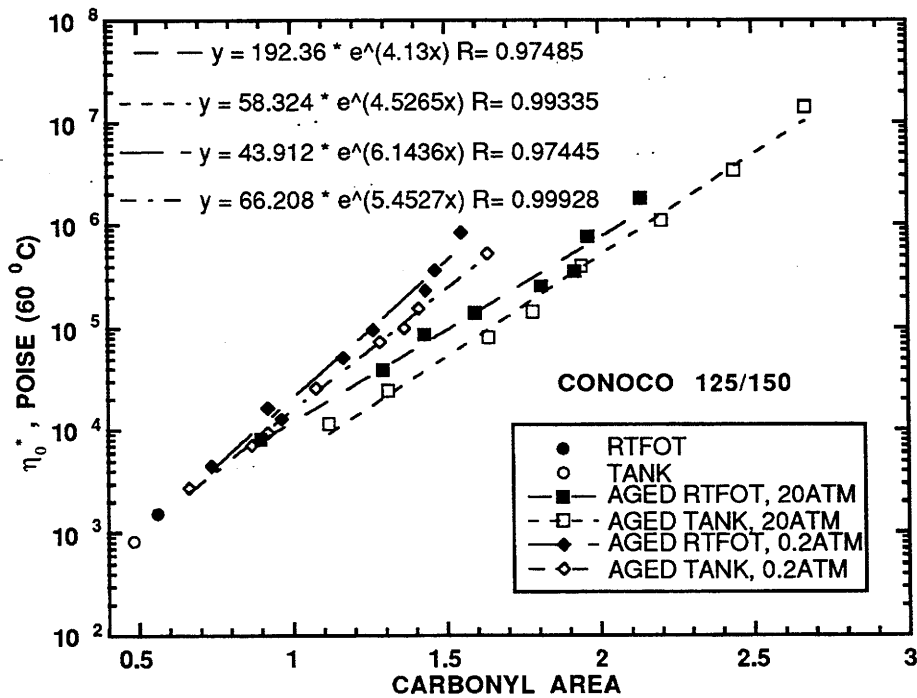


Figure 2-18. Hardening Susceptibility Versus Aging Pressure

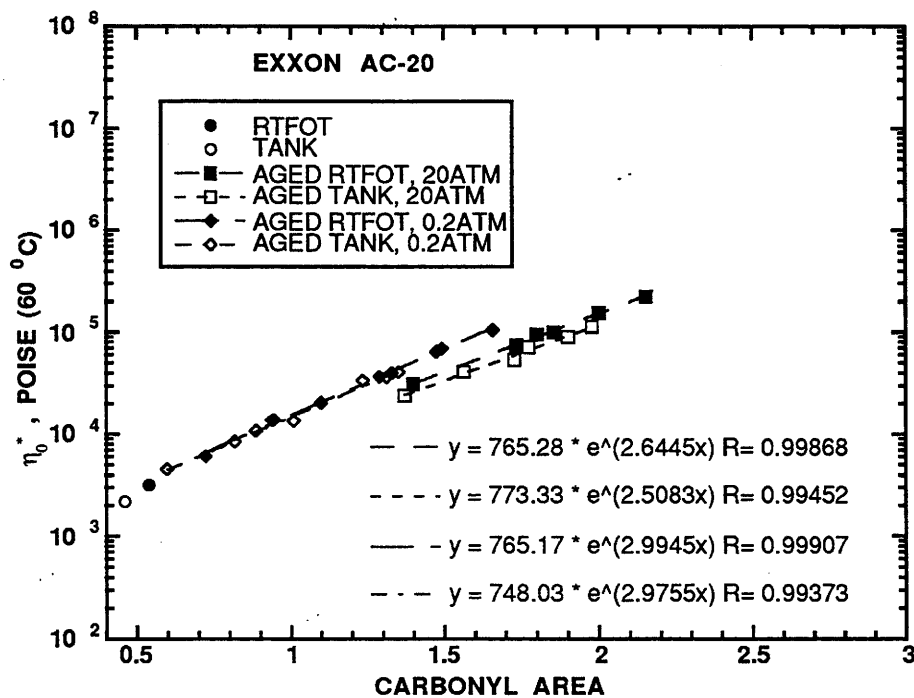


Figure 2-19. Hardening Susceptibility Versus Aging Pressure

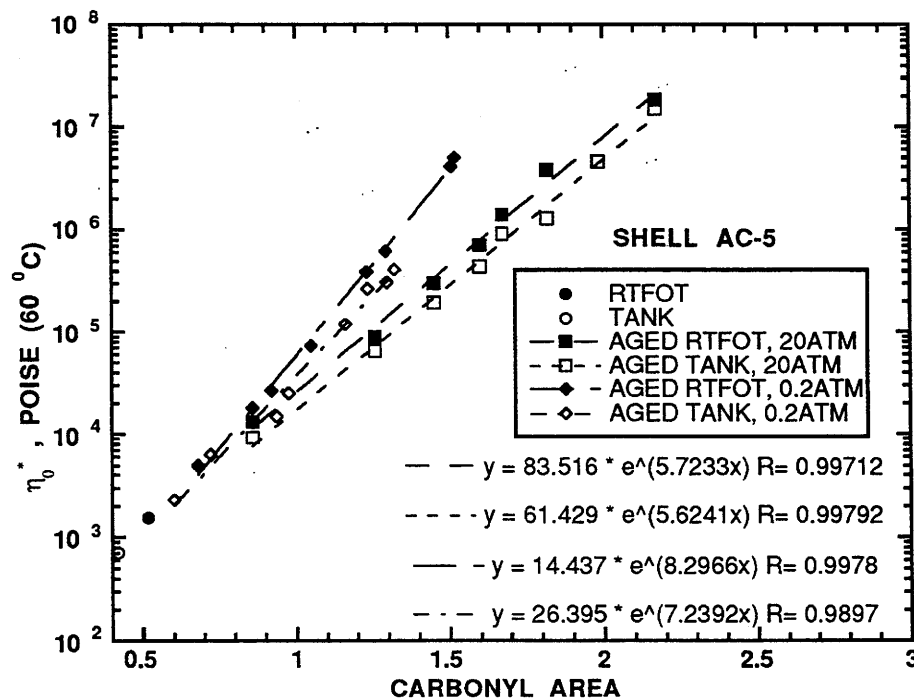


Figure 2-20. Hardening Susceptibility Versus Aging Pressure

Table 2-2b. Aging Test Results: Hardening Susceptibility Parameters^a

Asphalt	— 0.2 atm — HS	— m	— 20 atm — HS	— m
AAA-1	6.93	39.8	4.61	135
AAD-1	8.00	3.73	4.29	69.7
AAF-1	4.47	345	3.46	727
AAG-1	1.35	1400	1.22	986
AAM-1	4.91	318	4.62	123
AAB-1	5.87	87.3	4.12	235
AAS-1	5.31	306	4.38	417
Conoco	5.45	66.2	4.53	58.3
Exxon	2.98	847	2.51	773
Shell	7.24	26.4	5.62	61.4

^a $\ln \eta_o = (HS)(CA) + m$

The large pressure effects indicate that both CA_o and HS must be measured at 0.2 atm, the oxygen partial pressure to which roadways are subjected. Since it is known that there are diffusion effects at 0.2 atm, the question arose whether this would effect the HS. Obtaining HS requires mixing of the film to obtain material for viscosity measurement, and if diffusion limitations occurred, the film would have a viscosity and a carbonyl gradient. These two properties have different mixing rules (Chapter 8). Figures 2-21 and 2-22 show the carbonyl measurements for the exposed surface, bulk carbonyl measurement and the difference caused by diffusion. Fortunately, as shown in Figures 2-23 to 2-25, this appears to have negligible effect on the HS which, of course, must be based on bulk carbonyl and viscosity.

To obtain kinetic results from the rate data, Equation 1-3 was written

$$\ln r = \ln A + \alpha \ln P + E/RT \quad (2-1)$$

and the constants A , α and E were obtained for each asphalt by least square

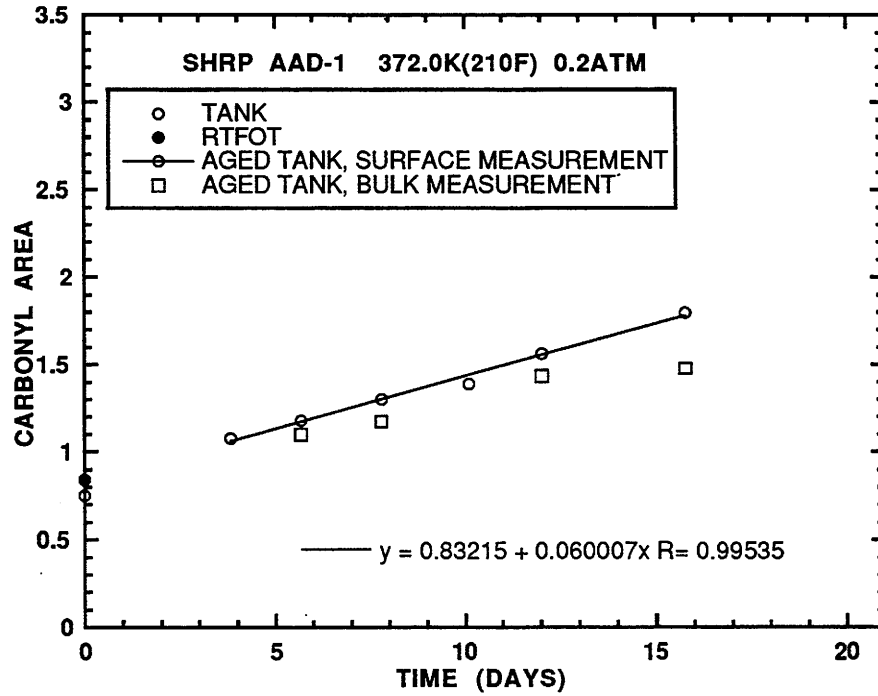


Figure 2-21. Comparison of Surface and Bulk Values, AAD-1

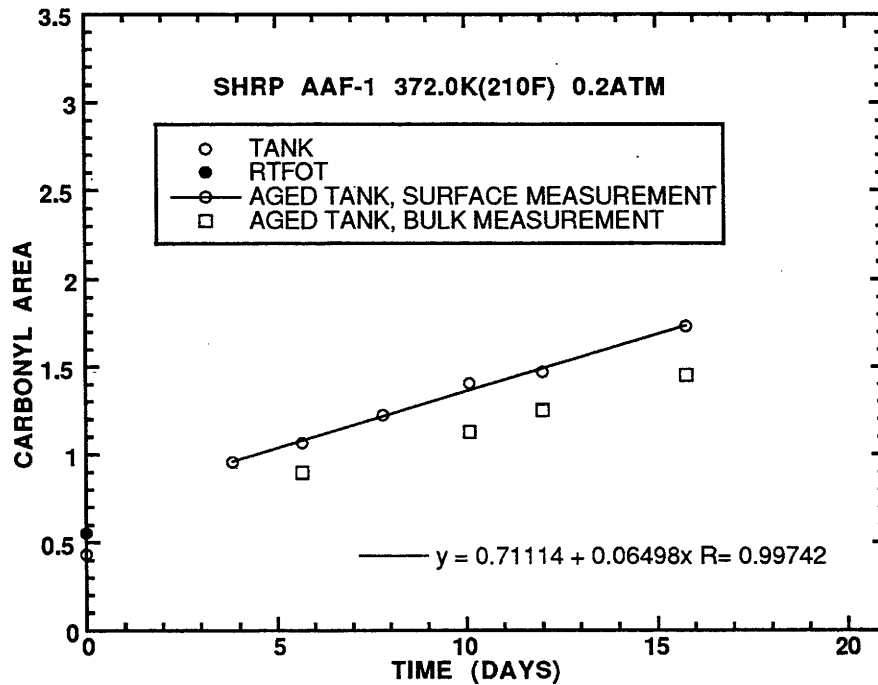


Figure 2-22. Comparison of Surface and Bulk Values, AAF-1

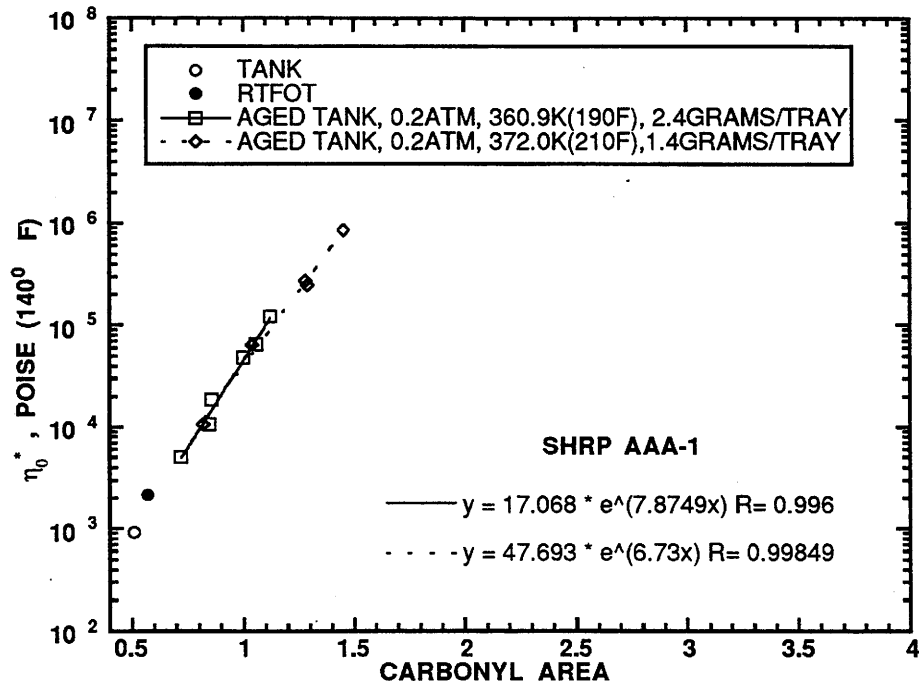


Figure 2-23. Hardening Susceptibility Versus Film Thickness

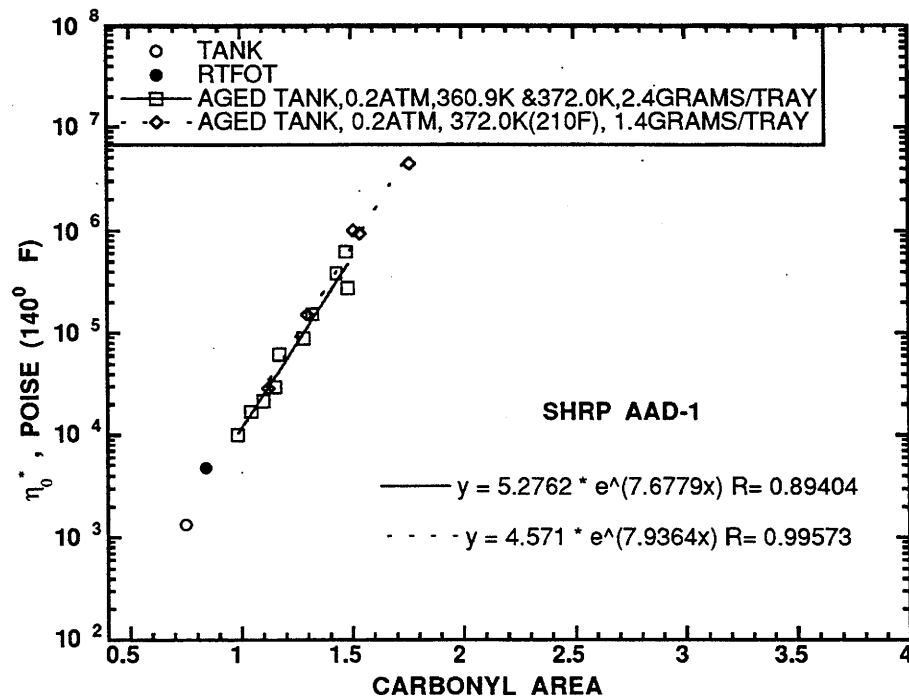


Figure 2-24. Hardening Susceptibility Versus Film Thickness

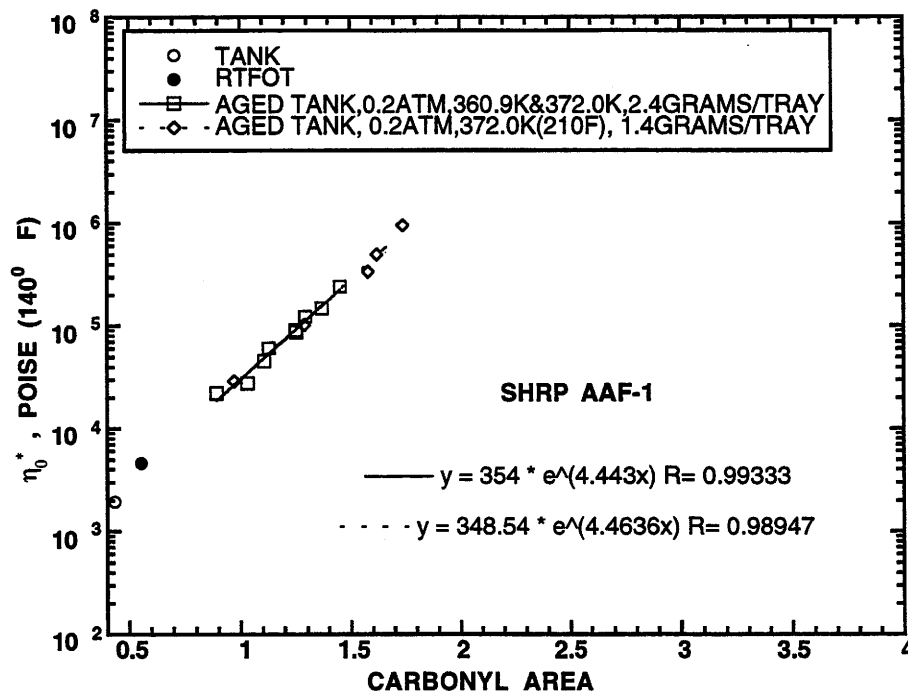


Figure 2-25. Hardening Susceptibility Versus Film Thickness

regression analysis, where A is the frequency factor, α the pressure dependence and E the activation energy. Table 2-2a shows the results.

All results were converted to 0.2 atm using their respective α and plotted on an Arrhenius plot. Set I results are in Figure 2-26 and Set II in Figure 2-27. Unlike the five asphalts studied in the previous section, these show wide variation in both activation energy and the pressure factor α . However, the one common asphalt, Exxon AC-20, yielded very similar results in both studies. The data in Figures 2-26 and 2-27 show the large differences in relative rates that can occur as extrapolation is made to lower temperatures. But these data have already been corrected for pressure, so that the differences between test conditions and road conditions are even larger. For instance, asphalts AAA-1 and AAD-1 show the highest rates at 372 K (210°F) and 20 atm, but the lowest at 349.8 K (170°F) and 0.2 atm.

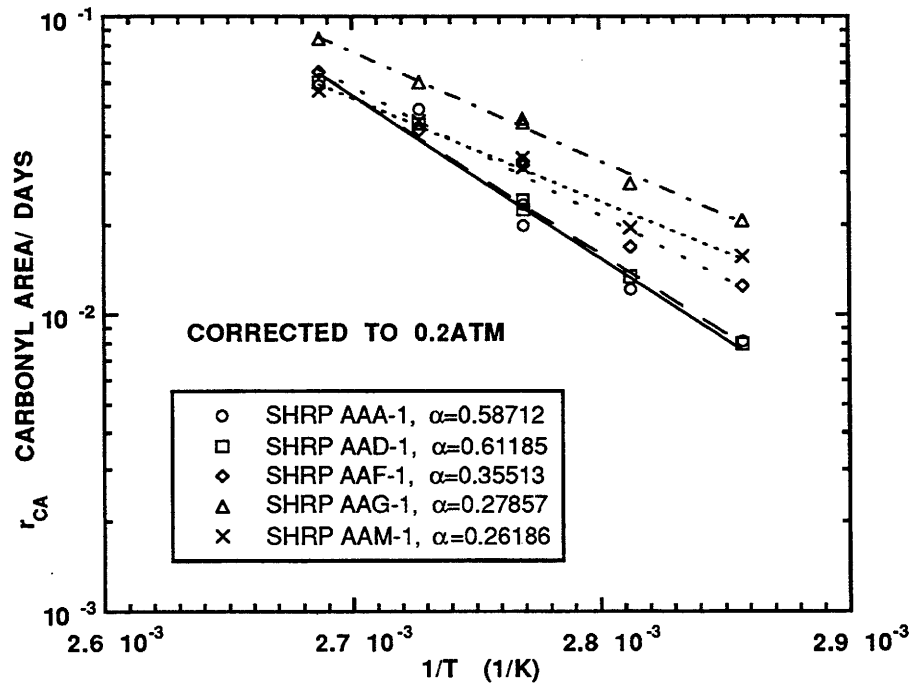


Figure 2-26. Arrhenius Plot of Set I Asphalts

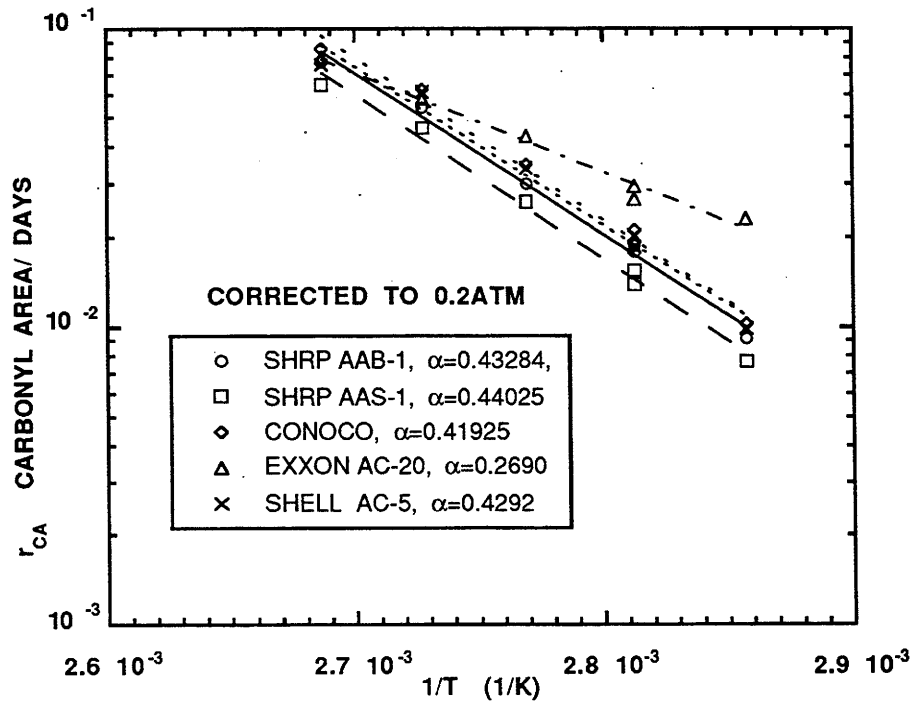


Figure 2-27. Arrhenius Plot of Set II Asphalts

Using the values of A , α and E in Table 2-2a, the carbonyl formation rate was calculated for each asphalt at 322 K (120°F) and 0.2 atm. These are also shown in Table 2-2a.

Next, using the 0.2 atm tank HS, the carbonyl value corresponding to 500,000 poise was calculated for each asphalt. Then, using the 322 K (120°F) 0.2 atm rates, the time to reach this viscosity was calculated for each asphalt by the following equation

$$\text{time (days)} = \frac{CA(0.5 \text{ M Poise}) - CA_0}{r_{120}} \quad (2-2)$$

These times (days) are shown in the first column of Table 2-3a. Using the same procedure but with 20 atm HS, the times to reach 500,000 poise at 366.5 K (200°F) and 20 atm were calculated and are presented in the second column of Table 2-3a. Next, all of the asphalts were aged using the SHRP PAV procedure at 366.5 K (200°F); the results are shown in the third column of Table 2-3a. The last column of Table 2-3b shows the time (in days) for an asphalt to reach its PAV residue viscosity, calculated using the A , α , and E kinetic parameters. Table 2-3b shows the relative rankings of the ten asphalts, with 1 being the best, according to the particular criterion used from Table 2-3a. In addition, the last two columns rank the asphalts on the basis of the viscosity reached after a fixed amount of time at the specified condition. The disagreement in these rankings demonstrates the impossibility of using high temperature, high pressure data to estimate road aging.

As part of the study described in Chapter 1, asphalts were aged at 322 K (120°F) and 20 atm for up to 80 days. The results are shown in Appendix B, Figures B-25 to B-28, and in Table B-6. These experimental rates were corrected to 0.2 atm and compared to calculated results obtained in both parts of this study. The data on the left of Figure 2-28, shown by open symbols, are from this chapter. Those on the right are from Chapter 1, with the exception of the hashed square for Exxon. Texaco shows only one symbol as the match is nearly exact. Considering the scatter in the 322 K (120°F), 20 atm data and the required extrapolations, the agreement is as good

Table 2-3a. Aging Tests: Time Comparisons

Asphalt	CT ^a at 120°F, 0.2 atm	CT at 200°F, 20 atm	PAV Aging Index ^b	PAVT ^c at 120°F, 0.2 atm
Conoco 125/150	2491	3.60	8.44	497.58
AAB-1	2437	3.60	9.99	493.65
AAS-1	2356	2.84	8.60	455.37
AAA-1	1958	2.03	10.68	375.17
Shell AC-5	1711	2.64	16.01	521.83
AAD-1	1491	1.88	17.32	477.71
AAG-1	1226	12.27	4.14	54.98
AAF-1	796.3	3.03	9.97	129.05
AAM-1	371.3	3.89	9.59	68.78
Exxon AC-20	296.8	5.12	3.81	22.07

- ^a critical time is defined as the time needed to reach viscosity of 0.5MM poise at the aging condition
- ^b PAV aging index is defined as the ratio of the viscosity after PAV aging to that of tank asphalt
- ^c calculated aging time at 120°F and 0.2 atm needed to reach PAV viscosity

Table 2-3b. Aging Tests: Rank Comparisons

Asphalt	Rank					
	CT at 120°F, 0.2 atm	CT at 200°F, 20 atm	PAV AI	PAVT	4 ^a	5 ^b
Conoco 125/150	1	5	3	7	1	3
AAB-1	2	4	7	5	4	4
AAS-1	3	7	4	6	6	7
AAA-1	4	9	8	0	3	9
Sh AC-5	5	8	9	9	2	6
AAD-1	6	10	10	1	5	10
AAG-1	7	1	2	3	7	1
AAF-1	8	6	6	2	8	8
AAM-1	9	3	5	4	9	5
Ex AC-20	10	2	1	8	10	2

- ^a rank by viscosity after aging at 120°F and 0.2 atm for 300 days
- ^b rank by viscosity after aging at 200°F and 20 atm for 2 days

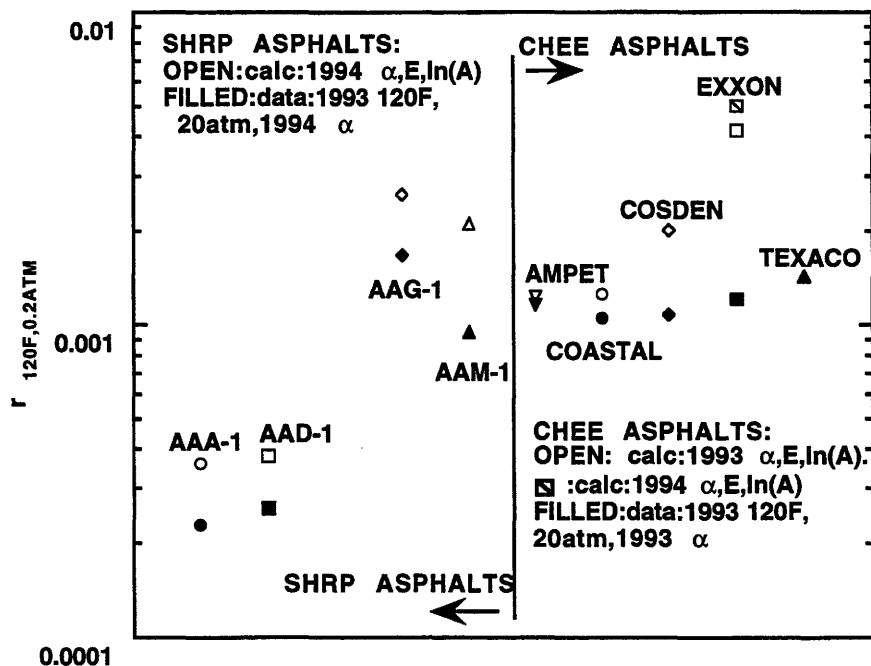


Figure 2-28. Calculated Rates Versus Pressure Corrected Experimental Rates

as could be expected, except for Exxon, where the two extrapolations are in close agreement but show much higher rates than the data measured at 322 K (120°F) and converted to 0.2 atm. There is no explanation.

In the following ten Figures, 2-29 to 2-33 for Set I, and 2-34 to 2-38 for Set II, the Arrhenius plot and data points are shown for each asphalt. For Set I, two points occur at 360.9 K (190°F): one for 0.2 atm and the other for 20 atm converted to 0.2. SHRP AAA-1 and AAA-D have large α , and, for AAA-1, the agreement is not good. For Set II, two points occur at 355.4 K (180°F): one at 10 atm and one at 20. Generally, these points look good but four of the five points at 372.0 K (210°F) are below the curve. These data also involve evaluation of the constants from six points. The pressure correction could be eliminated by running all data at 0.2 atm, but the lower temperatures would have to be eliminated requiring a larger temperature extrapolation.

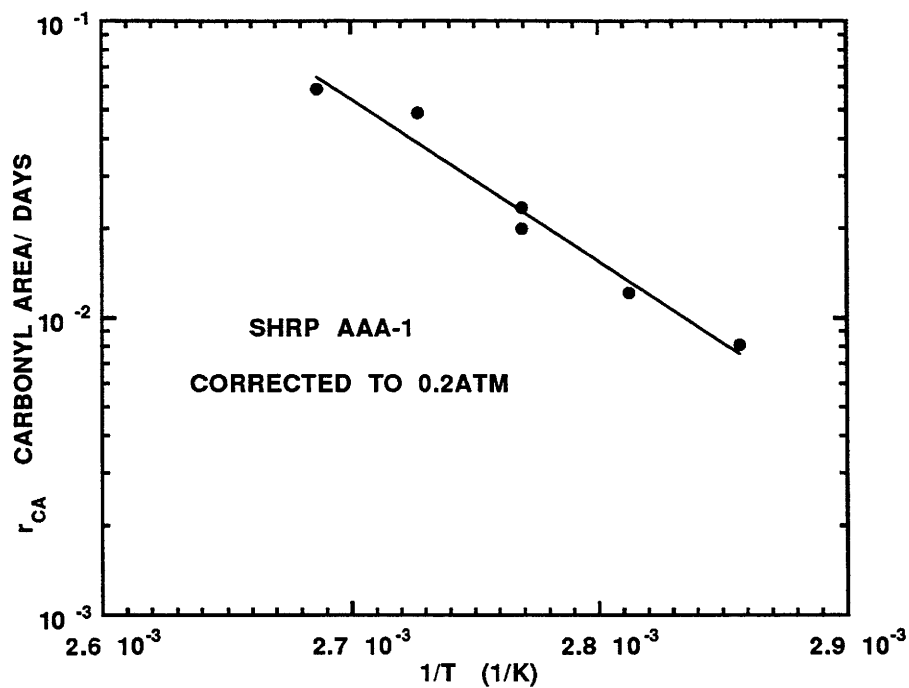


Figure 2-29. Pressure Corrected Rates and Arrhenius Plot by Linear Regression

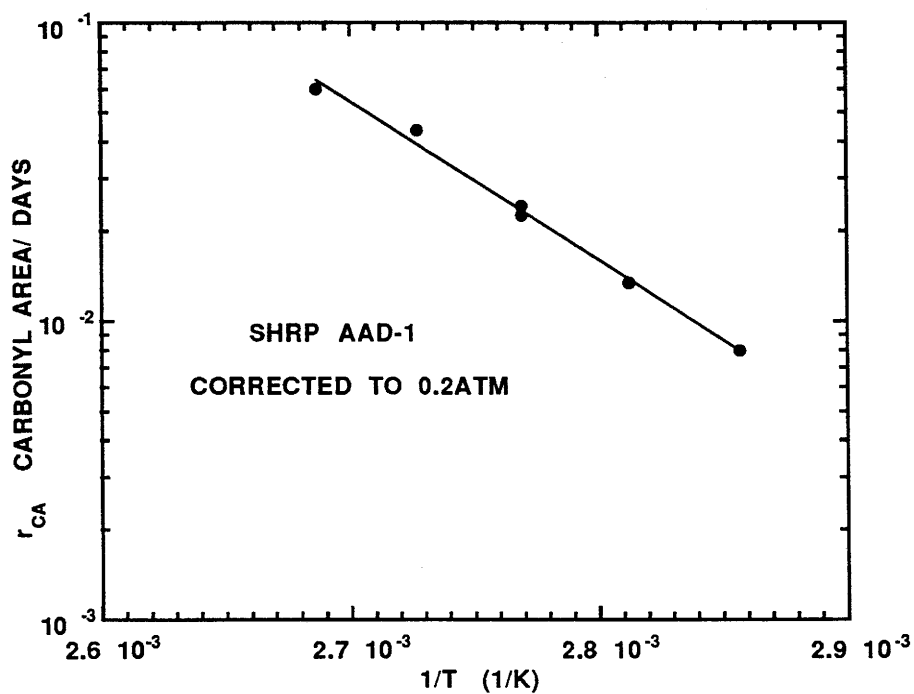


Figure 2-30. Pressure Corrected Rates and Arrhenius Plot by Linear Regression

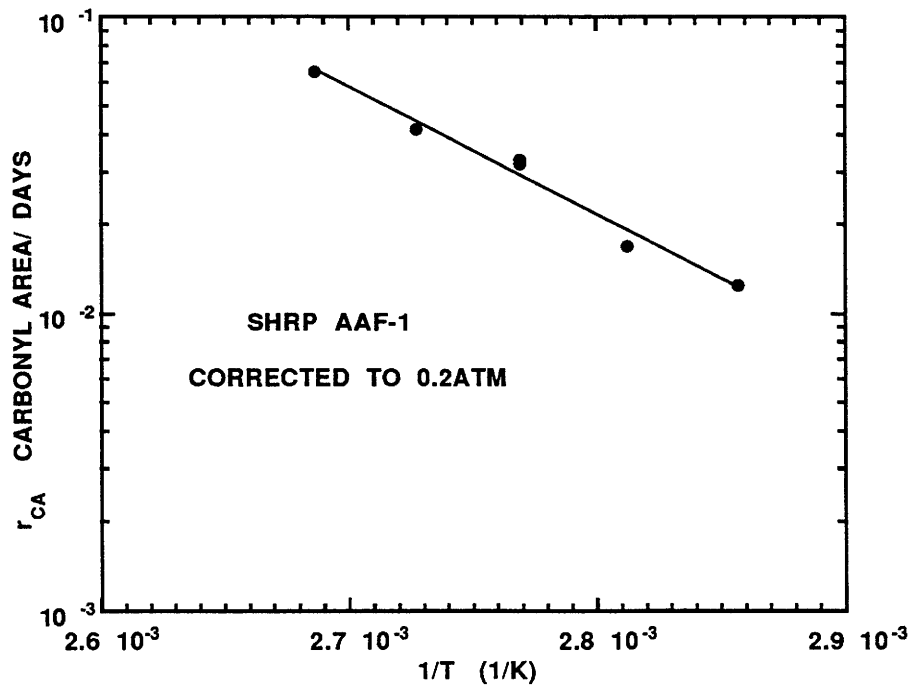


Figure 2-31. Pressure Corrected Rates and Arrhenius Plot by Linear Regression

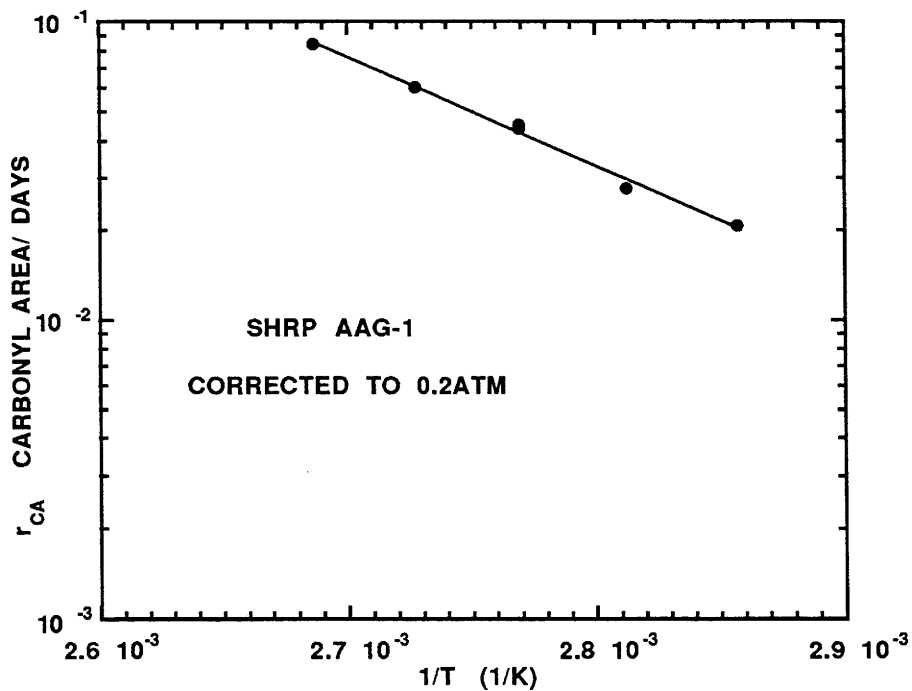


Figure 2-32. Pressure Corrected Rates and Arrhenius Plot by Linear Regression

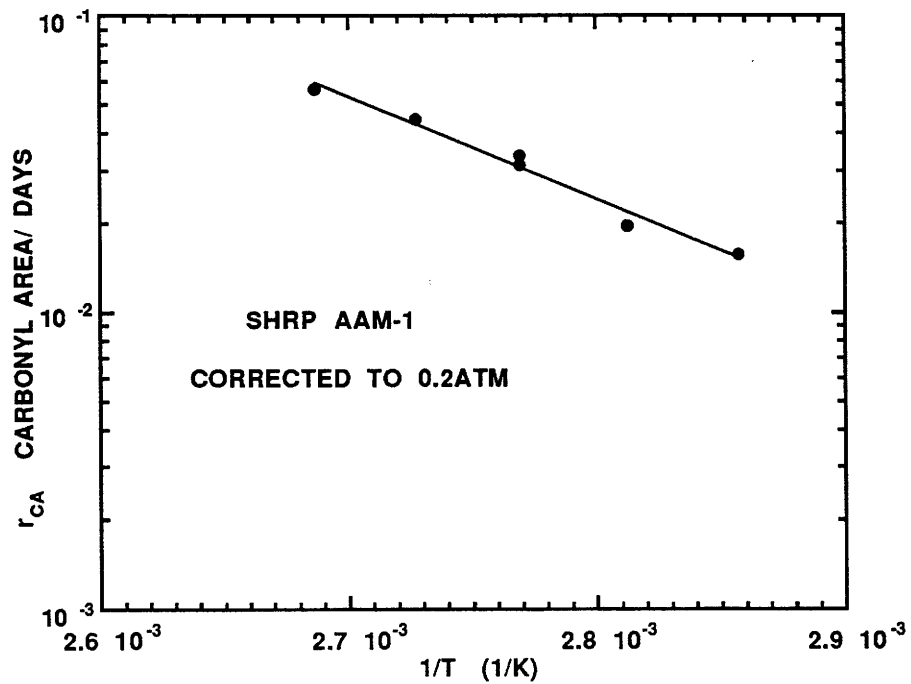


Figure 2-33. Pressure Corrected Rates and Arrhenius Plot by Linear Regression

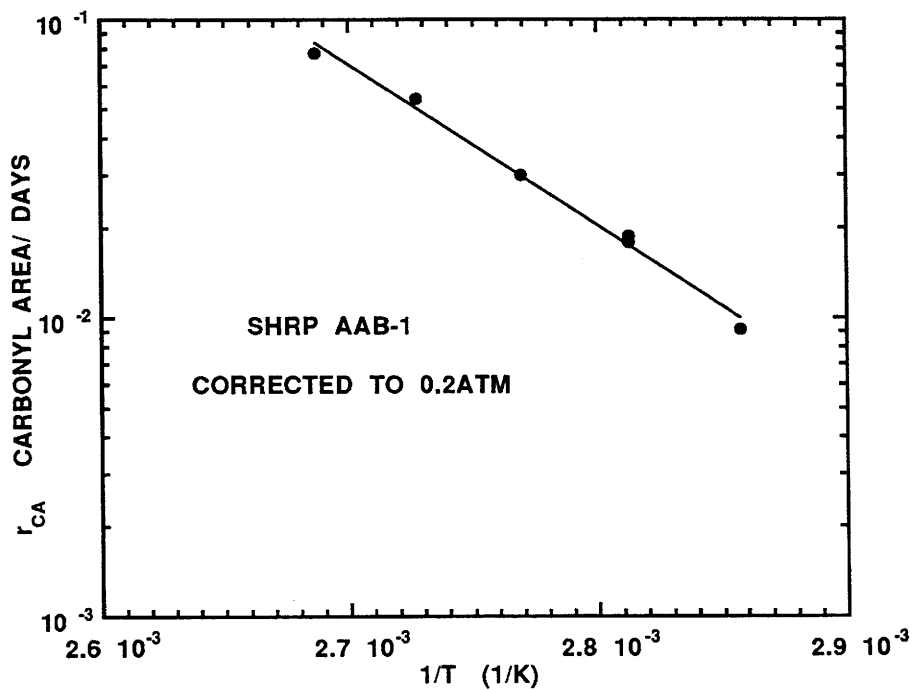


Figure 2-34. Pressure Corrected Rates and Arrhenius Plot by Linear Regression

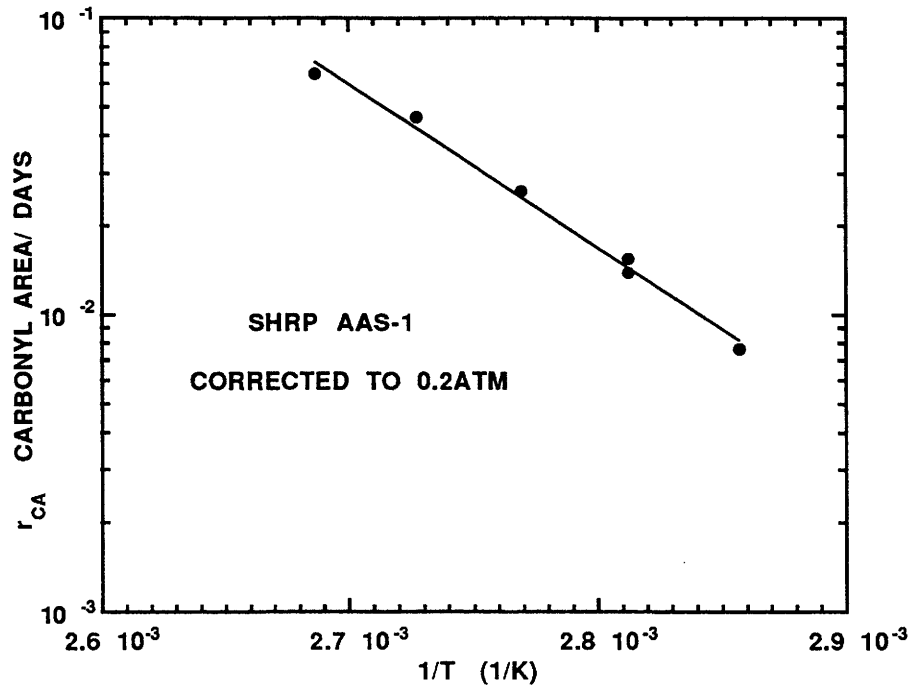


Figure 2-35. Pressure Corrected Rates and Arrhenius Plot by Linear Regression

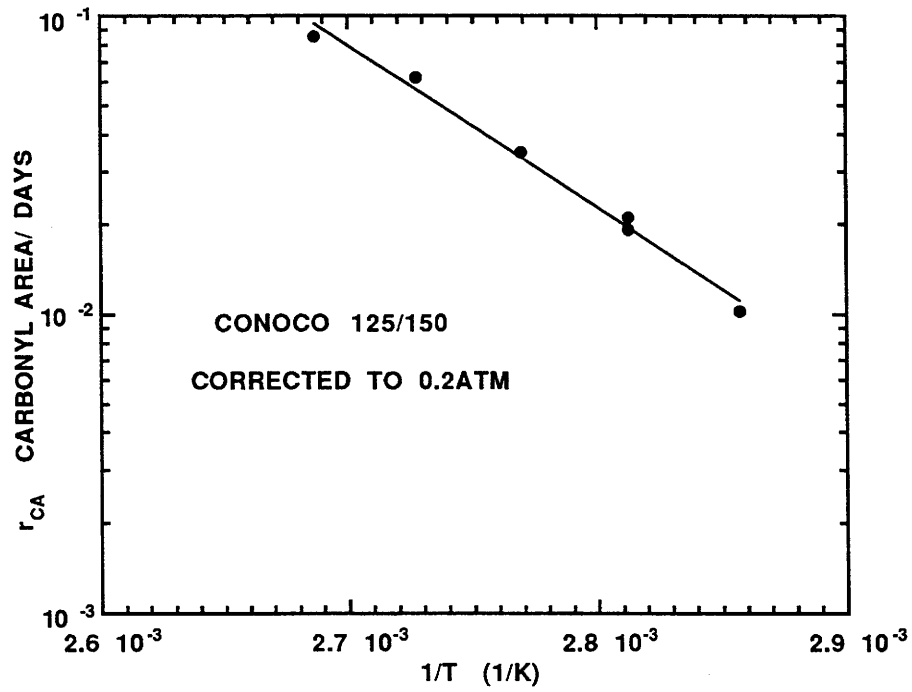


Figure 2-36. Pressure Corrected Rates and Arrhenius Plot by Linear Regression

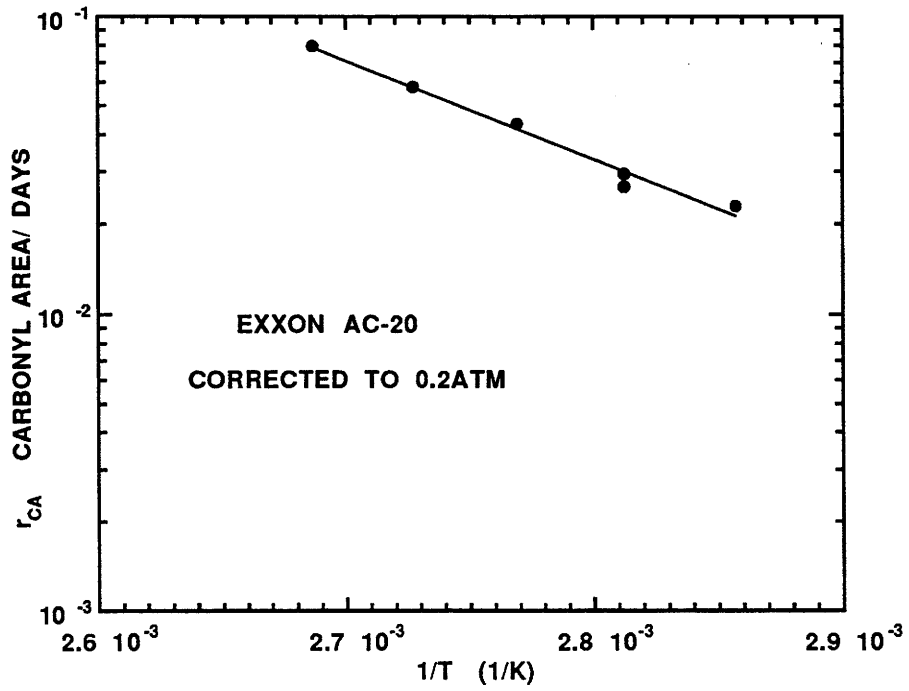


Figure 2-37. Pressure Corrected Rates and Arrhenius Plot by Linear Regression

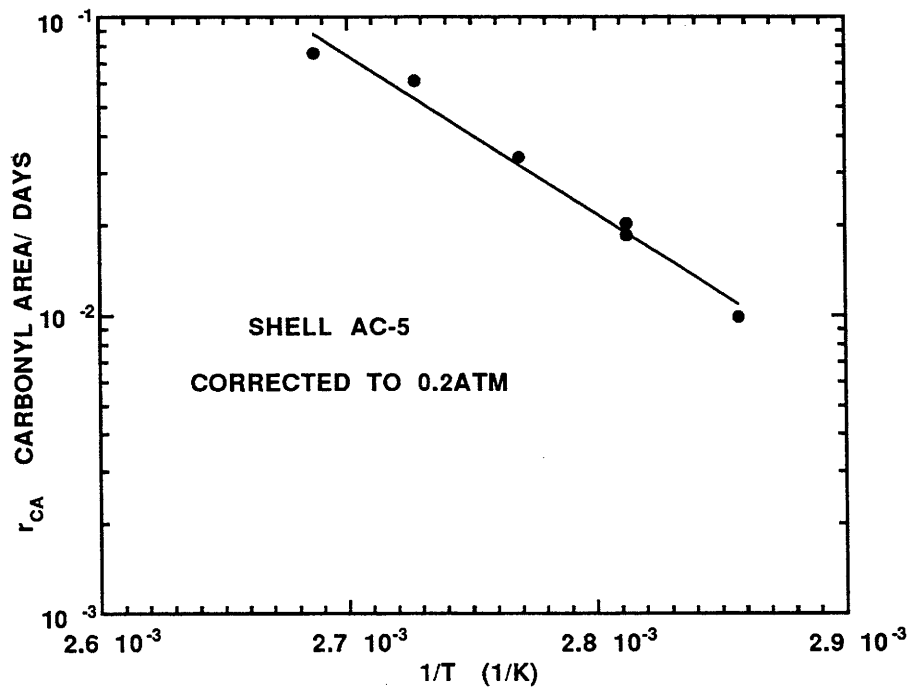


Figure 2-38. Pressure Corrected Rates and Arrhenius Plot by Linear Regression

There are a number of very interesting correlations between properties measured for the asphalts. In the following figures, open circles are the five Chapter 1 asphalts; the closed circles are the ten Chapter 2 asphalts. In Figure 2-39, α is plotted vs E where, in general, high α indicates high E and these asphalts would be particularly bad in high temperature, high pressure tests. Two distinct families of activation energies appear. There is an ever stronger correlation between $\ln A$ and E as shown in Figure 2-40. The HS generally increases with α (and thus with E). The data for 0.2 atm are shown in Figure 2-41. As mentioned previously, the initial jump, CA_0 , is pressure dependent. Figure 2-42 shows that this is particularly true for the low α asphalts. In fact, for $\alpha = 0.6$ the 0.2 atm data are actually higher than those at 20 atm, but this is probably error. In Figure 2-43, the 322 K (120°F) rate data are plotted vs α with the asphalts ranked. The actual hardening rate, however, is not so clearly defined because the HS increases with α . The results from Table 2-3 are shown in Figure 2-44 with rankings.

How much of this is cause-and-effect and how much is coincidence is still unknown. In Study 1249 (Davison et al., 1992) we were able to greatly reduce the HS, seemingly without having much effect on the oxidation rate, indicating that the relations shown above may be coincidental and thus offer opportunity for profitable property manipulation.

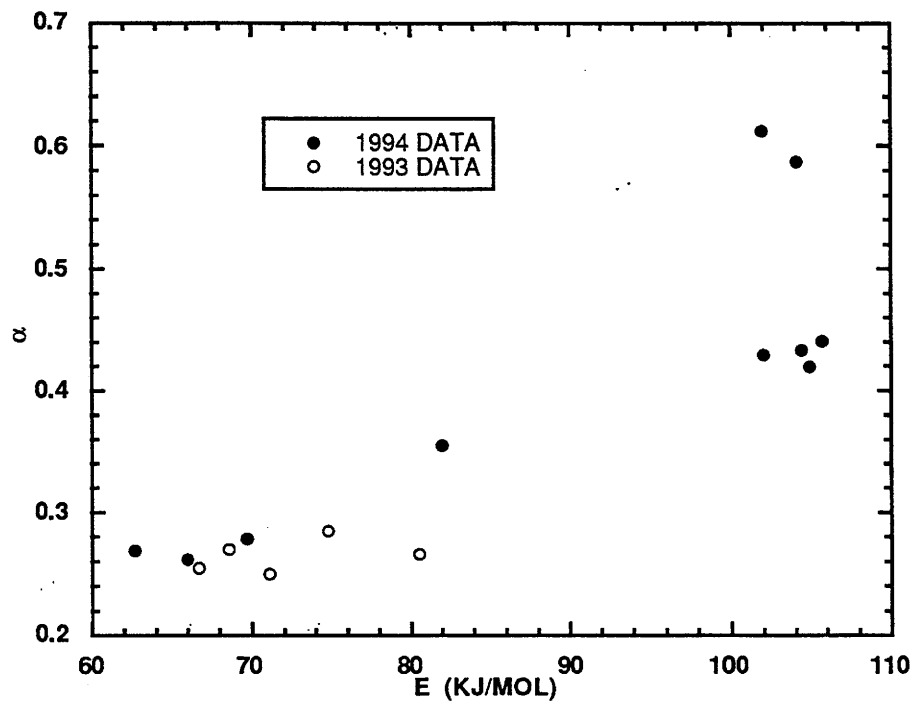


Figure 2-39. Pressure Dependence Factor Versus Activation Energy

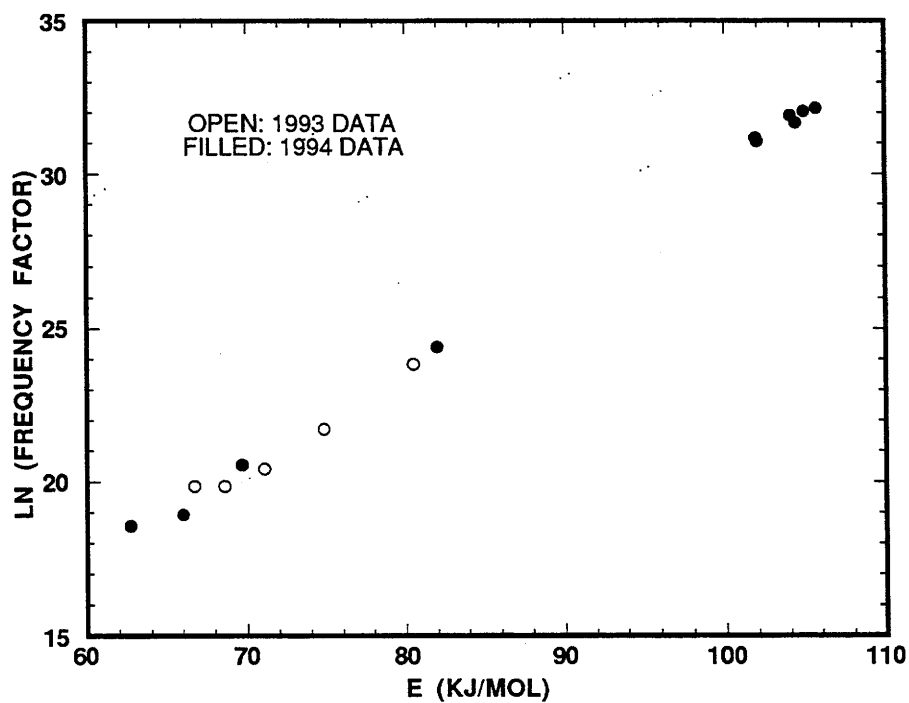


Figure 2-40. Log Frequency Factor Versus Activation Energy

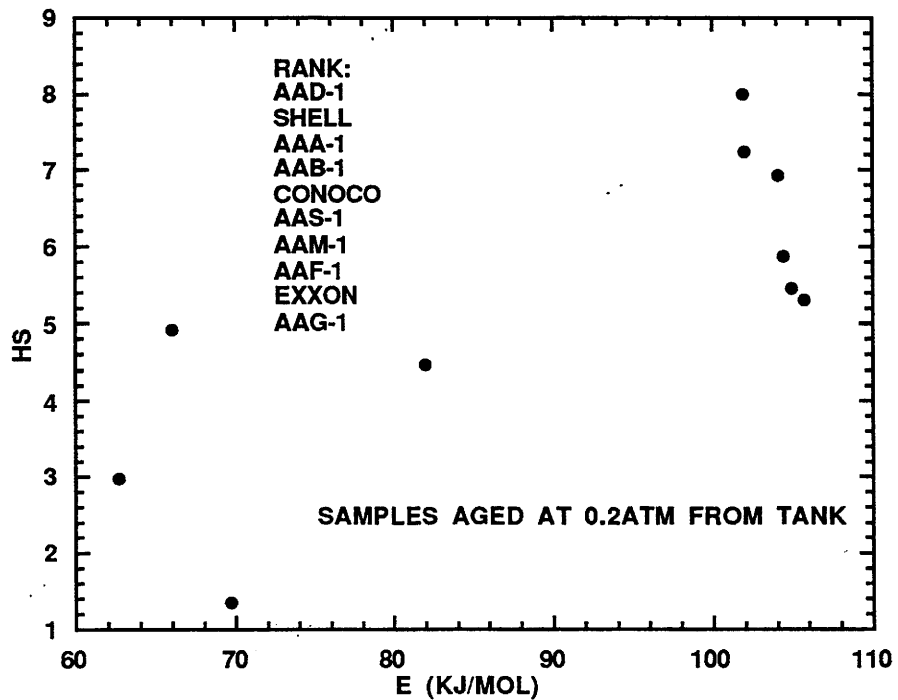


Figure 2-41. Hardening Susceptibility Versus Activation Energy

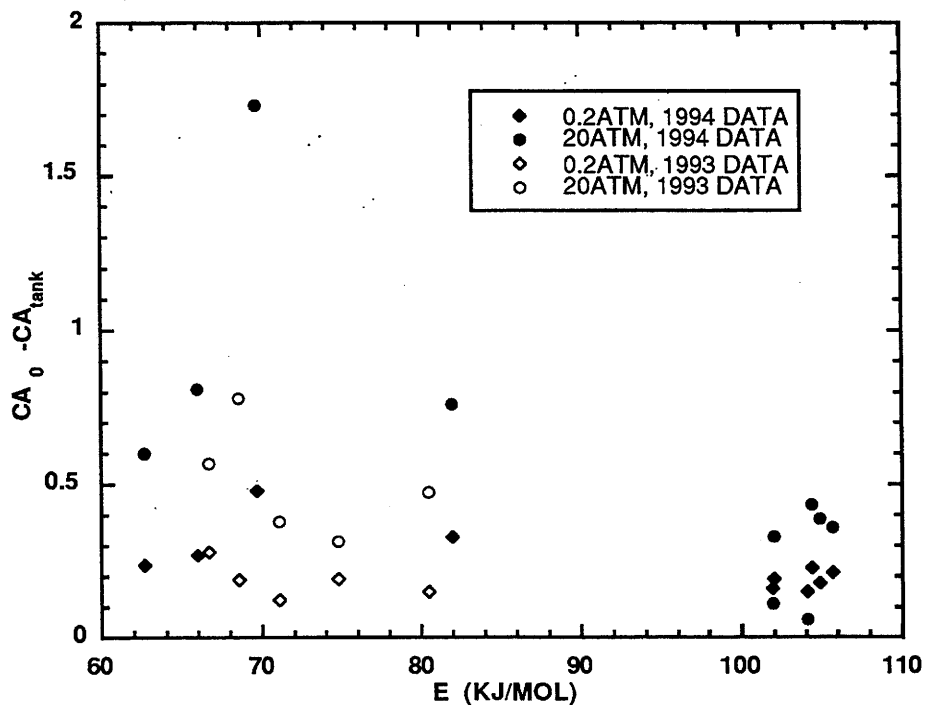


Figure 2-42. Initial Jump Versus Activation Energy

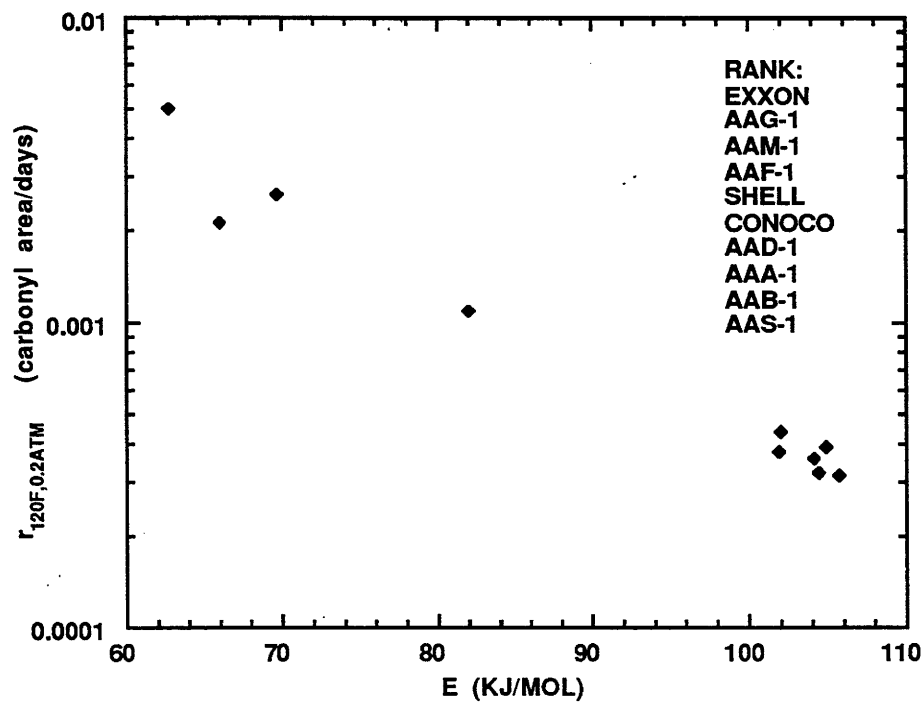


Figure 2-43. Calculated Reaction Rate Versus Activation Energy

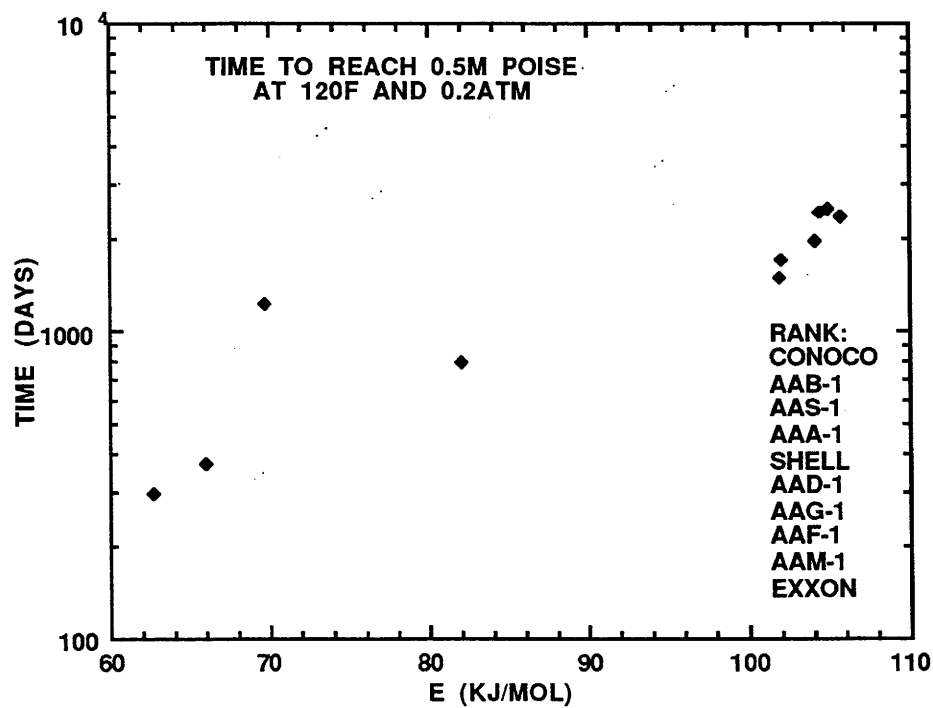


Figure 2-44. Critical Time Versus Activation Energy

SECTION II

THE EFFECT OF ASPHALTENE CONTENT ON ASPHALT HARDENING AND RECYCLING

The principal compositional change in asphalt hardening is the increase in asphaltene content resulting from the oxidation of polar aromatic components. Asphalt properties are extremely dependent on both the amount and characteristics of the asphaltene fraction. It has been shown by many that this is the most variable fraction and that the molecular weight varies over the greatest range. Indeed there is quite a lot of disagreement over what actually constitutes the molecular weight; see Glover et al. (1987) and Davison et al. (1991). Part of the reason for the variability is that, unlike other fractions, asphaltenes are separated purely by solubility in n-alkanes with differing n-alkanes used. For example, the asphaltenes obtained by n-pentane precipitation might contain much material that would be in the polar aromatics fraction if the Corbett separation scheme were used.

The asphaltenes contribute much more to viscosity than do other fractions. They may also improve temperature susceptibility. Altgelt and Harle (1975) have shown a decided effect of asphaltene molecular weight on viscosity. They separated asphaltenes into a range of apparent molecular weights and studied the effect of molecular weight, concentration, and solvency on viscosity. The effect of concentration was approximately linear at lower asphaltene molecular weights, but at higher molecular weights the viscosity increased dramatically with concentration. This was much more apparent in poor solvents and was found to vary quite significantly when different maltenes were used with a given asphaltene.

A large number of studies have shown that the principal change that occurs as an asphalt ages is an increase in the asphaltene content. This is also the principal change in the hot-mix step and in air blowing of asphalt. Corbett and Swarbrick (1960) showed that essentially all of this increase came from their heavy, multi-ring

aromatic fraction, which is essentially what they later called polar aromatics. Corbett and Merz (1975), examining the Michigan test roads after 18 years, found that the main factor was a change in naphthene aromatics to polar aromatics and a change of polar aromatics to asphaltenes. This was accompanied by an increase in viscosity and a decrease in ductility. Rostler and White (1962) showed that their nitrogen bases, which are largely equivalent to polar aromatics, and their first acidaffin fraction, which is the most reactive part of the naphthene aromatics, were most reactive with the nitrogen bases going to asphaltenes and the first acidaffins to nitrogen bases. Very interestingly, the first acidaffins that converted to nitrogen bases did not, in turn, convert to asphaltenes. GPC data from Glover et al. (1987) show that while the quantity of the Corbett fractions changed on road aging, their molecular size distribution changed little.

Since asphaltenes are a major factor in hardening and will always be present in excess in recycled pavement, the present study was undertaken to gain a deeper understanding of the asphaltene-maltene interactions that occur in recycling. This study has two parts. The first aims at a better understanding of the value of the asphaltene contribution to hardening and to compare the effects of original asphaltenes and those formed by oxidation. The second part explores the effects of blending maltenes and asphaltenes from different sources as occur during recycling.

CHAPTER 3

MODEL DEVELOPMENT FOR THE EFFECT OF ASPHALTENES ON VISCOSITY

Many researchers have studied the effect of original asphaltenes, as well as the effect of those produced from air-blowing, on the viscosity of the maltene and solvents. Eilers (1948) measured the relative viscosities of diethyl ether asphaltenes of several original and air-blown asphalts in carbon disulfide. The data from all of the asphalts were compared with the Eilers model but did not show good agreement. Eilers' model is an empirical correlation relating the volume fraction to the relative viscosity. Implicit in the equation, is the assumption that the particle is a perfect hard sphere. Eilers concludes that the deviations between the model and the measured data were associated with the fact that the asphaltenes were non-spherical particles, deformable particles, or polydisperse in size. Reerink and Lijzenga (1973) measured the solution viscosity of n-heptane asphaltenes from original and air-blown asphalts in toluene. The solution viscosities were related to the concentration and width of the molecular weight distribution of the asphaltenes as measured by Gel Permeation Chromatography. The data were compared to the Heukelom and Wijga (1971) model and did not show good agreement. The Heukelom and Wijga model is a simplification of the Eilers model assuming a linear relation between $1/(\eta_r)^{1/2}$ and the volume fraction. Relative viscosities calculated from the model were consistently lower than the measured values.

Altgelt and Harle (1975) measured the effect of heptane asphaltenes on the viscosity of organic solvents and maltenes. Increasing the asphaltene concentration increased the relative viscosity of the solution. Although no model was developed, the behavior followed a light and repeatable trend for blends of asphaltenes and maltenes taken from the same parent asphalt. However, when combining asphaltenes and maltenes from different sources, the data were highly scattered. Evidently, when cross mixing asphaltenes and maltenes, the effect on relative viscosity must not only include

the concentration of asphaltenes but also the solvation power of the maltene.

Recently, however, Branthaver et. al. (1991) studied the effect of unaged asphaltenes on unaged asphalt relative viscosity. The data at 60°C (140°F) for unaged asphalts from a variety of crude sources showed a very little difference between asphalts. This result seems to be contradictory to that of Altgelt and Harle and would seem to show that the solvation power of each maltene is the same.

Sheu et. al. (1991) relate the n-heptane asphaltene concentration of two Ratawi vacuum residues in toluene to the solution relative viscosity. In this paper, the authors discuss four different solution viscosity models. The solution viscosity data suggest that the asphaltenes associate to form larger particles as a result of solvation by the solvent phase. For the solution relative viscosity, the Pal and Rhodes (1989) model showed good agreement with the measured values. No data were reported for maltene/asphaltene systems.

The Pal-Rhodes equation is as follows:

$$\frac{\eta}{\eta_s} = (1 - K \Phi)^{-2.5} \quad (3-1)$$

where η and η_s are the viscosities of solution and solvent, respectively. The volume fraction of colloidal particles (asphaltenes) is Φ . K is the solvation constant. The Pal-Rhodes model assumes all the particles are solvated by the solvent phase and act like polydisperse hard spheres. Sheu et. al. point out that for non-spherical particles the exponent of -2.5 in the Pal and Rhodes model can be a free parameter to account for the particle asymmetry.

Storm and Sheu (1993) also use the Pal-Rhodes model to describe the dependence of the relative viscosity of Ratawi vacuum residues on the n-heptane asphaltene. However, in this paper, the concentration of asphaltene was bounded to that of original Ratawi vacuum residues. For aged asphalt materials, the concentration of asphaltene is usually much higher than that of the original.

To summarize, based on the reported literature for unaged and air-blown asphalt materials, the asphaltene concentration and maltene solvation power affect the relative viscosity of the solution. Furthermore, the Pal-Rhodes model is sufficient for describing the relative viscosity of organic asphaltene solutions.

Anderson et. al. (1976) compare the viscosity and n-pentane asphaltene content of 108 different field sections using 8 different asphalts after field aging in Utah for seven years. The data were compared with the Hoiberg (1964) model and did not show good agreement, probably because all of the asphalts were included in the regression. With laboratory oxidative aging, Plancher et al. (1976) oxidized 4 asphalts in the presence and absence of lime. The data show that the viscosity at 25°C (77°F) as a function of n-pentane asphaltene content depended on the crude source but was independent of lime treatment. Lee et al. (1973) also report that the absorbance in the carbonyl region increases linearly with n-heptane asphaltenes of four asphalts after field and laboratory aging.

Lau et. al. (1992) showed that for Pressurized Oxygen Vessel (POV) aging at temperatures from 60-104.4°C (77°F - 220°F) a linear relationship between log viscosity and carbonyl content is dependent only on the crude source and not on the aging conditions of temperature or pressure. The Hardening Susceptibility (HS) is defined as

$$HS = \left(\frac{d \ln \eta_0^*}{dCA} \right) \quad (3-2)$$

where η_0^* is the zero shear rate complex dynamic viscosity and CA is carbonyl content relative to unaged materials. Unfortunately, no asphaltene data were reported in this study.

Based on the previous work, oxidative aging changes the chemical composition and the rheological properties of whole asphalt. Girdler (1965) shows that the

produced asphaltenes from oxidative aging are chemically different from those originally present by elemental analysis; the produced asphaltenes have lower nitrogen and sulphur content and higher oxygen content. Because of chemical differences, the effect of the produced asphaltenes on the physical properties of the asphalt, compared to the original asphaltenes, may be different.

A rheological model relating the composition of the unaged and aged asphalt in terms of asphaltene and carbonyl content to rheological properties is desired. This model would provide a foundation for predicting asphalt behavior during pavement life.

EXPERIMENTS AND METHODOLOGY

Seven SHRP whole asphalts (AAA-1, AAB-1, AAC-1, AAD-1, AAF-1, AAG-1, AAK-2) were fractionated by solvent precipitation into asphaltenes and maltenes. Following precipitation, the whole asphalts and maltenes were laboratory aged. For one of the asphalts (AAA-1), unaged asphaltenes and maltenes were blended to different ratios from the parent unaged whole asphalt. All seven SHRP whole asphalts and their corresponding maltenes were aged in a POV at 20.7 bar pure oxygen, at temperatures of 60, 71.1, 82.2, 93.3, and 104.4°C (140, 160, 180, 200, and 220°F) for aging times from 0.25 to 50 days depending on aging temperature.

Blends were made using unaged maltenes, asphaltenes, and whole asphalts from AAA-1. Blend B1 was made from 59 weight percent maltene and 41 weight percent whole asphalt to make a 10 weight percent asphaltene mixture. Physical mixing was used to insure homogeneity. Blend B2 was made by adding 21% asphaltenes to 79% whole asphalt. To insure good mixing, the blend was dissolved with a 85%TCE/15% ethanol solution and then recovered. The final blend, B3, was made by adding 73.5% whole asphalt to B2. Physical mixing was used.

The changes in chemical, rheological, and compositional properties of the aged whole asphalts and maltenes and unaged blends were measured by FT-IR, DMA, and HPLC analysis.

Two rheological properties, the zero shear limiting viscosity (η^*_0) and the reciprocal of the loss compliance ($1/J''$), were determined from data measured at 60°C (140°F) using a 2.5 cm (1 in) composite parallel plate with a 500 μm gap. A 0.1 rad/sec frequency was used to approximate the η^*_0 for materials less than 100,000 poise at 60°C (140°F). For materials with higher viscosities the time-temperature superposition procedure was used. All of the $1/J''$ values were measured at 60°C (140°F) and 10 rad/sec in accordance with SHRP specifications (SHRP, 1992).

RESULTS AND DISCUSSION

For the unaged whole asphalts and maltenes and blends, Table 3-1 shows the percent asphaltenes, η^*_0 , and $1/J''$. The carbonyl areas are not shown because these are defined to be zero. For unaged whole asphalts and maltenes there appears to be no correlation between asphaltene content and rheological properties when comparing different crude sources. However, blends B1, B2, and B3 show a good correlation between asphaltene content and rheological properties since the blends were made by combining asphaltenes and maltenes from the same source.

Carbonyl areas versus aging times for POV aging temperatures of 71.1 and 104.4°C (160 and 220°F) for asphalt and maltene AAA-1 are shown in Figure 3-1. The whole asphalt is represented with the filled symbol while the maltene is the hollow symbol. For both asphalt and maltene the carbonyl area grows linearly with aging time. Furthermore, the rate of carbonyl formation increases with aging temperature as shown by Lau et. al. (1992).

Asphaltene content versus aging time for AAA-1 is shown in Figure 3-2. The aging conditions are the same as those described in Figure 3-1. Similar to carbonyl formation, the asphaltene content is a linear function of time. Obviously, the growth rate can not remain constant indefinitely since the maximum asphaltene content is finite. For the conditions studied the asphaltene growth rate also increases with aging temperature. Unlike the carbonyl formation, the whole asphalt shows a larger

Table 3-1. The Weight Percentage of n-Hexane Asphaltenes (%A), Zero Shear Rate Limiting Viscosities (η_0) and Reciprocal Loss Compliances ($1/J''$) of Whole Asphalts, Blends, and Maltenes

Samples	Whole Asphalt or Blend			Maltene		
	%A ^a	η_0^b	$1/J''^c$	%A ^a	η_0^b	$1/J''^c$
AAA-1	21.7	915	8.21×10^3	1.8	43.3	462.0
B1	10.0	120	1143.0	---	---	---
B2	38.2	2.4×10^5	9.31×10^5	---	---	---
B3	25.9	4420	3.70×10^4	---	---	---
AAB-1	22.2	1378	1.09×10^4	1.6	44.2	495.0
AAC-1	15.6	943	1.06×10^4	1.6	132.8	2811.0
AAD-1	26.3	1332	1.33×10^4	1.4	25.0	248.0
AAF-1	18.0	1950	2.99×10^4	2.1	170.0	1673.0
AAG-1	10.3	1925	1.91×10^4	1.8	756.0	8896.0
AAK-2	23.3	1420	1.12×10^4	1.1	35.0	352.0

^a %A weight percentage

^b η_0^* poise at 60°C (140°F).

^c $1/J''$ dyne/cm² at 60°C (140°F) and 10 rad/sec.

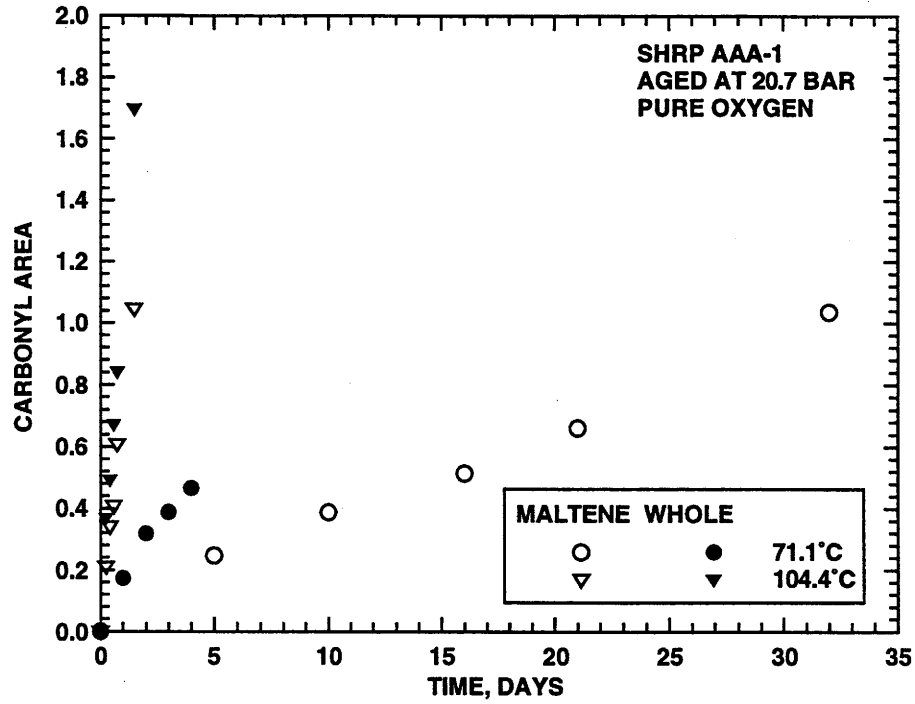


Figure 3-1. Carbonyl Area Versus Aging Time for SHRP AAA-1 Asphalt

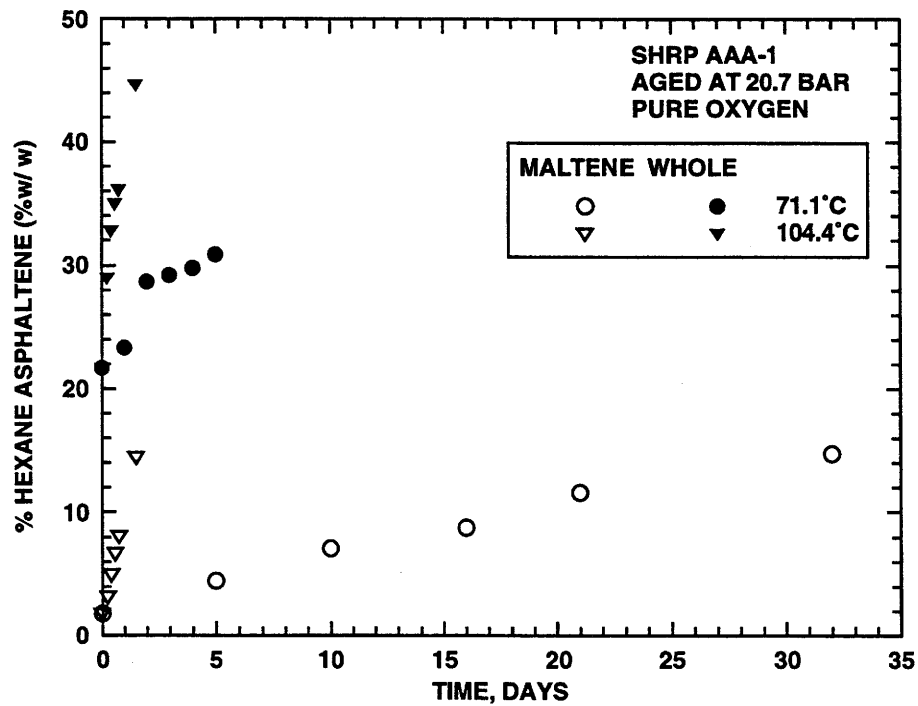


Figure 3-2. Asphaltene Content Versus Aging Time for SHRP AAA-1 Asphalt

asphaltene content than its respective maltene at the same aging temperature and time. This difference, of course, is explained by the presence of original asphaltenes in whole asphalt.

A cross plot of percent asphaltenes versus carbonyl area for AAA-1 whole asphalt and maltene for all aging temperatures and times is given in Figure 3-3. For both the maltene and whole asphalt, the total asphaltene percentage for a given carbonyl area is independent of aging temperature and time. This result suggests that the aging mechanism is independent of temperature for the aging temperature range studied. Both the asphalt and maltene show a linear relationship between carbonyl area and percent asphaltenes for carbonyl areas less than about 2.5. At high carbonyl areas, the asphaltene content appears to be independent of carbonyl formation. The whole asphalt shows a higher asphaltene content than the maltene at a given carbonyl area. Again, this is explained by the presence of original asphaltenes which show no well-defined carbonyl band in the whole asphalt.

Because of carbonyl formation due to oxidative aging and increases in asphaltene content in the whole asphalt and maltenes, the chemical composition of the produced asphaltenes must be different from those originally found in the whole asphalt. For example, the whole asphalt starts with 20 % asphaltene but zero carbonyl area. For the maltene to produce the same 20 % asphaltene content, the carbonyl area must be 1.8. However, it cannot be concluded that all of the carbonyl-containing species are found in the asphaltene phase. Both the maltene and asphaltene phases contain carbonyl compounds, indicating that the compositions of both the maltenes and asphaltenes are changing.

Next, considering only the asphaltenes that are produced from oxidative aging as a function of carbonyl area, Figure 3-4 shows a surprising result for AAA-1 at all aging conditions. The amount of asphaltenes produced by aging is not affected by the presence of the original asphaltene. That is, remarkably, both the whole asphalts and maltenes show the same production of new asphaltenes for a given amount of aging. This suggests that the presence of the original asphaltenes has no effect on the

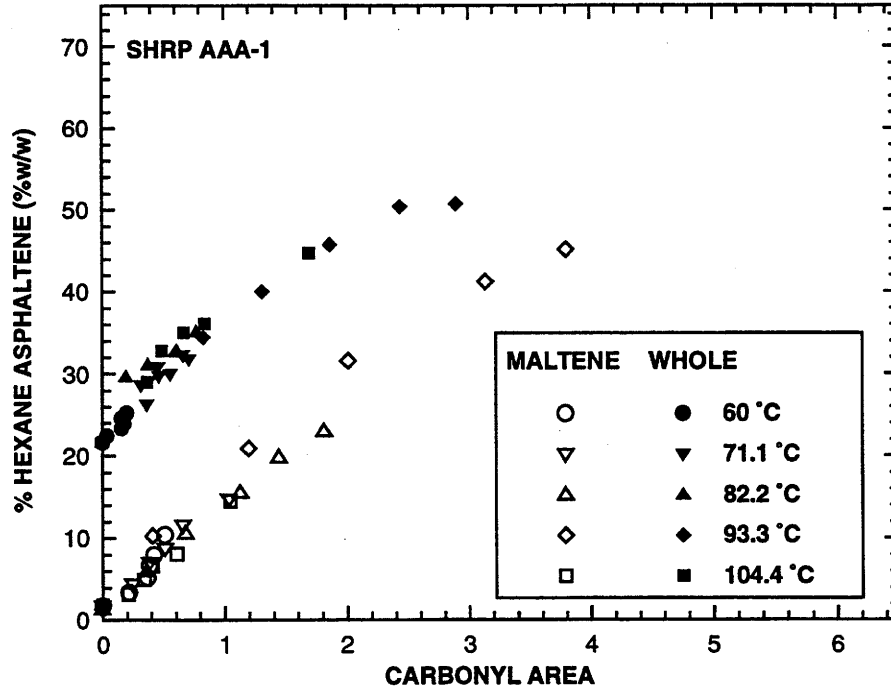


Figure 3-3. Total Asphaltene Versus Carbonyl Area for SHRP AAA-1 Asphalt

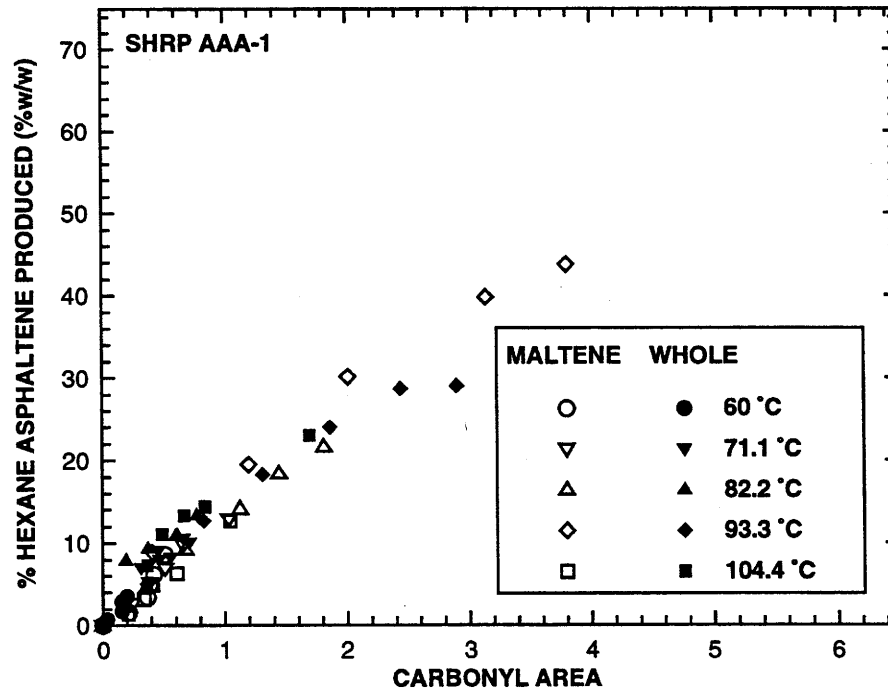


Figure 3-4. Produced Asphaltene Versus Carbonyl for SHRP AAA-1 Asphalt

production of the new asphaltene in the aged maltene environment. Therefore, for a given asphalt, the production of asphaltenes is determined solely by its maltenes. Furthermore, the relationship appears to be essentially linear up to moderate oxidation levels.

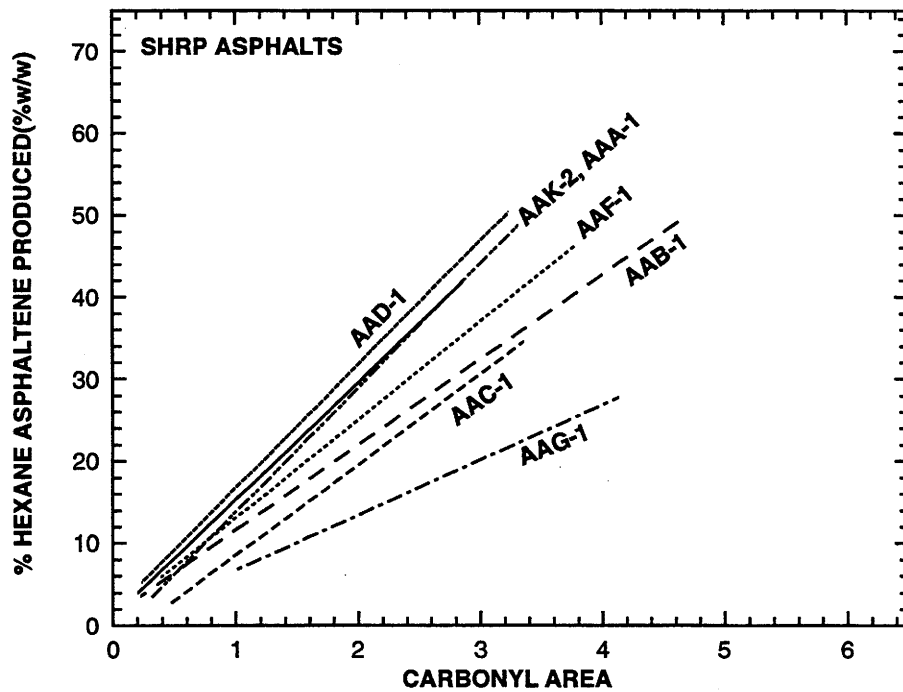


Figure 3-5. AFS for All of SHRP Asphalts and Maltenes Studied

For all asphalts studied, the produced asphaltene versus carbonyl area is shown in Figure 3-5. The lines represent a regression of the data within the linear region. The asphalts have different slopes, indicating that each maltene has a different tendency to form asphaltenes during aging. To quantify this, the asphaltene formation susceptibility (AFS), is defined by Equation 3-3

$$AFS = \left(\frac{d\%A}{dCA} \right) \quad (3-3)$$

Because this parameter does not change with oxidative aging, it is only dependent on the original maltene composition. Table 3-2 shows the AFS values for all the asphalts studied. Asphalt AAG-1 has a lower AFS than AAB-1; therefore, AAG-1 produces less asphaltene than asphalt AAB-1 for a given change of carbonyl content. Hence, AFS is a measure of productivity of new asphaltenes for a maltene.

Table 3-2. Asphaltene Formation Susceptibilities of Asphalts

Asphalt	AFS $\left(\frac{\% \text{ w/w}}{CA} \right)$
AAA-1	14.3
AAB-1	10.4
AAC-1	11.0
AAD-1	15.0
AAF-1	11.9
AAG-1	6.7
AAK-2	15.1

A primary concern in asphalt technology is the irreversible hardening as a result of oxidative aging. Figure 3-6 shows the 60°C (140°F) $\ln(\eta^*_o)$ versus aging time for AAA-1 at 71.1 and 104.4°C (160 and 220°F). This result agrees with Lau, et. al. (1992); $\ln(\eta^*_o)$ increases linearly with aging time at constant aging temperature over a very large range of viscosity increase. The viscosity of the whole asphalt compared to its maltene at equivalent times and temperatures is greater because of the presence of the original asphaltenes. Also, the time rate of change of $\ln(\eta^*_o)$ for the whole asphalt is greater than that for the maltene at a given aging temperature.

As described above, the oxidative aging causes chemical composition changes in the asphalt. The carbonyl formation results in more polar molecules, thus increasing the asphaltene content. This change in chemical composition must ultimately affect the

rheological properties.

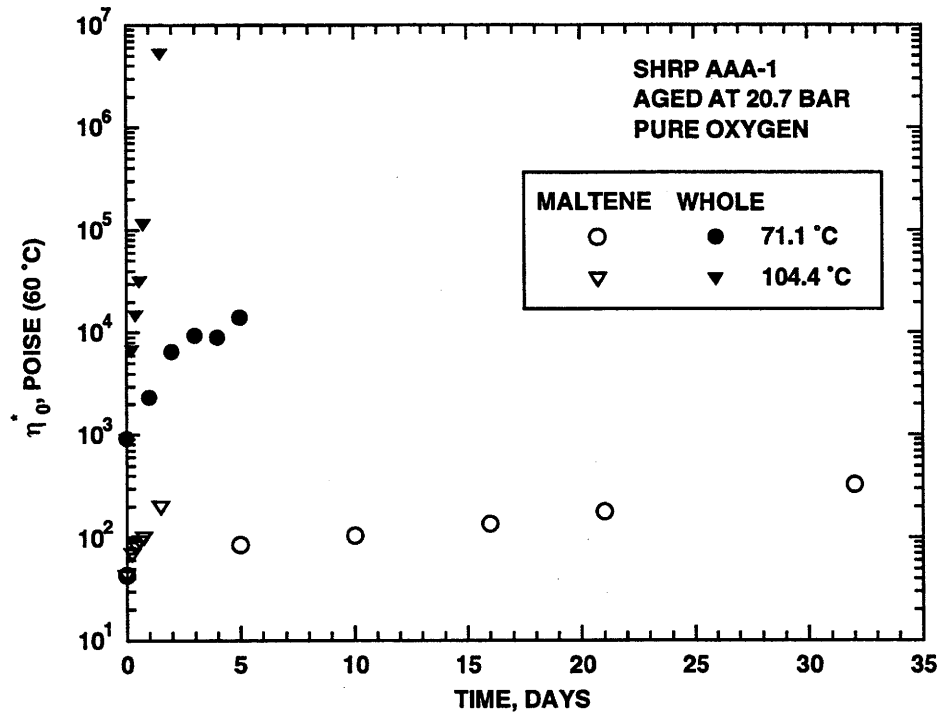


Figure 3-6. Viscosity Versus Aging Time for SHRP AAA-1 Asphalt

Figure 3-7 and Figure 3-8 give $\ln(\eta^*_0)$ versus total %A for AAA-1 and AAC-1, respectively, for the whole asphalts and maltenes at all aging temperatures and times. Again the maltenes are shown with hollow symbols and the solid symbols represent the whole asphalt. Surprisingly, the $\ln(\eta^*_0)$ as a function of total %A is essentially the same for both whole asphalt and maltene. Furthermore, the behavior is independent of aging conditions studied. Based on this result, the original asphaltenes and those produced from oxidative aging have almost the same effect on $\ln(\eta^*_0)$ even though they are chemically different.

In the previously described Pal-Rhodes model (Equation 3-1), asphaltenes form colloidal particles that are dispersed by a solvent phase. Furthermore, the asphaltenes were assumed to be solvated polydisperse hard spheres. For such systems, this theory describes the viscosity dependence on asphaltene concentration.

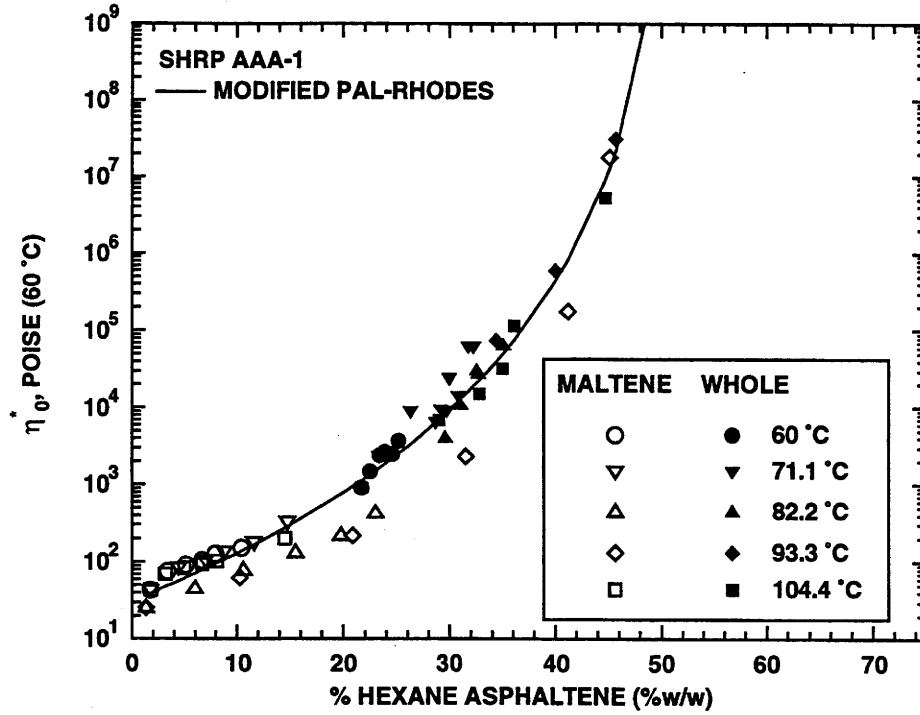


Figure 3-7. Modified Pal-Rhodes Model for SHRP AAA-1 Asphalt and Maltene

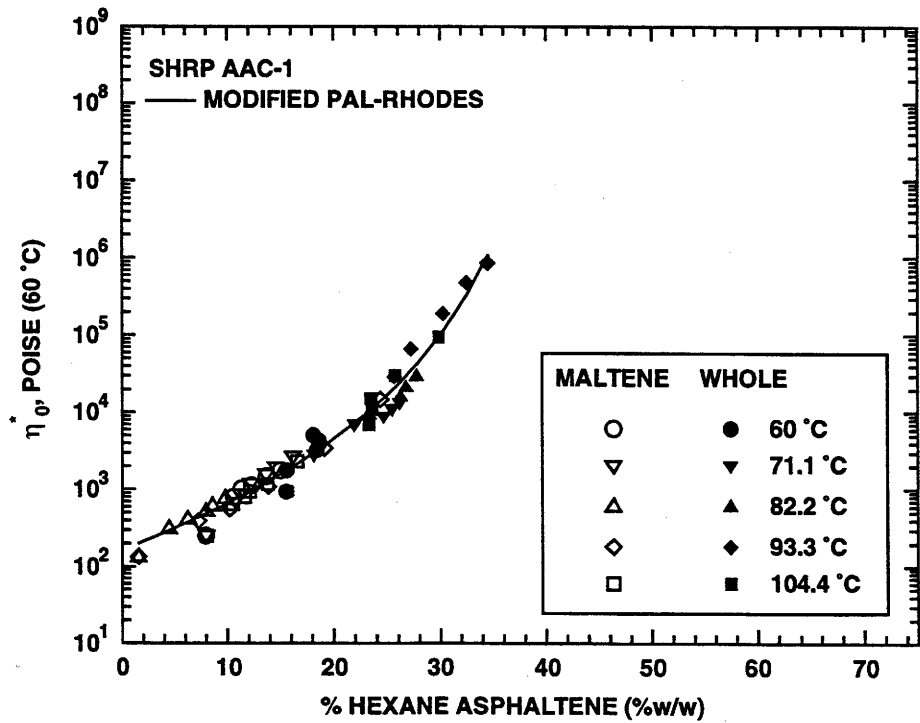


Figure 3-8. Modified Pal-Rhodes Model for SHRP AAC-1 Asphalt and Maltene

For asphalts, the asphaltene is assumed to be the solvated colloidal particle in the maltene phase. Because the interactions between asphaltenes and maltenes are not solely due to hydrodynamic effects, the assumption that the asphaltene is a solvated hard sphere is not valid in the maltene. Therefore, the exponent -2.5 in the original Pal-Rhodes model (Equation 3-1) can not adequately describe the relative viscosity dependence on asphaltene concentration for whole asphalts (Sheu et al., 1991; Storm and Sheu, 1993). Instead, the exponent, denoted as ν , is a parameter to be estimated from data. This modified Pal-Rhodes model is given in Equation (3-4)

$$\frac{\eta}{\eta_M} = (1 - K\Phi_A)^\nu \quad (3-4)$$

where η and η_M are the viscosities of asphalt and unaged maltene and K is the solvation constant. Because the asphaltene weight percent (%A) was measured and not the volume fraction, the volume fraction is defined by Equation 3-5.

$$\Phi_A = \left(\frac{\rho}{\rho_A} \right) \%A \quad (3-5)$$

Φ_A is the volume fraction of the asphaltene in the asphalt. ρ and ρ_A are the densities of asphalt and asphaltene, respectively. Substituting Equation 3-5 into Equation 4 gives Equation 3-6.

$$\frac{\eta}{\eta_M} = \left(1 - K \left(\frac{\rho}{\rho_A} \right) \%A \right)^\nu \quad (3-6)$$

Comparing Equation 3-6 to Equation 3-4, a solvation constant with respect to %A is defined in Equation 3-7.

$$K' = \left(\frac{\rho}{\rho_A} \right) K \quad (3-7)$$

Returning to Figure 3-7 and Figure 3-8, the modified Pal-Rhodes model was optimized for SHRP asphalt AAA-1 and AAC-1 by determining optimal (least squares) estimates of K' and v and the resulting calculated line. Even though the solvation constant (K') and v are assumed to be constant during the aging process, the agreement of the model to the data is excellent.

To verify this idea that the original asphaltenes and those produced from oxidative aging have a very similar rheological effect, three blends (B1, B2, and B3) from AAA-1 containing different levels of original asphaltenes were made. In Figure 3-9, these three blends are compared to the optimal modified Pal-Rhodes model based on the least squares regression of the data. The model predicts the blend viscosities reasonably well, confirming that there is a similarity, in terms of rheological response, between the asphaltenes produced by oxidation of maltenes and the asphaltenes originally present in the asphalt.

Figure 3-10 illustrates the optimal modified Pal-Rhodes model for each asphalt studied. Each asphalt gives unique K' and v as given in Table 3-3. The values of v range from 5.1 to 13.6, much larger than 2.5. Hence the assumption that other interactions beside hydrodynamic effects between the asphaltenes and maltenes affecting relative viscosity and relaxing the spherical shape on the asphaltene is validated. The values of K' range from 1.14 to 2.36. Low values of K' indicate that the maltene is a more powerful solvating agent.

Figure 3-11 gives the $\ln(\eta^*_0)$ versus carbonyl area for the AAA-1 whole asphalt and maltene for all aging conditions. The HS (Equation 3-2) for the whole asphalt and maltene are given in parenthesis in Figure 3-11. At low levels of aging or low asphaltene concentration, the HS of the maltene is lower than that of the whole asphalt.

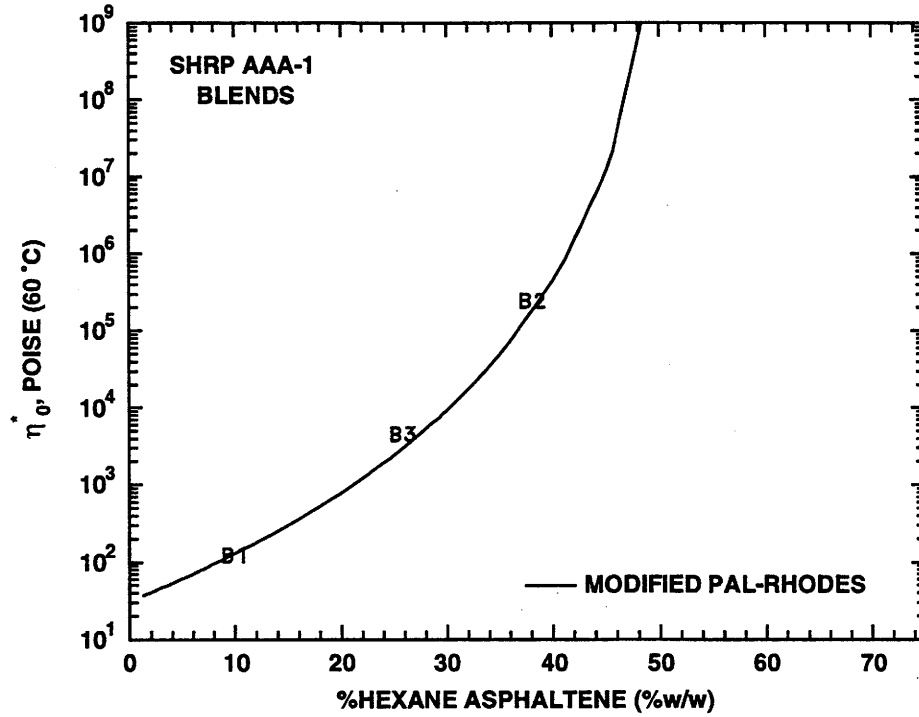


Figure 3-9. Viscosity Versus Asphaltene Content for Unaged SHRP AAA-1 Blends

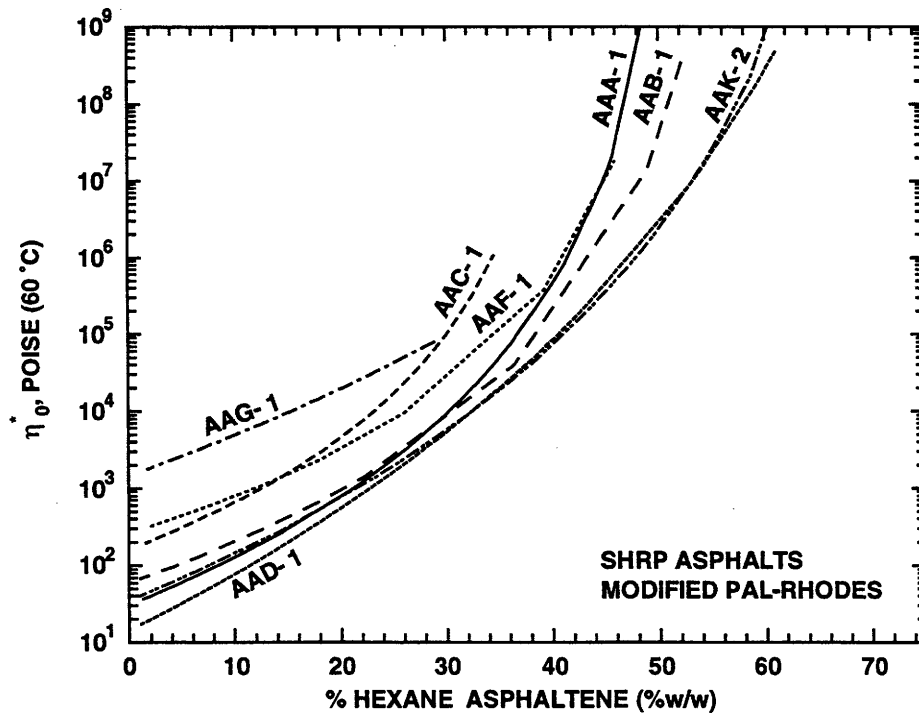


Figure 3-10. Modified Pal-Rhodes Model for All of Asphalts Studied

Table 3-3. Parameter ν and Solvation Constant (K') for Asphalts

Whole Asphalts	$\nu(60^\circ\text{C})$	K'
AAA-1	6.9	1.88
AAB-1	6.4	1.74
AAC-1	5.2	2.36
AAD-1	13.6	1.18
AAF-1	5.1	1.93
AAG-1	10.0	1.14
AAK-2	9.6	1.37

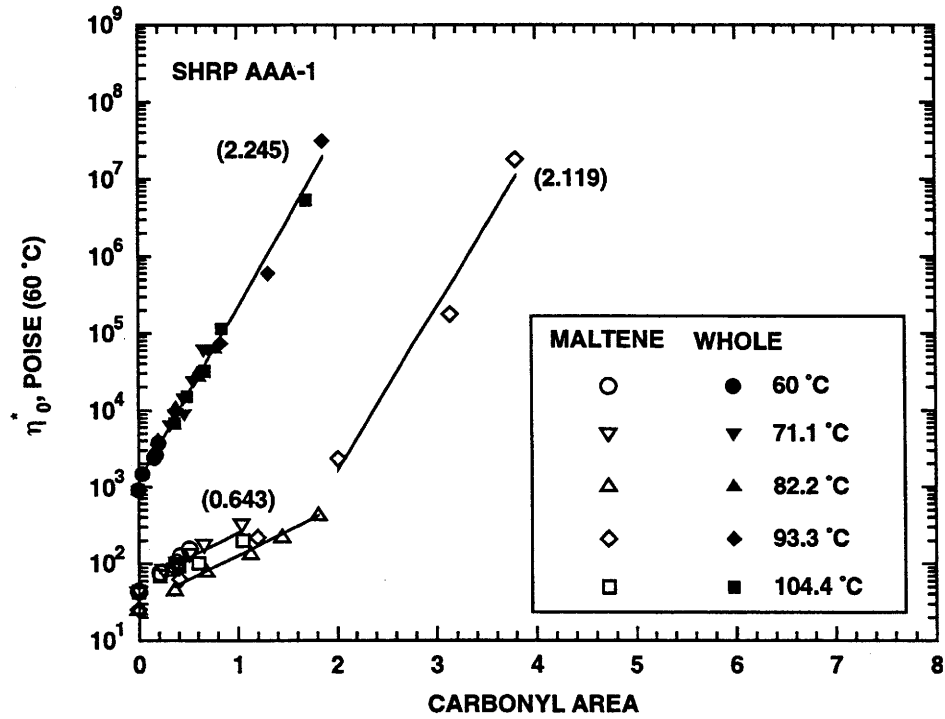


Figure 3-11. Hardening Susceptibility of SHRP AAA-1 Asphalt and Maltene

Only when the maltene reaches the same asphaltene content or viscosity as the whole asphalt, does the HS of the maltene approach that of the whole asphalt. All asphalts studied show similar behavior except for AAG-1 because the HS of the maltene and asphalt are the same.

There appears to be a break point where the HS of the maltene changes abruptly to the value of the whole asphalt. Table 3-4 shows the %A, CA and $\ln(\eta^*_o)$ where the HS of the maltene increases to that of the whole asphalt. For five of the asphalts, AAA-1, AAB-1, AAC-1 AAD-1, and AAF-1, the break point is located at the %A of the whole asphalt. However, the other two asphalts, SHRP AAG-1 and AAK-2, show no logical trend for the location of this break point. The viscosity/asphaltene relation for SHRP AAG-1 is further discussed in the next chapter.

Mathematically, the HS can be expressed in terms of Equation 3-3 and Equation 3-7. By applying the chain rule to Equation 3-2, the HS is the product of two quantities, the first described by the modified Pal-Rhodes model expressing the asphaltene content on $\ln(\eta^*_o)$, and the second the AFS (Equation 3-3).

$$HS = \left(\frac{d \ln \eta^*_o}{dCA} \right) = \left(\frac{d \ln \eta^*_o}{d\%A} \right) \left(\frac{d\%A}{dCA} \right) = \left(\frac{vK'}{1-K'\%A} \right) (AFS) \quad (3-8)$$

Actually, for the whole asphalt, the HS is surprisingly constant for certain ranges of carbonyl and is probably constant during the pavement life. Only in the maltenes studied does the HS change dramatically. This constant HS can be explained by the two competing factors on the right hand side of Equation 3-8. The first factor is the increasing rate of change of $\ln(\eta^*_o)$ with %A as described by the modified Pal-Rhodes model (shown in Figure 3-10), and the second is the decrease in AFS (shown in Figure 3-5) since the weight percent asphaltene has a limit of 100% while the carbonyl area still grows. Equation 3-8 also suggests that the HS for a given asphalt and maltene is a weak function of asphaltene concentration only.

Table 3-4. The Zero Shear Limiting Viscosities (η_0^*), Weight Percentage of n-Hexane Asphaltenes (%A), and Carbonyl Areas (CA) of Asphalts at Break Point

Asphalts	η_0^* (Poise,60°C)	%A(%w/w)	CA
AAA-1	1,000	23.0	1.8
AAB-1	1,150	22.0	2.4
AAC-1	900	12.0	1.5
AAD-1	900	26.0	1.8
AAF-1	2,000	19.0	1.5
AAG-1	---	---	---
AAK-2	20,000	51.0	4.7

Another rheological property ($1/J''$) correlates with the rut depth in pavement mixes (SHRP, 1992). This parameter is compared to %A for SHRP asphalt AAA-1 in Figure 3-12 and shows a similar result as that of Figure 3-7. Again, the original and produced asphaltenes from oxidative aging have the same effects on rheological properties.

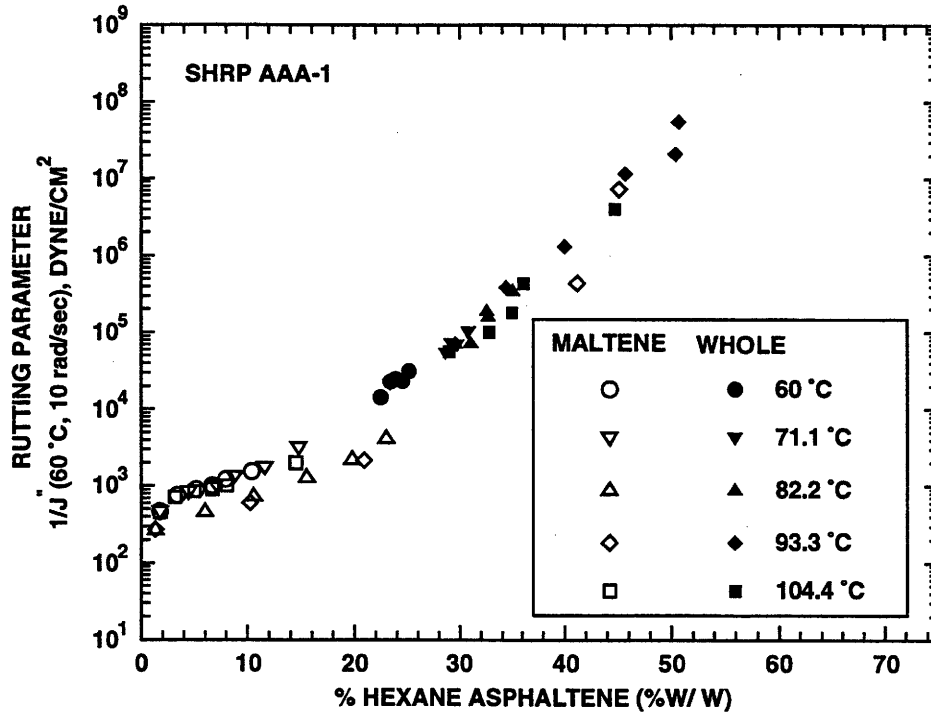


Figure 3-12. Rutting Parameter Versus Asphaltene for SHRP AAA-1 asphalt

CHAPTER 4

APPLICATION OF THE MODEL TO MIXTURES OF ASPHALTENES AND MALTENES FROM DIVERSE SOURCES

In the previous chapter, a model was developed for the effect of asphaltenes on viscosity, and the hardening susceptibility was related to this function and the (AFS), the rate of asphaltene formation with oxidation as measured by the growth of the carbonyl peak. It was concluded that AFS was the same whether whole asphalts or maltenes were oxidized. In other words, the existing asphaltenes have little, if any, effect in the formation of new asphaltene. However, this function is quite different in different asphalts and maltenes.

The present study was undertaken to explain the interaction of asphaltene and maltene from different sources, as would occur in recycling, and to better understand the difference, if any, between the original asphaltenes and those produced by oxidation.

EXPERIMENTS AND METHODOLOGY

Four asphaltenes fractionated from SHRP AAD-1, AAG-1, AAK-2 and a supercritical fraction of SHRP ABM-1 were blended with the maltenes fractionated from SHRP AAD-1 in 10/90, 20/80 and 40/60 asphaltene/maltene ratios by weight. In addition, three asphaltenes (from SHRP AAD-1, AAG-1 and AAK-2) were also blended with the maltenes from SHRP AAG-1 in the same ratios as those described above. A total of 21 blends were produced by this blending scheme. Blends of 10%, 20% and 40% asphaltenes from SHRP AAG-1 into the maltene from SHRP AAD-1 were designated GD1, GD2, and GD4, respectively. Similarly, blends of AAK-2 asphaltene in AAD-1 maltene were designated KD1, KD2, and KD4. Also formed were blends DD1, DD2 and DD4 by blending D asphaltenes with D maltenes. Other blends

were BMD1, BMD2, BMD4; DG1, DG2, DG4; KG1, KG2, K4; and GG1, GG2, GG4.

All blends, except the three blends made by adding asphaltene from SHRP AAD-1 into its own maltene (DD1, DD2, and DD4), were laboratory aged in a POV at 20.5 atm pure oxygen, at temperatures of 71.1, 82.2, and 93.3°C (100, 180 and 200°F) for aging times from 1 to 24 days, depending on the aging temperature. One and one-half gram samples were weighed into the aluminum trays giving an effective film thickness of 0.6 mm (0.024 in) to minimize oxygen diffusion effects.

The changes in compositional, chemical, and rheological properties of the aged blends were measured by HPLC, FT-IR, and DMA. GPC was used to characterize the difference between the molecular weight distributions of aging-produced asphaltenes and original asphaltenes from unaged asphalts. For maltenes, original asphaltenes, whole asphalts, and blends, 0.07±0.005 gram of sample was first dissolved in 10 mL THF. For produced asphaltenes, the filter-washed solution was injected directly into the column. Molecular weight and molecular weight distribution were calculated based on a calibration using polystyrene standards.

RESULTS AND DISCUSSION

For the unaged whole asphalts, maltenes, and blends, Table 4-1 shows the percent asphaltenes (measured by the procedure described in Appendix A), η_0^* , and the relative viscosity (η_r) (defined as the η_0^* for a blend divided by the η_0^* for the maltene from which the blend is made). The carbonyl areas are not shown because these are defined to be zero. For a given unaged asphaltene/maltene blend, the absolute viscosities increase with the amount of asphaltene blended. When comparing blends comprised of various maltenes, the absolute viscosity shows no correlation with asphaltene content because different maltenes have very different viscosities. However, in spite of some scatter, as shown in Figure 4-1, the relative viscosity of all blends regardless of the sources of asphaltenes and maltenes behave similarly with

Table 4-1. The Weight Percentage of n-Hexane Asphaltenes (%A), Low Frequency Limiting Viscosities (η_0^b), and Relative Viscosity of Maltenes, Whole Asphalts, and Blends

	10%			20%			40%			MALTENE OR ASPHALT		
	%A ^a	η_0^b	η_r^c	%A ^a	η_0^b	η_r^c	%A ^a	η_0^b	η_r^c	%A ^a	η_0^b	η_r^c
AAD-1 MALTENE										0.7	2.3	1.0
AAD-1 ASPHALT										23.2	133.2	57.9
GD	10.7	9.88	4.3	20.9	62.1	27.0	39.2	17400	75652.2			
KD	10.9	10.0	4.3	20.8	65.0	28.3	39.7	18700	8130.4			
DD	10.6	10.7	4.7	20.8	85.2	37.0	41.7	39300	17087.0			
BMD	10.0	7.0	3.0	20.0	36.3	15.8	40.0	6260	2721.7			
AAG-1 MALTENE										0.3	73.0	1.0
AAG-1 ASPHALT										6.2	192.5	2.6
GG	12.5	503.7	6.9	22.9	5610	76.8	42.3	4.0×10^6	54794.5			
KG	12.2	478.7	6.6	20.6	3190	43.7	37.2	5.58×10^5	6643.8			
DG	13.4	496.0	6.8	23.6	5160	70.7	40.1	1.13×10^6	15479.5			

^a %A weight percentage.

^b η_0^b in Pa·s at 60°C (140°F).

^c η_r^c dimensionless at 60°C (140°F).

respect to the total asphaltene content. In addition to the maltene viscosity, the maltene solvent power or ability to disperse the asphaltenes will affect the resulting rise in viscosity with asphaltene content. Therefore, Figure 4-1 suggests that the SHRP AAD-1 and AAG-1 maltenes may have similar solvation power, although they are very different in chemical nature, and that the asphaltene-maltene interactions do not vary widely for all materials studied in this work.

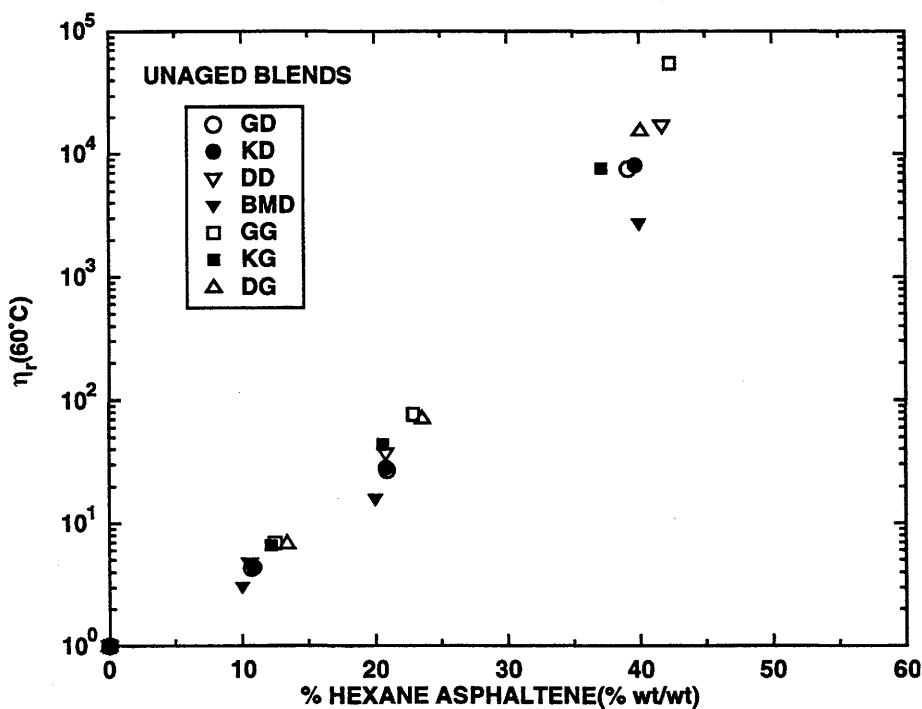


Figure 4-1. Viscosities of Unaged Blends as Function of Asphaltene Content

Figure 4-2 shows a plot of HS for SHRP AAD-1 and AAG-1 whole asphalt aged at 20.7 bar (300 psia) pure oxygen and various temperatures from 60 to 104.4°C (140 to 220°F). The HS is independent of aging temperature, which indicates that the aging mechanism stays the same within the temperature range studied. However, the HS of AAD-1 asphalt is significantly higher than that of AAG-1 asphalt. That is, for the same amount of carbonyl increase, one asphalt may exhibit much more hardening than the others. This indicates that the carbonyl groups formed during oxidative aging

do not directly cause an increase in the viscosity of asphalt. Many investigators such as Traxler (1961), Anderson et al. (1976), Plancher et al. (1976) and Lee and Huang (1973) have shown that the viscosity increase as an asphalt ages results from the formation of asphaltenes from oxidation. Figure 4-1 also suggests that the increase in asphaltene content directly results in the increase in the viscosity of blends with relatively slight dependence on asphaltene sources. As mentioned earlier (Chapter 3), the HS of an asphalt material can be further studied by considering separately the increase in viscosity due to the increase in asphaltene content and the increase in asphaltene content due to the increase in carbonyl formation (AFS).

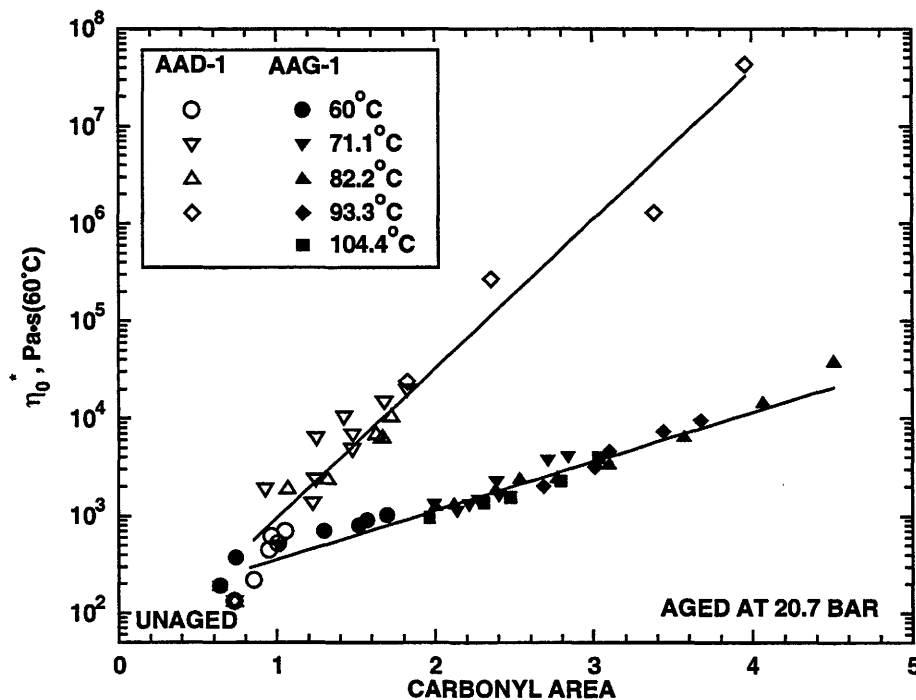


Figure 4-2. Hardening Susceptibilities of SHRP AAD-1 and AAG-1

First, consider the increase in asphaltene content due to the carbonyl formation. Girdler (1965) showed that asphaltenes produced by oxidation have a higher oxygen content than those originally present. This is shown in Figure 4-3, where the carbonyl area of asphaltene produced by aging SHRP AAD-1 maltene shows a much higher

value than that of the asphaltene originally present. Figure 4-3 shows a direct evidence that the carbonyl formation gives rise to the asphaltene formation by oxidative aging of maltene. Figure 4-4 shows a plot of produced asphaltene versus carbonyl area for AAD-1 maltene, AAD-1 whole asphalt, and blends made by adding various asphaltene into AAD-1 maltene. The slopes of the data, AFS, for each blend are quite different from one other. It was pointed out in the previous chapter that for a given maltene or asphalt, the asphaltene production for a given carbonyl formation approaches zero as the total asphaltene content increases. This is seen again in Figure 4-4, for all the blends studied, where the AFS decreases as the starting asphaltene content of blends increases. For example, the AFS of KD4 is smaller than that of KD2, the AFS of KD2 is smaller than that of KD1, and the AFS of KD1 is smaller than that of AAD-1 maltene. This result suggests that the AFS is a function of total asphaltene content including both produced and original asphaltene. This is not surprising as asphaltene should continue to react to produce carbonyl without producing more asphaltene, but this is also likely due to the depletion of the reactive polar aromatics.

To compare the difference in the AFS of blends having varied original asphaltene sources blended with the same maltene, the carbonyl area for a given blend is adjusted to that of the maltene with the same asphaltene content by adding a constant to the carbonyl area of the blend. However, the constant is different for each blend, depending on the original asphaltene content of the blend. The result is shown in Figures 4-5 and 4-6. For all of the blends, asphalts, and maltenes studied, all of the AFS values overlap and form a single curve for materials from the same maltene. This indicates that the AFS is not affected by the type of asphaltene which is produced by aging or originally present in different sources.

However, the AFS of SHRP AAG-1 maltene is much lower than that of SHRP AAD-1 maltene. Figure 4-7 compares the AFS of the blends made from SHRP AAG-1 maltene with that of the blends made from SHRP AAD-1 maltene. Evidently AFS is a strong function of the maltene in the blend and is a function of the total

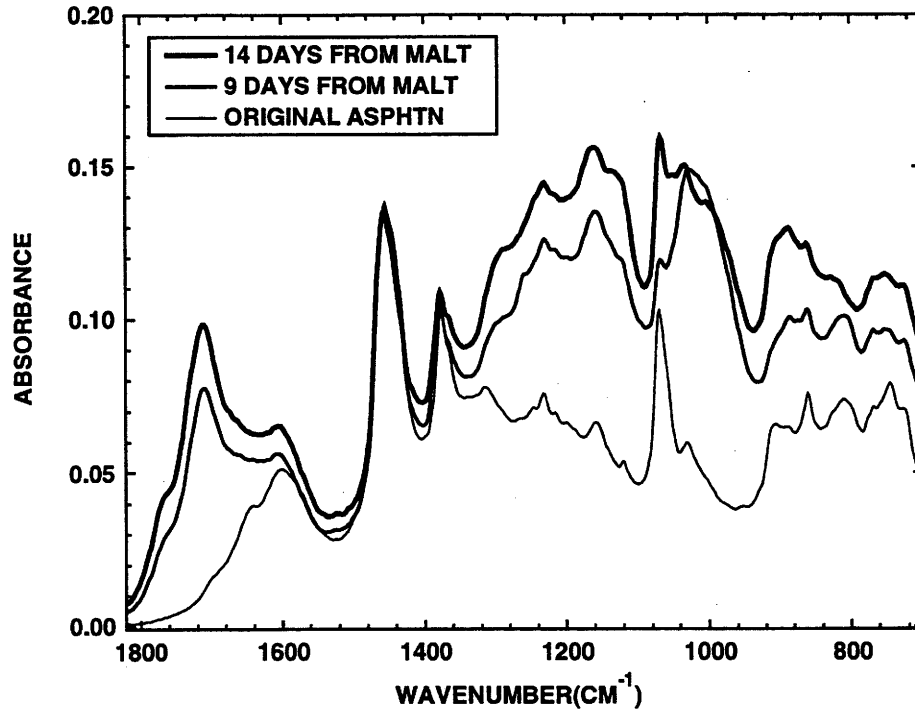


Figure 4-3. FT-IR Spectra of Produced Asphaltenes for SHRP AAD-1

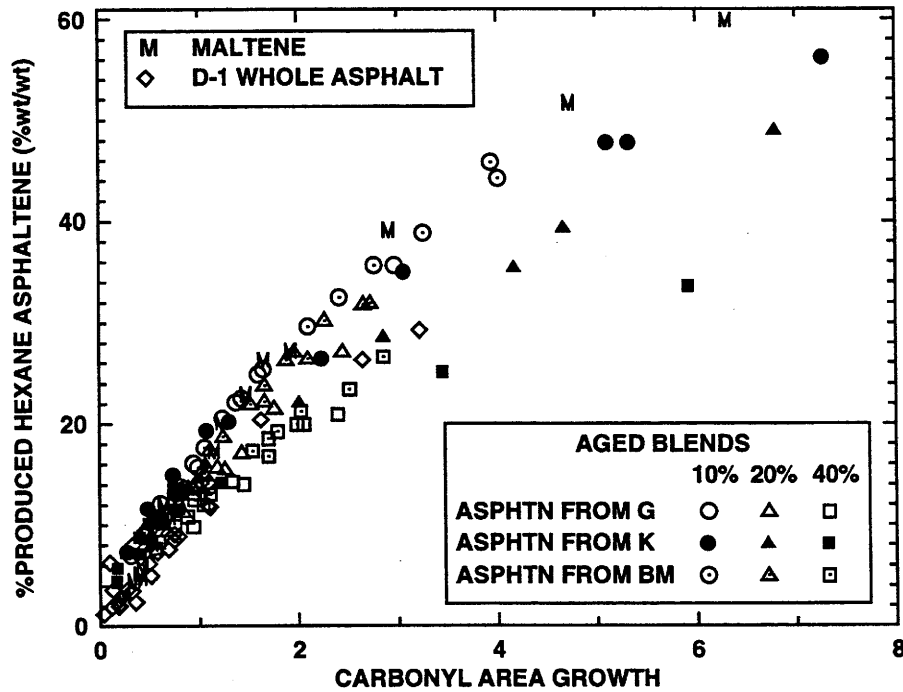


Figure 4-4. Produced Asphaltene Versus Carbonyl Area for SHRP AAD-1

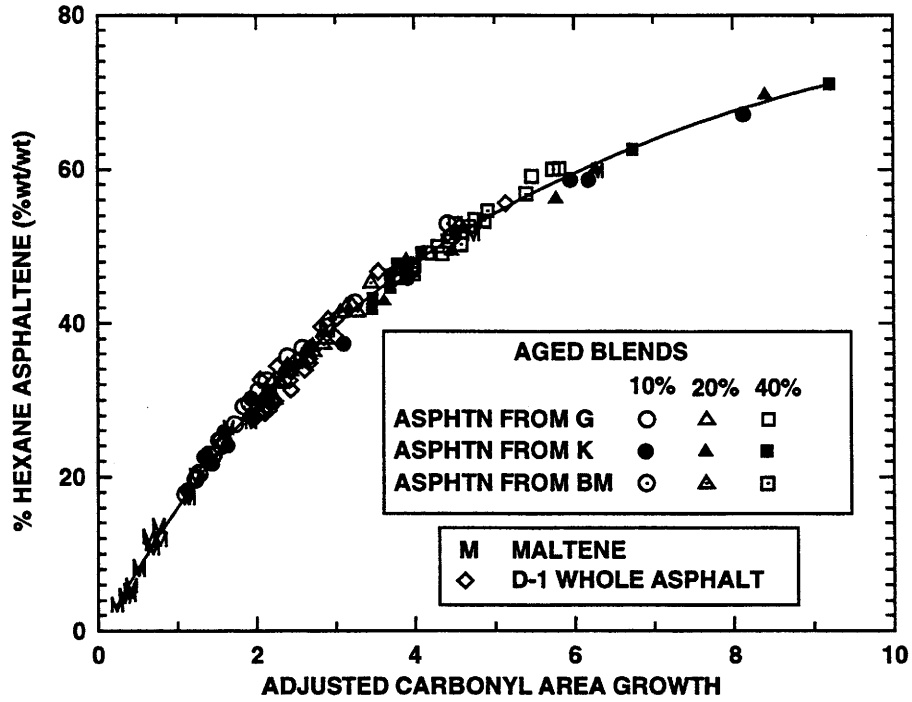


Figure 4-5. AFS for SHRP AAD-1 Asphalt and Asphaltene/Maltene Blends

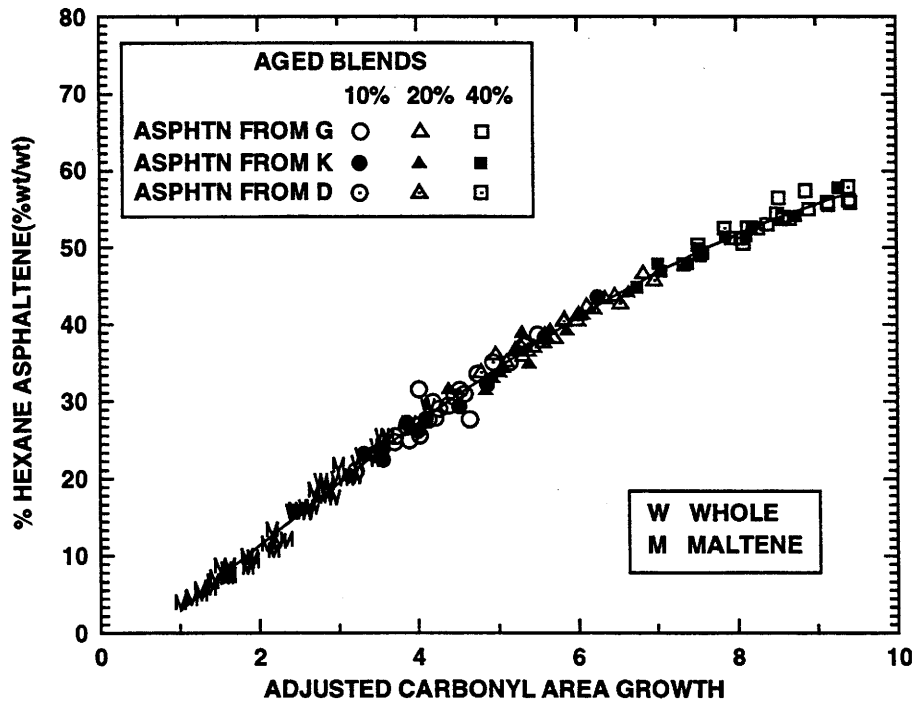


Figure 4-6. AFS for SHRP AAG-1 Asphalt and Asphaltene/Maltene Blends

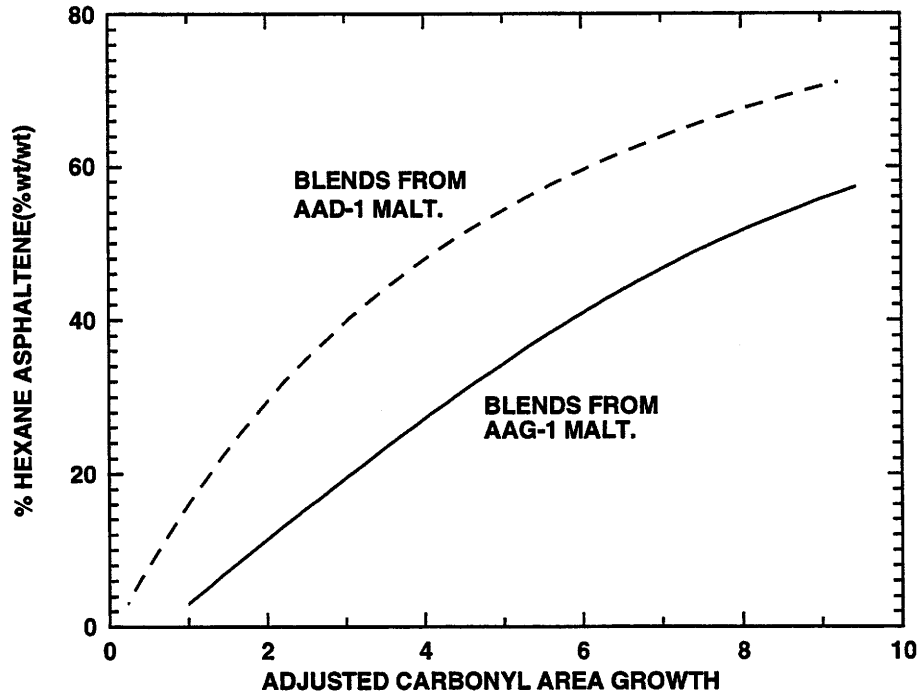


Figure 4-7. Comparison of AFS for SHRP AAD-1 and AAG-1

asphaltene content but not a strong function of the type of asphaltene.

Next, consider the increase in viscosity resulting from asphaltene formation. In Chapter 3 it was shown that the asphaltenes naturally present and those produced by oxidation have similar effects on the increase in the viscosity of the asphalt. However, the effect of asphaltene from different asphalts in a given maltene before and after aging the blends was not addressed. In this work, the effects of asphaltenes from several sources on the increase in the viscosity of the blend were studied and compared to the effects of those naturally occurring or produced by maltenes from AAG-1 and AAD-1. Figure 4-8 compares the difference in the viscosity/asphaltene behavior of blends made by adding AAD-1 original asphaltene into AAD-1 maltene and that of aged AAD-1 maltene. The symbols D1, D2, and D4 represent the blends made by adding approximate 10%, 20%, and 40% of AAD-1 original asphaltene into AAD-1 maltene while the symbol M represents the aged AAD-1 maltene. It should be noted that, as shown in Table 4-1, the asphaltene contents for the DD blends shown in Figure

4-8 are slightly different from 10%, 20%, or 40%, which are the percentages of asphaltenes mixed. That is because the asphaltene content used in this work was always determined by precipitation. The differences in the asphaltene contents determined by precipitation and mixing are due to the interaction of asphaltene and maltene even in dilute solution. However, the difference is not significant and usually within the error of asphaltene measurement.

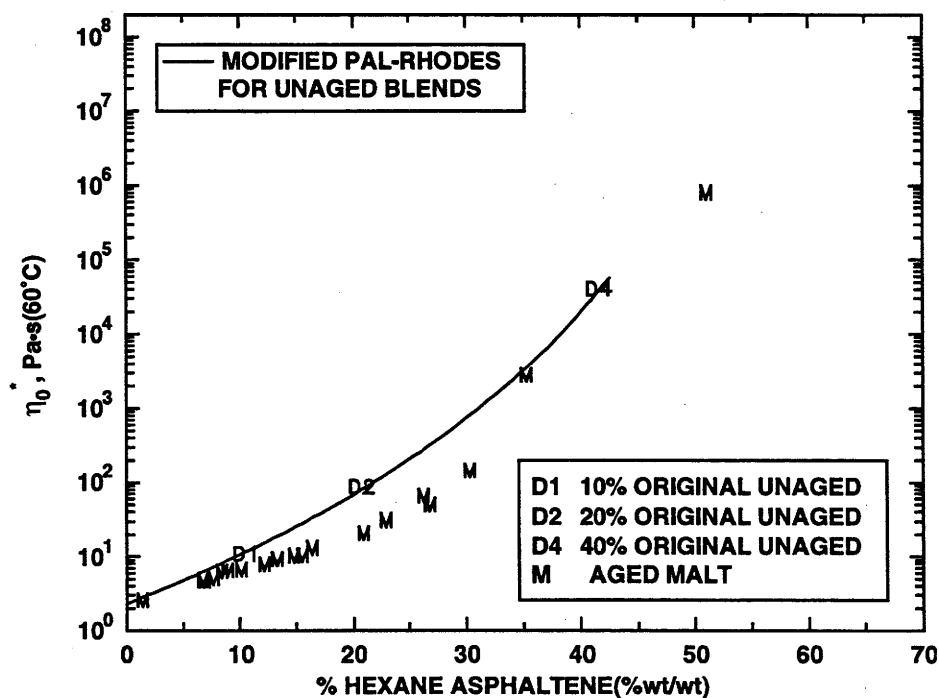


Figure 4-8. Viscosity/Asphaltene Relationship for Unaged DD and D Maltene

For the same amount of asphaltene content, the viscosity of aged maltene is consistently lower than that of the DD blends. To further understand the cause for this difference, GPC was implemented to measure the molecular size distribution of the AAD-1 original asphaltene and the maltene-produced asphaltene. Figure 4-9 shows that the AAD-1 maltene-produced asphaltenes have a much lower molecular size than the AAD-1 original asphaltene. Yen et al. (1961) showed that asphaltenes form aggregates through aromatic stacking. Upon oxidative aging, as shown in Figure 4-3,

the aging-produced asphaltene contains large numbers of carbonyl groups that can produce polar-polar interaction. Furthermore, Storm et al.(1990) also indicate that the asphaltene molecular weight measured by mass spectroscopy is usually significantly lower than that measured by VPO or GPC. Therefore, the molecular size of the asphaltene determined by GPC can be as a measure of the severity of the asphaltene aggregation. Furthermore, for viscosity of suspensions that form aggregates, Pal and Rhodes (1989) and Graham et al. (1984) showed that the effects of particle concentration on the suspension viscosity increase as the average number of particles per aggregate increases. This indicates that the viscosity of aged maltene is somewhat lower than that of the DD blends due to lower molecular weight of the produced asphaltene.

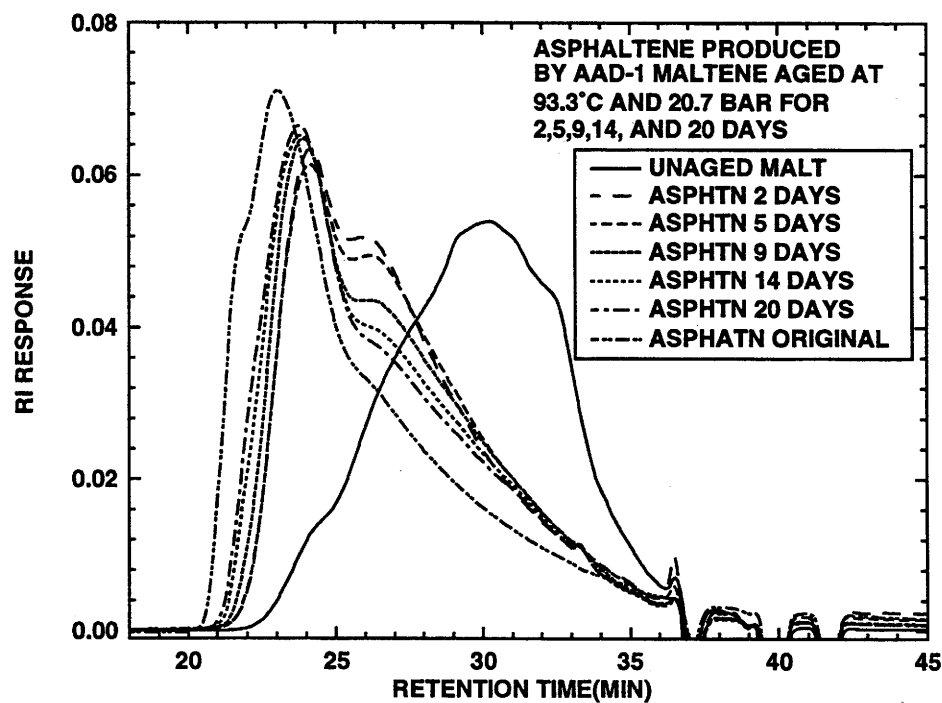


Figure 4-9. GPC of Original and Produced Asphaltene for SHRP AAD-1

Figures 4-10, 4-11, and 4-12 show the viscosity/asphaltene relationship for aged and unaged blends made by adding the original asphaltenes of SHRP AAG-1,

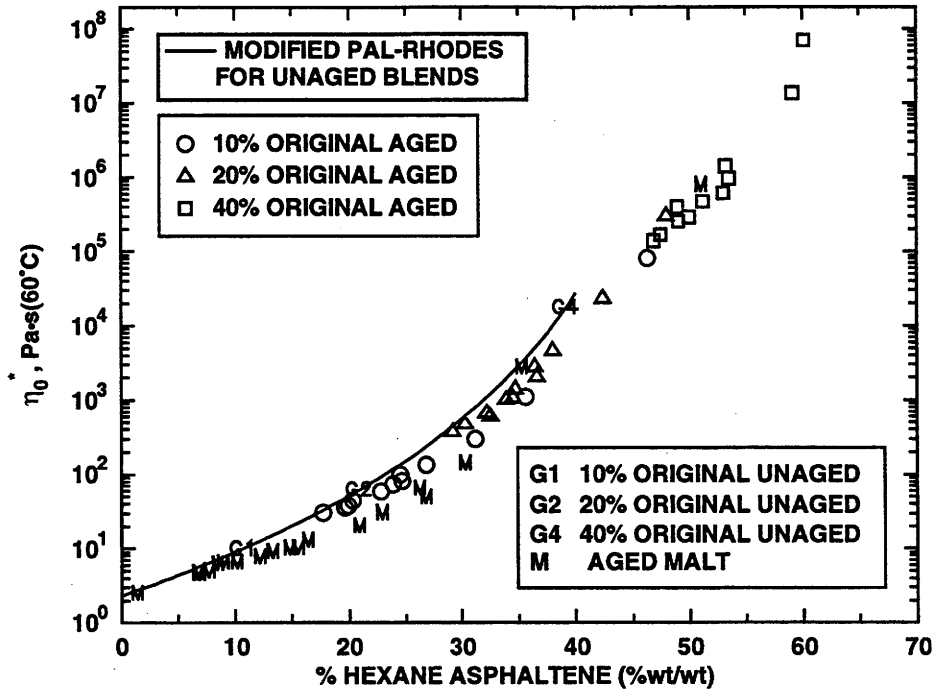


Figure 4-10. Viscosity/Asphaltene Relationship for GD and D Maltene

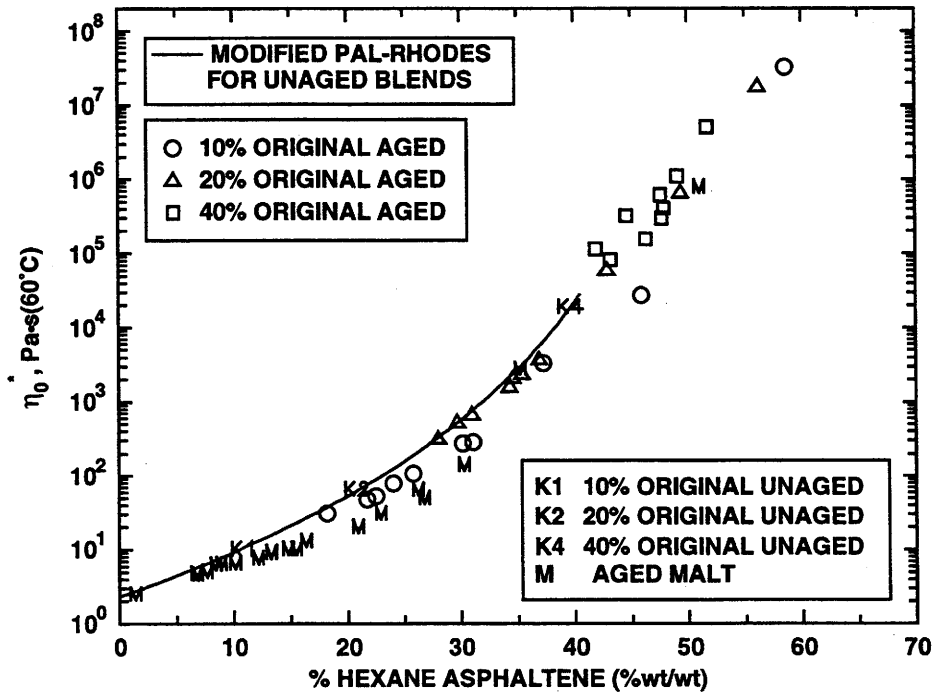


Figure 4-11. Viscosity/Asphaltene Relationship for KD and D Maltene

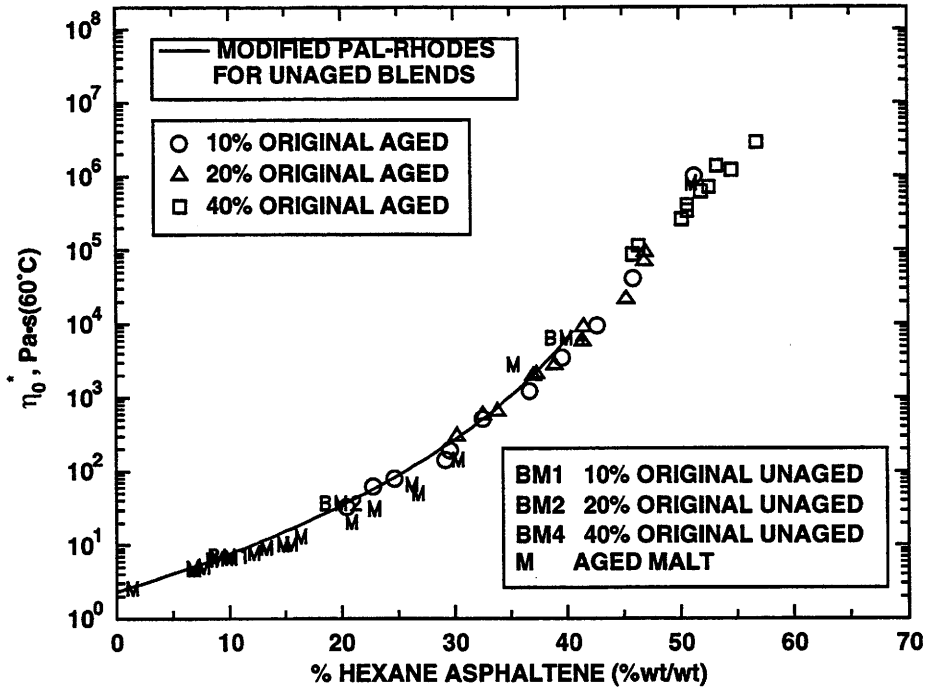


Figure 4-12. Viscosity/Asphaltene Relationship for BMD and D Maltene

SHRP AAK-2, and the supercritical fraction of SHRP ABM-1 to the SHRP AAD-1 maltene. Again, Figures 4-10, 4-11, and 4-12 show that the viscosities of unaged blends are higher than that of aged maltene. Furthermore, the difference in the viscosities of unaged blends and aged maltene is most severe for the DD blends and decrease in order of DD>KD>GD>BMD. This is consistent within the ranking of the GPC molecular weight of original asphaltenes: SHRP AAD-1>AAK-2>AAG-1>ABM-1 S2, as shown in Figure 4-13. However, for aged blends, the viscosities lie between the unaged blends and aged maltene because the asphaltenes of aged blends contain both original asphaltene and produced asphaltene. Figure 4-14 shows all the viscosity/asphaltene data for the blends made by adding the original asphaltenes studied into SHRP AAD-1 maltene. Although there are differences in the viscosity/asphaltene relationship for different blends, all data lie in a narrow band in the practical viscosity range of 1,000 to 500,000 poise. For asphaltenes in AAG-1 maltene, Figures 4-15 to 4-18 show similar behavior. However, for the GG blends, the viscosities of the aged

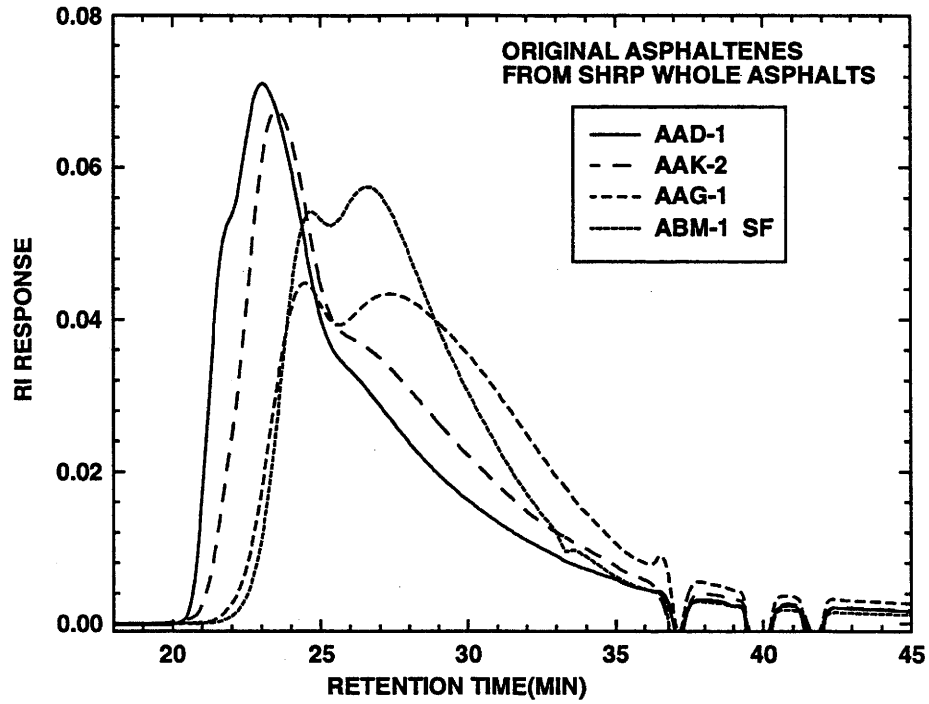


Figure 4-13. GPC of Original Asphaltenes for Four SHRP Asphalts

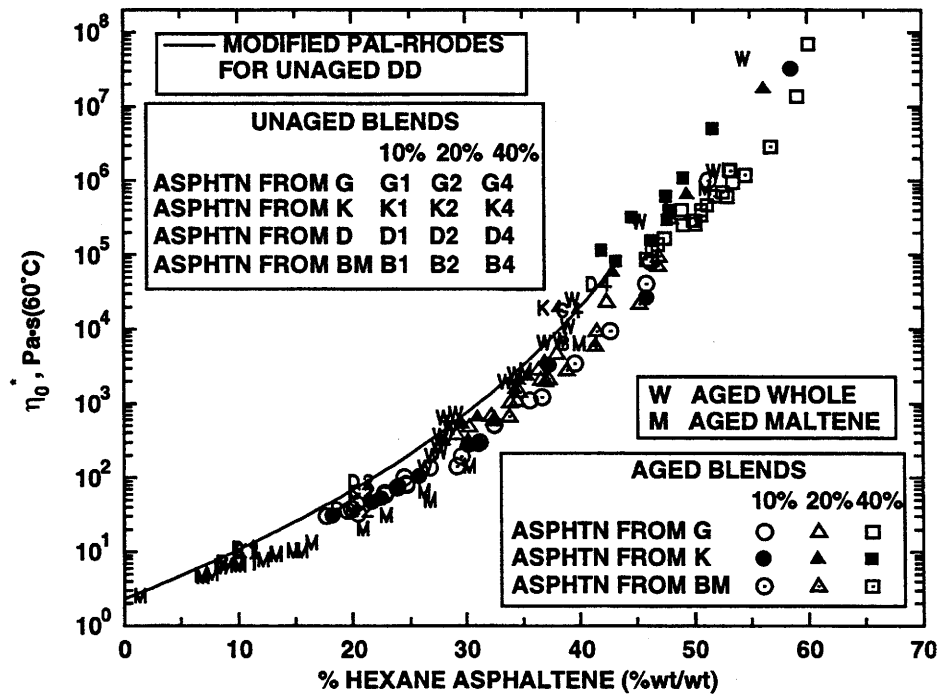


Figure 4-14. Viscosity/Asphaltene Relationship for DD, GD, KD and BMD

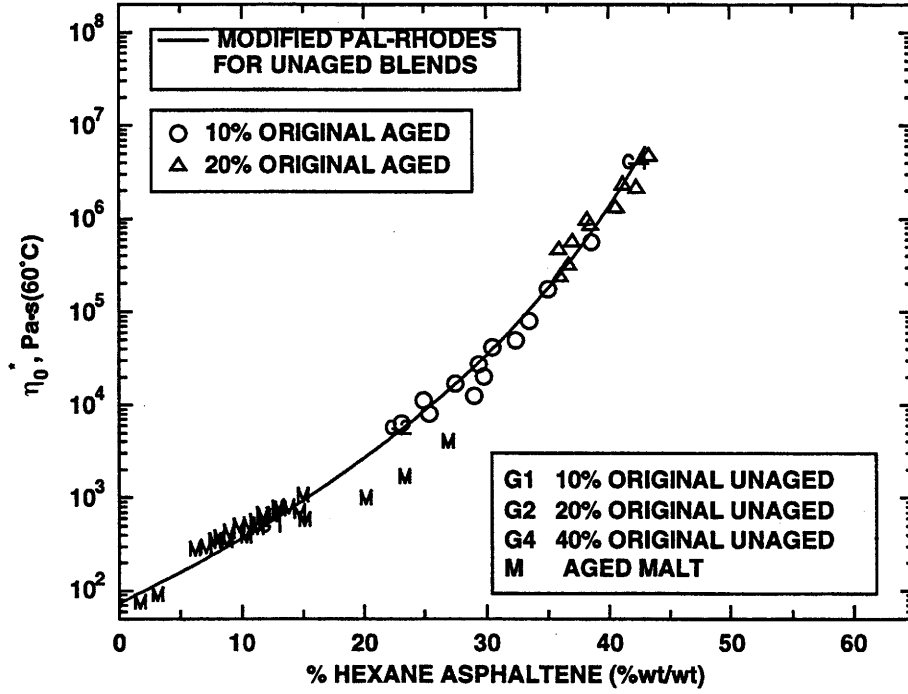


Figure 4-15. Viscosity/Asphaltene Relationship for GG and G Maltene

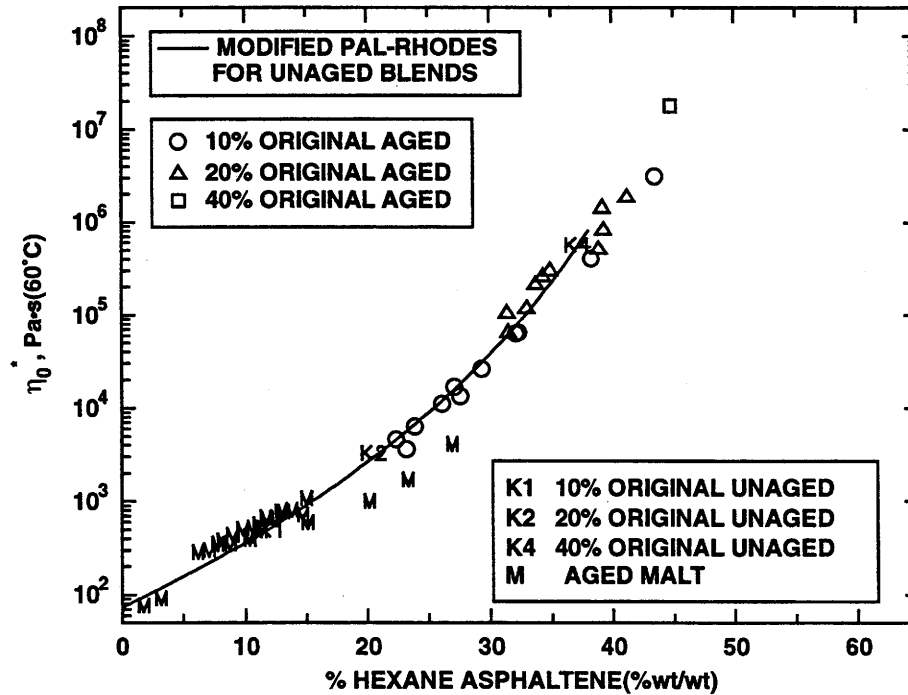


Figure 4-16. Viscosity/Asphaltene Relationship for KG and G Maltene

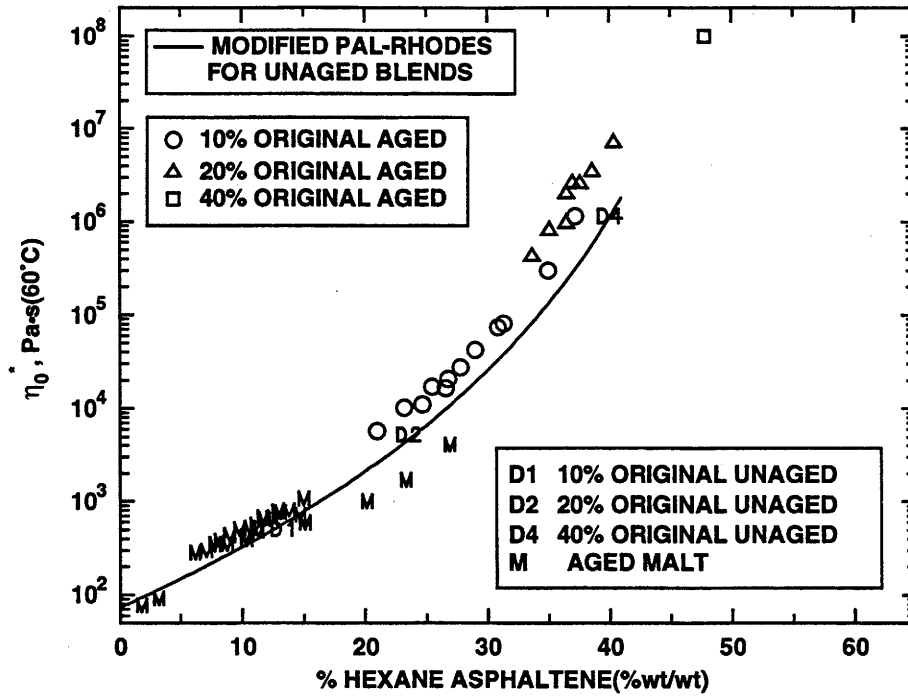


Figure 4-17. Viscosity/Asphaltene Relationship for DG and G Maltene

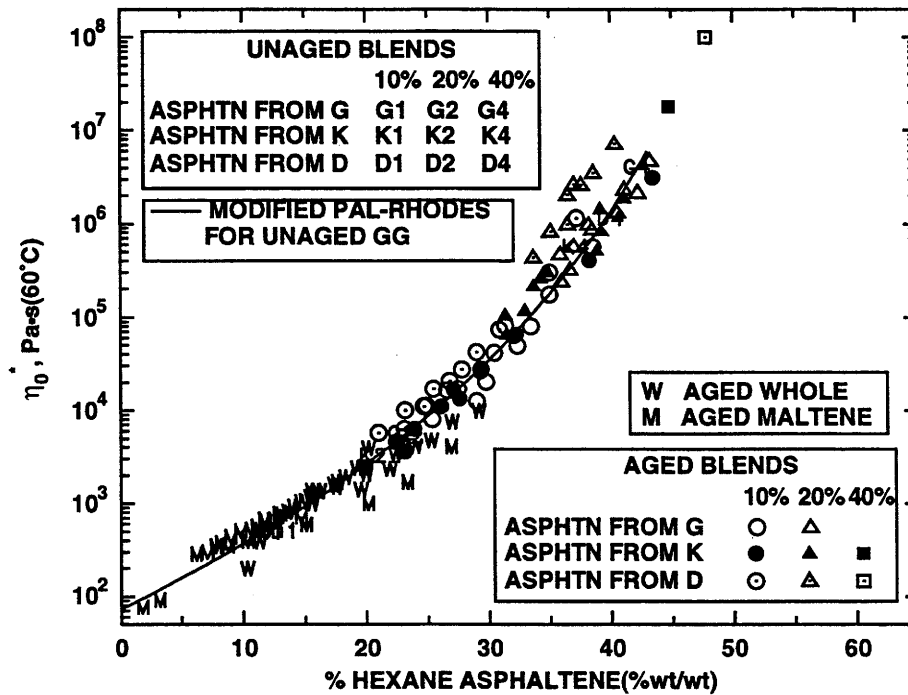


Figure 4-18. Viscosity/Asphaltene Relationship for GG, KG and DG

blends are essentially identical to that of unaged blend. This can be explained by the fact, as shown in Figure 4-19, that the molecular weight distribution of asphaltene produced by AAG-1 maltene is very similar to that of the original determined by GPC. Figure 4-20 shows all the reduced viscosity/asphaltene data for all the blends studied in this work. For aged blends, the maltene source alters the behavior of the increase in relative viscosity with asphaltene content. However, for a given maltene, all aged blends do not show significant difference with respect to asphaltene sources.

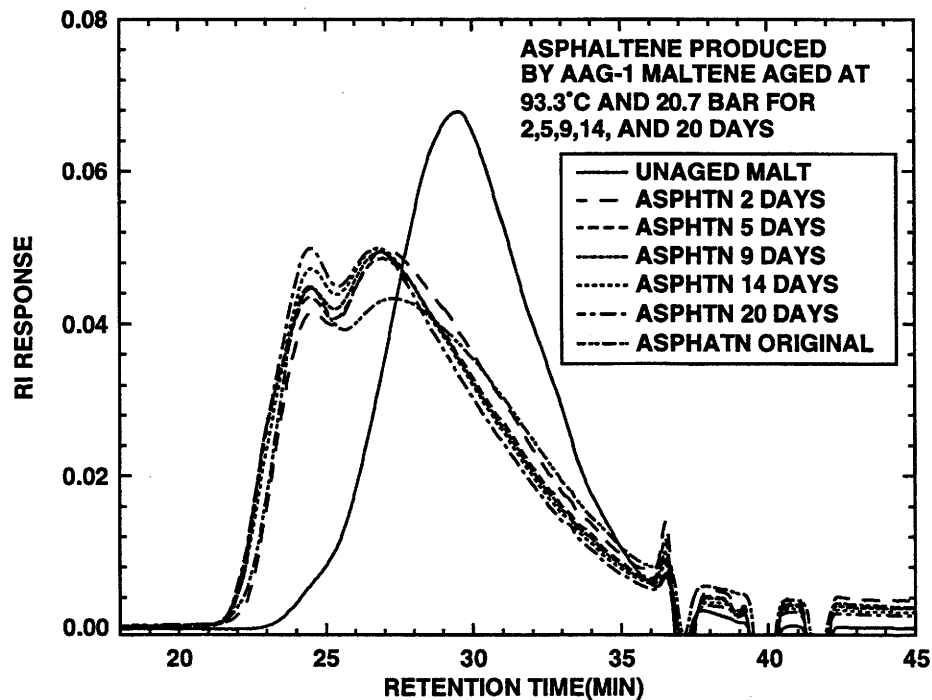


Figure 4-19. GPC of Original and Produced Asphaltene for SHRP AAG-1

As stated in Equation 3-1, HS can be considered as the product of two functions. Based on the results presented in this study, the first term in Equation 3-1 does not vary greatly with asphaltene sources for the two maltenes studied. However, the second term, AFS, is very different for AAD-1 maltene compared to AAG-1 maltene. This indicates that the main difference in HS for different asphalts is due to a different AFS. Therefore, for recycling, the recycling agent should be designed or

selected to have low AFS. Recycled pavement with a low AFS rejuvenator can significantly suppress the formation of asphaltenes during oxidation, and therefore, further improve the service life of the recycled pavement. However, for blends from different maltenes, the difference in the increase in relative viscosity with asphaltene content is less significant than the difference in AFS. In other words, asphaltenes, if produced, will ultimately cause hardening that does not depend heavily on maltene sources. Furthermore, dilution of asphaltene by the agent will decrease this hardening, because the increase in viscosity is much less with low asphaltene content than with high asphaltene. As shown in Figure 4-21, although the $(d \log \eta_0^*/d\%A)$ of AAG-1 asphalt is larger than that of AAD-1 asphalt at the same asphaltene content, the $(d \log \eta_0^*/d\%A)$ of AAG-1 asphalt is actually smaller than that of AAD-1 asphalt due to lower asphaltene content and lower level of asphaltene content in the entire service life.

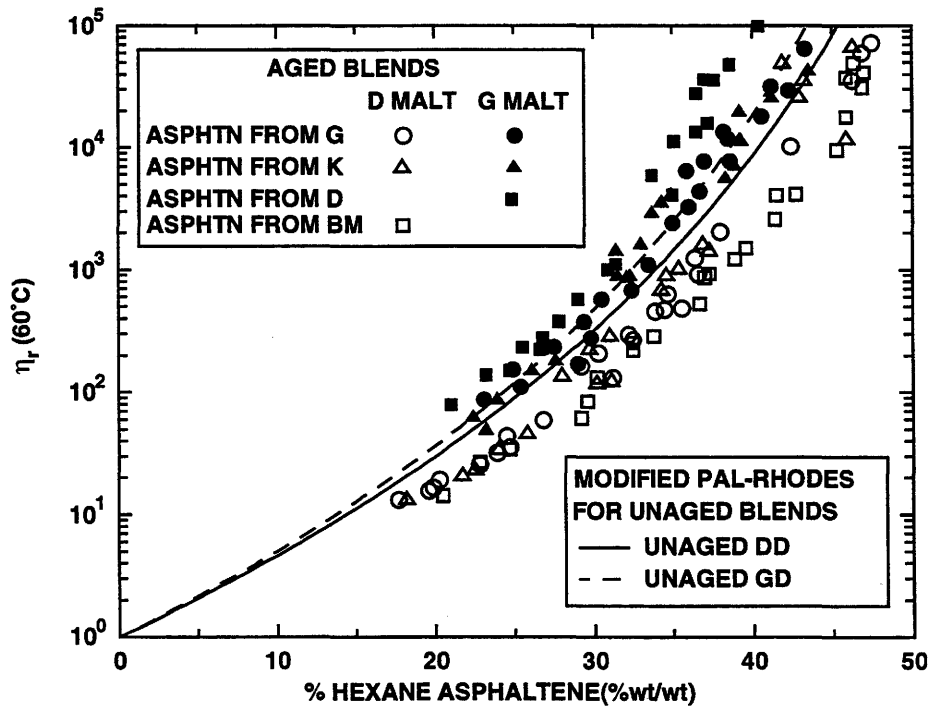


Figure 4-20. Reduced Viscosity Versus Asphaltene for Blends Studied

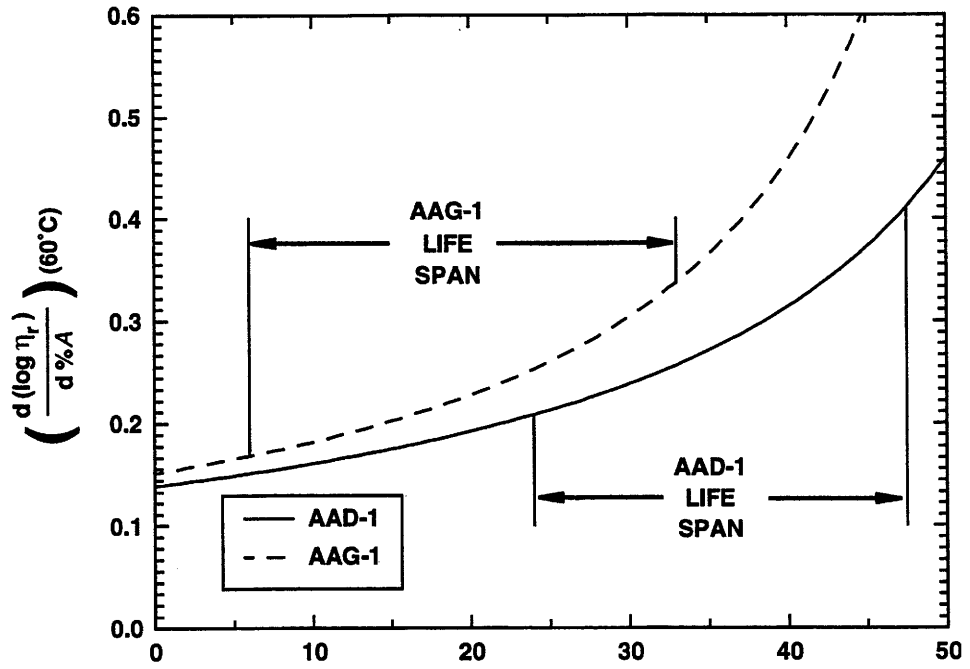
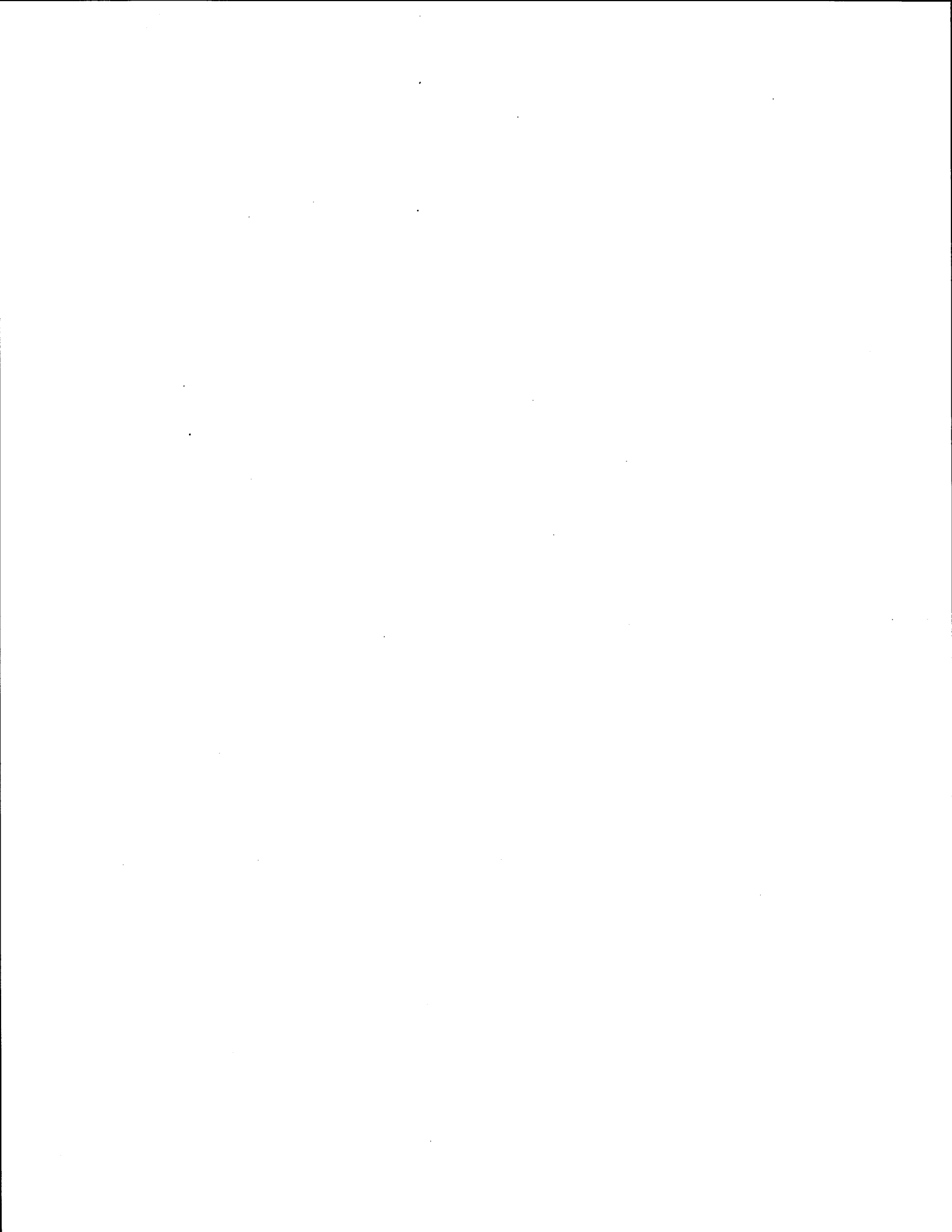


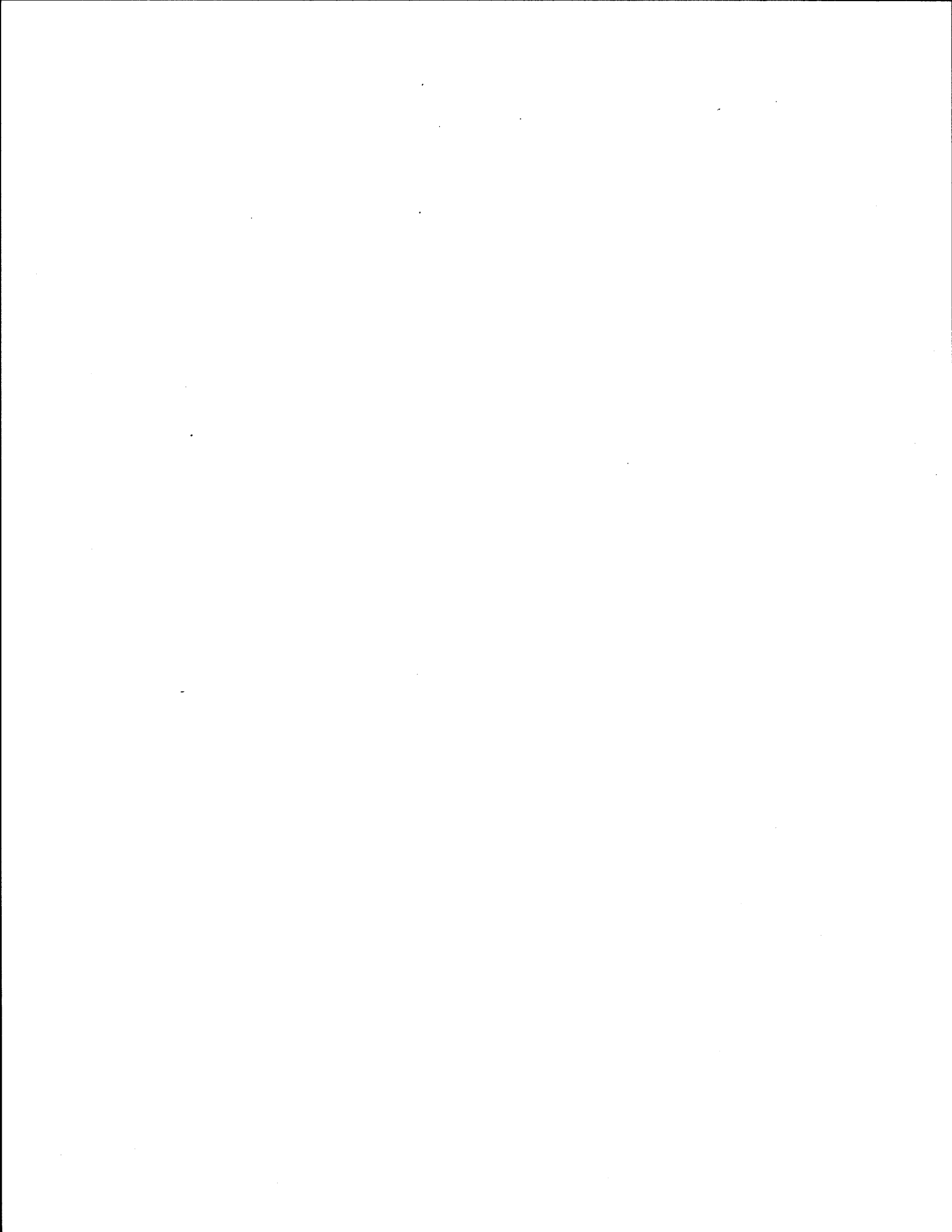
Figure 4-21. $(d \log \eta_r / d \%A)$ Versus Asphaltene for Blends Studied



SECTION III

RECYCLING

The previous two sections detail considerable effort to better understand the oxidation process of asphalt, to predict the relative rate of asphalt aging and to understand how asphaltene formation during oxidation results in asphalt hardening. This section describes methods used to produce asphalt fractions by supercritical extraction. Procedures are also developed to produce quantities of aged asphalt for recycling. The actual recycling work is developed in four chapters. The first is a preliminary study of the effect of saturate, asphaltene and metal content on recycled asphalt hardening. This is followed by a study in which two hardened asphalts are softened by an array of recycling agents and aged in the POV. The next chapter describes mixing rules for blending hardened asphalt and recycled agent, and the last chapter describes some studies done in connection with in-place recycling on I-45.



CHAPTER 5

MATERIALS PRODUCTION FOR RECYCLING

In order to conduct a systematic study of asphalt recycling it is necessary to have recycling agents with a variety of properties and compositions as well as aged asphalts from different sources and hardened to varying degrees. The agents have been obtained from several sources including low viscosity asphalt, commercial agents and agents obtained from the supercritical fractionation of asphalt. Rather than obtain aged asphalt from cores, which is very labor intensive and complicated by the extraction process, a method was developed for laboratory aging.

SUPERCritical FRACTIONATION

Davison et al. (1991, 1992) described the SC apparatus design and operation in detail. Modifications were made to the apparatus for Study 1314 because they were both necessary and convenient. However, the basic process and operating conditions remained unchanged. Brief descriptions of the process, operating conditions, and apparatus modifications follow.

Process Description

The following description is taken primarily from the Study 1249 (Davison et al., 1992) report with appropriate modifications. The unit operates at a constant pressure above the critical pressure of the solvent. The SC separation unit separates heavy petroleum products up to four fractions according to solubility in SC solvents. The temperatures of the separators determine the density of the solvent and, consequently, the solvent power in each vessel. Components of the feed precipitate when no longer soluble in the solvent. Decompression during solvent recovery removes the lightest, most soluble materials.

Figures 5-1 and 5-2 illustrate schematically the SC unit. The solvent is pumped to the operating pressure in S1-S3 by MP1. Several hours are required to bring the temperatures to the desired steady-state values. The steady-state operating temperature in S4 determines the steady state pressure for S4. Once steady-state conditions are achieved, MP2 is activated, introducing feed material into the circulating solvent stream. The temperature in each separator determines the solubility in the SC solvent. The insoluble material is transferred from the separator to its corresponding collector periodically to avoid potential plugging problems while the soluble material travels to the next separator. Finally, the overhead mixture from S3 passes through the control valve, where the pressure is reduced to a significantly subcritical value. At these gaseous conditions, none of the asphaltic material is soluble and complete separation of the solvent is achieved. The solvent then passes overhead, is condensed in WC1 and flows back into the solvent reservoir.

Operating Conditions

The fractionation in Study 1155 (Davison et al., 1991) employed n-pentane as the supercritical solvent. The major problem encountered with the use of n-pentane was that a large portion of the feed material remained insoluble even at supercritical conditions. The unit tended to become plugged and required much maintenance. To rectify this situation, cyclohexane was used to perform an initial fractionation of the asphalt (and reduced crudes) in Study 1249 (Davison et al., 1992). However, the use of cyclohexane resulted in other problems including reduced selectivity and higher operating pressures and temperatures. For Study 1314, n-pentane was chosen as the sole SC solvent. The operating pressures and temperatures were chosen based on the results obtained in Studies 1155 (Davison et al., 1991) and 1249 (Davison et al., 1992) and are given in Table 5-1. The use of n-pentane necessitated several modifications to the apparatus to eliminate potential problems.

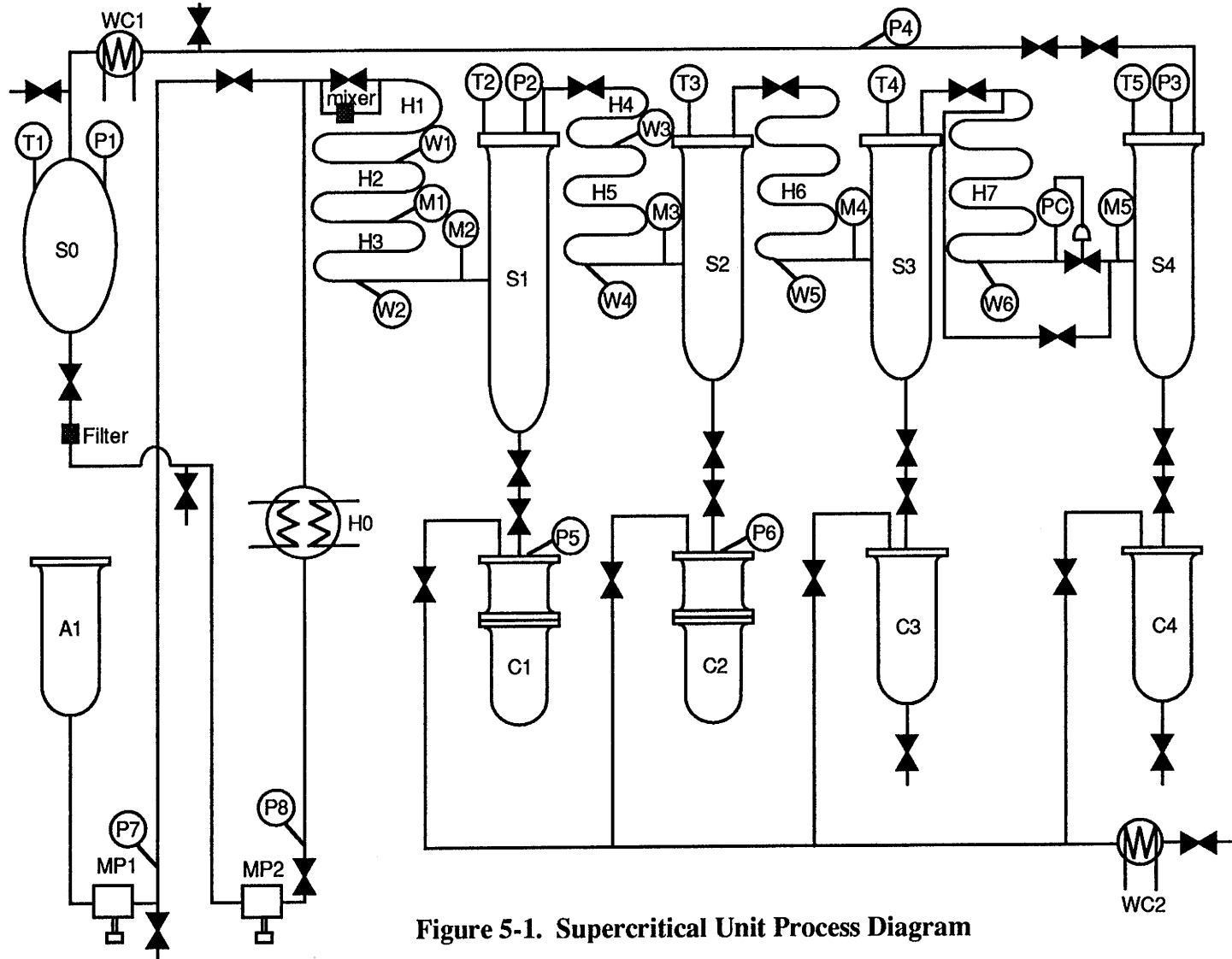


Figure 5-1. Supercritical Unit Process Diagram









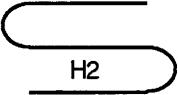

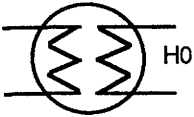

S0	Solvent Tank	S1-S4	Separators
C1-C4	Collectors	A1	Asphalt Tank
	In-line Filter/mixer		Valve
	Control Valve		Thermocouple
	Tubing Wall Temperature Thermocouple		Temperature Monitor and Controller
	Pressure Controller		Pressure Gauge
	Heating Tape Heater		Metering Pump
	Dual Purpose Heater/Cooler		Water Cooled Condenser

Figure 5-2. Legend for Supercritical Extraction Unit Diagram

Table 5-1. Supercritical Operating Conditions and Fraction Yields

Fraction	T (°C)	P (bar)	Fraction Percentage			
			YBF	ABM	AAF	AAA
F8	191	49.3	23.8±1.5	16.4±1.5	28.1±6.9	35.1±4.2
F7	204	49.3	9.6±3.9	8.2±1.2	6.4±0.5	4.0±0.2
F6	213	49.3	13.6±6.3	8.6±2.2	9.0±0.9	6.8±1.5
F5	149	3.3	53.6±4.0	66.9±3.2	56.6±5.4	54.1±2.5
F4	213	49.3	18.8	25.2±2.6	2.0	0.9±0.0
F3	221	49.3	18.8	25.2±2.6	30.3	17.0±3.7
F2	230	49.3	18.2	22.8±0.5	16.5	19.0±9.2
F1	149	3.3	6.4	16.3±1.2	7.8	17.0±12.5

Apparatus Modifications

The plugging problems encountered with the use of n-pentane are due mainly to settling effects resulting from mixing the solvent and the asphalt at low altitude and then pumping the mixture upward. This problem was eliminated by moving the mixing point to the top of the SC unit. Thus, insoluble material will settle into the separator and not the pump.

Moving the mixing point required redesigning the heaters between the pumps and the first separator. The previous heaters were removed and discarded after it was determined that a large amount of insoluble coke had built up in the tubing. This coke deposition was a direct result of the high operating temperatures necessary for cyclohexane separation. This coke build up also indicated that the modifications to the SC unit for Study 1249 (Davison et al., 1992) to reduce the heat load on the initial heaters were not wholly successful. To further reduce the heat load, a steam condensation preheater, H0, was installed between the solvent pump and the mixing point. Steam condensation is a safe, efficient, and uniform method for heat transfer.

Ideally, all of the heat input would be delivered by steam heaters. Electrical resistance heating tape heaters were installed between the asphalt pump and the mixing point to preheat the asphalt. New straight tubing heaters equipped with electrical resistance heating tapes and heat transfer cement were installed between the mixing point and the first separator. The number of heaters was not changed; however, the length for heat transfer was greatly increased. The net effect of installing the preheaters and redesigning the other heaters is more evenly distributed heat input. This, in combination with the use of n-pentane, should prevent coking from occurring again.

Once these initial modifications were made, the unit was tested. The test run ended when a fire occurred due to operator error. The pump had been shut off and no fluid was passing by the heaters. Without any mechanism for dissipation of heat, the temperature rose until the stainless steel tubing melted and ignited the solvent. The Halon fire suppression system described in Appendix A of Study 1155 (Davison et al., 1991) performed properly and the operator was not injured. As a direct result of this incident, extensive modifications were made to the apparatus to ensure that this could not happen again.

As an upgrade in the safety systems, relays were installed to prevent operation of the electrical resistance heaters when the solvent pump is not activated. In addition, thermocouples were installed between the heating tapes and the tubing wall in six locations. These thermocouples are connected to a high temperature alarm that will shut off the pump, and thus, interrupt the power to the heaters. The ultraviolet flame detectors were moved inside the apparatus hood, also. These modifications make the SC unit nearly foolproof.

As a precaution, every bank of electrical resistance heaters was replaced in case they had been stressed but had not failed. An additional heater was installed between separators 1 and 2 to reduce individual heater load. In addition, the unit was streamlined by removing all tubing allowing individual separator bypass. A binary or ternary cut may still be made by adjusting the operating temperatures accordingly. Tubing allowing periodic sampling of the overhead products and the

unused second asphalt feed tank was also removed.

Additionally, a much larger removable collection vessel was installed to assist in collection of the solid fraction collected in C1. In addition, the collection vessel C2 was replaced with a removable collection vessel. Ball valves were installed between S1 and C1 to eliminate plugging problems collecting the hardest fraction. Finally, rupture disks were installed to protect the relief valves from corrosion.

Even with these extensive modifications and tightened safety requirements, less than six months were lost. In the eighteen months of operation, the unit performed relatively problem free; only one heating tape burned out, requiring replacement.

ASPHALT FRACTIONATION

Four different asphalts were fractionated and analyzed in detail for this study. One asphalt was acquired from a local hot-mix contractor and three asphalts were obtained from the SHRP Materials Reference Library. A representative for the hot mix contractor indicated that the asphalt acquired was an AC-20 manufactured by the Fina Petrochemical Corporation in Fina's Baytown, Texas refinery. This asphalt is identified as YBF. We were unable to confirm the producer of YBF and we were also unable to determine the crude source or processing scheme. Furthermore, this asphalt was completely uncharacterized. We determined that the other asphalts for fractionation must be better documented and characterized to some extent.

The asphalts previously studied by our research group had been acquired in only small quantities for routine lab testing or had been exhausted in previous supercritical fractionation studies (Studies 1155 [Davison et al., 1991] and 1249 [Davison et al., 1992]). Therefore, we would either have to obtain additional quantities of these asphalts or completely characterize new asphalts. We decided that it would be preferable to acquire large quantities of asphalts that we had already characterized. Because refineries adjust operating conditions frequently, as well as switch crude sources, we decided that asphalts acquired in the past, such as those

used in Studies 1155 (Davison et al., 1991) and 1249 (Davison et al., 1992) would not be suitable for study in this work. We chose to study asphalts whose crude source and processing could not change: the SHRP asphalts. The asphalts acquired in conjunction with the SHRP program were sampled at one instant in time and can be considered the only 'standard' asphalts in the world. Furthermore, many of these asphalts have been studied extensively not only by our research group, but throughout the world as well. As such, a large database exists for these asphalts. Fifteen gallons each of these SHRP asphalts were acquired, however, not all of this material was used for fractionation studies. Some of these asphalts were used for other experiments for Study 1314.

Asphalt Properties

Table 5-2 tabulates the results of our analyses on the asphalts. Table 5-3 is a tabulation of data collected during the SHRP program on the SHRP asphalts studied.

Table 5-2. Tank Asphalt Data

Asphalt	Grade	Viscosity (Poise)	Saturate	Asphaltene	Aromatic
YBF	AC-20	3100	7.5	17.6	74.9
ABM-1	AR-4000	2200	6.8	6.7	86.5
AAF-1	AC-20	1950	11.1	14.8	74.1
AAA-1	150/200 Pen	915	9.8	16.9	73.3

Table 5-3. SHRP Data

Asphalt	Viscosity (Poises)	Saturate	n-Heptane Asphaltene	Napthene Aromatic	Polar Aromatic
ABM-1	2230	9.0	7.1	29.6	52.4
AAF-1	1872	9.6	13.3	37.7	38.3
AAA-1	864	10.6	16.2	31.8	37.3

The properties of interest are the viscosity and composition. The compositional information generated during this study is given for n-hexane asphaltene, saturate, and total aromatic content. No determination was made regarding the naphthene/polar or aromatic/resin content. It is immediately apparent from Tables 5-2 and 5-3 that the data are different from the SHRP data in all aspects. This is due to using a dynamic rheometer instead of a capillary viscometer to determine viscosity, precipitation of asphaltenes with n-hexane (C₆) instead of n-heptane (C₇), and saturate determination from HPLC analyses instead of traditional Corbett fractionation.

The asphalts chosen for this study were picked to represent the widest variation in hardening susceptibility, a reasonable indication of physicochemical properties. The HS has been determined (*prior* to the bulk of Study 1314) for more than 20 asphalts with values ranging from 1.0 to 5.3. AAA-1 has a 20.7 bar (300 psia) O₂ HS of 5.2, one of the highest ever determined. To represent an average HS, SHRP AAF-1 was selected. This asphalt has a 20.7 bar O₂ HS of 3.8. Finally, AAG-1 was selected to be fractionated because it possesses an anomalously low HS of 1.0. This HS is more than 1 point below the HS of any other asphalt ever studied. However, only a limited amount of this asphalt was available and we had to substitute with SHRP ABM-1. The HS for ABM-1 had not been determined but this asphalt was obtained from the same refinery using the same processing method and crude source as AAG-1, only at a different point in time. It would be necessary to invest at least some time to characterize this asphalt. However, the variations between AAG-1 and ABM-1 were thought to be small. Indeed, the 20.7 bar pure O₂ HS for ABM-1 was determined to be no different than the HS of AAG-1.

Fractionation

YBF was the first asphalt fractionated. This asphalt was fractionated four times with the standard operating conditions shown in Table 5-1. The data in this table also include the fraction yields for each of the asphalts fractionated. One trial

run was made with slightly adjusted operating conditions, but the difference between cuts was not significant, so no further experimentation was performed. F5 and F6 from the four runs with the same operating conditions were combined and fed through the unit for a second pass. The operating conditions were controlled such that the temperature for separation of F3 was the same as the temperature for separation of F6. This way, the F3 should contain all of the material from F6. In fact, second cut fractionation of the combined F5 and F6 material produced a much larger F3 than the sum of the F6 materials.

The next asphalt fractionated was SHRP ABM-1. This asphalt was fractionated four times using the same operating conditions as those used for the initial fractionation of YBF. A large overhead fraction, F5, containing approximately 65% of the asphalt was recovered from each run. A small amount of ABM-1 F5 was refractionated in a preliminary run using the same operating conditions as those used for refractionation of YBF combined F5 and F6. The yields in separators two and three (F3 and F2) were sufficient to warrant using these operating conditions. Nearly all of the remaining ABM-1 F5 was then fed through the unit for fractionation into F4-F1. A small clean-up fraction was obtained in the first separator. Two approximately equal sized fractions, F3 and F2, were collected.

Several problems were encountered with the fractionation of SHRP AAA-1. The transfer lines between S1 and C1 tended to plug with solid material. This was undoubtedly due to the large amount of asphaltenes (16.9% n-hexane and much more than this in n-pentane asphaltenes) present in the asphalt. The asphalt prompted the switch from needle valves to ball valves in the transfer line. Asphalt AAA-1 was fractionated four times using the standard operating conditions. However, two of these runs were aborted at various stages due to plugging problems. No mass balance was possible on these fractions; however, some F5 was obtained. The F5 materials from three of the runs were combined and refractionated separately from the F5 material from the fourth run. As such, the properties of the fractions from these second cuts vary quite drastically.

The final asphalt fractionated was SHRP AAF-1. By the time this asphalt was

fractionated, most of the operating problems had been worked out, so that only two runs were needed to produce a sufficient quantity of F5 for further fractionation. The F5 materials from these two runs were combined and refractionated in a single run.

Fraction Properties

The trends reported in Studies 1155 (Davison et al., 1991) and 1249 (Davison et al., 1992) were observed once again. Table 5-4 provides tabulations for the fraction viscosities, molecular weights (M_w), and composition data. The viscosities, M_w values, and asphaltene contents all increase nearly monotonically for F1-F4 and for F5-F8, while the content of saturates decreases nearly monotonically for F1-F4 and for F5-F8. The aromatic content increases for F1-F4 and for F5-F7. Deviations from a strictly monotonic trend are attributed to possible contamination in the recovery process and random errors in GPC or HPLC sample preparation. The discontinuity at F5 is due to refractionation of this material. This refractionation redistributes the material, concentrating the aromatics in F4 and the saturates in F1.

Figure 5-3 shows the trends in viscosity for all the asphalts, Figures 5-4 to 5-6 show the trend in composition for all asphalts, and Figure 5-7 shows fraction molecular weights. It is clear from these figures that there are significant differences between asphalts. Of particular importance are the differences in viscosities of F3 and F2 between the asphalts. For some reason, possibly the high aromatic and low saturate contents in the whole asphalt, the fractions obtained from ABM-1 are much more viscous than the fractions from the other asphalts.

The data are reported in Table 5-4 with statistical accuracy. Those data points with only a mean were measured once. The data points with standard deviation values may have been measured as many as 12 times (the viscosity of ABM-1 F3). Those values that have large deviations typically fall into one of two categories. The first category includes fractions where the residual pentane is difficult to remove. This will have a large effect on the viscosity and compositional

Table 5-4. Representative Supercritical Fraction Properties

Fraction	Viscosity (poise)	M _w	Saturates (wt %)	Asphaltenes (wt %)	Aromatics (wt %)
YBF F1	6	649	33.1	1.5	65.4
YBF F2	29.2 ± 7.3	895	22.7 ± 0.9	2.6 ± 0.4	74.8 ± 0.6
YBF F3	137.4 ± 9.0	1152	11.0	0.1	88.9
YBF F4	1040	1388	7.6	2.4	90
YBF F5	43.2 ± 5.2	986 ± 19	16.2 ± 3.0	2.4 ± 0.5	81.4 ± 3.2
YBF F6	1813 ± 835	1460 ± 51	6.2 ± 1.3	2.5 ± 1.1	91.3 ± 1.5
YBF F7	5.95 × 10 ⁵ ± 3.91 × 10 ⁵	1912 ± 182	1.3 ± 0.8	7.5 ± 1.8	91.2 ± 1.8
YBF F8	--	2668 ± 96	0.3 ± 0.3	63.4 ± 5.1	36.3 ± 5.2
ABM F1	11.1 ± 1.5	495 ± 9	17.5 ± 0.6	0.0 ± 0.0	82.6 ± 0.6
ABM F2	91.1 ± 8.0	748 ± 28	12.9 ± 0.6	0.0 ± 0.0	87.1 ± 0.6
ABM F3	627.3 ± 18.7	918	7.7 ± 0.7	0.0 ± 0.1	92.3 ± 0.7
ABM F4	1610	1085	9.5 ± 2.2	0.0 ± 0.0	90.6 ± 2.2
ABM F5	115.8 ± 17.1	758 ± 4	11.5 ± 0.5	0.0 ± 0.0	88.5 ± 0.7
ABM F6	8.21 × 10 ⁴ ± 1.32 × 10 ⁴	1266 ± 36	3.4 ± 0.2	0.3 ± 0.5	96.4 ± 0.5
ABM F7	1.44 × 10 ⁷ ± 1.10 × 10 ⁷	1531 ± 44	1.7 ± 0.1	6.7 ± 2.0	91.6 ± 2.0
ABM F8	--	2232 ± 63	1.0 ± 0.4	47.7 ± 1.7	51.4 ± 1.9
AAA F1	2.0 ± 0.1	572 ± 27	31.3 ± 3.4	0.5 ± 0.6	68.3 ± 2.8
AAA F2	14.5 ± 3.2	875 ± 6	20.0 ± 1.5	0.2 ± 0.3	79.8 ± 1.4
AAA F3	99.2 ± 28.5	1237 ± 5	11.0 ± 1.3	0.4 ± 0.5	88.6 ± 0.8
AAA F4	76.1 ± 81.8	1178 ± 285	16.2 ± 6.5	0.6 ± 0.6	83.2 ± 5.9
AAA F5	10.7 ± 0.5	902 ± 5	22.7 ± 0.3	0.2 ± 0.0	77.2 ± 0.2
AAA F6	250	1701 ± 304	7.6 ± 4.6	0.6 ± 0.2	92.0 ± 4.3
AAA F7	30,000	2257 ± 233	6.2 ± 0.6	6.5 ± 1.6	87.4 ± 1.0
AAA F8	--	4867 ± 83	1.8 ± 0.8	62.0	36.8
AAF F1	2.1	661	32.6	0.8	66.6
AAF F2	11.7 ± 1.6	928	23.5 ± 0.4	0.4 ± 0.1	76.2 ± 0.4
AAF F3	67.1 ± 8.0	1111	14.3 ± 0.1	0.4 ± 0.3	85.4 ± 0.4
AAF F4	315.6	1334	10.0	1.0	89.0
AAF F5	15.9 ± 0.2	966 ± 15	24.6 ± 0.4	0.1 ± 0.1	75.4 ± 0.4
AAF F6	3,000	1417 ± 27	8.1 ± 0.1	1.1 ± 0.1	90.9 ± 0.1
AAF F7	50,000	1696 ± 17	6.2 ± 1.7	7.4 ± 0.4	86.5 ± 1.3
AAF F8	--	2495 ± 1	1.2 ± 0.6	51.5 ± 2.1	47.3 ± 2.7

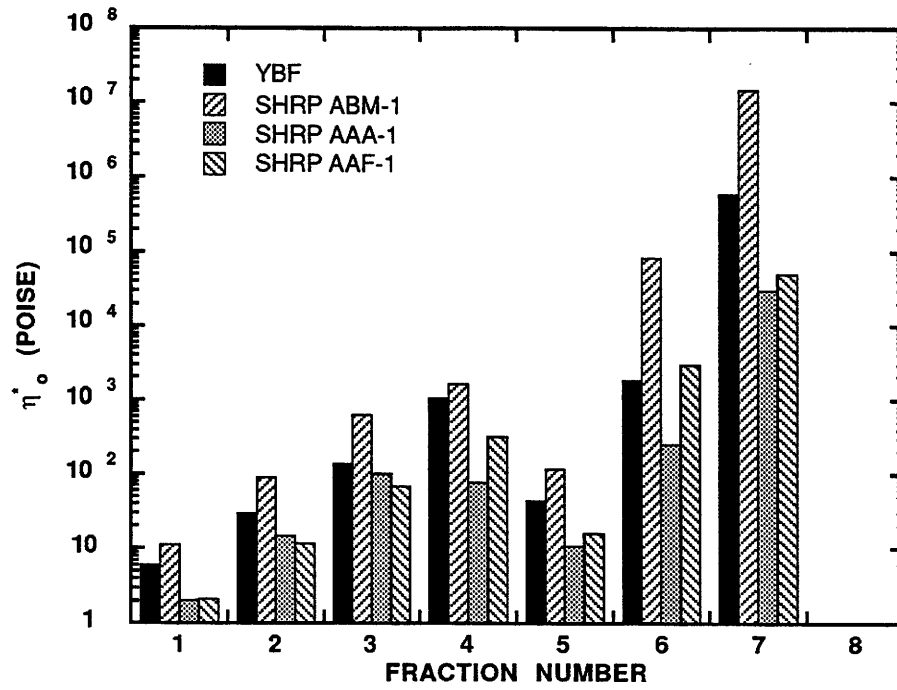


Figure 5-3. Fraction Viscosity Versus Fraction Number

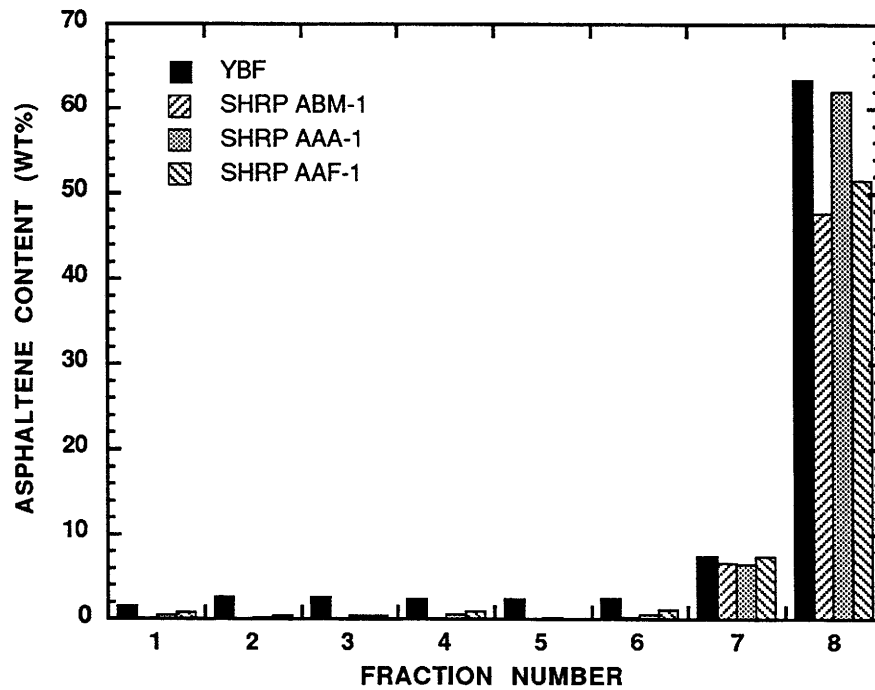


Figure 5-4. Asphaltene Content Versus Fraction Number

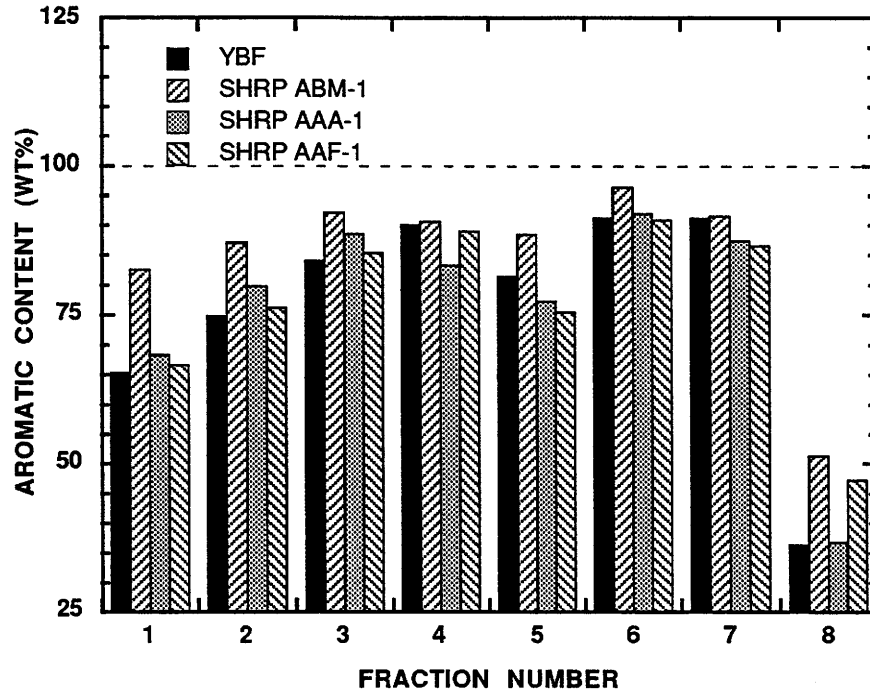


Figure 5-5. Aromatic Content Versus Fraction Number

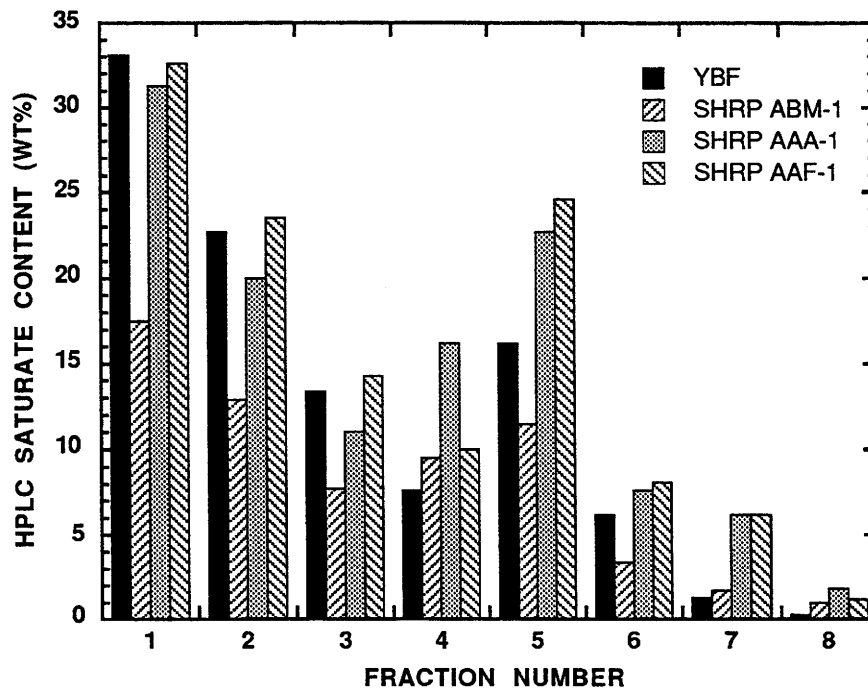


Figure 5-6. Saturate Content Versus Fraction Number

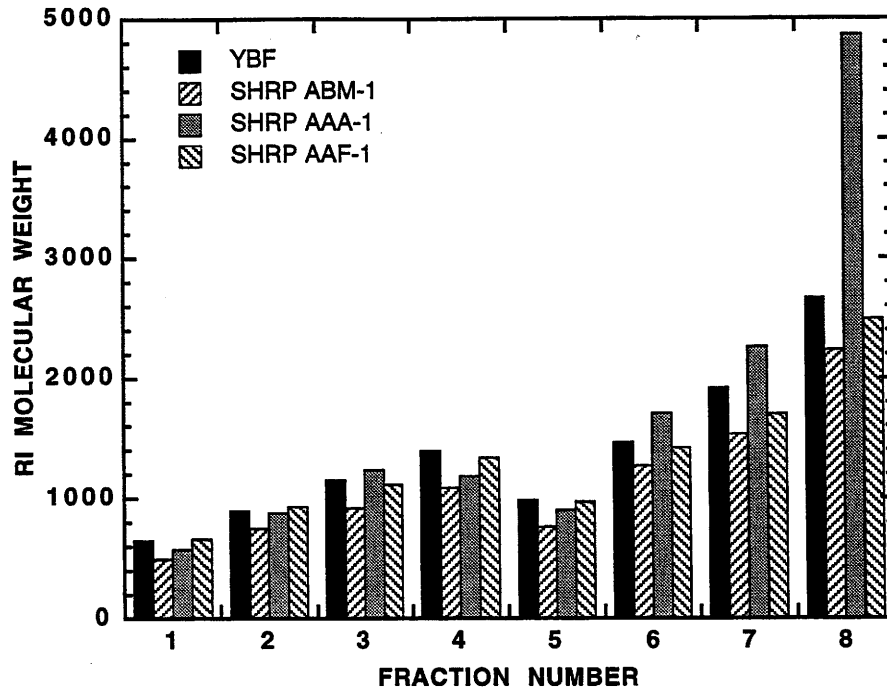


Figure 5-7. Molecular Weight Versus Fraction Number

analysis. F7 and F8 are highly subject to this problem. The second category is fractions with multiple samples such as YBF F5-F8. The data for these fractions represent at least four data points from the four different fractionation runs. These errors result from minor differences in operating conditions and from performing the different refractionation runs with potentially widely different materials. Many of these problems can be eliminated by operating a supercritical fractionation unit continuously, as occurs in industry.

Fraction Uses

YBF F3 and F2 were used for recycling experiments with two different asphalts. These fractions and YBF F5 were also used for the extensive mixing rules study. In addition to these fractions, ABM-1 F5, F3, and F2; AAA-1 F3 and F2; and AAF-1 F3

and F2 were utilized in the mixing rules study. Asphaltenes from ABM-1 F7 were used in the study to determine the effect of molecular size (weight) on the physicochemical properties of asphaltic materials.

AGED ASPHALT PRODUCTION

To produce large amounts of aged material suitable for recycling, tank asphalts from various sources were artificially hardened in the lab. This is a very straightforward procedure, the only requirements being heat and contact with oxygen. Four different methods were used to age material for this study. Early aged material was produced in the POV. Some tests were run using material aged on cookie sheets in a laboratory oven and some material was produced by bubbling air through an asphalt sample at elevated temperature. Finally, a new apparatus was developed for aging a large quantity of asphalt by bubbling air through a well mixed asphalt sample at moderate temperature.

Early aged materials were produced by aging in the POV. The material was weighed into trays (maximum of 5g per tray). These trays were then placed in the POV at 20.7 bar (300 psia) O₂ at temperatures between 87.8°C and 98.9°C (190°F and 210°F) for a predetermined amount of time. We had not yet become fully aware of the pressure effect on aging. Up to 350g (70 trays of a maximum of 5g) can be produced per POV. The material also has to be frozen with liquid nitrogen and then chipped into a new container. As such, the POV method for aging large quantities of asphalt is very labor intensive.

Two moderate improvements were made over POV aging. One interim aging method consisted of weighing asphalt onto cookie sheets and placing them in a laboratory oven to age at approximately 148.9°C (300°F). Other materials are placed into and removed from this oven periodically, so the temperature control is not optimum. The asphalt in the trays was stirred twice per day and the trays were rotated to ensure uniform aging. However, the quantity produced, the labor required and the loss of oven space hinder the use of this method for producing large quantities of material. The other temporary method entailed placing about 500g of asphalt in a 1000

mL round bottom flask and bubbling air through the asphalt at elevated temperature. Air was supplied from a building air source and the temperature was monitored using a thermocouple. The temperature was maintained below 232.2°C (450°F) to avoid thermal decomposition of the asphalt molecules. A small sample was removed periodically to determine the viscosity until the desired viscosity had been achieved. Some experiments used material aged in this manner. While the pressure dependence was removed by bubbling with air, the high temperature was later shown to drastically alter the products. Furthermore, there is considerable evidence that the air bubbling is not sufficient to ensure complete mixing and uniform aging.

The final method used to produce aged material is aging in a well mixed, air bubbled (AB) reaction vessel. An apparatus was built to age large quantities of asphalt in a uniform manner. The apparatus consists of a variable speed 1/15th horsepower motor which drives a 2.54 cm (2") diameter mixing shaft placed in a half full 3.8 L (1 gal) can of asphalt. Later, a second apparatus was constructed using a variable speed 1/4 horsepower motor. The can is wrapped with a heating tape connected to a variable transformer and a thermocouple-actuated on/off controller. Building air passes through a surge tank, filter, and a copper coil placed in a mineral oil controlled-temperature bath before being fed to the asphalt. The air is introduced to the asphalt through a 12.7 cm (5") diameter sparging ring made from 0.64 cm (1/4") stainless steel tubing with 14 nearly uniformly spaced 0.16 cm (1/16") holes. The inlet air temperature is controlled by adjusting both the temperature of the oil bath and the air flow rate. The operating temperature of the air-bubbled reaction vessel must be high enough for the oxidation to proceed at an appreciable rate, but not so high as to drastically alter the reaction mechanism or reaction products. Additionally, the temperature must be high enough to soften the asphalt so that the asphalt can be well mixed by the mixing paddle.

SHRP AAA-1 asphalt was aged at 149.8°C, 121.1°C, and 93.3°C (300°F, 250°F and 200°F) to study the effect of aging temperature on the reaction products. Samples were taken periodically to monitor the progress of oxidation. The viscosity and carbonyl areas were measured and plotted in Figure 5-8. This vessel is primarily responsible for determining that the hardening susceptibility is a function of pressure. The hardening

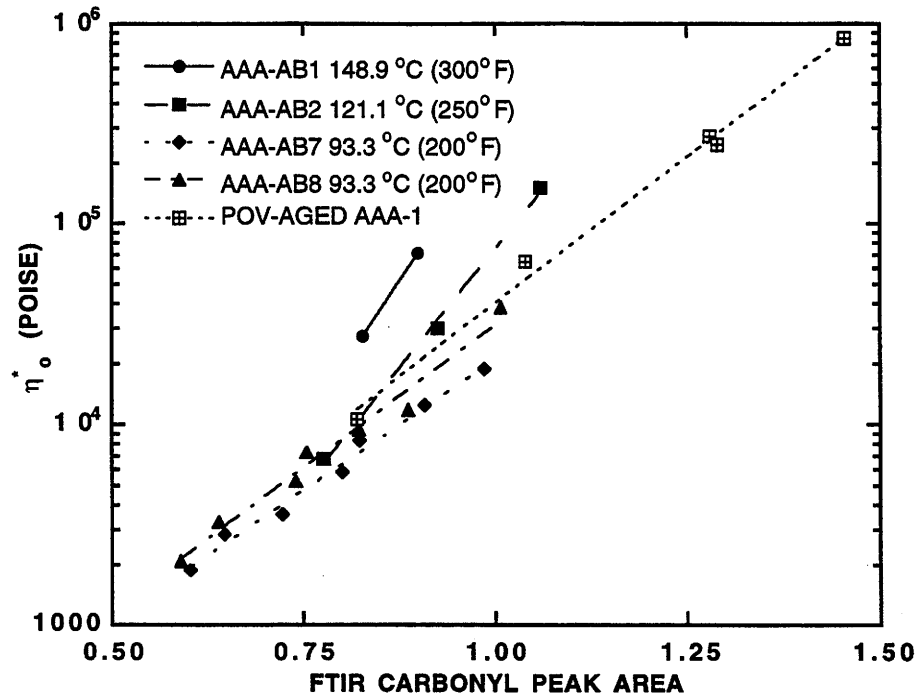


Figure 5-8. Effect of Air Bubbler Temperature on HS

susceptibilities, HS, (slope of \ln viscosity versus carbonyl area) were determined and compared to the HS values obtained from samples aged in the POV. Lau et al. (1992) showed that the POV HS is independent of aging temperature for temperatures up to 93.3°C (200°F). In addition, Martin et al. (1990) and Lunsford (1994) have shown that the POV HS is approximately representative of the relationship between viscosity and carbonyl area in asphalt binder extracted from pavement samples. However, the HS used by these researchers was the 20.7 bar (300 psia) O₂ HS. Comparison with the 0.2 bar (2.9 psia) O₂ HS may result in a different conclusion.

Figure 5-8 clearly shows that the AB HS is a function of temperature, with increasing deviation from the POV HS for increasing temperature. The POV HS shown in Figure 5-8 is the 0.2 bar (2.9 psia) O₂ HS. Initially, the AB HS was compared to the 20.7 bar (300 psia) O₂ POV HS. There was significant deviation, so it was thought that the AB apparatus was aging the material improperly. In fact, the AB aged HS is what

led us to the pressure dependence of the HS. The 93.3°C (200°F) HS measured for two different samples is equal to the POV HS. As a result of these data, it was determined that the products of oxidation at 149.8°C (300°F) are not the same as those formed through oxidation at 93.3°C (200°F) with respect to the relationship between viscosity and carbonyl area. This clearly implies that the previous method of producing aged material at 232.2°C (450°F) resulted in different products.

Large quantities of SHRP AAA-1 and SHRP AAF-1 were produced in the air-bubbling (AB) apparatus. Both asphalts were aged to two different viscosity levels. The aged AAA-1 samples are designated as AAA-AB7 (SHRP AAA-1 air-bubbled sample 7) and AAA-AB8, and the aged AAF-1 samples are designated as AAF-AB1 and AAF-AB2. To produce pavement-like materials, the reaction temperature was controlled at 93.3°C (200°F) initially. Effort was not expended to maintain this temperature precisely; however, the temperature was never allowed to exceed 110°C (230°F).

CHAPTER 6

COMPOSITIONAL EFFECTS IN ASPHALT RECYCLING

INTRODUCTION

The main objective of this research was to determine what types of materials are suitable for use as asphalt recycling agents. Any material under consideration must, of course, be low in viscosity, so that the aged material can be blended back to new asphalt viscosity, using the smallest amount of recycling agent possible. Furthermore, the material must be highly aromatic, to replace the aromatic materials which have been consumed by oxidation reactions. It must be low in asphaltenes, both to maintain low viscosity, and because the aged asphalt is already too rich in asphaltenes. Finally, recycle blends should have good aging characteristics.

The principal parameter for evaluation is the hardening susceptibility (HS). Data were taken to calculate oxidation rates, but poor temperature control ruined much of this. However, it is probable that in recycling, the HS will be easier to manipulate than the reaction rate.

METHODS

To produce recycling agents of specific compositions and to measure their effects on the aging properties of reblended asphalts, experiments were designed in which the various components were produced, mixed in controlled amounts, and artificially aged. Typically, the material used for recycling agents was fractionated using the Giant Corbett procedure. Tank asphalts were artificially aged, and recycling agents were mixed with these, yielding reblended asphalts which could be tested by artificial aging in a pressurized oxygen vessel (POV). The basic properties of interest in these experiments were the low frequency limiting dynamic viscosity, η_o^* , and the carbonyl area, an indicator of oxidation obtained through infrared

spectrometry. These properties were measured on aged and unaged blends. In one experiment it was also necessary to measure the nickel and vanadium content of the samples using atomic absorption.

Supercritical fractions were used to produce aromatics and saturates for this work. Two runs were made on the asphalt. The first run removed asphaltenes and produced a large lower molecular weight fraction. This fraction was rerun to produce four more fractions. The lightest of these fractions is designated as fraction 1, and the next fraction 2, and these were used in this study in several experiments.

To produce large amounts of aged material suitable for recycling, tank asphalts from various sources were artificially hardened in the lab by bubbling oxygen through molten asphalt at 232°C (450°F). Asphalts were also artificially aged in the POV. This was done at 87.8°C (190°F) and 20.7 bar (300 psia) oxygen for some previously determined time period.

Once suitable materials were obtained, or created using the preceding procedures, they were blended together in controlled ways to test the effect of each fraction on the overall properties. A typical test blend consisted of a recycling agent, either selected from some available material or blended from the various Giant Corbett fractions, which was mixed with an aged asphalt. A series of blends were designed in each experiment to test the various compositional effects, and were artificially aged in a POV as described by Lau et. al. (1992).

EXPERIMENTAL DESIGN AND RESULTS

To accomplish the goals of the research, several experiments were performed. These experiments involved selecting and/or producing materials, making blends from these materials, and performing POV aging tests on the blends. The experiments were designed to examine the following properties: effect of oils on aging of aromatic fractions, effect of metals and asphaltenes on aging, and effect of oils, waxes, and asphaltenes on reblended asphalt aging.

Temperature gradient problems made kinetic analysis impossible in several

experiments, but this does not affect the hardening susceptibility, which is independent of aging temperature.

Oils and Aromatics (Experiment 1)

Based on considerations already discussed, it was decided that the Giant Corbett aromatic fraction would be a good material to use as a recycling agent. However, it was found that aromatic fractions from asphalt had viscosities at 60°C (140°F) as high as 4000 poise, and that even aromatics from light supercritical fractions were a minimum of 100-200 poise. To bring the recycling agents into the required range, low viscosity (typically less than 2 poise) oils could be added, but their effect on aging would have to be examined. To do this, a Fina supercritical fraction #1 was fractionated into four components using the Giant Corbett. From the oils and aromatics, three blends were made. They contained 20, 40, and 60% oil, respectively. These blends were POV aged at 82.7°C (180°F) and 20.7 bar (300 psia), along with the pure oil and pure aromatic, for periods of 4, 8, 12, and 16 days. Both change in $\ln \eta_o^*$ and carbonyl are linear in time and a plot of $\ln \eta_o^*$ versus carbonyl (Figure 6-1) yields the hardening susceptibility as the slope.

The pure oil fraction experienced little or no aging during the test period. As the oil content of the blends decreased, the viscosity and carbonyl aging rates increased for all of the blends which contained oil. This trend did not apply to the pure aromatic fraction, which had lower aging rates after four days than the 20% oil blend, but this almost certainly was due to the temperature gradient in the POV, together with the hypothesis that the aging rates should actually have been an average of the rates for the pure components. This possibility is supported by the hardening susceptibilities (a property which is independent of aging temperature) and their linear dependence on oil content as shown in Figure 6-2. The hardening susceptibility of each blend is actually an average of the hardening susceptibility of its components.

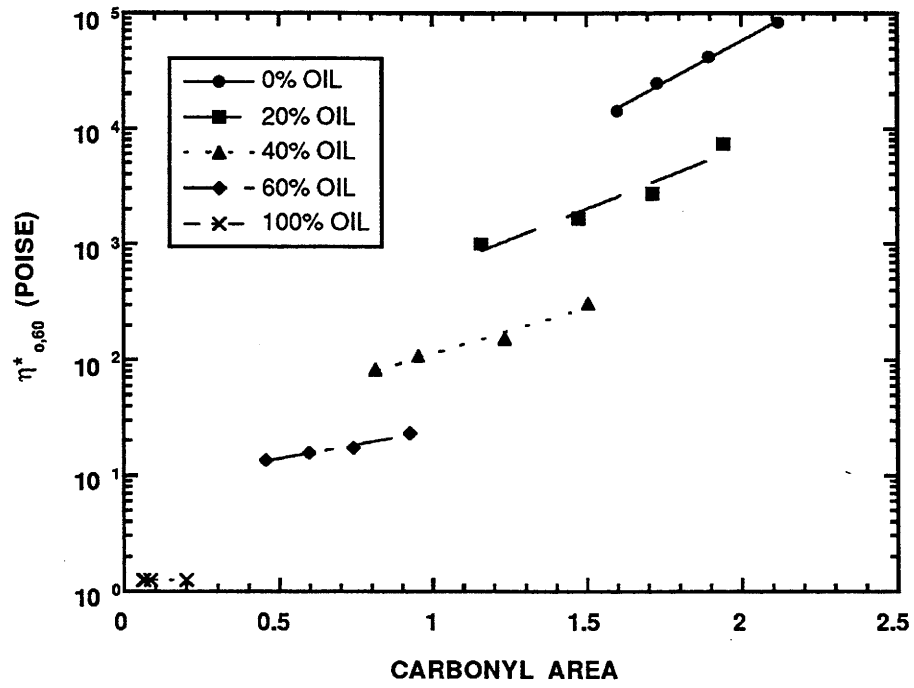


Figure 6-1. Experiment 1: Hardening Susceptibilities

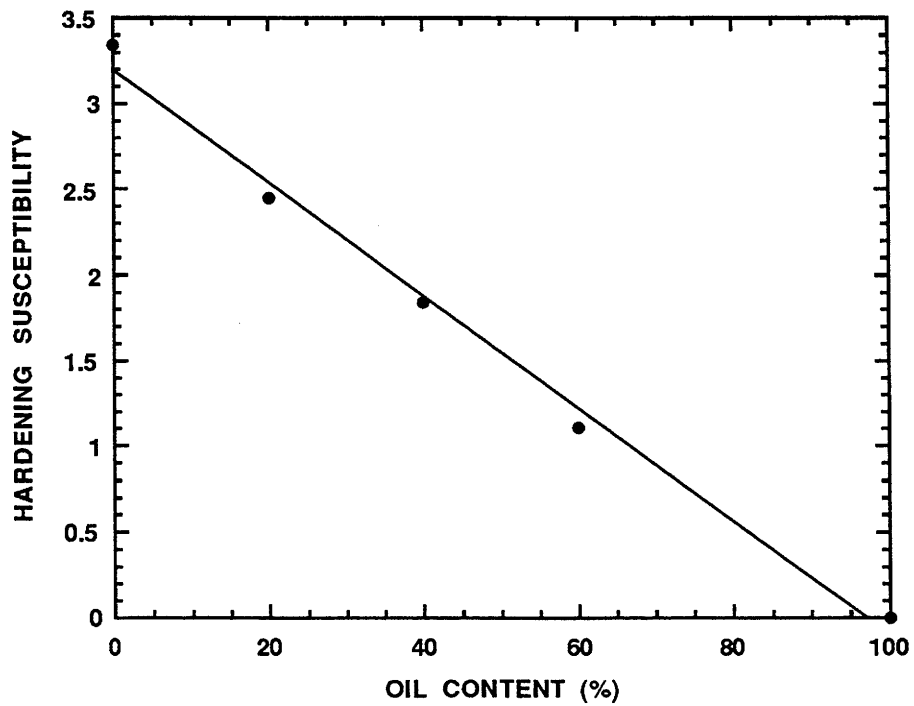


Figure 6-2. Hardening Susceptibility Versus Oil Content

Metals and Asphaltenes (Experiment 2)

This experiment was designed to examine the effects of trace metals and asphaltenes on aging. Jemison (1992) showed a strong correlation between hardening susceptibility and both trace metals (nickel and vanadium) and asphaltenes. There was some difficulty deciding how to isolate these two effects, since the asphaltenes typically contain almost all of the metals from the asphalt or fraction. The solution was to use asphaltenes from three different asphalts which all had different levels of metals. Blending these materials with an aromatic base would yield blends in which the asphaltene and metal contents would not be interdependent.

To perform the experiment, three tank asphalts were fractionated using the Giant Corbett: the McMillan low-metals AC-20; the intermediate-metals Exxon AC-20; and the Coastal AC-20 with high metals. The trace metal content, specifically nickel and vanadium, was determined using an atomic absorption method based on the method described by Davison (1989), but which allowed use of smaller sample size and more efficient sample preparation. To make the asphaltene measurement more consistent, the heptane asphaltenes were measured for the asphaltene and aromatic fractions. (Since the bulk asphaltene precipitation was not a careful analytical separation, there was a significant amount of asphaltene in the aromatic, and vice-versa.) Table 6-1 presents these data. The aromatic fractions were combined and used as a base, with 15% oil added to reduce viscosity. The three types of asphaltenes were blended with this material, producing nine blends with varying levels of metals and asphaltenes. The resulting blend compositions are shown in Table 6-2. These blends were all aged in the POV at 82.2°C (180°F) and 20.7 bar (300 psia) for periods of 4, 8, 11, and 14 days, and the viscosities and carbonyl areas were measured. The results show some scatter because of the temperature gradient problem, but are still quite interesting. Figure 6-3 shows no effect of metals on hardening susceptibility while Figure 6-4 shows a definite correlation with asphaltenes. This leads to the rather surprising result shown in

Table 6-1. Asphaltenes and Metals of Starting Fractions

Material	Starting % Asphaltenes	Nickel (PPM)	Vanadium (PPM)
Coastal Asphaltenes	78.1	142.1	966.7
Coastal Aromatics	2.2	32.1	160.9
Exxon Asphaltenes	80.6	20.5	32.1
Exxon Aromatics	2.8	9.0	13.3
McMillan Asphaltenes	48.1	82.5	288.7
McMillan Aromatics	3.6	22.1	60.7

Table 6-2. Compositions of Blends in Experiment 2

Blend	Base % Aromatic	Starting % Asphaltene	Nickel (PPM)	Vanadium (PPM)
L-10	88.67	11.33	45.3	54.6
L-20	83.21	16.79	22.2	46.8
I-10	89.79	10.21	24.2	88.5
I-20	80.05	19.95	27.6	83.3
I-30	73.15	26.85	26.7	75.1
H-10	89.96	10.04	29.2	137.7
H-20	82.19	17.81	32.7	128.1
H-30	74.37	25.63	36.3	118.5
Aromatic Base	97.38	2.62	16.9	47.3

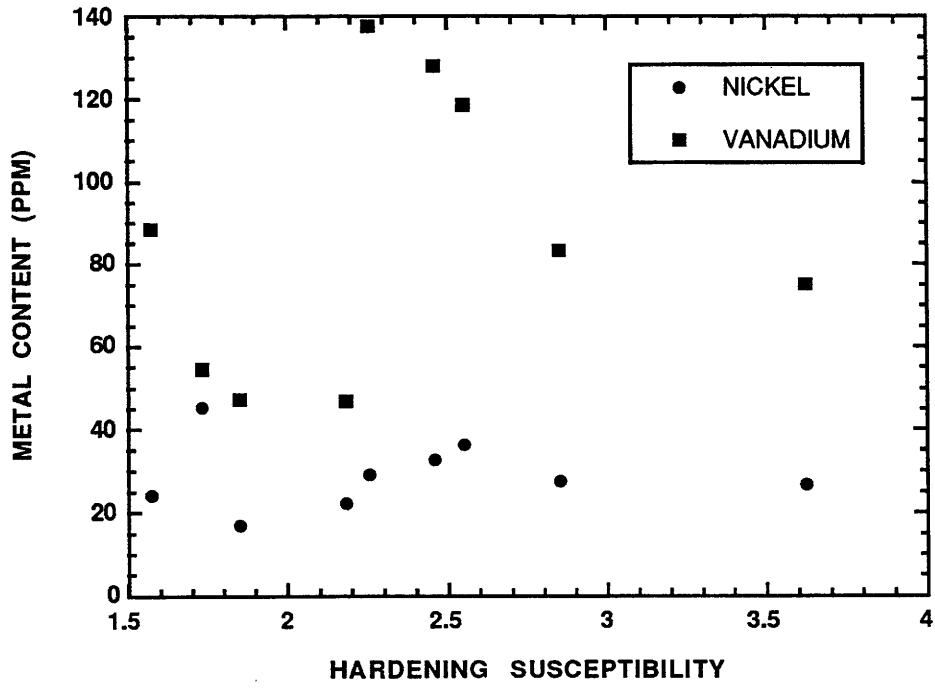


Figure 6-3. Effect of Metals on Hardening Susceptibility

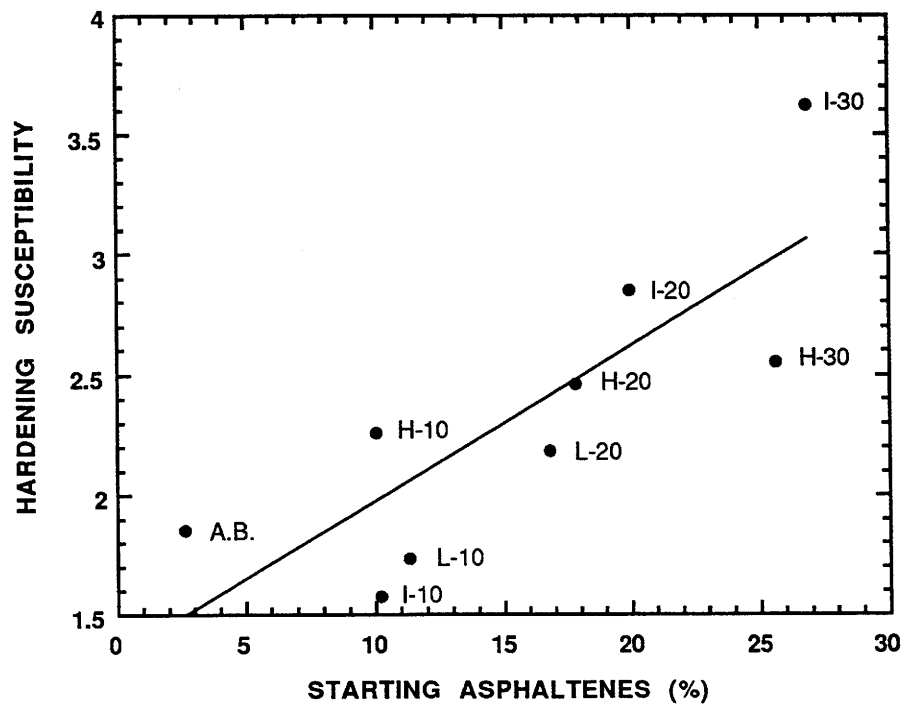


Figure 6-4. Effect of Asphaltene on Hardening Susceptibilities

Figure 6-5 that starting asphaltenes have essentially no effect on the oxidation rate but definitely increase the hardening rate through the adverse effect on hardening susceptibility.

Supercritical Fractions as Recycling Agents

Three sets of experiments were performed using light supercritical fractions either directly as recycling agents or after alteration of the oil, wax, and asphaltene content. In the first set of experiments (Experiment 3), two light supercritical fractions were chosen: a Fina fraction #2 and a Coastal fraction #1. In addition, the same fractions were dewaxed using the procedure for oil and wax separation from the Giant Corbett, and the dewaxed materials were used as two more recycling agents. These four agents were blended with five artificially aged asphalts to make ten blends. Table 6-3 shows the composition based on Corbett analysis and the

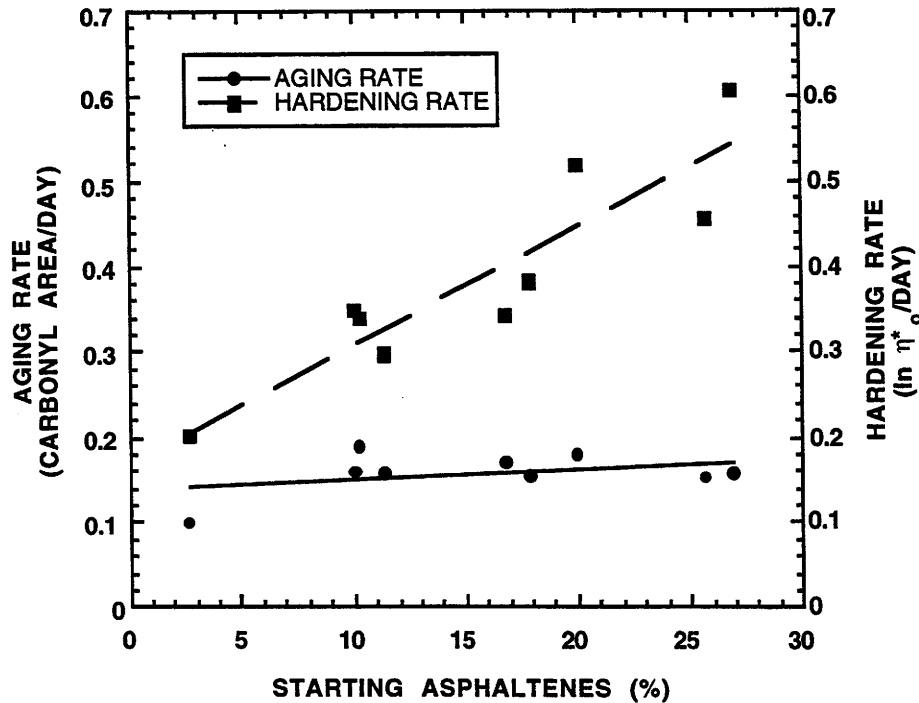


Figure 6-5. Effect of Asphaltenes on Hardening and Carbonyl Formation Rates

Table 6-3. Compositions and Viscosities of Materials in Experiment 3

Material	Blend Makeup	% Par.	% Orig. Asph.	Mix Ratio %	Hard. Susc.	Viscosity (P)
Coastal SC Fraction 1	NA	20.33	0.33	NA	NM	0.599
FINA SC Fraction 2	NA	33.67	0.67	NA	NM	0.631
DW Coastal SC Fraction	NA	18.04	0.35	NA	NM	1.358
DW FINA SC Fraction	NA	30.21	0.72	NA	NM	1.185
<hr/>						
Aged Ampet AC-20 #1	NA	8.33	12.33	NA	NM	83,000
Aged Ampet AC-20 #2	NA	8.33	12.33	NA	NM	260,000
Aged Ampet AC-20 #3	NA	8.33	12.33	NA	NM	160,000
Aged Cosden AC-20	NA	13.00	16.00	NA	NM	105,000
Aged Texaco AC-20	NA	8.22	18.41	NA	NM	230,000
<hr/>						
Blend R1	Ampet #2/ Coastal SC	13.57	8.95	56/44	NM	270
Blend R2	Ampet #2/ Fina SC	19.25	9.16	57/43	2.05	265
Blend R3	Ampet #3/ Fina SC	18.47	9.60	59/41	2.09	271
Blend R4	Ampet #3/ DW Coast.	12.07	8.95	61/39	2.25	333
Blend R5	Cosden/ DW Coast.	15.43	10.50	52/48	2.06	130
Blend R6	Cosden/ DW Fina	21.33	10.67	52/48	2.48	261
Blend R7	Texaco/ DW Fina	17.10	12.65	60/40	NM	568
Blend R8	Texaco/ Coastal SC	13.45	12.64	57/43	NM	470
Blend R9	Ampet #1/ Coastal SC	15.58	6.88	37/63	1.41	30.3
Blend R10	Ampet #1/ DW Coast.	14.67	5.09	35/65	1.90	70.2
<hr/>						
NA	Not Applicable					
NM	Not Measured					

viscosity of each recycling agent, aged asphalt, and rebled asphalt. The hardening susceptibilities are also given in Table 6-3, except for blends R1, R7, and R8, which were hardened either too little or too much because of a temperature control problem. The saturate content was much higher in this experiment than in the other two, and the hardening susceptibilities, as will be shown later, are anomalous.

Although the ductility was not measured in this research, there were samples from this experiment which had visibly poor ductility. At viscosities of only several thousand poise, the material from the POV trays would crumble, and had the texture of soft cheese. It is thought that the high paraffin content caused incompatibility, and the resultant loss in ductility. Evidence of this effect also came from the viscosity data. The frequency sweeps run to determine the zero-shear viscosities tended to become flat very soon in the run, as would be expected with these low viscosities, but would later jump to a higher viscosity and level out again. A typical frequency sweep and one exhibiting this behavior are shown in Figure 6-6. This effect was especially notable at higher saturate levels and became more pronounced as the blends aged.

In Experiment 4, a Coastal supercritical fraction #1 was fractionated and its oils, aromatics, and waxes were used to make four recycling agents. These agents contained 15.28% oil, 8.26% oil, 7.71% oil plus 4.09% wax, and no oil or wax. They were named A, B, C, and D, respectively. These were blended with four aged asphalts to make 11 blends. Table 6-4 shows the viscosities of the asphalts, agents, and blends, and the mixing ratios for each blend and its composition.

Unfortunately, continued temperature problems ruined much of the kinetic data from this experiment. However, the hardening susceptibilities of the blends could still be analyzed, and revealed some important results. Figure 6-7 shows combined viscosity vs carbonyl curves from all three aging temperatures for the blends which were made from the Coastal asphalt. In addition, the thick line above the blend data shows the viscosity/carbonyl relationship previously measured for the original asphalt alone. The slopes of these lines, the hardening susceptibilities, are actually lower in every case for the rebled material than for the original asphalt,

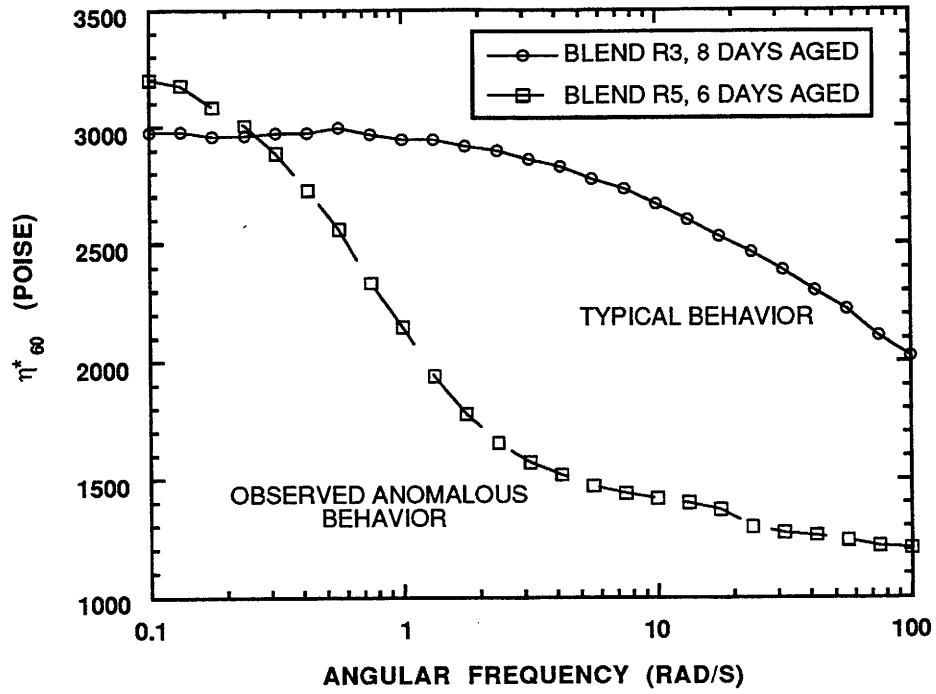


Figure 6-6. Asphalt Viscosity Frequency Sweep

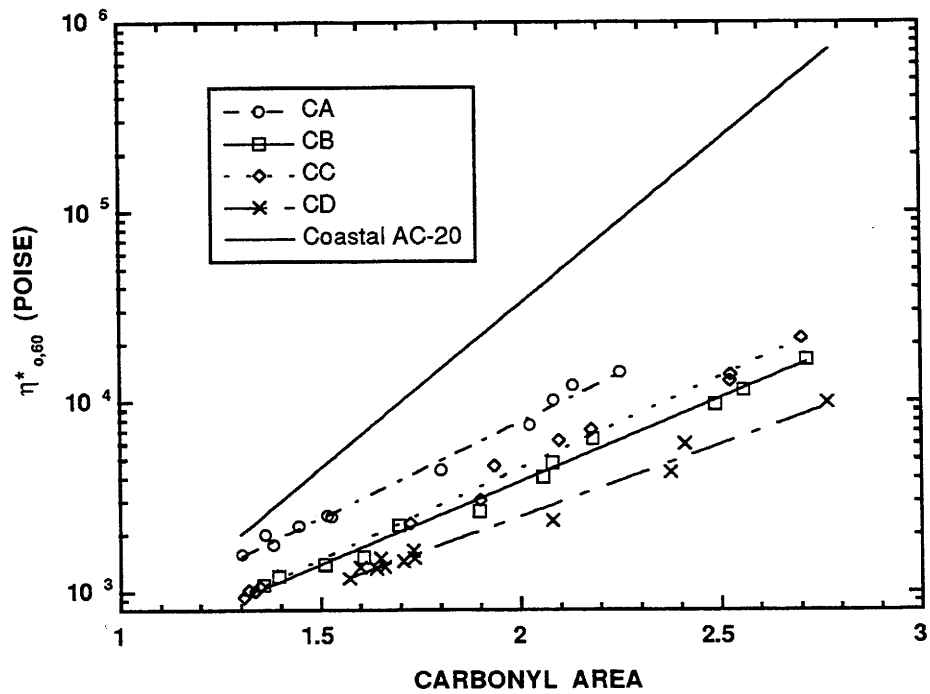


Figure 6-7. Coastal Blend Hardening Susceptibilities

Table 6-4. Viscosities and Blending Ratios for Experiment 4

Material	Visc. (P)	Mix Ratio (%) (Asph./Agnt.)	Hard. Susc.	Temp. Susc.	% Orig. Asph.	% Sat.
Agent A	20.2	NA	NM	NM	0	15.28
Agent B	47.7	NA	NM	NM	0	8.26
Agent C	37.6	NA	NM	NM	0	11.8
Agent D	183	NA	NM	NM	0	(7.71 oil, 4.09 wax) 0
Ampet AC-20	20,200	NA	NM	NM	12.33	8.33
Coastal AC-20	41,000	NA	NM	NM	19.41	8.91
Texaco AC-20	89,700	NA	NM	NM	18.41	8.22
Blend AA	1230	70/30	2.32	19746	8.63	10.41
Blend AB [†]	500	63/37	1.79	20597	12.22	8.30
Blend AC	1055	65/35	1.95	19242	8.02	9.54
Blend AA*	615	45/55	2.42	19000	5.55	12.15
Blend CA	750	64/36	2.33	18748	7.89	11.20
Blend CB	495	56/44	2.02	19046	10.87	8.62
Blend CC	535	58/42	2.21	18215	11.26	10.12
Blend CD	518	40/60	1.74	19231	7.76	3.56
Blend TA	436	58/42	1.79	17935	10.67	11.18
Blend TB	445	50/50	1.93	18876	9.21	8.24
Blend TC	450	52/48	1.90	18064	9.57	9.93
Blend TD	555	36/64	1.39	18970	6.63	2.95

(Notation for blends: A_ = Ampet, C_ = Coastal, T_ = Texaco;
 _A = Agent A, _B = Agent B, _C = Agent C, _D = Agent D;
 Example: Blend CB contains Coastal AC-20 and Agent B.)

NA Not Applicable

NM Not Measured

[†] Due to a shortage of material, a more highly aged Ampet asphalt was used for this blend, which had a viscosity of 260,000 Poise.

* Also due to a shortage of material, this blend contains the same recycling agent as blend AA.

indicating that the aged asphalt was actually improved by the recycling agent, at least from the standpoint of this analysis. There was less improvement for the Ampet materials than for the Texaco and Coastal, presumably because the Ampet was originally a better material. The improvements in hardening susceptibilities for the Texaco and Coastal asphalts are significant.

Experiment 5 was very similar to the fourth, in that recycling agents were designed to have specific compositions. This time, however, more variation was used in the amount of wax in the blends, and asphaltenes were included. Also, the temperature gradient in the POV had been eliminated. The materials for the recycling agents came from an Exxon Supercritical fraction #1, which was further fractionated by the Giant Corbett. Only one half of the paraffin fraction was separated into oil and wax; the other was left alone. Six recycling agents were made from these materials, containing varying amounts of oils, paraffins, aromatics, and asphaltenes. These were labeled E, F, G, H, I, and J, respectively. These agents were blended with an artificially aged Texaco asphalt. Table 6-5 shows the component viscosities, mixing ratios, and resulting viscosities and compositions for each reblend.

These recycled blends were aged in the POV at 20.7 bar (300 psia) and 71.1°C (160°F) for 8, 12, 14, and 16 days; at 79.4°C (175°F) for 10, 13, 16, and 19 days; and at 87.8°C (190°F) for 4, 6, 8, and 10 days. All of the blends displayed roughly the same aging rate, except for I and J, which contained wax. This behavior was observed at all three temperatures; moreover, at two temperatures the carbonyl growth rate decreased as wax content increased. (The actual wax content was not measured; the reblending agent which contained only paraffins would have approximately twice as much wax as the one containing paraffins and oil.) Examining the viscosity data reveals similar behavior. This would indicate that, although the aging rates seemed to be lower for the blends with waxes, the hardening susceptibilities should be close to the same. Arrhenius plots indicate no obvious effect of composition on activation energies.

Also of importance are the differences between the aging rates for the original

Table 6-5. Viscosity and Mixing Data for Experiment 5

Material/	% Sat.	% Asph.	Visc(P)	Hard. Susc.	Temp. Susc. (*10 ⁻⁴)	Mixing Ratio % (Asphalt) /Agent)
Agent E	20.4	0	36	NM	NM	NA
Agent F	14.9	0	37	NM	NM	NA
Agent G	10.2	2.8	111	NM	NM	NA
Agent H	9.9	5.4	132	NM	NM	NA
Agent I*	11.2 (6.1 oil, 5.1 paraffin)	0	37	NM	NM	NA
Agent J*	10.6 (all paraffin)	0	63	NM	NM	NA
Aged Texaco AC-20	8.22	18.41	160,000	NM	NM	NA
Blend E	13.1	11.0	358	2.25	1.87	60/40
Blend F	10.9	11.0	579	2.16	1.89	60/40
Blend G	8.9	13.4	945	2.02	1.92	68/32
Blend H	8.2	14.5	1169	1.97	1.97	70/30
Blend I	9.4	11.0	755	1.88	1.9	60/40
Blend J	9.1	11.8	865	2.03	1.93	64/36

NM Not Measured

NA Not Applicable

* Saturates in agent I are part oil and part unseparated paraffin. In agent J, saturates are all paraffin. The wax in these agents is contained in the paraffin.

and recycled asphalts. Aging data previously collected for the Texaco AC-20 (8) reveal very similar rates of carbonyl growth. At 71.1°C (160°F), the asphalt's carbonyl area increased by approximately 0.3 over ten days, while the blends in this experiment displayed increases of approximately 0.25 over nine days at the same temperature. At the same time, the asphalt's viscosity increased by about half of an order of magnitude, while the blends only hardened half that much (which is consistent with the hardening susceptibility). Furthermore, the 20-day, 71.1°C (160°F) aged asphalt had a viscosity of about 100,000 poise from a tank value of 2500; a typical blend viscosity from a similar aging time was 6000 poise from an initial 600.

The Effect of Saturates on Hardening Susceptibility and Temperature Susceptibility

In Experiments 3-5, hardening susceptibilities were measured for each blend. These are plotted versus saturate content in Figure 6-8. As would be expected there is considerable variation as a variety of aged asphalts and blending agents were used, but, in general, the hardening susceptibility is seen to increase with saturate content. This most clearly is seen in Experiment 5 where a single aged asphalt and a single recycling agent base stock were used. This result is contrary to the data in Experiment 1 where oils and aromatics were aged but confirms the adverse effect of asphaltenes in Experiment 2.

There is no apparent effect of wax in these experiments, which is not particularly surprising since these hardening susceptibilities are based on 60°C (140°F) viscosities while the detrimental effects of wax occur at low temperature.

Most of the Experiment 3 data appear anomalous. There are two possible explanations. The first is that experiment 3 composites are based on Corbett analysis while in Experiments 4 and 5, they were made by weight. Perhaps there is a systematic error. The other possibility is that the strange frequency sweeps seen in Figure 6-9 are giving erroneous viscosities as a result of phase separation.

In Experiments 4 and 5 viscosities were run from 0°C (32°F) to 60°C (140°F). The logs of the viscosities were plotted versus reciprocal absolute temperature. The

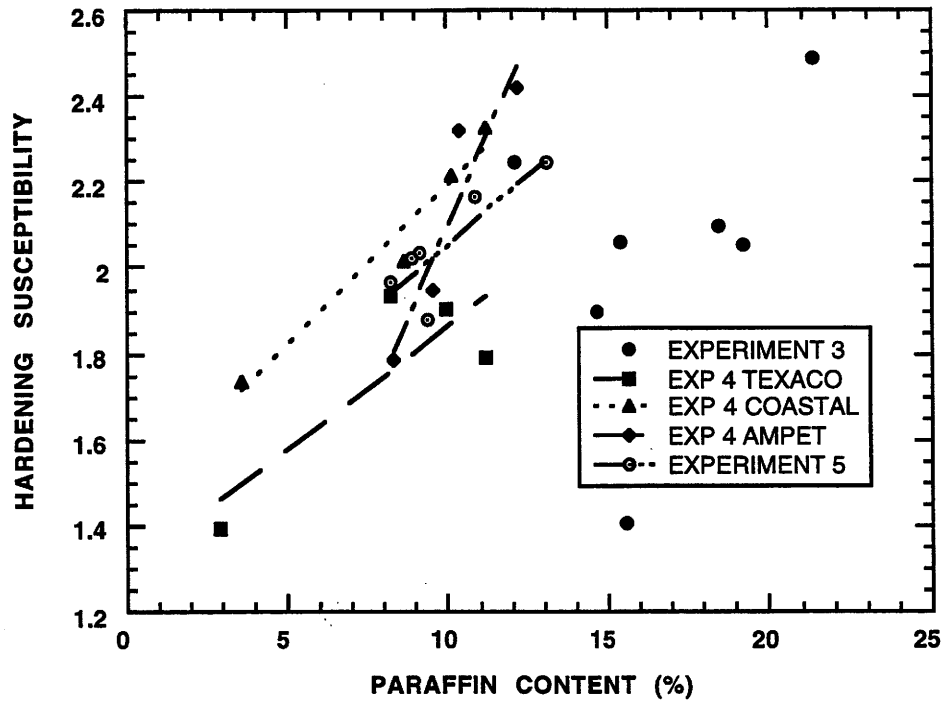


Figure 6-8. Effect of Paraffins on Hardening Susceptibilities

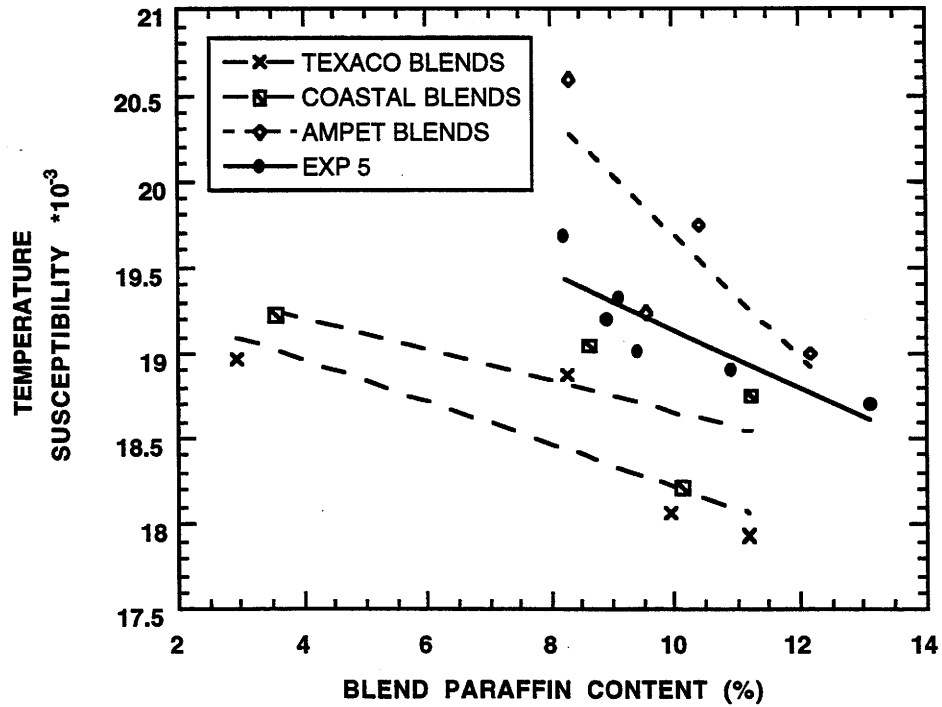


Figure 6-9. Effect of Paraffins on Temperature Susceptibilities

slopes of these lines, the temperature susceptibilities, are plotted as a function of paraffin content in Figure 6-9. The property shows no sensitivity to wax but does correlate with total saturate content. In all cases, temperature susceptibility decreases with paraffin content. It is also interesting to note that the temperature susceptibilities of the original asphalts are markedly larger than the reblended aged material.

CHAPTER 7

RECYCLING AGENT EXPERIMENTS

Two asphalts were POV-aged to provide the aged material for two recycling studies. Approximately 350g (0.772 lb) each of a Fina asphalt and a Coastal asphalt that had been well characterized by our lab were POV-aged for use in recycling studies. The Coastal asphalt was aged to approximately 250,000 poise and the Fina was aged to 100,000 poise. These two asphalts were blended with eight different softening agents. These softening agents included two supercritical fractions, five commercial recycling agents and one AC-3 asphalt. Table 7-1 lists the compositional information for these materials.

A viscosity of 5500 ± 1000 poise was chosen as the target viscosity for blending. The initial recycling agent content was calculated using an early mixing rule developed in the metals/asphaltenes study described in Chapter 6. Blending was accomplished by hand mixing using a procedure similar to that specified in ASTM D4887. The viscosity was measured, and additional asphalt (usually) or softening agent was added. This trial and error procedure was repeated until all blends were within the limits on viscosity. Once the specification blends were produced, compositional analyses of the materials were performed using the HPLC procedure. Table 7-2 lists the compositional data on these blends.

The mixtures were then aged in the POV at 71.1, 79.5, and 87.8°C (160, 180, and 200°F) under 20.7 bar O₂ (300 psia) for varying lengths of time. The carbonyl areas and viscosities of these aged samples were measured and the 20.7 bar HS were obtained.

AGED MATERIAL ANALYSES

Table 7-2 shows the 20.7 bar HS for each asphalt/softening agent blend in this experiment. Again, it is important to note that the data in Table 7-2 are not the

Table 7-1. Recycling Agent Table

Softening Agent	Viscosity (dPa·s)	Saturate	Asphaltene	Aromatic
YBF F3	137.4 ± 9.0	11.0	0.1	88.9
YBF F2	29.2 ± 7.3	22.7 ± 0.9	2.6 ± 0.4	74.8 ± 0.6
Witco Cyclogen	7.5 ± 1.4	24.9	0.8	74.3
Exxon Nuso 95	1.2 ± 0.2	28.0	0.5	71.5
Sun Hydrolene 110T	1.5 ± 0.3	30.3	0.7	69.0
Sun Hydrolene 125	3.5 ± 1.1	7.8 ± 1.0	0.3 ± 0.4	91.9 ± 1.3
Sun Hydrolene 600T	8.3 ± 1.5	20.8	1.2	78.1
Abilene AC-3	264 ± 23.3	11.1	11.8	77.1

Table 7-2. Final Mixture Table

Blend	Agent Content	Viscosity	Saturate	Asphal- tene	Aromatic	HS
Coastal-YBF F3	31.4	5540	14.6	21.5	63.9	3.67
Coastal-YBF F2	28.0	5030	17.6	23.3	59.1	4.79
Coastal-Cyclogen	17.0	5750	16.8	25.3	57.9	4.52
Coastal-Nuso 95	15.8	5040	16.9	27.0	56.0	5.60
Coastal-110T	18.0	5570	17.9	25.0	57.1	5.92
Coastal-125	14.8	5350	14.5	28.4	57.1	4.61
Coastal-600T	21.9	5340	17.4	25.3	57.3	5.06
Coastal-AC3	39.1	5320	15.0	25.2	59.7	4.11
Fina-YBF F3	32.0	6200	12.1	23.5	64.4	2.90
Fina-YBF F2	26.6	5780	14.5	23.6	61.9	3.45
Fina-Cyclogen	17.0	6330	13.7	26.5	59.7	3.39
Fina-Nuso 95	13.5	6140	12.8	26.8	60.4	3.37
Fina-110T	16.7	4790	15.7	26.7	57.6	3.61
Fina-125	15.5	5380	11.2	26.0	62.8	2.87
Fina-600T	21.5	4910	14.5	25.8	59.7	3.24
Fina-AC3	46.1	5240	13.0	23.2	63.7	3.21

correct low pressure HS. However, it is obvious that the HS for the Coastal blends show much more variation than the HS for the Fina blends.

Possible correlations between compositional variables and the HS were explored. Single correlations were explored first. Figure 7-1 shows the lack of correlation between HS and initial blend asphaltene content. This is due to the lack of variation in asphaltene content resulting from the approximately equal amounts of asphaltene free recycling agents added to rejuvenate the parent material. While a somewhat qualitative trend can be seen in Figure 7-2 for the HS as a function of total aromatic content, there is still much scatter. Figure 7-3 shows a much better correlation between HS and blend saturate content. However, two of the best correlations arise from combinations of these variables. The aromatic/saturate ratio is similar to the Rostler parameter N/P and correlates very well as shown in

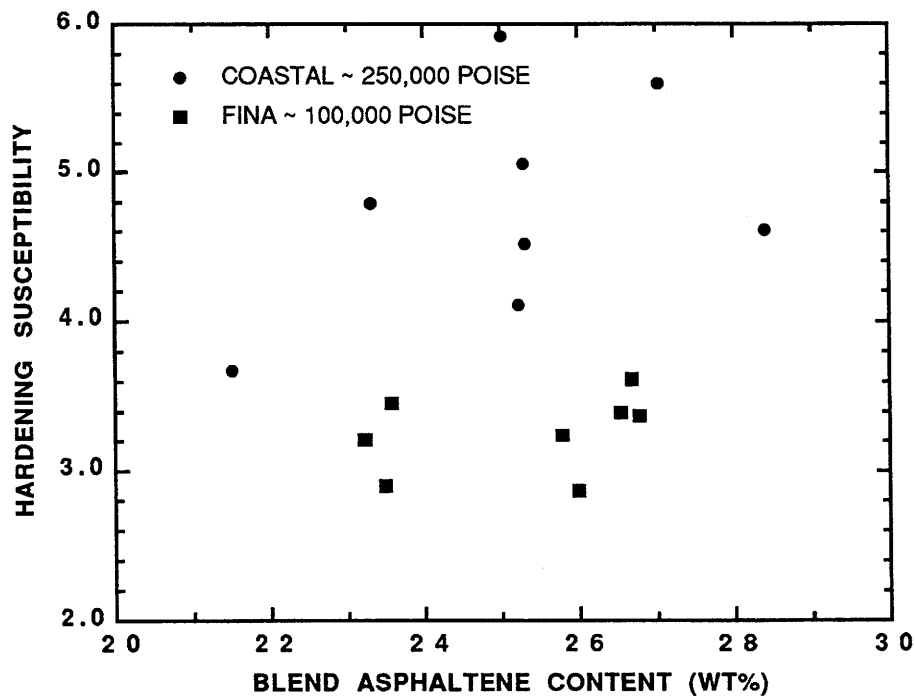


Figure 7-1. Blend HS Versus Initial Blend Asphaltene Content

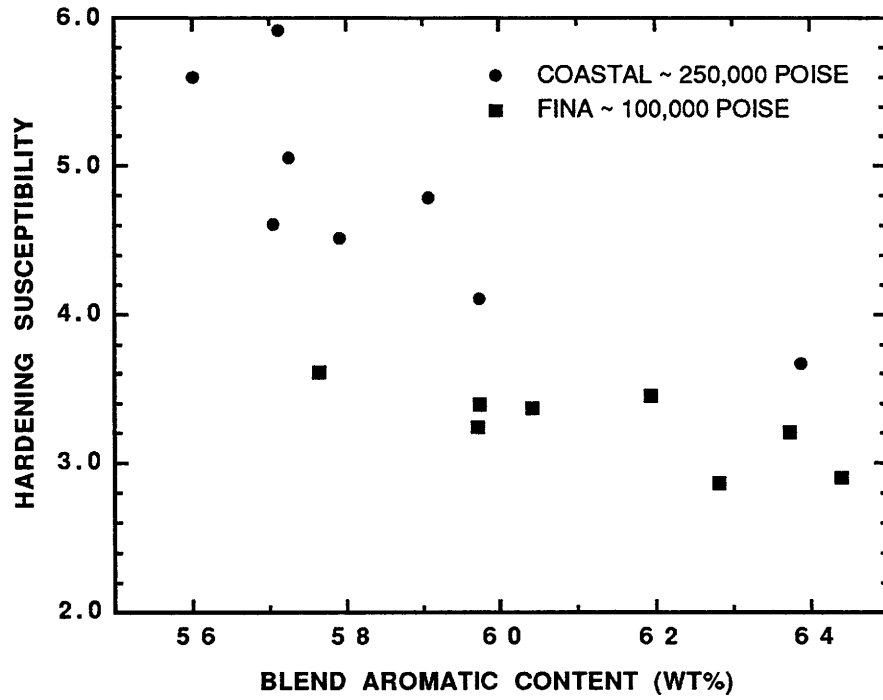


Figure 7-2. Blend HS Versus Initial Blend Aromatic Content

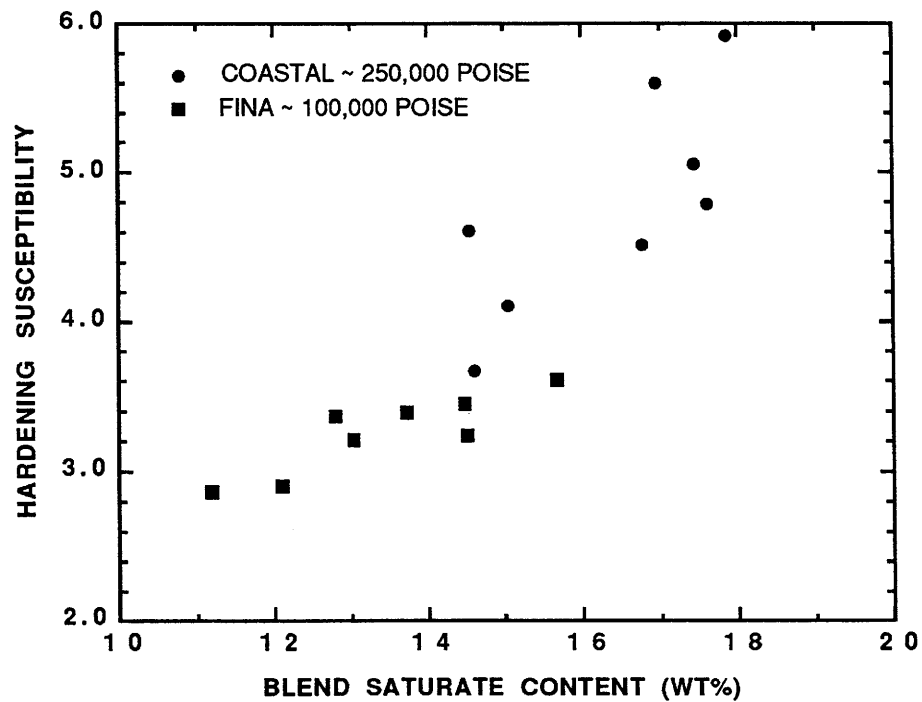


Figure 7-3. Blend HS Versus Initial Blend Saturate Content

Figure 7-4. The apparent continuous trend for the data is somewhat misleading. There are clearly two separate data sets: the data from the eight blends using the hardened Fina and the eight blends using the aged Coastal. There is relatively little difference in the HS of the Fina blends and a large difference in the HS for the Coastal blends with similar ranges in the AR/SA ratio.

The second compositional parameter that correlated reasonably well is the ratio of asphaltenes plus saturates divided by total aromatics $[(AS+SA)/AR]$. This grouping of data is referred to as the Gastel index or the colloidal stability index (I_c). Ishai et al. (1993) have shown that I_c correlates well with the viscosity of asphalts. This correlation is good not only for the viscosity of tank materials, but also for the viscosity of aged asphalts. Therefore, it is not surprising that this variable correlates with the HS as shown in Figure 7-5.

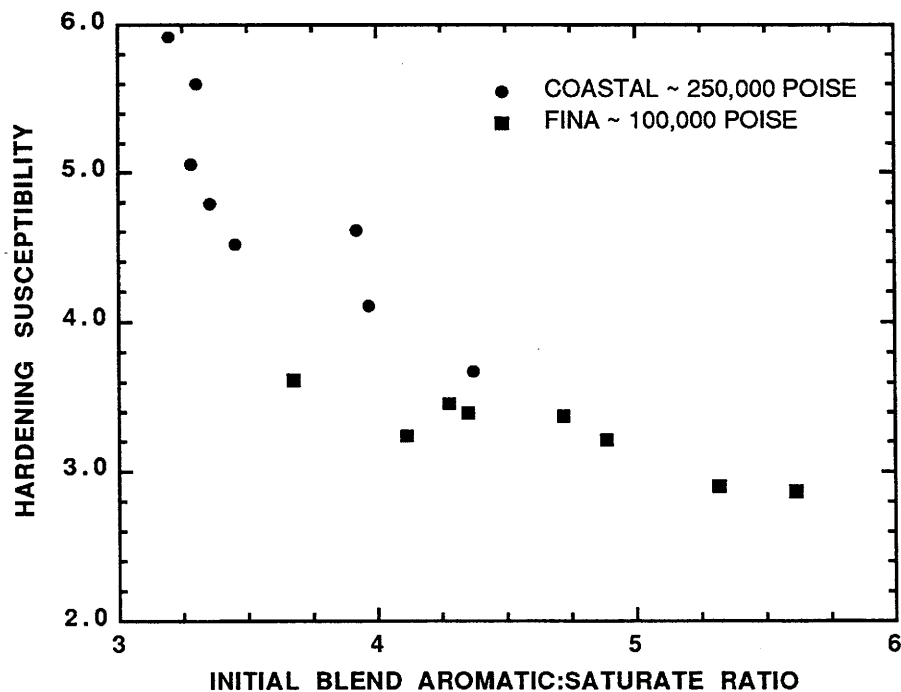


Figure 7-4. Blend HS Versus Initial Blend AR/SA Ratio

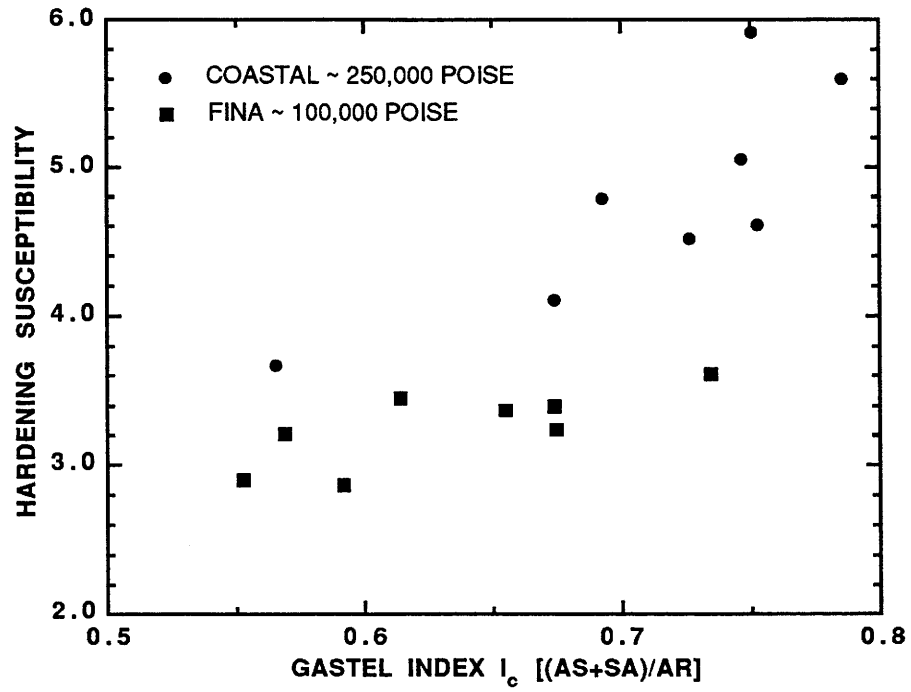


Figure 7-5. Blend HS Versus Initial Blend I_c

CHAPTER 8

MIXING RULES

Irving (1977a) conducted a survey of equations proposed to effectively describe the viscosity of binary liquid mixtures. This survey identified more than fifty equations proposed to predict either the dynamic or kinematic viscosity of binary liquid mixtures. Irving (1977b) also determined the effectiveness of the various mixture equations. Irving concluded that Equation 8-1, the equation proposed by Grunberg and Nissan (1949), was the best overall mixing rule in terms of accuracy and simplicity for predicting the viscosity of non-aqueous binary systems.

$$\ln \eta_m = x_1 \ln \eta_1 + x_2 \ln \eta_2 + x_1 x_2 G_{12} \quad (8-1)$$

The interaction parameter G_{12} is usually considered to be a constant; however, G_{12} may be a function of x_i where x_i may be mole, mass, or volume fraction. Irving determined that the viscosity of a mixture can be predicted to within 30% of the actual viscosity when an average, constant value of G_{12} was used for classes of mixtures (i.e. polar/polar). In addition, Irving's calculations (1977b) indicate that the choice of units for x_i (mole, mass, or volume fraction) make little difference in the accuracy of the model. Mehrotra (1990, 1992) has used the Grunberg equation to model bitumen/gas and bitumen/solvent systems. However, very little effort has been focused on using this equation to predict the viscosity of asphalt/softening agent mixtures. Instead, the majority of predictions are based on two other models.

The method proposed by Epps et al. (1980) is based loosely on the mixing rule of Roelands (1966). The nomograph presented by Epps suggests that $\log \log \eta$ for the mixture is a linear combination of $\log \log \eta$ for the pure components in terms of mass fraction or volume fraction and the Roelands model uses $\log \log 10\eta$. Other variations of the Roelands model have been proposed for recycled asphalts including

that proposed by Dunning and Mendenhall (1978). Although Epps' rule has received much attention, the rule most commonly used to estimate a recycled asphalt binder's viscosity is the procedure specified in ASTM D4887. This procedure, also suggested by The Asphalt Institute (1981), is the graphical representation of the equation proposed by Arrhenius (1887). The Arrhenius equation is a special case of the Grunberg equation with G_{12} equal to zero. Irving (1977b) concluded that using the Grunberg model with G_{12} equal to zero resulted in errors larger than those obtained using an optimized or average value of G_{12} , if it is available. Large errors may require actual blending to determine a mixture's viscosity. Epps and ASTM indicate that some degree of trial and error blending may be necessary to achieve an accurate viscosity for a recycled binder.

The results of Irving indicate that it is possible to use an average interaction parameter for the Grunberg model to describe certain classes of mixtures. The present study was undertaken to determine if the Grunberg equation can be used for describing aged asphalt/softening agent mixtures and if an average interaction parameter can be used for asphalt/softening agent pairs.

EXPERIMENTAL METHODS

To produce viscosity mixing rules, tank asphalts were artificially aged and then blended with softening agents in various ratios. Once the aged material had been produced, it was reheated in a laboratory oven and homogenized with a mixing paddle driven by a hand-held drill. Ideally, all of the aged material for a single asphalt was weighed at the same time so that all of the blends would have the same base material. For one asphalt, the sample was reheated, causing the viscosity to change. This viscosity change was taken into account and had no effect on the results of this study.

After the aged material was weighed into tins, the softening agent was added. Each blend contained a total of at least 30 g (1.06 oz) of material. It was determined that 30 g (1.06 oz) would be sufficient for viscosity testing and also minimize blend

homogeneity problems. Each blend was mixed using a procedure similar to that specified in ASTM D4887.

The primary property of interest was the 60°C (140°F) low frequency limiting dynamic viscosity. Table 8-1 lists representative viscosities for all materials examined in this study.

Compositional analyses of the softening agents were performed via HPLC analysis as described in Appendix A.

AGED ASPHALT PRODUCTION

Four asphalts were used in this study. Two of these asphalts were aged to multiple viscosities giving a total of seven aged materials. Three tank asphalts were obtained from the SHRP/LTPP MRL, and one tank asphalt was obtained from the Coastal refinery in Corpus Christi, Texas. Two samples were aged in a pressure oxygen vessel (POV) at 82.2°C (180°F) and 20.7 bar (300 psia) pure oxygen. One sample was produced by aging in a laboratory oven. The majority of the aged material was produced in the air-bubbled (AB) reaction apparatus.

Small amounts of SHRP AAA-1 and SHRP ABM-1 were POV-aged. The quantity of POV-aged AAA-1 produced was sufficient to blend with only one softening agent and the amount of POV-aged ABM-1 was sufficient for blending with two softening agents. The Coastal asphalt was aged in 6 mm (1/4") films on cookie sheets placed in a laboratory oven at approximately 110°C (230°F). The trays were rotated and the asphalt was stirred twice per day to encourage uniform aging. This oven-aged Coastal was blended with four softening agents. To produce the large amounts of material that were necessary for this study, a different aging procedure had to be developed.

Kilogram quantities of aged SHRP AAA-1 and SHRP AAF-1 were produced in the air-bubbling (AB) apparatus described in Chapter 5. Both asphalts were aged to two different viscosity levels. The aged AAA-1 samples are designated as AAA-AB7 (SHRP AAA-1 air-bubbled sample 7) and AAA-AB8, and the aged AAF-1

Table 8-1. Representative Viscosities for Aged Asphalts and Softening Agents

	MATERIAL	η_o^* (poise)
Aged Asphalts:	POV AAA-1	22,500
	AAA-AB7	22,900 ^a
	AAA-AB8	36,600
	AAF-AB1	52,500
	AAF-AB2	20,900
	Oven Coastal	100,000
	POV ABM-1	47,200
Recycling Agents:	NUSO 95	1.3
	Mobil 120	1.8
	Sun 125	3.0
	Cyclogen	8.9
	AAF F2	12
	AAA F2	13
	YBF F2	38
	YBF F5	47
	AAF F3	70
	AAA F3	79
	ABM F2	98
	ABM F5	100
	YBF F3	138
	Shell F3	165
ABM F3	650	
Low Viscosity Asphalts:	DS AC-3	310
	DS AC-5	500
	Shell AC-5	575
	SHRP AAV	630
	SHRP ABH	900

^a Initial value

samples are designated as AAF-AB1 and AAF-AB2.

SOFTENING AGENTS

Twenty-one different softening agents were utilized in this study. These twenty-one softening agents can be separated into two main classifications: low viscosity asphalts and recycling agents. The recycling agents can be further separated into commercial agents and supercritical fractions. Additionally, the n-hexane maltene of one of the asphalts was used for one experiment.

Two asphalts, AAV and ABH were obtained from the SHRP/LTPP MRL. An AC-3 and an AC-5 were obtained from the Diamond Shamrock (DS) refinery in Dumas, Texas and an AC-5 was acquired from the Shell refinery in Deer Park, Texas. Four non-emulsified commercial agents were obtained: Sun Hydrolene 125, Witco Cyclogen, Exxon NUSO 95, and Mobil Mobilsol 120. The supercritical fractions were produced in the four stage asphalt supercritical extraction pilot plant at Texas A&M University.

The supercritical fractions were produced from five source asphalts. These source asphalts for the supercritical fractionation were obtained from a local pavement contractor, Shell, and the SHRP/LTPP MRL. The asphalt acquired from the local contractor is an AC-20 asphalt and is identified as YBF. The YBF, SHRP AAA-1, ABM-1, and AAF-1 asphalts were fractionated in two runs. The first run removed the asphaltenes and heavy polar aromatic materials and produced a large low molecular weight fraction rich in naphthene aromatics and saturates. The majority of this fraction was further fractionated into four additional fractions. The lightest of the fractions is designated as fraction 1 (F1) and the heaviest is designated as fraction 8 (F8). The majority of the supercritical fractions used in this study are either F2 or F3 from these two run fractionations; however, some of the lightest fraction from the primary fractionation (F5) was used as a recycling agent. The Shell asphalt, an AC-20, was fractionated in only one run. As a result, the fraction used in this study, F3, contains a small amount of asphaltenes.

EXPERIMENTAL DESIGN AND RESULTS

The first two experiments were performed to determine the validity of the approach and to test the air-bubbling aging technique. The first experiment consisted of blending Sun Hydrolene 125, or simply Sun 125, with the POV AAA-1 in 10% increments of aged asphalt by mass. Figure 8-1 shows that 10% increments are not necessary to determine the relationship between viscosity and asphalt mass fraction. Furthermore, this experiment shows that the blends exhibit significant deviation from the viscosity predicted by the ASTM nomograph, the straight line connecting the pure materials.

The second experiment was performed using Sun 125 as the recycling agent and AAA-AB7 as the aged asphalt. AAA-AB7 has approximately the same viscosity as the POV AAA-1 used in the first experiment. Aged material content varied from 0% to 100% in 20% increments. The value of the Grunberg interaction parameter was determined by fitting the data from these two experiments in terms of \ln viscosity. Figure 8-1 shows that the Grunberg equation is capable of modeling the data for these first two experiments. The data for the AB-aged material show only minor differences from the POV-aged material data. The result of this experiment further supports the ability of the air-bubbling apparatus to produce quality aged material.

The first aged asphalt studied systematically was AAF-AB2. This material was blended with three asphalts and eight recycling agents. Each AAF-AB2/softening agent pair was blended at levels from 0% to 100% in 20% increments. The data for all AAF-AB2/softening agent pairs are adequately described by the Grunberg model. Although Figure 8-2 shows that there is some deviation between the data and the fit through the data, a single parameter for each asphalt/softening agent pair is able to model the data adequately. In addition, this parameter is constant, independent of aged asphalt mass fraction. It is immediately obvious from these data that there is a negative deviation from the straight line that would connect the pure-component endpoints for the recycling agents.

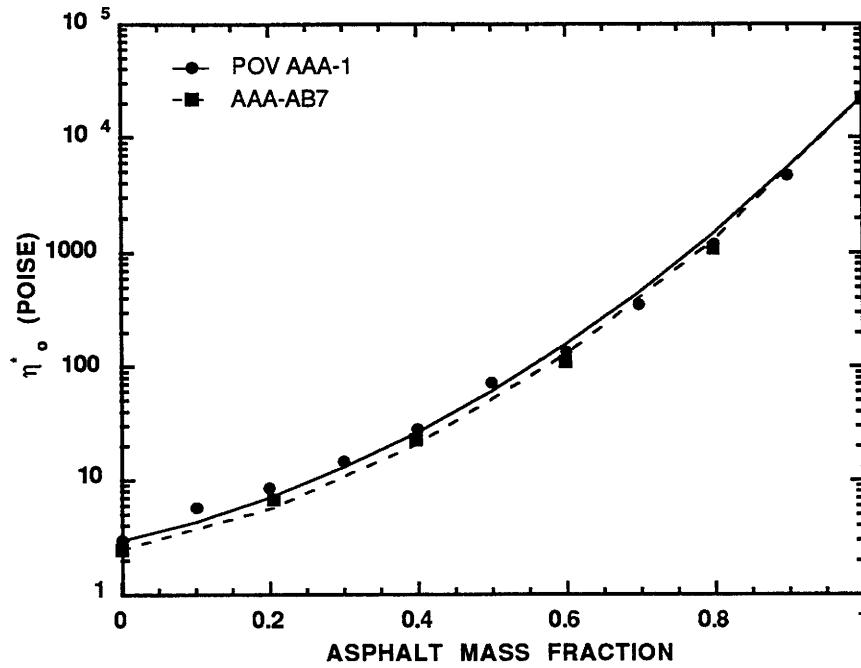


Figure 8-1. Viscosity for POV AAA-1 and AAA-AB7 Blends with Sun 125

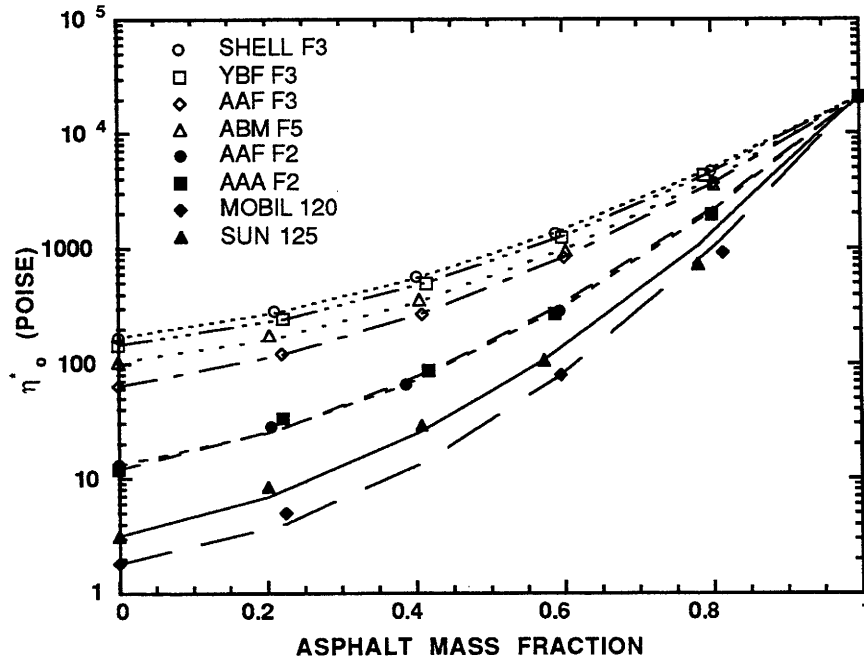


Figure 8-2. Viscosity for Blends of AAF-AB2 with 8 Recycling Agents

Figure 8-3 shows that the data for the asphalt/low viscosity asphalt pairs, however, are near or above the straight line representing the ASTM nomograph. This suggests that the recycling agent blends should be treated separately from the asphalt/low viscosity asphalt pairs.

Table 8-2 shows the value of the interaction parameter for each asphalt/softening agent pair. The interaction parameter varies considerably depending on the softening agent, indicating that using an average value for the interaction parameter would result in substantial error. The only noticeable trend from these data is that the interaction parameter decreases (i.e., becomes more negative) as the agent viscosity decreases for the recycling agents. From this, it was hypothesized that some of the variation in this parameter is due solely to the viscosity difference between the softening agent and the aged asphalt.

To eliminate this viscosity effect, it is necessary to normalize the data. The Grunberg equation may be rearranged such that the pure component endpoints are zero for the pure softening agent and unity for the pure aged asphalt. The

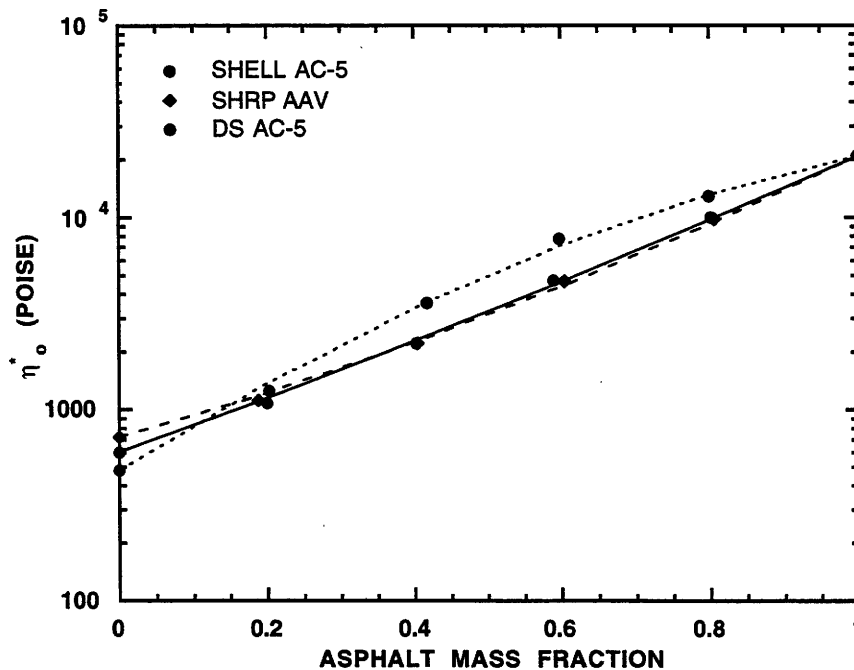


Figure 8-3. Viscosity for Blends of AAF-AB2 with 3 Low Viscosity Asphalts

Table 8-2. Aged Asphalt/Agent Grunberg Interaction Parameter G_{12}

ASPHALT	AGENT	G_{12}	ASPHALT	AGENT	G_{12}
POV AAA-1	Sun 125	-5.80	AAA-AB7	Sun 125	-6.31
AAA-AB7	Cyclogen	-6.28	AAA-AB7	YBF F2	-5.42
AAA-AB7	YBF F5	-4.28	AAA-AB7	ABM F2	-4.63
AAA-AB7	YBF F3	-3.45	AAA-AB7	ABM F3	-4.10
AAA-AB7	SHRP ABH	0.03			
AAA-AB8	Cyclogen	-6.33	AAA-AB8	AAA F2	-5.47
AAA-AB8	YBF F5	-4.03	AAA-AB8	AAA F3	-4.77
AAA-AB8	AAF F3	-4.52	AAA-AB8	DS AC-3	---
AAA-AB8	DS AC-3	---	AAA-AB8	Shell AC-5	1.14
	Maltene				
AAA-AB8	SHRP AAV	-0.46	AAA-AB8	NUSO 95	-6.23

AAF-AB1	NUSO 95	-8.42	AAF-AB1	AAF F2	-5.88
AAF-AB1	ABM F2	-4.88	AAF-AB1	AAA F3	-4.56
AAF-AB1	Shell F3	-3.64	AAF-AB1	ABM F5	-4.90
AAF-AB1	DS AC-5	2.57	AAF-AB1	SHRP ABH	0.08
AAF-AB1	DS AC-3	2.18	AAF-AB1	ABM F3	-3.99
AAF-AB1	Mobil 120	-7.69			
AAF-AB2	Sun 125	-6.24	AAF-AB2	Mobil 120	-7.50
AAF-AB2	AAA F2	-4.83	AAF-AB2	AAF F2	-5.26
AAF-AB2	ABM F5	-3.95	AAF-AB2	YBF F3	-3.39
AAF-AB2	AAF F3	-3.81	AAF-AB2	Shell F3	-3.12
AAF-AB2	Shell AC-5	-0.37	AAF-AB2	SHRP AAV	-0.88
AAF-AB2	DS AC-5	1.82			

Oven Coastal	Sun 125	-10.71	Oven Coastal	Cyclogen	-9.28
Oven Coastal	YBF F3	-6.54	Oven Coastal	YBF F5	-6.90
POV ABM-1	ABM F3	-1.48	POV ABM-1	ABM F2	-3.39

normalized Grunberg model is given as Equation 8-2, with the aged asphalt as component 2 and the recycling agent as component 1.

$$DLV = \frac{\ln (\eta_m / \eta_1)}{\ln (\eta_2 / \eta_1)} = \left(1 + \frac{G_{12}}{\ln (\eta_2 / \eta_1)}\right) x_2 + \left(\frac{-G_{12}}{\ln (\eta_2 / \eta_1)}\right) x_2^2 \quad (8-2)$$

The Dimensionless Log Viscosity (DLV) can be fit as a second order polynomial with respect to x_2 , the aged asphalt mass fraction. The coefficient on the second order term can be viewed as the normalized Grunberg interaction parameter. Figure 8-4 shows the normalized viscosity plotted as a function of mass fraction for the AAF-AB2/softening agent pairs. The data for the asphalt pairs show remarkably little difference when analyzed in this manner. Even though recycling agent saturate content varies from 8% to 23% and the aromatic content varies from 77% to 92%, all of the recycling agents produce the same DLV for a given aged asphalt mass

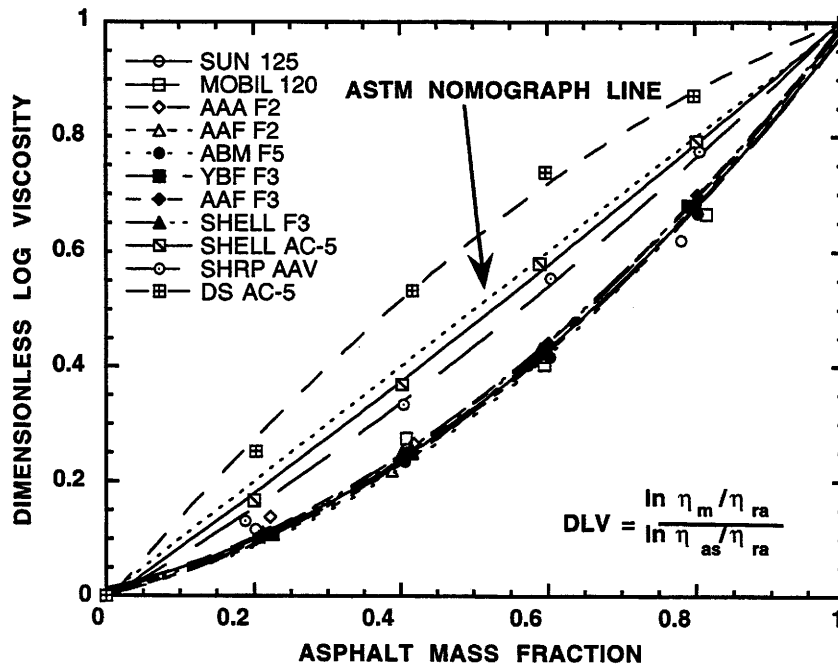


Figure 8-4. Dimensionless Log Viscosity for AAF-AB2 Blends

fraction. This result complicates the correlation of interaction parameter with recycling agent chemical composition.

The asphalt/low viscosity asphalt pairs do not collapse to a single grouping of data. SHRP AAV and the Shell AC-5 have similar interactions with AAF-AB2 and would be well predicted by the ASTM nomograph, but the DS AC-5 exhibits significant positive deviation. Even though these low viscosity asphalts do not exhibit behavior similar to the recycling agents, blends with all three asphalt softening agents can be modeled using the Grunberg equation in either the standard or normalized forms. Additionally, the AAF-AB2 data show that it may be possible to use an average value for the normalized interaction parameter for asphalt/low viscosity asphalt systems.

The next aged asphalt studied was AAF-AB1. This material was blended with three asphalts and eight recycling agents. Each asphalt/softening agent pair was blended at levels from 0% to 100% in 20% aged asphalt increments. Of these eleven softening agents, one of the asphalts and four of the recycling agents were the same as those blended with AAF-AB2. One of the recycling agents, ABM-1 F3, has a viscosity in the AC-5 range but with no asphaltenes and a low saturate content.

The Grunberg model describes the data for these asphalt/softening agent pairs well. As Table 8-2 shows, the value of the interaction parameter varies considerably from softening agent to softening agent and is different for an agent blended with AAF-AB1 and that same agent blended with AAF-AB2. Without exception, the absolute value of the interaction parameter was larger for an AAF-AB1 agent pair than for an AAF-AB2 agent pair. Once again, this suggests that there is some effect due solely to the viscosity difference between the aged asphalt and the softening agent.

The normalized viscosity data for the AAF-AB1/softening agent blends are plotted in Figure 8-5. There is more variation in the data for the AAF-AB1 recycling agent blends than there is for the AAF-AB2 recycling agent blends, but there is still remarkably little difference.

The AAF-AB1 recycling agent and AAF-AB2 recycling agent data are plotted

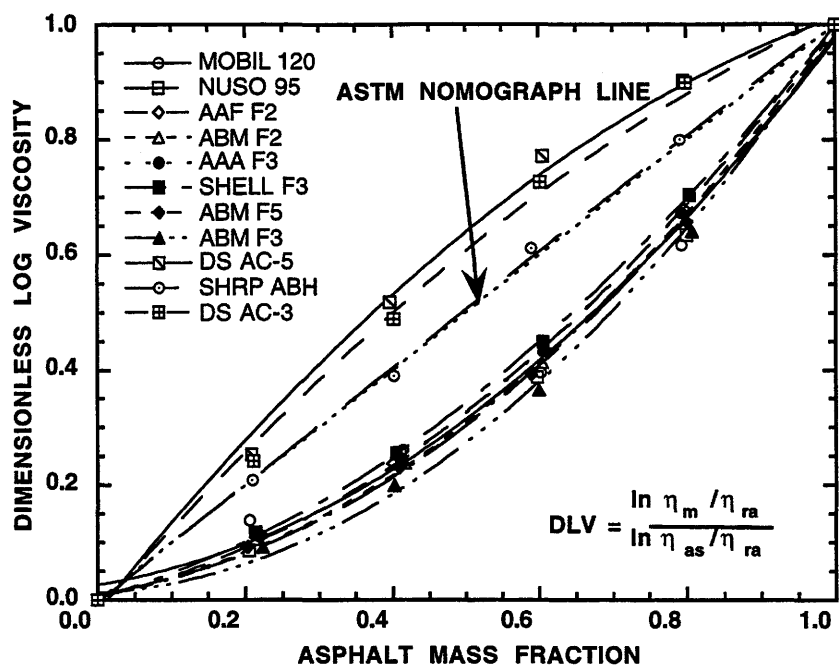


Figure 8-5. DLV Versus Aged Asphalt Mass Fraction for Blends Using AAF-AB1

together in Figure 8-6. It is clear that there is much similarity between the two sets of data. Blends of recycling agents with 20,900 poise AAF-1 and blends with 52,500 poise AAF-1 have essentially the same DLV for a given aged asphalt mass fraction, indicating that an average normalized interaction parameter can be used for AAF-1 recycling agent mixtures.

As was the case in the AAF-AB2 blends, the AAF-AB1/low viscosity asphalt pairs do not collapse to a single grouping of data. Figure 8-5 shows that the DS AC-3 and DS AC-5 exhibit similar positive deviations but that SHRP ABH shows no significant deviation from the behavior predicted by the ASTM nomograph. The behavior for the high viscosity supercritical fraction ABM-1 F3 is similar to the behavior of the recycling agents, demonstrating that a high viscosity material can exhibit negative deviations. Once again, the Grunberg model seems adequate to describe all of the data.

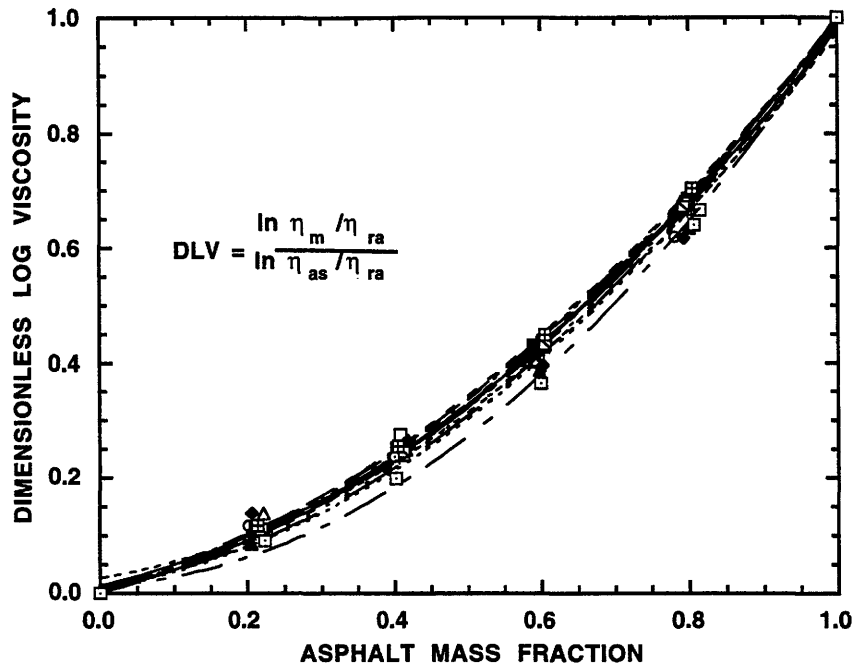


Figure 8-6. DLV for Blends of AAF-AB2 and AAF-AB1 with Recycling Agents

Next, AAA-AB7, which was blended with Sun 125 in the second experiment, was blended with seven additional softening agents. The normalized Grunberg equation is able to model the AAA-AB7 data, as shown in Figure 8-7. Again, there is significant deviation between the recycling agents and the low viscosity asphalts. There are two important features of these experiments. The first is that the ABM-1 F3 agent, a high viscosity supercritical fraction, shows moderate deviation from the rest of the recycling agents. The second noticeable feature is that there is more scatter among the mixture data for AAA-AB7 blends than for AAF-AB2 blends, even though these aged materials have similar viscosities. This implies that AAF-AB1 will exhibit similar recycling behavior independent of the recycling agent used and that the mixture viscosity behavior of AAA-AB7 can be altered by the choice of recycling agent.

Aged material AAA-AB8 was blended with six recycling agents, 3 asphalts,

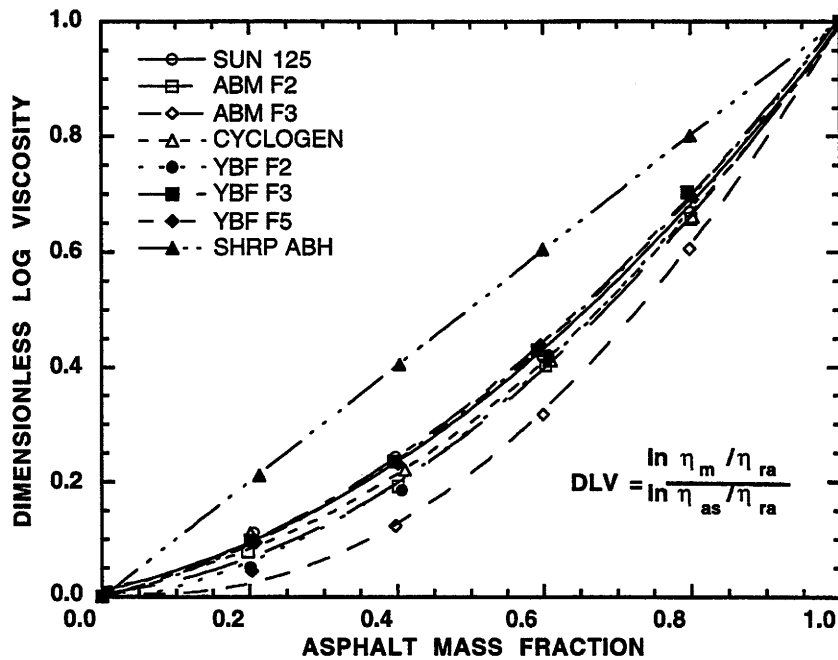


Figure 8-7. DLV for AAA-AB7 Blends

and DS AC-3's maltene. Once again, the recycling agents form a narrow band with respect to DLV, while the asphalts do not, as shown in Figure 8-8. There are two significant results from the AAA-AB8 data. First, with this asphalt, the Shell AC-5 shows positive deviation from the ASTM nomograph that it did not with AAF-AB2. Second, the Grunberg model fails miserably for the DS AC-3 and its maltene (Figure 8-9). In fact, the DS AC-3 and maltene data are highly sigmoidal, exhibiting negative deviation at low AAA-AB8 levels and positive deviation at high AAA-AB8 mass fractions. Additionally, Figure 8-9 shows that the DS AC-3 blends have larger DLV values than the maltene blends. Therefore, removing the asphaltenes from DS AC-3 has only a minor effect. This further complicates the correlation between viscous interaction and compositional parameters.

The oven-aged Coastal was blended with four different recycling agents. Aged asphalt content varied from 0% to 100% in 25% increments. The data from these

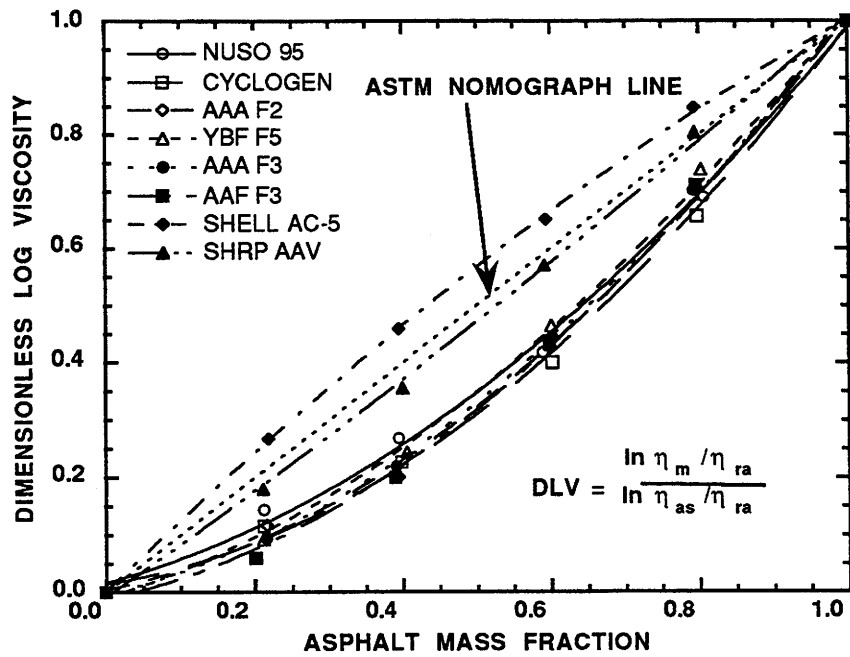


Figure 8-8. DLV for AAA-AB8 Blends

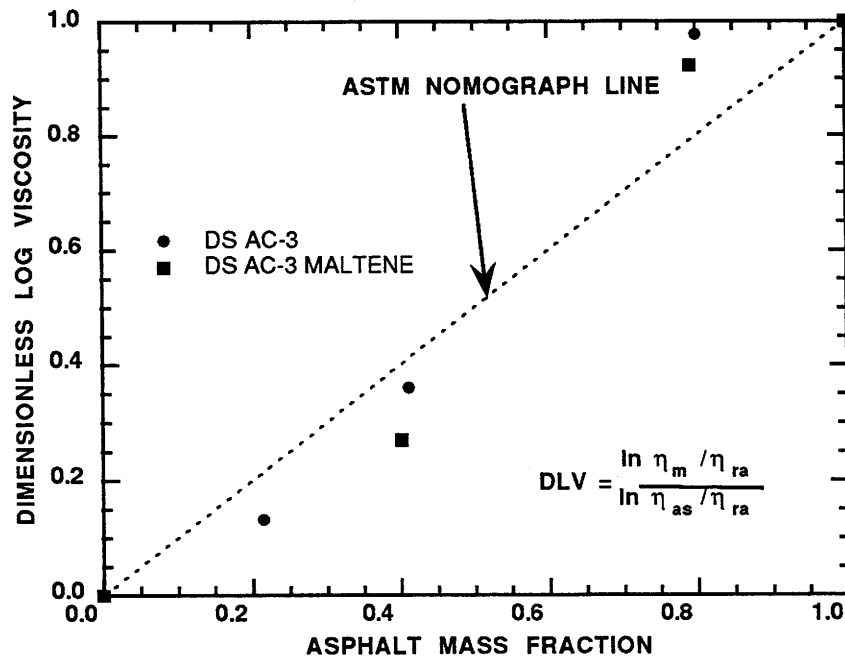


Figure 8-9. Anomalous Behavior of AAA-AB8/DS AC-3 Blends

blends also form a narrow band in terms of the DLV; however, this narrow band, shown in Figure 8-10, is significantly lower than the data for the other blends. Although these Coastal blends result in DLV's lower than the majority of the other asphalt blends, they are still not as low as the data for the AAA-AB7/ABM-1 F3 blends, Figure 8-7. The data obtained for the POV ABM-1 blends are somewhat higher than the average for the rest of the data. In fact, the POV ABM-1/ABM-1 F3 blend data shown in Figure 8-11 are closest to the diagonal line representing the ASTM suggested mixing rule. Thus, blends made with ABM-1 F3 as the recycling agent form both the high and low boundaries of data collected in this study.

DISCUSSION OF RESULTS

All of the recycling agent blend data collected in this study were placed on the same plot of DLV versus asphalt mass fraction. An overall mixing rule was determined by fitting the DLV data to a second order polynomial. Figure 8-12 shows the complete data and overall fit. This overall DLV mixing rule was used to predict the amount of recycling agent necessary to obtain specification blends for all of the asphalt/softening agent pairs used in this study with the exception of the AAA-AB7/DS AC-3 material blends. The log log η mixing rule suggested by Epps and the ASTM nomograph were used for comparison. Two target viscosities were also compared. A target viscosity of 2000 poise was chosen because this is the specification for an AC-20 asphalt and the probable target viscosity for Hot Mix Recycling. A target viscosity of 5000 poise was also chosen. This is a reasonable value for an AC-20's viscosity after Thin Film Oven Test (TFOT) treatment and a probable target viscosity for Hot-In-Place Recycling. The amount of recycling agent required was calculated for each mixing rule and then the actual mixture viscosity was determined from the Grunberg interaction parameter for the individual asphalt/softening agent pair. If the predicted softening agent content was less than 10%, the data were considered unreliable because unrealistically high actual viscosities resulted (mostly for the Epps rule). The resulting viscosities were

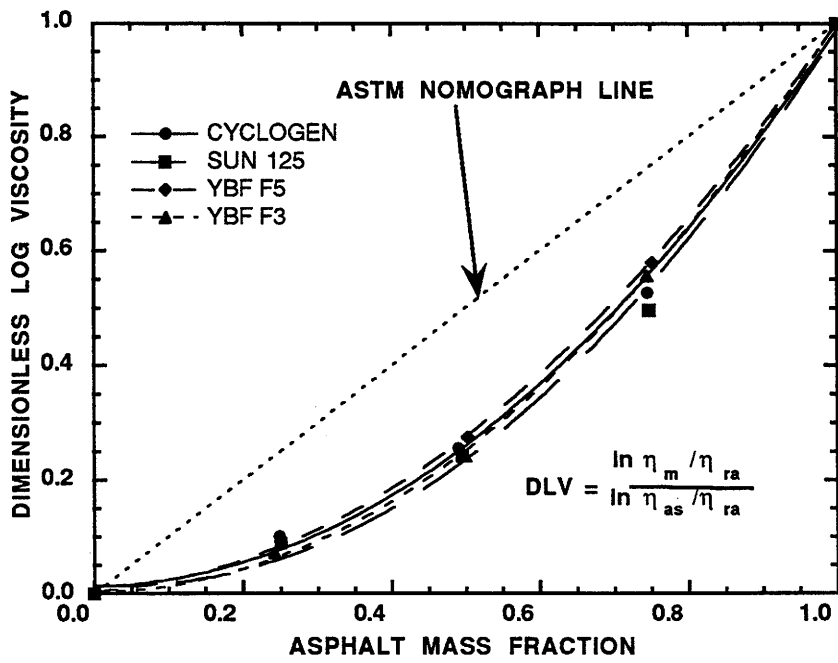


Figure 8-10. DLV for Oven Coastal Blends

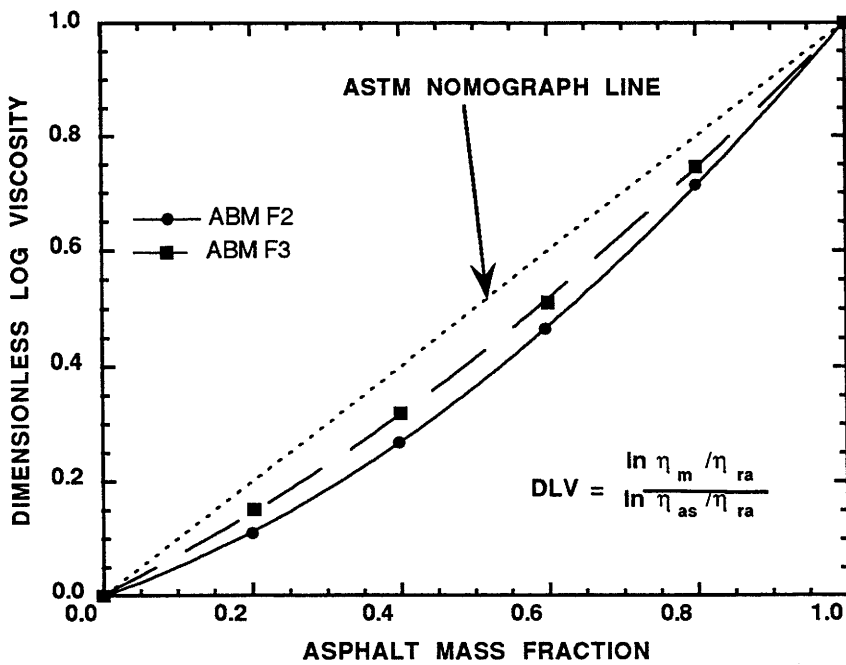


Figure 8-11. DLV for POV ABM-1 Blends

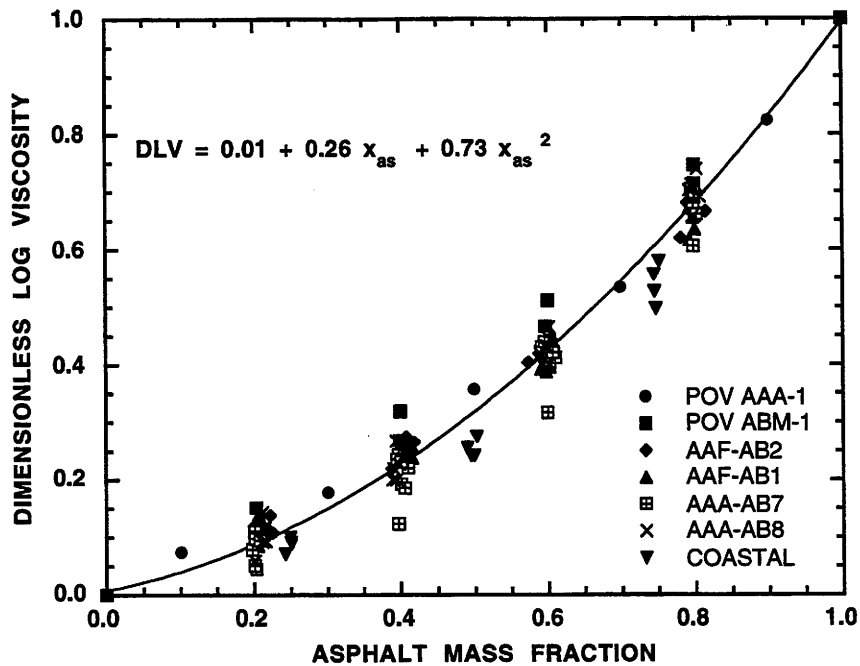


Figure 8-12. DLV Mixing Rule for All Recycling Agent Blends

calculated and an average value was obtained for the recycling agent blends as a group and for the low viscosity asphalts as a group.

The average viscosities that would result from prediction using each model are given in Table 8-3. In addition to the average viscosity, the range of viscosities resulting from each model are listed. From these data, it is obvious that the DLV mixing rule using an average normalized interaction parameter is superior to the other two mixing rules. This is to be expected because the DLV mixing rule is based on the very data that it is predicting. However, the ability of the DLV mixing rule to produce AC-20 blends nearly 95% of the time is an extraordinary result given the extreme variation, both in terms of standard deviation and range, for the other two models. This shows that the current methods are inadequate at predicting proper recycling agent content. In fact, the ASTM nomograph results in completely unacceptable viscosities for better than 95% of the hypothetical mixtures. This

Table 8-3. Comparison of Viscosities Resulting from Various Mixing Rules

Recycling Agent
Target Viscosity 2000 dPa·s (poise)

Model	Avg. Viscosity	Low	High
DLV	2040±390	1100	3000
Epps	1920±1200	780	6730
ASTM	700±370	160	2340

Recycling Agent
Target Viscosity 5000 dPa·s (poise)

Model	Avg. Viscosity	Low	High
DLV	5010±840	3120	7350
Epps	4380±1490	2140	9190
ASTM	1880±570	540	3460

Asphalt Softening Agents
Target Viscosity 2000 dPa·s (poise)

Model	Avg. Viscosity	Low	High
DLV	5320±2200	2960	8800
Epps	3310±1190	1910	5090
ASTM	2430±680	1660	3410

Asphalt Softening Agents
Target Viscosity 5000 dPa·s (poise)

Model	Avg. Viscosity	Low	High
DLV	11500±4300	6900	19200
Epps	8380±3000	4800	13000
ASTM	6180±2000	4030	9500

substantiates the findings of Irving (1977b) as to the accuracy using G_{12} equal to zero. Use of the ASTM nomograph would certainly result in much trial and error to obtain the correct viscosity for these asphalt/recycling agent blends.

For prediction of the asphalt softening agent data, the DLV mixing rule does not perform very well. The average, deviation, and range are all larger than those obtained by the other mixing rules. The ASTM nomograph procedure is best at predicting the asphalt softening agent data. In fact, this method is remarkably good considering that these data include the blends formed by the DS asphalts and the Shell AC-5.

CHAPTER 9

INTERSTATE 45 RECYCLING

A section of Interstate 45 (I-45) near Madisonville, Texas that was recycled in September and October 1993 was chosen as a recycling test section. The section of I-45 that was recycled starts at 1993 mile marker 137 and extends to mile marker 141. A two-mile stretch between mile marker 141 and mile marker 143 was not recycled, and then recycling continued for four miles between mile marker 143 and mile marker 147 using Hot-In-Place-Recycling (HIPR). Hot-In-Place-Recycling is a process where the existing material is heated in place, a set depth of the pavement is roto-milled, fresh hot mix and/or rejuvenator is added, and the mixture is placed on the road through the screed. All of this takes place in a continuous train of equipment. Addition of fresh hot mix allows the aggregate gradation of the pavement to be altered and slightly softens the pavement. Addition of rejuvenator reduces the viscosity and increases the penetration value. The final mixture should result in a pavement with the desired gradation and a viscosity similar to that of a fresh hot mix pavement.

SAMPLING

TxDOT personnel from the Bryan, Texas office assisted in obtaining 42 core samples of I-45 in the vicinity of Madisonville, Texas. Specifically, the cores were taken from the northbound outside lane in the sections of pavement that were recycled. These cores were taken at four locations, each location having different characteristics.

The first coring location starts exactly at 1993 mile marker 138 (MM138) and extends 4.6 m (15 ft) north. Ten cores were taken at this location. This section of pavement between MM137 and MM139 showed no obvious signs of distress. The pavement material from this location consisted solely of hot mix asphalt

overlay placed in 1987. The section between MM137 and MM139 appears to be a control section.

The second location that was cored starts 412 m (1352 ft) past 1993 mile marker 139 and extends 5.2 m (17 ft). The pavement in the vicinity of this location was suffering from severe rutting. To eliminate the ruts, maintenance crews had placed rubberized crack seal in large patches in the wheel ruts. This had resulted in some traction problems over the previous winter, so the maintenance crews had also placed some cold mix asphalt on top of the crack seal patches to improve traction. Eleven cores were taken from one patch of this crack seal from the right wheel path.

The third location that was cored was in the neighborhood of mile marker 140. The pavement in this location also was suffering from rutting and had been treated only with the rubberized crack seal in the wheel ruts. Again, the crack seal had only been used in patches. Eleven cores were taken from one crack seal patch located 19.7 m (64.5 ft) past MM140. The cores were taken over a distance of 5.5 m (18 ft).

The last location studied had been treated at some time with the crack seal to eliminate rutting. However, the entire section of road was later treated with a 0.64 cm ($\frac{1}{4}$ in) rubberized chip seal. The entire section of pavement between MM143 and MM147 was treated in this manner. Ten cores were taken starting 6.1 m (20 ft) past MM145 extending 5.8 m (19 ft).

The cores can be considered as the untreated material from their relative locations. In addition to these cores, samples were taken periodically throughout the recycling process to follow the physical property (viscosity) changes that occur in the pavement at different stages of the recycling process. By taking samples of the heated and milled material, or post-heater (PH) material, it is possible to determine the change in viscosity that takes place as a result of the heating conditions used in the HIPR process. In fact, this material, and not the untreated material, should be considered as the base starting material for recycling. Samples of the add hot mix or add mix and emulsified rejuvenating agent were also

obtained, but as yet have not been used for any analyses. Finally, samples of the rejuvenated asphalt were obtained from regions similar to those locations that were cored. The rejuvenated material was obtained prior to passing through the screed and is referred to as pre-screed (PS) material.

At least 0.0076 m³ (2 gal) of PH material, at least 0.0038 m³ (1 gal) of add hot mix, and at least 0.0038 m³ (1 gal) of PS material was obtained from locations near the cored areas. PH material was obtained 19.5 m (64 ft) south of MM138 and the PS material was obtained 25.3 m (83 ft) south of MM138. There were no major problems with the recycling of this untreated, undistressed pavement.

PH material was taken from 431 m (1414 ft) north of MM139 and PS material was taken 425 m (1394 ft) north of MM139. These MM139+ locations do not correspond exactly with the MM139+ cores, but were taken from locations having material similar to that in the cores. Some problems were encountered with recycling the material in the vicinity of this location. First, the location lies in a slight depression, so there was some trapped moisture which did not allow proper heating. The presence of the rubberized crack seal compounded this problem, which not only helped to trap the moisture, but also prevented good heat transfer from the heaters to the pavement. In addition, the crack seal patches tended to burn, rather than soften and be mixed in with the other bituminous material.

PS samples were taken from 95.4 m (313 ft) south of MM140 and PH samples were taken from 88.1 m (289 ft) south of MM140. These MM140-sampling locations do not correspond to the MM140 core locations, but were taken from pavement with similar crack sealed areas. The recycling in this area suffered mainly from the burning rubber problem. This section of pavement is located on the crest of a slight incline and had little of the moisture problems associated with the MM139+ location.

The final location where samples were acquired is located near 1993 MM145. Severe problems were encountered with recycling the material that had been treated with the chip seal coat. The moisture content was a serious problem in this section because the chip seal had trapped a large amount of water in the

pavement. In addition, the presence of continuous polymer modified chip seal caused the entire area of the pavement to burn and resulted in oily rejuvenated asphalt. For both safety reasons and to ensure high quality recycling, the top 1.9 cm ($\frac{3}{4}$ in) were milled off of the pavement between MM143 and MM147 before the recycling was completed. PS samples were taken from 3.66 m (12 ft) north of MM145 and PH samples were obtained from 6.10 m (20 ft) north of MM145. As a result of the milling, the recycled material mix was adjusted to include more add mix to accommodate for this lost material and keep a level driving surface.

ANALYSES AND SAMPLING

One 7.5 cm (3 in) core from each location was tested to determine the void content. Some difficulty was encountered trying to determine the void content of the cores with the crack or chip seal, but values were obtained. These values are tabulated in Table 9-1 and they indicate that the rutting problems were not a direct result of the void content.

Cores from each location were extracted and recovered using the process described by Burr (1993). The extracted binders were subjected to FTIR and GPC analyses to determine if the extraction process had altered the binder and to confirm that complete solvent removal had been achieved. Once it was determined that the binder was solvent free and unchanged by the solvent, the 60°C (140°F) limiting dynamic viscosity was measured. The viscosities of the extracted cores are listed in Table 9-1.

Some of the cores were cut into two 3.75 cm (1.5 in) sections to determine if there were significant variations in viscosity with depth. If variations do occur with depth, it is necessary for TxDOT and other highway departments across the nation to consider only the depth of material to be recycled when determining the initial pavement properties. This study shows that there is significant variation with depth. MM 138 Core #1, #2 and #6 have viscosities of 12,200, 21,300, and 21,800 poise, respectively. These values were obtained from full 7.5 cm (3 in)

Table 9-1. I-45 Extraction Data

Sample	Viscosity	Void Content
MM 138 Core #3	21,300	3.8
MM 138 Core #1	12,200	-
MM 138 Core #6	21,800	-
MM 138 Core #9 Bottom	10,100	-
MM 138 Core #9 Top	58,000	-
MM 138 Core #10 Top	43,500	-
MM 138 PH Ext. #1	44,200	-
MM 138 PH Ext. #2	52,000	-
MM 138 PS Ext. #1	9,600	-
MM 138 PH	53,000	-
MM 139 Core #3	37,800	5.6
MM 139 PH Ext. #1	80,600	-
MM 139 PH Ext. #2	73,000	-
MM 139 PS Ext. #1	16,800	-
MM 139 PH	90,000	-
MM 140 Core #7	29,500	7.0
MM 140 PH Ext. #1	30,700	-
MM 140 PH Ext. #2	32,500	-
MM 140 PS Ext. #1	17,600	-
MM 140 PH	38,000	-
MM 145 Core #1	31,000	6.1
MM 145 PH Ext. #1	49,000	-
MM 145 PH Ext. #2	42,000	-
MM 145 PS Ext. #1	7,320	-
MM 145 PH	54,000	-

core samples. MM138 Core #9 top and #10 top have viscosities of 58,000 and 43,500 poise, respectively. MM138 Core #9 bottom has a viscosity of 10,100 poise. Although these data are limited, it is clear that there are significant differences in pavement properties with depth.

Similarly, the post-heater (PH) material was extracted and analyzed. The viscosities of the PH materials are also given in Table 9-1. From a limited amount of data on only MM138 samples, it is clear that the PH material has a viscosity similar to that of the top part of the cores that were extracted. MM138 Core #9 top and #10 top have viscosities of 58,000 and 43,500 poise while MM138 PH Extraction #1 has a viscosity of 44,200 poise and the combined binder from MM138 PH Extractions #1 and #2 has a viscosity of 53,000 poise. From the core extractions and the post-heater extractions, it is clear that TxDOT probably underestimated the viscosity (overestimated the pen) of the binder to be recycled. This would undoubtedly result in recycled asphalt that is hard and brittle.

To examine this possibility, pre-screed (PS) materials were also extracted and recovered. The viscosity of the recycled material from MM138 PS Extraction #1 is around 10,000 poise compared to the TxDOT target viscosity of 3,800 poise. This confirms that either TxDOT underestimated the viscosity of the binder to be recycled or the contractor did not add enough of the add mix or rejuvenating agent. The data for MM138 should be considered as solid, reliable data; however, the data from the other locations may be unreliable due to the presence of the rubberized crack seal. This rubber complicates the extraction and recovery process and may influence the properties of the recovered binder. As a result, no specific conclusions have been made concerning material from the MM139+, MM140-, and MM145 locations, even though the chip seal was removed from the MM145 location.

RECYCLING STUDIES

The extracted PH materials were blended with 6 softening agents. Two of

the recycling agents are supercritical fractions, YBF F3 and YBF F2. The other four softening agents are two commercial recycling agents and two AC-3 asphalts from different refineries. Each PH/softening agent pair was mixed using a procedure similar to that specified in ASTM D4887. The amount of softening agent required was not determined from the suggested mixing rule in ASTM D4887. Instead, the necessary amount of softening agent was determined from early mixing rules, not the mixing rules described in Chapter 8. The criteria for an acceptable blend was that the blend viscosity should be within 10% of the viscosity for the PS material at the same location. Tremendous difficulty was encountered in achieving this target viscosity with one of the AC-3 asphalts, so the recycled blends using this softening agent were not studied further.

Five samples of the five laboratory blends and the contractor's blend for each of the four I-45 locations (24 total blends, 120 total samples) were aged in the POV at 82.2°C (180°F) and 20.7 bar O₂ (300 psia). These aged materials were characterized by FTIR and their viscosities were determined. From these data, the hardening susceptibility (HS) for each recycled blend was determined. The 20.7 bar O₂ HS was chosen as the property for comparison between laboratory blends and the contractor's blend because the HS is a good representation of the physicochemical properties of the asphalt. Poor temperature control in the POV, the elevated oxygen pressure, and the small amount of sample prevented comparison on the basis of oxidation or hardening rate. However, some conclusions can be drawn from the viscosity of similarly aged materials.

The HS for each recycled mixture is given in Table 9-2. The 'Abilene' AC-3 softening agent blends have the worst HS for three of the four locations. The rest of the agents yield blends that have low HS for some locations and yield blends with high HS at others. These comparisons are based strictly on a relative scale. It is clear that there is little difference between the laboratory blends and the contractor's mix. Additionally, there is little difference between the commercial agents and the supercritical fractions in terms of HS.

The viscosities of the most highly-aged samples for each blend are also

Table 9-2. Blend HS and Most-Highly-Aged Sample Viscosity

PH Location	Rejuvenating Agent	HS	Highest Viscosity 10 ⁵ Poise
MM 138	Contractor	2.37	5.32
	YBF F3	2.66	4.55
	YBF F2	2.21	4.72
	Sun 125	2.02	3.61
	Exxon NUSO 95	2.25	4.44
	'Abilene' AC-3	2.54	13.3
MM 139+	Contractor	2.80	8.98
	YBF F3	2.20	8.91
	YBF F2	2.51	7.50
	Sun 125	2.28	5.95
	Exxon NUSO 95	2.56	8.61
	'Abilene' AC-3	2.95	24.4
MM 140-	Contractor	2.63	10.6
	YBF F3	2.49	14.7
	YBF F2	2.41	15.9
	Sun 125	2.44	17.0
	Exxon NUSO 95	2.61	19.1
	'Abilene' AC-3	2.99	25.2
MM 145	Contractor	2.63	4.36
	YBF F3	2.44	2.76
	YBF F2	2.60	3.51
	Sun 125	3.1	3.20
	Exxon NUSO 95	2.83	3.02
	'Abilene' AC-3	3.24	10.6

given in Table 9-2. All of the most highly aged samples were aged for the same amount of time at the same temperature, so comparisons are valid. These data show that the AC-3 softening agent blends age far more than any of the other blends for each location and that the aged contractor's blends have the second highest viscosity for three of the four locations. The common link between the AC-3 blends and the contractor's blends is that these blends were made by blending an asphalt, with its own asphaltenes, with an aged asphalt. This results in blends with higher asphaltene levels than the blends made with the supercritical fractions and the commercial agents alone. These conclusions further confirm that asphaltene content is a critical variable to consider in recycling.

The blends made using commercial agents and those produced using supercritical fractions follow no systematic pattern. Although the HS for the contractor's blends are similar to those of the other recycling agents, the single point viscosity comparison shows that using recycling agents alone is superior to using an asphalt in combination with a rejuvenating agent. However, no clear distinction between the supercritical fractions and the commercial agents exists using these limited analyses. Clearly some additional criterion for comparison is needed in the future. The aging test described in Chapter 2 would be an excellent criterion.

CORE TESTING

Based on the HS obtained from the aging of the laboratory recycled blends and the single point viscosity comparison, two recycling agents were chosen for further study. Supercritical fraction YBF F2 and Sun Hydrolene 125, or Sun 125, were chosen to be blended with the remaining unextracted PH material from all four I-45 locations. The blending and all subsequent core tests were performed by TTI personnel. The blending was performed according to standard procedures using recycling agent content determined from the blending experiments above. The blends made by mixing the commercial agent and the supercritical fraction

with the contractor's pre-screed material were compacted into laboratory cores using the Texas gyratory method (TEX 206F). Three cores were made for each recycled material. The cores were tested to determine air voids by ASTM methods D2041 and D2726. Finally, the cores were subjected to indirect tension (ASTM D4123), resilient modulus (ASTM D4123), and Hveem stability testing (ASTM D1560).

The void content for all the cores was extremely low. Typical laboratory cores have voids near 3.0%. Only four cores out of thirty-six had voids above 3.0%, with several having voids of 2.0% or less. The average void content for each recycled mixture is shown in Figure 9-1. From the voids data, it is likely that the mixes were over-asphalted. This was to be expected from the laboratory mixes, which were blended using pure recycling agent and unaltered post-heater material; however, the contractor's mix should have had the proper asphalt content.

All of the cores had non-passing initial Hveem stabilities. It was decided that the cores might require time to cure, or let the recycling agent fully disperse into the aged asphalt. The cores were allowed to cure for several weeks before they were retested. The retesting results show that curing had little or no effect on the Hveem stabilities as shown in Figure 9-2. These generally poor Hveem stabilities indicate that the aggregate used is of poor quality, or of the wrong gradation. Too many fines would result in the poor stabilities and the low voids observed. The aggregate gradation was not determined in this study, and this conclusion is purely speculation.

Once the Hveem stabilities were measured, the cores were subjected to resilient modulus testing. Resilient moduli for some of the laboratory cores are shown in Figure 9-3. These data are within the normal values for typical core specimens. Finally, the cores were subjected to destructive indirect tension testing. The average tensile strength at failure is plotted in Figure 9-4. These IDT results are also within the usual range.

The results of the core tests indicate that mixes made with the supercritical

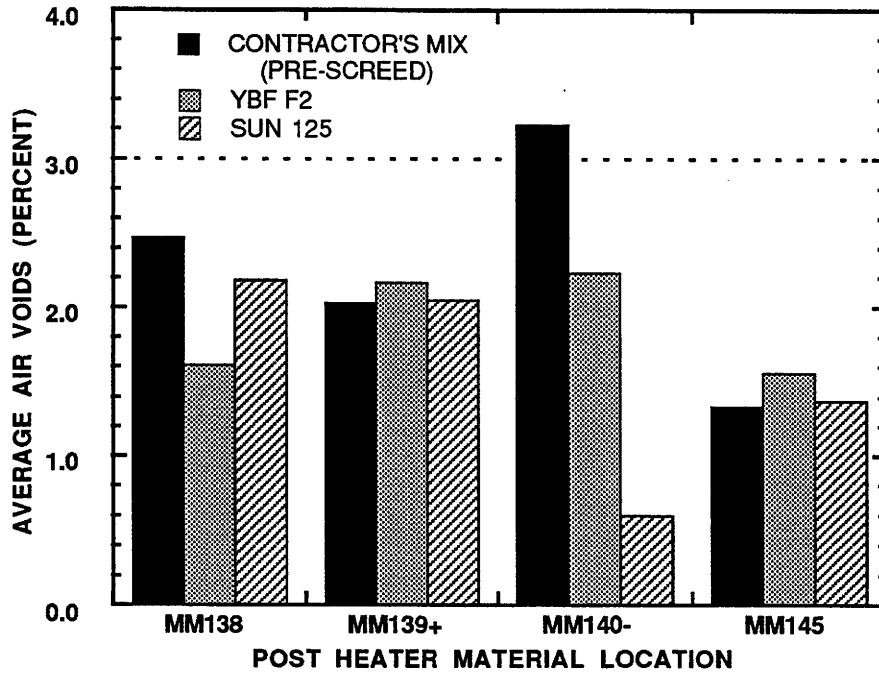


Figure 9-1. Laboratory Core Air Voids

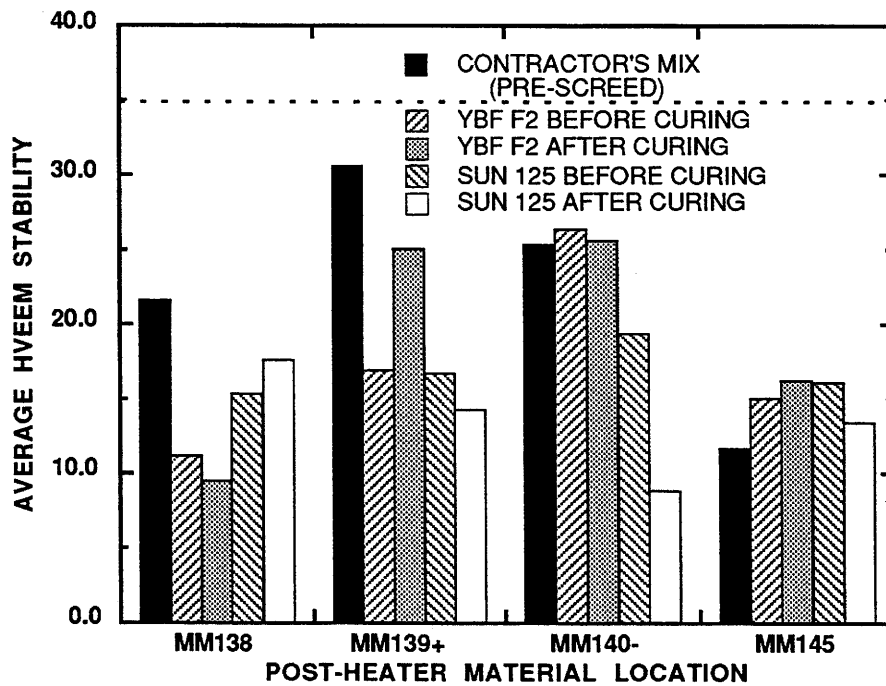


Figure 9-2. Laboratory Core Hveem Stabilities

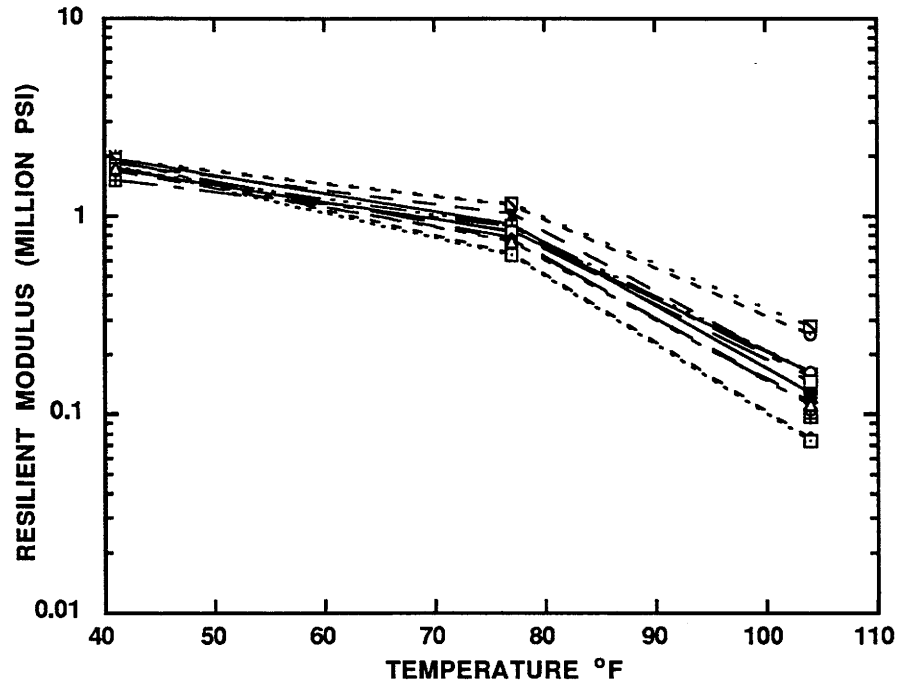


Figure 9-3. Laboratory Core Resilient Moduli

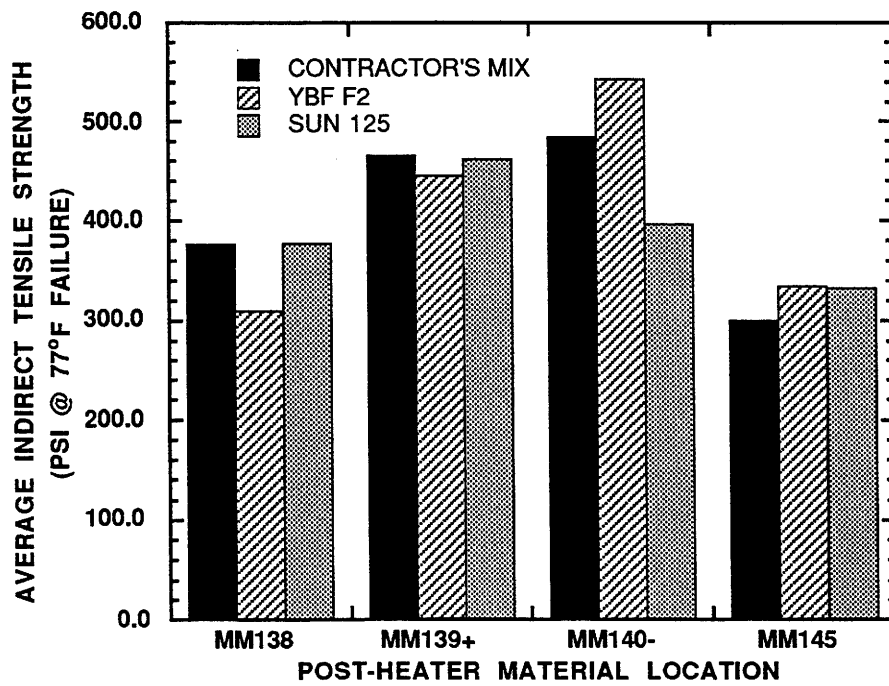
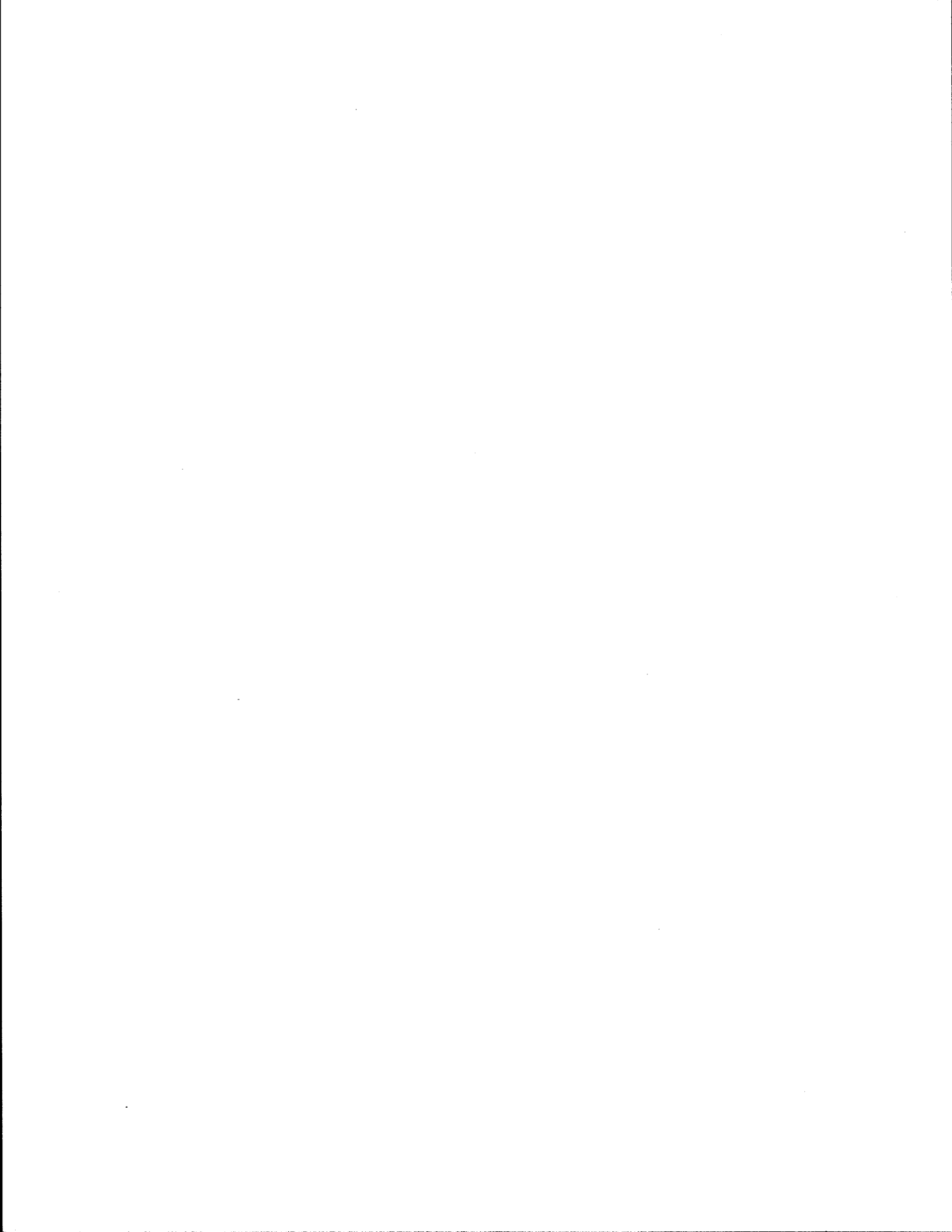


Figure 9-4. Laboratory Core Indirect Tensile Strength

fraction recycling agent YBF F2 and Sun 125, although over-asphalted, are no worse than those made from the contractor's mix in terms of physical properties, and may be better in terms of the limited aging data collected.



SECTION IV

HIGHWAY MODELING

An ultimate objective of our research is to understand the chemical and physical properties of asphalt binders well enough to be able to make long-term predictions of asphalt binder aging and subsequent pavement performance. In order to do this, we must understand, with some detail, the quantitative nature of the diffusion of oxygen and subsequent reaction in the asphalt binder. We must also understand the resulting consequences of this aging on the physical properties of the binder.

Chapter 10 details work which resulted in estimates of the diffusivity of oxygen in asphalt films. The work also produced a model for the diffusion and reaction of oxygen in thin, flat asphalt films and calculations of how such a film might age under given conditions of oxygen pressure and ambient temperature. This is a very important first step in developing a highway pavement aging model.

Chapter 11 then describes comparisons between pavement-aged binder and laboratory-aged POV material. Such comparisons are necessary to determine if the same reaction mechanisms are occurring in the pavement as are occurring in the laboratory. Then, the thin-film aging model is adapted to make a first-effort development of a pavement aging model.

CHAPTER 10

FUNDAMENTALS OF A HIGHWAY AGING MODEL

OBJECTIVES

The broad objectives of our research effort are to understand asphalt chemical and physical properties well enough to be able

- To select pavement binders to meet specific physical criteria at the time of placement,
- To predict changes to a road's physical behavior as a result of climate and use as an aid in scheduling maintenance and replacement,
- To design pavement binders for optimum life cycle costs.

In order to be able to accomplish these objectives, results of the previous chapters are essential. We need to understand the role and effect of asphaltenes which are initially present and which are formed during aging. When recycling asphalt materials, we need to understand how the physical properties of the recycled material will depend upon the blend of the recycled pavement with a recycling agent. And, for a range of temperatures, we need to understand the reaction kinetics of aging well enough to be able to predict reaction rates at road conditions, and the effect of aging on the asphalt's physical properties.

While the results of the earlier chapters are necessary, they are not sufficient. In addition, researchers must understand oxidation rates in asphalt films, not just as they are affected by reaction kinetics, but also as they are controlled by diffusion kinetics.

Consequently, the immediate goal of the work reported in this chapter was to propose a physical model of diffusion and reaction of oxygen in asphalt films and to measure the diffusivity of oxygen in asphalt. Such a model, together with the data, would then provide the basis for making predictive calculations of the oxidation of asphalt in thin films and in highway pavements and of the resulting changes in the physical properties of the pavement as it ages. Such calculations are demonstrated in the next chapter and compared to actual field aging.

Accordingly, this chapter contains additional background in the form of a literature review of asphalt oxygen diffusion measurements, a discussion of the phenomenological model which describes oxygen transport and reaction in thin asphalt films, data on oxygen diffusion which were obtained using this model, and calculations based upon these data and this model which describe trends in asphalt properties with time as a thin film might age.

LITERATURE SURVEY

The literature is limited with regard to oxygen transport properties in asphalt. The fundamental transport property for oxygen is diffusivity, D_{O_2} . Other transport properties, such as permeability and oxygen absorption, used primarily to characterize non-homogenous matrices, have also been studied. The difficulty in performing these experiments and analyzing the data is separating the transport from the reaction effect. Anderson and Wright (1941) measured both the permeability of oxygen and water vapor in an asphalt film. Based on the permeability data, the researchers concluded that water diffuses much faster than oxygen through asphalt films. Krchma et al., (1960) measured oxygen absorption at 333.3 K (140 °F) for 48 hrs and 372.2 K (210 °F) for 8 hrs. They concluded that for different asphalts there was no relationship between the amount of absorbed oxygen and the degree of hardening. Knoterus (1972) reported on oxygen absorption experiments with asphalt toluene solutions. He reports that an organic solution was used to minimize the diffusion effect.

Even less work has been attempted in the theoretical development of aging models for asphalt films including both reaction and diffusion of oxygen. Van Oort (1956) describes the combined effects of diffusion and reaction of oxygen in an asphalt film. By starting from fundamental transport and reaction equations, a theoretical model was proposed. Assumptions in this model include a first order reaction in oxygen concentration and that \mathcal{D}_{O_2} varies across the film, due to oxidation, by Equation 10 – 1.

$$\mathcal{D}_{O_2} = D_o \left(1 - \frac{g}{G_o} \right) \quad (10 - 1)$$

D_o is the oxygen diffusivity for the unaged tank material; g is the concentration of chemically bound oxygen; G_o is the theoretical maximum concentration of chemically bound oxygen. Experimental observations based on oxygen absorption were used to confirm the theory. Actual determinations of G_o were achieved after 100 hours of aging. Based on the model, the layer of exposed asphalt film near the surface forms a skin of high viscosity and retards the aging of the asphalt below the skin. Van Oort reported a \mathcal{D}_{O_2} of $8.6 \times 10^{-16} \text{ m}^2 / \text{s}$ in a neat asphalt film at 323.2 K (122 °F). Although theoretically sound, the values of G_o for different asphalts are not known and cannot be measured.

Measuring oxygen absorption and asphalt viscosity, Blokker and van Hoorn (1959) confirmed a skin formation but stated that the order of reaction in terms of oxygen concentration was 0.6. The depth of bound oxygen penetration was 2.5 mm (0.1 in) for 10 days aging at 323.2 K (122 °F) , 1 atm pure oxygen. Comparisons between field-aged samples led to the conclusion that aging at 20 atm oxygen, 323.2 K (122 °F) for one day is equivalent to 1/2 year of actual service. They report a \mathcal{D}_{O_2} of $12 \times 10^{-11} \text{ m}^2 / \text{s}$ in neat asphalt films at 323.2 K (122 °F) . The authors argue that \mathcal{D}_{O_2} in the film is not really changing. The reactivity of the components in the asphalt decreases with time. The values reported by Blokker and van Hoorn are four orders of magnitude higher than that reported by Van Oort. In terms of model development, these works are significant, and little model development has occurred since then. However, using these procedures in a laboratory simulation is not practical.

Dickinson et al., (1958) studied the absorption of oxygen in asphalt films. They used a model with first order reaction and constant \mathcal{D}_{O_2} . They concluded that at highway-pavement conditions, the process was diffusion controlled. Furthermore, the rate of oxygen absorption decreased with increasing viscosity and film thickness. The rate increased with temperature and the activation energy for the process is 42 kJ/gmol. However, their model is only valid for the initial rate of absorption because the properties of the asphalt change as a result of oxidation. Lee and Dickinson (1962) also concluded that the absorption of oxygen was continuously modified by high viscosity skin formation. For aging at 303.2 K (86 °F) under atmospheric pressure, the absorption of oxygen was diffusion controlled. Unfortunately, actual experimental measurements of the surface of the films were never reported.

Verhasselt and Choquet (1991), give an empirical kinetic equation which they apply to several asphalt physical and chemical properties that supposedly includes the effect of oxygen transport. However, the equation does not account for changes in \mathcal{D}_{O_2} as a function of CA in the film. Comparison with field aging for two asphalts was not very good. Furthermore, their equation is not a realistic model for field aging. It predicts an infinite change in the measured property as aging time goes to infinity. Actual field aging is asymptotic or diffusion limited.

Only two literature sources report \mathcal{D}_{O_2} in asphalts at one temperature, 323.2 K (122 °F). More importantly no quantitative model relating \mathcal{D}_{O_2} to other measurable properties such as temperature, η , or CA exists. Since research has shown that field aging is diffusion limited, only a fundamental aging model containing both oxygen diffusion and reaction has any hope of providing accurate predictions of field aging.

To summarize, the effect of temperature and pressure on the rate of asphalt aging has not been satisfactorily determined. Some theoretical and experimental work has been accomplished for diffusion and reaction of pure oxygen in an asphalt film; however, models relating oxygen diffusivity to measurable changes in an asphalt film have not been studied. The development of an asphalt-aging model including both oxygen diffusion and reaction has not been attempted. Furthermore, comparisons between POV- and field-aged materials have not conclusively shown that POV aging simulates field aging.

OVERVIEW OF THE THIN-FILM MODEL

Consider the section of asphalt concrete pavement depicted in Figure 10-1. Aggregate materials of various sizes form the bulk of the pavement (95% by weight). This solid rock performs the function of supporting the load. The asphalt binder together with air voids, fill the interstices between the aggregate materials (fine aggregate material also is small enough to exist within the asphalt binder). The function of the binder is to seal the pavement from moisture and to adhere the aggregate matrix into a single composite pavement material. In the simplified schematic, we show the aggregate material, coated on its surface by a binder film. Air voids then occupy additional volume. The asphalt binder typically is 5% by weight of the entire pavement. In this simplified model we imagine an aggregate surface with a film of asphalt material coated onto it, plus air in contact with the binder at the air void interface. This air void may or may not have access to the atmosphere through porous channels in the pavement.

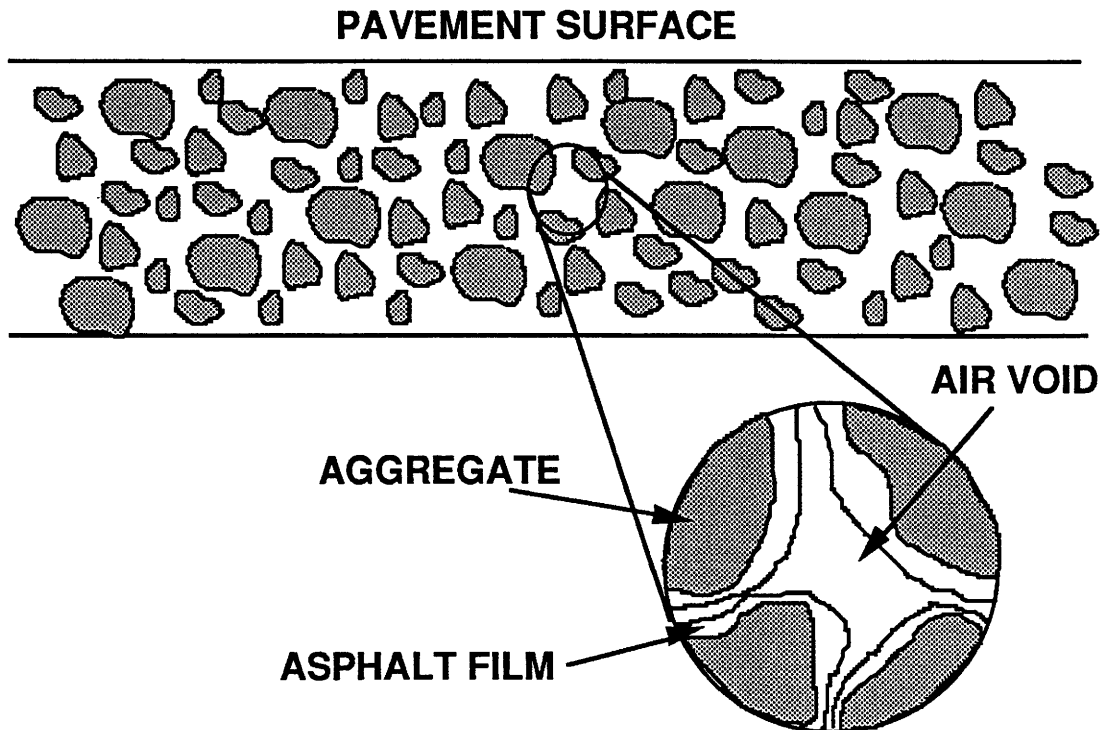


Figure 10-1. Highway Pavement Cross-Section

This is a complicated model and the picture we show is actually simplified compared to the actual situation. Nevertheless, the basic elements of the model can be incorporated into Figure 10-2. Here we show a flat asphalt film coated onto an impermeable substrate. The other surface of the asphalt is exposed to a gaseous phase which contains oxygen. In the schematic of Figure 10-1, if the aggregate radius of curvature at the aggregate particle surface is large compared to the thickness of the asphalt film, then this flat-film model of Figure 10-2 is not a bad approximation to the actual case, and this simplified model may well have pertinence to the prediction of aging in asphalt pavements.

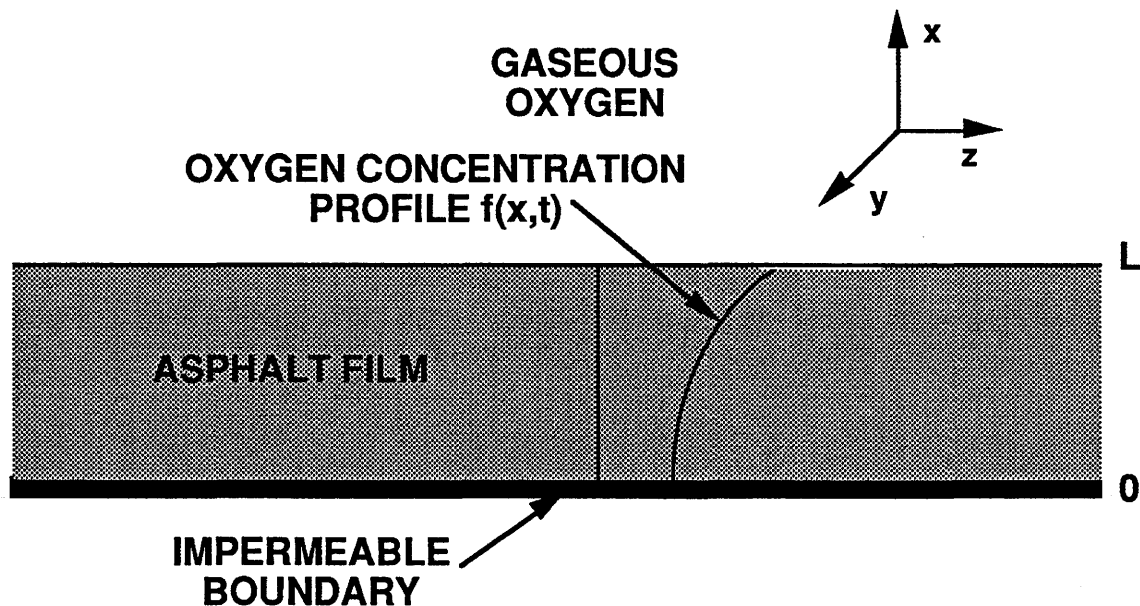


Figure 10-2. Oxygen Diffusion and Reaction in a Thin Asphalt Film

The primary purpose in this chapter, however, was to use such a flat-film model as a means of measuring the diffusivity in asphalt rather than predicting aging in asphalt pavements. This latter purpose will be discussed in the next chapter.

Consider now, qualitatively, what happens within this asphalt film over a period of time when the gas phase at the exposed surface contains oxygen, i.e., consider the qualitative shape of the oxygen concentration profile within the asphalt film (Figure 10-2). Oxygen will react with the asphalt at this gas/asphalt interface, in accordance with the

reaction kinetics, which depend upon temperature and oxygen pressure at this interface. The kinetics of this reaction were described earlier in Section I. Deeper in the film, the oxygen concentration will be less than at the surface because (1) oxygen must diffuse from the surface into the film and (2) because oxygen reaction within the film tends to deplete the oxygen as it arrives. Hence, we expect to see the oxygen concentration decrease with depth in the film. The actual oxygen concentration at a point in the film depends upon the competing effects of oxygen supply by diffusion and oxygen depletion by reaction. If the reaction is slow compared to the diffusion rate, then the oxygen concentration within the film can be essentially the same as at the surface. If the oxygen reaction is fast compared to the diffusion rate, however, then the oxygen concentration will be much less than at the surface. At the substrate surface (the asphalt-aggregate interface, e.g.) the oxygen concentration profile must be flat because at this interface there can be no diffusion of oxygen, assuming that the diffusivity of oxygen through the substrate is zero and that there is no reaction of oxygen with the aggregate.

So the concentration of oxygen and, hence, of carbonyl varies across the film and over time, due to the combined effects of diffusion and reaction. With an adequate quantitative model and measurements of carbonyl concentration within the film over time, the diffusivity of oxygen can be determined.

The procedure is described in more detail in Appendix C, but, basically, the carbonyl area (measured by FT-IR) as a function of time is measured at both the exposed surface (ES) and at the substrate interface (SI). The ATR zinc selenide prism is uniquely suited for this measurement; the exposed surface of a film is pressed onto a prism for the ES measurement and then the substrate interface side is used for a second measurement. With these measurements and the kinetic data relating reaction rate to oxygen pressure, the diffusivity can be measured. The numerical procedure is rather involved, however.

RESULTS

As described above, the fact that oxygen must diffuse through an asphalt film while undergoing reaction to carbonyl compounds implies that the carbonyl formation rate at the substrate interface will be lower than at the exposed surface. Figures 10-3 through 10-8 show example data. Note that the asphalt at the substrate interface is less oxidized, at a given time, than that at the exposed surface. Also, there are obvious differences for the same asphalt exposed to different oxygen pressures at the same temperature (compare Figures 10-3 and 10-4) and for the same asphalt at different temperatures but the same pressure (compare Figures 10-3 and 10-5). These effects must be accounted for by the model through the asphalt's different physical and reactive properties.

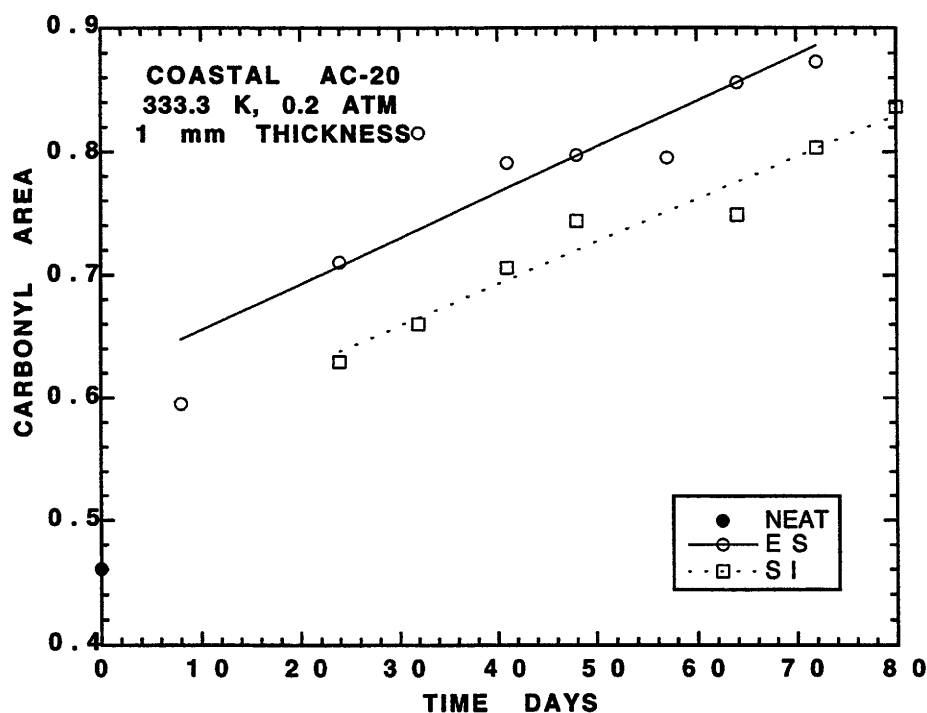


Figure 10-3. Measured *CA* Growth at the *ES* and *SI* (333.3 K, 0.2 atm)

It should also be noted that in all the data shown the rate of carbonyl formation after an initial jump at an early time period is essentially constant over the length of the experiment. This constancy suggests that, for all practical purposes, the diffusion

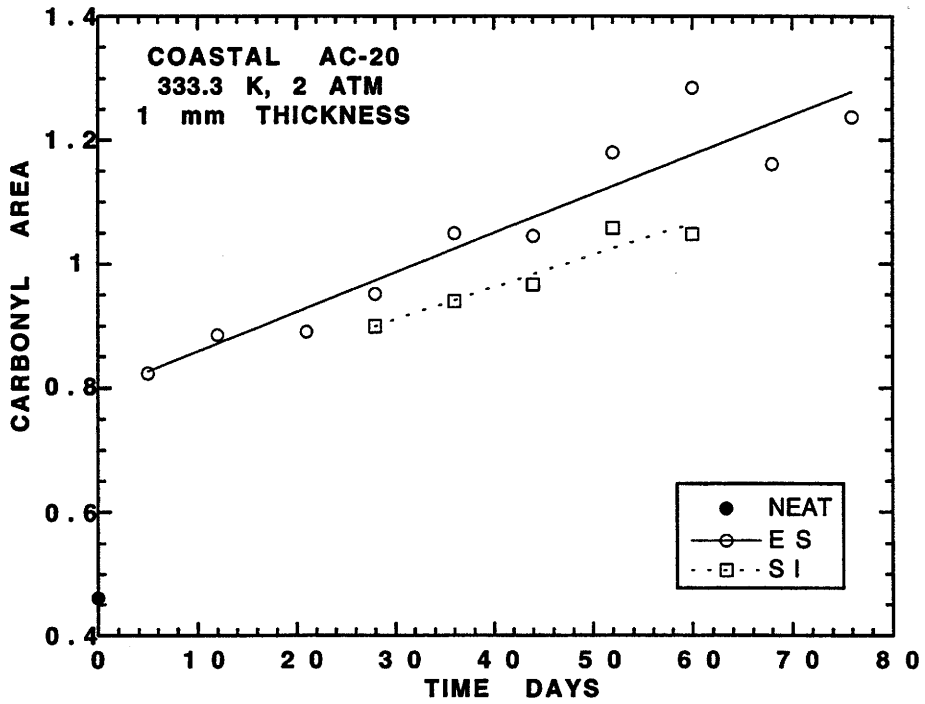


Figure 10-4. Measured *CA* Growth at the *ES* and *SI* (333.3 K, 2 atm)

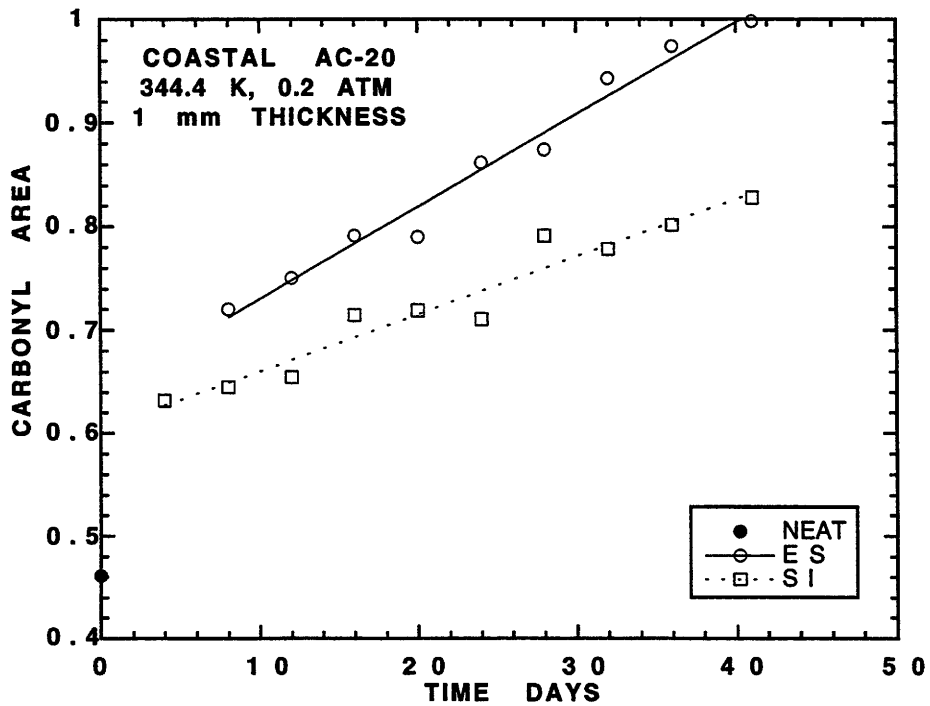


Figure 10-5. Measured *CA* Growth at the *ES* and *SI* (344.4 K, 0.2 atm)

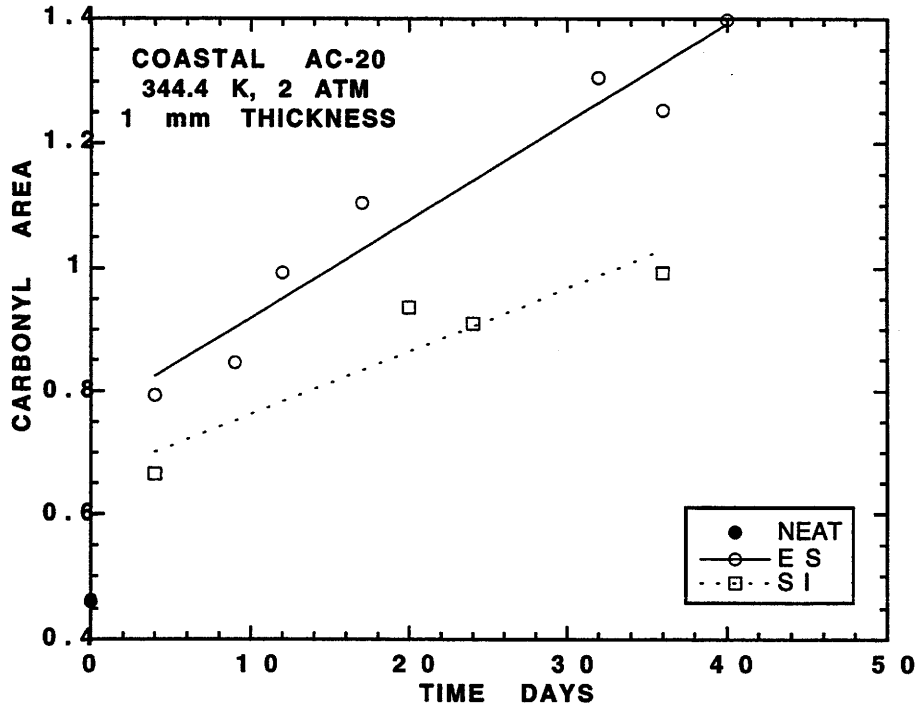


Figure 10-6. Measured *CA* Growth at the *ES* and *SI* (344.4 K, 2 atm)

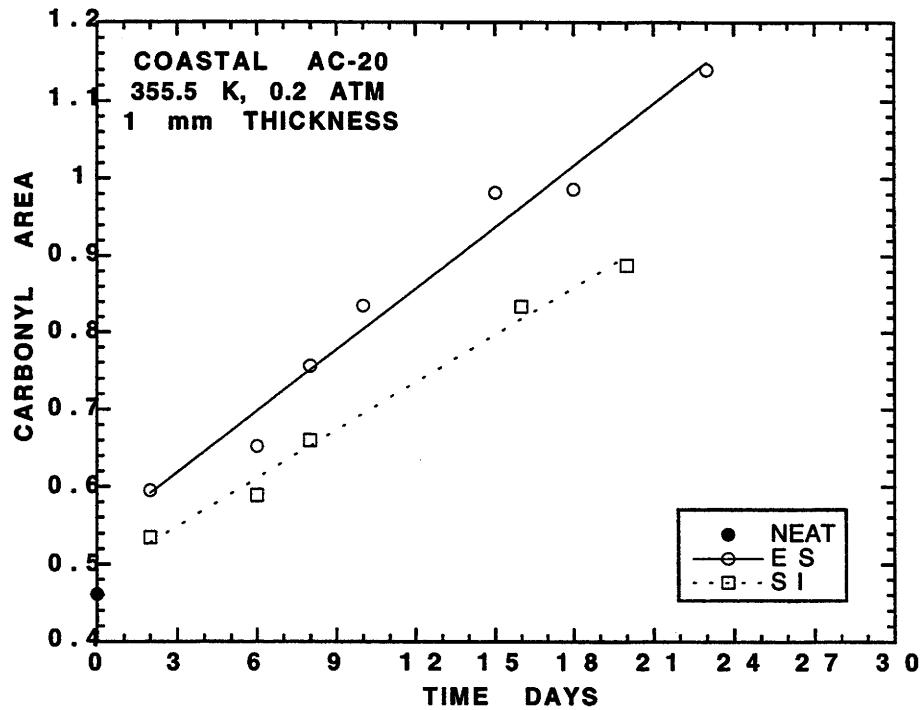


Figure 10-7. Measured *CA* Growth at the *ES* and *SI* (355.5 K, 0.2 atm)

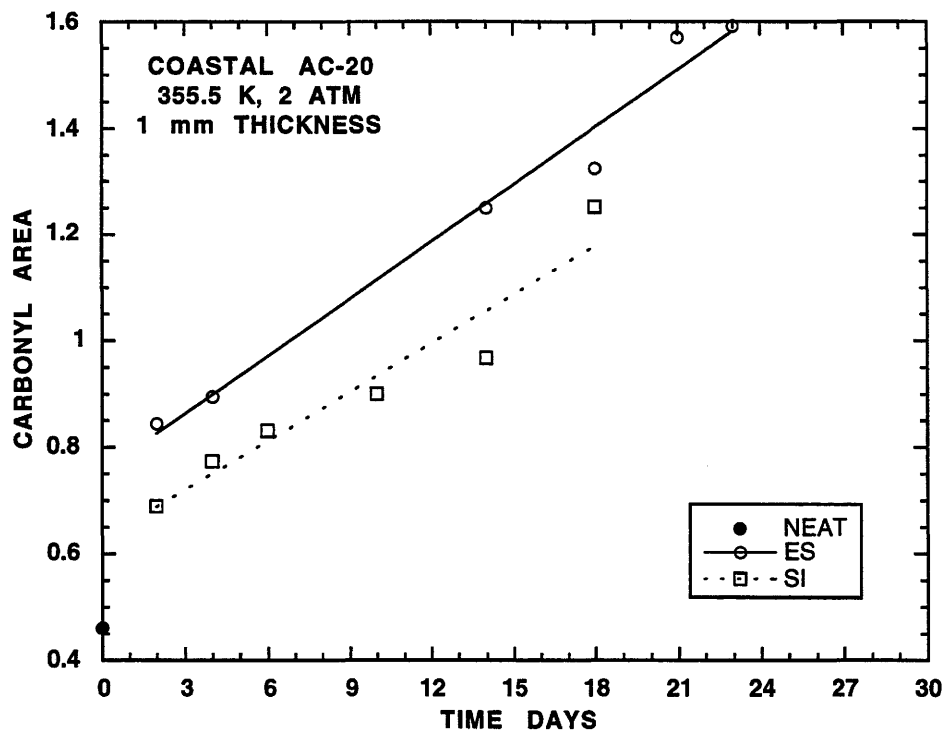


Figure 10-8. Measured CA Growth at the ES and SI (355.5 K, 2 atm)

coefficient is constant during the aging process even though the oxidation of the film likely causes some increase in the viscosity. This apparent constancy of diffusivity was used to obtain estimates of the diffusivity.

The carbonyl area versus time data at the substrate interface were used to determine the oxygen pressure in the film at the interface as a function of time. Because the rate is essentially constant, this pressure was also essentially constant. From the reaction kinetic work reported in Chapter 1, the pressure is readily determined; the temperature of the film is known and the reaction rate is measured from the carbonyl data. Therefore, the only remaining factor is the oxygen pressure.

To be specific, the work in Chapter 1 showed that Equation 1 – 3 related oxygen pressure and temperature to r_{CA} :

$$r_{CA} = AP^{\alpha} e^{-E/RT} \quad (1-3)$$

For isothermal aging and a given asphalt, measured r_{CA} as a function of time can be

used to estimate oxygen pressure, P , as a function of time. This idea is applied to the SI of the POV-aged asphalt film. P_{SI} is estimated from the difference in the r_{CA} at the ES and SI through Equation 1 – 3 with pre-determined kinetic parameters.

This estimation of P_{SI} required experimental data from POV aging at low oxygen pressure and moderate temperatures. The data set consisted of five AC-20 asphalts studied by Lau et al., (1992). Three aging temperatures of 333.3, 344.4, and 355.5 K (140, 160, and 180 °F) and two oxygen pressures of 0.2 and 2 atm were used. Aging times ranged from 2 to 80 days depending on the aging temperature. These asphalts were chosen because kinetic information had already been determined, as shown in Chapter 1. Pure oxygen was the oxidizer. For air, diffusion of oxygen gas through the nitrogen gas film at the free surface would complicate the analysis. Asphalt films, 1 mm (0.039 in) thick, were made by weighing 2.4 grams (0.085 oz) of material into pre-made aluminum trays as described in Appendix A. For each aging condition, ten trays per asphalt were used. FT-IR measurements were used to monitor carbonyl formation at the ES and SI of the POV-aged asphalt film. Appendix A describes the procedure.

Tables of CA at the ES and SI for aging pressures of 0.2 and 2 atm and temperatures of 333.3, 344.4 and 355.5 K (140, 160, and 180 °F) for all the asphalts studied are given in Appendix C of Lunsford (1994). Figures 10-3 through 10-8 show example graphs for the Coastal asphalt. Figures C-1 through C-24 (Appendix C) show data for the other asphalts.

Estimation of Oxygen Diffusivity

Using the reaction and diffusion model detailed in the Appendix C together with the pressure data given in the previous section, the diffusivity of oxygen in the asphalt films was determined. It was assumed that at any instant in time the diffusivity was essentially constant through the film. While we know this isn't really correct from subsequent calculations which allow for variable diffusivity, it appears to be reasonable under the conditions of the experiment conducted. With the model and the pressures at the exposed surface and at the substrate interface known as a function of time (that at

the exposed surface, of course, is constant for a given experiment), the diffusivity in the film was determined. This required a numerical computational procedure, and details are given by Lunsford (1994).

Table 10-1 shows the values of diffusivity estimated from the data together with the corresponding exposed surface and estimated substrate interface values of pressure for the asphalts and temperatures of the experiments. Note that for these calculations a single value for α of 0.27 was used to represent all of the data.

For isobaric conditions and a given asphalt, \mathcal{D}_{O_2} increases with temperature in all cases studied except Coastal AC-20 and Exxon AC-20 at 0.2 atm from 333.3 to 344.4 K (140 to 160 °F) and Texaco AC-20 at 2 atm from 333.3 to 344.4 K (140 to 160 °F). For isothermal conditions and a given asphalt, \mathcal{D}_{O_2} decreases with increasing pressure except for Exxon AC-20 at 355.5 K (180 °F). These anomalies probably result from errors in determining P_{SI} based on $(r_{CA})_{SI}$.

From estimated \mathcal{D}_{O_2} and P_{SI} , oxygen pressure profiles in the films were calculated based upon the diffusion and reaction model. Figure 10-9 shows the oxygen pressure profiles of 1 mm (0.039 in) thick Ampet AC-20 at P_{ES} of 0.2 atm and three temperatures. For increasing temperature, the profile is less steep; P_{SI} approaches P_{ES} . This figure shows that diffusion resistance decreases with increasing temperature. In comparison, Figure 10-10 shows calculated oxygen pressure profiles for Cosden AC-20 at P_{ES} of 2.0 atm. From this figure, one would conclude that diffusion resistance decreases from 333.3 to 344.4 K (140 to 160 °F). This is not physically reasonable, and one of the profiles obviously is incorrect. Thus, comparing only the values of \mathcal{D}_{O_2} in Table 10-1, holding other measurable aging variables constant, may not be sufficient to detect errors in the data. A combination of both P_{SI} and \mathcal{D}_{O_2} must be considered.

Even though there are some unrealistic data, a comparison of estimated \mathcal{D}_{O_2} with literature values validates the technique of using r_{CA} . There are only two sources reporting \mathcal{D}_{O_2} in asphalt. Van Oort (1956) gives \mathcal{D}_{O_2} of 8.0×10^{-16} m² / s for neat asphalt at 323.2 K (122 °F). In 1959, Blokker and van Horn (1959) report \mathcal{D}_{O_2} as 1.2×10^{-10} m² / s at 323.2 K (122 °F). These literature values range six orders of magnitude. Estimated \mathcal{D}_{O_2} values in Table 10-1 are within the range of literature values.

Table 10-1. Estimated D_{O_2} for Steady-State Constant D_{O_2} Oxygen Diffusion and Reaction^a

Asphalt	T K	P_{ES} atm	P_{SI} atm	$D_{O_2} \times 10^{13}$ m^2 / s
Ampet AC-20	333.3	0.2	0.0673	20.0
	344.4	0.2	0.115	88.5
	355.5	0.2	0.161	486.0
	333.3	2	0.393	2.80
	344.4	2	0.857	11.5
	355.5	2	1.80	176.1
Coastal AC-20	333.3	0.2	0.149	64.9
	344.4	0.2	0.0345	39.3
	355.5	0.2	0.0789	160.0
	333.3	2	0.925	5.16
	344.4	2	0.408	7.83
	355.5	2	1.105	43.2
Cosden AC-20	333.3	0.2	0.0331	20.0
	344.4	0.2	0.130	141.0
	355.5	0.2	_b	-
	333.3	2	0.937	7.07
	344.4	2	0.363	8.86
	355.5	2	1.48	86.1
Exxon AC-20	333.3	0.2	0.175	150.0
	344.4	0.2	0.108	99.3
	355.5	0.2	0.0775	127.0
	333.3	2	1.09	6.88
	344.4	2	1.17	20.8
	355.5	2	1.86	249.0
Texaco AC-20	333.3	0.2	0.124	38.9
	344.4	0.2	0.122	92.5
	355.5	0.2	0.170	598.3
	333.3	2	1.39	9.11
	344.4	2	0.57	8.04
	355.5	2	1.28	44.6

^a α of 0.270 and 1 mm (0.039 in) thick films

^b This calculation was not done.

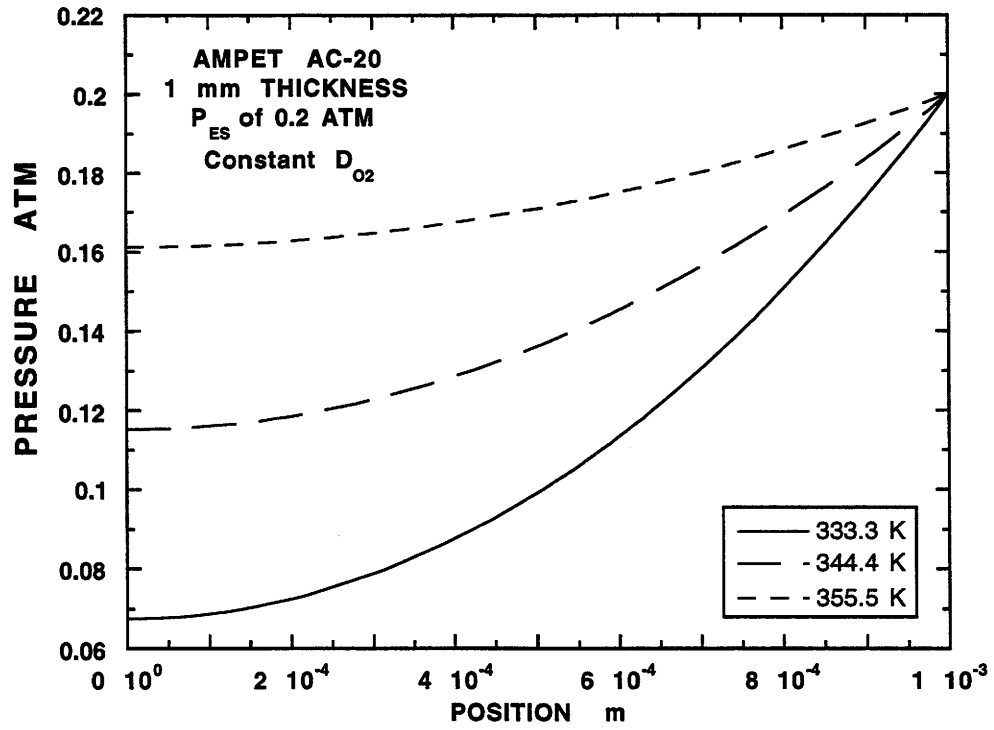


Figure 10-9. Calculated Oxygen Pressure Profiles in a 1 mm Thick Film (0.2 atm)

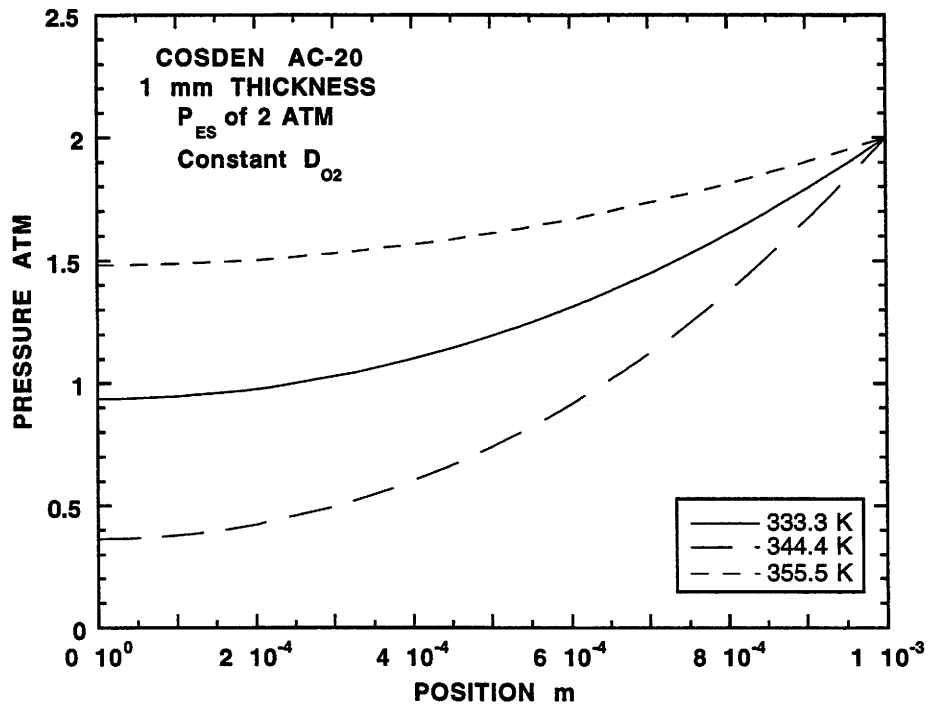


Figure 10-10. Calculated Oxygen Pressure Profiles in a 1 mm Thick Film (2 atm)

In both literature sources, no surface properties were measured. Van Oort assumed a first order reaction with \mathcal{D}_{O_2} varying inversely proportional to bound oxygen. Blokker and van Horn assumed \mathcal{D}_{O_2} did not change with oxidative aging, but the reactivity of the asphalt decreased with aging time. They assumed the order of reaction in oxygen concentration to be 0.6.

The propagation of errors is a significant problem since $(r_{CA})_{SI}$ was used to determine P_{SI} and to estimate \mathcal{D}_{O_2} . Table 10-1 contains some unrealistic values. With a 10% uncertainty in $(r_{CA})_{SI}$, the corresponding error band for P_{SI} is 40%. This results from the small value of α . To determine the error in estimated \mathcal{D}_{O_2} , a range of $\pm 40\%$ was established for P_{SI} . \mathcal{D}_{O_2} was estimated at each end of the range. The calculation was not possible for some cases since P_{SI} exceeded P_{ES} . The calculated \mathcal{D}_{O_2} are given in Table 10-2. The error in \mathcal{D}_{O_2} is directly related to the magnitude of \mathcal{D}_{O_2} . Small \mathcal{D}_{O_2} shows a small error band. The range of error varies from asphalt to asphalt and across aging conditions. For example, the error band in \mathcal{D}_{O_2} is from 4.35 to $86.4 \times 10^{-13} \text{ m}^2/\text{s}$ for Texaco AC-20 at 333.3 K and 2 atm at the *ES*. In contrast, Coastal AC-20 at the same aging conditions shows a range of \mathcal{D}_{O_2} from 3.48 to $8.43 \times 10^{-13} \text{ m}^2/\text{s}$.

Establishing a suitable criterion to discard data is next to impossible since the actual values of estimated \mathcal{D}_{O_2} are still unknown. Screening the data in an attempt to remove anomalous points before the estimation of \mathcal{D}_{O_2} was difficult. Using a criterion of large variability in \mathcal{D}_{O_2} may not be best, either. For example, values of P_{SI} that err on the low side tend to produce low variability in \mathcal{D}_{O_2} . From P_{SI} and \mathcal{D}_{O_2} together, Table 10-3 lists questionable \mathcal{D}_{O_2} and P_{SI} for the asphalts and specified aging conditions. Since most of the questionable data were at 2 atm, the diffusion resistance was probably extremely low. The difference in r_{CA} at the *SI* and *ES* could be accounted for by measurement error. However, these data points are not removed from the data set at this time.

The variation of \mathcal{D}_{O_2} with pressure for isothermal aging of a given asphalt, in Table 10-1, suggests that \mathcal{D}_{O_2} varies in the asphalt film as a result of aging, i.e., that changes in η_o^* as a result of *CA* formation affect changes in \mathcal{D}_{O_2} . A model relating \mathcal{D}_{O_2}

Table 10-2. Estimated D_{O_2} at $\pm 40\%$ P_{SI} for Steady-State Constant D_{O_2} Oxygen Diffusion and Reaction^{a,b}

Asphalt	T K	P_{ES} atm	P_{SI} atm	$D_{O_2} \times 10^{13}$ m^2 / s		
				-40% P_{SI}	P_{SI}	+40% P_{SI}
Ampet AC-20	333.3	0.2	0.0673	15.2	20.0	26.9
	344.4	0.2	0.115	51.8	88.5	207.5
	355.5	0.2	0.161	164.3	486.0	-
	333.3	2	0.393	2.35	2.80	3.29
	344.4	2	0.857	8.06	11.5	17.6
	355.5	2	1.80	35.0	176.1	-
Coastal AC-20	333.3	0.2	0.149	26.8	64.9	-
	344.4	0.2	0.0345	33.5	39.3	45.5
	355.5	0.2	0.0789	115.4	160.0	231.6
	333.3	2	0.925	3.48	5.16	8.43
	344.4	2	0.408	6.54	7.83	9.26
	355.5	2	1.105	26.1	43.2	91.7
Cosden AC-20	333.3	0.2	0.0331	17.1	20.0	23.0
	344.4	0.2	0.130	73.3	141.0	579.4
	355.5	0.2	-	-	-	-
	333.3	2	0.937	4.74	7.07	11.7
	344.4	2	0.363	7.52	8.86	10.3
	355.5	2	1.48	36.0	86.1	-
Exxon AC-20	333.3	0.2	0.175	35.0	150.0	-
	344.4	0.2	0.108	61.2	99.3	199.8
	355.5	0.2	0.0775	92.0	127.0	181.8
	333.3	2	1.09	4.19	6.88	14.3
	344.4	2	1.17	12.0	20.8	50.7
	355.5	2	1.86	35.2	249.0	-
Texaco AC-20	333.3	0.2	0.124	21.3	38.9	118.4
	344.4	0.2	0.122	51.1	92.5	270.2
	355.5	0.2	0.170	166.1	598.3	-
	333.3	2	1.39	4.35	9.11	86.4
	344.4	2	0.57	6.34	8.04	10.2
	355.5	2	1.28	23.4	44.6	170.0

^a α of 0.270 and 1 mm (0.039 in) thick films

^b - Signifies the values were not determined.

Table 10-3. Suspect D_{O_2} and POV-Aging Conditions for Steady-State Constant D_{O_2} Oxygen Diffusion and Reaction^a

Asphalt	T K	P_{ES} atm	P_{SI} atm	$D_{O_2} \times 10^{13}$ m^2/s
Ampet AC-20	333.3	2	0.393	2.80
	344.4	2	0.857	11.5
Coastal AC-20	333.3	0.2	0.149	64.9
	355.5	0.2	0.0789	160.0
	344.4	2	0.408	7.83
	355.5	2	1.105	43.2
Cosden AC-20	344.4	2	0.363	8.86
Exxon AC-20	333.3	0.2	0.175	150.0
	355.5	0.2	0.0775	127.0
	344.4	2	1.17	20.8
Texaco AC-20	344.4	2	0.57	8.04
	355.5	2	1.28	44.6

^a α of 0.270 and 1 mm (0.039 in) thick films

to η_o^* is given in Equation 10 - 2 for isothermal conditions.

$$D_{O_2} = D_o(\eta_o^*)^B \quad (10-2)$$

Comparing estimated D_{O_2} with average η_o^* on a log-log plot should yield a straight line if Equation 10 - 2 models the asphalt behavior.

The calculation of average η_o^* for a given asphalt film, aging temperature, and ES pressure is based upon the hardening susceptibility concept which relates η_o^* to CA according to Equation 10 - 3:

$$\eta_o^* = \exp\{HS \cdot CA + m\} \quad (10-3)$$

Of course, η_o^* varies according to the temperature of the asphalt film so that HS and m obviously are functions of the film temperature, as well. This relationship is discussed in more detail in Appendix C but, for the purposes of this discussion, values of HS and m for all five asphalts at all three temperatures studied were determined and are presented in

Table 10-4. Then, from the measured data at the *ES* and *SI*, the average *CA* in the film during the aging experiment was approximated by the arithmetic average of the minimum and maximum *CA*. Unaged tank *CA* was not used. Using *HS* and *m* of the different asphalts and aging temperatures from Table 10-4, average η_o^* of the asphalt during the aging experiment was calculated from Equation 10 – 3. Table 10-5 reports average *CA*, η_o^* , and estimated D_{O_2} at the aging conditions for all the asphalts studied. The data denoted with * in the table are from the questionable data set given in Table 10-3.

Table 10-4. *HS* and $\exp(m)$ at 333.3, 344.4, and 355.5 K for All POV-Aged Asphalts Studied^a

Asphalt	333.3 K ^b (140 °F)		344.4 K ^c (160 °F)		355.5 K ^c (180 °F)	
	<i>HS</i> 1 / <i>CA</i>	$\exp(m)$ p	<i>HS</i> 1 / <i>CA</i>	$\exp(m)$ p	<i>HS</i> 1 / <i>CA</i>	$\exp(m)$ p
Ampet AC-20	3.03	1126	2.84	168.0	2.68	26.8
Coastal AC-20	3.97	655	3.82	95.3	3.69	14.9
Cosden AC-20	2.95	1032	2.85	140.0	2.77	20.4
Exxon AC-20	2.63	1377	2.51	200.0	2.40	31.8
Texaco AC-20	3.39	687	3.14	116.0	2.92	21.0

^a Model: $\eta_o^* = \exp(m) \exp(HS \cdot CA)$

^b Measured

^c Calculated

Figure 10-11 shows estimated D_{O_2} with error bars versus average η_o^* for all asphalts. Circles, squares and diamonds denote aging temperatures 333.3, 344.4, and 355.5 K (140, 160, and 180 °F), respectively. Even with the questionable data, the conclusion can be reached that increases in η_o^* decrease D_{O_2} . For modeling, a specific mathematical relationship must be developed from this generality. For the purpose of obtaining a quantitative relation between D_{O_2} and η_o^* , the questionable data discussed above and presented in Tables 10-3 and 10-5 are omitted. Filled symbols indicate these data in Figure 10-11. Hollow symbols represent the data used in the parameter estimation. With the questionable data removed, Equation 10 – 2 models the asphalt behavior quite well. Surprisingly, the D_{O_2} vs η_o^* relationship appears to be independent of the asphalts

Table 10-5. Estimated D_{O_2} , Average CA and η_o^* , and POV-Aging Conditions for Steady-State Constant D_{O_2} Oxygen Diffusion and Reaction^{a,b}

Asphalt	T K	P_{ES} atm	CA_{avg} CA	$\eta_o^*_{avg}$ P	$D_{O_2} \times 10^{13}$ m^2 / s
Ampet AC-20	333.3	0.2	0.729	10200	20.0
	344.4	0.2	0.726	1320	88.5
	355.5	0.2	0.806	230	486.1
	333.3*	2	1.001	23400	2.80
	344.4*	2	0.985	2760	11.5
	355.5	2	1.099	510	176.1
Coastal AC-20	333.3*	0.2	0.734	12100	64.9
	344.4	0.2	0.815	4350	39.3
	355.5*	0.2	0.837	330	160.0
	333.3	2	1.030	39100	5.16
	344.4*	2	1.032	4910	7.83
	355.5*	2	1.140	1000	43.2
Cosden AC-20	333.3	0.2	0.834	12100	20.0
	344.4	0.2	0.778	1290	141.0
	355.5	0.2	—	—	—
	333.3	2	1.172	32800	7.07
	344.4*	2	1.098	3200	8.86
	355.5	2	1.302	750	86.1
Exxon AC-20	333.3*	0.2	0.802	11400	150.0
	344.4	0.2	0.839	1640	99.3
	355.5*	0.2	0.970	330	127.0
	333.3	2	1.096	24600	6.88
	344.4*	2	1.066	2900	20.8
	355.5	2	1.065	410	249.0
Texaco AC-20	333.3	0.2	0.669	6600	38.9
	344.4	0.2	0.736	1170	92.5
	355.5	0.2	0.746	190	598.3
	333.3	2	0.876	13400	9.11
	344.4*	2	0.904	1990	8.04
	355.5*	2	1.009	400	44.6

^a α of 0.270 and 1 mm (0.039 in) thick films

^b — Signifies the values were not determined.

* These data were not used to estimate parameters in Figure 10-11.

studied. Furthermore, the temperature dependence on D_{O_2} appears to be incorporated within the dependence on η_o^* . From the parameter estimation, a value of -0.84 is determined for B . This value lies in the range of literature values, -1 to -0.5 . The pre-exponential factor, D_o in Equation 10 - 2, is $4.039 \times 10^{-9} \text{ m}^2/\text{s}^2$.

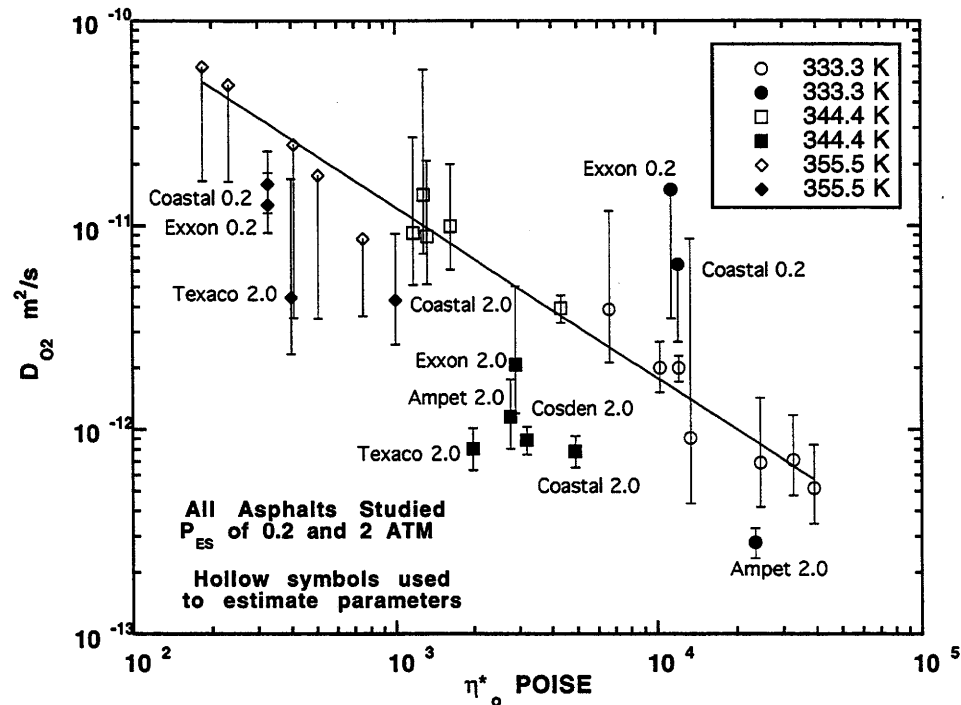


Figure 10-11. Estimated D_{O_2} for all 1 mm Thick Films

To summarize, for steady-state constant D_{O_2} , Equation 10 - 2, describing the dependence of D_{O_2} on η_o^* was used. D_{O_2} vs η_o^* showed significant scatter when all data were included. Questionable data were removed and the errors could be traced to the estimation of $(r_{CA})_{SI}$. The model parameters are B of -0.838 and D_o of 4.0389×10^{-9} for η_o^* in poise and D_{O_2} in m^2/s . The parameters are independent of asphalt film temperature and asphalt for the asphalts studied. Furthermore, the parameter B was in the range of literature values. The D_{O_2} vs T dependence is adequately accounted for by the dependence on η_o^* . This does not suggest that all asphalts have the same D_{O_2} in the film during aging. Asphalt-dependent parameters determine r_{CA} , CA_o , HS , and m . These are used to calculate η_o^* , and each asphalt has unique η_o^* from oxidative aging.

With unique η_o^* and asphalt-independent parameters B and D_o , unique values of \mathcal{D}_{O_2} are calculated for each asphalt.

Steady-State Variable Diffusivity

Previous calculations were based upon a constant diffusivity through the film. Even so, this led to a reasonable model for diffusivity as a function of asphalt viscosity (Figure 10-11). In reality then, assuming that this diffusivity model holds, as an asphalt ages, its viscosity will change and, therefore, the diffusivity will change. Furthermore, the aging rates at the exposed surface and the substrate interface will be different, leading to variable diffusivity throughout the film instead of constant, as was assumed in the previous section. Rather than actually estimating the diffusivities using a variable diffusivity parameter estimation model, the values for diffusivity that were obtained in the previous section were used to make calculations assuming that the diffusivity did, in fact, vary throughout the film. The calculations reported here still followed a steady-state model, however.

Using the model of diffusivity as a function of viscosity (Equation 10 – 2) and the diffusion and reaction model of Appendix C, values of oxygen pressure in the film as a function of position were calculated for various values of substrate interface pressure. Results are shown in Figures 10-12 through 10-14. In each figure the pressure profile is calculated by using the diffusivity at the exposed surface (to establish the slope of the pressure versus position profile at the ES) together with the zero gradient condition at the substrate interface. Consequently, this method allows the calculation of pressure versus position profiles for a given amount of aging without using a time dependent model.

The qualitative aspects of the calculations which were obtained match very well the kind of profiles that one would expect, predicting decreases in pressure at the substrate interface with increasing aging time. The diffusivity at the exposed surface decreases due to increases in η_o^* as the carbonyl area increases with aging. This phenomenon limits further oxygen transport into the asphalt film.

For comparison, average values of P_{SI} (averages of initial and final aging time), calculated based on variable D_{O_2} , and the values calculated from the kinetic data for $(r_{CA})_{SI}$ are given in Table 10-6. All of the asphalts and aging conditions are given, excluding those for 20 atm. The initial and final aging times are 10, 5, 2, and 80, 40, 20 (days), for 333.3, 344.4, 355.5 K (140, 160, and 180 °F), respectively. The percent differences are also shown. The sets of questionable data show the largest percent differences. These sets were not used to estimate D_{O_2} vs η_o^* model parameters.

Figures 10-12, 10-13, and 10-14 show that P_{SI} decreases with increasing aging time for all asphalts and aging conditions studied. For example, in Table 10-6 for Ampet AC-20 at 333.3 K (140 °F) and P_{ES} of 2 atm, P_{SI} is 1.66 atm at ten days and 1.41 atm at 80 days.

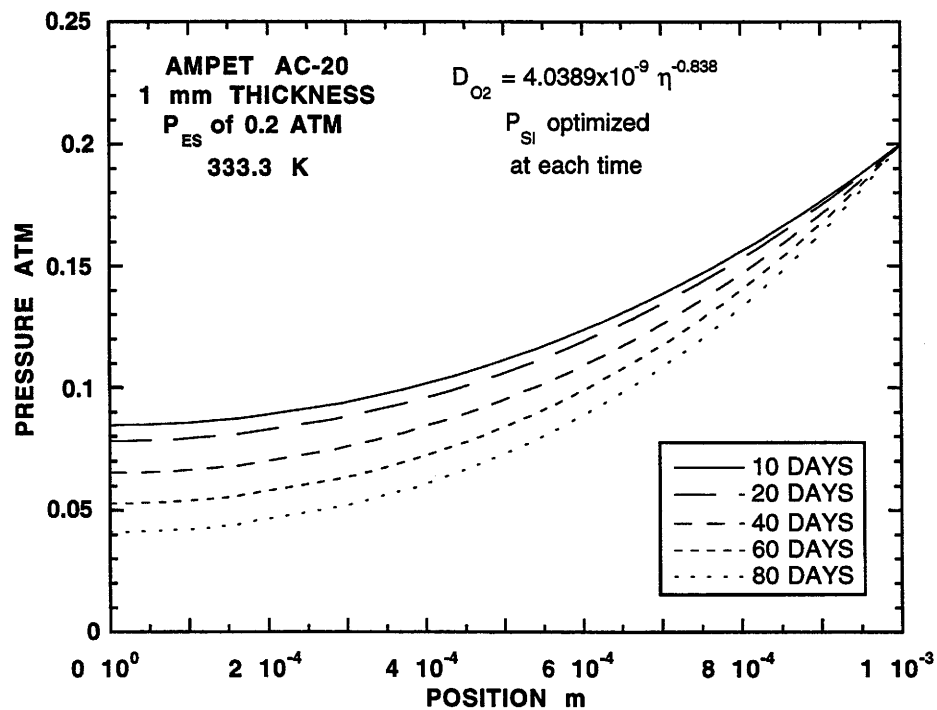


Figure 10-12. Calculated Oxygen Pressure Profiles (333.3 K)

Table 10-6. Comparisons Between P_{SI} Estimated from r_{CA} and Calculated for Steady-State Variable \mathcal{D}_{O_2} ^a

Asphalt	T K	P_{ES} atm	P_{SI}				% Diff ^b
			Initial atm	Kinetics atm	Final atm	Avg atm	
Ampet AC-20	333.3	0.2	0.0846	0.0673	0.0411	0.0629	7
		2.0	1.66	0.393*	1.16	1.41	-72
	344.4	0.2	0.138	0.115	0.0967	0.117	-2
		2.0	1.83	0.857*	1.49	1.66	-48
	355.5	0.2	0.170	0.161	0.142	0.156	3
		2.0	1.92	1.80	1.72	1.82	-1
Coastal AC-20	333.3	0.2	0.0820	0.149*	0.0290	0.0555	168
		2.0	1.49	0.925	0.630	1.06	-13
	344.4	0.2	0.132	0.0345	0.0698	0.101	-66
		2.0	1.74	0.476*	0.918	1.33	-64
	355.5	0.2	0.163	0.0789*	0.105	0.134	-41
		2.0	1.86	1.10	1.12	1.49	-26
Cosden AC-20	333.3	0.2	0.0444	0.0331	0.0063	0.0254	30
		2.0	1.33	0.936	0.403	0.868	8
	344.4	0.2	0.117	0.130	0.0576	0.0873	49
		2.0	1.70	0.363*	0.962	1.33	-73
	355.5	0.2	0.160	0.400*	0.121	0.140	186
		2.0	1.87	1.48	1.35	1.61	-8
Exxon AC-20	333.3	0.2	0.0686	0.175*	0.0284	0.0485	260
		2.0	1.54	1.09	0.958	1.25	-13
	344.4	0.2	0.120	0.108	0.0696	0.0948	14
		2.0	1.75	1.17*	1.21	1.48	-21
	355.5	0.2	0.169	0.0776*	0.146	0.158	-51
		2.0	1.91	1.86	1.74	1.82	2
Texaco AC-20	333.3	0.2	0.119	0.124	0.0749	0.0970	28
		2.0	1.74	1.38	1.28	1.51	-9
	344.4	0.2	0.157	0.122	0.123	0.140	-13
		2.0	1.87	0.570*	1.58	1.72	-67
	355.5	0.2	0.178	0.170	0.155	0.166	2
		2.0	1.94	1.28 *	1.75	1.84	-30

^a α of 0.270 and 1 mm (0.039 in) thick films

^b % Diff = $100 \left(\frac{P_{rea} - P_{avg}}{P_{avg}} \right)$

* These data were not used in the parameter estimation in Figure 10-11.

It should be noted that the values of P_{SI} determined from $(r_{CA})_{SI}$ and the average P_{SI} values estimated from the steady-state variable \mathcal{D}_{O_2} and reaction model are not entirely consistent. The range of initial and final P_{SI} should bound the reaction

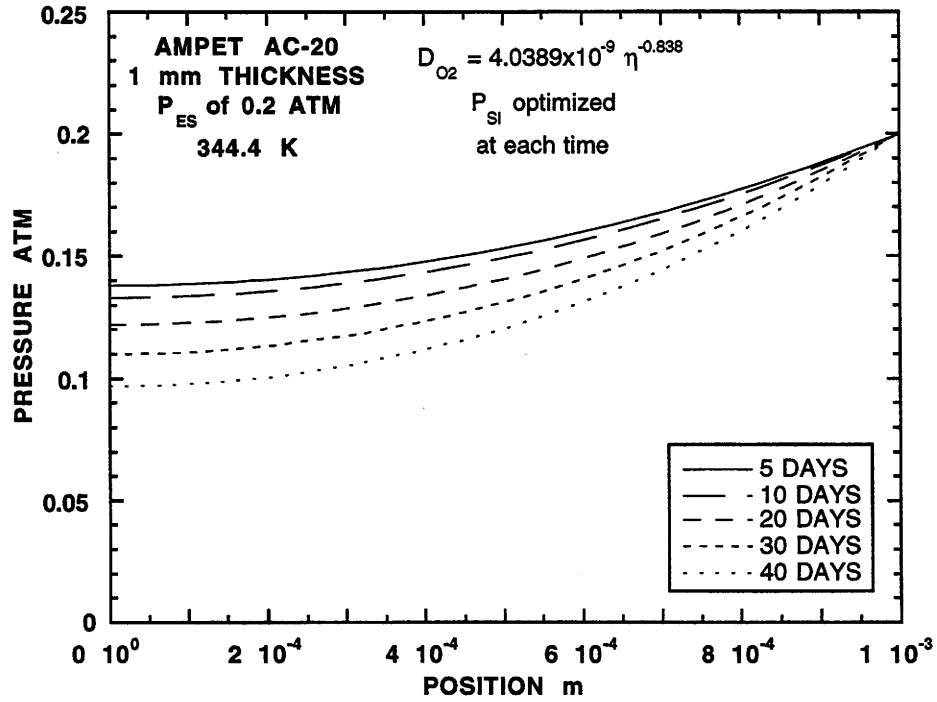


Figure 10-13. Calculated Oxygen Pressure Profiles (344.4 K)

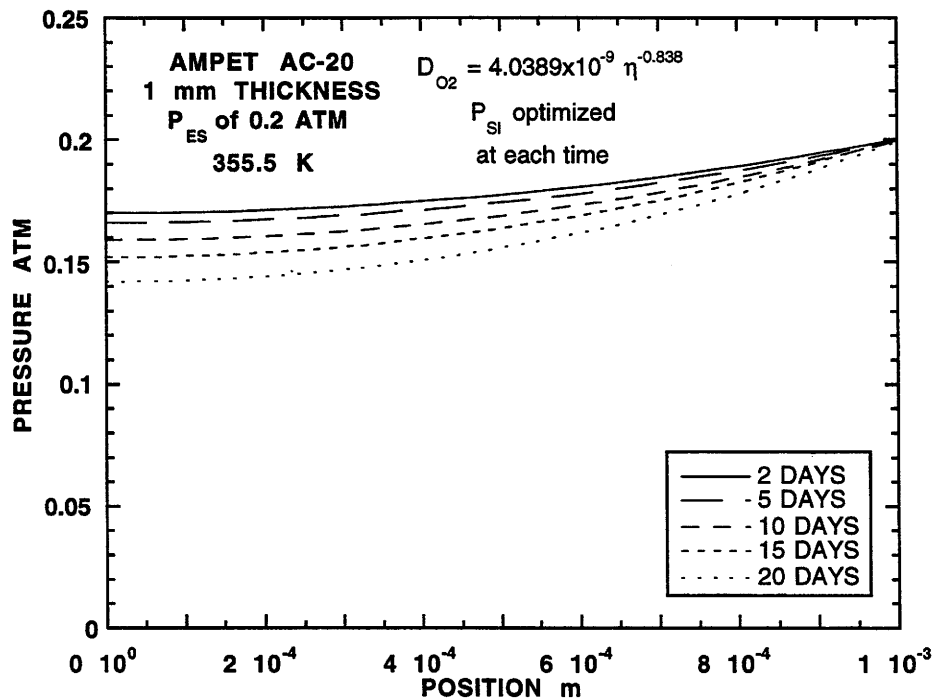


Figure 10-14. Calculated Oxygen Pressure Profiles (355.5 K)

values. This is not always the case, even for the “best” data, those which were included in the parameter estimation of the \mathcal{D}_{O_2} vs η_o^* model. (P_{SI} values estimated from $(r_{CA})_{SI}$ were outside initial and final P_{SI} for all questionable data that were not used to estimate \mathcal{D}_{O_2} vs η_o^* model parameters.) For example, the range of initial and final P_{SI} values does not bracket the kinetic P_{SI} value at 333.3 K (140 °F) and 0.2 atm for Texaco AC-20; at 344.4 K (160 °F) and 0.2 atm for Coastal AC-20, Cosden AC-20, and Texaco AC-20; and at 355.5 K (180 °F) and 2.0 atm for Coastal AC-20. These errors may result from the steady-state assumption or from the estimation of CA_o . CA_o was not in the model when steady-state constant \mathcal{D}_{O_2} was determined, and the \mathcal{D}_{O_2} vs η_o^* model was developed.

Unsteady-State Oxygen Diffusion and Reaction

From the calculations reported above and from considerations of the aging process it is clear that as time goes on the material becomes harder, the diffusivity less, and therefore, the pressure in the film less. Hence, in reality the oxidation process is an unsteady state phenomenon. Accordingly, to model it most correctly an unsteady-state calculation is called for. In this section such calculations are reported. Note again, however, as was true for the variable diffusivity situation, calculations based upon diffusivities obtained and reported earlier are used even though they were obtained for the steady state constant diffusivity model.

For this situation, the diffusivity is allowed to be a function of position through the film, and, furthermore, the pressure and all further physical and chemical (i.e. carbonyl area) properties of the asphalt are allowed to vary with time. The model is as reported in Appendix C and calculation procedures are outlined by Lunsford (1994).

A comparison between measured and calculated CA at the ES and SI gives an indication of the model's ability to predict aging characteristics. Figures 10-15 through 10-20 compare Texaco AC-20 at 333.3, 344.4, and 355.5 K (140, 160, and 180 °F), and P_{ES} of 0.2 and 2 atm. Comparisons for the other asphalts are shown in Appendix C. Measured CA values are designated with the hollow symbols; calculated CA values are shown with the solid or dashed line. It appears that calculated CA_{ES} is always lower

than measured CA_{ES} for the same aging times, temperatures, and P_{ES} . At the SI , calculated CA is higher than the measured value for some cases and lower for others. The agreement is best in Figures 10-16 and 10-18. While there are significant differences between measured and calculated CA , agreement in r_{CA} (slope of the lines) is better.

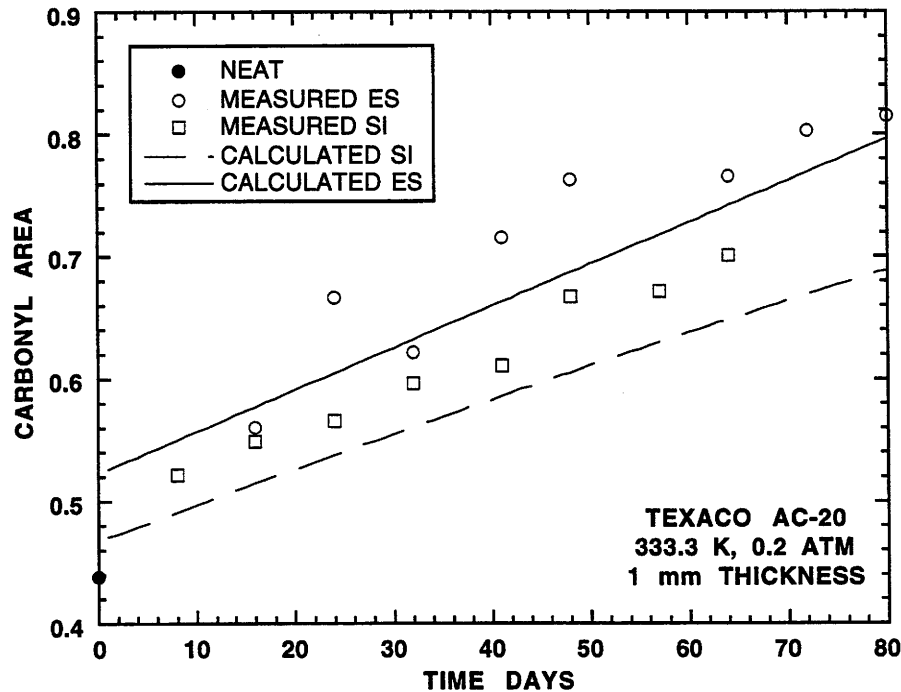


Figure 10-15. Comparisons of Measured and Calculated CA (333.3 K, 0.2 atm)

An averaged P_{SI} was determined from calculated P_{SI} for the aging simulation. Average P_{SI} values agree closely with those reported in Table 10-7 for steady-state and variable \mathcal{D}_{O_2} .

Figures 10-21 through 10-24 show the oxygen pressure, CA , $\log \eta_o^*$, and $\log \mathcal{D}_{O_2}$ profiles for Texaco AC-20 at 333.3 K (140 °F) and P_{ES} of 0.2 atm. These figures provide a qualitative understanding of the aging phenomenon. Similar figures were not generated for the other asphalts and aging conditions studied.

In Figure 10-21, the maximum P_{SI} occurs at about six days. This suggests that, initially, the rate of oxygen diffusion exceeds that of reaction. After the maximum, P_{SI} decreases as a result of an increase in CA_{ES} and a resultant decrease in \mathcal{D}_{O_2} at the ES .

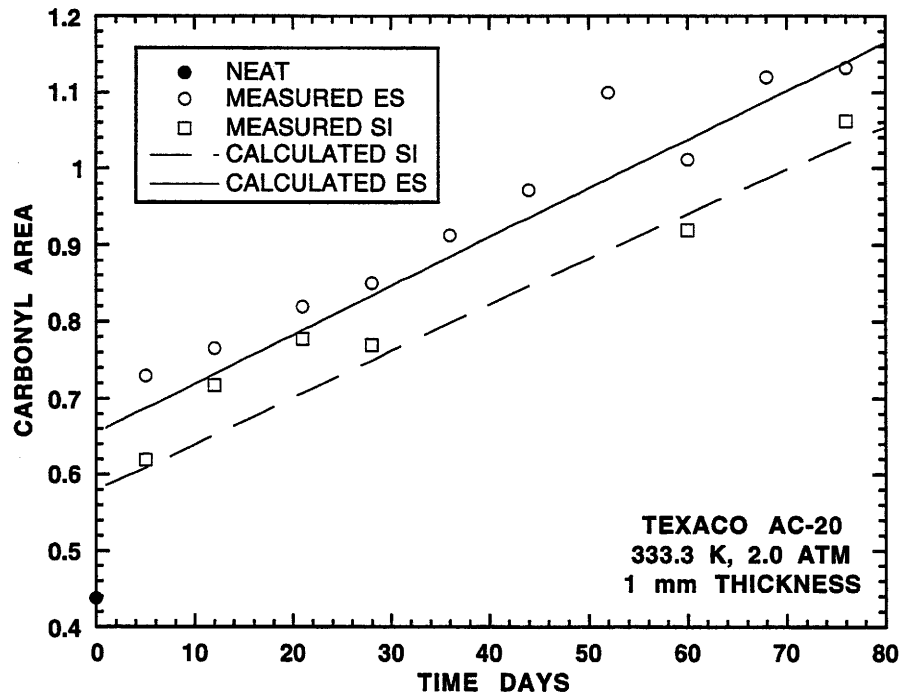


Figure 10-16. Comparisons of Measured and Calculated CA (333.3 K, 2 atm)

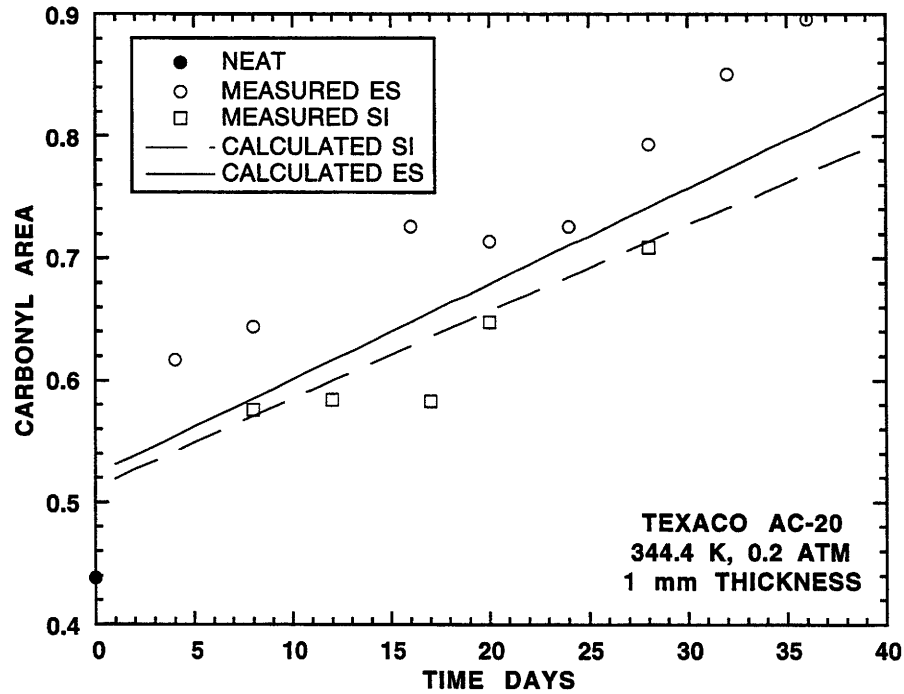


Figure 10-17. Comparisons of Measured and Calculated CA (344.4 K, 0.2 atm)

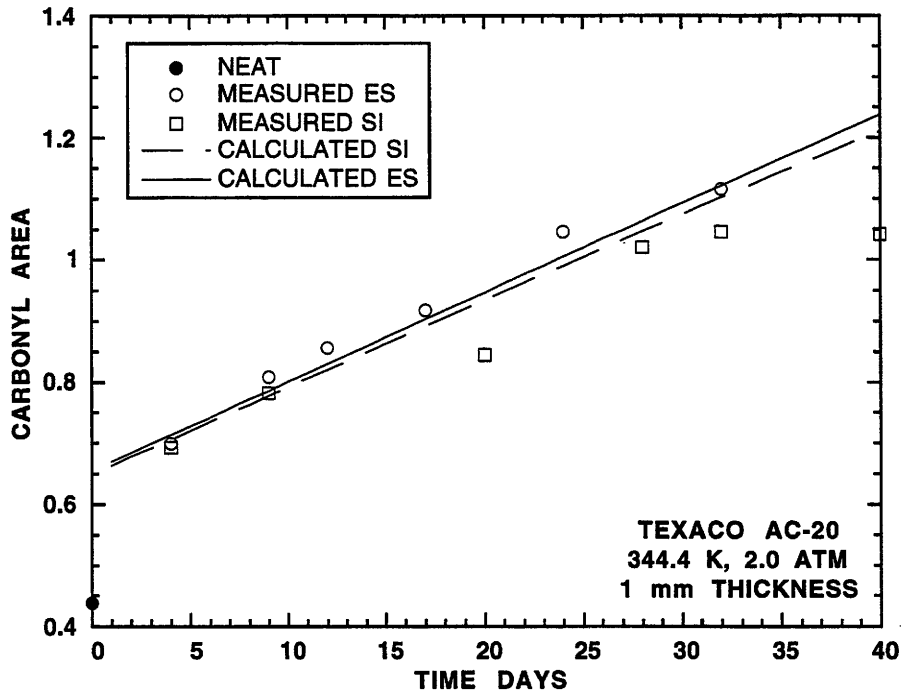


Figure 10-18. Comparisons of Measured and Calculated CA (344.4 K, 2 atm)

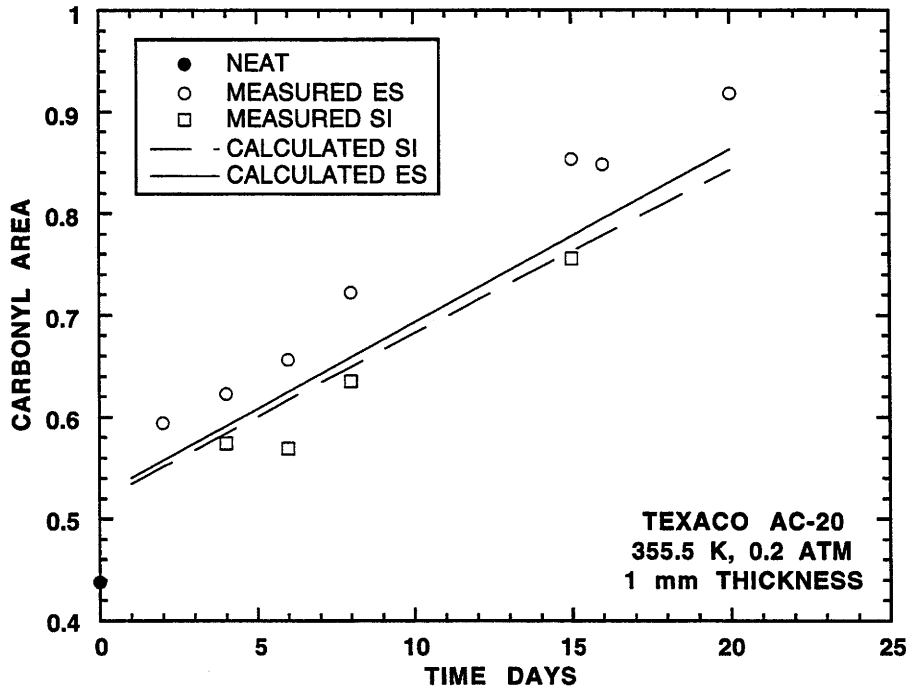


Figure 10-19. Comparisons of Measured and Calculated CA (355.5 K, 0.2 atm)

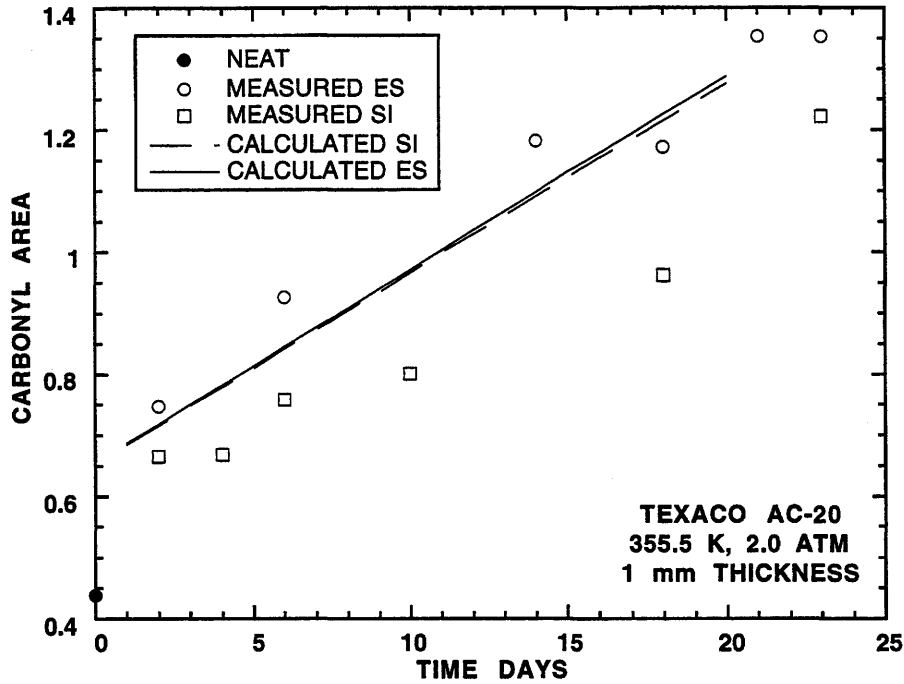


Figure 10-20. Comparisons of Measured and Calculated CA (355.5 K, 2 atm)

Figure 10-22 shows CA profiles. The difference increases between CA_{ES} and CA_{SI} with aging time at isothermal aging conditions. This results from decreasing P within the film.

Log η_o^* profiles in Figure 10-23 show similar trends as CA profiles. HS and m along with CA were used to calculate log η_o^* profiles.

Finally, Figure 10-24 shows log \mathcal{D}_{O_2} profiles. In this figure, note that the maximum \mathcal{D}_{O_2} is at the SI instead of at the ES ; this profile is inverted compared with the other profiles, of course. Furthermore, note that values of \mathcal{D}_{O_2} do not intersect at $t = 0$ because the integration over time was divided into two separate regions. The difference between the ES and SI increases with aging time, as with CA and log η_o^* . For the other asphalt and aging conditions, similar phenomena are expected; however, profiles were not generated.

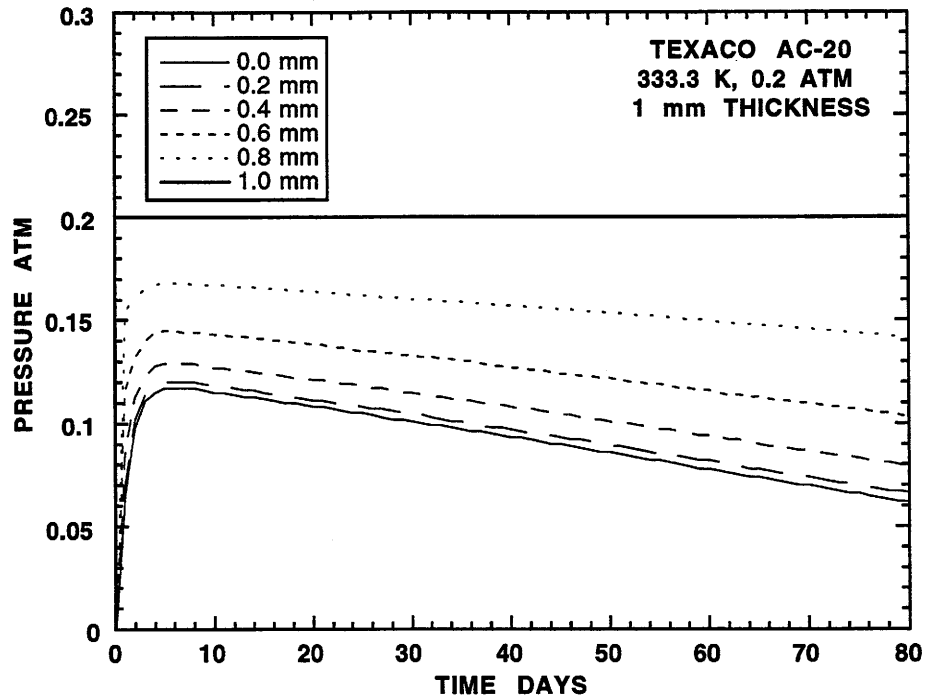


Figure 10-21. Calculated Oxygen Pressure Profiles Change over Time

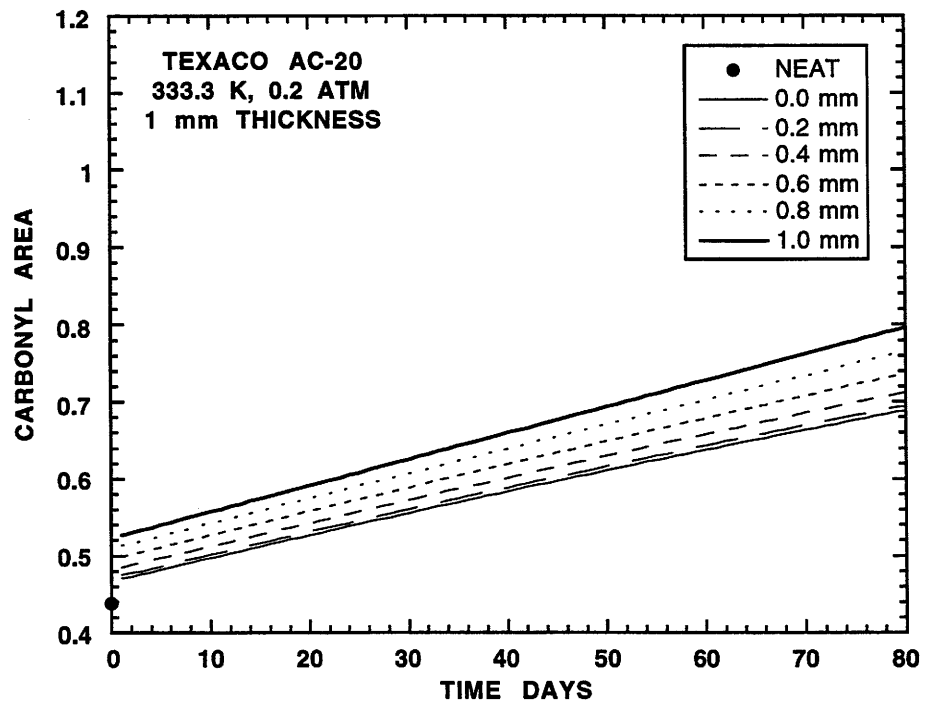


Figure 10-22. Calculated CA Growth

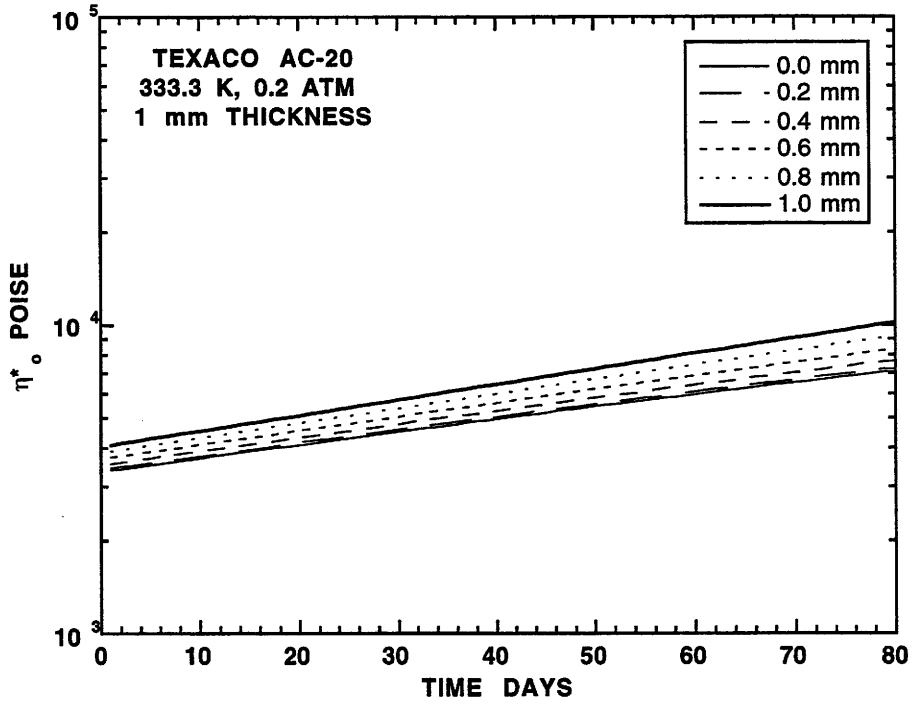


Figure 10-23. Calculated η^* Growth

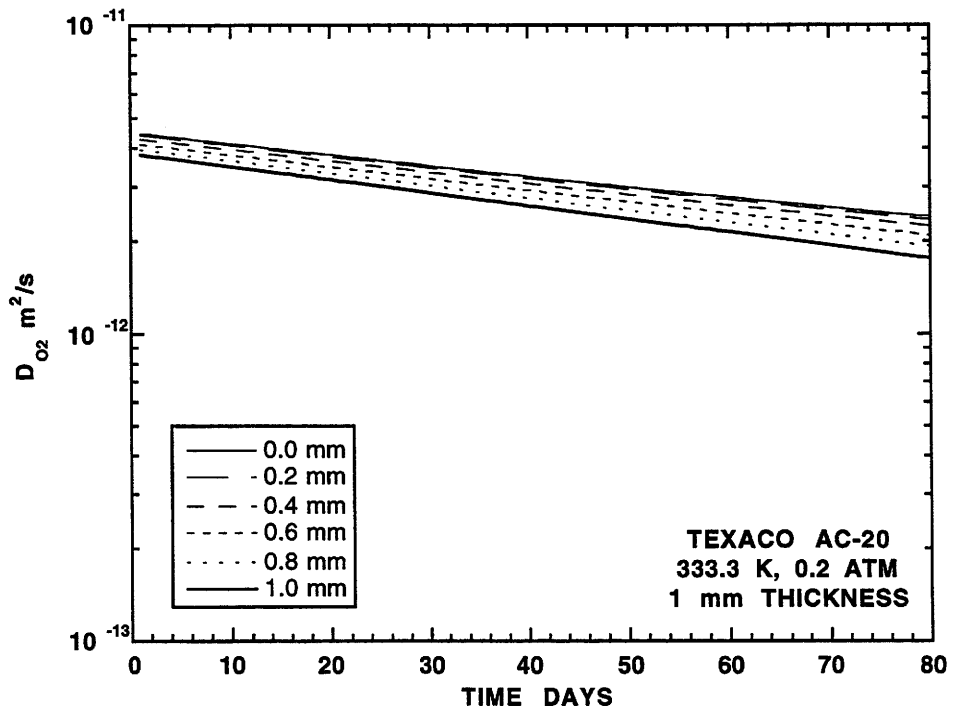


Figure 10-24. Calculated D_{O_2} Decrease over Time

DIFFUSION AND REACTION IN ASPHALT AGING TESTS

Davison et al., (1992) proposed an asphalt aging test. From kinetic parameters determined by POV aging at several temperatures and physicochemical property relationships, the authors calculated the time required to reach a certain pre-defined failure criterion. A relative ranking of the asphalts studied was provided. The POV experiments were at 20 atm.

This test showed the dramatic difference that oxidation temperature has on the ability of an asphalt to resist aging. However, the test neglected certain critical factors. First, POV data were only at one elevated pressure. No pressure correction to atmospheric conditions was provided. This does not change the relative rankings of the asphalts in this work, since they all had essentially the same oxygen order of reaction. Second, the authors assumed that CA_o for all of the asphalts was the same. Current data have shown that this is not true. CA_o is asphalt and pressure dependent. Since the change in CA relates to the time required to reach the failure criterion, the relative rankings of the asphalts could possibly change when atmospheric aging pressures and asphalt specific CA_o are taken into account. Finally, the previous aging test neglected diffusion resistance.

Using this same idea with the data and model presented in this chapter and in Appendix C, results for an isothermal aging test including diffusion and reaction were computed. The isothermal aging temperature was 322.2 K (120.3°F), P_{ES} was constant 0.2 atm, kinetic parameters were taken from Table 1-6, CA_o was determined from parameters in Table C-3, and four different calculations were done. The first assumed no oxygen diffusion resistance, while the last three calculations included diffusion resistance for film thicknesses of 0.8, 1.0, and 1.2 mm (0.031, 0.039, and 0.047 in). Table 10-7 shows the years required to reach a 500 kP η_o^* at 333.3 K (140 °F).

For these calculations, inclusion of the diffusion resistance resulted in an increase of about threefold in the required time for all of the asphalts studied. For a given asphalt, the time required was also increased by increasing film thickness. In addition, including the effect of diffusion resistance changed the relative rankings. Of the asphalts studied,

Table 10-7. Comparisons Between Calculated Time to Reach 500 kP η_o^* at 333.3 K (140 °F), Aging at 322 K (120 °F) and P_{ES} of 0.2 atm with and without Diffusion Resistance for Three Film Thicknesses

Asphalt	No Diff yrs	Film Thickness		
		0.8 mm yrs	1.0 mm yrs	1.2 mm yrs
Ampet AC-20	3.01	6.55	7.32	10.38
Coastal AC-20	2.30	3.10	4.30	5.45
Cosden AC-20	1.88	4.36	6.33	7.15
Exxon AC-20	2.59	5.51	9.45	9.73
Texaco AC-20	2.75	4.30	7.10	7.97

for example, Cosden AC-20 was the least resistant to oxidative aging at 322.2 K (120 °F), with no diffusion resistance. However, with oxygen diffusion through a 0.8 mm (0.031 in) thick film, Coastal AC-20 is the least resistant to oxidative aging relative to the other asphalts at 322.2 K (120 °F). This change in the rankings is caused by the two competing rate phenomena, oxygen diffusion versus reaction, further complicated by the hardening susceptibility physicochemical property relation. From the simulation, it appears that asphalts with a low HS show a more significant increase in aging resistance when diffusion is included than do those with a higher HS . For example, Coastal AC-20 has the highest HS (3.9), and its failure time changes the least when diffusion is included. On the other hand, Exxon AC-20 has the lowest HS (2.5) and its failure time increase is larger.

The previous table shows some peculiar results, however. It is difficult to explain why Ampet AC-20 is the best asphalt at 0.8 mm (0.031 in), the second best asphalt at 1.0 mm (0.039 in), and the best asphalt again at 1.2 mm (0.047 in). The reverse is true for Exxon AC-20. The other asphalts do not exhibit this rather erratic behavior. Although this is only a preliminary study, one conclusion can be made. It appears that asphalt film thickness and diffusion must be included in an asphalt-aging test.

SUMMARY

The work of this chapter consisted of two parts. The first part was to develop a fundamentals-based model for the aging of asphalt in pavements and to use this model to make estimates of \mathcal{D}_{O_2} in asphalt at a variety of conditions of temperature and asphalt oxidation. The second part was to use this model and the diffusivity values to calculate qualitative changes in asphalt properties across a thin film and during aging.

From these data, a relation of \mathcal{D}_{O_2} as a function of temperature and asphalt viscosity was obtained.

Growth of the infrared carbonyl peak at both the *ES* and *SI* was measured for POV-aged asphalt films. From these data, estimates of \mathcal{D}_{O_2} were calculated for a steady-state, constant \mathcal{D}_{O_2} model. Due to error propagation of $(r_{CA})_{SI}$ to P_{SI} , errors in \mathcal{D}_{O_2} in some cases were large. Nevertheless, the data were sufficient to allow the determination of the two parameters in a \mathcal{D}_{O_2} vs η_o^* model. With these two values and knowledge of how a particular asphalt's viscosity changes with aging, diffusivity can be related to the degree of aging of an asphalt, a necessary step in being able to make predictive calculations of aging in pavements.

To illustrate, with a model relating \mathcal{D}_{O_2} to η_o^* , along with the estimated model parameters, the change in P_{SI} during the POV aging experiment was calculated from the steady-state, variable \mathcal{D}_{O_2} model of oxygen diffusion and reaction. Average P_{SI} and P_{SI} determined from $(r_{CA})_{SI}$ compared favorably.

To further illustrate, an unsteady-state, variable \mathcal{D}_{O_2} model of oxygen diffusion and reaction was numerically integrated for the POV aging conditions studied. From these integrations, calculated *CA* at the *ES* and *SI* were compared to measured *CA*. For one asphalt and one aging condition, examples of oxygen pressure, *CA*, $\log \eta_o^*$, and $\log \mathcal{D}_{O_2}$ profiles from oxidative aging in an asphalt film were produced.

As another use of such a model, an aging test was evaluated. The time to reach a pre-determined failure criterion of $\eta_o^* = 500$ kP at 333.3 K (140 °F) was calculated for isothermal aging at 322.2 K (120 °F) and constant P_{ES} of 0.2 atm. For the thickest films, inclusion of the diffusion resistance increased the required time five fold in some

asphalts, as compared to aging without diffusion resistance. The relative ranking of the asphalts changed when diffusion resistance was included. Including both diffusion and reaction has a more significant effect on the calculated failure time for asphalts with relatively low HS as compared to those asphalts with relatively high HS .

Finally, the model developed in this chapter is the foundation for an asphalt-aging model. This model of oxygen diffusion and reaction in an asphalt film accounts for both temperature and pressure variation and for unsteady-state, variable \mathcal{D}_{O_2} .

CHAPTER 11

COMPARISON BETWEEN LABORATORY AND FIELD AGING

As reported in previous chapters, we have devoted much effort to developing kinetic and diffusion models for laboratory-aged asphalts. These models, together, form an asphalt-aging model. The ultimate objective is to develop a highway-pavement aging model using this fundamental asphalt-aging model. The highway-pavement aging and asphalt-aging models would allow highway engineers to monitor and predict field aging. Also, these models could be used to rank asphalts by their predicted resistance to field aging. With the knowledge from accurate aging models, highway engineers and governments can better allocate resources for improving and maintaining the highway system.

A favorable comparison between field- and POV-aged material would confirm that laboratory oxidation simulates field aging. Unfortunately, previous comparisons have been flawed by extraction and recovery procedures (Burr et al., 1990; Burr et al., 1991), or the complete lack of a kinetic model or data. However, in this work, the field- and POV-aged asphalts are compared by two different methods, reported in two sections in this chapter. The first method takes advantage of the physicochemical relationship developed by Lau et al., (1992). This relationship was independent of the diffusion and reaction kinetics of the aging process but does depend upon the chemical reaction and physical interaction mechanisms that occur within the asphalt. Having the ability to separate kinetics from mechanism is very important. The second method of comparison includes diffusion and reaction kinetics. From laboratory-determined kinetic and diffusion parameters along with climatic data, estimates of the effective asphalt film thickness, L_{eff} , and effective oxygen pressure in the void, P_{eff} , were made by comparing field-aged data to values calculated from the asphalt-aging model.

In order to achieve an accurate laboratory simulation of field aging the oxidation products obtained from POV aging over a relatively short time period should be the same as those which occur during field aging over a long period of time. Only the rate at which the products are formed should differ. If the same oxidation products are formed, the same physicochemical relationship should result. If both aging methods produce the same physicochemical model parameters, the laboratory simulation is correct. This confirmation must be completed before proceeding with the asphalt-aging model.

Once positive confirmation between field- and laboratory-aged materials is obtained from physicochemical properties, the field-aged data and asphalt-aging model can be used to develop a highway-pavement aging model. Laboratory experiments yield the asphalt-specific parameters, E_A , A , HS , and m . Assuming that α and the diffusivity parameters are independent of asphalt composition, these values can be taken from Chapters 1 and 10. The parameters relating CA_o to aging P are not determined for these asphalts. With the known kinetic and diffusion parameters and climatic information for the specific region, L_{eff} and P_{eff} can be estimated by comparing field-aged data with model-calculated values. The model relating L_{eff} and P_{eff} to measurable core properties then is the highway-pavement aging model.

LITERATURE SURVEY OF FIELD AGING

During laboratory aging, the temperature, oxygen pressure, and film thickness can be accurately monitored and controlled. In the field, these factors can only be estimated. Furthermore, the presence of aggregate in contact with the asphalt may also result in different mechanisms and different oxidation products. When modeling field aging, climatic conditions and measurable core properties must be included. These measurable core properties then must be related to the fundamental quantities in an asphalt-aging model.

The study of asphalt oxidation in the presence of different aggregates has led to many different conclusions. Petersen et al., (1974) studied asphalt oxidation on mineral surfaces with inverse gas liquid chromatography. They concluded that a majority of the

oxidation resulted from components naturally present in the asphalt. By comparison, the catalytic effect of the aggregate is significantly reduced. Plancher et al., (1976) concluded that hydrated lime decreases the rate of asphalt hardening. Edler et al., (1985) confirm this result using lime treatment and Extended RTFOT and POV aging. These last two studies suggest that the kinetics of oxidation may be affected by the type of aggregate. With limited data, Lau et al., (1992) concluded that the physicochemical relationships were independent of aggregate type by comparing POV-aged materials. This suggests that the products formed as a result of oxidation and their effect on physical properties is independent of aggregate. However, this says nothing of the nature of the kinetics.

Highway-pavement temperature is a very significant factor in field aging (Kemp and Predoehl, 1981). This affects both the rate of reaction and the rate of oxygen transport. The estimation of the maximum surface temperature, T_{sur} , based on ambient temperatures, T_{air} and latitude, ψ , is given by Solaimanian and Kennedy (1993). Based on field measurements and the conservation of energy for steady-state heat flow at the asphalt surface, the difference between the maximum T_{sur} and T_{air} is a quadratic function of ψ given in Equation 11 – 1:

$$(T_{\text{sur}} - T_{\text{air}})_{\text{max}} = -0.01113\psi^2 + 0.41202\psi + 43.877 \quad (11 - 1)$$

For Equation 11 – 1 the temperatures are in units of °F. The temperature of the pavement below the surface is also important. By comparing measured and estimated temperatures, the top 20.3 cm (8 inches) of the pavement are within 2.8 to 3.3 K (5 to 6 °F) of the surface temperature. At greater depths, the temperature difference increases. Using ambient temperature data from different locations and Equation 11 – 1 the annual temperature cycle of the pavement can be estimated. Verhasselt and Choquet (1993) discuss an interesting approach of including the annual temperature variation in the reaction kinetics. Integrating the Arrhenius equation over the annual temperature profile, they calculate a kinetic mean temperature. However, they do not discuss the fact that the kinetic mean temperature is not only a function of location but also asphalt, since the Arrhenius parameters are asphalt dependent.

The measurable core properties of percent voids, % V , asphalt content, % Asp , and aggregate gradation affect the rates of oxidation and hardening in the field. For field aging, Davison et al., (1989) provide an exhaustive literature review showing the % V is the single most dominant factor in the rate of asphalt oxidation and hardening. This work shows that the effect of air voids is greater than the difference in asphalt composition. Heithaus and Johnson (1958) concluded that a linear relationship existed between % V and binder hardening rate based on measured viscosity.

Goode and Lufsey (1965) conducted a study of the effect of voids, air permeability, asphalt content, and aggregate gradations on oven aging of asphalts using molded test specimens. For a given gradation, aging and permeability increased with voids. At high void content, the permeability was affected more than the aging. They found that aging increased as asphalt film thickness decreased. At fairly low voids, all gradations could be correlated with the ratio of voids to obtain an averaged film thickness. This ratio, called the voids-bitumen index, was suggested as a possible design parameter, permitting a range of air voids depending on the aggregate. Halstead (1963) noted the tendency for lower hardening with higher asphalt content based on the Zaca-Wigmore test sections.

In terms of oxidative aging in the field, permeability is critical, but at low void levels becomes very difficult to measure (Chipperfield et al., 1940). Permeability is very low at the top of the pavement from compaction due to traffic. Yet, oxidative aging is much greater at the top of the pavement relative to positions below the surface primarily due to elevated surface temperatures. At this position in the pavement with such low permeability, oxygen transport occurs primarily from diffusion. Goode and Lufsey (1965) found that air permeability was a function of aggregate gradation as well as % V . At high air voids, the effect of gradation was more pronounced than at low air voids. At void levels of 4-5%, the measured values of air permeability were very low and independent of aggregate gradation.

Based on experience, Campen et al., (1959) stated that asphalt film thicknesses of 6 to 8 microns are most desirable for pavement mixtures. This film thickness provides a thick asphalt film and, at the same time, the desired void content and stability. Kumar and Goetz (1977) report on a study of aging as a function of permeability and film thickness.

Laboratory compacted cores were prepared with graded and ungraded aggregate at varying asphalt content and compaction levels. The cores were aged by passing 333.3 K (140 °F) air through the cores. The aging was monitored periodically by a non-destructive creep test. For the single-size mixtures, the best correlation was the ratio of asphalt film thickness to permeability alone. The ratio of film thickness to voids did not correlate well, even though there was a strong correlation between voids and permeability. Surprisingly, for graded mixtures, everything correlated. The authors admitted that this is not very logical. Based on microscopic studies, they decided the idea of film thickness is not applicable to graded mixtures, and correlations were made only with permeability and voids. They discuss dividing the total air voids into two groups, accessible voids and non-accessible voids. Neither of these studies provides a fundamental model for calculating film thickness. Instead, film thickness is determined from empirical models based on % *Asp*. The authors did not provide any relation between the total voids, permeability, and non-accessible voids. Furthermore, the authors did not discuss the relationship of the permeability and void levels to the time-dependent oxygen pressure in the air voids.

There are few systematic and successful attempts to include other variables such as percent asphalt or aggregate gradation in correlations of road aging. Krchma and Groening (1959), in analyzing data of Pauls and Halstead (1958), showed that both percent asphalt and voids affect the asphalt hardening. As mentioned earlier, Kumar and Goetz (1977) correlated aging of lab samples in terms of film thickness but obtained poor results for dense mixtures. Goode and Lufsey (1965) used asphalt content to calculate a bitumen index that also included aggregate gradation and is supposedly a measure of film thickness. The best correlation was with percent air voids divided by the bitumen index. They also showed a relation between percent voids, asphalt gradation and permeability.

Similar to the laboratory aging tests, the main focus has been on the attempt to develop empirical correlations between measured core properties and degree of aging. No researcher has successfully used any of these models to predict field aging based solely on the current laboratory tests and empirical correlations. Unfortunately, these empirical models do not contain sufficient information to accurately predict field aging based on

the measured core properties at some initial time. A more fundamental approach is to relate the measured core properties to fundamental quantities in an asphalt-aging model. Then, in the context of the model, accurate predictions of field aging based on initial measured core properties are possible.

To summarize, a pavement aging model including climatic conditions and measurable core properties has not been investigated. With the development of an accurate asphalt-aging model and implementation of laboratory tests designed to estimate the model parameters, researchers will be able to reliably predict highway aging, potentially saving millions of dollars.

HIGHWAY SAMPLES AND LABORATORY EXPERIMENTAL DESIGN

Tank asphalts and field-aged material from three test sections located in the state of Texas were acquired. The test sections are located in Dickens, Pineland, and Bryan. For the Dickens test section, the original pavement was placed in 1982, and seven asphalts were used (Adams and Holmgreen, 1986). The Pineland test section was an overlay in 1983, where six asphalts were used. The aggregates at Dickens and Pineland were river gravel and limestone/iron ore mix, respectively. The Dickens and Pineland test sections are important for two reasons: different asphalts were used in the same test section, and several literature sources describe the test section aging (Adams and Holmgreen, 1986; Martin et al., 1990; Davison et al., 1989). The Bryan test section was placed in 1987 and was constructed of asphalt from one refinery. Tank asphalt and hot-mix were sampled at different locations during construction. Table 11-1 gives the asphalts used at each location; the numbers following the Bryan Exxon AC-20 designation correspond to the sample locations.

Tank asphalts from the test sections were POV-aged using procedures described in Appendix A. The POV aging temperature and time were selected such that the measured field-aged properties should lie within the range of laboratory data for comparison of physicochemical properties. The aging pressure in all cases was 20 atm pure oxygen. Table 11-2 gives viscosity, η , percent air voids, % V , and percent asphalt, % Asp , for

Table 11-1. List of Asphalts Studied for Field Aging^a

Location	Asphalts
Dickens ^b	Cosden 10, Cosden 20, Diamond Shamrock, Dorchester, Exxon, MacMillan
Pineland ^b	Cosden, Dorchester, Exxon, MacMillan, Texaco
Bryan ^c	Exxon #8, #15, #16, #18, #19, #1B

^a Asphalts are AC-20 grade unless noted in the table.

^b From Adams and Holmgreen (1986)

^c From Davison et al., (1989)

Dickens and Pineland asphalts from extracted cores in 1987 (Davison et al., 1989). Carbonyl content was also measured in this report, but the KBr method was used. Comparing IR spectra obtained by two different techniques was not attempted or recommended. From the data in Table 11-2, POV aging temperatures for Dickens and Pineland asphalts were 355.5 and 333.3 K (180 and 140 °F), respectively. For both, the maximum aging time was 22 days. From the Bryan test section, six asphalts were aged at 344.4 K (160 °F), and three of the six were aged at 355.5 K (180 °F). Aging times ranged from 40 and 20 days for 344.4 and 355.5 K (160 and 180 °F) experiments. Ten trays per asphalt per temperature were prepared for all of the POV aging experiments. Changes in *CA*, rheological properties, and *MW* were measured by FT-IR, DMA, and GPC, respectively.

The cores from Dickens and Pineland were extracted by two different methods: the auto extraction by Burr (1993) and a modification of method A (ASTM D-2172-81). The modified method is called the micro extraction since one core was partitioned into four equal masses. The four masses were extracted independently. The final recovery of the asphalt for both methods used a rotary evaporator. The cores from Bryan were extracted using the auto extraction method only. All extractions used a solvent solution of 25% ethanol and 85% TCE by volume. After extraction and recovery, GPC analysis confirmed that solvent removal was complete (Burr et al., 1990; Burr et al., 1991).

Table 11-2. Properties of 1987 Samples from Dickens and Pineland Test Sections^{a,b}

Location	Asphalt	η (333.3 K) Poise	% V	% Asp
Dickens	Cosden AC-10	342000	12.0	5.6
	Cosden AC-20	376000	11.0	4.0
	Diamond Shamrock AC-20	260000	12.0	—
	Dorchester AC-20	222000	13.0	4.6
	Exxon AC-20	900000	9.0	5.1
	MacMillan AC-20	159000	8.0	6.2
Pineland	Cosden AC-20	5400	1.8	6.9
	Dorchester AC-20	—	—	—
	Exxon AC-20	2500	2.5	7.7
	MacMillan AC-20	—	—	—
	Texaco AC-20	—	—	—

^a From Davison et al., 1989

^b — Signifies the values were not determined.

Furthermore, GPC data were used to identify and verify the asphalts. This determined whether the samples were cored in the correct location (Glover et al., 1987).

POV- AND FIELD-AGING COMPARISONS: EXPERIMENTAL DATA

In this section, POV- and field-aged asphalts are compared by physicochemical relationships. Based on the agreement in the comparisons, a tentative conclusion about the ability of POV aging to simulate field aging is reached. Since field-aged asphalt requires extraction and recovery, GPC confirmed complete solvent removal and verified the coring location and asphalt. The η_o^*-CA relationship for POV aging is compared to that for field aging. Extensive data for these and other property comparisons are given in Appendix E of Lunsford (1994).

Confirming Complete Solvent Removal and Coring Location

The extracted asphalt and the POV-aged material were analyzed by GPC. This

confirmed complete solvent removal during extraction and recovery and verified the location with POV-aged neat asphalt.

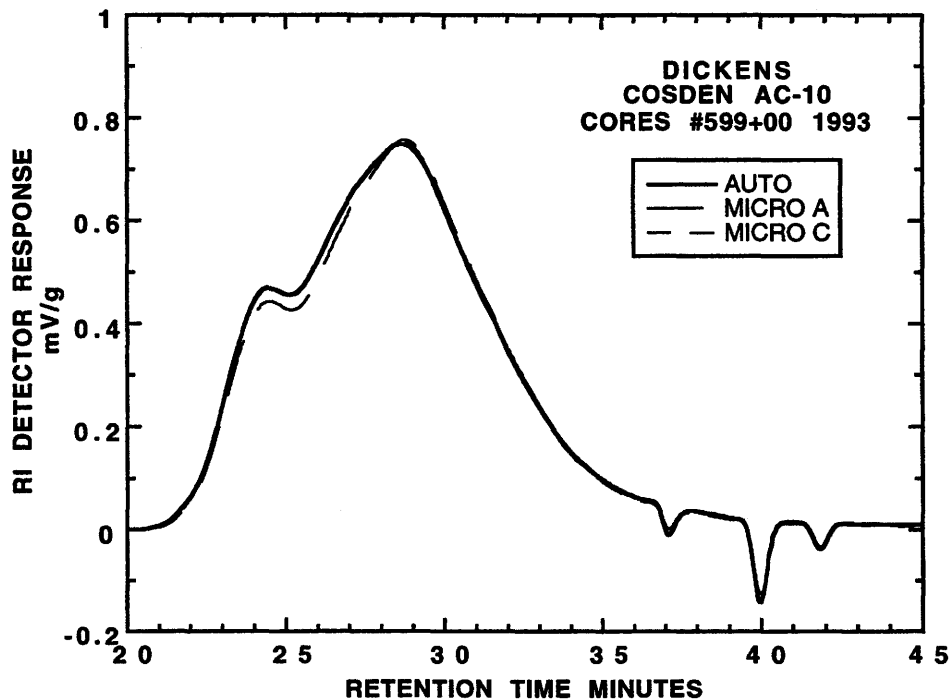


Figure 11-1. GPC Chromatograms of Field-Aged Cores (Dickens Cosden AC-10)

Figure 11-1 shows GPC chromatograms for field-aged Dickens Cosden AC-10. The bold line designates the auto extraction method, and the thin dashed lines represent the micro extractions. The two micro extraction chromatograms overlay each other. The chromatogram is divided into three sections for descriptive purposes. The first section, between 21 and about 26 minutes, represents the asphalt molecules of large molecular size. This is designated the *LMS* region. The second section, from 26 minutes to 35 minutes, is the medium molecular size, *MMS*. The third and final section, from 35 to 45 minutes, is the solvent and dissolved gases region. The negative peaks at 37, 40, and 42 minutes represent water, nitrogen, and oxygen, respectively. Since the *RI* of these compounds is less than the *RI* of the carrier solvent, THF, negative peaks result. The presence of the extraction solvent produces a positive peak at about 38 minutes between the water and nitrogen peaks.

From the absence of the solvent peak at 37 minutes, it was concluded that solvent removal was complete. The shape of chromatograms suggests that the auto extraction method either removed or produced more *LMS* than the micro extractions for this asphalt. Other than that discrepancy, the shapes of the chromatograms are nearly identical. Chromatograms of the extracted asphalt from the other locations are shown in Appendix E of Lunsford (1994). There appears to be no residual solvent present after extraction and recovery for any of the field-aged asphalts. Furthermore, the difference between the auto and micro extraction methods appears to be random with respect to the *LMS* region.

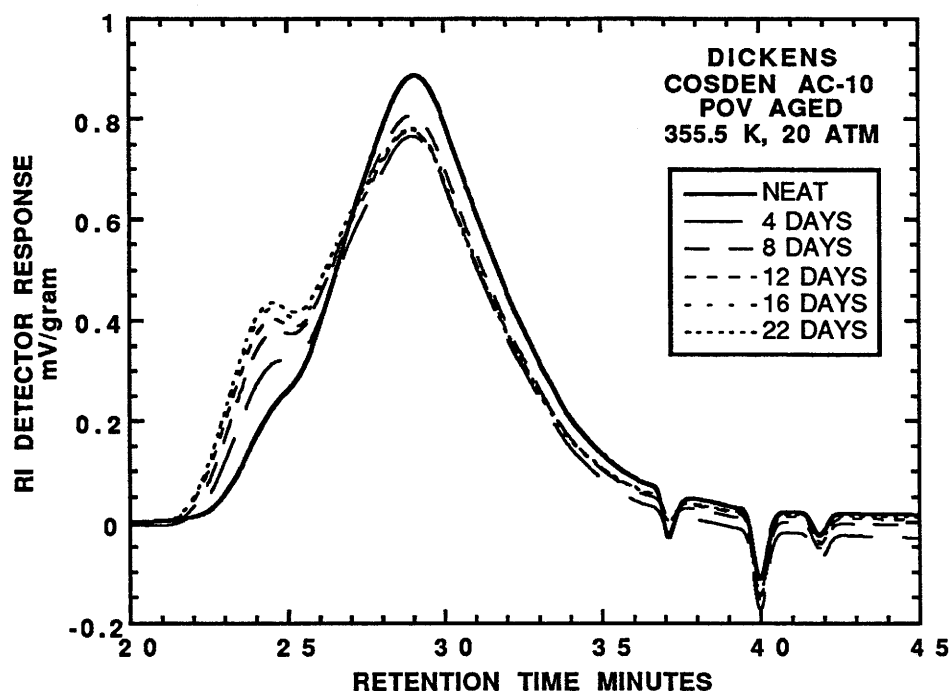


Figure 11-2. GPC Chromatograms of Tank and POV-Aged Dickens Cosden AC-10

Some of the POV-aged asphalts were analyzed by GPC to generate a fingerprint of the asphalt as described by Glover et al., (1987). POV- and field-aged fingerprints were compared, verifying that equivalent asphalts were being examined. Discrepancies in the comparison would indicate that the asphalts are different, and that physicochemical comparisons with such samples would not be valid. Figure 11-2 shows GPC chromatograms of tank and POV-aged Dickens Cosden AC-10. The tank sample is designated by the

solid, bold line. The POV-aged samples are designated by the thin, dashed lines. This figure shows that at isobaric and isothermal aging conditions, increases in aging time increase *LMS* and decrease *MMS*. These results confirm Lau's (1992) observations for POV aging. GPC chromatograms of the other POV-aged asphalts are shown in Appendix E of Lunsford (1994).

Figure 11-3 overlays POV- and field-aged GPC chromatograms for Dickens Cosden AC-10. The bold, solid line designates the auto extracted sample; the thin, dashed lines represent the POV-aged material. Overall, the chromatograms are very similar. The extracted field-aged material has a much higher peak and broader shoulder in the *LMS* region than the POV-aged samples. Furthermore, the extracted sample has larger shoulder at 27 minutes in the *MMS* region compared with POV-aged samples. Despite these differences, it is concluded that these asphalts are equivalent, based on the overall shape.

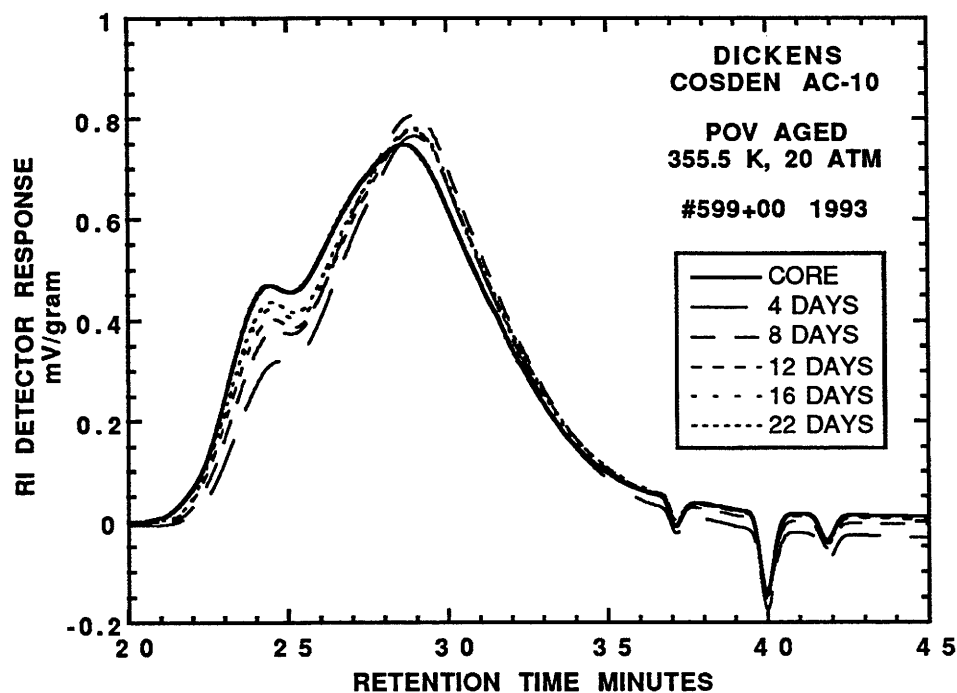


Figure 11-3. POV- and Field-Aged Dickens Cosden AC-10

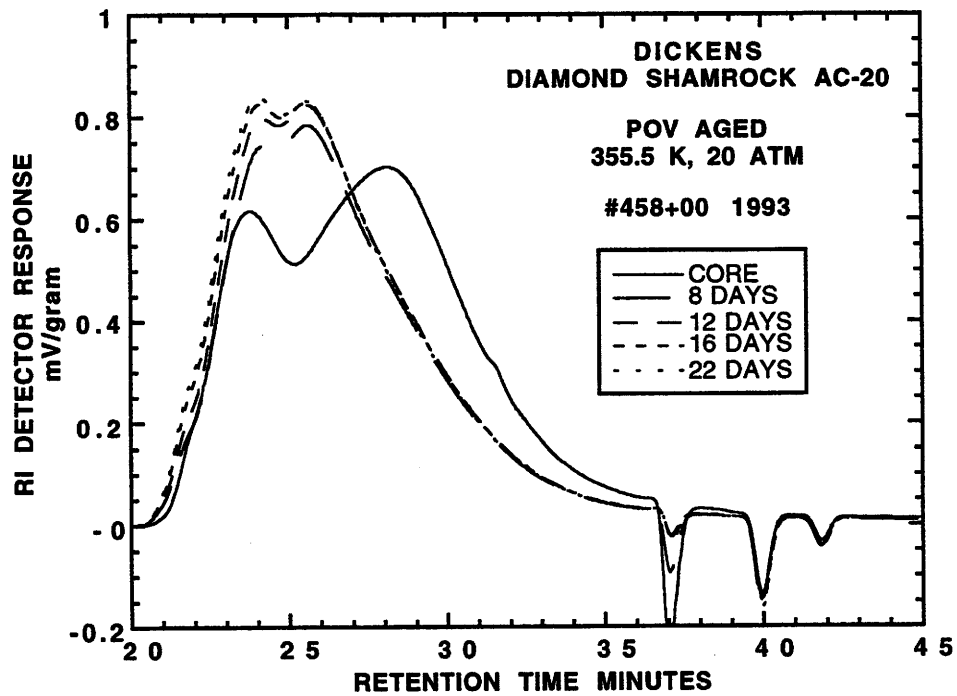


Figure 11-4. POV- and Field-Aged Dickens Diamond Shamrock AC-20

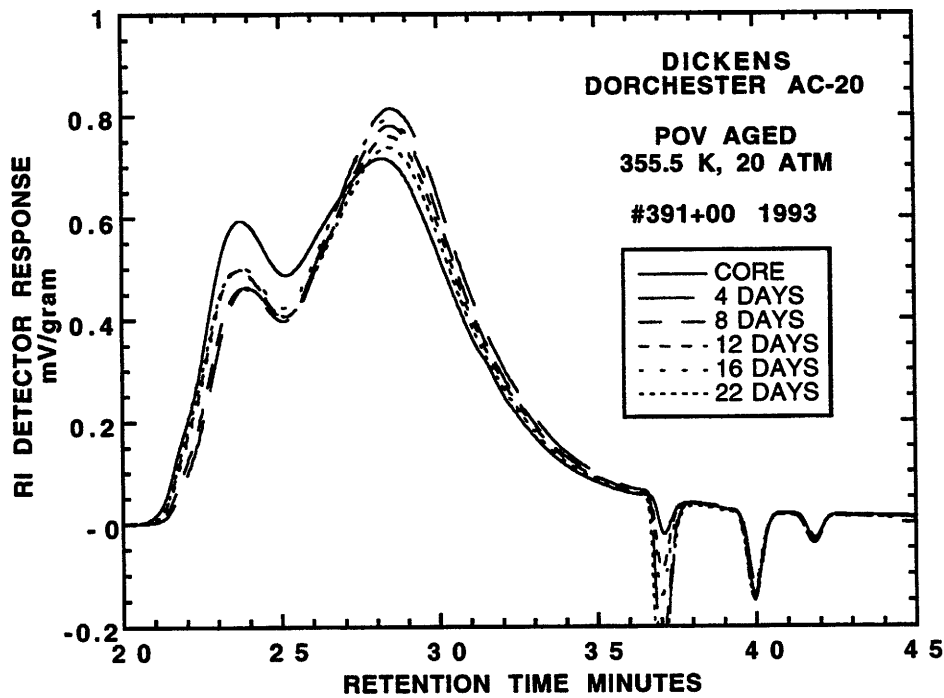


Figure 11-5. POV- and Field-Aged Dickens Dorchester AC-20

For Dickens Diamond Shamrock AC-20 and Dickens Dorchester AC-20, the comparisons are not as favorable. Figures 11-4 and 11-5 show the overlays of POV- and field-aged GPC chromatograms. The characteristic very high *LMS* peak is shown for POV-aged Dickens Diamond Shamrock AC-20 (Davison et al., 1989). The field-aged material extracted from station #458+00, reported to be Diamond Shamrock AC-20, does not show this characteristic. POV-aged Dorchester AC-20 shows a narrow *MMS* peak with a sharp *LMS* peak. However, field-aged material from station #391+00 shows a broad *MMS* peak and a large, dispersed *LMS* peak. The POV aging experiments were designed such that field-aged data would lie in the range of laboratory data. The field-aged *LMS* exceeds the range of POV-aged *LMS* for this asphalt. It was concluded that the field-aged samples for these two asphalts were not equivalent to the POV-aged material. The field-aged samples could have been contaminated, or the coring location might have been incorrect. It was concluded that all of the other asphalts and locations from the Dickens, Pineland, and Bryan test sections were equivalent based on GPC analysis.

The *LMS* region of the field-aged material is larger than that of the POV-aged material for the same *CA* or η_o^* for all of the asphalts studied. Jemison et al., (1991) also report on the differences of GPC chromatograms by comparing extracted hot-mix and oven-aged residue. For the same viscosity increase, the extracted hot-mix shows a larger *LMS* region compared to the oven-aged residue. The oven-aged residue was not extracted and recovered. More work is needed to understand these comparisons.

Comparisons Between η_o^* and *CA*

GPC analysis provides a qualitative characterization of asphalt based on unique chromatographic features, but the information contained in the chromatogram is difficult to correlate with chemical and physical properties. A much better relationship between η_o^* and *CA* due to oxidative aging exists. Lau et al., (1992) showed that for POV aging, Equation 10-3 describes the η_o^* -*CA* relationship. The model parameters, *HS* and *m*, are

dependent on asphalt composition.

$$\eta_o^* = \exp\{HS \cdot CA + m\} \quad (10 - 3)$$

GPC analysis has confirmed that similar asphalts from field- and POV-aged samples are equivalent. Agreement between POV- and field-aged HS and m should provide evidence that POV experiments are simulating field aging.

Figure 11-6 shows η_o^* at 333.3 K (140 °F) versus CA for Dickens Cosden AC-10. POV-aged data are represented by the hollow circle; the tank material is depicted by the filled circle, and the field-aged samples are designated by the square with slash symbol. The parameter estimation is based only on POV-aged data. This figure shows excellent agreement between the POV- and field-aged asphalt. The η_o^* of the field-aged material is slightly higher relative to POV-aged material for equivalent CA . Figure 11-7 shows η_o^* at 333.3 K (140 °F) versus CA for Dickens Cosden AC-20. The field-aged extracted asphalt has higher η_o^* for the same CA as compared with POV-aged asphalt. The difference is approximately 30% in η_o^* . However, HS for both POV- and field-aged asphalt appears to be the same. Figure 11-8 shows the POV- and field-aged data for Exxon AC-20. Agreement is better than for the Cosden AC-20; however, the field-aged asphalt has lower η_o^* relative to POV-aged asphalt for the same CA . For MacMillan AC-20, field-aged asphalt shows slightly lower η_o^* for equivalent CA relative to POV-aged asphalt, as illustrated in Figure 11-9. Except for Cosden AC-20, these asphalts show very good agreement based on this η_o^* - CA relationship.

Figures 11-10 and 11-11, however, show dramatic differences between field- and POV-aged asphalts for Dickens Diamond Shamrock AC-20 and Dorchester AC-20. These differences are reasonable, based on the conclusion that for these asphalts the extracted binder was not the same material as the tank asphalt, based on GPC analysis (Figures 11-4 and 11-5).

These figures show the differences between physicochemical properties of two different asphalts. Compared to the figures where the asphalts are equivalent these differences are enormous. Therefore, even though there are errors in the equivalent asphalts when comparing POV and field aging, the errors are relatively small.

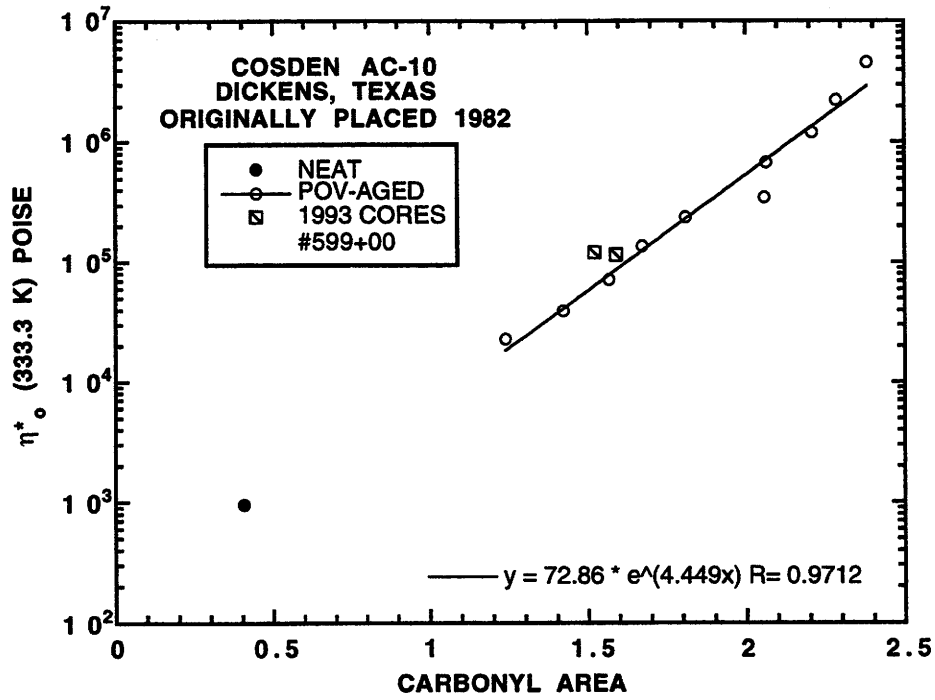


Figure 11-6. η_0^* Versus CA for Dickens Cosden AC-10

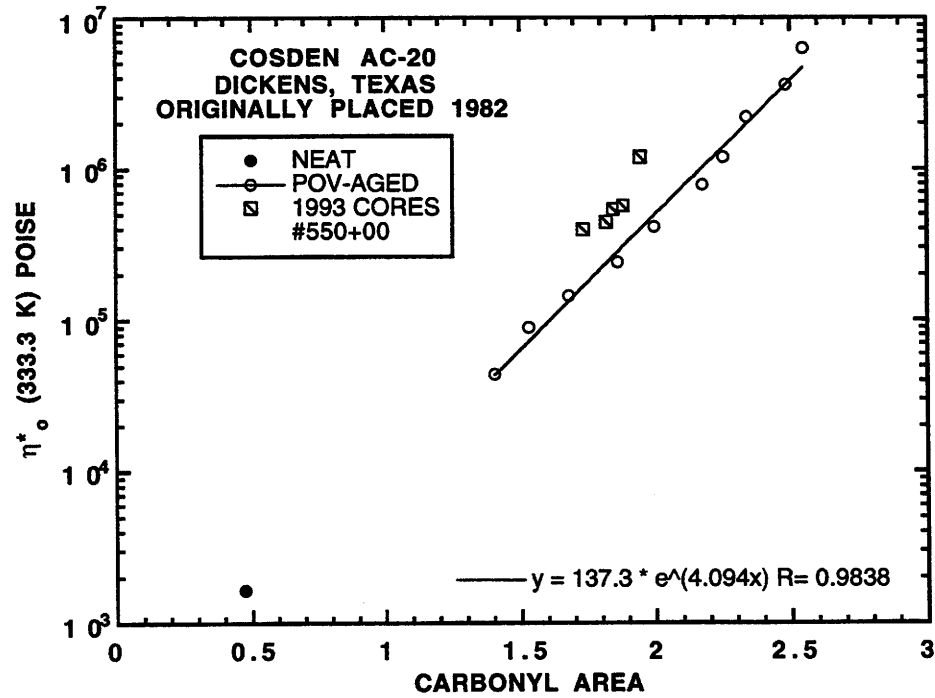


Figure 11-7. η_0^* Versus CA for Dickens Cosden AC-20

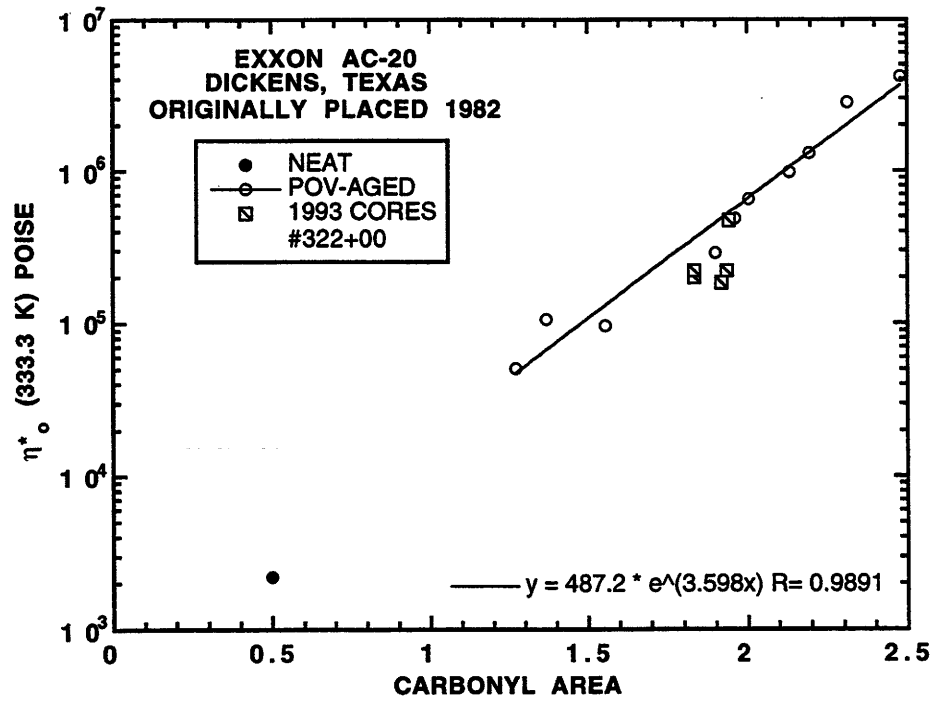


Figure 11-8. η_0^* Versus CA for Dickens Exxon AC-20

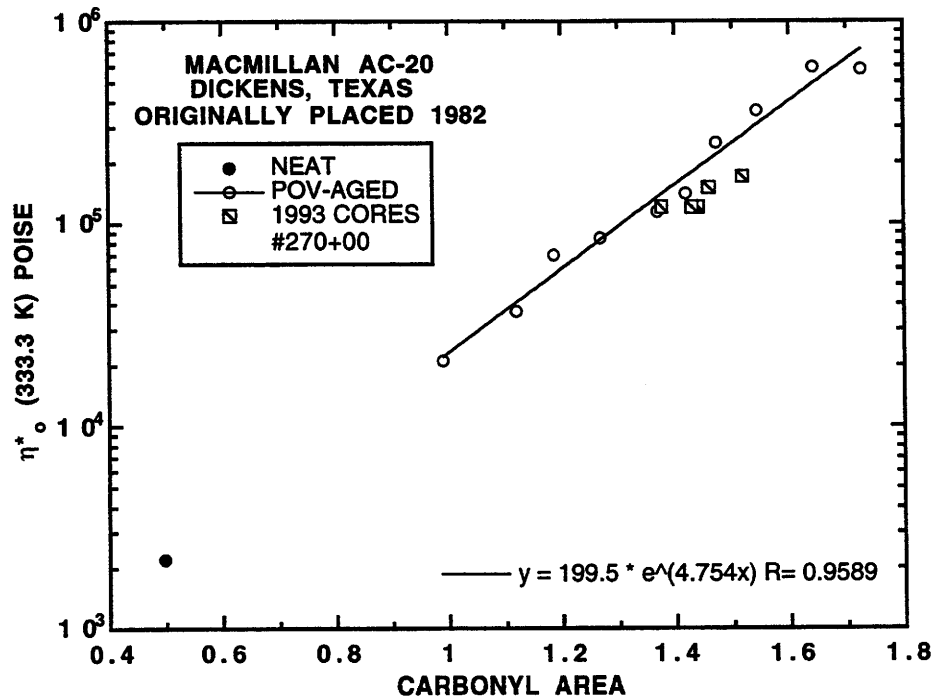


Figure 11-9. η_0^* Versus CA for Dickens MacMillan AC-20

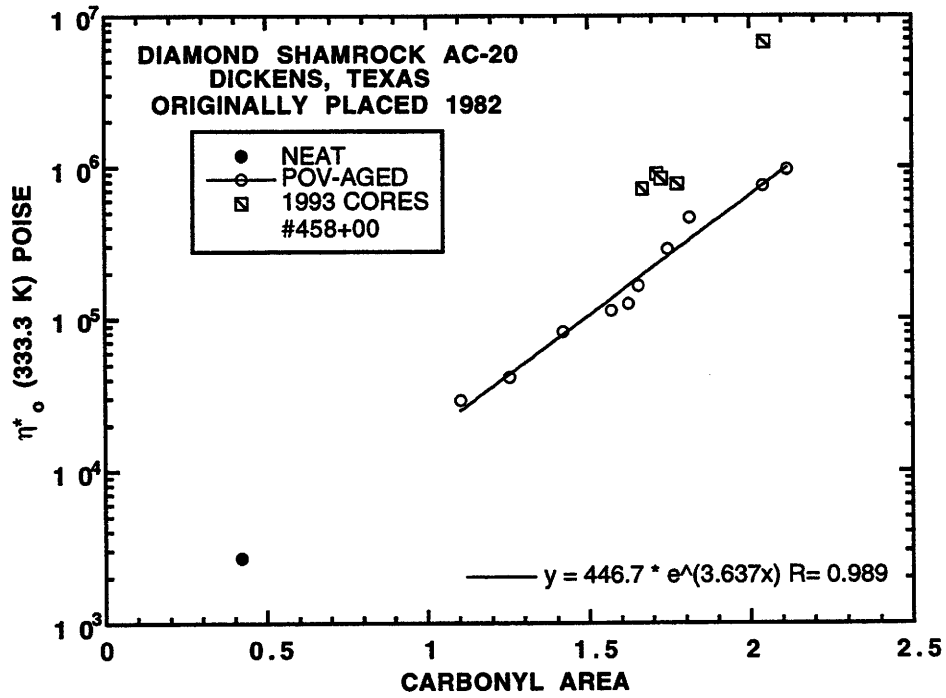


Figure 11-10. η_0^* Versus CA for Dickens Diamond Shamrock AC-20

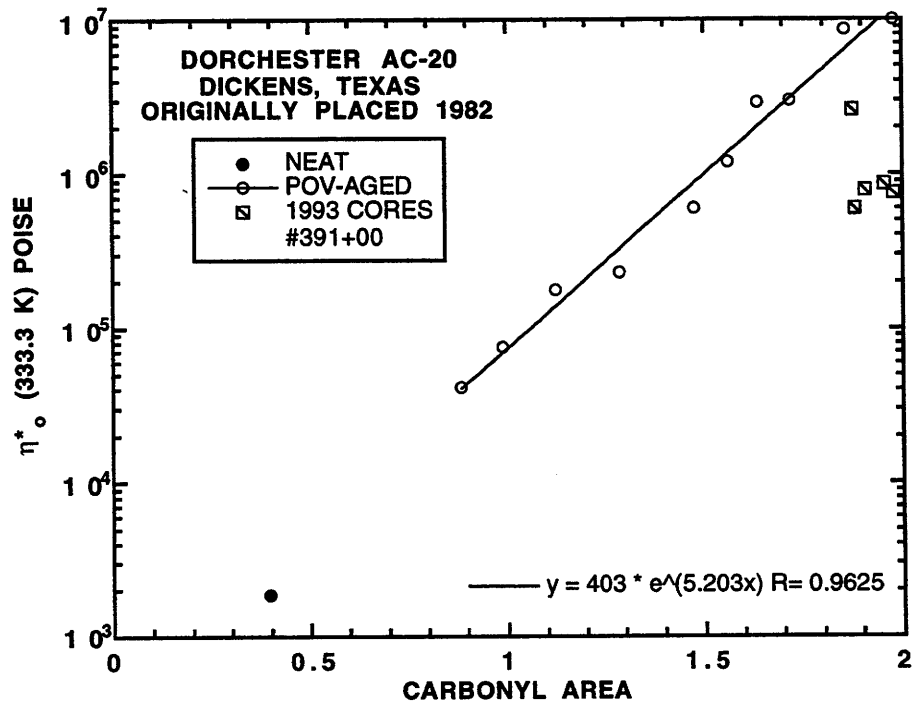


Figure 11-11. η_0^* Versus CA for Dickens Dorchester AC-20

Figures 11-12 through 11-16 compare the asphalts from Pineland. From the magnitude of η_o^* , the asphalts at this test section aged much less than the Dickens test section. For example, the POV simulation at 333.3 K (140 °F) and 20 atm for one day was more severe than ten years of service for Cosden AC-20 at Pineland, shown in Figure 11-12. Since the field-aged data are outside the range of the laboratory data, conclusions about the field- and POV-aged asphalt have not been made. However, it appears that field-aged asphalt has slightly lower η_o^* relative to POV-aged asphalt at the same *CA*. Figure 11-13 gives data for Dorchester AC-20. The field-aged asphalt shows about 40% higher η_o^* , compared with POV-aged asphalt at the same *CA*. *HS* appears to be the same in both cases. For Exxon AC-20, shown in Figure 11-14, agreement between the field- and POV-aged data is better. Field-aged asphalt has 20% lower η_o^* at the same *CA* compared to POV-aged asphalt. MacMillan AC-20, in Figure 11-15, shows field-aged asphalt with lower η_o^* by about 25% relative to POV-aged asphalt. *HS* for both field- and POV-aged asphalt appears to be equivalent. Texaco AC-20, in Figure 11-16, shows excellent agreement between field- and POV-aged asphalt. Since GPC confirmed that there was no residual solvent after extraction and recovery, lower η_o^* for field-aged Exxon AC-20 and MacMillan AC-20 compared to POV-aged material results from other undetermined factors.

Sixteen different extractions were performed for the Bryan test section. Six different Bryan Exxon AC-20 asphalts were POV aged. A clearer picture emerges with many extractions in determining if POV aging is simulating field aging. Figure 11-17 shows all of the field-aged extracted asphalt and three of the POV-aged asphalts. These POV-aged asphalts were selected since they have the highest, lowest, and median *HS* of the six asphalts studied for this test section. These asphalts give the variability of *HS* for the Bryan Exxon AC-20 asphalts studied. The extracted asphalts, shown by the slashed square, have significant scatter with respect to η_o^* at a given *CA* compared to the POV-aged asphalts. The scatter is random with respect to the mean defined as the POV-aged asphalt. A parameter estimation with the 1992 extraction data appears to give the same parameters as the POV-aged data. POV simulation at 344.4 K (160 °F), 20 atm and four days produced material that was more severely aged than two years of field

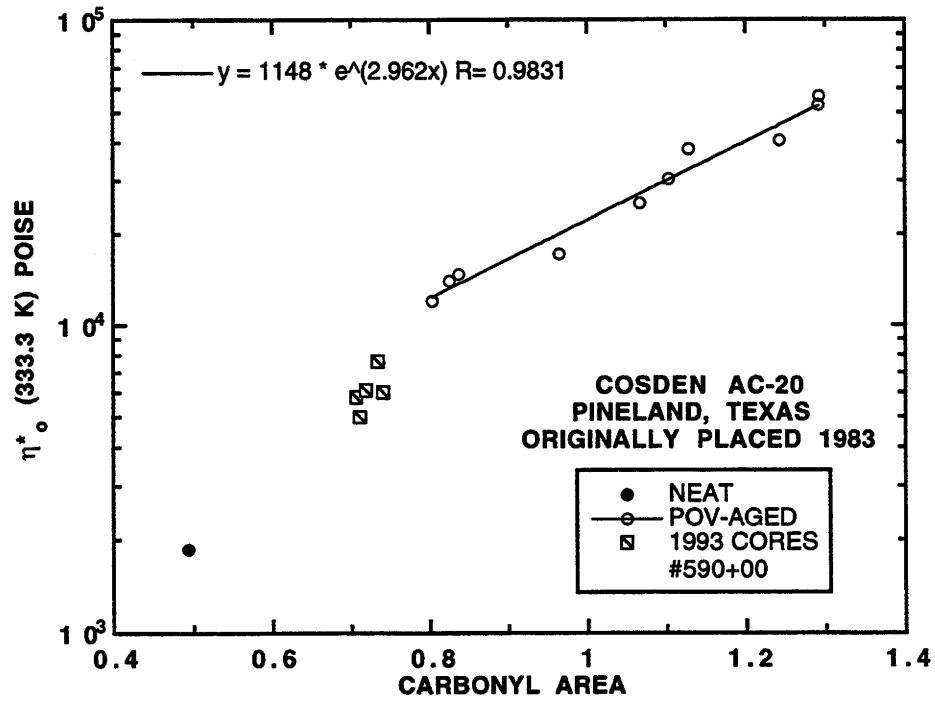


Figure 11-12. η_0^* Versus CA for Pineland Cosden AC-20

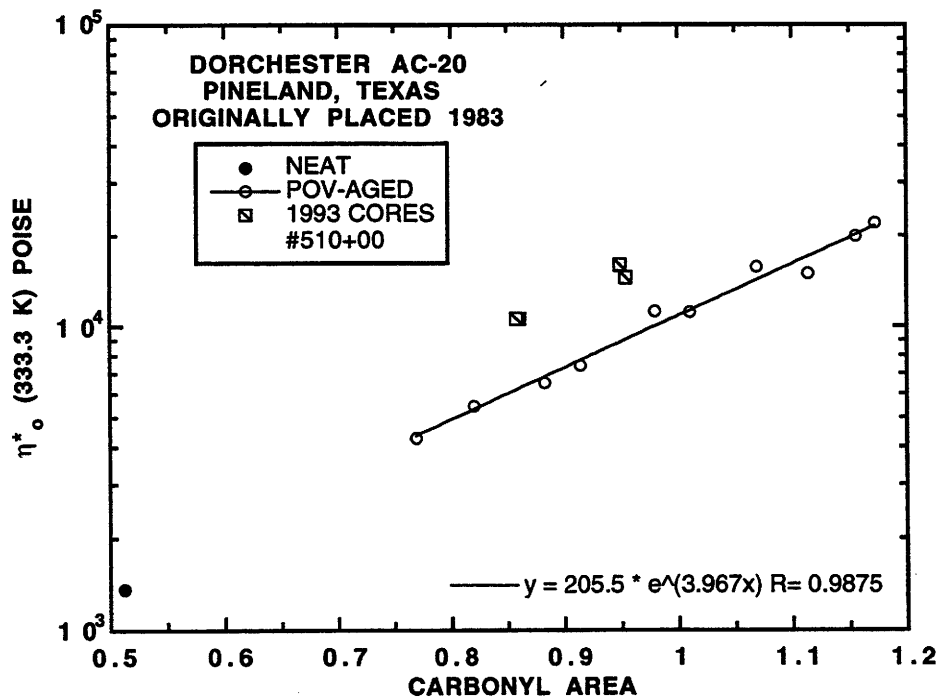


Figure 11-13. η_0^* Versus CA for Pineland Dorchester AC-20

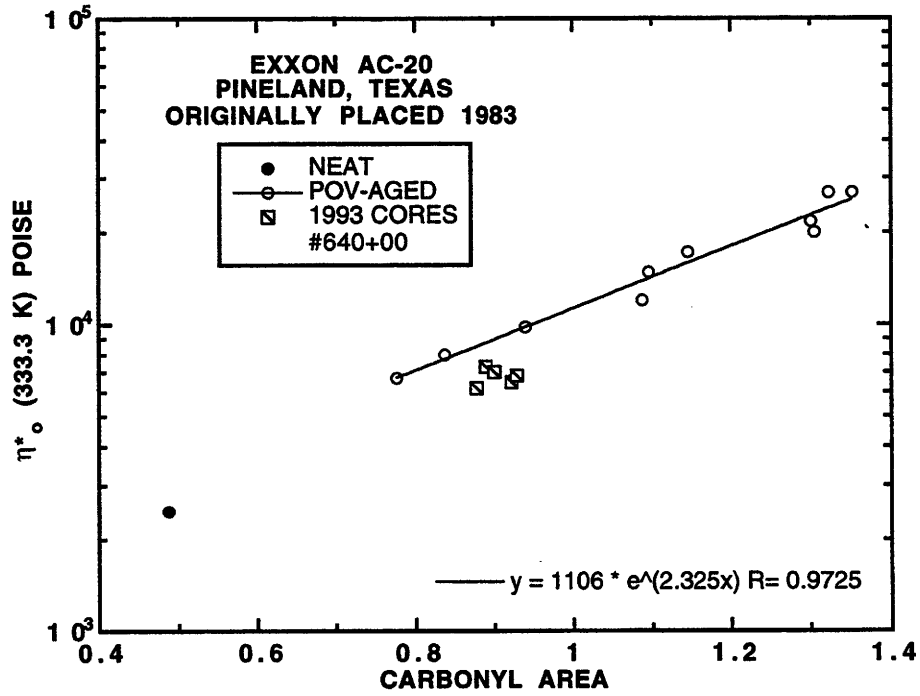


Figure 11-14. η_0^* Versus CA for Pineland Exxon AC-20

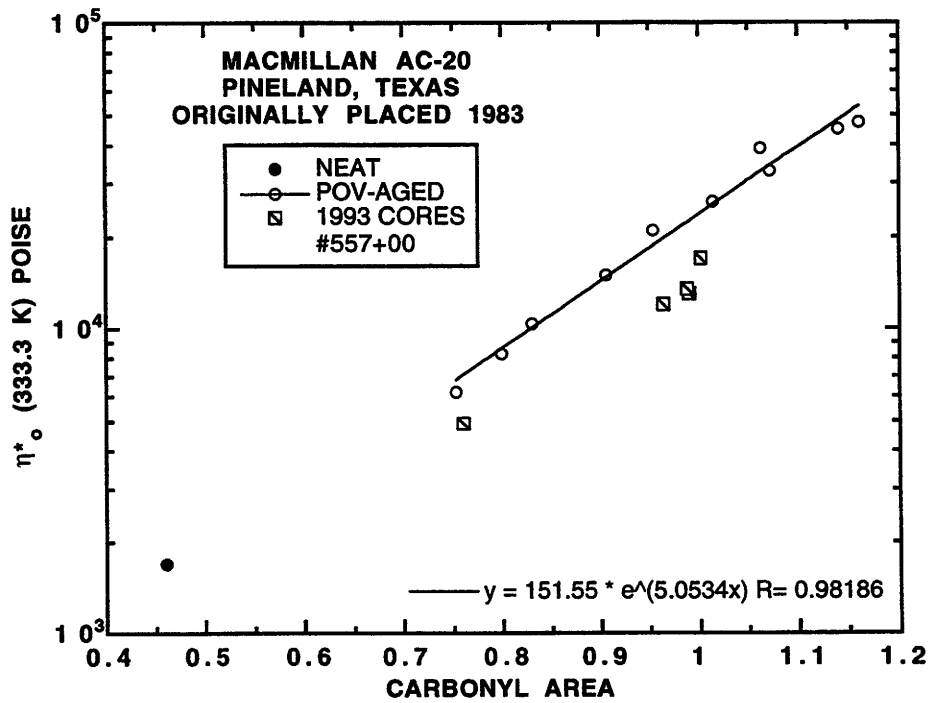


Figure 11-15. η_0^* Versus CA for Pineland MacMillan AC-20

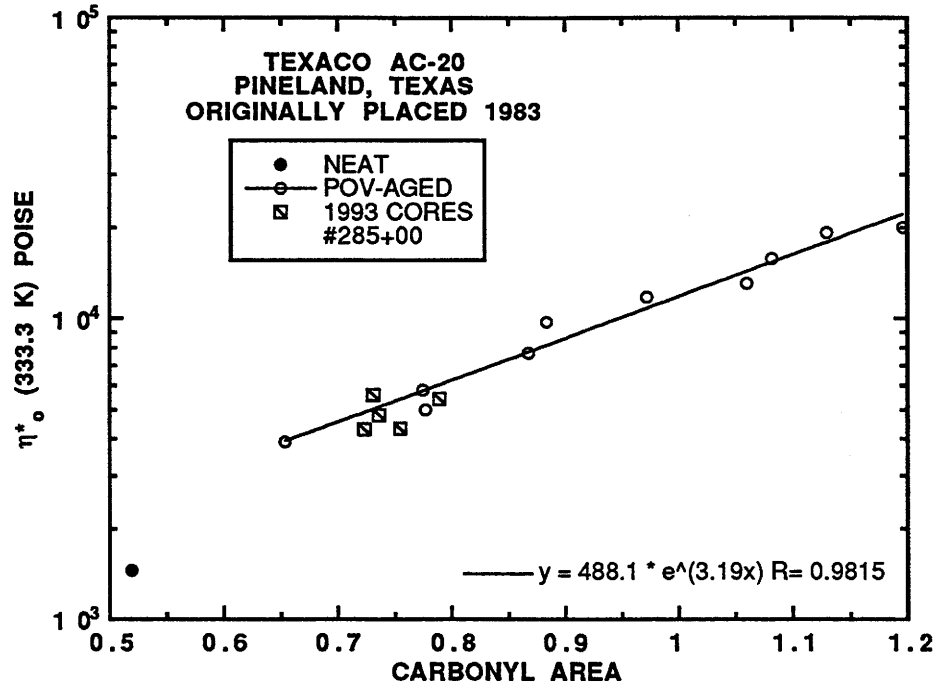


Figure 11-16. η_o^* Versus CA for Pineland Texaco AC-20

aging at this location.

Although POV experiments are simulating field aging, based on the agreement between η_o^* and CA , other aspects of the data need to be addressed. First, there is rather large variability in the properties of the extracted asphalt for the same age and location. For example, Dickens Cosden AC-20 has a range of CA from 1.7 to 1.95. η_o^* at 333.3 K (140 °F) ranges from 600 to 1,500 kP. Also, Pineland Dorchester AC-20 and Pineland MacMillan AC-20 show large variability with respect to the measured properties for field-aged extracted asphalt. It is unrealistic to suggest that the properties of the asphalt in the cores change so dramatically within a few inches of each other. A more realistic explanation is that the variability results from the extraction and recovery procedures. Second, the products of asphalt oxidation are independent of aggregate composition. At Dickens, Pineland, and Bryan the aggregate is river gravel, limestone/iron ore mix, and limestone, respectively. POV simulation accurately describes changes in η_o^* and CA for all test sections studied within a tolerance of error. Even though aggregate composition

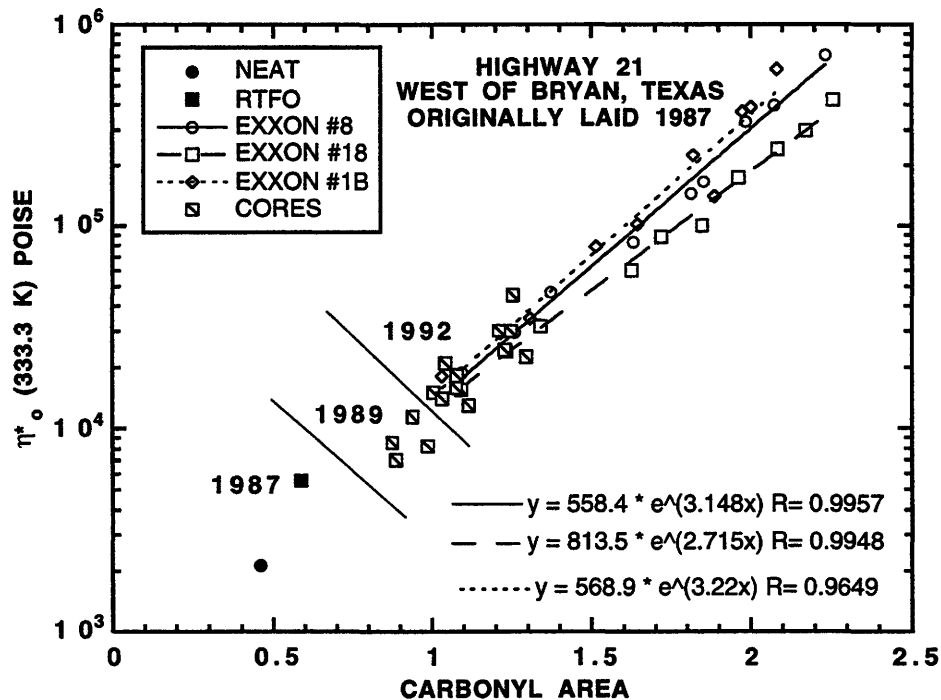


Figure 11-17. η_0^* Versus CA for Bryan Exxon AC-20

does not affect the oxidation products, the rate at which the oxidation products form may depend on aggregate composition. Unfortunately, the data shown thus far contain no information about the kinetics of field aging. Finally, ultimate precision in comparing POV- and field-aged asphalt at this point is unrealistic. From the data, HS is independent of aging method. However, the parameter m is more sensitive to field-aging or extraction and recovery since some of the field-aged data are shifted off the POV-aged model. The direction of the shift is somewhat random. Two asphalts, Dickens Cosden AC-20 and Pineland Dorchester AC-20, shift up; two asphalts, Pineland Exxon AC-20 and Pineland MacMillan AC-20, shift down; and the rest have no shift at all. Dickens Diamond Shamrock AC-20 and Dorchester AC-20 are excluded from this list. The downward shift is not caused by residual solvent after extraction and recovery. GPC analysis confirmed complete solvent removal. Since field-aged asphalts required extraction and recovery and POV-aged asphalts did not, more work is needed to confirm that this offset in the field-aged data is not an artifact of the extraction and recovery process.

POV- AND FIELD-AGING COMPARISONS: ASPHALT-AGING MODEL

In this section we begin the effort of developing a pavement aging model. This is a relationship between measurable core properties, such as % *V* or % *Asp*, and unmeasurable properties, such as the effective asphalt film thickness, L_{eff} , and the effective oxygen pressure in the voids, P_{eff} . L_{eff} and P_{eff} can then be used in the asphalt-aging model to predict field aging both qualitatively and, with the addition of more experimental data to refine the model parameters, quantitatively.

A comparison between POV- and field-aged asphalt was given in the previous section. It was concluded that POV experiments simulate field-aging reasonably well, although there are some differences which we do not fully understand, as yet. These comparisons only show to what extent the physical and chemical properties change. With these physicochemical relationships determined from laboratory data, monitoring the aging of a highway requires fewer measurable variables. For example, with *HS* and *m* determined from POV data, η_o^* can be calculated from a *CA* measurement. These physicochemical relationships greatly reduce the burden of monitoring highway aging. Unfortunately, these comparisons between physicochemical properties provide no kinetic information. With the data given thus far, it is impossible to predict how fast the chemical and physical properties change with time especially at other aging temperatures. It is this rate prediction capability that we wish to add through a highway aging model.

This section is divided into several sub-sections as described below. The first sub-section details the laboratory experiments required to estimate kinetic parameters for each field-aged asphalt. The next describes the estimation of pavement-surface temperature as a function of time from climatic data and latitude. The following section uses the kinetic information and field temperature, calculating a theoretical minimum time, t_{theor} , to reach the measured properties of field-aged asphalt. This calculation assumes that oxygen diffusion resistance is negligible or, equivalently, that asphalt film thickness is infinitely thin. t_{theor} qualitatively measures an asphalt's susceptibility to age in a given climate. Using t_{theor} , asphalts can be ranked. Finally, the last section describes an attempt to correlate the measurable core properties of % *V* and % *Asp* to the unmeasurable

properties L_{eff} and P_{eff} . These correlations are the pavement aging model. L_{eff} is estimated by comparing measured chemical properties to those predicted by the asphalt-aging model.

Experimental Design to Determine Kinetic Parameters

Multi-temperature POV experiments were designed to determine kinetic parameters for the asphalts from Dickens and Pineland. Aging temperatures were 333.3, 344.4, and 355.5 K (140, 160, and 180 °F), and pressure was 20 atm pure oxygen. Aging times ranged from one to forty-four days depending on the aging temperature. Results are given in detail in Appendix E of Lunsford (1994). Arrhenius parameters, E_A and A , for all of the asphalts studied are given in Table 11-3. Multi-pressure experiments were not designed. It was assumed that these asphalts have the same order of reaction with respect to oxygen pressure, α of 0.27, as those asphalts reported in Chapter 1.

The effects of P on CA_o and T on η_o^* , also asphalt-specific relationships, were not determined. Instead, a set of equivalent asphalts was established from those asphalts discussed in Chapter 10 and these asphalts. The criterion was based on the refiner. The equivalency is only for β and s as presented in Table C-3 and γ and δ given in Table C-2 for the Lau et al., (1992) asphalts. Cosden AC-20 and AC-10, Exxon AC-20, and Texaco AC-20 asphalts are equivalent. Dorchester AC-20 at Dickens and Pineland is equivalent to Ampet AC-20 from Chapter 10. For MacMillan AC-20, an arithmetic average for the individual parameters of the asphalts studied in Chapter 10 is used. Bryan Exxon AC-20 is assumed to have the same parameters as that of Lau et al., (1992) Exxon AC-20.

Estimation of Pavement Surface Temperature

Latitude and minimum and maximum ambient air temperatures of the location are needed to estimate an annual temperature cycle for the pavement. With this information, Solaimanian and Kennedy (1993) provide a method to estimate the highest surface

Table 11-3. Arrhenius Parameters of POV- and Field-Aged Asphalts^a Estimated from POV Data

Location	Asphalt	$A \times 10^{-8}$ $CA / \text{day atm}^\alpha$	E_A kJ / gmol
Dickens	Cosden AC-10	6132	87.5
	Cosden AC-20	5567	87.1
	D.S. AC-20 ^b	2893	85.9
	Dorchester AC-20	2516	85.4
	Exxon AC-20	382	79.4
	MacMillan AC-20	310	80.0
Pineland	Cosden AC-20	705	80.9
	Dorchester AC-20	6695	87.7
	Exxon AC-20	604	80.4
	MacMillan AC-20	436	80.2
	Texaco AC-20	1977	83.8
Bryan	Exxon AC-20	1.71	66.7

^a From Davison et al., 1989.

^b D.S. represents Diamond Shamrock

temperature as given in Equation 11 – 1:

$$(T_{\text{sur}} - T_{\text{air}})_{\text{max}} = -0.01113\psi^2 + 0.41202\psi + 43.877 \quad (11 - 1)$$

ψ is the latitude, and the temperatures are in °F. Minimum and maximum air temperatures are from the National Oceanic and Air Administration (NOAA, 1988). Table 11-4 gives the latitude, maximum and minimum air temperatures, the correction factor for estimating the maximum surface temperature from Equation 11 – 1, and the pavement surface maximum and minimum temperatures. The Dickens, Pineland, and Bryan air temperatures are approximated with NOAA data from Lubbock, Lufkin, and Austin, respectively.

A sinusoidal function, given in Equation 11 – 2,

$$T(t)_{\text{sur}} = T_{\text{avg}} + (T_{\text{max}} - T_{\text{avg}}) \cos(\omega t) \quad (11 - 2)$$

approximates the annual temperature variation. The model parameters, T_{max} and T_{avg} are determined from surface data in Table 11-4. T_{avg} is the arithmetic average of T_{min}

Table 11-4. Location and Climatic Data for Dickens, Pineland, and Bryan, Texas

Location	Latitude	Air T			Surface T	
		T_{\min} °F	T_{\max} °F	$(T_{\text{sur}} - T_{\text{air}})_{\max}$	T_{\min} °F	T_{\max} °F
Dickens	33	25	92	45	25	137
Pineland	30	41	92	46	41	138
Bryan	30	41	95	46	41	141

and T_{\max} at the surface. The frequency, ω , is defined such that for one year, the product of ωt is 2π . For example, if t is in units of days, ω is $2\pi / 365 \text{ day}^{-1}$. The variation of temperature in the pavement as a function of depth is not included.

Calculation of t_{theor} to Reach Measured CA

With the laboratory-determined kinetic parameters and an estimation of the annual temperature cycle of the pavement surface, Equation C – 4 can be integrated to give CA as a function of time.

$$\left(\frac{\partial CA}{\partial t}\right) = r_{CA} \quad (\text{C} - 4)$$

The integration constant, CA_o , is calculated from Equation 1 – 4 with model parameters from Table C-3 (Appendix C). The time period is from CA_o to CA measured at the time of coring. Thus, the unknown in this calculation is time. Equation C – 4 can be integrated directly only when diffusion resistance is negligible. This is probably not valid, but the solution gives t_{theor} , the theoretical minimum time to reach measured CA in the cores. Table 11-5 gives the calculated t_{theor} , the actual time, t_{act} , and the ratio of t_{act} to t_{theor} for all of the asphalts studied.

The table shows that t_{act} is over five times t_{theor} for Dickens and over nine times t_{theor} for Pineland. t_{act} is 2.5 times t_{theor} for Bryan Exxon AC-20 1992. These data suggest that oxygen diffusion resistance is significant and cannot be neglected in modeling pavement aging. Diffusion resistance increases with age as the ratio of t_{act} to

Table 11-5. Comparisons Between t_{act} and t_{theor} for Measured CA of Field-Aged Asphalt^a

Location	Asphalt	t_{theor} days	t_{act} days	t_{act} / t_{theor}
Dickens	Cosden AC-10	730	4015	5.5
	Cosden AC-20	770	4015	5.2
	Exxon AC-20	730	4015	5.5
	MacMillan AC-20	770	4015	5.2
Pineland	Cosden AC-20	310	3650	11.8
	Dorchester AC-20	370	3650	9.9
	Exxon AC-20	350	3650	10.4
	MacMillan AC-20	370	3650	9.9
	Texaco AC-20	330	3650	11.1
Bryan	Exxon AC-20 1989	530	730	1.4
	Exxon AC-20 1992	730	1825	2.5

^a From Davison et al., 1989.

t_{theor} increases for Bryan Exxon AC-20 from 1989 to 1992. The ratio of t_{act} and t_{theor} provides a measure of diffusion resistance for a given location. For example, diffusion resistance at Pineland is higher compared to Dickens. The Bryan test section appears to have the lowest diffusion resistance. This probably means that it will harden very quickly.

t_{theor} could be used to rank a set of asphalts. For example, a hypothetical failure criterion is established based on a maximum value of CA or η_0^* . A worst case scenario, no diffusion limitation, is tested with Equation C-4. With laboratory-determined kinetic parameters and climatic data from specific locations, the asphalt requiring the longest time to reach the failure criterion is most resistant to oxidative aging at that specific climate. Since the values of t_{theor} in Table 11-5 are not based upon a specific physical failure criterion, it cannot be concluded that asphalts with higher t_{theor} are more resistant to oxidative aging relative to the other asphalts from the same location.

The Asphalt-Aging Model and Pavement Aging

Oxygen diffusion and reaction are significant in modeling pavement aging. Therefore, only a model including both reaction and diffusion can be successful. A preliminary study examined how the cyclical annual temperature variation affects asphalt-aging model calculations. The model used was that of Chapter 10 and Appendix C.

With isothermal and isobaric conditions the oxygen pressure profile steadily decreased in an asphalt film after an initial maximum (Figure 10-21). The pressure gradients at the surface increased with aging time; however, oxygen transport was limited by decreases in D_{O_2} . For isothermal and isobaric conditions, the carbonyl profile grows at an ever decreasing rate at every point in the film except the *ES* (Figure 10-22). r_{CA} at the *ES* is constant for isothermal and isobaric conditions. The oxygen pressure and *CA* profiles in an asphalt film are different with a periodic temperature than with isothermal conditions. These profiles are fundamental to understanding the aging characteristics of asphalts.

Figure 11-18 shows the oxygen pressure profile in a 1 mm (0.039 in) film of Ampet AC-20 asphalt for seven years aging. (The *ES* is at 1 mm [0.039 in] and the *SI* is at 0 mm [0 in].) With elevated temperature, in summer, the rate of oxygen diffusion exceeds that of reaction. The oxygen pressure in the film increases. With time, D_{O_2} decreases as a result of *CA*, and the magnitude of oxygen pressure in the film decreases with each successive summer. When the temperature is low, during the winter, the oxygen pressure in the film goes to zero. η_0^* is extremely high at low temperature and decreases D_{O_2} further. Even though r_{CA} is very slow at these low temperatures, the rate of oxygen transport is even slower. Oxygen does not enter the film fast enough to replace that consumed by reaction.

With cyclical temperature variation, *CA* in a 1 mm (0.039 in) thick film of Ampet AC-20 is given in Figure 11-19. r_{CA} at low temperature during winter is practically zero even at the *ES*. In winter, r_{CA} in the film below the *ES* is close to zero, not only from low temperature but also from lack of oxygen. The lack of oxygen in the film below the *ES* becomes more significant with aging time. Only at the *ES* is the change in *CA* the

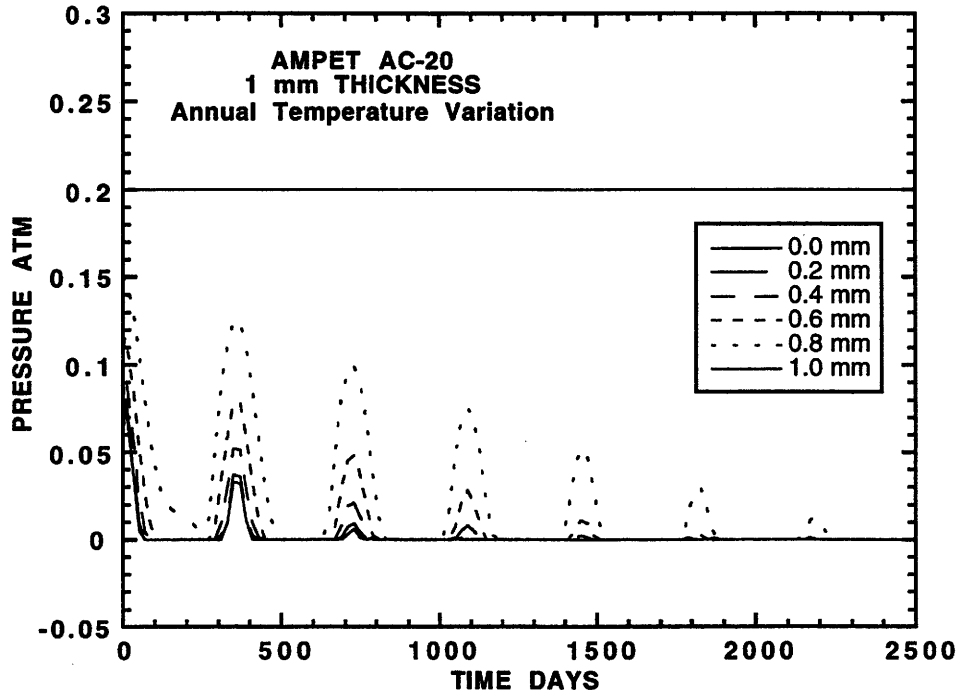


Figure 11-18. Temperature Effected Oxygen Pressure Profiles in Ampet AC-20

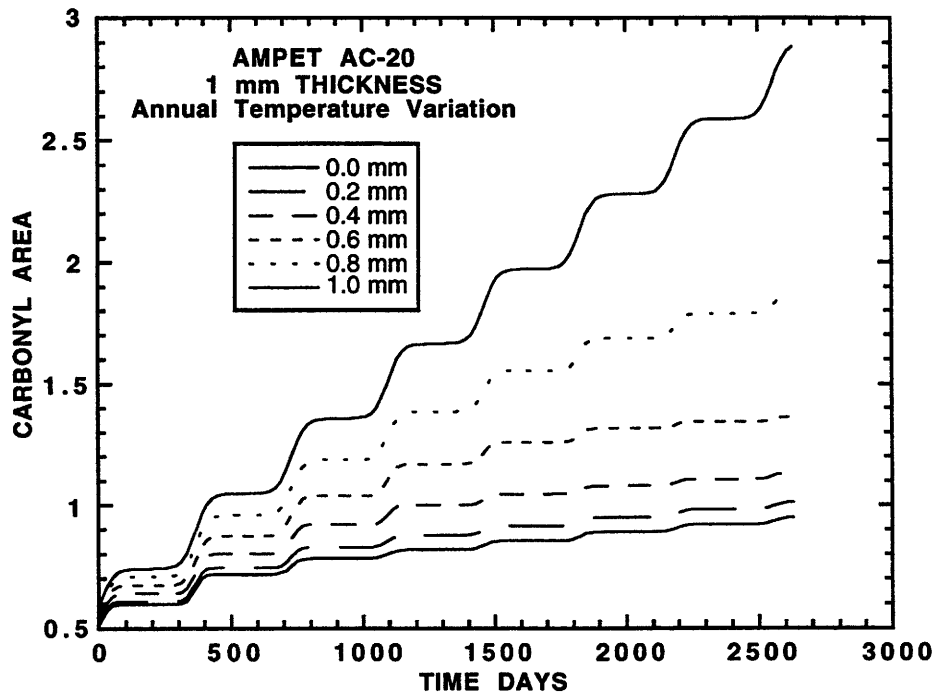


Figure 11-19. Temperature Effected CA Profiles in Ampet AC-20

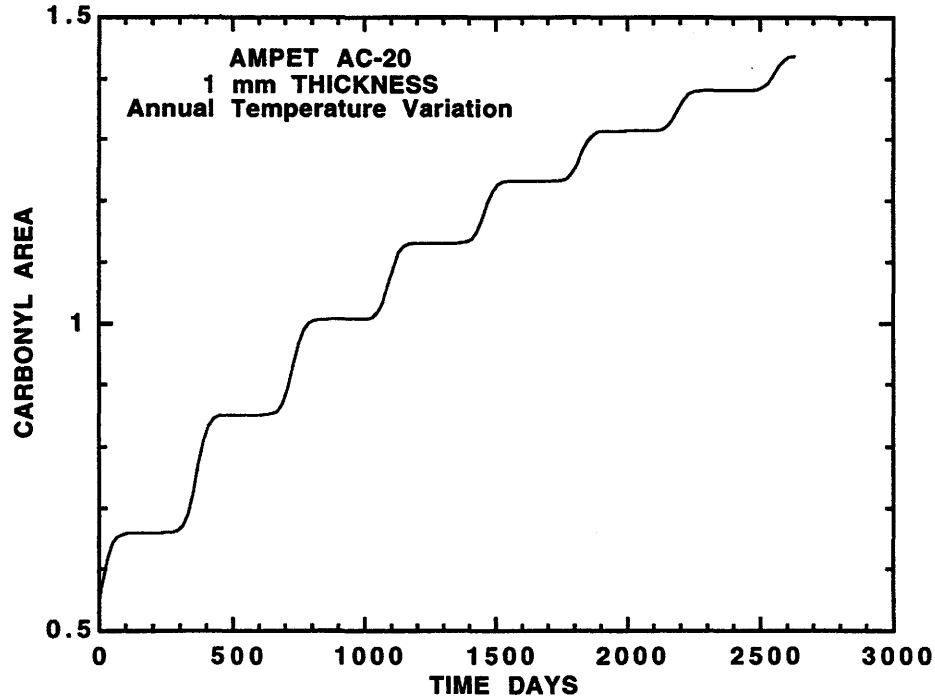


Figure 11-20. Temperature Effected CA_{avg} in Ampet AC-20

same over a one year period. P_{ES} is assumed to be constant. In the film, P decreases with time. Therefore, the change in CA at points inside the film for a one year period decreases with aging time.

Since bulk properties of highway-pavement samples are measured, the integral average CA in the film was determined. This was calculated from Equation 11 - 3.

$$CA_{avg} = \frac{1}{L_{eff}} \int^{L_{eff}} CA(x) dx \quad (11 - 3)$$

This represents a thoroughly mixed asphalt film measurement or bulk analysis. Figure 11-20 shows CA_{avg} in a 1 mm (0.039 in) film of Ampet AC-20 as a function of aging time with a cyclical temperature variation. From profiles in Figure 11-19 and decreasing average P in the film, average annual r_{CA} decreases with age. This figure suggests that asphalts age faster when initially placed compared with aging rates after several years of service. Even for summer months, the rate of aging decreases as the asphalt becomes harder every successive year.

The asphalt-aging model has the same asymptotic behavior as has been noted from

field data. However, the asymptotic nature was not achieved by empirically correlating field-aged data or devising empirical kinetic equations. Instead, the asphalt-aging model is based on fundamental principles, both carbonyl formation and unsteady-state variable \mathcal{D}_{O_2} oxygen diffusion and reaction. With the parameters estimated from laboratory data, the asphalt-aging model predicts the similar phenomenon of field aging. This is an important feature, separating this work from the previously developed empirical aging models. The same type of behavior would be predicted for η_o^* , since CA relates to rheological properties (Equation 10 – 3).

The asphalt-aging model is based on fundamental principles whenever possible. Applying the model to actual field aging should be more successful than previously developed empirical correlations. However, before the asphalt-aging model is applied to field aging, correlations between measurable core properties, % V and % Asp , and fundamental quantities in the asphalt-aging model, L_{eff} and P_{eff} , must be developed. These correlations form the pavement aging model.

Pavement Aging Model Development

Models relating the measurable core properties of % V and % Asp to fundamental quantities in the asphalt model can also be developed. These models form the pavement aging model. Equations 11 – 4 and 11 – 5, respectively, give the hypothesized models for P_{eff} and L_{eff} .

$$P_{eff} = f(\% V, t) \quad (11 - 4)$$

$$L_{eff} = f(\% Asp, \% V) \quad (11 - 5)$$

CA of field-aged asphalt are measured and reported in Appendix E of Lunsford (1994). The placement and coring times are known for these asphalts. The climatic conditions for these locations are also known (Table 11-4). The asphalt-aging model has been developed for POV-aged asphalt films. This model includes carbonyl formation (Equation C–4) and unsteady-state variable \mathcal{D}_{O_2} oxygen diffusion and reaction (Equation C – 11). However, to use the asphalt-aging model, asphalt specific model parameters

must be estimated from laboratory experiments. A series of three POV experiments at three different temperatures and one pressure yielded the necessary data to estimate the parameters, A , E_A , HS , and m . The other asphalt-specific model parameters, β , s , δ , and γ , were taken from equivalent asphalts in Chapter 10. c , α , B , and D_o are assumed to be independent of asphalt composition. Furthermore, a comparison of POV- and field-aged asphalt showed that POV experiments simulate field aging with respect to physicochemical properties. With all of these conclusions, observations, and discoveries, the strategy of estimating L_{eff} is given.

L_{eff} in an asphalt-pavement core is estimated by comparing field-aged data with calculations from the asphalt-aging model. A trial and error procedure is used. First, a thickness of L_{eff} is assumed. Equations C – 4 and C – 11 are integrated simultaneously from the time of placement to the time of coring. These integrations include the variation of temperature from the climatic data and the asphalt specific model parameters. When the time of coring is reached, CA_{avg} is calculated from Equation 11 – 3. CA_{avg} is compared to measured CA for the field-aged asphalt. If CA_{avg} is greater than the measured CA , the assumed film thickness is too small. Conversely, if CA_{avg} is less than the measured CA , the film thickness is too large. The value of L_{eff} is updated until measured CA and CA_{avg} are within a pre-defined tolerance. An incremental search and method of false position was used to estimate L_{eff} . The source code for this program is given in Appendix F of Lunsford (1994). This calculation assumes that oxygen diffusion resistance through the nitrogen gas in the air is negligible. Including the diffusion of oxygen through the nitrogen gas film should decrease the value of L_{eff} determined in this study.

Estimation of L_{eff} with Constant P_{eff}

In the first estimation of L_{eff} it is assumed that P_{eff} is constant, 0.2 atm. Table 11-6 shows estimated L_{eff} , % V , and % Asp for the Dickens and Bryan asphalts. It was not possible to determine reasonable values of L_{eff} for the Pineland asphalts with constant P_{eff} .

Table 11-6. Estimated L_{eff} for Dickens and Bryan Asphalts with Constant P_{eff} of 0.2 atm^a

Location	Asphalt	L_{eff} mm	% V	% Asp
Dickens	Cosden AC-10	3.12	8.3	5.96
	Cosden AC-20	1.44	8.7	5.94
	Exxon AC-20	1.16	9.4	—
	MacMillan AC-20	1.79	5.8	6.10
Bryan	Exxon AC-20 1989	3.70	6.9	—
	Exxon AC-20 1992	2.92	6.4	—

— Signifies the values were not determined.

From the table, higher % V tends to yield lower L_{eff} for all asphalts except for Dickens MacMillan AC-20. Not enough data were collected for % Asp to make any conclusion about this property. The field-aged asphalts from Pineland show very little CA growth. From the numerical calculation, r_{CA} at the surface is so great with constant P_{ES} that estimated L_{eff} is unreasonable. Since no realistic values for L_{eff} could be determined for the Pineland test section asphalts, the assumption that P_{eff} is constant may not be valid, especially for pavements with very low % V. Therefore, calculations with variable P_{eff} were performed. In order to compare Pineland field-aged data with the laboratory determined properties, it was assumed that P_{eff} decreases with time.

Estimation of L_{eff} with Variable P_{eff}

From conservation of mass in a void, the oxygen concentration in an inaccessible void decreases with time from oxygen diffusion and reaction in the asphalt film. At low enough % V levels, the number of inaccessible voids is significant. At high % V, the permeability of the core is such that most voids are accessible; the oxygen pressure in the void approaches 0.2 atm. A model relating P_{eff} as a function of time is hypothesized and given in Equation 11 – 6.

$$P_{\text{eff}} = (P_{\text{eff}})_o \exp(-\lambda t) \quad (11 - 6)$$

The model parameter $(P_{\text{eff}})_o$ is the oxygen pressure at the initial time and is assumed to

be 0.2 atm. The time constant, λ , is a function of % V . λ is large at low % V and small at high % V . Another model relating λ to % V is hypothesized in Equation 11 - 7.

$$\lambda = \lambda_o(\%V)^l \quad (11 - 7)$$

With no experimental data, the model parameters λ_o and l were based on the numbers in Table 11-7. An estimation gives λ_o of 0.154 1/day and l of -2.41. Figure 11-21 shows the hypothesized function and numbers.

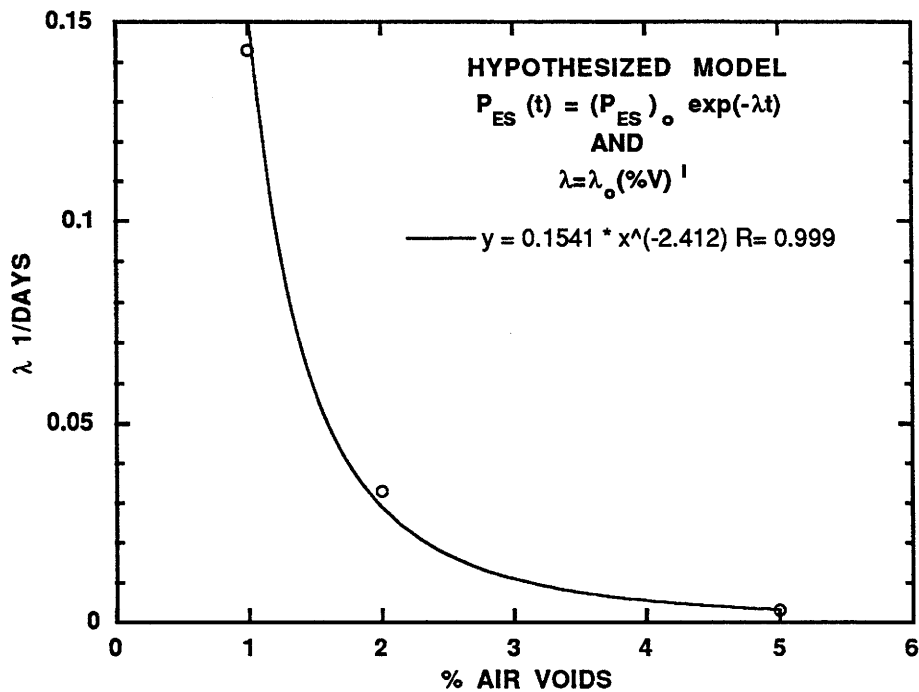


Figure 11-21. Hypothesized P_{eff} Time Constant λ Versus Percent Air Voids

Table 11-7. Hypothesized Model Between % V and λ

% V	λ 1/day
1	1/7
2	1/30
5	1/365

L_{eff} was estimated for the Dickens, Pineland, and Bryan asphalts with P_{eff} as the hypothesized function of time and % V , and with the hypothesized model parameters. Table 11-8 reports L_{eff} , % V , and % Asp for all the asphalts studied. Under the assumptions imposed by Equations 11 – 6 and 11 – 7, all of the asphalts studied show L_{eff} of about 1 mm (0.039 in) except for Pineland Cosden AC-20. L_{eff} for this asphalt is 4.18 mm (0.165 in). However, the field-aged data for Pineland Cosden AC-20 was outside the range of POV-aged data as shown in Figure 11-12. This calculation may not be accurate. For Dickens and Bryan asphalts, L_{eff} for constant P_{eff} of 0.2 atm is greater than L_{eff} for variable P_{eff} from Tables 11-6 and 11-8. For equivalent CA at the end of the time period, constant P_{eff} requires a larger diffusion length compared with decreasing P_{eff} .

Table 11-8. Estimated L_{eff} for Dickens, Pineland, and Bryan Asphalts with Variable P_{eff} ^a

Location	Asphalt	L_{eff} mm	% V	% Asp
Dickens	Cosden AC-10	1.86	8.3	5.96
	Cosden AC-20	0.94	8.7	5.94
	Exxon AC-20	0.74	9.4	–
	MacMillan AC-20	1.16	5.8	6.10
Pineland	Cosden AC-20	4.18	1.8	6.10
	Dorchester AC-20	1.60	2.2	6.30
	Exxon AC-20	1.70	2.6	6.36
	MacMillan AC-20	1.15	2.8	6.20
	Texaco AC-20	1.57	1.4	5.87
Bryan	Exxon AC-20 1989	1.93	6.9	–
	Exxon AC-20 1992	1.97	6.4	–

^a– Signifies the values were not determined.

An attempt to correlate L_{eff} with % Asp is made with L_{eff} determined under the assumptions of Equations 11 – 6, 11 – 7, and the model parameters. From Table 11-8, a relationship between L_{eff} and % Asp probably exists. However, the data set in this study is too small to make a conclusive development and parameter estimation. Most of the asphalts studied have % Asp ranging from 5.87 to 6.36. This is only an 8% difference.

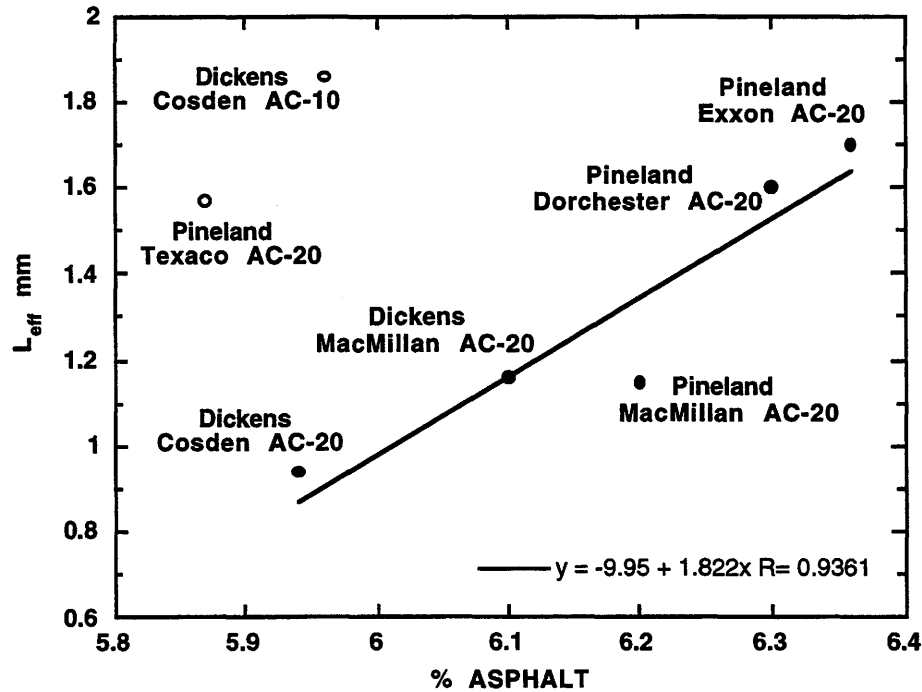


Figure 11-22. Hypothesized L_{eff} Versus Percent Asphalt

Unfortunately, % *Asp* for Bryan Exxon AC-20 was not measured.

Figure 11-22 shows % *Asp* and L_{eff} . Data for Pineland Cosden AC-20 are not shown on this figure. From this figure, two conclusions may be drawn. The first conclusion is that L_{eff} , estimated under the assumptions of Equations 11 – 6, 11 – 7 and the model parameters, is independent of % *Asp*. The second conclusion is based on the exclusion of the Dickens Cosden AC-10 and Pineland Texaco AC-20 data. These data show unusually high L_{eff} for the given % *Asp*. With these data excluded, it appears that there is a crude linear relationship between L_{eff} and % *Asp* as given by Equation 11 – 8.

$$L_{eff} = a(\% Asp) + e \quad (11 - 8)$$

The model parameters are given in the figure with a of 1.82 mm/% *Asp* and e of -9.95 mm (a of 0.0717 in/% *Asp* and e of -0.392 in). Based on this model and parameters, pavements with asphalt contents less than approximately 5% could not be used to predict valid L_{eff} .

From limited data, the initial development of the pavement aging model relates

P_{eff} to % V and t by Equations 11 – 6 and 11 – 7. L_{eff} is related to % Asp by Equation 11 – 8. These are very crude models and need further refinement with larger data sets.

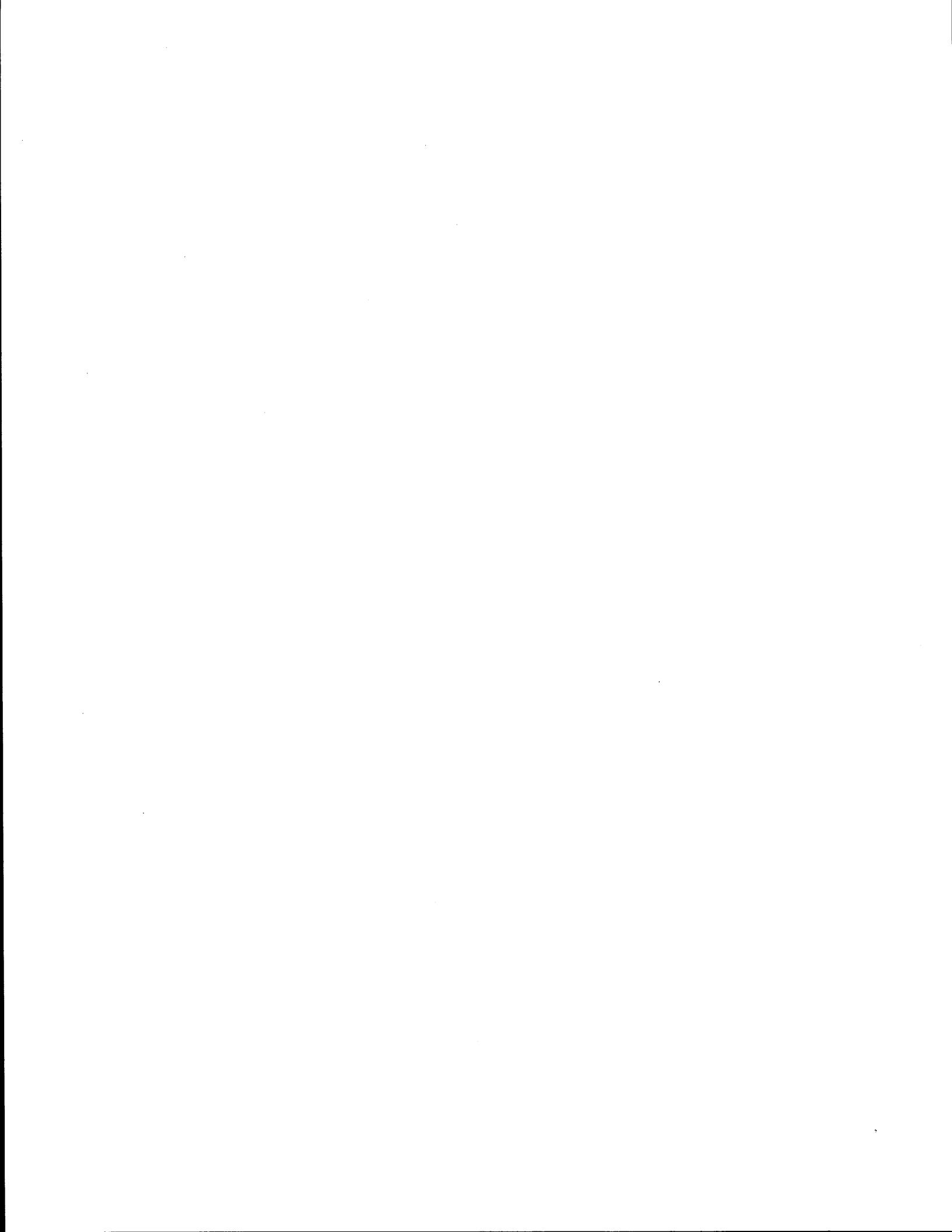
SUMMARY

A comparison between POV- and field-aged asphalts was performed. In the first comparison, only physicochemical relationships were considered. These properties are independent of the kinetics of the aging process. From rheological properties and CA , it was concluded that POV aging approximates field aging reasonably well, although more study is needed. GPC and IR spectra analysis showed there were slight chemical differences. It was not determined if these differences resulted from extraction and recovery procedures or from field aging.

A comparison between field-aged asphalt and calculations from the asphalt-aging model was used to develop a pavement aging model. A theoretical minimum time, t_{theor} , was calculated using an asphalt-aging model with no diffusion and resistance for each asphalt and location. The ratio of t_{act} and t_{theor} was five for Dickens and ten for Pineland. This ratio is a qualitative measure of diffusion resistance. From this, it was concluded that diffusion resistance is significant in field aging.

Using the asphalt-aging model and field data, L_{eff} was estimated by two different calculations. First, P_{eff} was assumed to be constant, 0.2 atm. Reasonable values of L_{eff} were calculated for pavements with relatively high % V , as at Dickens and Bryan. However, no reasonable L_{eff} could be determined for Pineland, a pavement with low % V . The assumption of constant P_{eff} was probably not valid, especially for cases with low % V .

While the model developed in this study needs more evaluation with laboratory and field data, it appears to be a very reasonable first step. Qualitatively, calculations agree well with field cores and quantitative calculations are also quite reasonable.



SECTION V

CONCLUSIONS AND RECOMMENDATIONS

CONCLUSIONS

- No accelerated aging test run at a single elevated temperature or pressure can reliably simulate relative asphalt road hardening rates.
- Accelerated aging tests must be run at several temperatures and at atmospheric oxygen pressures, or, if elevated pressure is used, sufficient data must be obtained to correct for pressure. The higher temperature data may then be extrapolated to lower road temperatures.
- The rate of oxidation or carbonyl formation can be expressed by the equation

$$\text{rate} = AP^\alpha e^{-E/RT} = \frac{\partial CA}{\partial \theta}$$

where P and T are pressure and temperature and A , α and E are asphalt dependent constants, θ is time, and CA is the infrared measured carbonyl peak.

- These constants correlate strongly; a high value of α accompanies a high value of E . Such asphalts, which may be quite good at ambient conditions, will generally look very poor in an accelerated test at higher temperature or pressure.
- Earlier work had indicated that for each asphalt there exists a constant relation between \ln viscosity increase and carbonyl formation called the hardening susceptibility (HS). It was shown to be independent of oxidation temperature up to at least 100°C (212°F). In this work, however, it is shown to be pressure dependent, and to be useful in road aging studies the oxidation must take place at atmospheric oxygen pressure.
- It is also shown that the HS correlates with the kinetic functions α and E .

- The hardening rate of asphalt may be expressed as the product of HS and oxidation rate or carbonyl formation rate

$$\frac{\partial \ln \eta}{\partial \theta} = \text{HS} \cdot \frac{\partial \text{CA}}{\partial \theta}$$

where η is viscosity, θ is time and CA carbonyl.

- The HS may be expressed as the product of two independent functions

$$\text{HS} = \frac{\partial \ln \eta}{\partial \text{CA}} = \frac{\partial \ln \eta}{\partial A_s} \cdot \frac{\partial A_s}{\partial \text{CA}}$$

where A_s is asphaltene content.

- The first term $\frac{\partial \ln \eta}{\partial A_s}$ obeys a modified Pal-Rhodes type equation $\eta/\eta_m = (1 - KA_s)^\alpha$ where η_m is maltene viscosity and K and α asphalt dependent constants. Thus

$$\frac{\partial \ln \eta}{\partial A_s} = \frac{K\alpha}{1 - KA_s}$$

This obviously increases with asphaltene content, but it also increases with asphaltene molecular weight and is maltene dependent. This relation indicates that asphaltenes in maltenes behave as a colloidal or particle-like mixture.

- The second term $\frac{\partial A_s}{\partial \text{CA}}$ is very maltene dependent and has a major effect on HS. It seems to be affected by asphaltenes only to the extent that new carbonyl formation is from existing asphaltenes rather than from formation of new asphaltenes, i.e., the reaction of the maltenes to form asphaltenes is not

affected by the presence of asphaltenes.

- The HS increases with saturate content as well as with asphaltene content, so that recycling agents should be low in both and, preferably, contain no asphaltenes.
- Since old asphalts contain too much asphaltenes, an asphaltene-free recycling agent will improve the HS through dilution.
- Recycling agents should be highly aromatic.
- As both HS and oxidation kinetics are very maltene dependent, the recycling agent crude source and aromatic composition are important.
- Metals have little, if any, effect on either the HS or oxidation rate.
- The viscosity of asphalt-recycling agent blends can be represented by the Grunberg equation

$$\ln \eta_m = x_1 \ln \eta_1 + x_2 \ln \eta_2 + x_1 x_2 G_{12}$$

Where η_m , η_1 , and η_2 are viscosities of the mixture, old asphalt and recycling agents, x_1 and x_2 are fractions of old asphalt and recycling agents, and G_{12} is a constant.

- If this equation is viscosity normalized so that

$$\frac{\ln(\eta_m / \eta_1)}{\ln(\eta_2 / \eta_1)} = \left[1 + \frac{G_{12}}{\ln(\eta_2 / \eta_1)} \right] x_2 + \left[\frac{-G_{12}}{\ln(\eta_2 / \eta_1)} \right] x_2^2$$

the expression $\frac{G_{12}}{\ln \eta_2 / \eta_1}$ is very nearly the same when asphaltene free recycling agents are used, and the value of G_{12} is negative. For agents containing asphaltenes, G_{12} may be less negative, or even positive.

- For some aged asphalts the recycled material can have a lower HS than the original asphalt.
- Studies relating hardening and oxygen diffusion showed that road aging is diffusion limited so that aging comparisons based on relative oxidation rates will exaggerate differences in asphalt performance, though the relative

rankings are not likely to change.

- A preliminary model relating field and laboratory aging is promising. The model includes asphalt properties, percent voids and asphalt content.

RECOMMENDATIONS

- Since a reliable accelerated aging test is much more complicated than supposed, studies should be made to optimize test conditions to minimize testing time and equipment.
- Studies are needed to confirm that benefits obtained in reduced viscosity hardening with low asphaltene and saturate content recycling agents extend to low-temperature properties such as ductility and creep stiffness.
- Work is needed on the effect of recycling on adhesion and water susceptibility.
- Further studies of the effect of recycling agents on subsequent oxidation rates are needed.
- While there is evidence that recycling agents should be highly aromatic, the optimum increase of naphthene and polar aromatics has not been determined.
- Mix time during recycling is short. Studies should determine how incomplete mixing affects performance.

REFERENCES

- Asphalt Hot-Mix Recycling*. Report MS-20. The Asphalt Institute, Lexington, KY (1981).
- SHRP Binder Specification, Draft No. 7G.*, SHRP, Federal Highway Administration, Washington D.C. (1992).
- Adams, C.K. and R.J. Holmgren, *Asphalt Properties and Pavement Performance*, Report FHWA-TX-86/287-4. Texas Transportation Institute, College Station, TX (1986).
- Altgelt, K.H. and O.L. Harle, "The Effect of Asphaltenes on Asphalt Viscosity," *Ind. Eng. Chem. Prod. Res. and Dev.*, vol. 14, pp. 240-246 (1975).
- Anderson, A.P. and K.A. Wright, "Permeability and Absorption Properties of Bituminous Coatings," *Ind. and Eng. Chem.*, vol. 33, p. 992 (1941).
- Anderson, D.I., D.E. Peterson, and M. Wiley, *Characteristics of Asphalts as Related to the Performance of Flexible Pavements*. Report UDOT-MR-76-6, Utah Department of Transportation, June 1976.
- Andrade, E.N., "The Viscosity of Liquids," *Nature*, vol. 125, p. 309 (1930).
- Arrhenius, S., The Viscosity of Aqueous Mixtures (In German). *Z. Phys. Chem.*, vol. 1, pp. 285-298 (1887).
- Bateman, L., "Olefin Oxidation," *Quart. Rev.*, vol. 8, p. 147 (1954).
- Bird, R.B., W.E. Stewart, and E.N. Lightfoot, *Transport Phenomena*, Wiley, New York, NY (1960).
- Bishara, S.W. and E. Wilkins, "Rapid Method for the Chemical Analysis of Asphalt Cement: Quantitative Determination of the Naphthene Aromatic and Polar Aromatic Fractions Using High Performance Liquid Chromatography," *Trans. Res. Rec.*, vol. 1228, pp. 183-190 (1989).
- Blokker, P.C. and H. van Hoorn, "Durability of Bitumen in Theory and Practice," *5th World Petroleum Congress*, pp. 417-429 (1959).
- Bolland, J.L., "Kinetics of Olefin Oxidation," *Quart. Rev.*, vol. 3, p. 1 (1949).

- Branthaver, J.F., J.C. Petersen, J.J. Duvall, and P.M. Harnsberger, "Compatibilities of Strategic Highway Research Program Asphalts," *Trans. Res. Rec.*, vol. 1323, pp. 22-31 (1991).
- Burr, B.L., "Improved Methods for Extracting and Recovering Asphalts from Pavement Samples," Texas A&M University, Department of Chemical Engineering, College Station, TX, PhD Dissertation, (1993).
- Burr, B.L., R.R. Davison, C.J. Glover, and J.A. Bullin, "Solvent Removal from Asphalt," *Trans. Res. Rec.*, vol. 1269, pp. 1-8 (1990).
- Burr, B.L., R.R. Davison, H.B. Jemison, C.J. Glover, and J.A. Bullin, "Asphalt Hardening in Extraction Solvents," *Trans. Res. Rec.*, vol. 1323, pp. 70-76 (1991).
- Campen, W.H., J.R. Smith, L.G. Erickson, and L.R. Mertz, "The Relationships Between Voids, Surface Area, Film Thickness and Stability in Bituminous Paving Mixtures," *Proc. AAPT*, vol. 28, p. 149 (1959).
- Chipperfield, E.H., J.L. Duthie, and R.B. Girdler, "Asphalt Characteristics in Relation to Road Performance," *Proc. AAPT*, vol. 39, p. 575 (1940).
- Corbett, L.W. and P.E. Merz, "Asphalt Binder Hardening in the Michigan Test Road After 18 Years of Service," *Transportation Research Board*, vol. 544, pp. 27-34 (1975).
- Corbett, L.W. and R.E. Swarbrick, "Composition Analysis Used to Explore Asphalt Hardening," *Proc. AAPT*, vol. 29, pp. 104-114 (1960).
- Davison, R.R., J.A. Bullin, C.J. Glover, B.L. Burr, H.B. Jemison, H.B., A.L.G. Kyle, and C.A. Cipione, *Development of Gel Permeation Chromatography, Infrared and Other Tests to Characterize Asphalt Cements and Correlate with Field Performance*, Research Report FHWA/TX-90/458-1F. State Department of Highways and Public Transportation, Austin, Texas (1989).
- Davison, R.R., J.A. Bullin, C.J. Glover, J.R. Stegeman, H.B. Jemison, B.L. Burr, A.L.G. Kyle, and C.A. Cipione, *Design and Manufacture of Superior Asphalt Binders*, Texas Dept. of Trans. Research Report No. 1155 (1991).
- Davison, R.R., J.A. Bullin, C.J. Glover, H.B. Jemison, C.K. Lau, K.M. Lunsford, and P.L. Bartnicki, *Design and Use of Superior Asphalt Binders*, Texas Dept. of Trans. Research Report No. 1249 (1992).
- Dickinson, E.J. and J.H. Nicholas, "The Reaction of Oxygen with Tar Oils," *Road*

Research Technical Paper No. 16, p. 1 (1949).

- Dickinson, E.J., J.H. Nicholas, and S. Boas-Traube, "Physical Factors Affecting the Absorption of Oxygen by Thin Films of Bituminous Road Binders," *J. Appl. Chem.*, vol. 8, p. 673 (1958).
- Dunning, R.L. and R.L. Mendenhall, *Design of Recycled Asphalt Pavements and Selection of Modifiers*. STP 662, ASTM, Philadelphia, PA, (Nov. 1978).
- Edler, A.C., M.M. Hattingh, V.P. Servas, and C.P. Marais, "Use of Aging Tests to Determine the Efficacy of Hydrated Lime Additions to Asphalt in Retarding its Oxidative Hardening," *Proc. AAPT*, vol. 54, p. 118 (1985).
- Eilers, H.J., "The Colloidal Structure of Asphalt," *J. Phys. Colloid Chem.*, vol. 53, pp. 1195-1211 (1948).
- Epps, J.A., D.N. Little, R.J. Holmgreen, and R.L. Terrel. *Guidelines for Recycling Pavement Materials*. Report 224. NCHRP, TRB, National Research Council, Washington D.C. (1980).
- Ferry, J., *Viscoelastic Properties of Polymers*, John Wiley and Sons, 4th ed., New York, NY (1985).
- Girdler, R.B., "Constitution of Asphaltenes and Related Studies," *Proc. AAPT*, vol. 34, pp. 45-79, 1965.
- Glover, C.J., J.A. Bullin, J.W. Button, R.R. Davison, G.R. Donaldson, M.W. Hlavinka, and C.V. Philip, *Characterization of Asphalts Using Gel Permeation Chromatography and Other Methods*, Texas State Dept. of Highways and Public Trans. Research Report No. 419 (1987).
- Goode, J.A. and L.A. Lufsey, "Voids, Permeability, Film Thickness vs. Asphalt Hardening," *Proc. AAPT*, vol. 34, p. 430 (1965).
- Graham, A.L., R.D. Steele, and R.B. Bird, "Particle Clusters in Concentrated Suspensions. 3. Prediction of Suspension Viscosity," *Industrial and Engineering Chemistry Fundamentals*, vol. 23, pp. 420-425 (1984).
- Grunberg, L. and A.H. Nissan, "Mixture Law for Viscosity," *Nature*, vol. 164, pp. 799-800, (Nov. 5 1949).
- Halstead W.J., "The Relation of Asphalt Ductility to Pavement Performance," *Proc. AAPT*, vol. 32, p. 247 (1963).

- Heithaus, J.J. and R.W. Johnson, "A Microviscometer Study of Road Asphalt Hardening in the Field and Laboratory," *Proc. AAPT*, vol. 27, p. 17 (1958).
- Heukelom, W. and P.W.O. Wijga, "Viscosity of Dispersions as Governed by Concentration and Rate of Shear," *AAPT*, vol. 40, pp. 418-437 (1971).
- Hoiberg, A.J., *Bituminous Materials, Asphalts, Tars, and Pitches*, vol II, part 1, A. J. Hoiberg (ed.), Interscience Publishers, New York, NY (1964).
- Hoiberg, A.J. and W.E. Garris Jr., "Analytical Fractionation of Asphalts," *Ind. and Eng. Chem. Anal. Ed.*, vol. 16, pp. 294-302 (1944).
- Irving, J.B.. *Viscosities of Binary Liquid Mixtures: A Survey of Mixture Equations*, Report 630, National Engineering Laboratory, U.K. Department of Industry (1977a).
- Irving J.B.. *Viscosities of Binary Liquid Mixtures: The Effectiveness of Mixture Equations*, Report 631, National Engineering Laboratory, U.K. Department of Industry (1977b).
- Ishai, I., Y.A. Tuffour, and J. Craus, "Some Aspects of the Effect of Asphalt Chemical Composition on Material Behavior and Pavement Performance," *Trans. Res. Rec.*, vol. 1391, pp. 39-55 (1993).
- Jemison, H.B., "Supercritical Refining of Asphalts," Texas A&M University, Department of Chemical Engineering, College Station, Texas, PhD Dissertation, (December 1992).
- Jemison, H.B., R.R. Davison, C.J. Glover, and J.A. Bullin, "Evaluation of Standard Oven Tests for Hot-Mix Plant Aging," *Trans. Res. Rec.*, vol. 1323, p. 77 (1991).
- Kemp, G.R. and N.H. Predoehl, "A Comparison of Field and laboratory Environments on Asphalt Durability," *Proc. AAPT*, vol. 50, p. 492 (1981).
- Knoterus, J., "Bitumen Durability-Measurement by Oxygen Absorption," *Ind. and Eng. Chem. Prod. Res. Dev.*, vol. 11, p. 411 (1972).
- Krchma, L.C., D.E. Allison, C.E. Quiring, and T. Groening, "A Laboratory Exposure for Study of Asphalt Hardening," *Proc. AAPT*, vol. 29, p. 362 (1960).
- Krchma, L.C. and T. Groening, "Influence of Pavement Voids, Asphalt Content and Asphalt Grade on Asphalt Performance," *Proc. AAPT*, vol. 28, p. 34 (1959).
- Kumar, A. and W.H. Goetz, "Asphalt Hardening as Affected by Film Thickness,

- Voids, and Permeability in Asphaltic Mixtures," *Proc. AAPT*, vol. 46, pp. 571-605 (1977).
- Lau, C.K., K.M. Lunsford, C.J. Glover, R.R. Davison, and J.A. Bullin, "Reaction Rates and Hardening Susceptibilities as Determined from POV Aging of Asphalts," *Trans. Res. Rec.*, vol. 1342, pp. 50-57 (1992).
- Lee, A.R. and E.J. Dickinson, "The Weathering of Bituminous Materials," in *Bituminous Materials in Road Construction*, W.H. Glanville, ed., Her Majesty's Stationery Office, London, p. 176 (1962).
- Lee, D.Y. and R.J. Huang, "Weathering of Asphalts as Characterized by Infrared Multiple Internal Reflectance Spectra," *Applied Spectroscopy*, vol. 27, pp. 435-440 (1973).
- Lin, M.S., K.M. Lunsford, C.J. Glover, R.R. Davison, and J.A. Bullin, "The Effect of Asphaltenes on the Oxidative Characteristics of Asphalts," *The Fine Particle Society*, Preprints at 24th Annual Meeting (1993).
- Lunsford, K.M., "The Effect of Temperature and Pressure on Laboratory Oxidized Asphalt Films with Comparison to Field Aging," Texas A&M University, Department of Chemical Engineering, College Station, TX, PhD Dissertation, (May 1994).
- Martin, K.L., R.R. Davison, C.J. Glover, and J.A. Bullin, "Asphalt Aging in Texas Roads and Test Sections," *Trans. Res. Rec.*, vol. 1269, p. 9 (1990).
- Mehrotra, A.K., "Development of Mixing Rules for Predicting the Viscosity of Bitumen and Its Fractions Blended with Toluene," *Can. J. Chem. Eng.*, vol. 68, pp. 839-848 (Oct. 1990).
- Mehrotra, A.K., "Mixing Rules for Predicting the Viscosity of Bitumens Saturated with Pure Gases," *Can. J. Chem. Eng.*, vol. 70, pp. 165-172 (Feb. 1992).
- NOAA, "Local Climatological Data, Annual Summary with Comparative Data," National Oceanic and Atmospheric Administration, Asheville, NC (1988).
- Pal, R. and E. Rhodes, "Viscosity/Concentration Relationships for Emulsions," *J. Rheology*, vol. 33, pp. 1021-1045 (1989).
- Pauls, J.T. and W.J. Halstead, "Progressive Alteration of Sheet Asphalt Pavement Over a Long Period of Service," *Proc. AAPT*, vol. 58, p. 123 (1958).
- Pearson, C.D. G.S. Huff, and S.G. Gharfeh, "Technique for the Determination of

- Asphaltenes in Crude Oil Residues," *Anal. Chem.*, vol. 58, p. 3266 (1986).
- Petersen, J.C., F.A. Barbour, and S.M. Dorrence, "Catalysis of Asphalt Oxidation by Mineral Aggregate Surfaces and Asphalt Components," *Proc. AAPT*, vol. 43, p. 162 (1974).
- Petersen, J.C., J.F. Branthaver, R.E. Robertson, P.M. Harnsberger, J.J. Duvall, and E.E. Ensley, "Effects of Physicochemical Factors on Asphalt Oxidation Kinetics," *Trans. Res. Rec.*, vol. 1391, p. 1 (1993).
- Plancher, H., E.L. Green, and J.C. Petersen, "Reduction of Oxidative Hardening of Asphalts by Treatment with Hydrated Lime--A Mechanistic Study," *Proc. Association of Asphalt Paving Technologists*, vol. 45, pp. 1-24 (1976).
- Reerink H. and J. Lijzenga, "Molecular Weight Distributions of Kuwati Asphaltenes as Determined by Ultracentrifugation. Relation with Viscosity of Solutions," *J. Inst. Pet.*, vol. 59, pp. 211-222 (1973).
- Reid, R.C., J.M. Prausnitz, and T.K. Sherwood, *The Properties of Gases and Liquids*, McGraw-Hill, 4th ed., New York, NY (1983).
- Roelands, C.J.A. *Correlational Aspects of the Viscosity-Temperature-Pressure Relationship of Lubricating Oils*. Doctoral Thesis, Delft University of Technology, Delft, The Netherlands (1966).
- Rosen, S.L., *Fundamental Principles of Polymeric Materials*, John Wiley and Sons, New York, NY (1982).
- Rostler, F.S. and White, R.M., "Composition and Change in Composition of Highway Asphalts, 85-100 Penetration Grade," *Proc. AAPT*, vol. 31, pp. 35-72 (1962).
- Sheu, E.Y., M.M. De Tar, and D.A. Storm, "Rheological Properties of Vacuum Residue Fractions in Organic Solvents," *Fuel*, vol. 70, pp. 1151-1156 (1991).
- Solaimanian M. and T.W. Kennedy, "Predicting Maximum Pavement Surface Temperature Using Maximum Air Temperature and Hourly Solar Radiation," *Trans. Res. Rec.*, Preprint #930671 at 72nd Annual Meeting (1993).
- Storm, D.A., S.J. DeCanio, M.M. DeTar, and V.P. Nero, "Upper Bound on Number Average Molecular Weight of Asphaltenes," *Fuel*, vol. 69, pp. 735-738 (June 1990).
- Storm, D.A. and E.Y. Sheu, "Rheological Studies of Ratawi Vacuum Residue at 366K," *Fuel*, vol. 72, pp. 233-237 (1993).

- Thenoux, G., C.A. Bell, J.E. Wilson, D. Eakin, and M. Schroeder, "Experiences with the Corbett-Swarbrick Procedure for Separation of Asphalt into Four Generic Fractions," *Trans. Res. Rec.*, vol. 1171, pp. 66-70 (1988).
- Traxler, R.N., "Relation Between Asphalt Composition and Hardening by Volatilization and Oxidation," *Proceeding of Association of Asphalt Paving Technologists*, vol. 36, pp. 359-377 (1961).
- Van Oort, W.P., "Durability of Asphalt, Its Aging in the Dark," *Ind. and Eng. Chem.*, vol. 48, p. 1196 (1956).
- Verhasselt, A.F. and F.S. Choquet, "A New Approach to Studying the Kinetics of Bitumen Aging," *Proceedings of the International Symposium Chemistry of Bitumens, Vol. II*, p. 686 (1991).
- Verhasselt, A.F. and F.S. Choquet, "Comparing Field and Laboratory Aging of Bitumens on a Kinetic Basis," *Trans. Res. Rec.*, vol. 1391, p. 30 (1993).
- Yen, T.E, J.G. Erdman, and S.S. Pollack, "Investigation of the Structure of Petroleum Asphaltenes by X-Ray Diffraction," *Analytical Chemistry*, vol. 33, pp. 1587-1594 (1961).



APPENDIX A

EXPERIMENTAL METHODS

SUPERCRITICAL EXTRACTION

Study 1155 (Davison, 1991) and Study 1249 (Davison, 1992) describe the supercritical extraction unit. Chapter 5 discusses recent modifications as well as the operating conditions used in this work.

PRESSURE OXYGEN VESSEL (POV) CONFIGURATION II

This unit is described in Lau (1992) and Davison (1992). In order to improve on aging simulation capacity, four additional units were constructed and a central control panel was installed, as shown in Figure A-1. Because of temperature gradient problems, an additional heating tape was installed to increase the heat input near the vessel bottom. Operation of the unit in this mode is as follows: asphalt samples of 2.4 grams (0.085 oz) are prepared in aluminum trays. The dimensions of the tray are 7.0 cm (2.75 in) by 3.5 cm (1.38 in). When the asphalt is evenly distributed by slight heating, the effective film thickness is 1 mm (0.039 in). After preparing the asphalt samples, loading the sample rack, and allowing the temperature in the POV to reach equilibrium, the operator places the rack inside the POV and bolts the cover flange to the top. The vent valves, oxygen feed valves, and vacuum valves are closed. A vacuum pump evacuates the air in the vessel to a pressure of 0.03 atm absolute. The vessels are slowly pressurized to the desired level by manipulating the oxygen cylinder regulator and oxygen feed valves. Once the desired oxygen pressure is reached, the cylinder, regulators, and feed valves are closed. The vessel is isolated for the experimental time period.

During the experiment, samples are periodically removed. To obtain samples, the pressure in the vessel is decreased by slowly venting off the oxygen to the

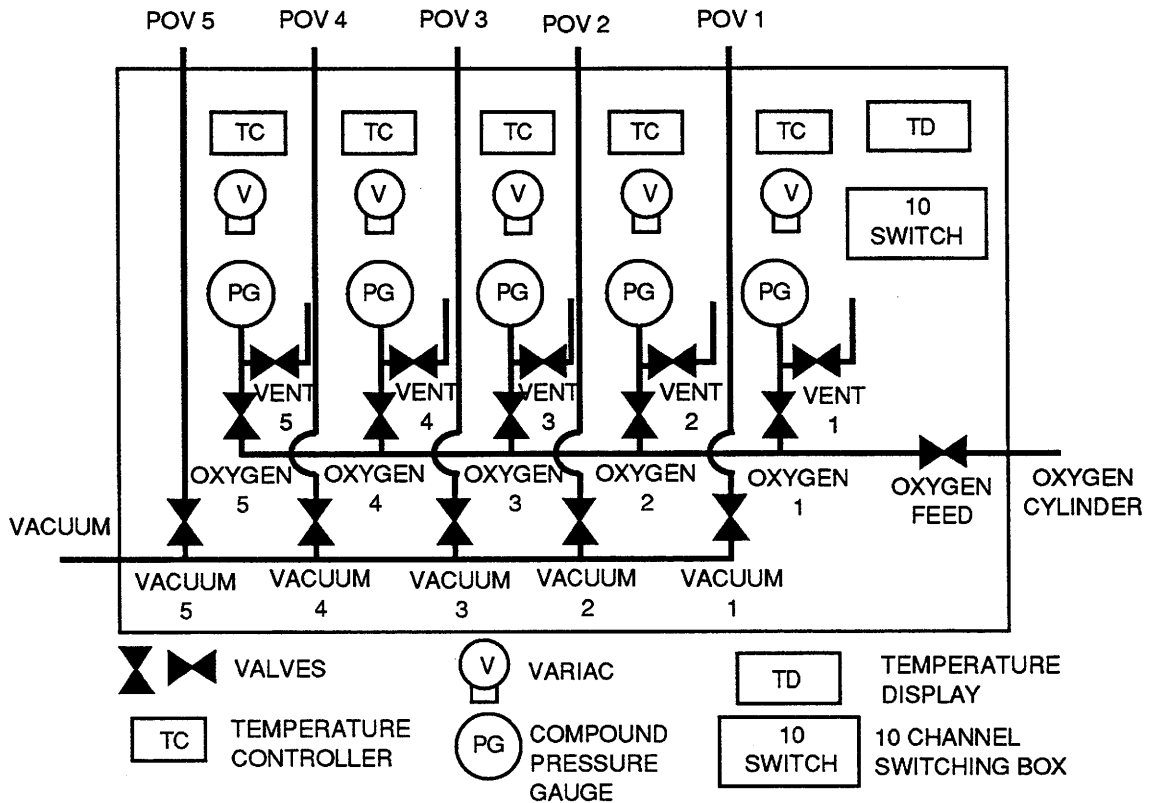


Figure A-1. Pressure Oxygen Vessel Control Panel

atmosphere until the pressure gauge reads zero. The operator removes the top insulation, unbolts the cover flange, and collects the samples. Samples to be aged further are loaded back into the vessel, and the process is repeated. The aged samples are saved for chemical and physical analysis.

POV CONFIGURATION III

Temperature gradient problems were still encountered in Configuration II, so it was decided to immerse the vessels in glycol-water baths which eliminated the problem.

Figure A-2 shows a schematic of one of the POVs. The actual vessels are

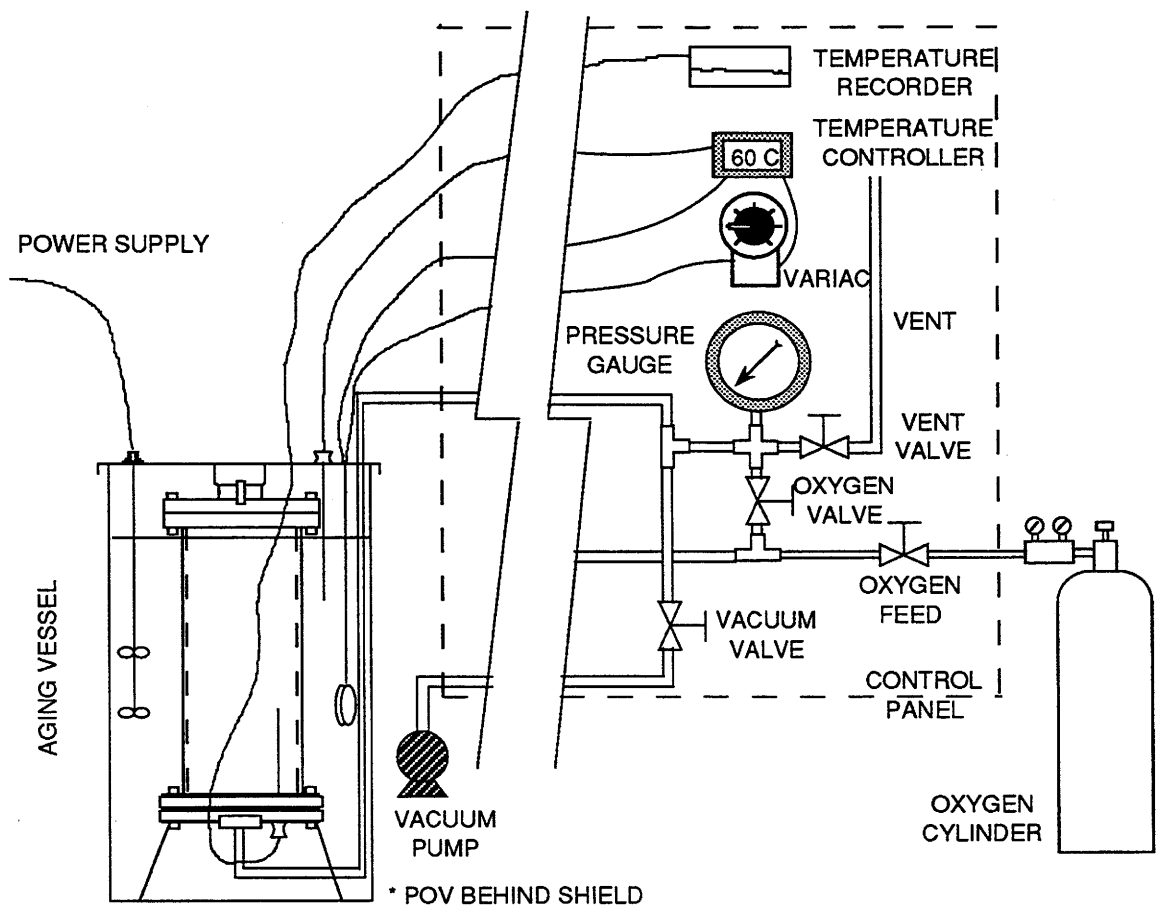


Figure A-2. Pressure Oxygen Vessel and Control Panel

behind a steel wall in an explosion proof hood. Each vessel is contained in a steel barrel which is enclosed in a four-sided shield made of *Lexan*™. The vessel is monitored and controlled from a panel outside the explosion proof hood. The control panel uses a compound pressure gauge to monitor the pressure, a variable transformer to control the amount of electrical power to the heating elements in the water/triethylene glycol bath, an on/off temperature controller, and a recorder to monitor the temperature within the POV. A stirrer is employed in the bath for even temperature distribution. To the left of the control panel is the vacuum pump that evacuates the vessels before charging with oxygen. Three valves per vessel, as labeled in Figure A-1, are used for venting to atmospheric pressure, evacuating to low pressure to remove the air, and charging with oxygen. The oxygen feed valve

isolates the POVs from the oxygen cylinder when closed.

CORBETT ANALYSIS

Corbett analyses (ASTM D 4124) separated the components of the samples according to polarity. Some modifications of the Corbett procedure were implemented to reduce sample size and increase efficiency as suggested by Thenoux et al. (1988).

GIANT CORBETT APPARATUS

This apparatus (Figure A-3) was constructed to separate larger samples corresponding roughly to the Corbett fractions: Asphaltenes, aromatics (polar aromatics plus naphthene aromatics) and saturates. The column contains about 1 kg (2.2 lbm) of alumina and is fed samples up to 250 grams (0.55 lbm).

The sample to be fractionated, either asphalt or supercritical fractions, is dissolved in 10-20 mL (0.34-0.68 fl oz) of hexane per gram (0.035 oz) of material and vacuum filtered. If asphaltenes are present, they are collected on the filter. The material still dissolved is then recovered using the Abson procedure, ASTM D-1856-79, and redissolved in n-heptane or hexane. This solution is poured over a bed of activated alumina. A mixture of paraffin and solvent flows into a reboiling flask, where the solvent is boiled away, recondensed, and allowed to flow back into the top of the column, and into the alumina bed. Over a period of three hours this removes all of the paraffinic material, which, when recovered, resembles petrolatum in appearance and texture.

Once the paraffins have been removed from the bed, the column is drained of heptane. A new solvent composed of 85% trichloroethylene and 15% ethanol dissolves the aromatic material adsorbed on the bed. Over a period of another three hours, this fraction, which contains both the naphthene and polar aromatics, is recovered and reported as aromatics.

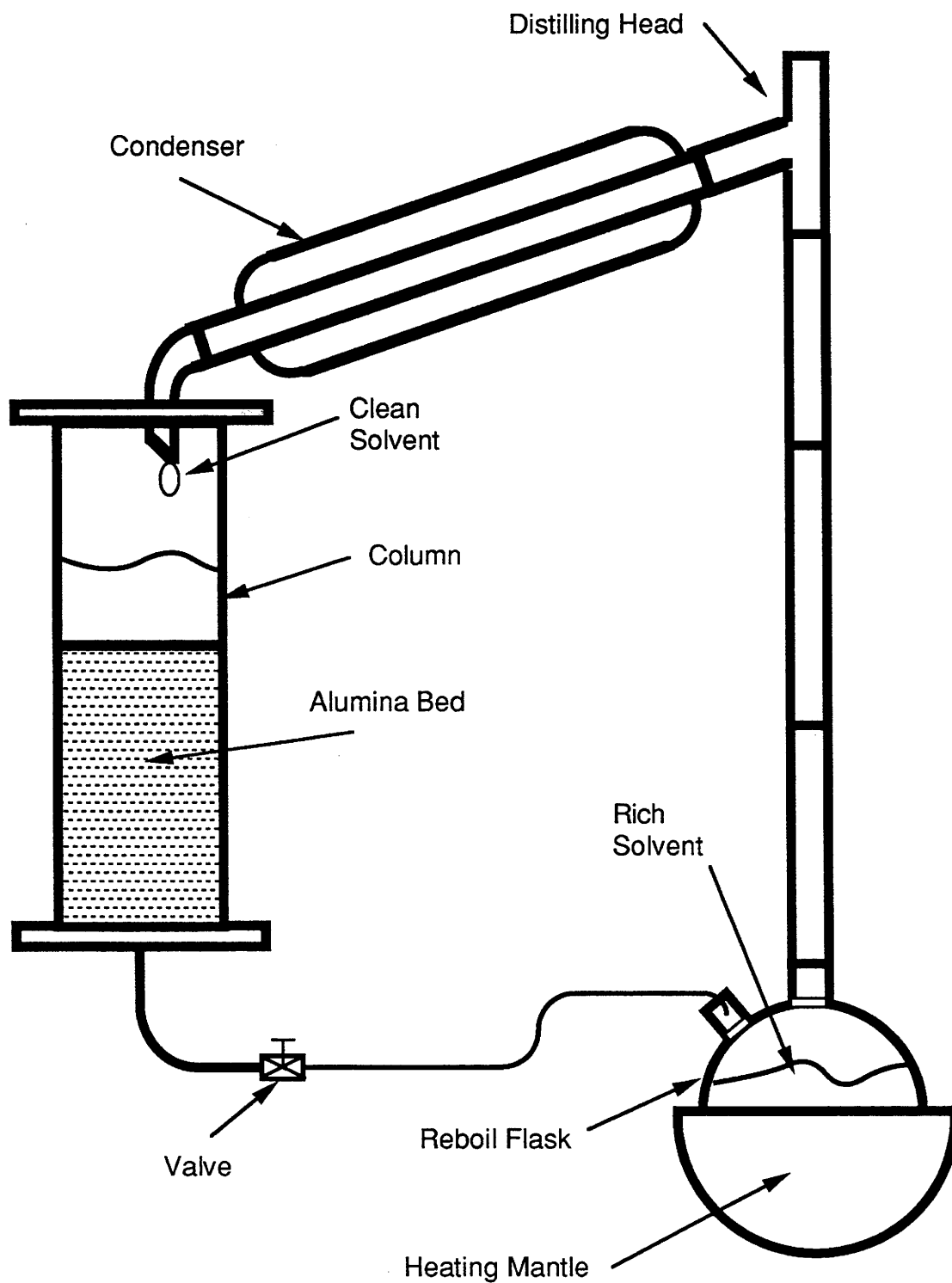


Figure A-3. Giant Corbett Apparatus

Although the asphaltenes may be slightly different from Corbett's asphaltenes due to the use of hexane rather than heptane for the precipitation, the difference is one of necessity. To insure that all of the heptane-insolubles, which will plug the alumina column very quickly, are removed, it is necessary either to precipitate the asphaltenes from a highly dilute (100 mL [3.38 fl oz] solvent per 1 gram [0.035 oz] of asphalt) solution, or to use a weaker solvent.

It was discovered that the recovered saturates still gave some UV absorption indicating the presence of aromatics. In some later work the saturate fractions were put through a standard Corbett column and flushed with hexane until aromatic material just began to appear. Recovery of the dissolved material from the diluted hexane yielded pure saturates.

SEPARATION OF SATURATES INTO OILS AND WAXES

This is a procedure described by Hoiberg and Garris (1944). The paraffins are dissolved in a solvent composed of two parts dichloromethane and one part acetone. The solution is chilled to 0°C (32°F) and vacuum filtered. The solid collected is a white or yellowish wax and is reported as waxes. The material that remains dissolved is a light yellow or brown oil and is reported as oils.

CORBETT ANALYSIS USING HPLC

Bishara and Wilkins (1989) developed an analytical method for analyzing the Corbett-type composition for asphalts using high performance liquid chromatography (HPLC). The HPLC method provides a rapid and high-repeatability analysis for determining the composition of an asphalt.

Asphalt samples are weighed to 0.2 ± 0.01 gram (0.0071 ± 0.00035 oz) in a scintillation vial and mixed with 20 mL (0.68 fl oz) of n-hexane. The asphalt/n-hexane solution is then sonicated for five minutes to ensure good mixing and is allowed to equilibrate overnight. A $0.45 \mu\text{m}$ PTFE membrane syringe filter is first

pre-dried in an oven at 100°C (212°F) for an hour prior to use and the weight of the filter is recorded. The asphaltene fraction is removed by filtering the solution through the syringe filter. After filtering, the filter is further dried in an oven at 100°C (212°F) for an hour. The weight difference between the filter before and after filtering is the weight of the asphaltene. The asphaltene content is equal to the weight of asphaltene divided by the weight of the asphalt sample.

After removal of the asphaltenes, 20 μL of the filtered solution is injected into a Waters 3.9x300 mm (0.15x11.8 in) 125 Å $\mu\text{Bondapak NH}_2$ steel column. A flow rate of 2.0 mL/min (0.068 fl oz/min) is used and the column is maintained at a temperature of 35°C (95°F). Saturates elute at 1.7 minutes and are detected by a refractive index (RI) photometer, while polar and naphthene aromatics are detected by an ultraviolet (UV) photometer. Naphthene aromatics elute shortly after the saturates; however, the polar aromatics will strongly absorb on the column and need to be backflushed out 15 minutes after injection. The saturate content is determined from a calibration of the RI response of pure saturates from the traditional Corbett column. The total aromatics content, the sum of polar aromatics and naphthene aromatics, is obtained by difference.

FOURIER TRANSFORM INFRARED SPECTROSCOPY, FTIR

A Mattson Galaxy series 5020 Spectrometer at 4 cm^{-1} resolution and 64 scans is used to measure the infrared absorbance spectra of the samples. The Attenuated Total Reflectance, ATR, method with a Zinc Selenide prism is used (Jemison et al., 1992). To quantify the changes in the spectra, the integrated absorbance from 1820 to 1650 cm^{-1} with respect to the baseline at the absorbance of 1820 cm^{-1} is calculated. This area is called the *Carbonyl Area* or *CA*. The range of wave numbers includes the following carbonyl compounds: esters, ketones, aldehydes, and carboxylic acids. The primary absorbance peak for the oxidized asphalt is located at 1700 cm^{-1} and corresponds to ketone formation.

At low aging pressures of 2 and 0.2 atm oxygen, an oxygen diffusion problem

may be significant. To partially eliminate this diffusion problem, only the exposed surface, *ES*, of the film is analyzed for kinetic data. The depth of penetration of the IR beam for the ATR prism is 1 micron. For analysis, a quarter of the material in the aluminum tray is removed and the *ES* placed on the prism face. To insure good contact at the sample/prism interface, the sample is compressed. Heating of the sample is avoided if possible.

For oxygen diffusion determinations in the asphalt film it is necessary to measure FTIR spectra at both the *ES* and the substrate interface, *SI*. This procedure requires two ATR prisms. Spectra of POV-aged asphalts and model compounds containing carbonyl groups were analyzed with both prisms. The agreement in the two ATR prisms was within 2% based on *CA* determinations, and it was concluded that the two prisms were equivalent.

The actual procedure for measuring the *ES* and *SI* spectra with the two ATR prisms is explained. First, the *ES* spectrum is measured with one of the ATR prisms. The second prism is placed in the sample compartment and the required backgrounds and purge references are collected. The aluminum is removed, and the *SI* surface is ready for analysis. The second prism face is placed on the *SI* surface creating a sandwich configuration with the asphalt film. Good surface contact between the second prism and the *SI* surface is sometimes difficult to achieve, since heating of the samples should be avoided, and excessive compression will damage the prism. When sufficient contact is achieved, the prism configuration is placed in the sample compartment, and the *SI* spectrum is collected.

For measuring the spectra of asphaltenes, a sample of asphaltene material is dissolved in THF and the solution is deposited on the ATR prism drop-by-drop, allowing the THF to evaporate. When the film is sufficiently thick it is further dried with a heat gun.

DYNAMIC MECHANICAL ANALYSIS, DMA

The rheological properties of neat and aged asphalt were measured on a Carri-Med 500 Controlled Stress Rheometer. The specific properties used to characterize the asphalts were the limiting zero shear complex viscosity, η_o^* , and the reciprocal of the loss compliance, $(1/J'')$. Both properties were measured at a temperature of 333.3 K (140°F) and values of $(1/J'')$ are reported at a frequency of 10 rad/s. The value of η_o^* is independent of frequency or shear rate (Lau et al., 1992). The geometry consisted of a 2.5 cm (1 in) parallel plate with a 0.5 mm (0.02 in) gap. Torque levels were such that the behavior of the asphalt was linearly viscoelastic in the frequency range of 100 to 0.1 rad/s. η_o^* was not measurable at 333.3 K (140°F) and 0.1 rad/s on samples with viscosity higher than 200,000 poise. For these hard samples, rheological measurements were performed at both 333.3 and 363.2 K (140° and 195°F). The moduli curves were superimposed at 333.3 K (140°F) using time-temperature superposition (Ferry, 1985) and η_o^* was calculated.

HEXANE ASPHALTENE DETERMINATION

Asphaltenes are the insoluble portion of the asphalt in a paraffinic solvent. The hexane asphaltenes of neat and aged asphalts were precipitated as described by Pearson et al., (1986). Solutions of 0.2 grams (0.0071 oz) of asphalt in 20 mL (0.68 fl oz) of hexane were made, sonicated for 30 minutes, and precipitated for 12 hours. The solutions were filtered through pre-weighed 0.4 micron membranes. After drying for approximately three days, the membranes were post weighed. The difference in the weight of the membrane relative to the sample weight multiplied by 100 is the %A.

GEL PERMEATION CHROMATOGRAPHY, GPC

A WATERS GPC 600E system was used to determine the molecular weight, *MW*, distributions of asphalts and to detect for trace amounts of solvent after extraction and recovery (Burr et al., 1991). Three columns in order of decreasing pore size of 1000, 100, and 50 Å separated the sample based on molecular size or hydrodynamic volume. The first two columns were 305 mm (12 in) long and were obtained from WATERS. The final column, from PLGel, was 610 mm (24 in) long. Solvent detection after extraction and recovery required this final column (Burr et al., 1991). The mobile phase was tetrahydrofuran, THF, at a flow rate of 1 mL/min (0.34 fl oz/min). The injection volume was 100 μL. A Differential Refractive Index detector, RI, monitored the elution of the sample through system. Isothermal operation of the columns and detectors was at 313.2 K (104°F).

The system was calibrated with a known set of polystyrene, PS, standards at a concentration of 0.025 g/mL (0.026 oz/fl oz). Based on the retention time or elution volume of the PS and the known *MW*, a calibration curve was constructed and a high order polynomial was used to fit the data points providing a smooth function through the data. Furthermore, the retention times for the asphalt samples were in the range of the PS standards. Errors introduced from extrapolation of the polynomial outside of the calibration range were eliminated, since this calibration curve was not used for retention times outside the range of the standards.

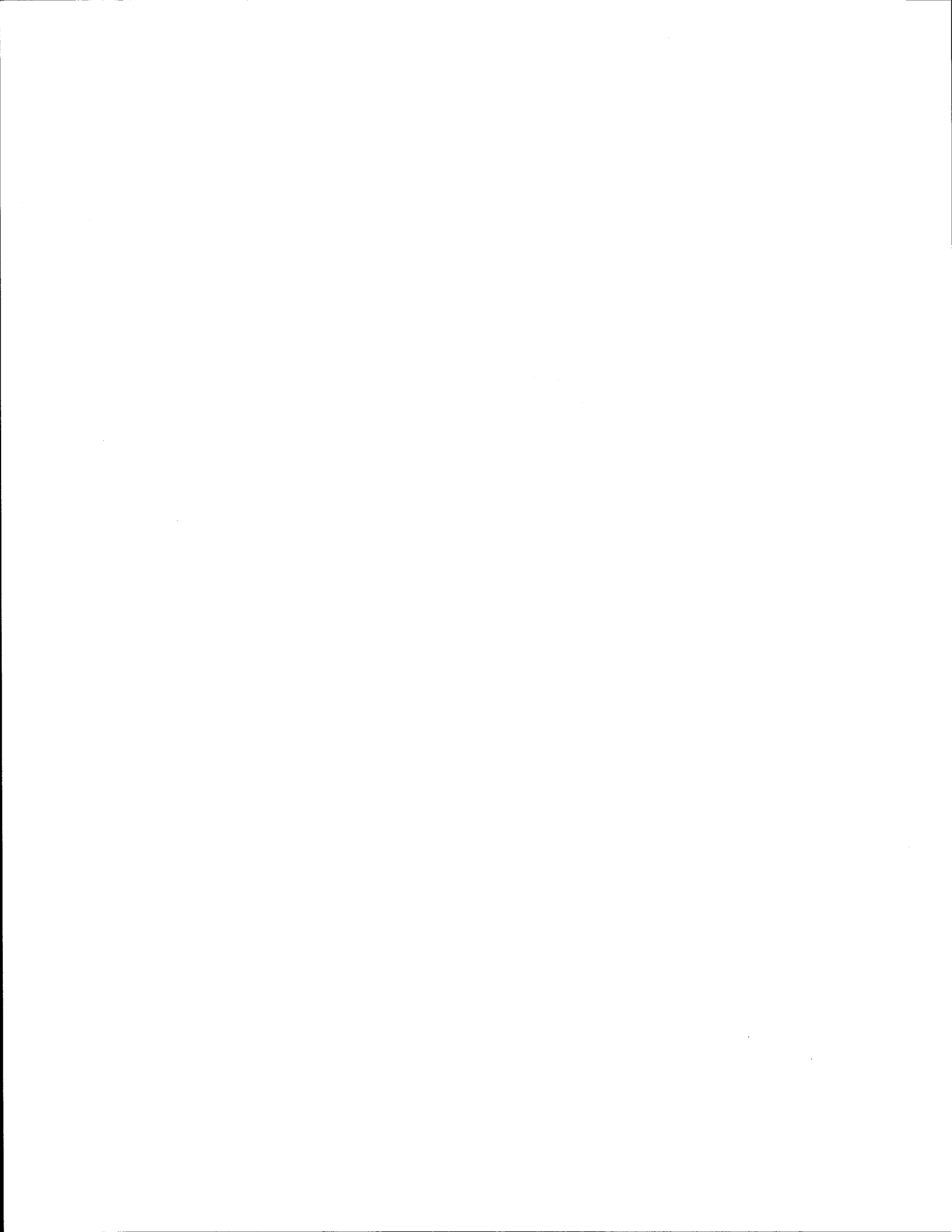
After calibration, samples were prepared at a concentration of 0.020 g/mL (0.021 oz/fl oz). The samples were sonicated for 30 minutes and filtered through 0.4 micron membranes, removing insoluble particles that could damage the GPC columns. Samples were analyzed within two days of preparation decreasing the effect of solvent aging (Burr et al., 1991). The weight-averaged molecular weight, based on RI *MW*, was calculated from the measured chromatogram and calibration curve.

VOID CONTENT OF FIELD-AGED CORES, % V

Percent air voids, % V, was the only core property measured. This procedure is designated ASTM D 3203-83, a combination of measuring the bulk specific gravity of the core, D 2726-83, and the theoretical maximum specific gravity, D 2041-78.

EXTRACTION AND RECOVERY OF FIELD-AGED ASPHALT

Two different procedures were used for extraction and recovery. The extracting solvent for both procedures was the same, a mixture of 15% ethanol and 85% TCE by volume. The first procedure is an automated system that continuously feeds and removes solvent (Burr, 1993). The second procedure is a manual method, extracting the asphalt with discrete volumes of solvent. The manual or micro method is similar to ASTM D 2172-81 Method A. In both procedures, a rotary evaporator recovered the asphalt from the extraction solution. To minimize the solvent effects on the asphalt during recovery, the asphalt concentrations were kept as high as possible, and the oil bath temperature was maintained at 388.9 K (240°F). For final recovery, the temperature was increased to 444.4 K (340°F). To ensure sufficient solvent removal, the final recovery process was extended 30 minutes beyond the detection of the last drop of solvent in the collection flask. To verify complete solvent removal, all of the extracted asphalts were analyzed with GPC (Burr et al., 1991).



APPENDIX B
DATA FOR CHAPTER 1

Table B-1. Ampet AC-20 Kinetic Data^a

<i>t</i> days	0.2 atm ^b			2 atm ^b			20 atm ^c		
	333.3 ^d CA	344.4 CA	355.5 CA	333.3 CA	344.4 CA	355.5 CA	333.3 CA	344.4 CA	355.5 CA
2	-	-	0.637	-	-	-	-	-	0.890
4	-	-	0.679	-	0.745	0.917	-	-	-
5	-	-	-	0.764	-	-	-	-	1.046
6	-	0.681	0.698	-	-	-	-	0.941	-
7	-	-	-	-	-	-	0.752	-	-
8	0.712	0.705	0.797	-	-	-	-	-	-
9	-	-	-	-	0.772	1.014	-	-	-
10	-	-	0.777	-	-	1.063	-	-	-
12	-	0.730	-	0.793	0.882	-	-	-	-
13	-	-	-	-	-	-	-	1.247	1.496
14	-	-	-	-	-	1.276	-	-	-
17	-	-	-	-	0.917	-	-	-	-
20	-	0.814	0.975	-	0.927	-	1.017	1.424	1.995
21	-	-	-	0.902	-	1.468	-	-	-
24	0.728	-	-	-	-	-	-	-	-
27	-	-	-	-	-	-	-	-	2.583
28	-	0.821	-	0.925	1.056	-	-	-	-
30	-	-	-	-	-	-	1.060	1.697	-
32	0.753	0.882	-	-	1.212	-	-	-	-
36	-	-	-	-	1.151	-	-	-	-
40	-	-	-	-	1.262	-	-	-	-
41	0.815	-	-	-	-	-	-	-	-
44	-	-	-	0.993	-	-	-	2.078	-
50	-	-	-	-	-	-	1.310	-	-
57	0.865	-	-	-	-	-	-	-	-
58	-	-	-	-	-	-	-	2.436	-
68	-	-	-	1.237	-	-	-	-	-
70	-	-	-	-	-	-	-	2.567	-
72	0.885	-	-	-	-	-	-	-	-
76	-	-	-	1.218	-	-	-	-	-
80	0.938	-	-	-	-	-	-	-	-

^a - Signifies the values were not determined.

^b Exposed surface analysis

^c Bulk analysis

^d Units of K

Table B-2. Coastal AC-20 Kinetic Data^a

<i>t</i> days	0.2 atm ^b			2 atm ^b			20 atm ^c		
	333.3 ^d CA	344.4 CA	355.5 CA	333.3 CA	344.4 CA	355.5 CA	333.3 CA	344.4 CA	355.5 CA
2	—	—	0.595	—	—	0.845	—	—	1.037
4	—	—	0.710	—	0.793	—	—	—	—
5	—	—	—	0.823	—	0.894	—	—	1.224
6	—	—	0.652	—	—	—	—	1.138	—
7	—	—	—	—	—	—	0.992	—	—
8	0.595	0.720	0.756	—	—	—	—	—	—
9	—	—	—	—	0.846	—	—	—	—
10	—	—	0.835	—	—	—	—	—	—
12	—	0.750	—	0.885	0.992	—	—	—	—
13	—	—	—	—	—	—	—	1.386	1.754
14	—	—	—	—	—	1.250	—	—	—
15	—	—	0.982	—	—	—	—	—	—
16	—	0.791	0.773	—	—	—	—	—	—
17	—	—	—	—	1.104	—	—	—	—
18	—	—	0.986	—	—	—	—	—	—
20	—	0.790	0.918	—	—	—	1.235	1.682	2.464
21	—	—	—	0.890	—	1.570	—	—	—
23	—	—	1.140	—	—	1.591	—	—	—
24	0.710	0.862	—	—	—	—	—	—	—
28	—	0.874	—	0.951	—	—	—	—	—
30	—	—	—	—	—	—	1.326	1.934	—
32	0.815	0.943	—	—	1.306	—	—	—	—
36	—	0.974	—	1.049	1.253	—	—	—	—
40	—	—	—	—	1.398	—	—	—	—
41	0.791	0.998	—	—	—	—	—	—	—
44	—	—	—	1.044	—	—	—	2.493	—
48	0.797	—	—	—	—	—	—	—	—
50	—	—	—	—	—	—	1.517	—	—
52	—	—	—	1.180	—	—	—	—	—
57	0.795	—	—	—	—	—	—	—	—
58	—	—	—	—	—	—	—	2.845	—
60	—	—	—	1.285	—	—	—	—	—
64	0.856	—	—	—	—	—	—	—	—
68	—	—	—	1.161	—	—	—	—	—
70	—	—	—	—	—	—	1.753	3.100	—
72	0.873	—	—	—	—	—	—	—	—
76	—	—	—	1.237	—	—	—	—	—

^a — Signifies the values were not determined.

^b Exposed surface analysis

^c Bulk analysis

^d Units of K

Table B-3. Cosden AC-20 Kinetic Data^a

<i>t</i> days	0.2 atm ^b			2 atm ^b			20 atm ^c		
	333.3 ^d CA	344.4 CA	355.5 CA	333.3 CA	344.4 CA	355.5 CA	333.3 CA	344.4 CA	355.5 CA
2	--	--	0.646	--	--	0.946	--	--	1.290
4	--	--	0.767	--	0.833	--	--	--	--
5	--	--	--	0.856	--	--	--	--	1.688
6	--	--	0.762	--	--	1.006	--	--	--
7	--	--	--	--	--	--	1.052	1.468	--
8	0.694	0.763	0.912	--	--	--	--	--	--
9	--	--	--	--	0.943	1.209	--	--	--
12	--	0.778	--	0.945	--	--	--	--	--
13	--	--	--	--	--	--	--	--	2.385
14	--	--	--	--	--	1.375	--	2.020	--
16	0.739	--	1.041	--	--	--	--	--	--
17	--	0.788	--	--	1.088	--	--	--	--
18	--	--	1.069	--	--	1.426	--	--	--
20	--	0.822	1.095	--	1.153	--	1.598	--	3.026
21	--	--	--	1.053	--	1.769	--	--	--
24	0.831	0.951	--	--	--	--	--	--	--
26	--	--	--	--	--	--	--	2.270	--
27	--	--	--	--	--	--	--	--	3.497
30	--	--	--	--	--	--	1.904	--	--
32	0.765	1.015	--	--	1.393	--	--	--	--
35	--	--	--	--	--	--	--	2.465	--
36	--	--	--	--	--	--	--	--	--
44	--	--	--	1.249	--	--	--	--	--
48	0.929	--	--	--	--	--	--	--	--
50	--	--	--	--	--	--	2.166	--	--
52	--	--	--	1.318	--	--	--	--	--
57	0.917	--	--	--	--	--	--	--	--
60	--	--	--	1.430	--	--	--	--	--
64	0.975	--	--	--	--	--	--	--	--
70	--	--	--	--	--	--	2.292	--	--
72	1.031	--	--	--	--	--	--	--	--
76	--	--	--	1.487	--	--	--	--	--
80	1.027	--	--	--	--	--	--	--	--

^a -- Signifies the values were not determined.

^b Exposed surface analysis

^c Bulk analysis

^d Units of K

Table B-4. Exxon AC-20 Carbonyl Areas^a

<i>t</i> days	0.2 atm ^b			2 atm ^b			20 atm ^c		
	333.3 ^d CA	344.4 CA	355.5 CA	333.3 CA	344.4 CA	355.5 CA	333.3 CA	344.4 CA	355.5 CA
2	--	--	0.740	--	--	0.871	--	--	0.953
4	--	0.745	0.853	--	0.813	--	--	--	--
5	--	--	--	0.875	--	--	--	--	1.471
6	--	--	--	--	0.918	0.955	--	--	--
7	--	--	--	--	--	--	0.949	1.268	--
8	--	0.759	0.966	--	--	--	--	--	--
9	--	--	--	--	--	1.146	--	--	--
10	--	--	1.033	--	--	--	--	--	--
12	--	0.826	--	0.988	--	--	--	--	--
13	--	--	--	--	--	--	--	--	1.727
14	--	--	--	--	--	1.267	--	1.465	--
16	0.744	0.894	1.089	--	--	1.283	--	--	--
17	--	--	--	--	1.037	--	--	--	--
18	--	--	--	--	--	1.400	--	--	--
20	--	0.866	1.149	--	1.051	--	1.315	--	2.074
21	--	--	--	1.009	--	--	--	--	--
23	--	--	1.200	--	--	--	--	--	--
24	0.819	0.922	--	--	--	--	--	--	--
26	--	--	--	--	--	--	--	1.872	--
27	--	--	--	--	--	--	--	--	2.651
28	--	0.889	--	1.032	1.192	--	--	--	--
30	--	--	--	--	--	--	1.547	--	--
32	--	1.033	--	--	--	--	--	--	--
35	--	--	--	--	--	--	--	2.071	--
36	--	0.958	--	1.226	--	--	--	--	--
40	--	--	--	--	1.319	--	--	--	--
41	--	1.056	--	--	--	--	--	--	--
44	--	--	--	1.218	--	--	--	--	--
48	0.909	--	--	--	--	--	--	--	--
50	--	--	--	--	--	--	1.707	--	--
52	--	--	--	1.314	--	--	--	--	--
60	--	--	--	1.412	--	--	--	--	--
68	--	--	--	1.386	--	--	--	--	--
70	--	--	--	--	--	--	1.775	--	--
76	--	--	--	1.426	--	--	--	--	--
80	1.027	--	--	--	--	--	--	--	--

^a -- Signifies the values were not determined.

^b Exposed surface analysis

^c Bulk analysis

^d Units of K

Table B-5. Texaco AC-20 Kinetic Data^a

<i>t</i> days	0.2 atm ^b			2 atm ^b			20 atm ^c		
	333.3 ^d CA	344.4 CA	355.5 CA	333.3 CA	344.4 CA	355.5 CA	333.3 CA	344.4 CA	355.5 CA
2	—	—	0.594	—	—	0.747	—	0.731	0.946
4	—	0.617	0.623	—	0.699	—	—	—	—
5	—	—	—	0.729	—	—	—	—	1.130
6	—	—	0.656	—	—	0.927	—	0.973	—
7	—	—	—	—	—	—	0.782	—	—
8	—	0.644	0.722	—	—	—	—	—	—
9	—	—	—	—	0.809	—	—	—	—
10	—	—	0.772	—	—	—	—	—	—
12	—	—	—	0.765	0.856	—	—	—	—
13	—	—	—	—	—	—	—	1.247	1.620
14	—	—	—	—	—	1.182	—	—	—
15	—	—	0.853	—	—	—	—	—	—
16	0.560	0.726	0.848	—	—	—	—	—	—
17	—	—	—	—	0.918	—	—	—	—
18	—	—	—	—	—	1.172	—	—	—
20	—	0.714	0.918	—	—	—	1.048	1.374	1.985
21	—	—	—	0.819	—	1.353	—	—	—
23	—	—	—	—	—	1.354	—	—	—
24	0.667	0.726	—	—	1.045	—	—	—	—
27	—	—	—	—	—	—	—	—	2.363
28	—	0.793	—	0.850	—	—	—	—	—
30	—	—	—	—	—	—	1.195	1.730	—
32	0.622	0.851	—	—	1.115	—	—	—	—
36	—	0.896	—	0.912	—	—	—	—	—
41	0.716	0.878	—	—	—	—	—	—	—
44	—	—	—	0.971	—	—	—	2.002	—
48	0.763	—	—	—	—	—	—	—	—
50	—	—	—	—	—	—	1.364	—	—
52	—	—	—	1.100	—	—	—	—	—
58	—	—	—	—	—	—	—	2.315	—
60	—	—	—	1.011	—	—	—	—	—
64	0.766	—	—	—	—	—	—	—	—
68	—	—	—	1.120	—	—	—	—	—
70	—	—	—	—	—	—	1.505	2.687	—
72	0.803	—	—	—	—	—	—	—	—
76	—	—	—	1.132	—	—	—	—	—
80	0.815	—	—	—	—	—	—	—	—

^a — Signifies the values were not determined.

^b Exposed surface analysis

^c Bulk analysis

^d Units of K

Table B-6. Kinetic Data for Asphalts
Aged at 322.2 K and 20 atm^a

AC-20 Asphalts					
<i>t</i> days	Ampet <i>CA</i>	Coastal <i>CA</i>	Cosden <i>CA</i>	Exxon <i>CA</i>	Texaco <i>CA</i>
7	0.752	0.746	0.882	0.832	0.710
21	0.876	0.887	1.042	0.973	0.785
35	0.965	0.940	1.178	1.110	0.855
54	1.081	1.018	1.282	1.199	0.935
72	1.110	1.058	1.311	1.268	—
82	1.144	1.114	1.367	1.292	—

^a — Signifies the values were not determined.
 Bulk analysis

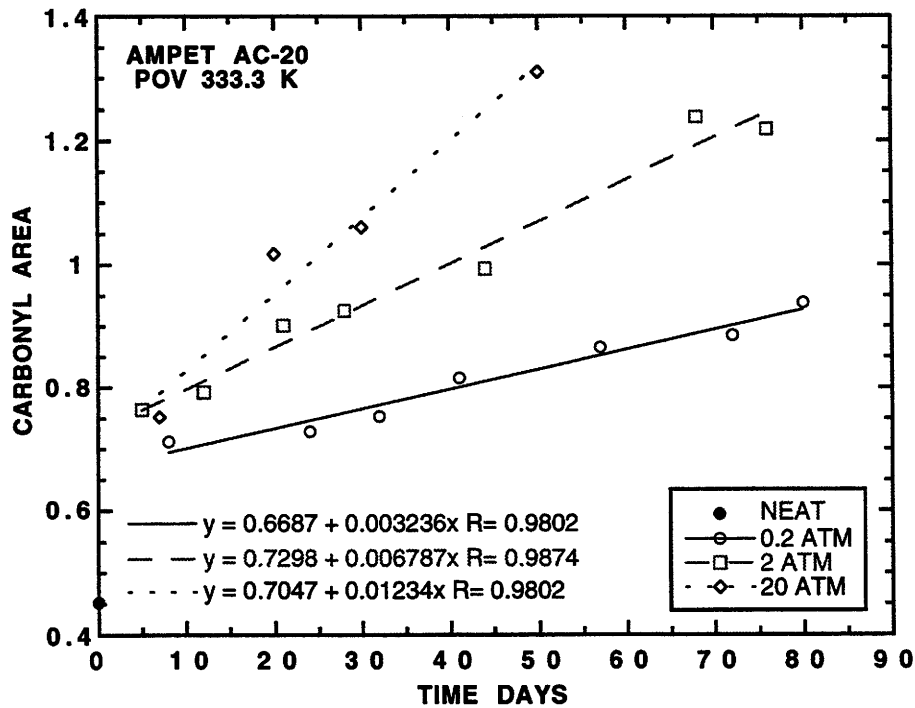


Figure B-1. CAs of Tank and POV-Aged Ampet AC-20 at 333.3 K

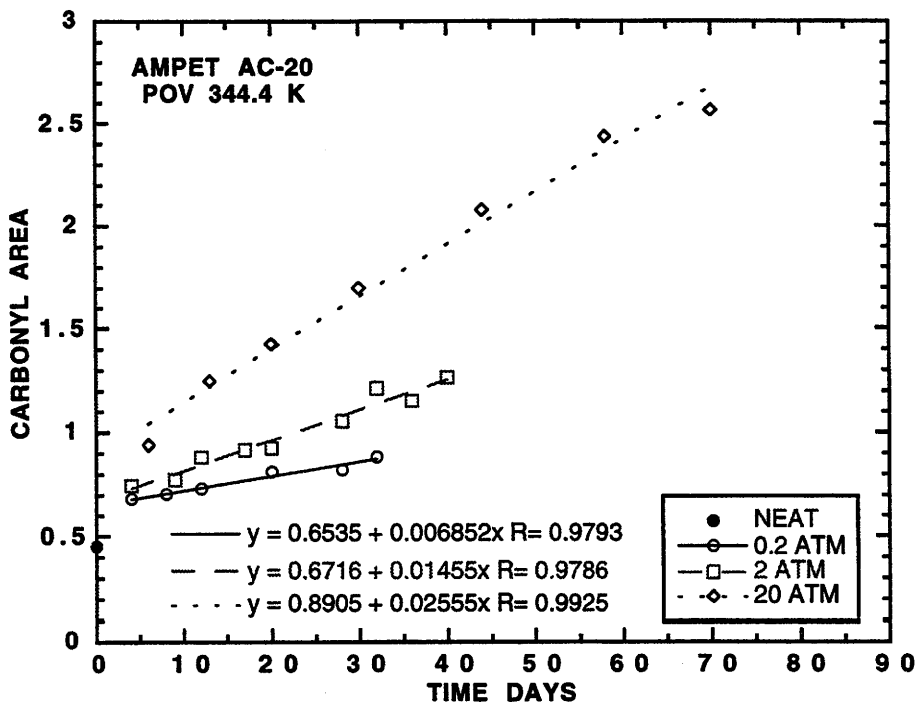


Figure B-2. CAs of Tank and POV-Aged Ampet AC-20 at 344.4 K

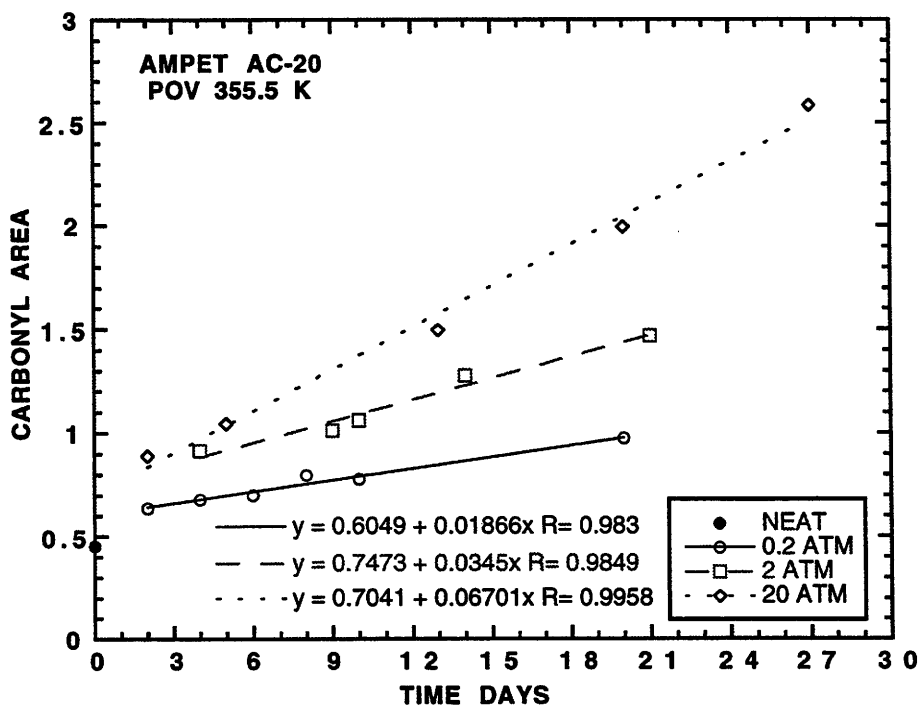


Figure B-3. CAs of Tank and POV-Aged Ampet AC-20 at 355.5 K

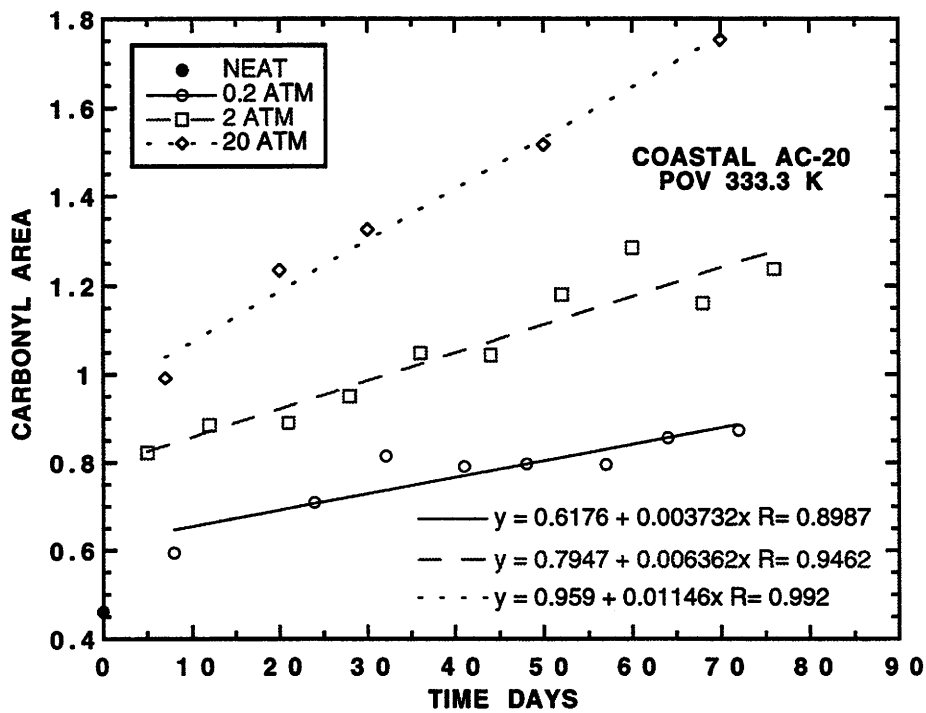


Figure B-4. CAS of Tank and POV-Aged Coastal AC-20 333.3 K

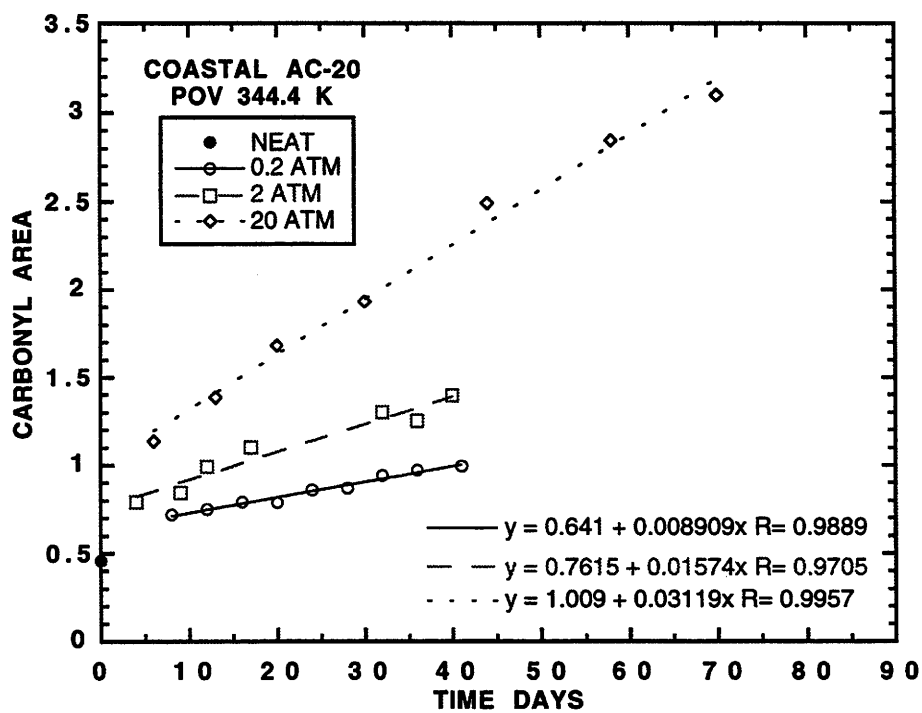


Figure B-5. CAS of Tank and POV-Aged Coastal AC-20 at 344.4 K

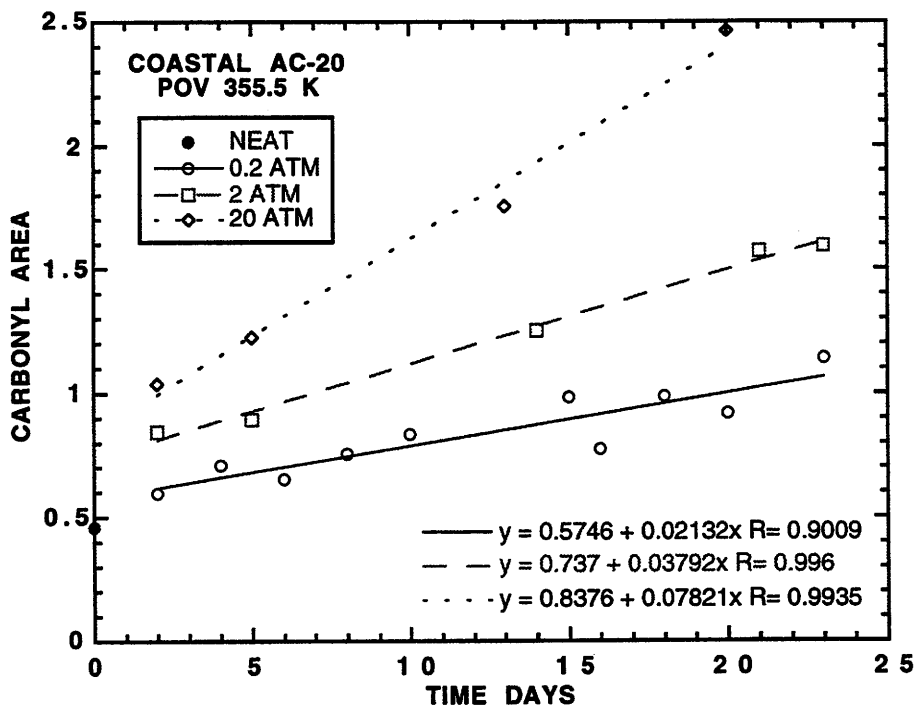


Figure B-6. *CAs* of Tank and POV-Aged Coastal AC-20 at 355.5 K

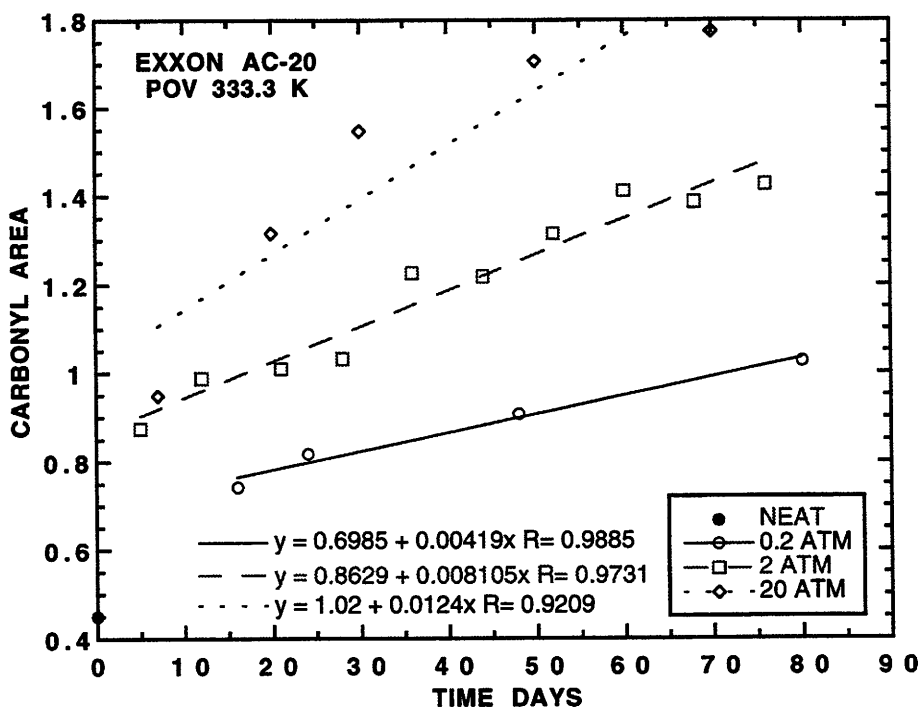


Figure B-7. *CAs* of Tank and POV-Aged Exxon AC-20 at 333.3 K

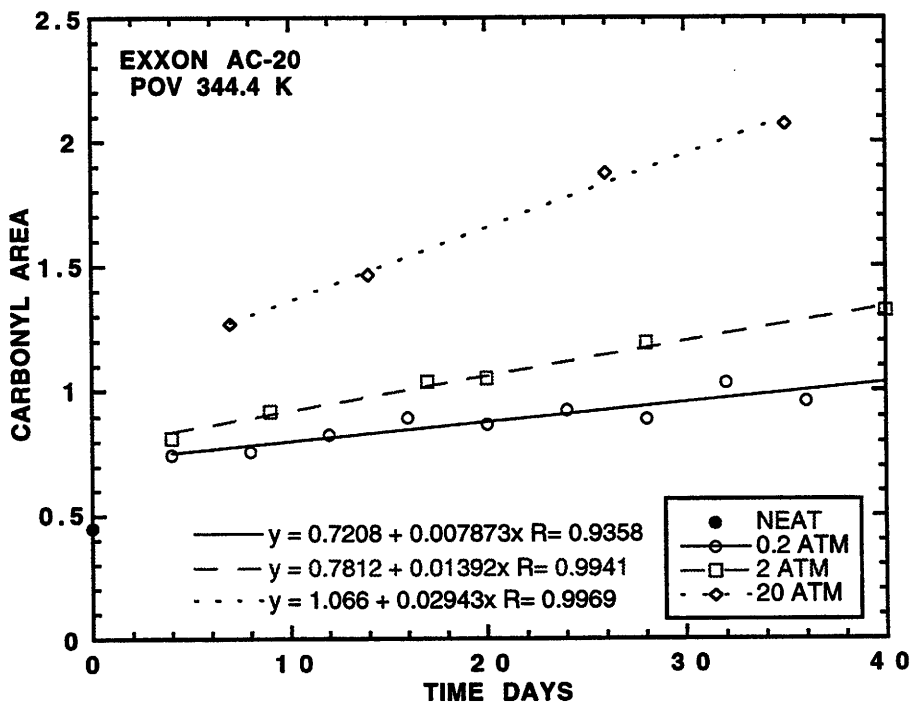


Figure B-8. CAs of Tank and POV-Aged Exxon AC-20 at 344.4 K

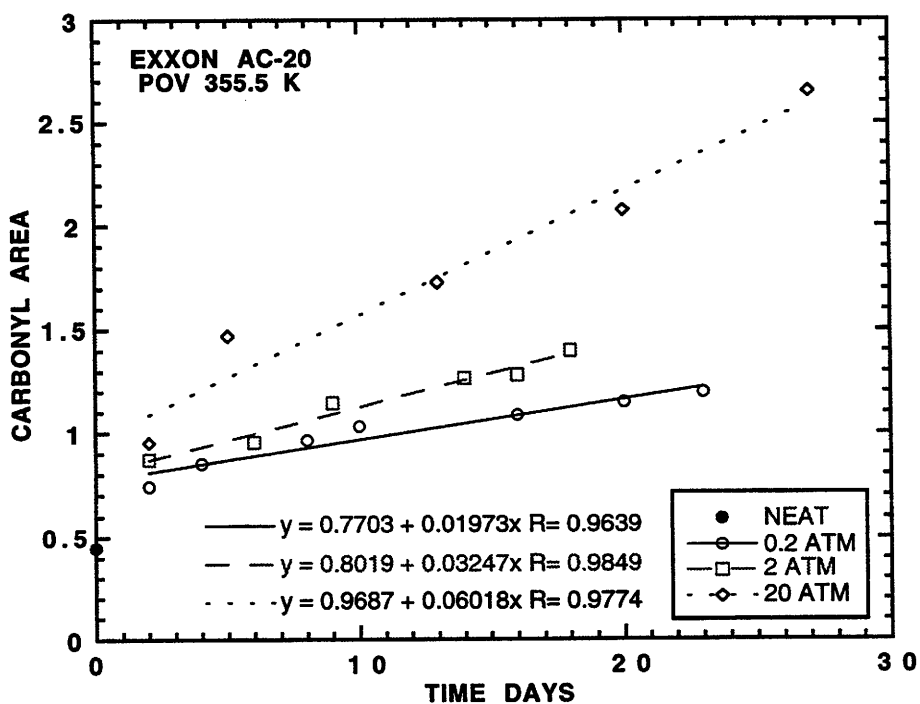


Figure B-9. CAs of Tank and POV-Aged Exxon AC-20 at 355.5 K

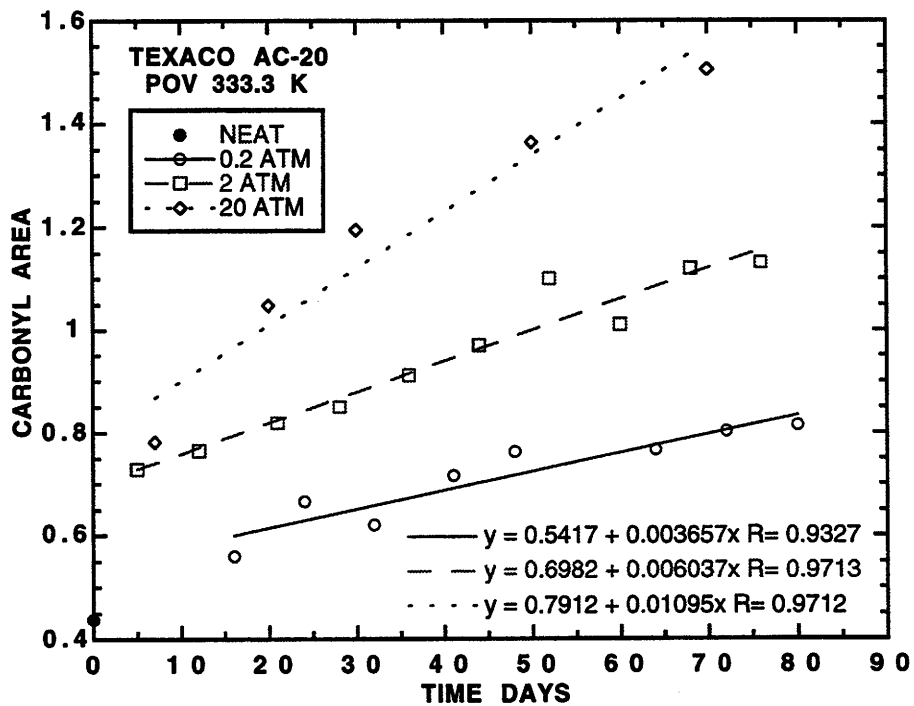


Figure B-10. CAs of Tank and POV-Aged Texaco AC-20 at 333.3 K

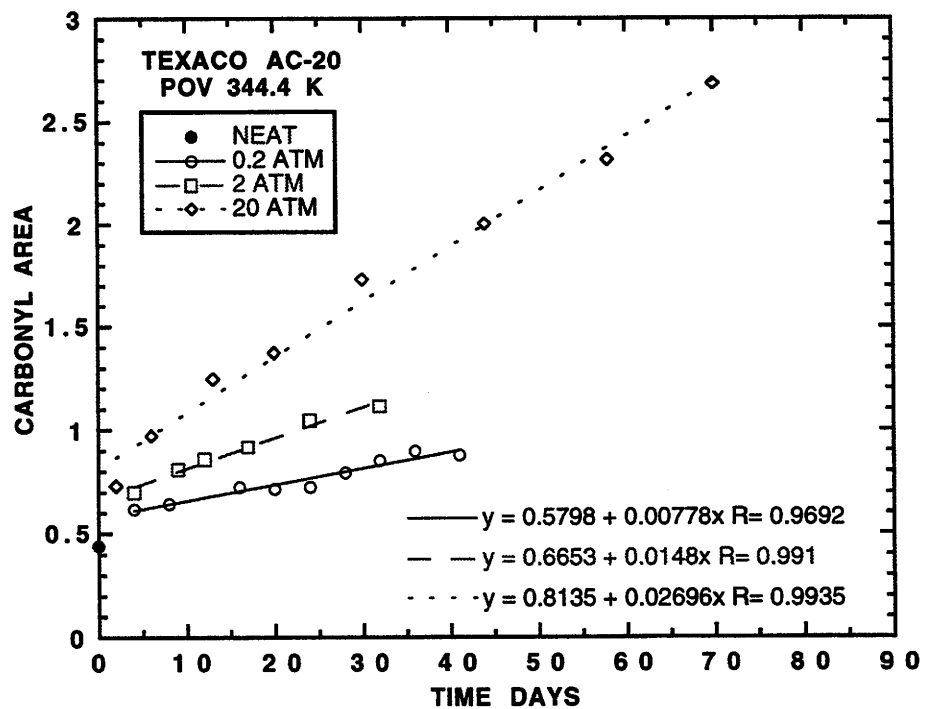


Figure B-11. CAs of Tank and POV-Aged Texaco AC-20 at 344.4 K

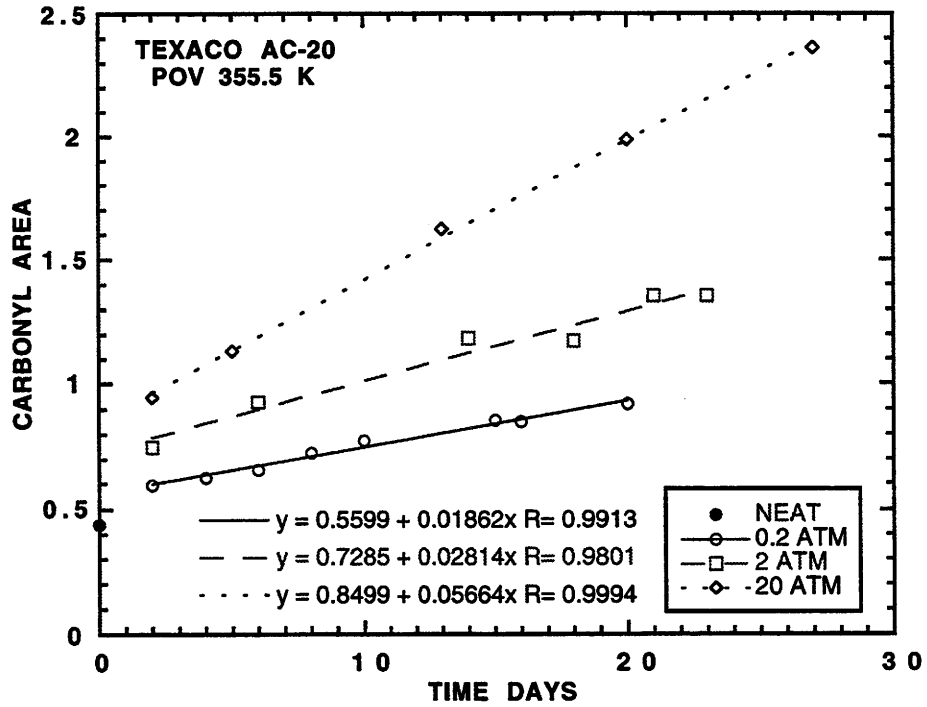


Figure B-12. CAs of Tank and POV-Aged Texaco AC-20 at 355.5 K

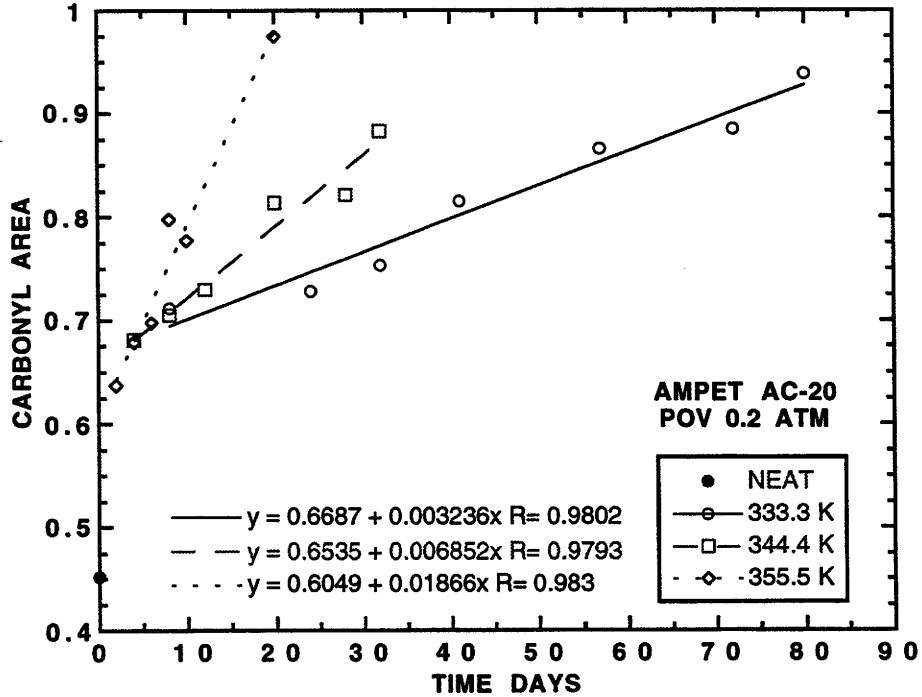


Figure B-13. CAs of Tank and POV-Aged Ampet AC-20 at 0.2 atm

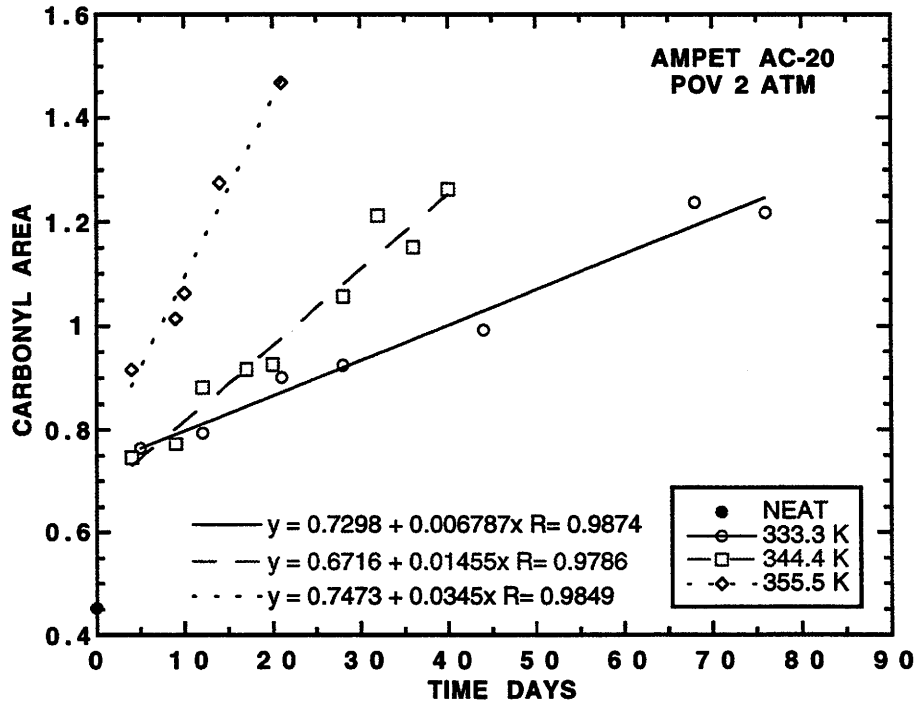


Figure B-14. CAs of Tank and POV-Aged Ampet AC-20 at 2 atm

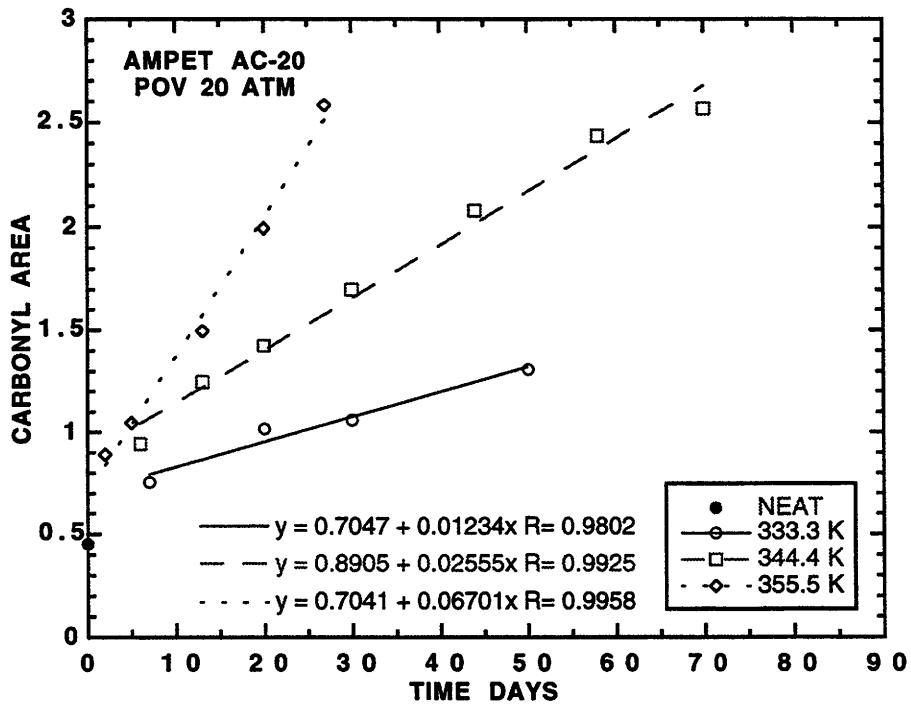


Figure B-15. CAs of Tank and POV-Aged Ampet AC-20 at 20 atm

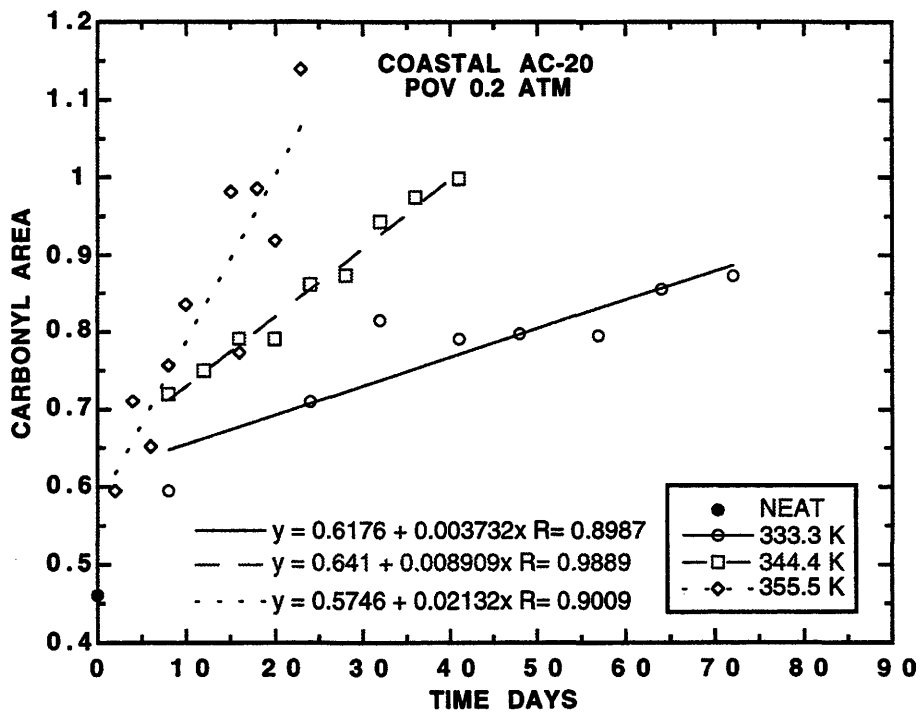


Figure B-16. CAS of Tank and POV-Aged Coastal AC-20 at 0.2 atm

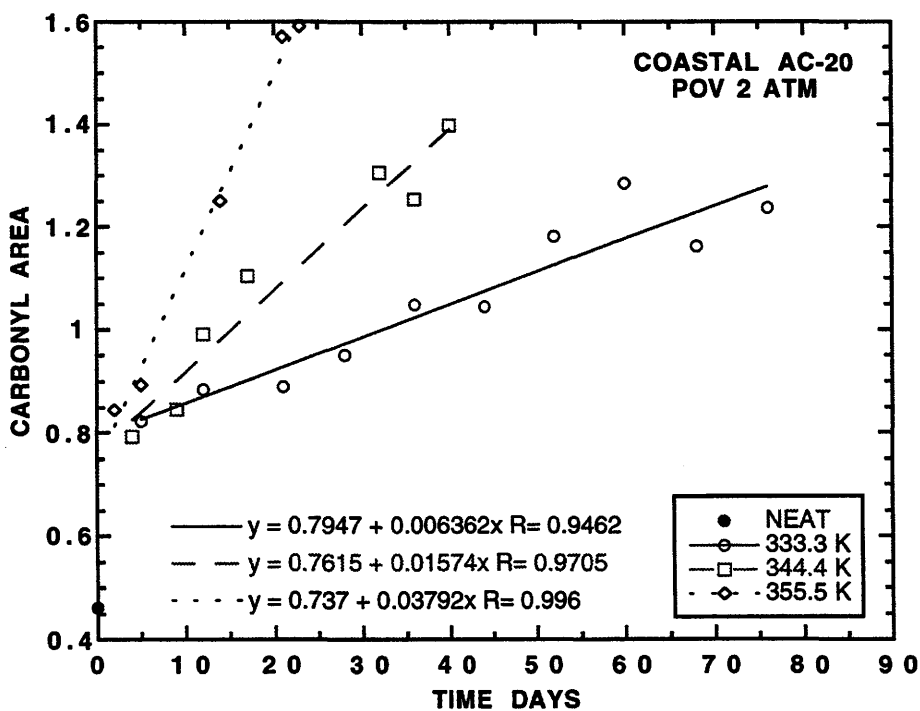


Figure B-17. CAS of Tank and POV-Aged Coastal AC-20 at 2 atm

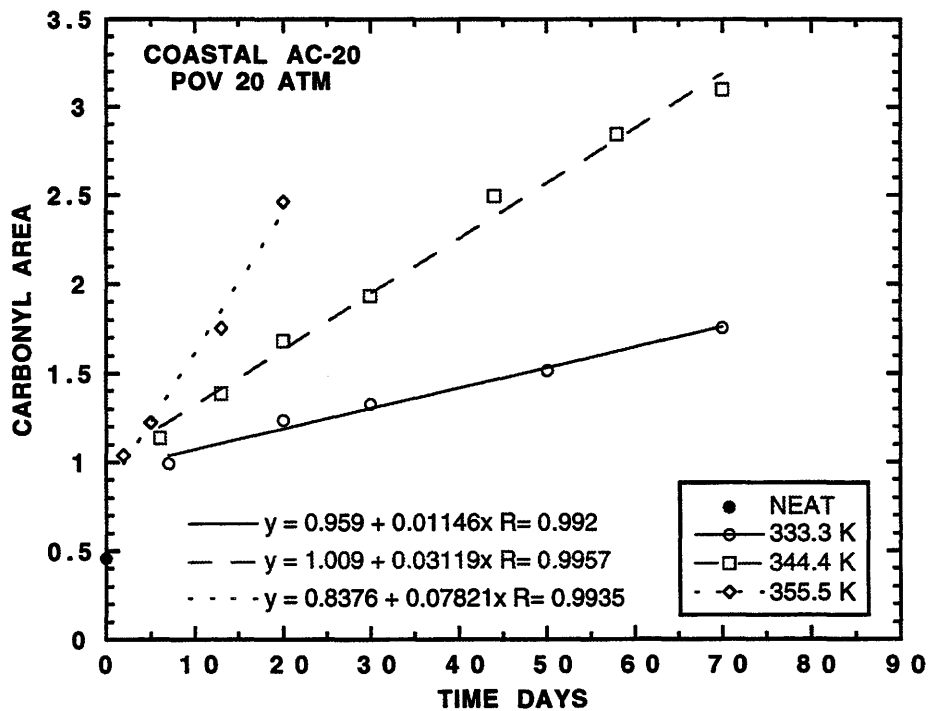


Figure B-18. CAs of Tank and POV-Aged Coastal AC-20 at 20 atm

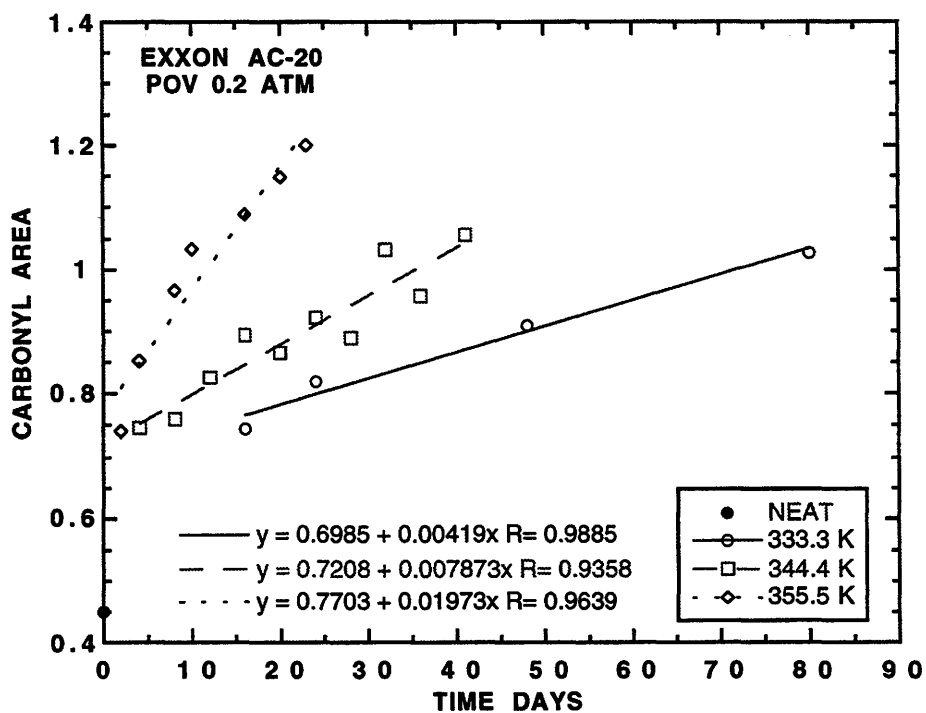


Figure B-19. CAs of Tank and POV-Aged Exxon AC-20 at 0.2 atm

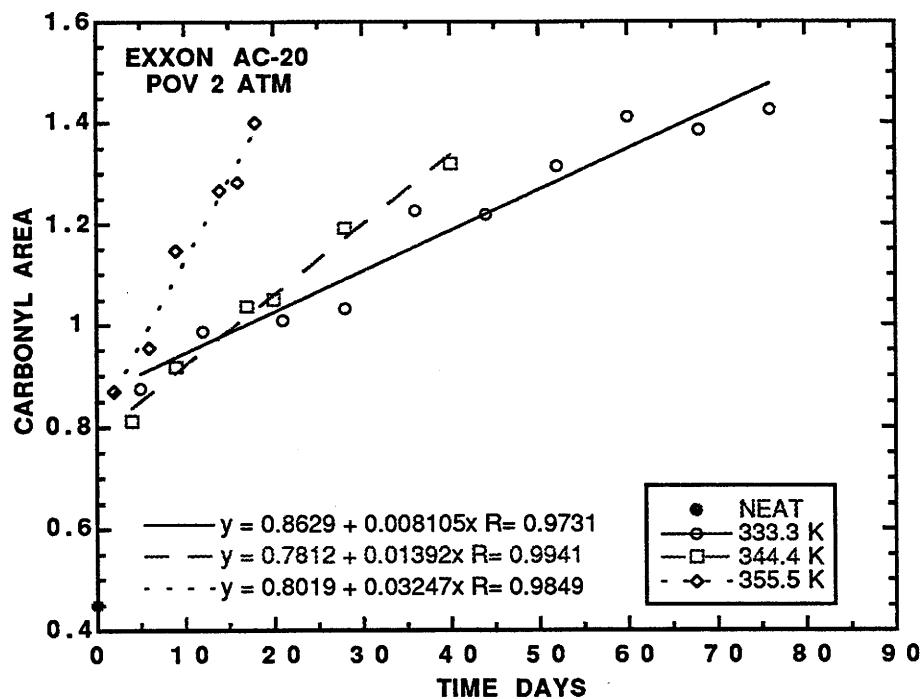


Figure B-20. CAS of Tank and POV-Aged Exxon AC-20 at 2 atm

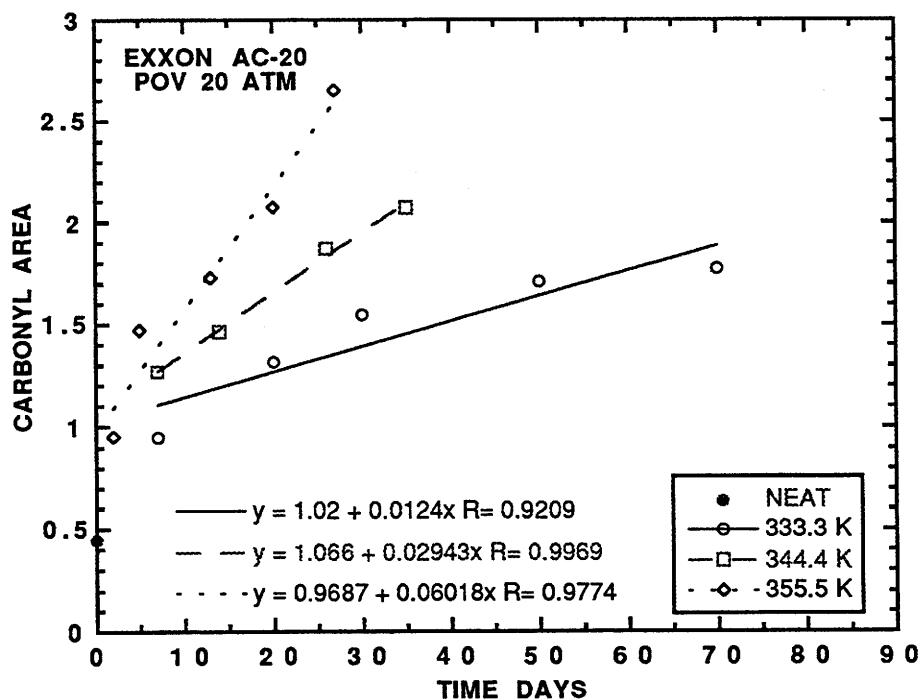


Figure B-21. CAS of Tank and POV-Aged Exxon AC-20 at 20 atm

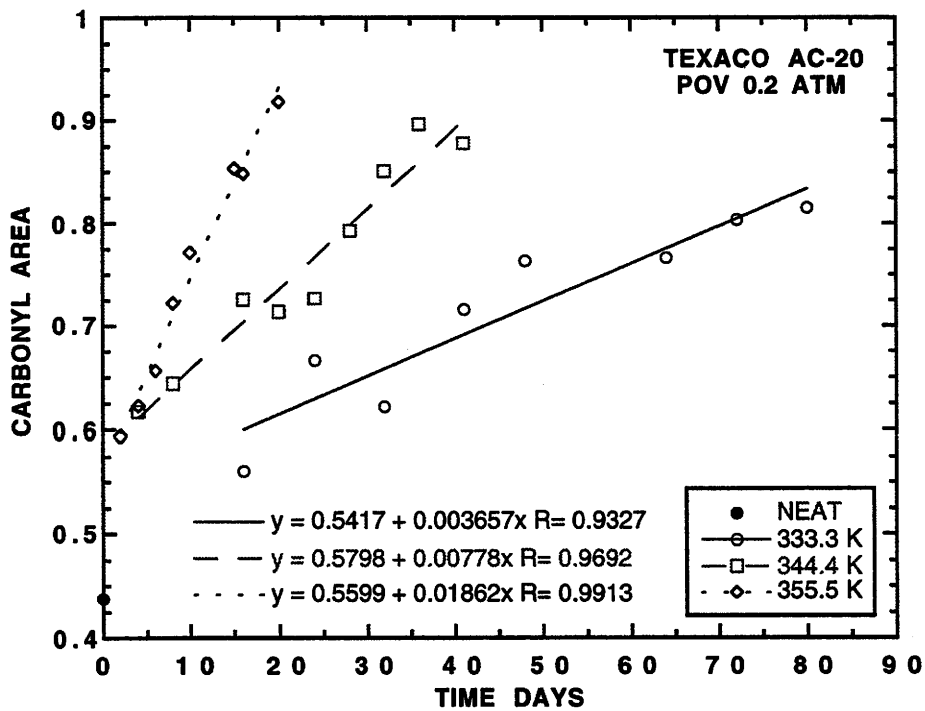


Figure B-22. CAs of Tank and POV-Aged Texaco AC-20 at 0.2 atm

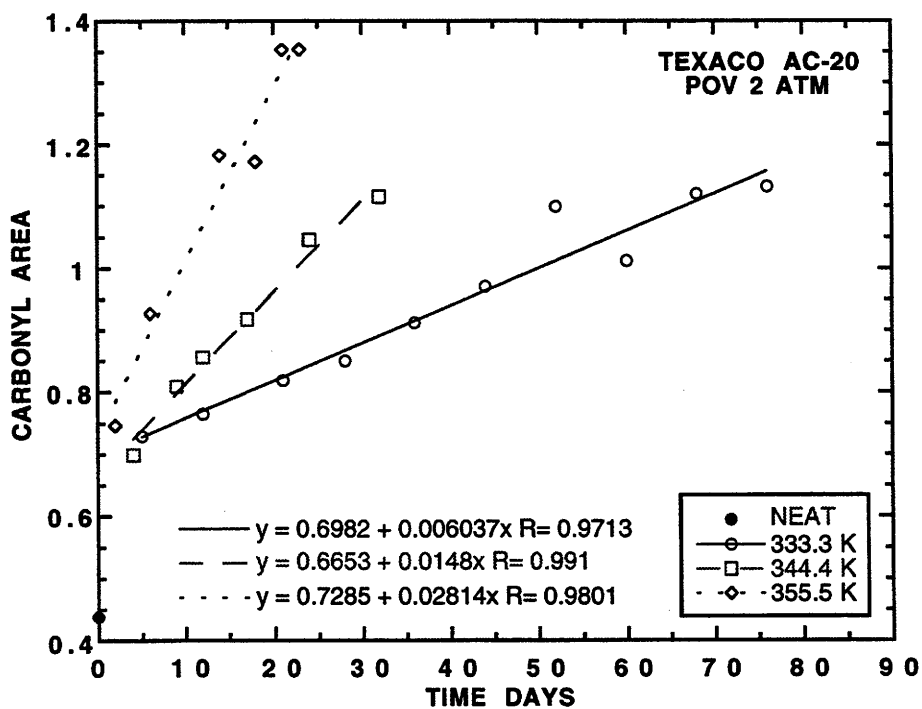


Figure B-23. CAs of Tank and POV-Aged Texaco AC-20 at 2 atm

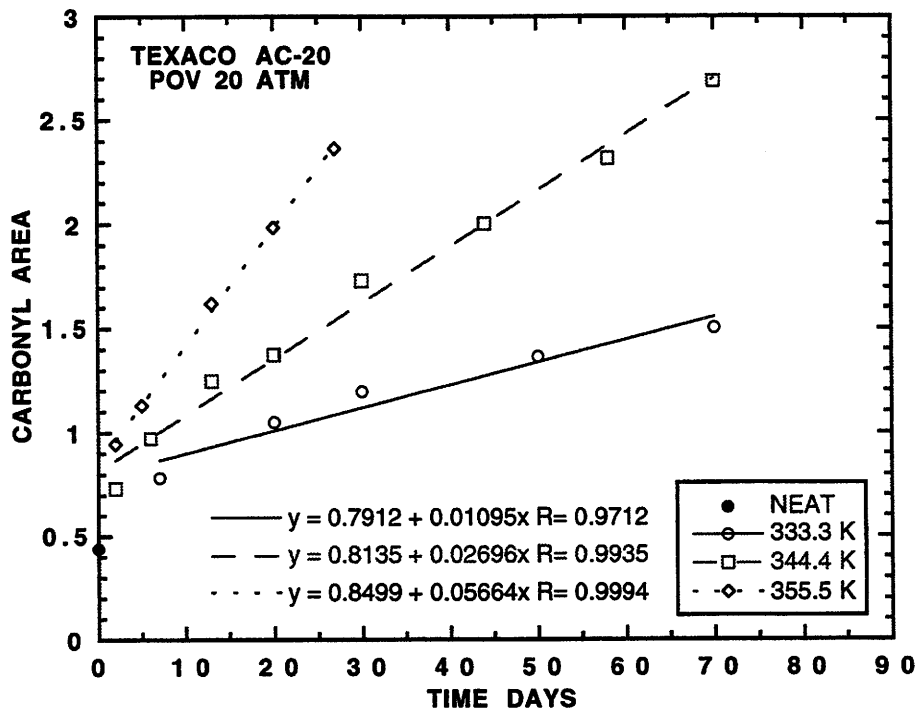


Figure B-24. *CAs* of Tank and POV-Aged Texaco AC-20 at 20 atm

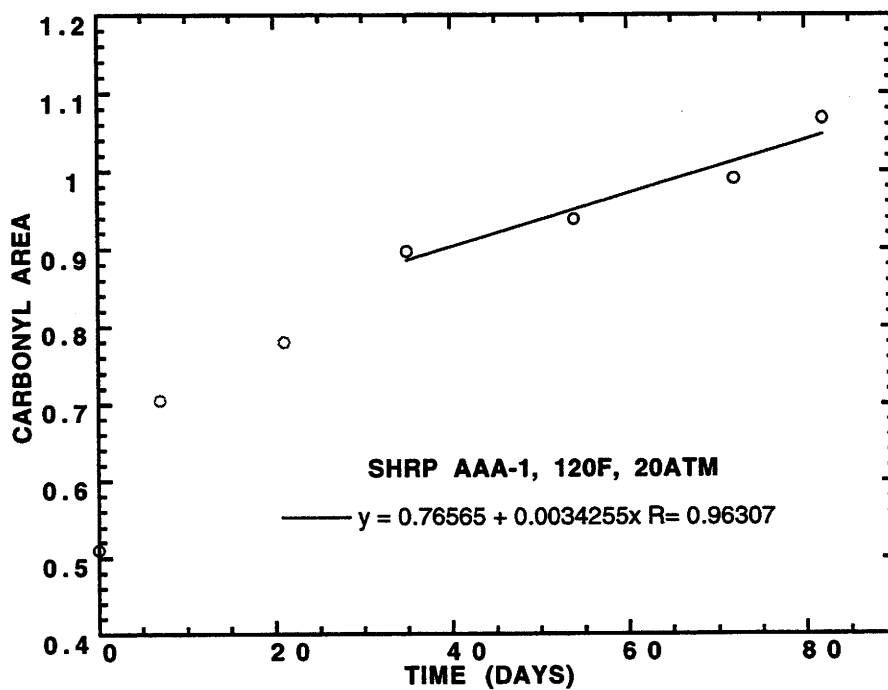


Figure B-25. *CAs* of Tank and POV-Aged SHRP AAA-1

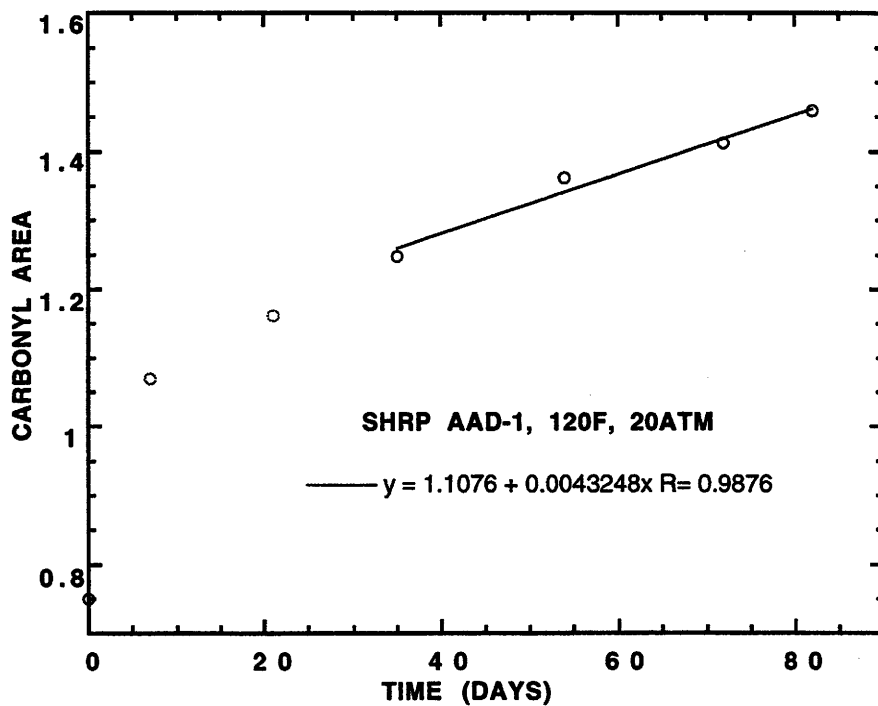


Figure B-26. CAs of Tank and POV-Aged SHRP AAD-1

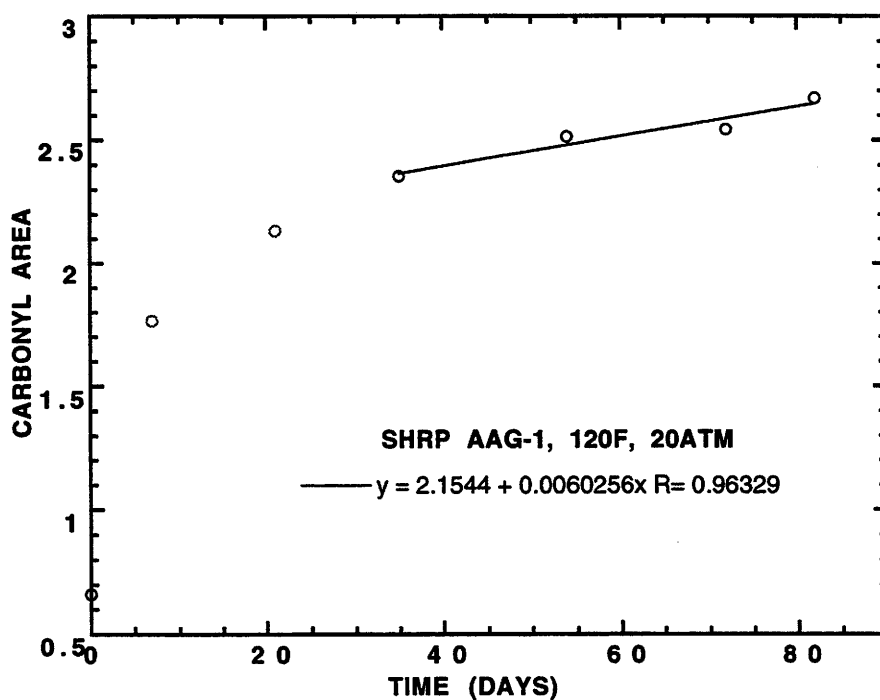


Figure B-27. CAs of Tank and POV-Aged SHRP AAG-1

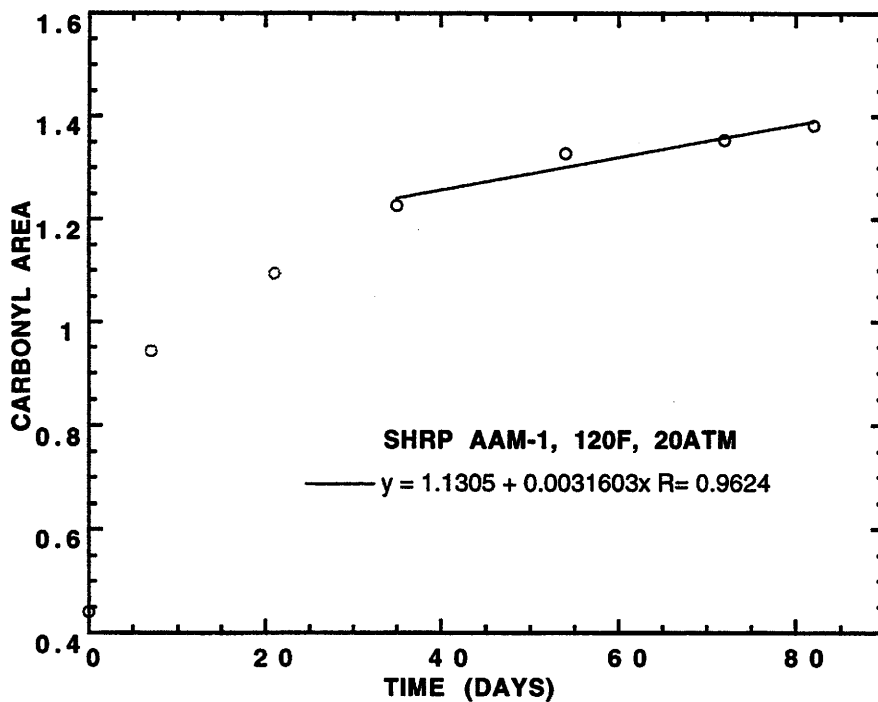


Figure B-28. *CAs* of Tank and POV-Aged SHRP AAM-1

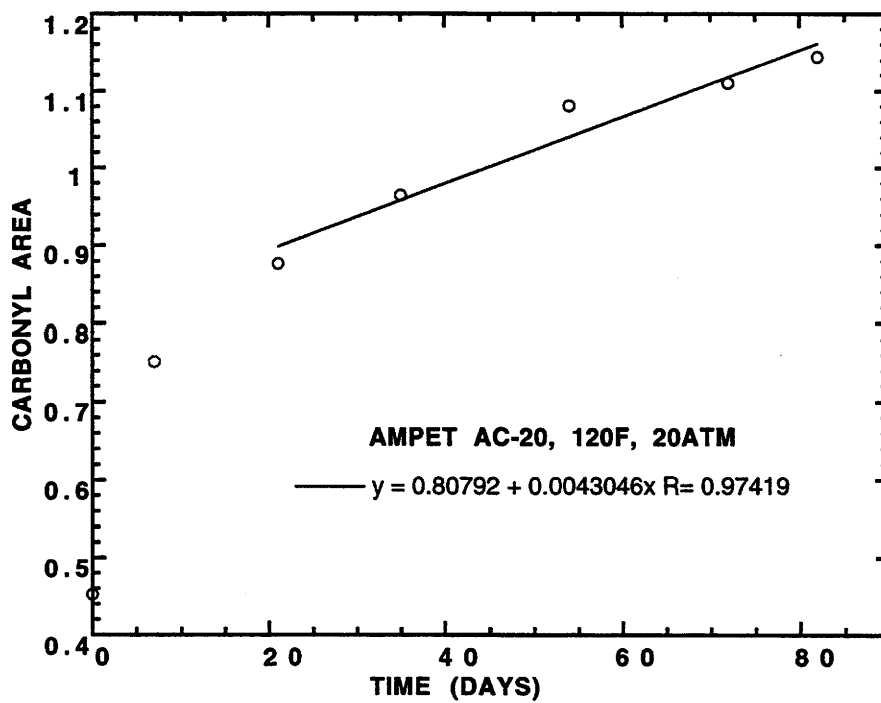


Figure B-29. *CAs* of Tank and POV-Aged Ampet AC-20

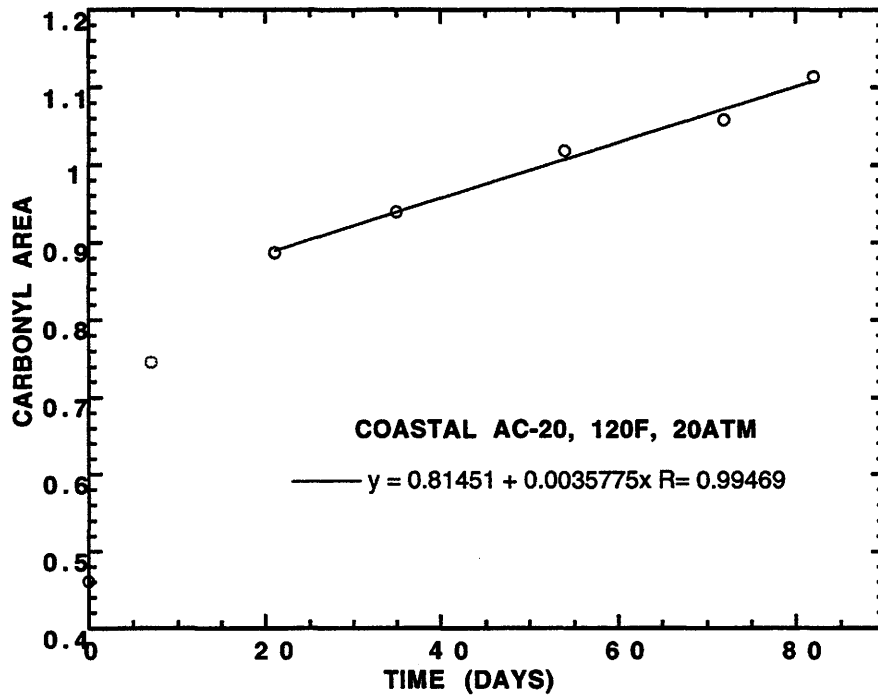


Figure B-30. CAS of Tank and POV-Aged Coastal AC-20

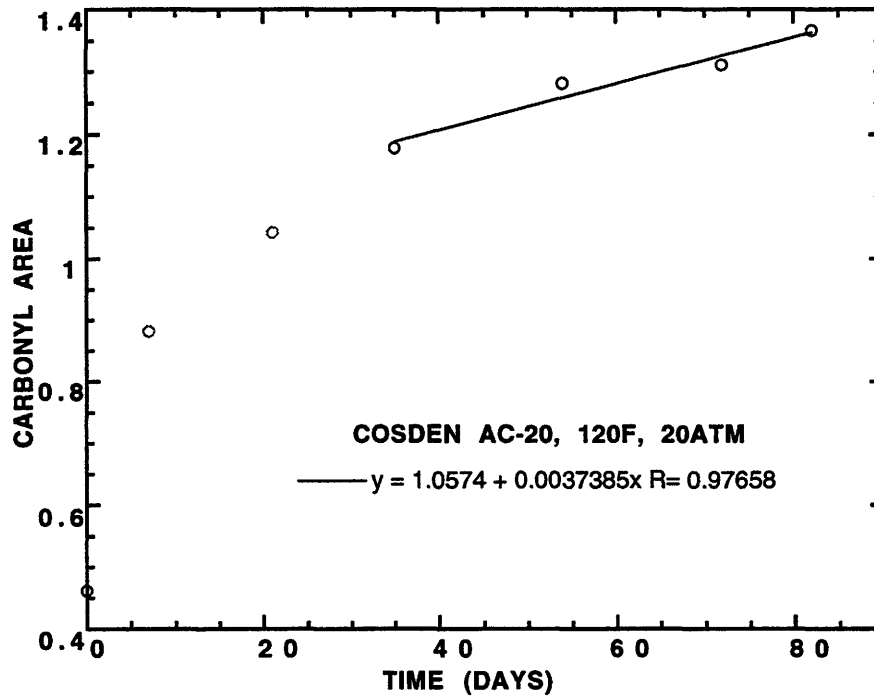


Figure B-31. CAS of Tank and POV-Aged Cosden AC-20

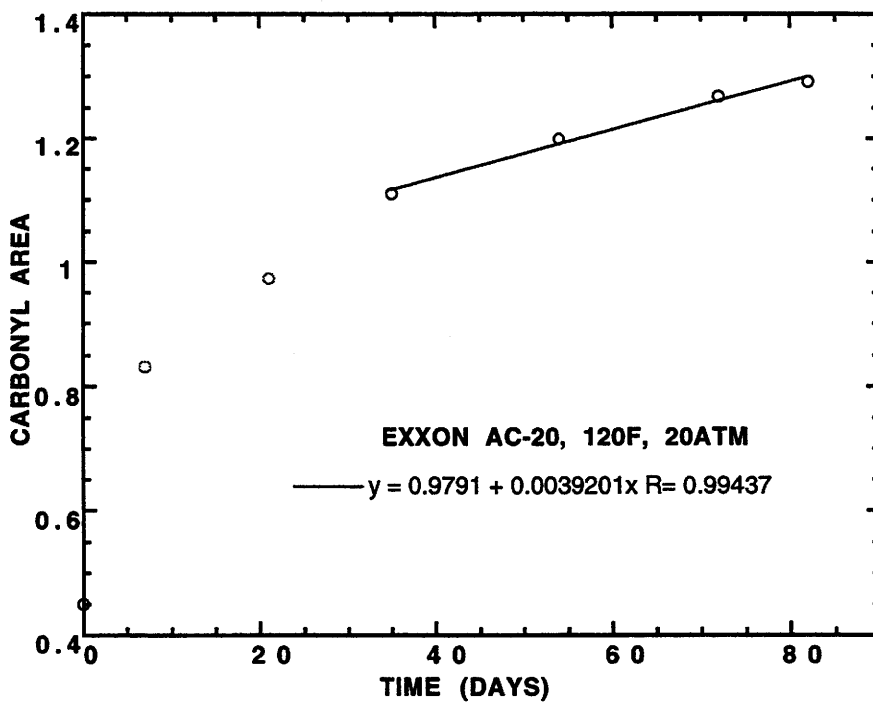


Figure B-32. CAs of Tank and POV-Aged Exxon AC-20

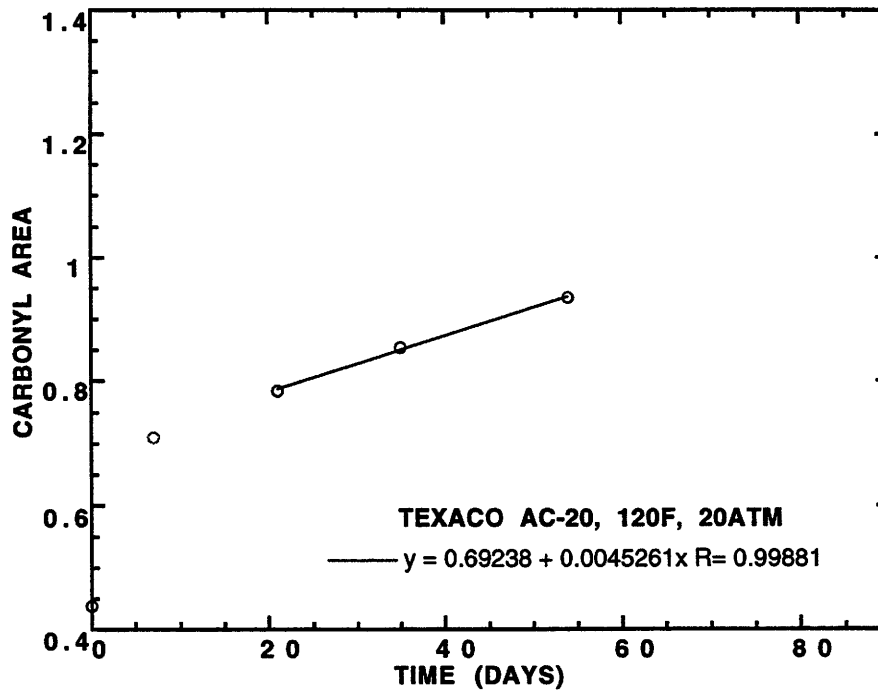


Figure B-33. CAs of Tank and POV-Aged Texaco AC-20

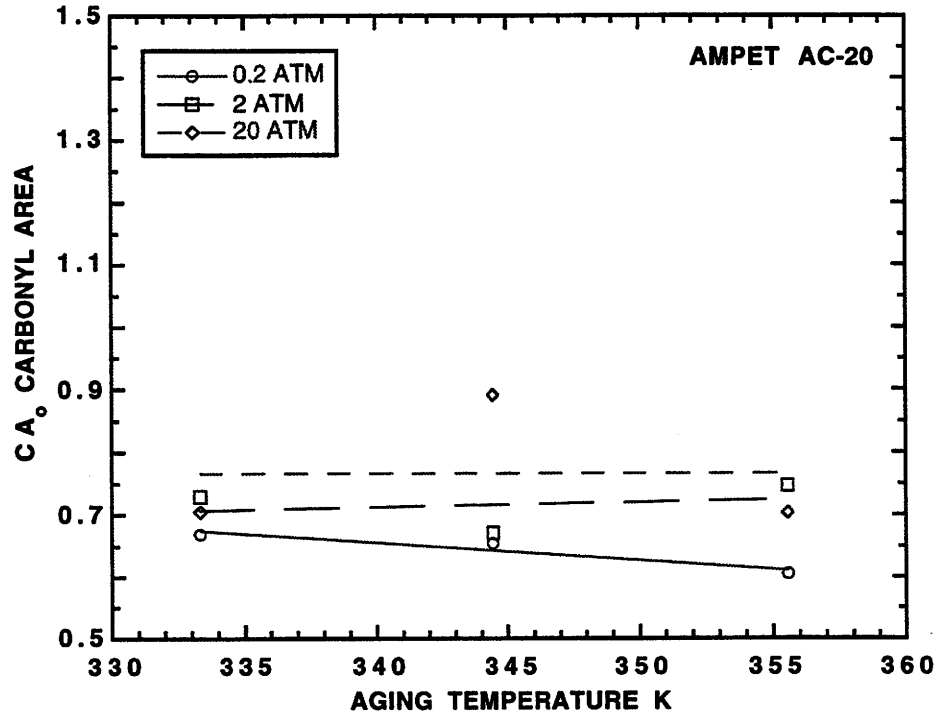


Figure B-34. Initial Jump Versus Aging Temperature for Ampet AC-20

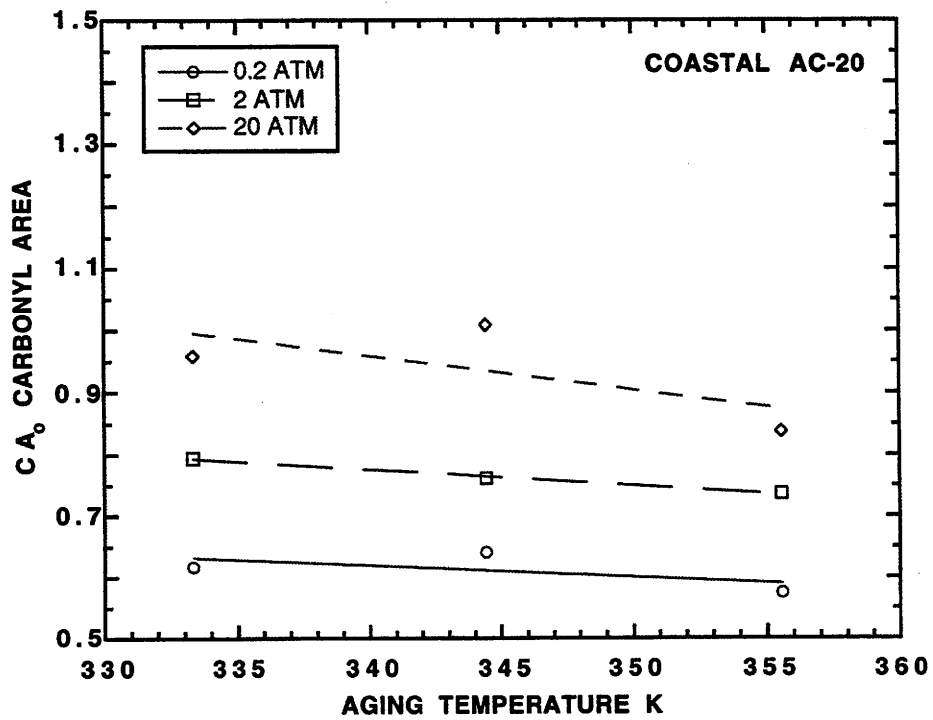


Figure B-35. Initial Jump Versus Aging Temperature for Coastal AC-20

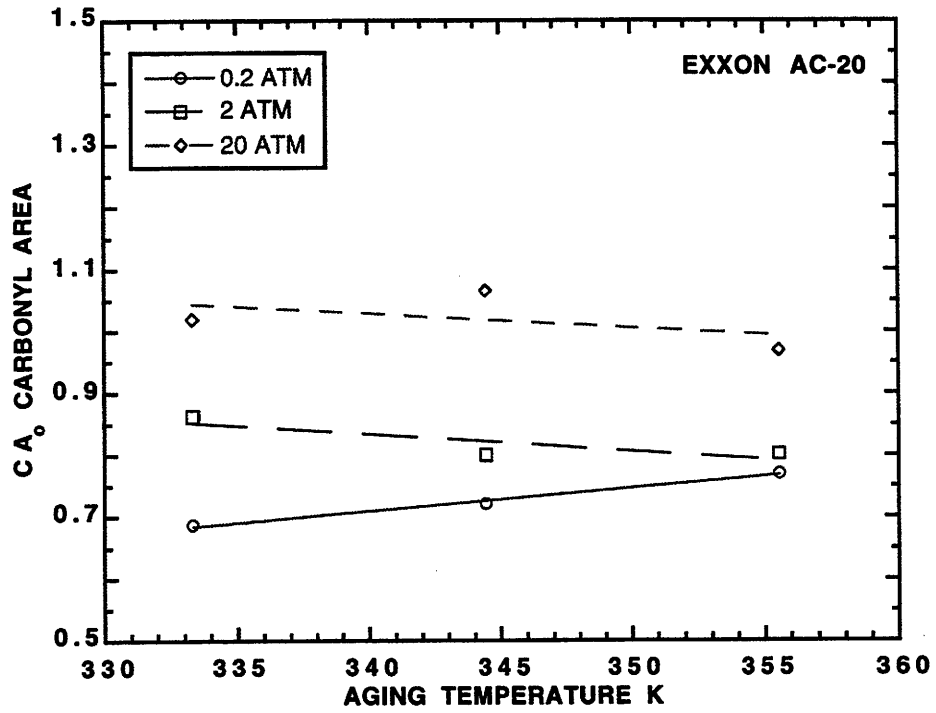


Figure B-36. Initial Jump Versus Aging Temperature for Exxon AC-20

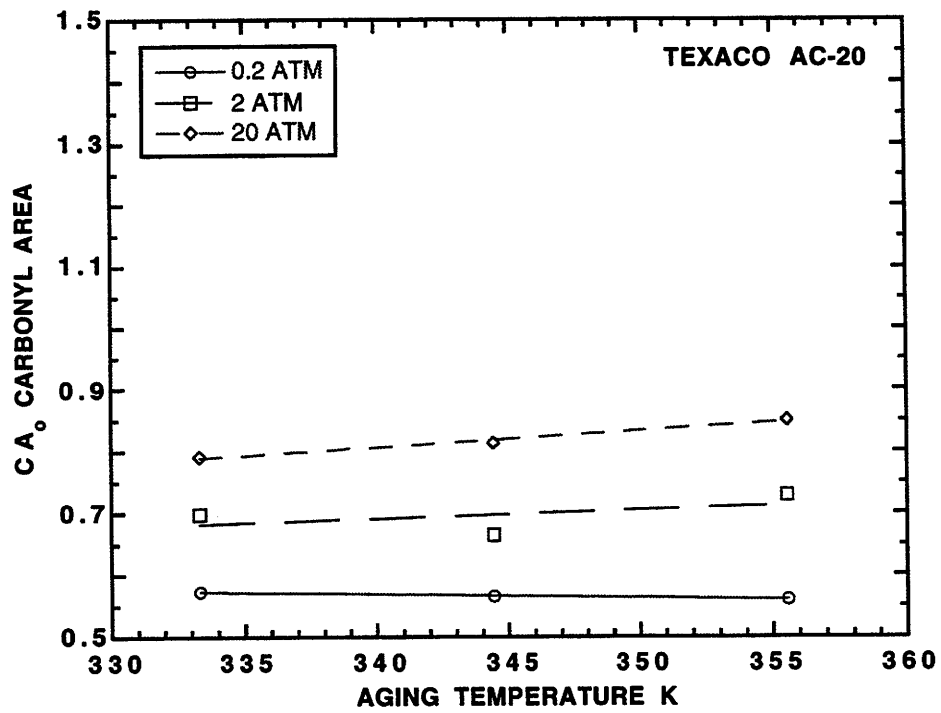


Figure B-37. Initial Jump Versus Aging Temperature for Texaco AC-20

APPENDIX C

HIGHWAY AGING MODEL AND DATA

OVERVIEW

Ultimately, when dealing with binders in asphalt pavements over an extended period of time, we would like to know how the physical properties of these binders change over time or, to put it more practically, we would like to know how long the binders will be serviceable. Using viscosity, as one example, it is a function of the temperature of the material and of the extent of aging of the sample. In the context of earlier chapters, the viscosity is a function of temperature (T) and infrared carbonyl area (CA)

$$\eta_o^* = \eta_o^*(T, CA) \quad (C-1)$$

where the temperature varies during the year (and during the day, for that matter) in the film and, as a consequence, depends upon time (t) and position (x)

$$T = T(t, x) \quad (C-2)$$

Also, of course, because the material ages, the carbonyl area is a function of time (t) and position (x) in the film:

$$CA = CA(t, x) \quad (C-3)$$

If we knew T and CA throughout the film as a function of time, then the problem would be finished. But of course, we don't. The carbonyl area at a point in the film increases due to the reaction of oxygen with the asphalt material:

$$\left(\frac{\partial CA}{\partial t}\right) = r_{CA} \quad (C-4)$$

where r_{CA} is the rate of formation of carbonyl at a point in the film. The reaction rate, as was discussed in earlier chapters, depends upon the temperature (T) but also upon the amount of oxygen in the material and, hence, upon the oxygen pressure (P)

$$r_{CA} = r_{CA}(T, P) \quad (C-5)$$

This relation is embodied in a transport partial differential equation for oxygen which must be solved, and this PDE is the heart of the problem.

Oxygen Transport and Reaction

Bird et al., (1960) provide a mathematical model accounting for oxygen in a differential volume:

$$\left(\frac{\partial C_{O_2}}{\partial t}\right) = -\nabla \cdot \mathbf{N}_{O_2} - r_{O_2} \quad (C-6)$$

\mathbf{N}_{O_2} is the molar flux of oxygen. In an asphalt, there is no bulk flow of oxygen, and the molar flux is expressed by Fick's law of diffusion as given in Equation C-7.

$$\mathbf{N}_{O_2} = -\mathcal{D}_{O_2} \nabla C_{O_2} \quad (C-7)$$

Substituting back into Equation C-6 gives Equation C-8.

$$\left(\frac{\partial C_{O_2}}{\partial t}\right) = -\nabla \cdot (-\mathcal{D}_{O_2} \nabla C_{O_2}) - r_{O_2} \quad (C-8)$$

Equation C-8 is expanded for variable \mathcal{D}_{O_2} :

$$\left(\frac{\partial C_{O_2}}{\partial t}\right) = \nabla \mathcal{D}_{O_2} \cdot \nabla C_{O_2} + \mathcal{D}_{O_2} \nabla^2 C_{O_2} - r_{O_2} \quad (C-9)$$

Equation C-9 accounts for changes in \mathcal{D}_{O_2} in the film as a result of changes in physical properties due to oxidation. Unfortunately, it is not known how significant these changes are to oxygen transport in asphalt. Obviously, changes in \mathcal{D}_{O_2} as a function of position in the film further affect the oxygen concentration profile.

The thin asphalt film which was depicted in Figure 10-2 extends infinitely wide and deep (into the page). Furthermore, for laboratory aging, the oxygen transport in the asphalt film is assumed to occur in only one direction based on the experimental procedures described in Chapter 1 and Appendix A. Hence, the three-dimensional model of Equation C-9 reduces to a one-dimensional model as given in Equation C-10.

$$\left(\frac{\partial C_{O_2}}{\partial t}\right) = \left(\frac{\partial \mathcal{D}_{O_2}}{\partial x}\right) \left(\frac{\partial C_{O_2}}{\partial x}\right) + \mathcal{D}_{O_2} \left(\frac{\partial^2 C_{O_2}}{\partial x^2}\right) - r_{O_2} \quad (C-10)$$

x is the spatial variable.

Using Equation C – 20 along with experimental data from laboratory aging, an estimation of \mathcal{D}_{O_2} in an asphalt film is possible. For constant \mathcal{D}_{O_2} , this is a one parameter estimation. For variable \mathcal{D}_{O_2} , the estimation is more complex depending on the relationship between \mathcal{D}_{O_2} and the asphalt properties in the film.

The problem is complex, however, in that the various terms in the PDE all must be expressed in terms of measurable quantities. First, the oxygen concentration in the film (C_{O_2}) must be expressed in terms of oxygen pressure (P). Second, the oxygen reaction rate in the film must be related to the measured CA . Finally, the diffusivity itself must be related to temperature (T) and degree of aging (CA). Actually, this will be done through the dependence of viscosity (η_o^*) on T and CA .

These relations are discussed more fully in the next section but the bottom-line system of PDEs to be solved is:

$$\left(\frac{\partial P}{\partial t}\right) = \left(\frac{\partial \mathcal{D}_{O_2}}{\partial x}\right) \left(\frac{\partial P}{\partial x}\right) + \mathcal{D}_{O_2} \left(\frac{\partial^2 P}{\partial x^2}\right) - \left(\frac{cRT}{h}\right) r_{CA} \quad (C-11)$$

$$\left(\frac{\partial CA}{\partial t}\right) = r_{CA} \quad (C-4)$$

For this final form, the boundary conditions and initial conditions are specified.

$\left(\frac{\partial P}{\partial x}\right) = 0$	at	$x = 0$	Substrate interface
$P = P_{gas}$	at	$x = L$	Exposed surface
$P = 0$	at	$t = 0$	Initial condition
$CA(t, 0) = CA_{ES}(t)$	at	$x = L$	Exposed Surface

\mathcal{D}_{O_2} in Equation 10 – 33 is not known and must be estimated. An infinite number of values of \mathcal{D}_{O_2} satisfy the initial and boundary conditions. A unique determination of \mathcal{D}_{O_2} is not possible based on the initial and boundary conditions given above. An additional specification, either P at the substrate interface, SI , or the pressure gradient at the exposed surface, ES , is required. In this study the additional specification is P_{SI} through the measurement of CA at SI .

QUANTITATIVE DETAILS OF THE MODEL

Oxygen Film Concentration in Terms of Oxygen Pressure

Since the measurable variables in the laboratory experiments are temperature and pressure and the experiments are designed at low oxygen pressure, the ideal gas law converts the concentration of oxygen C_{O_2} to an expression in terms of T and P .

$$C_{O_2} = h \left(\frac{P_{O_2}}{RT} \right) \quad (C - 12)$$

h is the Henry's law constant, relating the oxygen pressure to the concentration of oxygen in the asphalt.

r_{O_2} Versus r_{CA}

In the laboratory experiments, the rate of oxygen consumption, r_{O_2} , is not measured; however, the production rate of CA , r_{CA} , is. To estimate D_{O_2} , the r_{O_2} is required. From the conservation of mass, r_{O_2} is equal to the rate of production of all oxygen-containing compounds as a result of oxidation.

$$r_{O_2} = n_{CA}r_{CA} + n_{SO}r_{SO} + \dots \quad (C - 13)$$

The rate of sulfoxide formation is r_{SO} . n_{CA} and n_{SO} are required stoichiometric coefficients to satisfy conservation of elemental oxygen. The dots symbolize all of the other oxygen reactions in the asphalt. The formation of sulfoxides as measured by FTIR did not increase after an initial growth for long-term (Lau et al., 1992) and highway-pavement (Martin et al., 1990) aging. In other words, r_{SO} for long-term aging is approximately zero. However, CA continued to increase. From this information, long-term r_{O_2} is approximated as being proportional to the r_{CA} .

$$r_{O_2} = cr_{CA} \quad (C - 14)$$

c is an experimentally determined parameter accounting for the differences in the FTIR measurement for CA and the true mass of oxygen. For aged asphalts, CA is compared

Table C-1. CA and Wt% O₂ for Tank and POV-Aged SHRP AAA-1 at 344.4 K and 20 atm

Time days	CA	wt%O ₂ FISON	wt%O ₂ LECO
0	0.492	0.59	0.78
4	0.863	1.34	1.55
12	1.054	1.78	1.98

with oxygen content as determined from elemental analysis to determine c in Equation C - 14. Measurements were made on one asphalt and are given in Table C-1.

D_{O_2} as a Function of T and CA

To account for changes in D_{O_2} as a result of CA due to reaction and η_o^* increase by HS , a mathematical relationship between D_{O_2} and the amount of aging must be developed. Only with such a function can Equation C - 11 be numerically integrated. Reid et al., (1983) provide models relating diffusivity to viscosity and temperature as given in Equation C - 15.

$$D_{O_2} = f(\eta_o^*, T) \quad (C - 15)$$

In the literature, for isothermal conditions, the diffusivity of oxygen in liquids is dependent on the viscosity of the liquid by Equation C - 16.

$$D_{O_2} = D_o(\eta_o^*)^B \quad (C - 16)$$

B ranges from -1 to -0.5 for organic liquids (Reid et al., 1983). The values for B in the literature are based on diffusion measurements of carbon dioxide in various organic solvents and n -hexane in hydrocarbons. The viscosity of the solvents ranged from 0.5 to 5000 cP in the later case. Although the viscosity of asphalt is much higher, in the neighborhood of 2000 P at 333.3 K (140 °F) for tank material, this model provides a reasonable starting point. For the asphalts studied, D_o and B are the estimated parameters. These were reported in Chapter 10 and Figure 10-11.

The temperature dependence of the diffusivity is expressed by two different models (Reid et al., 1983). The first model relates the diffusivity and temperature:

$$D \propto T \quad (C - 17)$$

while the second model relates the log of diffusivity to reciprocal temperature.

$$\ln D \propto \frac{1}{T} \quad (C - 18)$$

Since η_o^* of asphalt is such a strong function of temperature, Equation C - 16 may be sufficient to describe D_{O_2} as a function of asphalt material properties, and this appeared to be true, as was discussed in Chapter 10.

Relationships Between η_o^* and CA for Multiple Temperatures

Lau et al., (1992) showed that for long-term oxidative aging η_o^* and CA are related by Equation 10 - 3.

$$\eta_o^* = \exp\{HS \cdot CA + m\} \quad (10 - 3)$$

However, only estimated parameters for η_o^* at one temperature, 333.3 K (140 °F) were provided. The parameter m does not necessarily correspond to the tank η_o^* . Furthermore, the authors suggest that the HS is independent of temperature.

A model is developed, relating the parameters HS and m to measurement temperature. At the reference temperature, T_o , and any other temperature, T , η_o^* as a function of CA is given in Equation C - 19.

$$\begin{aligned} \ln(\eta_o^*(T_o)) &= HS(T_o) \cdot CA + m(T_o) \\ \ln(\eta_o^*(T)) &= HS(T) \cdot CA + m(T) \end{aligned} \quad (C - 19)$$

Jemison (1992) measured η_o^* from 273.15 to 333.3 K (32 to 140 °F). He used the Andrade equation (Andrade, 1930) to model η_o^* as a function of temperature as given in Equation C - 20.

$$\ln\left(\frac{\eta_o^*(T)}{\eta_o^*(T_o)}\right) = E_V \left(\frac{1}{T} - \frac{1}{T_o}\right) \quad (C - 20)$$

E_V is the viscosity activation energy divided by the universal gas constant, and is also called the Andrade parameter. By comparing Equations C - 19 and C - 20:

$$E_V \left(\frac{1}{T} - \frac{1}{T_o} \right) = \left(HS(T) - HS(T_o) \right) CA + \left(m(T) - m(T_o) \right) \quad (C - 21)$$

Hence, E_V must be a linear function of CA :

$$E_V = \gamma CA + \delta \quad (C - 22)$$

From Equation C - 22, with known model parameters, γ , δ , $HS(T_o)$, and $m(T_o)$, HS and m at other temperatures can be determined:

$$\begin{aligned} HS(T) &= HS(T_o) + \gamma \left(\frac{1}{T} - \frac{1}{T_o} \right) \\ m(T) &= m(T_o) + \delta \left(\frac{1}{T} - \frac{1}{T_o} \right) \end{aligned} \quad (C - 23)$$

For linear viscoelastic behavior, values of η_o^* are not required at other temperatures in order to estimate the model parameters γ and δ . Ferry (1985) describes time-temperature superposition where the horizontal shift factor, a_T , relates the response time and frequency to temperature by Equation C - 24.

$$a_T = \frac{t_T}{t_{T_o}} = \frac{\omega_{T_o}}{\omega_T} \quad (C - 24)$$

T and T_o represent any temperature and the reference temperature, respectively.

The complex viscosity, η^* , at the reference temperature is defined by Equation C - 25 in terms of the storage, G' , and loss, G'' , moduli. η_o^* is defined when G' is negligible compared with G'' .

$$\eta_{T_o}^* = \frac{1}{\omega_{T_o}} \sqrt{(G')^2 + (G'')^2} \quad (C - 25)$$

For any temperature, T , η^* is given by C - 26.

$$\eta_T^* = \frac{1}{\omega_T} \sqrt{(G')^2 + (G'')^2} \quad (C - 26)$$

Table C-2. E_V Model Parameters for All Asphalts Studied

Asphalt	$K \frac{\gamma}{CA}$	δ K
Ampet AC-20	1920	20400
Coastal AC-20	1520	20600
Cosden AC-20	1000	21400
Exxon AC-20	1280	20400
Texaco AC-20	2560	19000

^a Model: $E_V = \gamma CA + \delta$

Substituting Equation C – 24 into Equation C – 26 yields:

$$\eta_T^* = \frac{a_T}{\omega_{T_o}} \sqrt{(G')^2 + (G'')^2} \quad (C - 27)$$

Since the moduli are the same at the two different temperatures because of the horizontal shift only, the ratio of η^* at T to η^* at T_o is a function of a_T only.

$$\frac{\eta_T^*}{\eta_{T_o}^*} = a_T \quad (C - 28)$$

Comparing Equation C – 20 and C – 28, a_T must have the same temperature dependence as η^* as given in Equation C – 29.

$$\ln a_T = E_V \left(\frac{1}{T} - \frac{1}{T_o} \right) \quad (C - 29)$$

For asphalts at different degrees of aging or CA , the dynamic mechanical properties are measured at different temperatures. Shift factors, a_T , are determined as functions of T , and E_V is calculated at different degrees of aging. The model parameters, γ and δ , are estimated by comparing E_V and CA through Equation C – 22. From these results, η_o^* at any CA and T can be calculated from the reference temperature HS and m and the E_V model parameters, γ and δ . Extending the η_o^*-CA relationships to multiple temperatures is required to formulate an asphalt oxygen diffusion and reaction model. Furthermore, this development is needed to apply the physicochemical property relationships to highway-pavement aging. Measure values for γ and δ are given in Table C-2. Shift factors are given by Lunsford (1994).

Carbonyl Formation Rate

The carbonyl formation rate was discussed extensively in Chapters 1 and 2. A rate expression is given in Equation 1 – 3

$$r_{CA} = AP^\alpha e^{-E/RT} \quad (1-3)$$

This equation contains three adjustable parameters A , E_A , and α describing r_{CA} . The parameters may be determined from experimental data as described in Chapter 1. Furthermore, the experimental data must be such that P is known. The pressure of the gas is measured; however, the oxygen pressure at the surface should be proportional to the pressure in the gas. For lack of accurate oxygen solubility data in this study, the proportionality constant is assumed to be unity. For aging asphalts in thin films, the only place P is known or a function of thermodynamic variables, is at the *ES* in Figure 10-2. Unfortunately, P in the film is not known because of diffusion and reaction.

To calculate CA , the integration constant, CA_o , in Equation 1 – 1 must also be determined. Based on Lau et al., (1992) for aging at 20 atm oxygen pressure, the initial conditions of the tank asphalt did not correspond to the long-term aging characteristics because of an initial non-linearity. Petersen et al., (1993) also reports this initial non-linearity with POV and TFAAT aging. Fortunately, Equation C – 4 suggests that CA_o may be of the following form.

$$CA_o = f(T, P) \quad (C-30)$$

Only through experimental data can the exact nature and functionality and the model parameters in Equation C – 30 be determined.

In Chapter 1, an attempt to relate CA_o and P led to the development of equation 1 – 4.

$$CA_o = sP^\beta \quad (1-4)$$

Surprisingly, this relationship was independent of T . The parameters were found to depend on asphalt as reported in Table C-3. Then, using these parameters together with the kinetic parameters for Equation 1-3, the carbonyl area can be calculated, provided T and P as functions of time are known.

Table C-3. CA_o Model Parameters from Measured and Estimated P for All POV-Aged Asphalts and Conditions Studied^a

Asphalt	s CA / atm^β	β
Ampet AC-20	0.652	0.063
Coastal AC-20	0.704	0.113
Cosden AC-20	0.805	0.104
Exxon AC-20	0.740	0.097
Texaco AC-20	0.612	0.098

^a Model: $CA_o = sP^\beta$

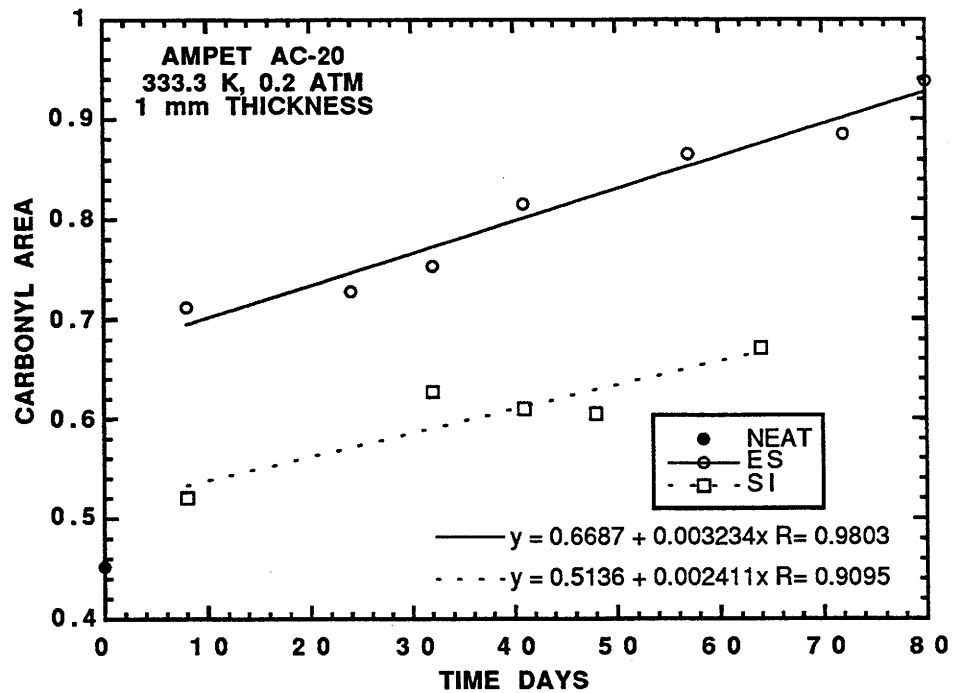


Figure C-1. CA s of Tank, ES and SI (Ampet AC-20, 333.3 K, 0.2 atm)

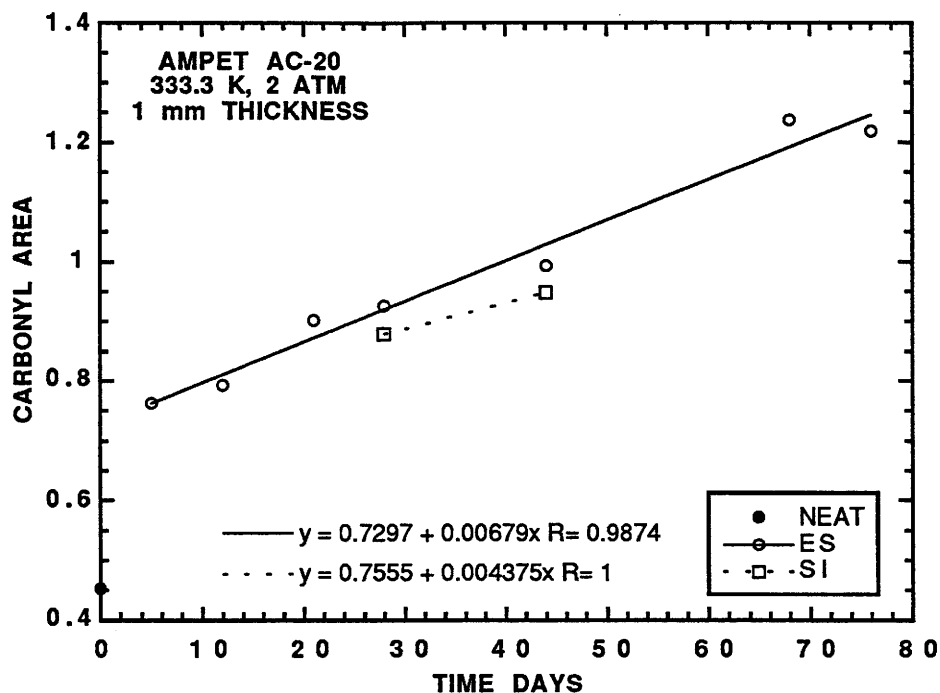


Figure C-2. CAs of Tank, *ES* and *SI* (Ampet AC-20, 333.3 K, 2 atm)

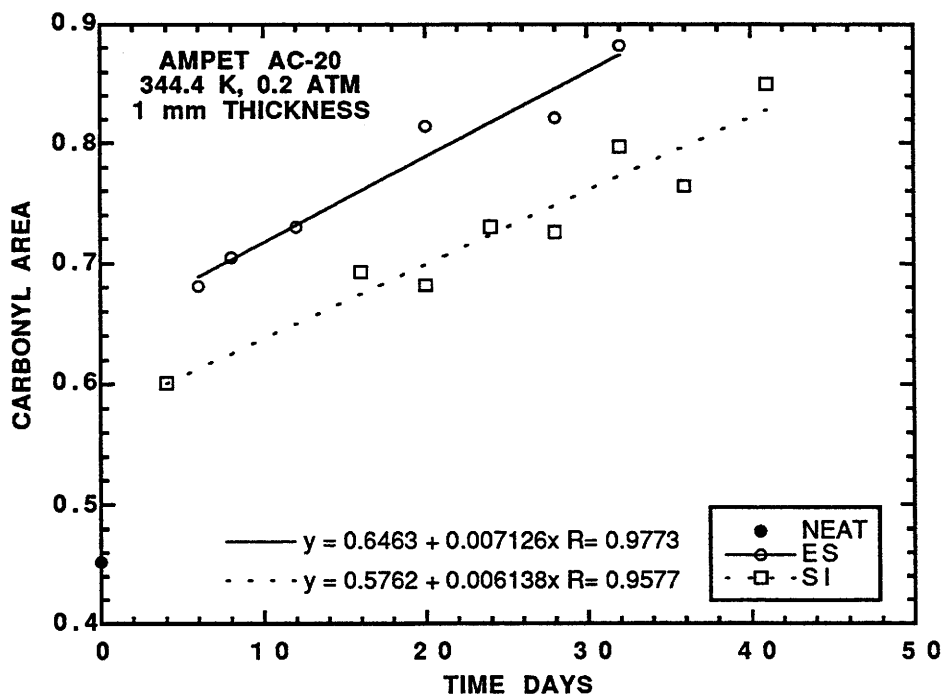


Figure C-3. CAs of Tank, *ES* and *SI* (Ampet AC-20, 344.4 K, 0.2 atm)

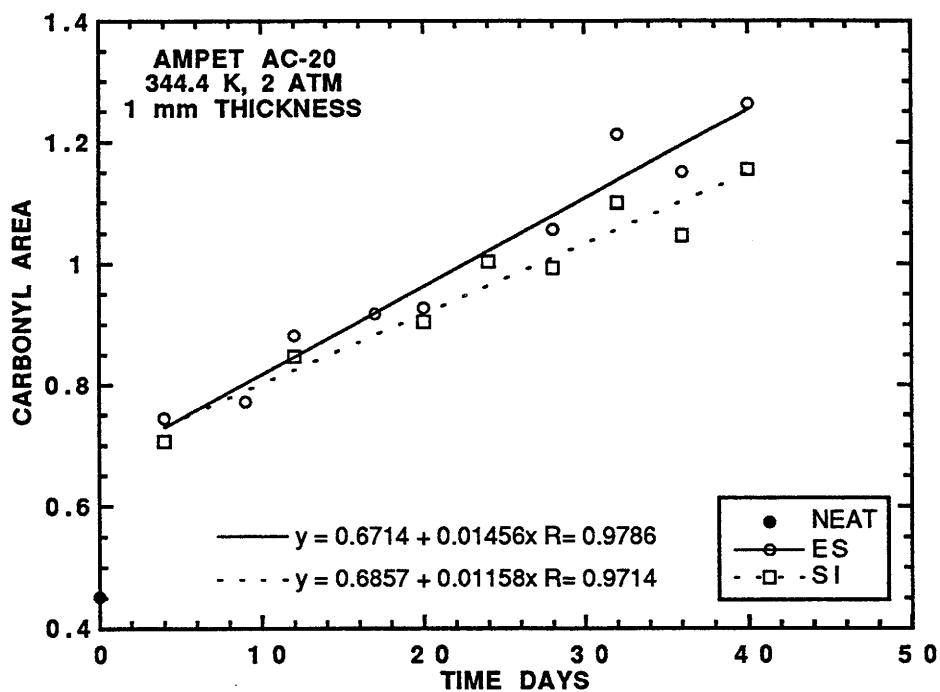


Figure C-4. CAs of Tank, *ES* and *SI* (Ampet AC-20, 344.4 K, 2 atm)

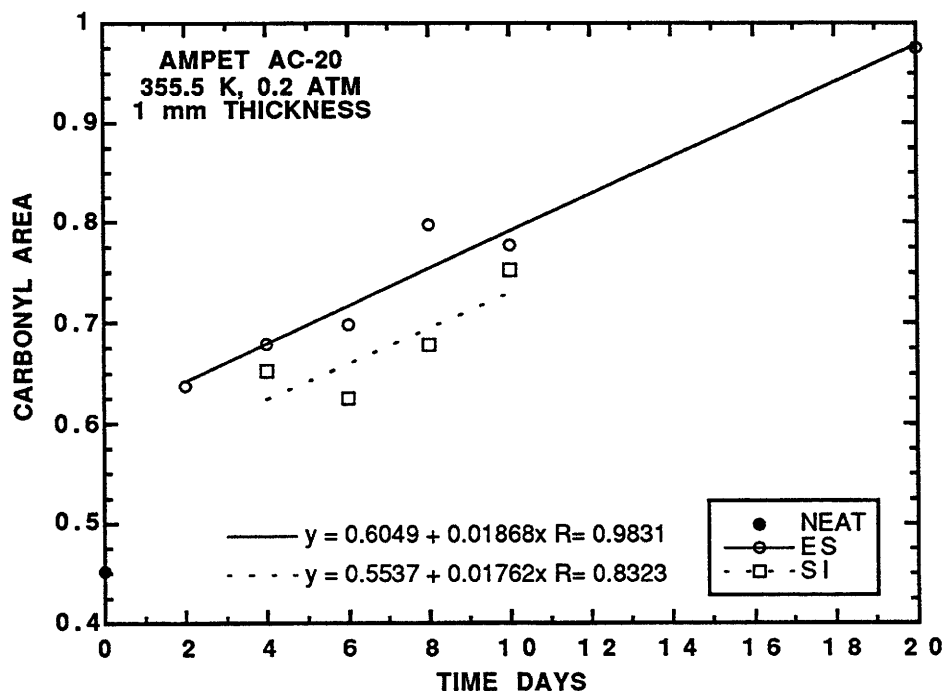


Figure C-5. CAs of Tank, *ES* and *SI* (Ampet AC-20, 355.5 K, 0.2 atm)

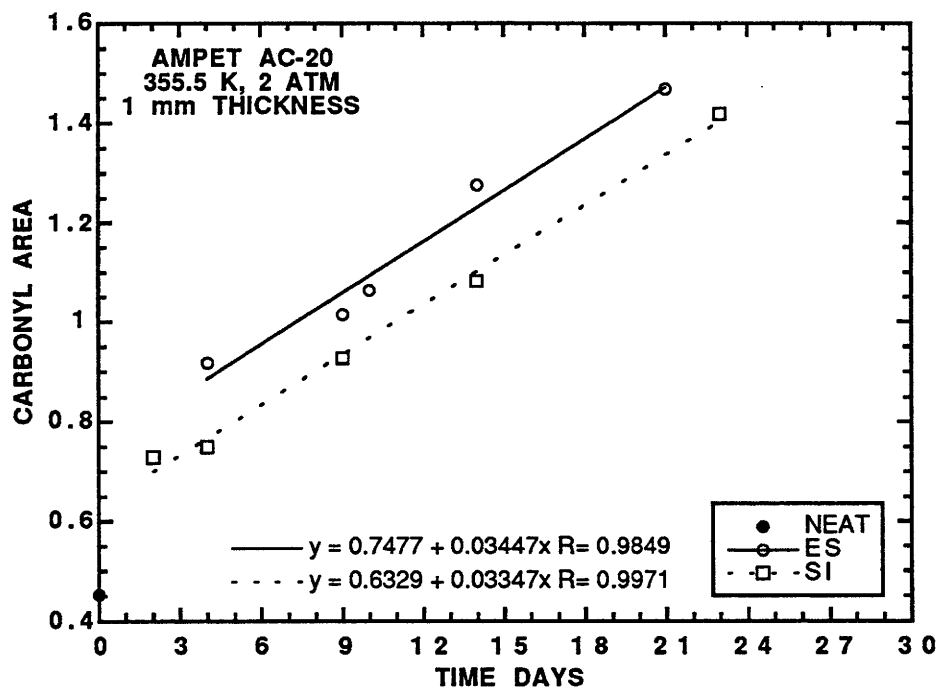


Figure C-6. CAs of Tank, *ES* and *SI* (Ampet AC-20, 355.5 K, 2 atm)

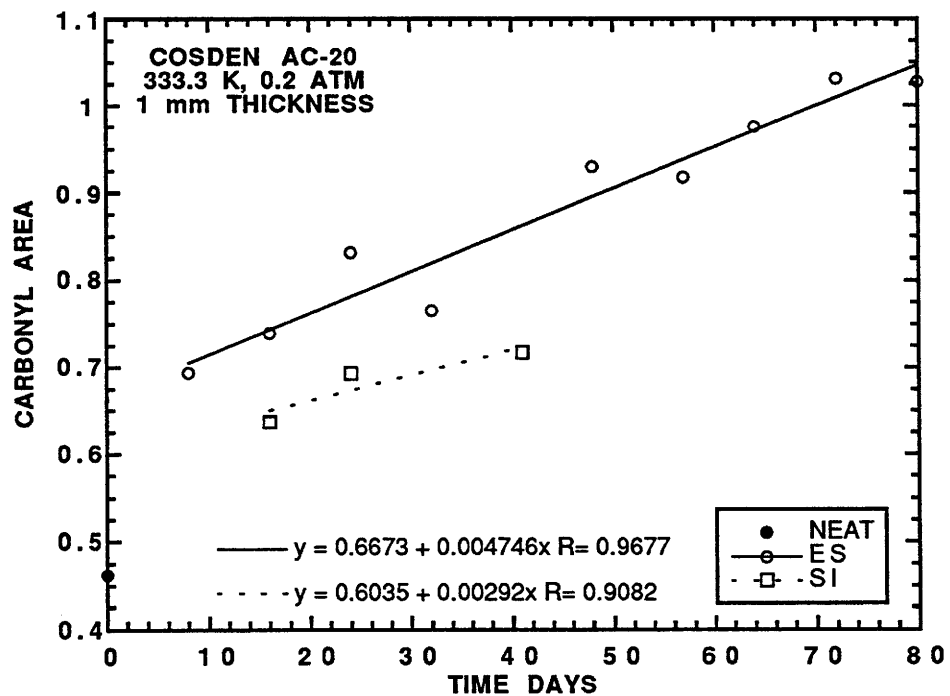


Figure C-7. CAs of Tank, *ES* and *SI* (Cosden AC-20, 333.3 K, 0.2 atm)

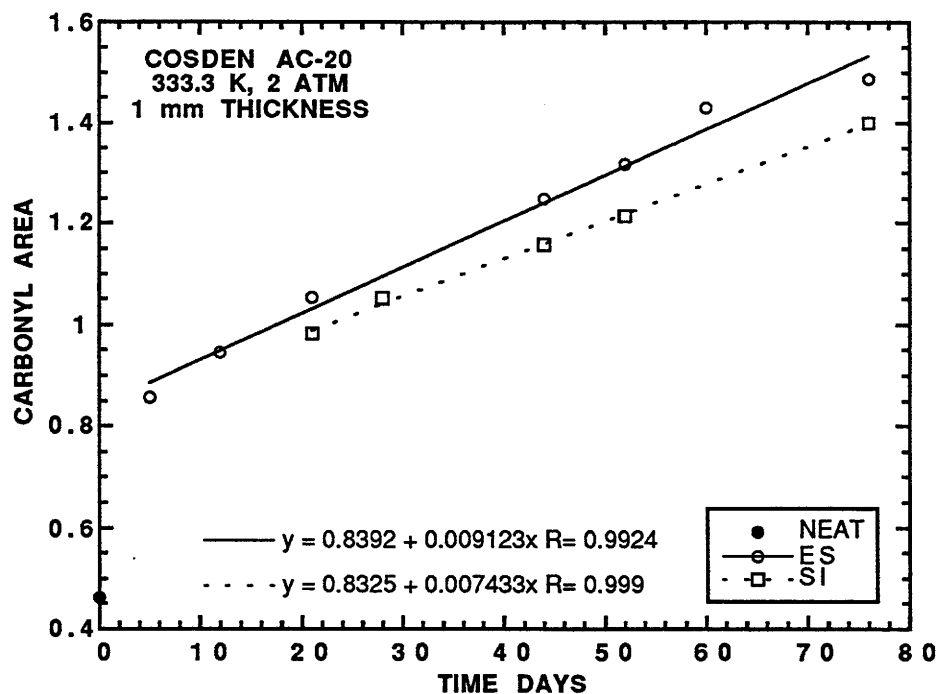


Figure C-8. *CAs* of Tank, *ES* and *SI* (Cosden AC-20, 333.3 K, 2 atm)

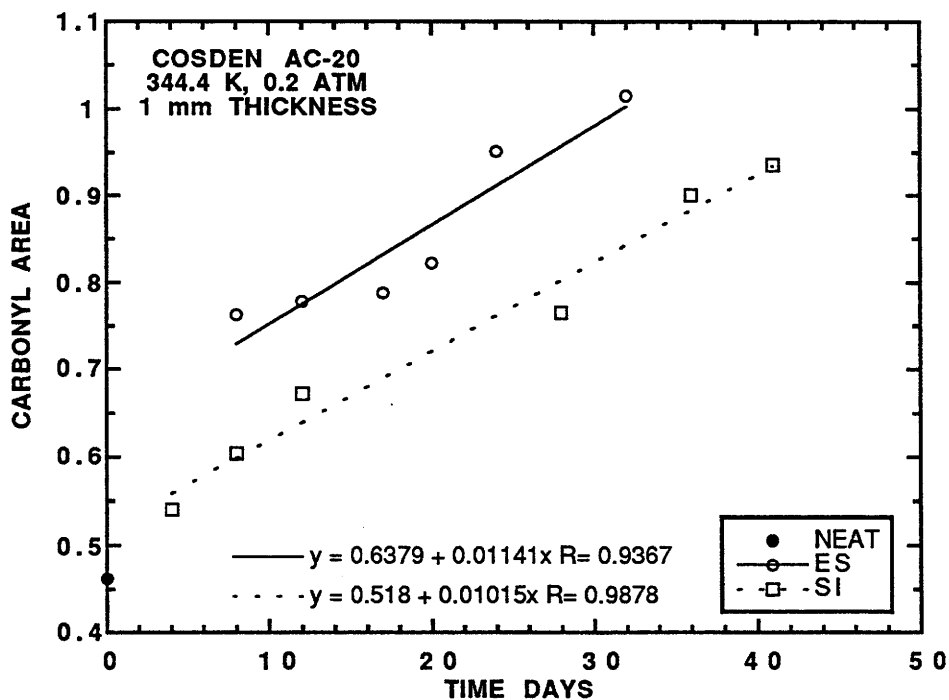


Figure C-9. *CAs* of Tank, *ES* and *SI* (Cosden AC-20, 344.4 K, 0.2 atm)

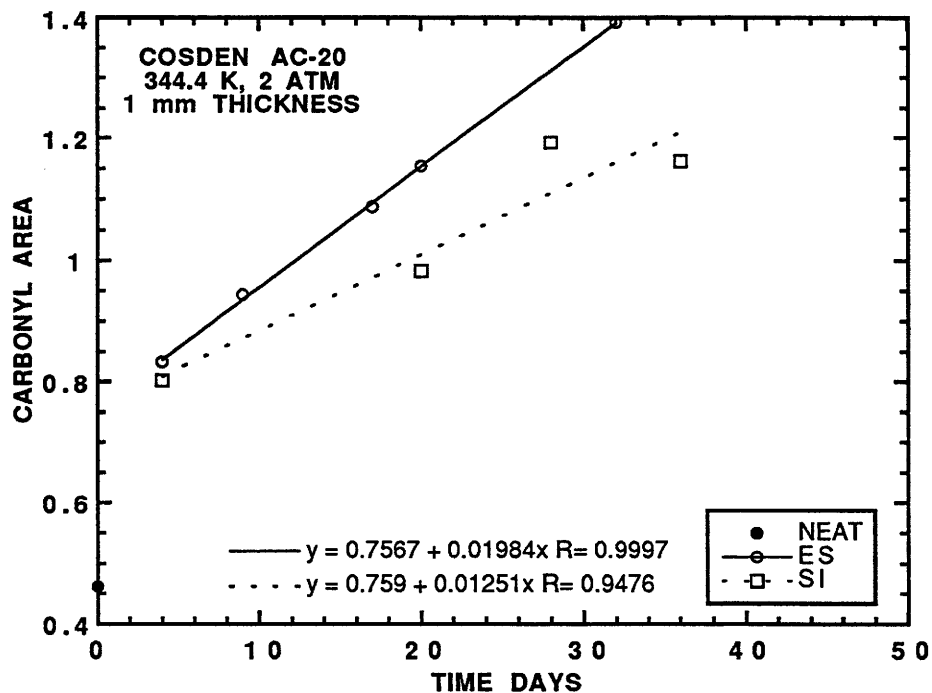


Figure C-10. CAs of Tank, *ES* and *SI* (Cosden AC-20, 344.4 K, 2 atm)

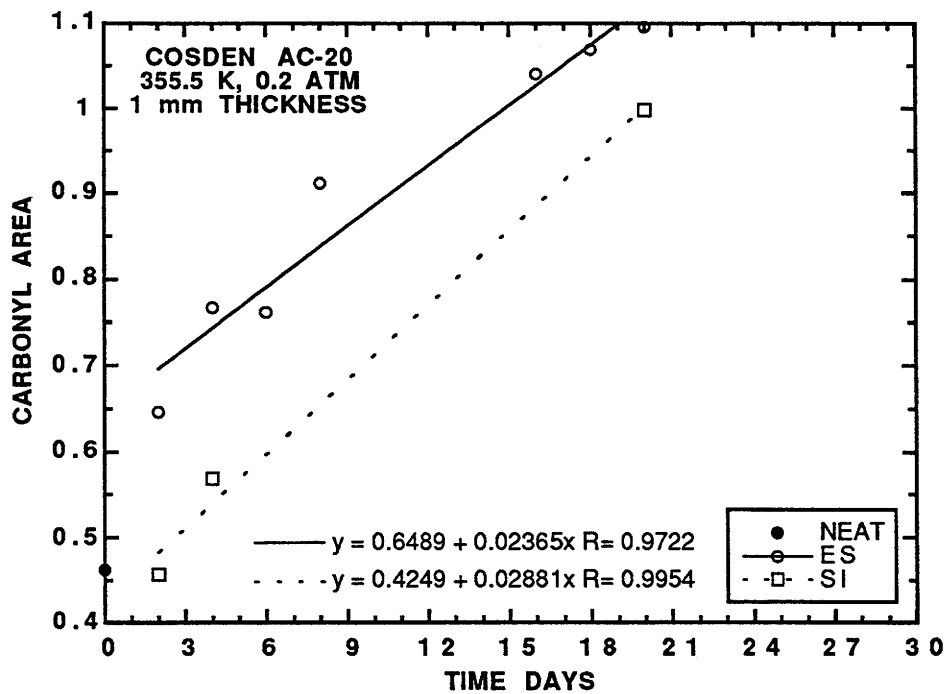


Figure C-11. CAs of Tank, *ES* and *SI* (Cosden AC-20, 355.5 K, 0.2 atm)

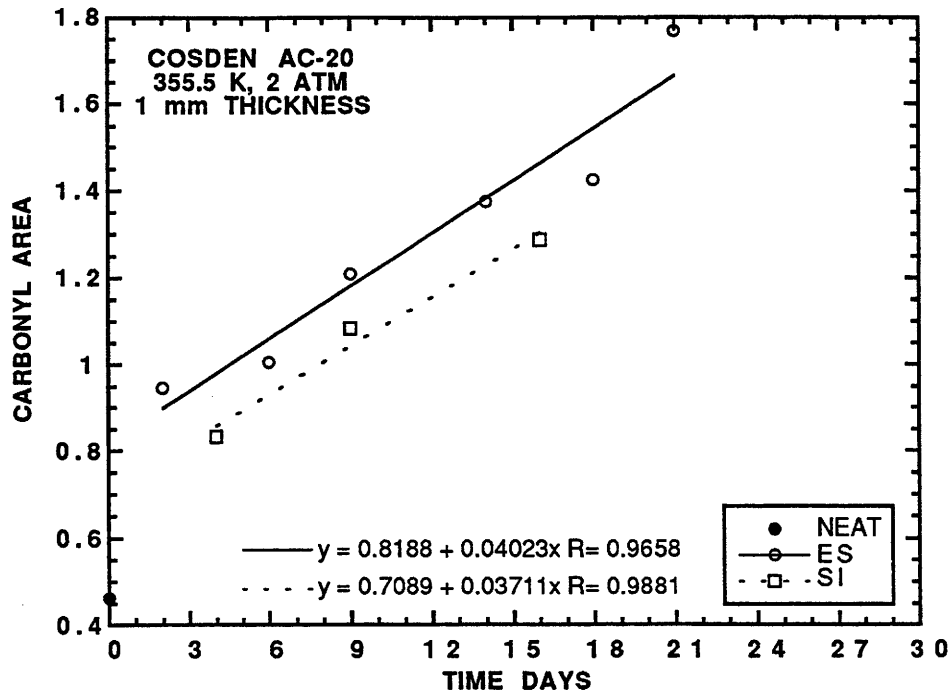


Figure C-12. CAs of Tank, *ES* and *SI* (Cosden AC-20, 355.5 K, 2 atm)

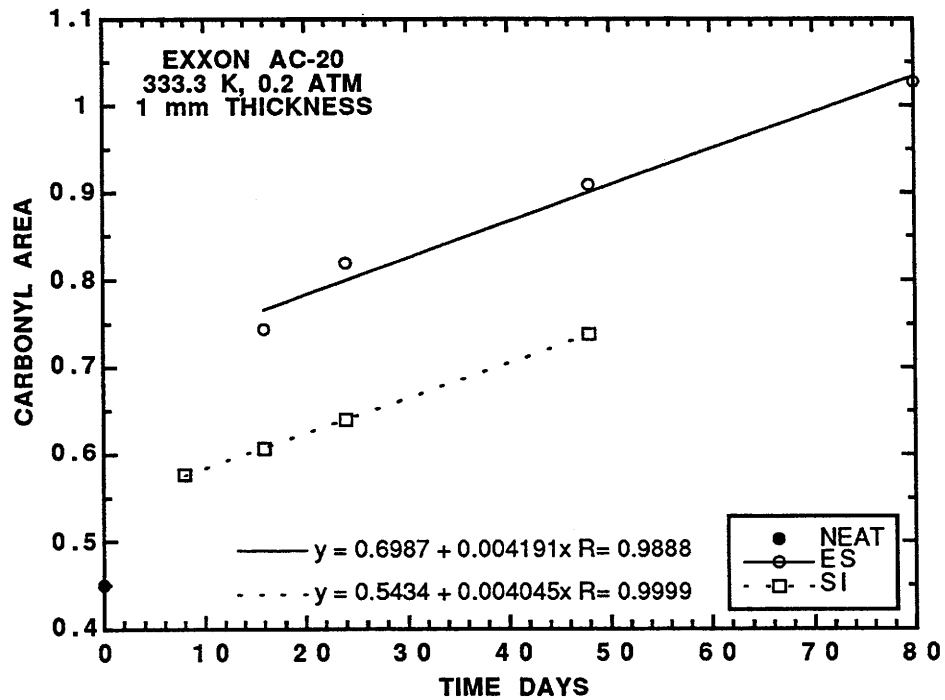


Figure C-13. CAs of Tank, *ES* and *SI* (Exxon AC-20, 333.3 K, 0.2 atm)

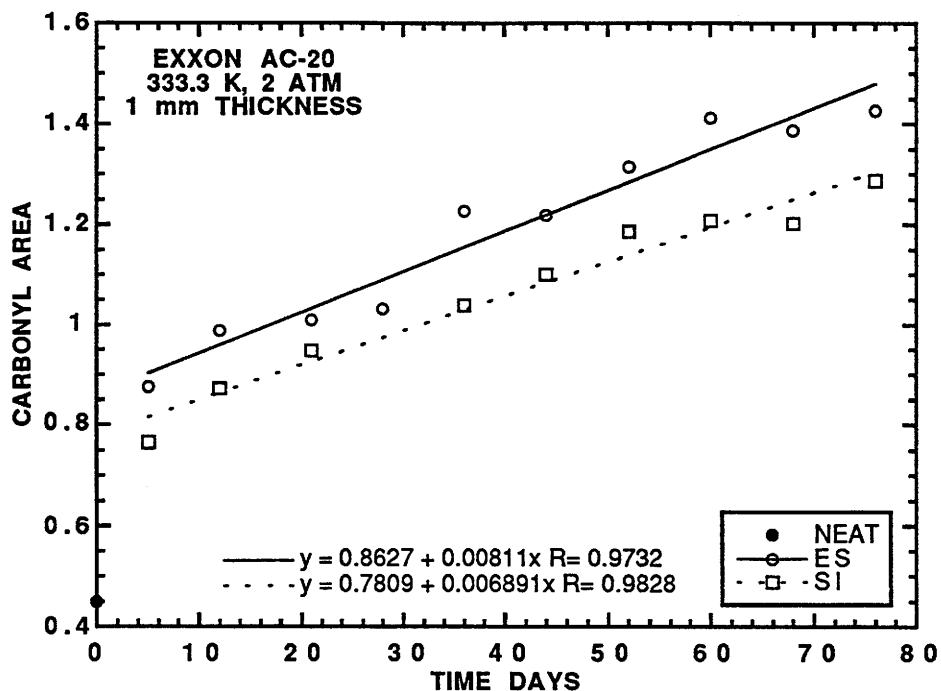


Figure C-14. CAs of Tank, ES and SI (Exxon AC-20, 333.3 K, 2 atm)

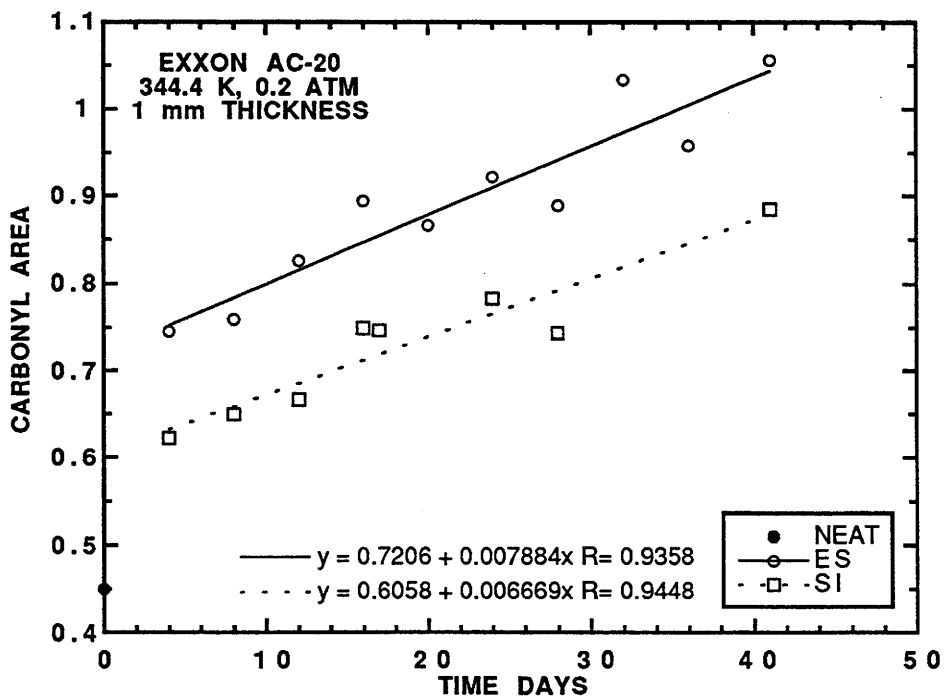


Figure C-15. CAs of Tank, ES and SI (Exxon AC-20, 344.4 K, 0.2 atm)

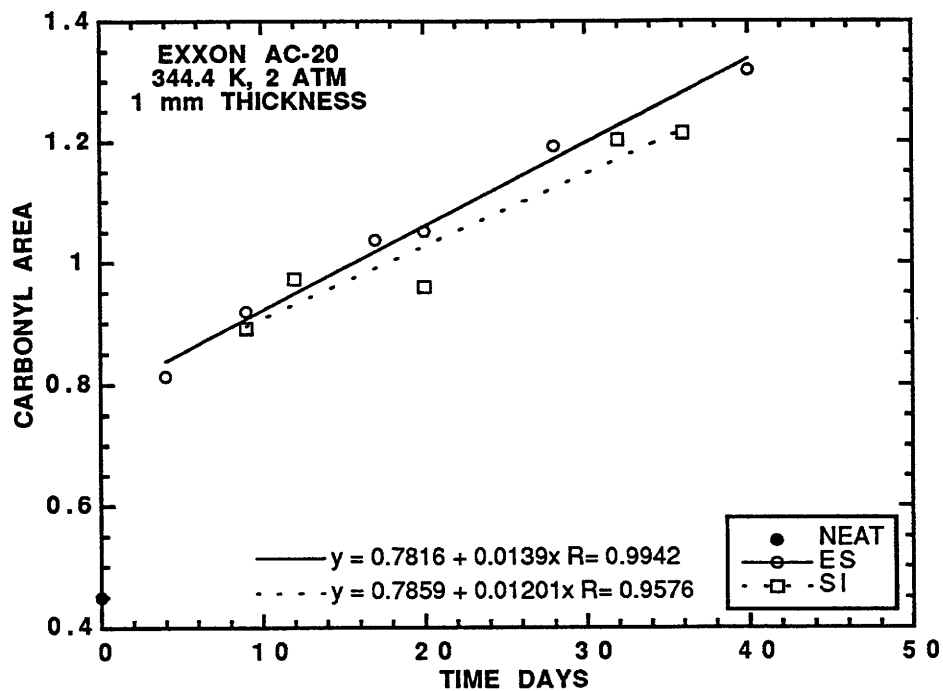


Figure C-16. CAs of Tank, ES and SI (Exxon AC-20, 344.4 K, 2 atm)

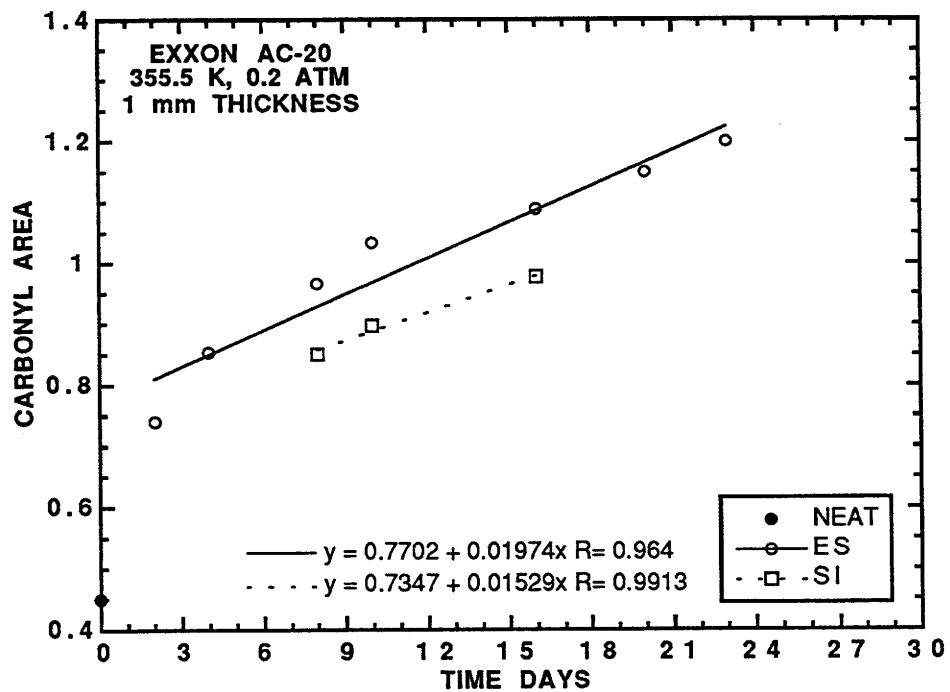


Figure C-17. CAs of Tank, ES and SI (Exxon AC-20, 355.5 K, 0.2 atm)

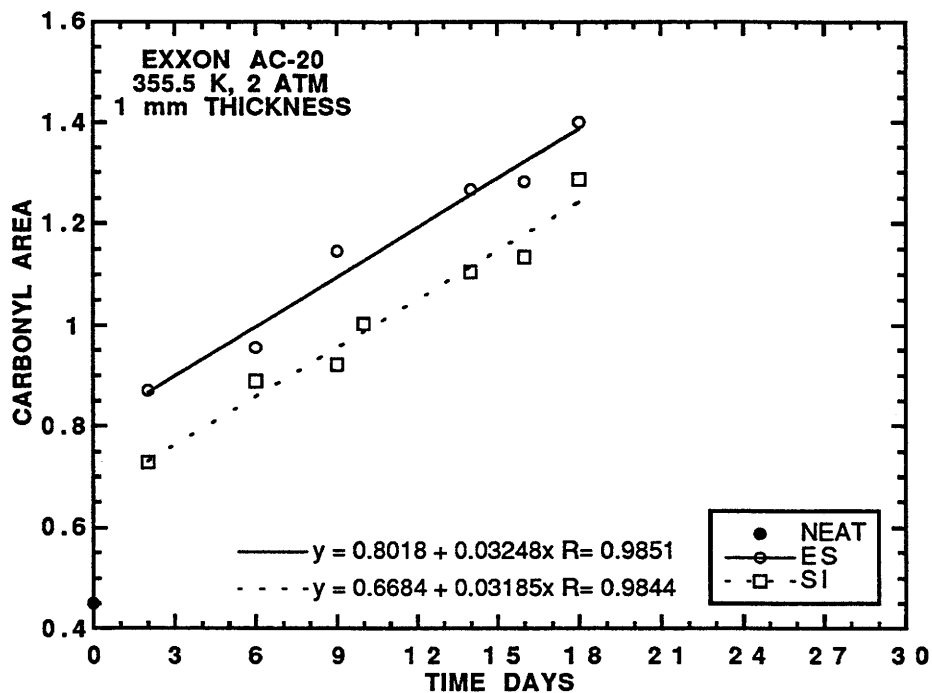


Figure C-18. CAs of Tank, ES and SI (Exxon AC-20, 355.5 K, 2 atm)

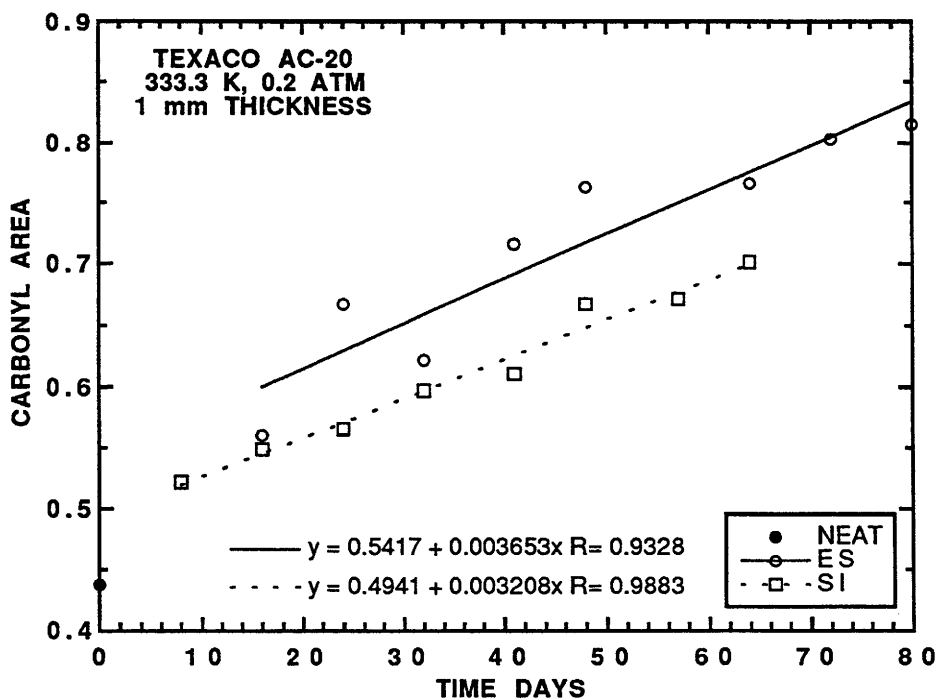


Figure C-19. CAs of Tank, ES and SI (Texaco AC-20, 333.3 K, 0.2 atm)

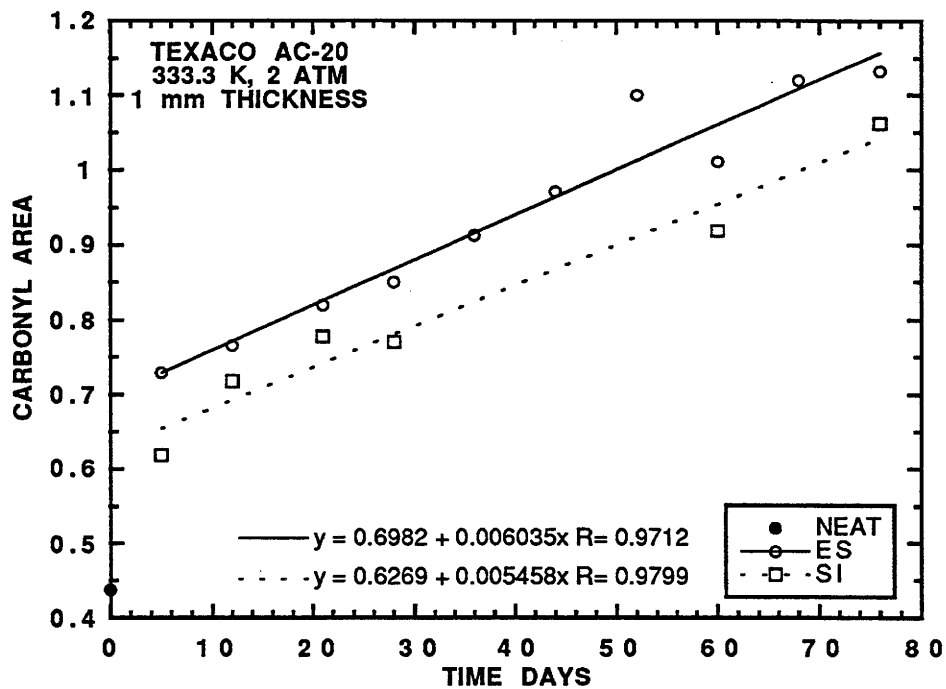


Figure C-20. CAs of Tank, *ES* and *SI* (Texaco AC-20, 333.3 K, 2 atm)

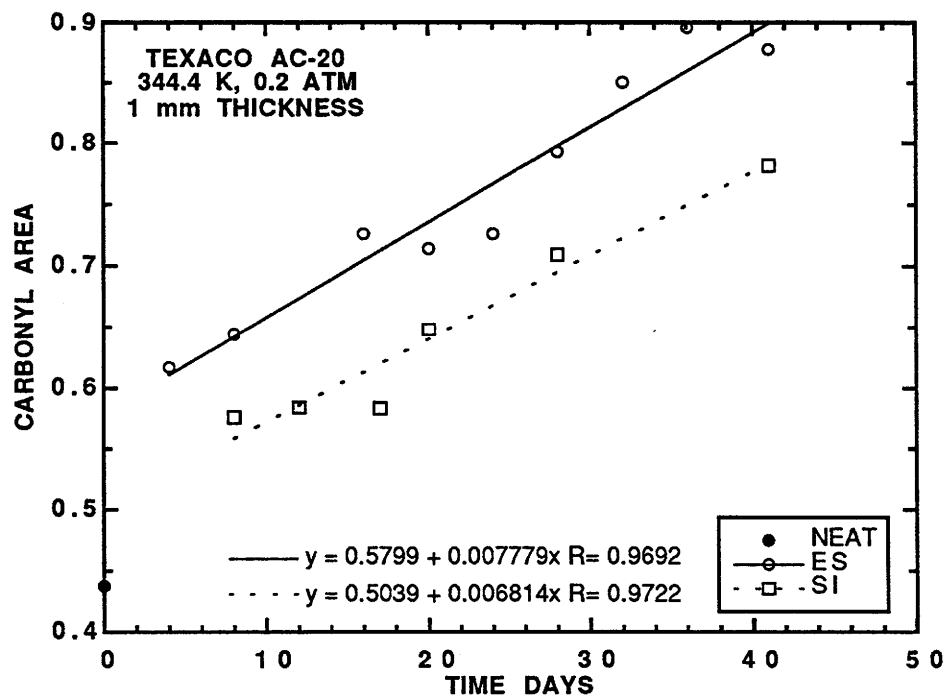


Figure C-21. CAs of Tank, *ES* and *SI* (Texaco AC-20, 344.4 K, 0.2 atm)

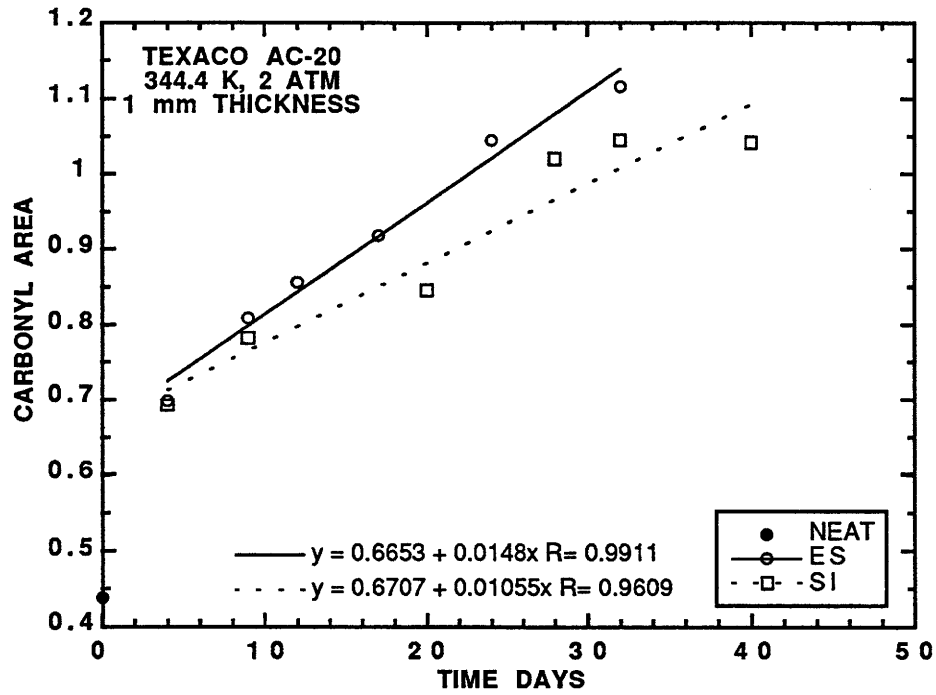


Figure C-22. CAs of Tank, *ES* and *SI* (Texaco AC-20, 344.4 K, 2 atm)

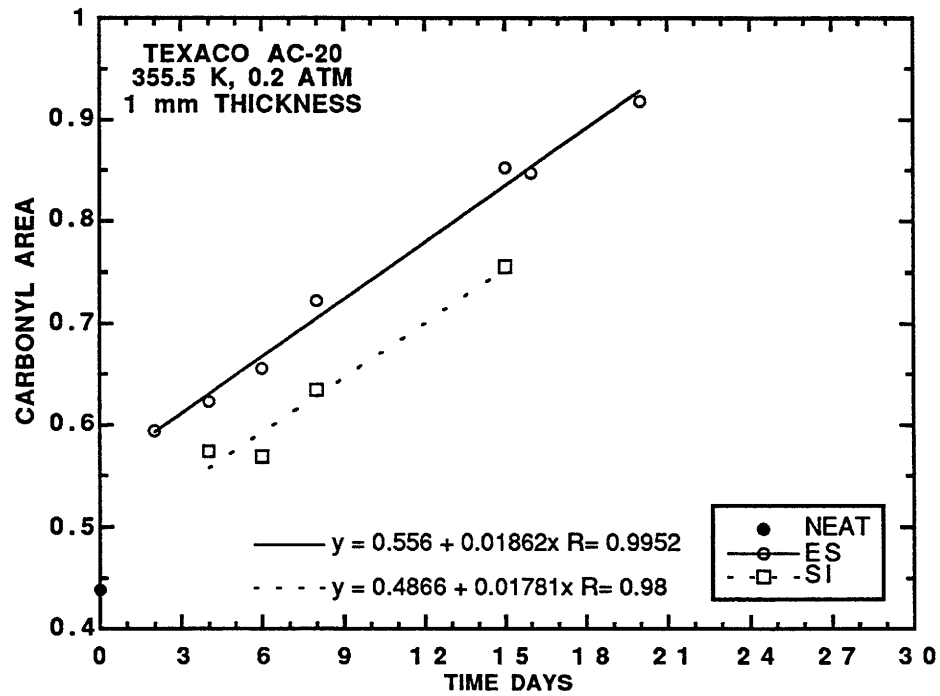


Figure C-23. CAs of Tank, *ES* and *SI* (Texaco AC-20, 355.5 K, 0.2 atm)

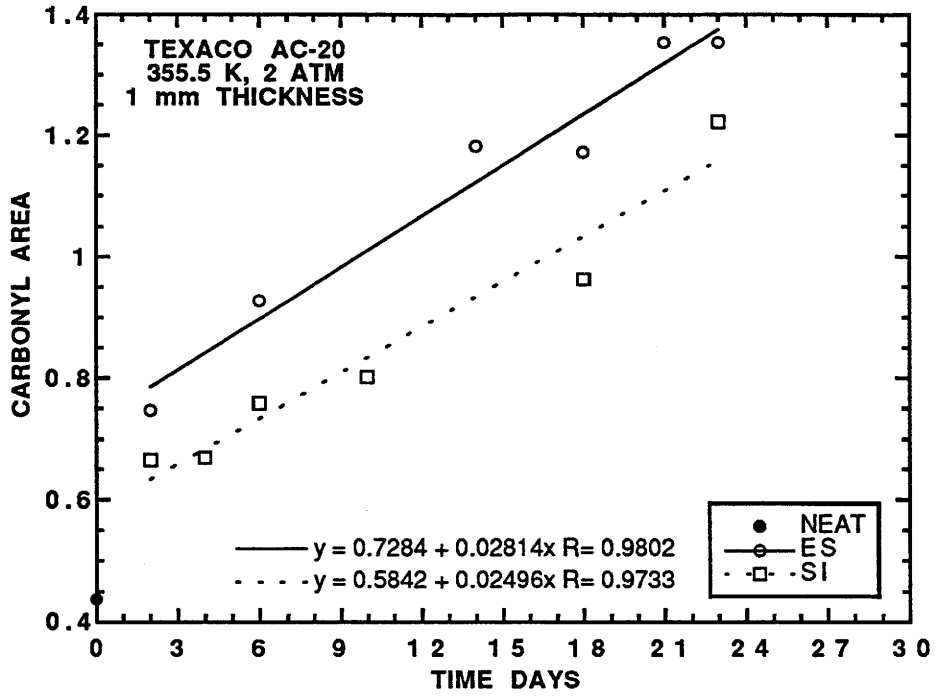


Figure C-24. CAs of Tank, *ES* and *SI* (Texaco AC-20, 355.5 K, 2 atm)